istituto nazionale di fisica nucleare
laboratori nazionali di frascati

2008
ANNUAL REPORT

Scientific Editor
D. Babusci

Technical Editor
L. Invidia

Editorial Office
D. Bifaretti
A. Cupellini

Cover: "Natural Order"
Cover artwork: Claudio Federici

istituto nazionale di fisica nucleare
laboratori nazionali di frascati

2008
ANNUAL REPORT

LNF-09/04 (IR)
April, 2009

Published by
SIDS-Publications & Library
P.O. Box 13 – I–00044 Frascati (Italia)

Available at www.lnf.infn.it/rapatt

Mario Calvetti
LNF Director

Vitaliano Chiarella
Head, Research Division

Pantaleo Raimondi
Scientific Head, Accelerator Division

Claudio Sanelli
Technical Head, Accelerator Division

LNF Scientific Coordinators

Riccardo de Sangro
Particle Physics

Marco Ricci (*until April 2008*) – Francesco Terranova
Astroparticle Physics

Pasquale Di Nezza
Nuclear Physics

Calogero Natoli *(until April 2008)* – Gino Isidori
Theory and Phenomenology

Roberto Cimino
Technological and Interdisciplinary Research

FOREWORD
Laboratori Nazionali di Frascati-Frascati National Laboratories (LNF)
Present and Future

1 Introduction

The Frascati National Laboratories (LNF) is the largest laboratory of the Italian Institute of Nuclear Physics (INFN). It is composed by the Accelerator Division, the Research Division and the Administration, for a total of about 380 staff members.

The Accelerator Division runs the DAΦNE accelerator complex, an $e^+ \, e^-$ storage ring, used to produce ϕ-mesons at a high rate. Three experiments, KLOE, FINUDA and SIDDHARTA, study the ϕ decays, the charged and neutral kaon decays, the kaonic nuclei, produced when a negative kaon is absorbed in a nucleus, and the properties of any other of the particles produced in the ϕ decay chain. A linear accelerator (the Linac) accelerates electrons and positrons to fill the storage rings. The very clean electron and positron beams, with variable energy in the interval between 50 MeV and 850 MeV, variable intensity from 1 to 10^{10} electrons per bunch, at a rate of 50 Hz, can be deflected into an experimental area, the Beam Test Facility (BTF), where a photon tagged beam, of variable energy, is also available. The BTF facility is continuously used by internal and external users. Experiments with cryogenic detectors, channelling of positron with undulated crystals for X-ray production, and other experiments, are planned for the coming years. The Accelerator Division participates in the construction of the CNAO (Centro Nazionale di Adroterapia Oncologica), a 1.2 GeV proton synchrotron used for cancer therapy in Pavia. A free electron laser, named SPARC, is in operation at the LNF, in collaboration with ENEA (the Italian National Agency for New Technologies, Energy and the Environment). The scientific goal of the SPARC project consists in producing 10 ps electron bunches, with emittance smaller then 2 mm $\cdot$ mrad, able to induce the self amplified green synchrotron laser light in the magnetic undulators placed downstream the electron gun. The laser light has been recently observed. A very intense Laser, able to produce 300 TW of 0.8 micron wavelength for 20 fs (the Frascati Laser for Acceleration and Multidisciplinary Experiments, FLAME) is going to be assembled this year. The possibility to accelerate a bunch of electrons in the plasma waves produced by the light in a gaseous target will be explored. The proton synchrotron in Pavia (CNAO) and the laser FLAME should be operational by the end of the year 2009.

Physicists and engineers of the Accelerator Division also participate to the research and development in the field of accelerator technology. The construction of CTF3, the CLIC Test Facility at CERN, the work for the future Linear Collider and the study for a possible future Super B-factory as well, are

part of our research program. The DAΦNE accelerator, which is continuously being improved, produces synchrotron radiation light used by many experimental groups. The very intense infrared light from a synchrotron source is available at DAΦNE. At the moment we have three lines running, the Infra Red line, the X ray line and the UV line, a second X-ray line is under construction. More than a hundred users, in the context of the European research funding TARI program, used this facility last year.

The Research Division is composed of physicists and engineers working in many experiments at the LNF, at CERN (ATLAS, LHCb, DIRAC, ALICE, CMS), at FNAL (CDFII), at JLAB (AIACE), at DESY (HERMES), in Grenoble (GRAAL), at the Gran Sasso National Laboratories LNGS (OPERA, ICARUS), in space borne experiments within the WIZARD program, and also, locally, in the search for gravitational waves with a cryogenic bar (NAUTILUS).

DAΦNE is a beautiful opportunity to study machine physics at its cutting edge. Several modifications of the accelerator have been implemented to increase the luminosity. New technologies will be applied, like the use of fast kickers, to increase the injection efficiencies, kickers that could be used for the ILC damping rings, crab cavities, wigglers with shaped poles and so on. An adequate fraction of the beam time will be dedicated to machine studies, because it is important to understand the machine limits, the new technologies and the new ideas. The LNF are also very active in the field of scientific communication. In fact, every year we have many visitors, mainly students and teachers. Every autumn we organize a week long meeting, with lectures, discussions, visits to the labs, attended by more than 250 secondary school teachers of physics and philosophy.

Prof. Mario Calvetti
Director of LNF

2008 ANNUAL REPORT
CONTENTS

1 – Particle Physics

2 – Astroparticle Physics

3 – Nuclear Physics

4 – Theory and Phenomenology

5 – Technological and Interdisciplinary Research

6 – Accelerator Physics

General Informations

1 – Particle Physics

ATLAS

A. Annovi, M. Antonelli, M.M. Beretta, H. Bilokon,
E. Capitolo (Tecn.), F. Cerutti, V. Chiarella, M. Curatolo,
B. Esposito (Resp.), M.L. Ferrer, C. Gatti, S. Giovannella,
P.F. Laurelli, G. Maccarrone, A. Martini, W. Mei, S. Miscetti,
G. Nicoletti, G. Pileggi (Tecn.), B. Ponzio (Tecn.), V. Russo (Tecn.),
A. Salvucci (Laur.), A. Sansoni, M. Testa (Ass. Ric.),
T. Vassilieva (Tecn.), E. Vilucchi, V. Zambrano (Bors.)

In collaboration with: C. Soprano (Centro di Calcolo)

1 Introduction

In the year 2008 the preparation of the Atlas detector for the first beams in LHC has been completed. In September 2008, when the first beams have been circulated in the LHC, Atlas was ready and data has been collected. Unfortunately, because of an accident occurred to the machine, the running of LHC had to be stopped before beam collisions could be achieved, and the data taken is only interesting for detector commissioning and not for physics. The activity on the detector of the LNF group has mostly concerned the MDT chambers and the muon system, and in part the TDAQ system. The status of the MDT chambers and of the TDAQ system is described in paragraphs 2 and 3. In view of first data from LHC, during the year 2008 an intense activity has been carried on the preparation of the physics analysis and the commissioning of the computing resources and software. In paragraphs 4, 5, 6 and 7 the activity done at LNF on the analysis studies, including the detector calibration in situ, is briefly reported. Paragraph 8 concerns the LNF Tier-2 activity. Finally in paragraph 9 the activity for the upgrade of the track trigger is reported.

2 Status of MDT muon chambers

The commissioning of the precision chambers of the Muon Spectrometer with cosmic rays progressed in 2008 including more and more chambers into the Atlas DAQ. At the LHC startup in September 2008 the percentage of active tubes in all the MDT chambers was about 98.5%. In the shutdown following the LHC incident, in the last weeks of 2008 when the cavern was opened again, the detector maintenance work was resumed and the percentage of dead channels was lowered to less than 0.5%. During the cosmic runs in 2008 several millions of muons have been collected and recorded with magnets ON and OFF and the muon tracking has been performed by means of the MDT chambers. For the processing of these events the whole calibration chain has been used. It makes use of a calibration data stream at the second level trigger, which is sent to three different Tier-2 calibration centers, where it is processed. One of the calibration centers is in Roma 1. With the cosmic data collected the performance of the sagitta measurement with the spectrometer was studied. The chamber positions do not correspond to the nominal geometry, which is determined by the metrology survey with a precision not adequate to the muon precision tracking. The MDT chambers are equipped with a complex and sophisticated alignment system. For the End Cap

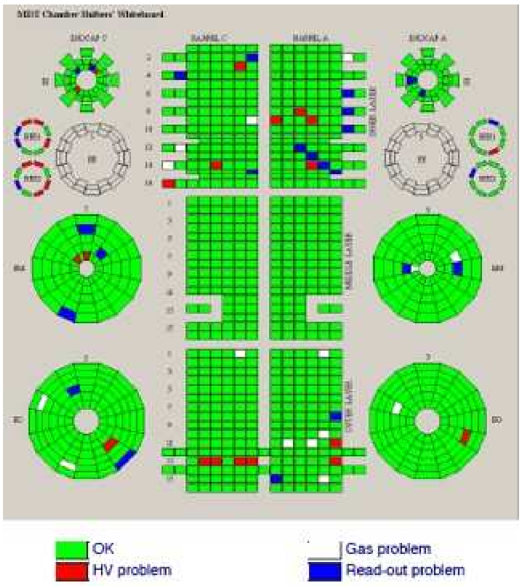

Figure 1: *Status of Barrel MDT chambers. From top are shown Inner, Middle (the large sectors done at LNF), Outer Chambers.*

chambers it was shown that it provides the absolute alignment already at the level of better than 50 microns, as necessary. In the case of the barrel chambers it turned out that the optical alignment could not provide an absolute alignment better than a few 100 microns, which by itself is not adequate. For this reason a track based alignment has been performed. With it, the average sagitta obtained was better than 50 microns (Fig. 2). This was done only for the sectors traversed by the cosmic rays, but it proved the adequateness of the absolute alignment with straight tracks. Runs with magnets OFF are to be performed with the LHC running. The reconstruction of the cosmic data has been compared with the MC simulation and a good agreement was found (Fig. 3). During the first beam experience many splash events have been recorded in Atlas, with thousands of tracks hitting the MDT chambers in the same event. The detector behaved very well and those events demonstrated the very good capabilities of the Read-Out / DAQ system (Fig. 4). As a contribution to the MDT calibration we partecipate to the development of the Oracle database hosted in Rome, Munich and Michigan. During the year 2008 a big effort was dedicated to develop a new schema able to meet the new calibration software requirements. This activity was presented to international conference and workshops [3], [6], [7].

3 DAQ Commissioning

The activity on the Trigger and Data Acquisition (TDAQ) system has been focused, during the year 2008, on the following aspects [3], [4], [5] :

1. Developments of the Event Building (EB) sub-system;
2. Technical runs for TDAQ commissioning and first data;

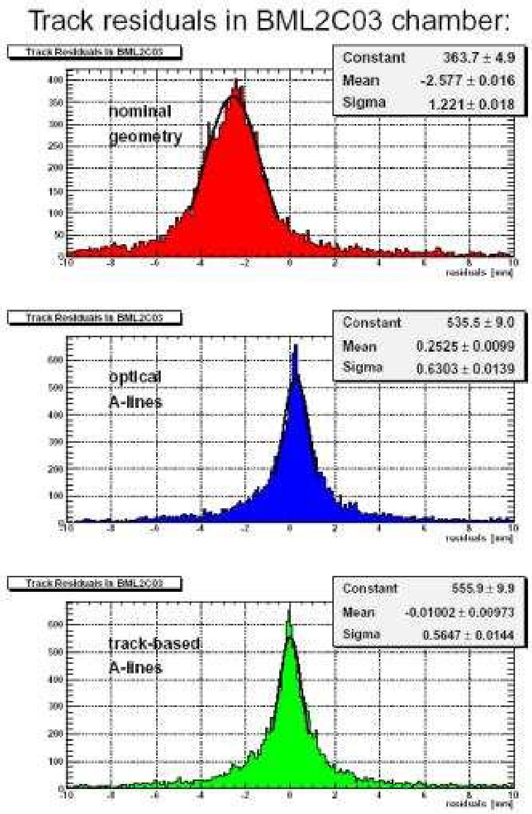

Figure 2: *Residual distribution for the track fit in the Muon Spectrometer. From top: Ideal Geometry, Optical Survey Correction, Track Alignment.*

The Event Builder sub-system was running with minimal interventions during all the TDAQ and detectors commissioning activities and the first LHC data. In the meantime important facilities were added. Events are now fully or partially built depending on run requests. The partial building can contains a specific list of sub-detectors or specific readout drivers (ROBs) or both, and are of interest for calibration runs when higher acquisition rates are needed. How the Event Building provides events to monitoring processes was also improved. The main modification in the protocol is that an event is provided to multiple monitoring processes. In the previous version every event was given to only one monitor and in case the event did not fullfil the selection criteria it was unused, making big inefficiencies in particular in case of rare events. The event monitor was also unriched producing online histograms. The LNF group has been involved in the definition and implementations of those components. There are not previsions to include new developments in the TDAQ-02-00-0* release that will be built starting 2009 and will be used in the first physical runs.

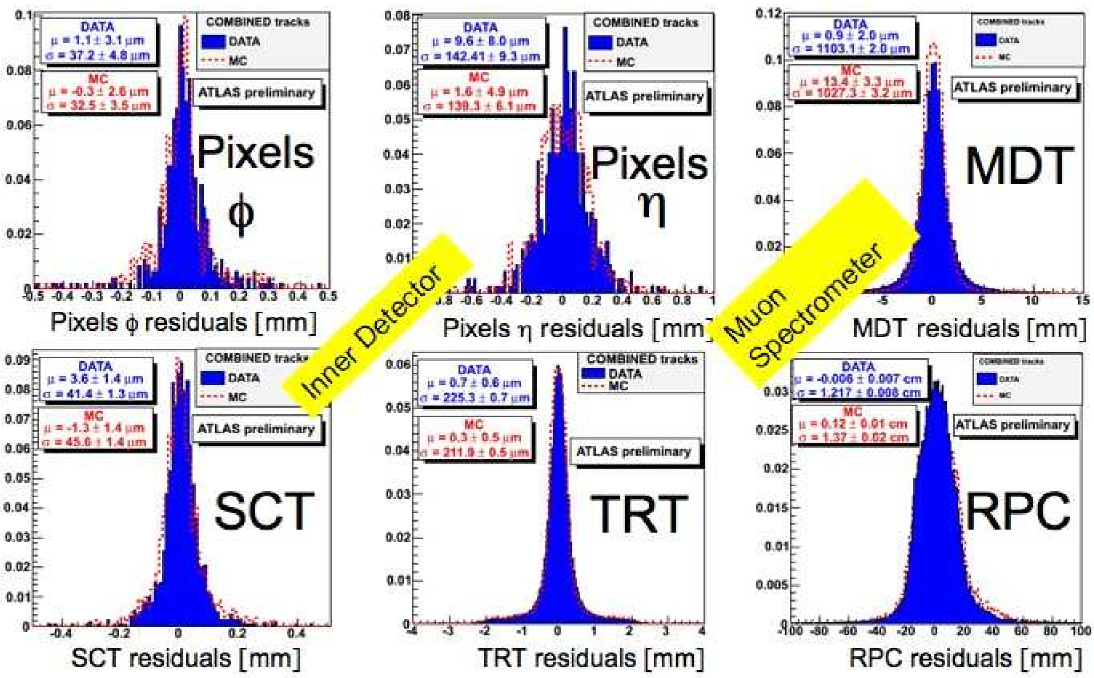

Figure 3: *Residual distribution for the track fit in the combined recontruction. All the detectors involved are showed.*

4 Report of the analysis activity

In the last LNF Report [1] we have shown that part of our analysis activity was dedicated to the understanding and the determination "in-situ" of the detector performance, with particular interest for the muon spectrometer. This activity covers the measurement of reconstruction efficiencies, determination of the energy scale and resolution, correction and monitoring of the miscalibrations due to, for instance, misalignments between detector elements. In Sec. 5, we present an update of this work. In order to test and refine all these methods, and to understand their limits, we decided to apply them to a benchmark measurement. We then chose to measure the ratio $\sigma(pp \to Z \to \mu\mu)/\sigma(pp \to W \to \mu\nu)$. This quantity has a relatively small error (few %) and will be performed with the first data at LHC (O(100 pb^{-1}) expected). We would like to stress here that this activity seeded a fruitful collaboration among several INFN sections, mainly Cosenza, Frascati, Pavia, Roma2, and Roma3. This activity is described in Sec. 6. Finally, all the experience gained with this analysis, from the detector understanding to the data handling, must be adressed to the search of physics beyond the Standard Model. Still here the main interest is for multi-muon channels. Of particular interest are some general models of electroweack simmetry breaking based on the higher symmetry $SU(2)_L \times SU(2)_R$. In these models, new physics may show up as new heavy resonances deaying into couple of vector bosons. A strong interest on this field was also shown by the Frascati theory group, with which we have started a series of meetings for defining which measurements

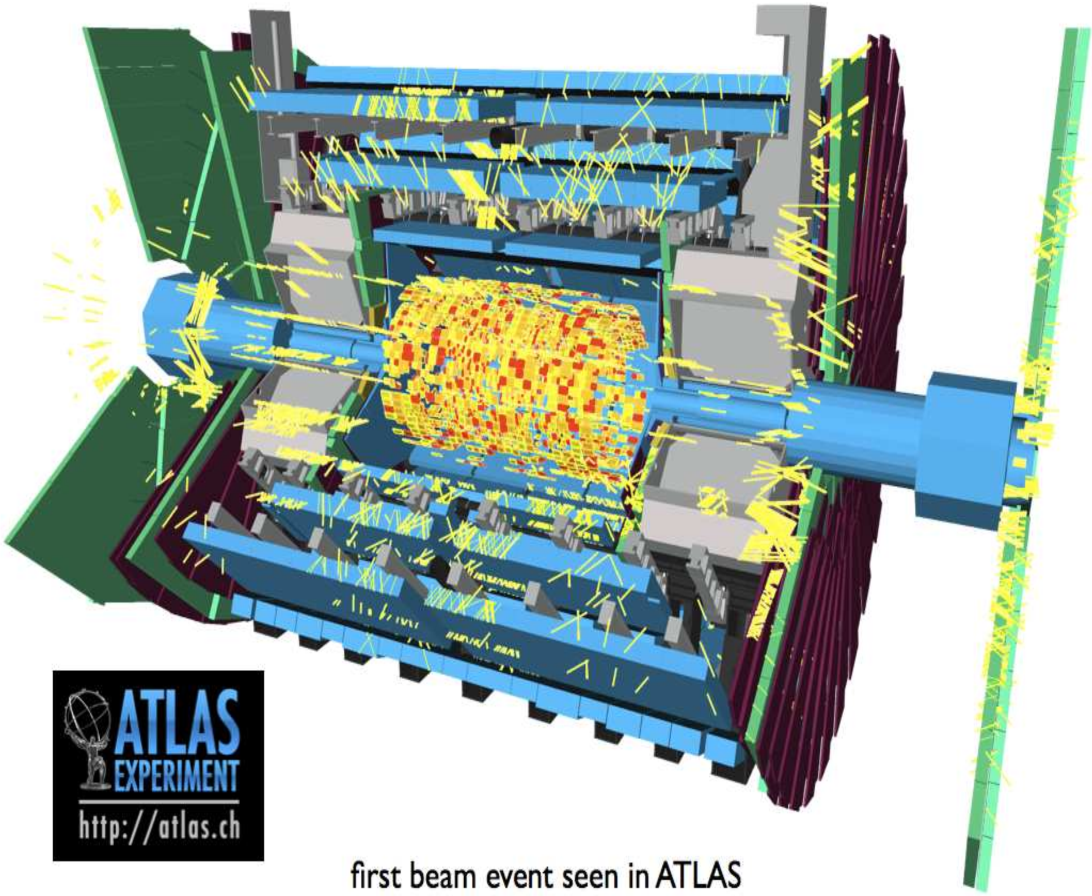

Figure 4: *Event Display of one of the first "Splash" Events seen in ATLAS.*

are possible according to a given integrated luminosity. From the experimental point of view, we are interested, first of all, in understanding the spectrometer behavior at high momenta, above several hundred GeV. The simplest benchmark channel is the decay of a Z' into two muons. This is discussed in Sec. 7.

5 Calibration and monitoring with $Z \to \mu\mu$

In the previous report [1], we have shown how the Z mass constraint can be imposed to re-determine the muon momenta and correct errors in the reconstruction due to misalignments in the muon-spectrometer chambers. For this study, we have used a sample of about 100 thousand $Z \to \mu\mu$ decays reconstructed with a detector geometry in which the muon spectrometer chambers have been rotated (O(1mrad)) and shifted (O(1mm)) with respect to the nominal position. The effect of the misalignments have been investigated within the projective towers. For this scope we have defined about 360 towers.

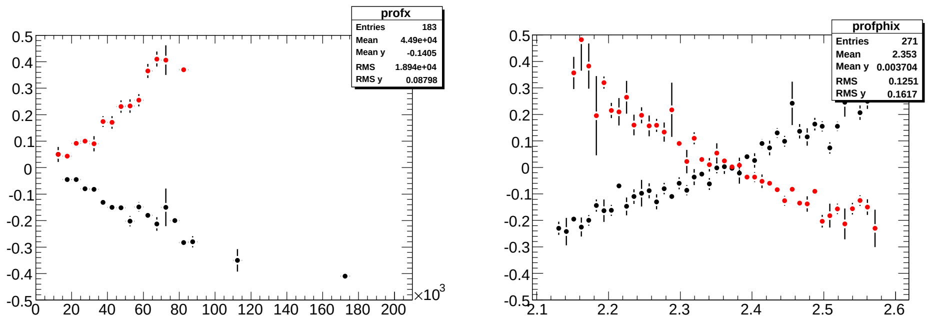

Figure 5: *Left Panel: percent residuals of reconstructed muon momenta, dp/p, as a function of the MC momentum for positive (red) and negative (black) muons. Right Panel: dp/p as a function of the angular coordinate along the chamber tubes (ϕ).*

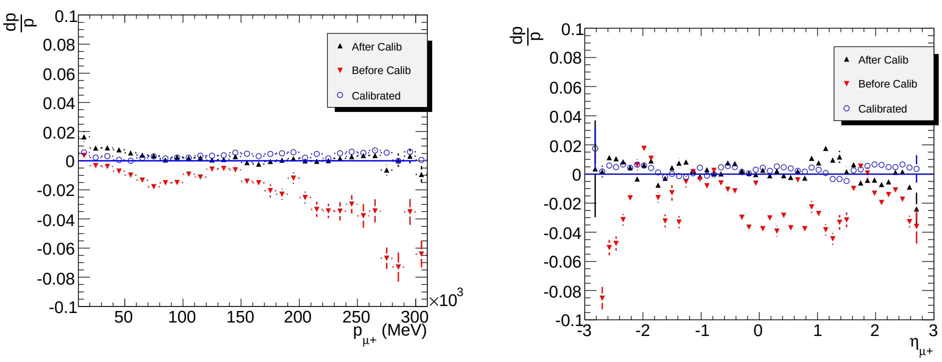

Figure 6: *Percent momentum residuals as a function of the muon momentum (Left Panel) and pseudorapidity η, (Right Panel), before the calibration (red triangles), after the calibration (black triangles), and for ideally-alligned sample (blue circles).*

The effect of chamber shifts and rotations on the momentum reconstruction is shown in Fig. 5. Here, the percent error on the momentum (with respect to the true MC momentum) is shown as a function of the momentum itself (left panel) and as a function of the angular coordinate along the chamber tubes (ϕ) (right panel). In the first case, the relative shift among the three tower chambers leads to an error on the sagitta measurement and to the typical linear behavior on the momentum residuals. Moreover, the effect has opposite sign for positive and negative muons. In the second case, the chamber relative rotations lead to an error on the sagitta measurement that is proportional to the distance from the center of the chamber. Again the effect has an opposite sign for the two muon charges.

Parametrizing these effects, and re-determining the muon momenta with a kinematic fit, event by event, we determine for each projective tower the effective corrections to the reconstructed momenta. The result of the calibration procedure can be appreciated in Fig. 6, where the percent residuals of the reconstructed momenta are shown as a function of the momentum itself (right

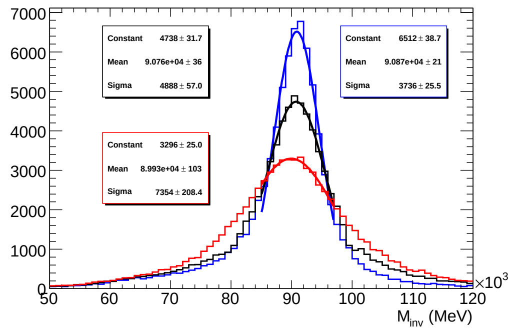

Figure 7: *Z reconstructed invariant mass, before the calibration (red histogram), after the calibration (black histogram) and for ideally-alligned sample (blue histogram).*

panel) and as a function of the pseudorapidity η. The residuals before the calibration are shown in red downward triangles, while those after the calibration are shown with black upward triangles. We can see how the average residuals improve after the calibration and how any non-linearity is removed.

Finally, the effect on the reconstruction of the Z invariant mass is shown in Fig. 7. The width of the Z lineshape goes from about 7.4 GeV, before the calibration, to 4.7 GeV after the calibration, while in the ideal case it should be 3.7 GeV. The residual miscalibration is under study, but is mainly due to the overlapping regions between projective towers that break the approximations in our parametrization. However, it must be stressed that we expect to apply this procedure after the alignment with the optical system and and with single muon tracks. In this case, the residual misalignments should be within 100 μm and the effect of the overlapping regions should be much smaller. Then, while the optical and single-track alignment provides only indirect checks on the spectrometer calibration, since they are not based on an absolute momentum measurement, this method provides, beside a fine calibration of the momenta, a direct way of monitoring the calibration status as a function of any kinematical variable (η, ϕ, and p_T).

6 Measurement of the cross section for the processes $pp \to Z \to \mu\mu$ and $pp \to W \to \mu\nu$

Electroweak boson production has a large cross section at LHC, and the ratio of the two cross sections is known with an uncertainty of few %. This means that with early data, on the order of 100 pb^{-1}, with about 100,000 $Z \to \mu\mu$ decays and 1 million $W \to \mu\nu$ decays, we will be able to perform a precise measurement of this ratio. Therefore, this measurement allows us to test our methods for measuring efficiency, and calibrating the momenta at least to the same accuracy level. Moreover, performing a complete analysis, even if only on MC samples, will allow us to set up all the required software tools to read the ATLAS data, run jobs on the grid and get ready for the

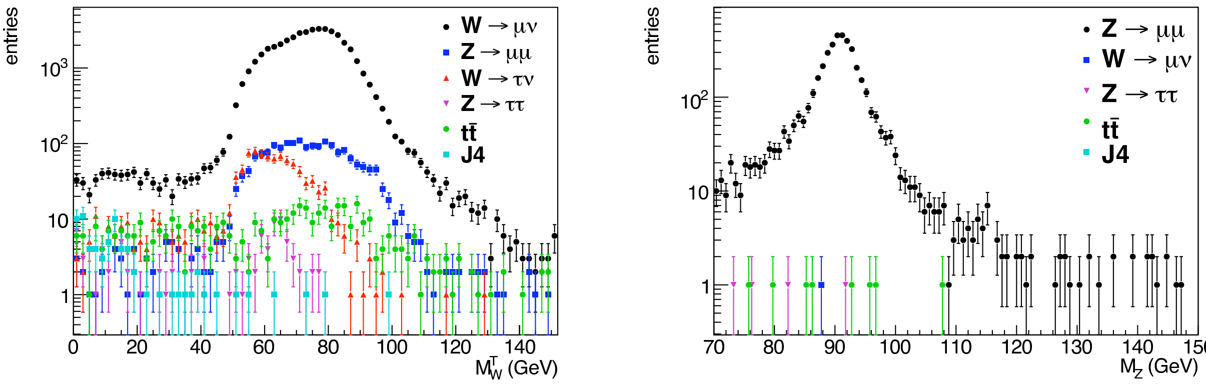

Figure 8: *Left Panel: tranverse mass after the selection of $W \to \mu\nu$ events. Right Panel: Reconstructed invariant mass after the selection of $Z \to \mu\mu$ events.*

first data-taking.

This work is done in collaboration with several INFN sections (Cosenza, Pavia, Roma2 and Roma3). In particular, it is based on a software framework EWPA [2] developed in Pavia. Our goal is to produce two different MC samples with an equivalent integrated luminosity of 100 pb^{-1}. The first sample will be reconstructed with the same geometry used in the simulation (ideal case), while the second sample will be reconstructed with misalignments in the inner detector and in the spectrometer. This last sample will be used as a "data" sample. We have already tested the reconstruction with different geometries and we are now producing the first datasets with these misalignaments.

In the meantime, we have performed the signal selection within the EWPA framework determining the signal efficiencies and the amount of residual background (see Fig. 8). The efficiencies are dominated by the geometrical acceptance. The background are negligible for the Z channel, while are at the level of few % for the W channel.

The work is ongoing for determining tracking and trigger reconstruction efficiencies from $Z \to \mu\mu$ sample (Fig. 9), for measuring the momentum resolution as explained in the previous report [1], and for combining all these information together to correct the MC simulation.

7 Search for $Z' \to \mu\mu$

The study of the process $pp \to Z' \to \mu\mu$ have been considered as a benchmark measurement for investigating the ATLAS performance in reconstructing muon tracks at high momenta, and to understand how to extrapolate the reconstruction efficiencies, energy scale and resolution determined with the Z samples to the TeV region.

We considered Z' bosons within the SSM model, where the new boson is an exact replica of the SM Z boson, i.e. same couplings, but with higher mass (1 TeV in this case). The signal selection is quite easy and the only relevant background is due to the continuum Drell-Yan process. The production cross section is on the order of 0.5 pb, and the selection efficiency is about 60% in a detector with an ideal alignment. In Fig. 10 (left panel), we show the discovery plot for such a boson at ATLAS. Here we test the background-only hypothesis on background only and signal plus

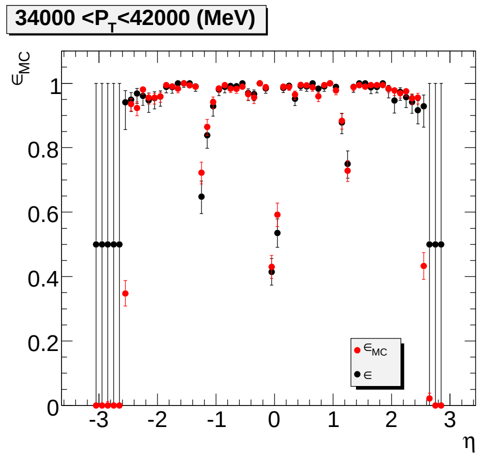

Figure 9: *Example of tracking efficiency determined using $Z \to \mu\mu$ events. The comparison is done between the true MC efficiency (red points) and the efficiency measured with the method (black points).*

background pseudo-experiments. The green line crosses the red line for an integrated luminosity of about 10 pb^{-1}, corresponding to the expected integrated luminosity needed for a 5σ discovery.

Further studies are ongoing for understanding the effect on the discovery potential of detector miscalibrations. For instance, in Fig. 10 (right panel), we show the effect on the momentum resolution of 500 μm shifts in the nominal position of the muon chambers, for muon tracks reconstructed with the muon spectrometer standalone, and combining inner detector with the muon spectrometer measurements. In this case the inner detector is ideally aligned so that most of the miscalibration is recovered by combining the two measurements. However, we are now also testing the effect of misalignments in the inner detector. Of particular interest is the effect of such misalignments in the reconstruction of combined tracks and in particular on the trigger efficiency. A preliminar study shows that if for the trigger we are using only combined tracks, in presence of miscalibrations, the efficiency drops down by a large ammount, spoiling the potential discovery for these kind of particles.

8 LNF Tier-2 activity

The LNF Tier-2 computing farm is considered a proto-Tier-2 by INFN and is still in the process of getting officially approved. However, during 2008 it worked at full efficiency providing computing power and data storage for official and private ATLAS simulation production campaigns. Because of LHC starting delay, ATLAS accepted a reduction of the financial support dedicated to computing resources, and in particular the LNF Tier-2 received less than the 10% of the total assignments. The configuration was increased by using also local resources.

- The computing power increased from 80 KSI2k to 170 KSI2k;

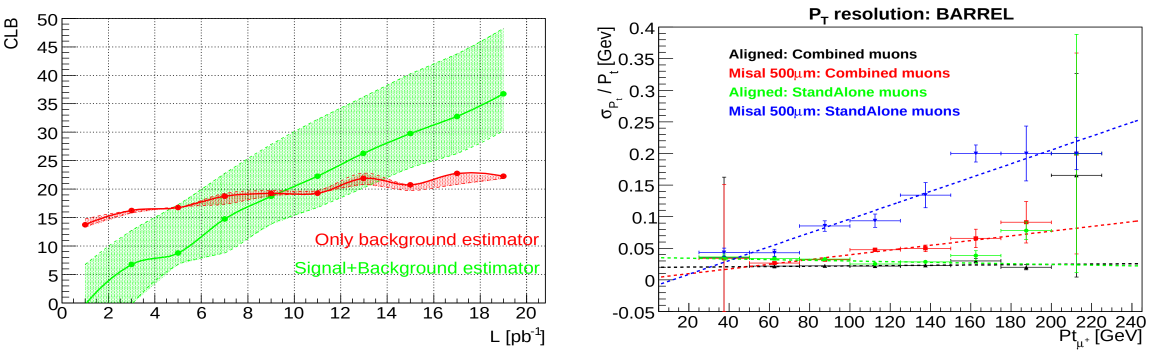

Figure 10: *Left Panel: Discovery plot for a SSM Z' in the muon channel. The background-only hypothesis is tested on background and signal plus background pesudo-experiments. The point where the green line crosses the red line corresponds to the integrated luminosity for a potential 5σ discovery. Right Panel: Momentum resolution for stand-alone and combined muon tracks for an aligned detector and in presence of shifts of the muon chambers with respect to the nominal position on the order of $500\mu m$.*

- The storage capability increased from 33 TB to 46 TB usable, corresponding to 63 TB raw.

At present the Tier-2 has a dedicated man-power equivalent to 2 FTE: 0.2 FTE from the Computing Service, responsible for hardware installations, configurations and network management, and 1.8 FTE from the ATLAS group, responsible of software installation and management and all ATLAS related interventions and users support. For example, a new farm monitoring system was installed and configured.

Some of the most relevant periodic activities we cite:

- Two people partecipates to the ATLAS Italy shifts for cloud monitoring;
- The group partecipates to phone conferences like SA1, accounting, Tier-2 federation, analysis activities;
- The group provides and validates accounting data;

The group suffered a sustantial reduction of dedicated manpower. In particular a fulltime dedicated to the DDM central management as INFN contribution, did not get contract renewal. The plot 11 shows in red, day by day, the Computing time used during 2008. The plot indicates the trend of the computing resources increment.

9 Report on Fast Track

The trigger is a fundamental part of any experiment at hadron colliders needed to select on-line the low cross-section physics from the huge QCD background. Experience at high luminosity hadron collider experiments shows that controlling trigger rates can be extremely challenging as the luminosity increases, physics goals change in response to new discoveries, and the detector ages. It is thus essential that the trigger system be flexible and robust, and have redundancy and

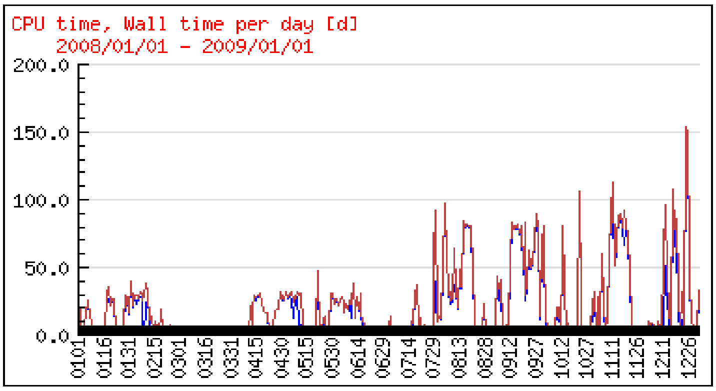

Figure 11: *Day by day CPU usage during the year 2008.*

significant operating margin. Providing high quality track reconstruction over the full ATLAS Inner Detector by the start of processing in the level-2 computer farm can be an important element in achieving these goals. With the goal to improve and make more robust the ALTAS trigger, during summer 2007 the group joined the Fast-Track proposal for "A hardware track finder for the ATLAS trigger". This is a proposal to build a hardware track finder (FTK) as an upgrade to the ATLAS trigger. It will provide global reconstruction of tracks above 1 GeV/c in the silicon detectors, with high quality helix parameters, by the beginning of level-2 trigger processing. FTK can be particularly important for the selection of 3rd-generation fermions (b and). These have enormous background from QCD jets, which can be quickly rejected in level-2 if reconstructed tracks are available early. This RD proposal is aimed at producing a full technical design report for FTK. The Fast-Track proposal has been approved for RD by the ATLAS experiment on February 2008. The Frascati's group is developing a hardware-implementable clustering algorithm for the pixel detector. The clustering for the pixel detector is one piece of Fast-Track that needs RD from scratch. Clustering in the pixel detector is a non trivial computational problem because of the 2D nature of the pixel detectors and of the huge amount of data involved. The pixel detector's RODs deliver data with 132 S-link fibers each with a 1.2 Gbits bandwidth. The clustering algorithm must identify and clusterized hits as well as calculate the center of the cluster. During 2007 we implemented a first offline simulation of a first clustering algorithm. This algorithm will not necessarily be the final algorithm but is used a first reference for the clustering performances. During 2008, we studied in detail two candidate algorithms to be implemented in hardware. After considering several options and comparing the simulation results we have found an algorithm that solves the clustering problem. It achieves the same resolution as the offline and it is implementable within reasonable time and cost. The algorithm is based on a few main ideas: - it uses FPGA distributed logic (CLB) in order to recognize the association between contiguous clusters; - this logic reproduces internally to the FPGA the structure of the pixel detector; - in order to save a factor in excess of 10 on the amount of logic and thus on the cost, the logic doesn't implement the full grid of a pixel module (328x144 for the ATLAS' pixels), but it corresponds to a window (328x8) that virtually slides over the pixel module while data is received. The essential feature of this approach is that the processing time is proportional to the number of received hits. Thus, we avoid completely the combinatorial problem of software-based clustering algorithms that have processing time worse than quadratic in the number of hits. Mapping the pixel module onto the FPGA, allows to obtain a processing time that is linear with respect ot the number of hits. Thus making the algorithm intrinsically stable with respect to luminosity. In fact, as instantaneous luminosity increase, generating higher hit density, the processing time will scale linearly with the number of hits, in the same way as the readout does. For this reason clustering will not be a bottleneck for the system. These ideas have been studied and resulted in a first implementation of the algorithm that solves the clustering problem with a sensible amount of hardware that is one FPGA (xc5vlx155) for each one of the 132 S-Links which carry the data of the pixel detector (each S-Link sends 1.2 Gbits of data). As of today, we have a FPGA implementation of the algorithm core. It is a proof of feasibility in the FPGA simulation framework. These results have just been submitted for presentation at "16th IEEE NPSS Real Time Conference - RT09, IHEP, Beijing, China, 10-15 May, 2009".

10 Conclusions

In the year 2008 LHC started and Atlas was ready for data. In the year 2009, after a long shut down, LHC is foreseen to restart in the fall. Atlas eagerly waits for first collisions in the LHC.

References

1. LNF Report 2007.

2. Bellomo, M.
`http://indico.cern.ch/getFile.py/access?contribId=4&resId=0&materialId=slides&confId=36008`

3. The ATLAS collaboration, JINST **3** S08003 (2008).

4. A. Abdesselam, *et al.*, JINST **3** P01003(2008).

5. A. Abdesselam, *et al.*, JINST **3** P02007 (2008).

6. P. Bagnaia *et al.*, Nucl. Phys. B **177-178** 269-270 (2008).

7. P. Bagnaia *et al.*, "Calibration model for the MDT chambers of the ATLAS Muon Spectrometer", ATLAS Note: ATL-MUON-PUB-2008-004; ATL-COM-MUON-2008-006.- Geneva: CERN, 2008 - 23 p.

BaBar

F. Anulli (Art. 23), R. Baldini Ferroli, A. Calcaterra, L. Daniello (Tecn.), R. de Sangro, G. Finocchiaro, S. Pacetti (Bors. PD), P. Patteri, I. Peruzzi (Ass., Resp.), M. Piccolo, M. Rama, A. Zallo

1 Introduction

BaBar has run at the SLAC asymmetric B-factory PEP-II till April 2008; the physics program of *BaBar* is centered on, but not limited to, the study of the CP violation in the decay of neutral B mesons. The B system is the best suited to study CP violation because the expected effects are large, appear in many final states and, most importantly, can often be directly related to the Standard Model parameters. The datasample collected at the $\Upsilon(4S)$ resonance has allowed significant advances in a large number of topics in B, charm and tau lepton physics; all three angles of the Unitarity Triangle have been measured, direct CP violation has been observed in B decays, several new B decay modes have been measured, and new charmed states have been discovered.

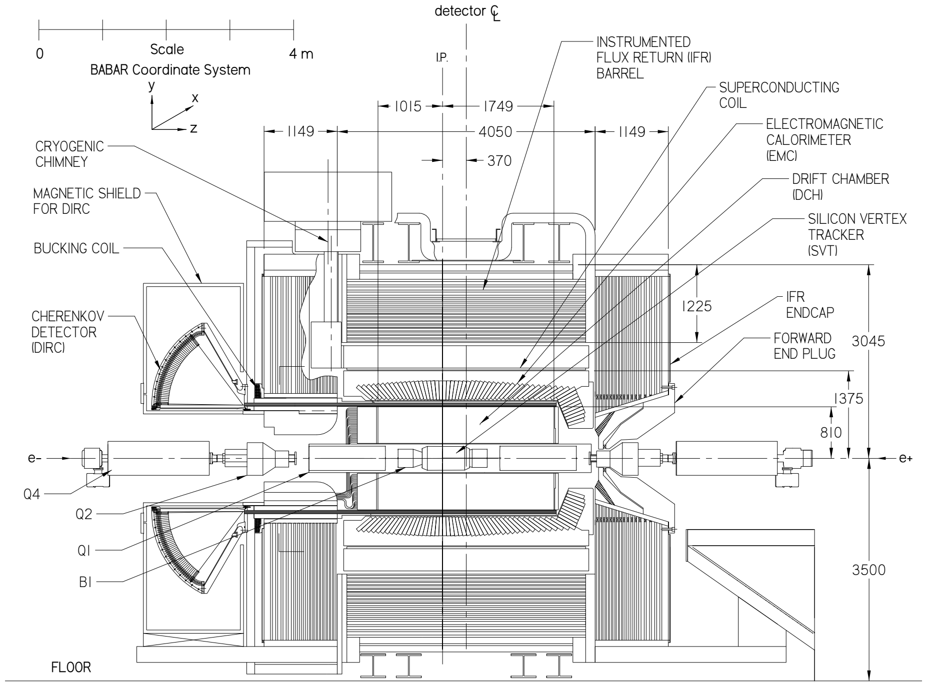

Figure 1: *Elevation view of the BaBar Detector.*

The PEP-II asymmetric e^+e^- collider has operated mainly at a center-of-mass energy of 10.58 GeV corresponding to the mass of the $\Upsilon(4S)$ resonance, which decays 50% in B^+B^- and 50% in $B^0\ \overline{B}^0$. The electron beam of 9.0 GeV collides head-on with the positron beam of 3.1 GeV resulting in a Lorentz boost ($\beta\gamma = 0.56$) to the $\Upsilon(4S)$ resonance, making possible the measurement of the time-dependent CP violation of the neutral B's. The PEP-II operations stopped in April 2008 after a budget cut has shortened the original schedule.

The *BaBar* detector (Fig. 1) has been designed primarily for *CP* violation studies, but it has also served well for the other physics objectives of the experiment. The asymmetry of the beam energies is reflected in the detector design: the apparatus is centered 37 cm ahead of the collision point, along the direction of the high-energy beam, to increase forward acceptance. Charged particles are detected and their momenta measured with the combination of a five-layer silicon vertex tracker (SVT) and a 40-layer drift chamber (DCH), both operating in a 1.5 T solenoidal magnetic field. Photons are detected by a CsI(Tl) electromagnetic calorimeter that provides high detection for energies above 20 MeV. Charged particle identification is provided by the ionization loss measurements in the SVT and DCH, and by an internally reflecting ring-imaging Cherenkov detector covering the central region of the detector. Muons and neutral hadrons are identified in the iron magnet's yoke, where a total thickness of 65 cm of Fe plates has been segmented and instrumented with Resistive Plate Counters and Limited Streamer Tubes. This system is called Instrumented Flux Return, or IFR.

2 Activity

As a consequence of the budget cut to the US HEP field in 2008, the *BaBar* data taking was reduced to about three months (from January to April 6) as opposed to the previously planned ten months. Since running at the $\Upsilon(4S)$ for just three months would have determined a modest relative increase of the overall $\Upsilon(4S)$ sample, it was decided to make the best use of the data collected by *BaBar* by running at center-of-mass energies corresponding to the $\Upsilon(3S)$ and $\Upsilon(2S)$ resonances, and by scanning the energy region between 10.54 and 11.20 GeV. While the Upsilon meson and its excited states were discovered over twenty years ago, little was actually known about the potentially rich spectroscopy of bottomonium. In particular, key states predicted by the Standard Model, such as the ground state η_b or the h_b, had never been observed before. In addition, heavy quarkonium is an excellent place to search for new physics effects. Scanning energies above the $\Upsilon(4S)$ is important to search for bottomonium-like exotic states that would give indications on new forms of aggregation states not fitting the ordinary interpretation of quark-antiquark bound states.

With these motivations *BaBar* collected 30.22 fb^{-1} at the $\Upsilon(3S)$ (10^8 $\Upsilon(3S)$ decays), 14.45 fb^{-1} at the $\Upsilon(2S)$ (10^8 $\Upsilon(2S)$ decays) and a total of 3.9 fb^{-1} scanning the energy range between 10.54 and 11.20 GeV. The integrated luminosity as function of time is reported in Fig. 2. The major result is the first observation of the bottomonium ground state, the η_b, performed by *BaBar* and published in [18].

Besides the study of bottomonium states, the analysis activity by *BaBar* in 2008 continued covering a very wide spectrum of measurements, including updates on the angles of the Unitarity Triangle β, α, γ, branching ratios and CP-violation of rare B decays, $|V_{ub}|$, $|V_{cb}|$, the extensive study of charm and τ decays (*BaBar* is also a charm and τ factory), and the most extensive systematic study up to now of low-energy meson spectroscopy in the energy range between 1 and 4 GeV, possible at *BaBar* using the technique of Initial State Radiation (ISR).

A total of 41 papers were published in the same year on major journals and Babar continued as a major contributor at all HEP Conferences In the next sections the analysis items which led to publications in 2008 and in which the Frascati group is more directly involved are shortly described.

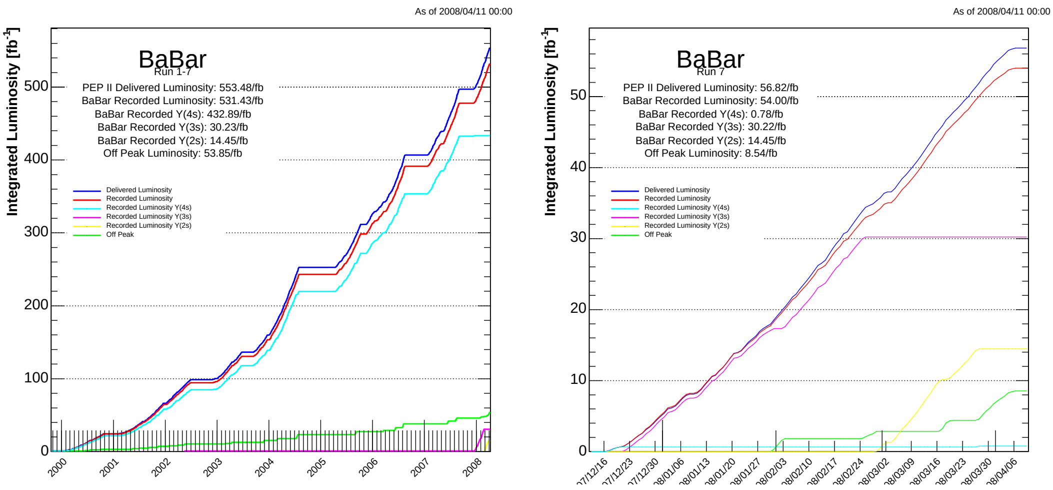

Figure 2: *Left: BABAR integrated luminosity from the start of the data taking in 1999 till the end of PEP-II operations in 2008. Right: BABAR integrated luminosity in Run7 collected between December 2007 and April 2008.*

The group has also been active in participating to the Design Study for a detector at the SuperB Factory, a proposed e^+e^- asymmetric collider with 100 times more luminosity than PEP-II. More details are given in Section 5.

3 Measurement of the angle γ with $B^\pm \to D^{(*)0}K^{(*)\pm}$ decays

The measurement of the angle γ of the Unitarity Triangle using the $B \to D^{(*)0}K^{(*)-}$ decays with $D^0 \to K^0_S h^+h^-$ $(h = \pi, K)$ has been performed. This family of decay channels gives the most precise measurement of γ among the methods which have been explored so far. Our result, based on a data sample of 383×10^6 $B\bar{B}$, is $\gamma = (76 \pm 22(stat) \pm 5(syst) \pm 5(model))^\circ$ (Fig. 3). The third uncertainty comes from the model assumptions for the Dalitz plots of the flavour-tagged D^0. Details on the analysis technique can be found in the journal article which has been published in Phys. Rev. D in 2008 [29].

4 Light hadron spectroscopy with initial state radiation events

Initial state radiation (ISR) events can be effectively used to measure e^+e^- annihilation at a high luminosity storage ring, such as the B-factory PEP-II. A wide mass range is accessible in a single experiment, contrary to the case of fixed energy colliders, which are optimized only in a limited energy region. In addition, the broad-band coverage may result also in greater control of systematic effects because only one experimental setup is involved.
Measurements of the main hadronic final states in the energy range between thresholds and 6 GeV have been carried out at BABAR.
Besides the study of the $KK\pi$ and $KK\eta$ final states [41], we are now finalizing the analysis of various $K_SK_L\pi + n\pi^0$ channels, with one, two and three additional π^0's.

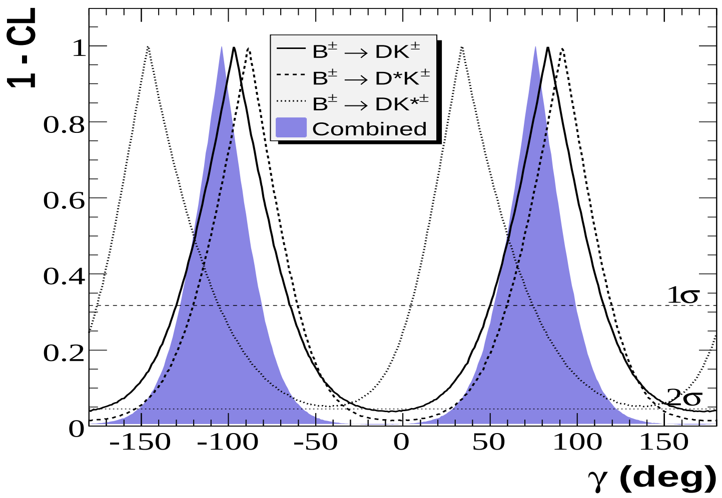

Figure 3: $\alpha = 1 - \mathrm{CL}$ *as a function of* γ *for* $B^- \to D^0K^-$, $B^- \to D^{*0}K^-$, *and* $B^- \to D^0K^*$ *decays separately, and their combination, including statistical and systematic uncertainties and their correlations. The dashed (upper) and dotted (lower) horizontal lines correspond to the one- and two-standard deviation intervals, respectively.*

4.1 Unexpected threshold behavior in baryon-antibaryon cross sections

Recent *BABAR* data on baryon-antibaryon cross sections show an unexpected threshold behavior. In particular the cross sections for $e^+e^- \to p\overline{p}$, $\Lambda\overline{\Lambda}$, $\Sigma^0\overline{\Sigma^0}$, and $\Lambda\overline{\Sigma^0}$ have monotonically decreasing behaviors starting from the threshold, where they take non vanishing values, up to about 4 GeV. Generally the baryon-antibaryon cross section should be zero at threshold due to the vanishing of the phase space. In the $p\overline{p}$ case the phase space vanishing is cancelled by the Coulomb correction. Moreover, using such a correction we get a unitary normalization for the common proton form factor at the production threshold, i.e. for time-like square momentum $q^2 = (2M_p)^2$ [a1].
Also in the case of $e^+e^- \to \Lambda_c\overline{\Lambda_c}$, as recently measured by Belle for the first time, a point-like behavior is suggested for the charmed charged baryon, being the form factor at threshold $|G^{\Lambda_c}(4M^2_{\Lambda_c})| \simeq 1$, even if within a large error [a2]. The same argument can not be used in the case of neutral baryons, where the non-vanishing cross section at threshold is interpreted as a remnant of quark pair Coulomb interaction before the hadronization, taking into account the asymmetry between attractive and repulsive Coulomb factors.
A complete study of the other crucial channels: $\Sigma^+\overline{\Sigma}^-$ and $\Delta^{++}\overline{\Delta}^{--}$ is underway. In the first case we expect a cross section which, after correcting for the $p - \Sigma^+$ mass difference, should behave like the $p\overline{p}$ one, showing the Coulomb threshold enhancement. In the case of Δ^{++}, instead, the Coulomb enhancement should play a dominant role at the production threshold, being stronger by a factor of four, with respect to typical charge $+e$ baryons.

5 The SuperB project

A conceptual design report of a next generation asymmetric-energy e^+e^- collider (SuperB) capable of delivering about 100 times the luminosity of the current B factories has recently been compiled [sb1]. This report discusses the physics motivation, detector, and accelerator designs for the next generation B factory at an e^+e^- collider.

5.0.1 R&D for the SuperB Drift Chamber

In 2007 the *BABAR* Frascati group has started the R&D activities that lead towards the design and construction of the tracking detector for the SuperB.

Since the *BABAR* drift chamber has performed excellently throughout the course of the experiment, we chose it as the baseline design for the SuperB tracking detector. However, at a luminosity of at least $10^{36}\,\mathrm{cm}^{-2}\mathrm{s}^{-1}$ we expect the occupancy in the drift chamber volume, especially in the forward region, to be considerably higher than in *BABAR*. The gas mixture and the cell shape need therefore to be optimized for faster operation.

As a general consideration the *BABAR* design of the drift chamber did not emphasize low mass end-plates, so this would be the typical area of improvement. We envisage an all-Carbon Fiber conical or dome shaped structure to minimize the material in front of the outer detector components. The engineering of the front-end electronics also needs complete rework.

As mentioned in the previous paragraphs, experimental activities were started during 2008: an external tracker to measure space time relations in different gases and spatial resolution in prototype devices was refurbished and is being commissioned. A dedicated small dimension prototype has been designed and engineered, once built it will be exposed to cosmic rays and to the Frascati BTF to experimentally check simulation results obtained with MAGBOLTZ and/or GARFIELD.

5.1 *Development of Simulation Tools for Detector Design and Physics Studies*

The design of the SuperB detector and the study of the physics reach of the experiment require specific simulation tools. Depending on the nature of the study, a detailed simulation (Geant4) or a fast simulation is needed. The Frascati group has been involved in the development of both tools.

Three different GDML models of the drift chamber (differing on the endplates shape) have been implemented and plugged into the Geant4 simulation of the machine interaction region and the detector to study the hit rates from Touschek, radiative Bhabha and $e^+e^- \to e^+e^-e^+e^-$ background events. This is the first step of a study which aims at designing the drift chamber layout to keep the background rates down to an acceptable level.

To optimize the overall SuperB detector geometry and to study the reach of the main physics channels, a simulation tool which is both highly flexible in the detector description, and very fast, is needed. These requirements are not met by a detailed simulation based on Geant4. For this reason a fast Monte Carlo (FastSim) was developed, which includes a simplified detector element description (cylinders, rings, cone, ...), a full modeling of particle passage through the detector (energy loss, multiple scattering, showering, ...), the parameterization of the detector response (track hit resolution, cluster shape, Cherenkov ring resolution, ...) and particle reconstruction (tracks, clusters, photon rings, ...). In addition FastSim has been designed in such a way that the output is compatible with the *BABAR* analysis tools (vertexing, tagging, etc.). The Frascati group is coordinating the development of the SuperB fast simulation and of the physics tools.

5.2 *Detector Geometry Working Group*

The SuperB detector as described in the Conceptual Design Report (CDR) [sb1] has a number of options not yet defined that have a large impact on the overall detector geometry. A Detector Geometry Working Group (DGWG) has been setup at the end of 2008 to study the physics tradeoffs of the open CDR detector options with the goal of being able to finalize the global geometry and define the subsystems of the SuperB detector. The DGWG will help evaluating the impact of several detector options and designs, such as a) a forward PID detector compared to a longer drift chamber (DCH), b) a backward EM calorimeter vs. no backward EM calorimeter, c) the internal geometry of the Silicon Vertex Tracker (SVT), d) the SVT-DCH transition radius, e) the distribution and amount of absorber in the muon system. The Frascati group is co-coordinating the DGWG.

6 Talks at Conferences in 2008

- G. Finocchiaro, "CKM unitarity triangle: mixing and CP violation", presented at the Second Workshop on Theory, Phenomenology and Experiments in Heavy Flavour Physics, June 16-18 2008, Capri, Italy.
- S. Pacetti, "Charmed Particles Production in $e^+e^- \to c\bar{c}$ at 10.6 GeV" presented at the Workshop on parton fragmentation processes in the vacuum and in the medium, February 25-29, 2008, ECT* Trento, Italy.
- S. Pacetti, "Initial state radiation at BaBar" presented at the Workshop on parton fragmentation processes in the vacuum and in the medium, February 25-29, 2008, ECT* Trento, Italy.
- S. Pacetti, "Mesoni leggeri e fattori di forma del nucleone a BaBar" presented at the Mini-Workshop sulle prospettive di Fisica adronica al Jefferson Lab e in altri laboratori, February 27-29, 2008, Genova, Italy.
- S. Pacetti, "Unexpected features of $e^+e^- \to$baryon-antibaryon cross sections near threshold" Hadron Electromagnetic Form Factors Workshop, May 12-23, 2008, ECT* Trento, Italy.
- S. Pacetti, "Unexpected features of $e^+e^- \to$baryon-antibaryon cross sections near threshold and analysis of G_E^p/G_M^p" presented at the Hadron Structure and QCD: from LOW to HIGH energies, June 30 - July 4, 2008, Gatchina, Russia.
- P. Patteri, "Initial state radiation physics at *BABAR* and Belle", presented at the Workshop on Hadron Structure and QCD 2008, June 30 - July 4, Gatchina, Russia.

7 *BaBar* Publications in 2008

References

1. B. Aubert *et al.* [BaBar Coll.], Phys. Rev. Lett. **102**, 012001 (2009).
2. B. Aubert *et al.* [BaBar Coll.], Phys. Rev. D **79**, 012002 (2009).
3. B. Aubert *et al.* [BaBar Coll.], Phys. Rev. D **78**, 071101 (2008).
4. B. Aubert *et al.* [BaBar Coll.], Phys. Rev. D **78**, 091101 (2008).
5. B. Aubert *et al.* [BaBar Coll.], Phys. Rev. D **78**, 112001(2008).
6. B. Aubert *et al.* [BaBar Coll.], Phys. Rev. D **78** 072007, (2008.,
7. B. Aubert *et al.* [BaBar Coll.], Phys. Rev. D **78**, 091102 (2008).
8. B. Aubert *et al.* [The BaBar Coll.], Phys. Rev. D **78**, 092008 (2008).
9. B. Aubert *et al.* [BaBar Coll.], Phys. Rev. Lett. **101** 261802 (2008),
10. B. Aubert *et al.* [BaBar Coll.], Phys. Rev. D **78**, 071104 (2008).
11. B. Aubert *et al.* [BaBar Coll.], Phys. Rev. D **78**, 112003 (2008).
12. B. Aubert *et al.* [BaBar Coll.], Phys. Rev. Lett. **102**, 091803 (2009).
13. B. Aubert *et al.* [BaBar Coll.], Phys. Rev. Lett. **101**, 201801 (2008).
14. B. Aubert *et al.* [BaBar Coll.], Phys. Rev. D **78**, 071102 (2008).
15. B. Aubert *et al.* [BaBar Coll.], Phys. Rev. D **78**, 092002 (2008).
16. B. Aubert *et al.* [BaBar Coll.], Phys. Rev. D **78**, 112002 (2008).
17. B. Aubert *et al.* [BaBar Coll.], Phys. Rev. D **78**, 051101 (2008).
18. B. Aubert *et al.* [BaBar Coll.], Phys. Rev. Lett. **101**, 071801 (2008), Erratum *ibid.* **102**, 029901 (2009).
19. B. Aubert *et al.* [BaBar Coll.], Phys. Rev. D **78**, 051103 (2008).
20. B. Aubert *et al.* [BaBar Coll.], Phys. Rev. Lett. **101** 161801 (2008).
21. B. Aubert *et al.* [BaBar Coll.], Phys. Rev. D **78**, 071103 (2008).
22. B. Aubert *et al.* [BaBar Coll.], Phys. Rev. Lett. **101**, 171804 (2008).
23. B. Aubert *et al.* [BaBar Coll.], Phys. Rev. Lett. **101**, 081801 (2008).
24. B. Aubert *et al.* [BaBar Coll.], Phys. Rev. D **79**, 011102 (2009).
25. B. Aubert *et al.* [BaBar Coll.], Phys. Rev. D **78**, 011104 (2008).

26. B. Aubert *et al.* [BaBar Coll.], Phys. Rev. D **78**, 011103 (2008).
27. B. Aubert *et al.* [BaBar Coll.], Phys. Rev. D **79**, 031102 (2009).
28. B. Aubert *et al.* [BaBar Coll.], Phys. Rev. D **78**, 011107 (2008).
29. B. Aubert *et al.* [BaBar Coll.], Phys. Rev. D **78**, 034023 (2008).
30. B. Aubert *et al.* [BaBar Coll.], Phys. Rev. D **78**, 012006 (2008).
31. B. Aubert *et al.* [BaBar Coll.], Phys. Rev. Lett. **101**, 021801 (2008).
32. B. Aubert *et al.* [BaBar Coll.], Phys. Rev. Lett. **101**, 091801 (2008).
33. B. Aubert *et al.* [BaBar Coll.], Phys. Rev. D **78**, 012004 (2008).
34. B. Aubert *et al.* [BaBar Coll.], Phys. Rev. D **78**, 032005 (2008).
35. B. Aubert *et al.* [BaBar Coll.], Phys. Rev. D **77**, 111101 (2008).
36. B. Aubert *et al.* [BaBar Coll.], Phys. Rev. D **78**, 034008 (2008).
37. B. Aubert *et al.* [BaBar Coll.], Phys. Rev. D **77**, 112002 (2008).
38. B. Aubert *et al.* [BaBar Coll.], Phys. Rev. D **77**, 111102 (2008).
39. B. Aubert *et al.* [BaBar Coll.], Phys. Rev. D **78**, 051102 (2008).
40. B. Aubert *et al.* [BaBar Coll.], Phys. Rev. D **77**, 091104 (2008).
41. B. Aubert *et al.* [BaBar Coll.], arXiv:0710.4451, accepted by Phys. Rev. D.

Other publications related to *BaBar*

a1 . R. Baldini, S. Pacetti, A. Zallo, and A. Zichichi, Eur. Phys. J. A **39**, 315 (2009).

a2 . R. Baldini, S. Pacetti, and A. Zallo, arXiv:0812.3283.

SuperB publications

sb1 . The SuperB Conceptual Design Report, arXiv:0709.0451.

sb2 . Proceedings of the SuperB Workshop VI, January 7-15 2008, Valencia, Spain, arXiv:0810.1312.

CDF-2

A. Annovi, M. Cordelli (Resp.), P. Giromini, F. Happacher (Art. 23)

1 Introduction

The Tevatron, with a $p\bar{p}$ collision energy of 1.96 TeV in the center of mass system, is running with a record instantaneous luminosity, L, delivered to the experiments of 350×10^{30} cm^{-2} s^{-1} ($vs.$ $\sim 10^{31}$ of Run I). At the end of year 2008, the Tevatron has delivered to the experiments ~ 5600 pb^{-1}; CDF experiment has collected on tape ~ 4800 pb^{-1} (see Figure 1); during the whole Run I we collected ~ 109 pb^{-1}. The CDF data taking is expected to continue through all of year 2010 and likely also through 2011.

The CDF group of Frascati has built the central hadronic calorimeter (the iron-scintillator based calorimeter in the central and end-wall region, CHA and WHA) and is responsible for the hardware maintenance and for the energy scale calibration.

Since year 2005 we are also responsible of the Silicon Vertex Trigger operations.

The analysis interest of the Frascati group focuses on the measurements of b quark production cross sections. Indeed, the bottom quark production at the Fermilab Tevatron has been called one of the few instances in which experimental results appear to challenge the ability of perturbative QCD to accurately predict absolute rates in hadronic collisions. We are repeating the most significant b quark cross section measurements from Run I in order to clarify the current situation.

2 Calibration of the central hadron calorimeter

The Frascati group plays a leading role in the calibration of the central hadron calorimeters, CHA/WHA.

For the WHA calorimeter the original Run I ^{137}Cs Sources system is fully working and therefore it can be used to set the absolute energy scale for all the towers; we have taken two ^{137}Cs Source runs during 2007 and we have accordingly computed a set of Linear Energy Response:

$$LER = \frac{^{137}Cs(test - beam)e^{-\Delta t/\tau}}{^{137}Cs(today)}$$

that have been downloaded in the front end electronics to correct the raw ADMEM counts. This system effectively probes the behavior of the calorimeter since the source runs in front of the inner scintillator plane of the wedges thus irradiating few of the scintillator/absorber layers of the calorimeter. In this way we monitor aging phenomena of the scintillator together with PM gain variations.

We calibrate the CHA calorimeter looking at the energy deposition of Minimum Ionizing Particles (i.e. muons from J/ψ decays).

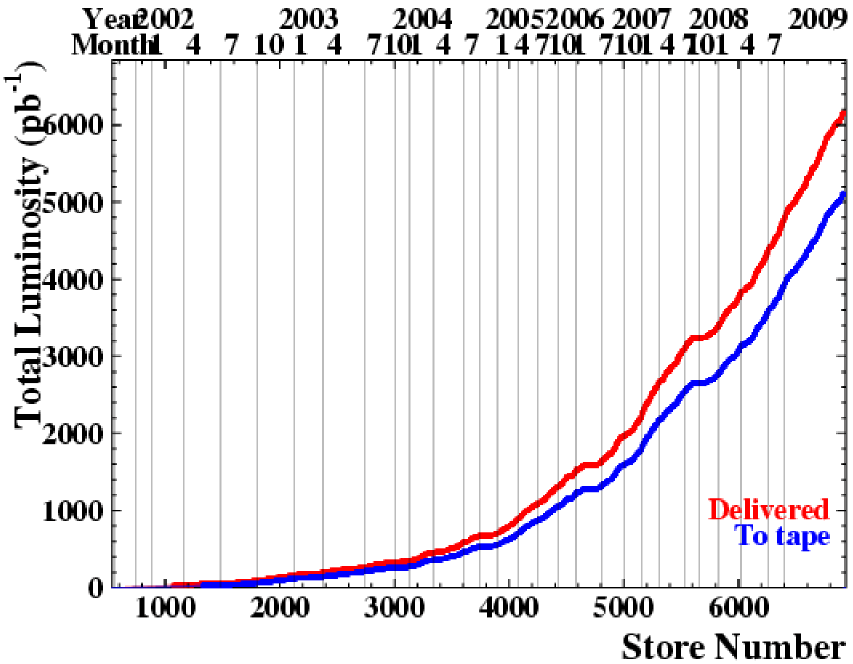

Figure 1: *Integrated Luminosity vs time.*

We briefly recall the procedure to set the absolute calorimeter energy scale using Mip's. Looking at μ's from the $\sim$ 81 pb^{-1} dimuon trigger sample collected in Run Ib, we determined the necessary statistics to determine the peaks of μ's hadronic energy, HadE, distributions with enough precision per every CHA tower. With a statistics of $\sim$ 40 pb^{-1} we find that the tower by tower peak is determined with a precision of $\sim$ 1.5%. The LER's correction factors are derived comparing tower by tower the HadE deposition for Run I and Run II mips every 30-40 pb^{-1} of data; the LER at a given time time t are defined as the previous set of LER (t-1) multiplied by the observed ratio of the Mip's at a time t and in Run I:

$$LER(t) = LER^{t-1} \times \frac{MIP(RunI)}{MIP(t)}$$

We look at Mip's peaks response every $\sim$ 100 pb^{-1} and the typical response shows a tiny 1.5% gain variations on average and few channels that drift more than 5%.

The laser system represents a quick tool to follow the trend of the PM's gains. We have continuously acquired laser runs since year 2003 to monitor the gain variations of each photo-multiplier; the CHA is stable within $\sim$ 2%.

2.1 ONLINE-OFFLINE energy scale calibration

At CDF with the current luminosity the data are being processed through the OFFLINE reconstruction every couple of months. Before producing the fully reconstructed events from the raw information of the detector we first produce small dedicated calibration samples to derive the calibrations constants for all the sub detectors. Every 6-8 weeks we run an executable called CalibExe which produces all the data ntuples for different data sets, including the dimuon trigger data sample where we reconstruct J/ψ events; then the various calibrators use these samples to derive the calibrations. We made all this procedure automatic during the year 2006.

Usually for the Hadron calorimeters we produce two set of calibrations: ONLINE calibrations are directly downloaded in the ADMEM electronics and are intended to correct the energy response for data that have to be acquired afterward; the OFFLINE calibrations attempts to propagate back to the data already acquired the needed corrections. The calibration constants are then filled in appropriate ORACLE data base tables called CHALINERESPONSE and CHAOFFLER. To validate the OFFLINE calibrations, the same data sets are reconstructed again picking the right calibration tables for every run range they have been produced for and the calibrators have to repeat their analysis to check that the calibrations are correct.

With this procedure the calorimeter response is kept constant at $\sim 2\%$ level over the running period.

3 SVT

The Silicon Vertex Trigger (SVT) is part of the L2 trigger of CDF II. The SVT reconstructs tracks by associating Silicon hits to Central Tracker (COT) tracks reconstructed by the L1 trigger. By using the hits in the silicon, SVT is able to measure the impact parameter of the tracks so that this information can be used by the L2 to select data enriched of heavy flavor decays. Data collected using the SVT processor made possible the first measurement of the B_s mixing.

During 2008 we contributed to the operations and maintence of the Silicon Vertex Trigger. In order to optimize the maintenance we continue to improved the online and offline monitoring allowing for a better understanding of the problems and a quicker reaction when they appear during data taking. An upgrade of the track fitting boards of the SVT is being evalutated with the goal to increase tracking quality and efficiency. This upgrade is based on a new board, being developed in Pisa, that is called Giga fitter for its ability to perform one fit per nanosecond. We contributed to the tests of the board in Pisa and at Fermilab.

4 Studies of b quark cross section

4.1 Status of the Tevatron measurements

The bottom quark production at the Fermilab Tevatron has been called one of the few instances in which experimental results appear to challenge the ability of perturbative QCD to accurately predict absolute rates in hadronic collisions. In general, the data are underestimated by the exact next-to-leading-order (NLO) QCD prediction. The most recent measurement from the Tevatron is however in very good agreement with an improved QCD calculation (FONLL), and has prompted a number of studies suggesting that the apparent discrepancy has been resolved with incremental improvements of the measurements and predictions. The increase of the cross-section predicted by FONLL with respect to original NLO calculatiuons, which results into a better agreement with data, is mostly coming from new structure functions and fragmentation functions that have been computed at next-to-leading-order, in order to match the perturbative order of the FONLL

Table 1: Ratio R of measured single b cross sections to a prediction based on the exact NLO calculation.

channel	R for $p_T^{\min}$ (GeV/c) =					
	6	$8-10$	$12-15$	$19-21$	$\simeq 29$	$\simeq 40$
$J/\psi K^+$		$4.0 \pm 15\%$	(3.4)			
$J/\psi K^+$		$2.9 \pm 23\%$	(1.9)			
$\mu\, X$				$2.5 \pm 26\%$	(1.9)	
$e\, X$			$2.4 \pm 27\%$			
eD^0				$2.1 \pm 34\%$		
$J/\psi\, X$		$4.0 \pm 10\%$	(3.4)			
$J/\psi\, X$		$3.1 \pm 9\%$	(2.7)			
$\mu\, X$	$2.1 \pm 27\%$		(1.7)			
$\mu\, X$	$2.5 \pm 25\%$		(3.5)			
b jets (μ)				$2.4 \pm 20\%$		(2.0)

calculation. The measured single b-quark cross-section is also in agreement with the prediction of LL shower MC, with an *ad hoc* tuning.

Because of the experimental difficulty inherent to each result, we reviewed all measurements of the single b cross section performed at the Tevatron, and then compared their average to the standard and to the improved QCD predictions. We have also compared the cross sections for producing both b and $\bar{b}$ quarks - centrally and above a given transverse momentum cut - to theoretical predictions. The single b-quark cross section is inferred from the measurement of the production rate as a function of the transverse momentum, p_T, of B hadrons; or some of their decay products (leptons or ψ mesons); or jets produced by the hadronization of b quarks. Most of the Tevatron measurements correspond to b quarks produced centrally (rapidity $|y^b| \leq 1$) and with $p_T \geq 6$ GeV/c (up to $p_T \simeq 100$ GeV/c). We have performed a consistency check of all available data. For that purpose, we use the value of the single b-quark cross section extracted from the data and integrated from the p_T threshold of each experiment. We determined the ratio R of each measurement to the same theoretical prediction. We have then evaluated the average R and its dispersion. As benchmark prediction of the b-quark parton-level cross section we choose the exact NLO calculation implemented with old but consistent sets of parton distribution functions (PDF), since it has been used in most published works, convoluted with the Peterson fragmentation function; B-hadron decay are modeled with the QQ Monte Carlo generator program.

There are 10 measurements of the single b cross section performed by the CDF and DØ collaborations at the Tevatron. The ratios of these measurements to the standard theory are summarized in Table 1.

Using the measurements listed in Table 1, we derive an average ratio of the data to the standard theory that is $< R >= 2.8$; the RMS deviation of the 10 measurements in Table 1 is 0.7

Table 2: Ratio R_{2b} of $\sigma_{b\bar{b}}$, the observed cross section for producing both b and $\bar{b}$ quarks, centrally and above a given $p_T^{\min}$ threshold, to the exact NLO prediction.

channel	R_{2b} for $p_T^{\min}$ (GeV/c) =			
	$6-7$	10	15	$\simeq 20$
$b+\bar{b}$ jets			$1.2 \pm 25\%$	
$b+\bar{b}$ jets				$1.0 \pm 32\%$
$\mu + b$ jet		$1.5 \pm 10\%$		
$\mu^+ + \mu^-$	$3.0 \pm 20\%$			
$\mu^+ + \mu^-$	$2.3 \pm 33\%$			

It has to be noticed that all the measurement involving the J/ψ reconstruction, experimentally the cleanest, are consistently much higher than the ones based on the detection of a semileptonic decay.

The new measurement of the $B^+ \to J/\psi(\to \mu^+\mu^-)K^+$ differential cross section (see next paragraph) carried on by the Frascati group finds a ratio R with the theory of 2.80 ± 0.24, somehow closer to the average of all measurements.

Leading-order (LO) and higher-than-LO terms are sources of b and $\bar{b}$ quarks with quite different topological structure. The production of events with both a b and $\bar{b}$ quark with $p_T \geq 6$ GeV/c and $|y| \leq 1$ is dominated by LO diagrams and the parton-level cross sections predicted by the exact NLO calculation is comparable to that predicted by LL Monte Carlo generators.

R_{2b}, the ratio of $\sigma_{b\bar{b}}$ measured at the Tevatron to the exact NLO prediction, $\simeq 1$ would imply that the parton-level cross section predicted by LL generators (NLO) is correct and that the contribution of higher-than-LO terms has to be a factor of two larger than in the present NLO or FONLL prediction. If the ratio R_{2b} is much larger than one, then the agreement between the observed single b cross section and the prediction of LL Monte Carlo generators is fortuitous and agreement with the data may be found by using harder fragmentation functions as in the FONLL calculation.

We review five measurements, listed in Table 2, and derive a value of $< R_{2b} >= 1.8$ with a 0.8 RMS deviation. Such a large RMS deviation indicates that the experimental results are inconsistent among themselves. Additional measurements are certainly needed to clarify the experimental situation.

4.2 $B^+ \to J/\psi(\to \mu^+\mu^-)K^+$

We have repeated the Run I analysis that measures the B^+ differential cross section as a function of p_T, reconstructing the decay $B^+ \to J/\psi(\to \mu^+\mu^-)K^+$. We search for $B^\pm \to J/\psi K^\pm$ candidates in the data set selected by the $J/\psi \to \mu^+\mu^-$ trigger. We search for J/ψ candidates by using pairs of muons, reconstructed in the CMU detector, with opposite charge, and $p_T \geq 2$ GeV/c. The invariant mass of a muon pair is evaluated by constraining the two muon tracks to originate from a common point in three-dimensional space (vertex constrain) in order to improve the mass resolution. All muon pairs with invariant mass in the range $3.05 - 3.15$ GeV/c^2 are considered J/ψ

candidates. If a J/ψ candidate is found, we search for $B^{\pm}$ mesons by considering all charged particle tracks in the event as possible kaon candidates. The invariant mass of the μ^+ μ^- $K^{\pm}$ system is evaluated constraining the corresponding tracks to have a common origin while the μ^+ μ^- invariant mass is constrained to the value of 3096.9 GeV/c^2. In Fig. 2 we show the comparison of the recent RUN II CDF b cross section result with the FONLL theoretical predictions.

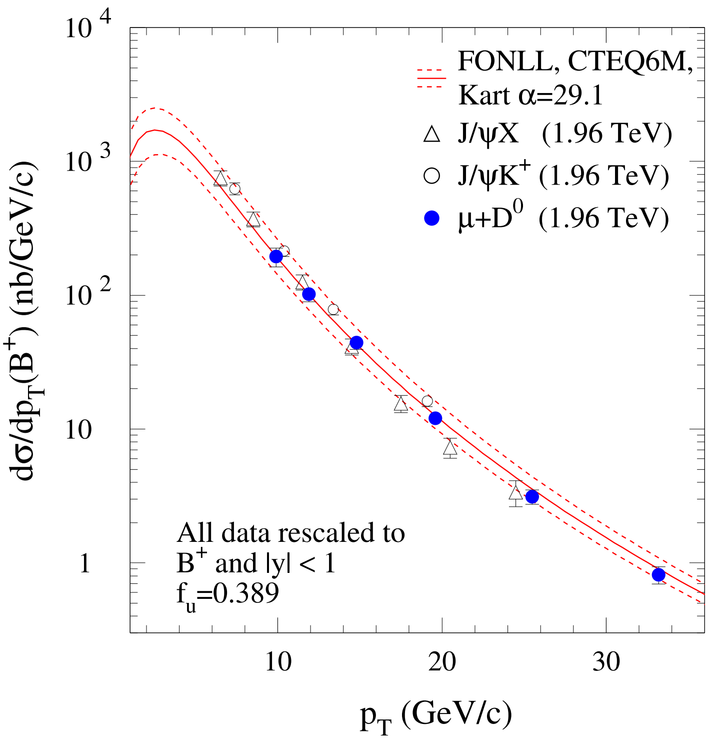

Figure 2: *Comparison of the CDF b cross section results with the FONLL theory as a function of the B hadron p_T.*

To measure the B^+ differential cross section as a function of p_T, we divide the sample of $B^{\pm}$ candidates into five p_T bins: $6-9$, $9-12$, $12-15$, $15-25$, and ≥ 25 GeV/c. In each p_T bin, we fit the invariant mass distribution of the B^+ candidates with a binned maximum likelihood method to determine the number of B^+ mesons. We use a first order polynomial function to model the combinatorial background and gaussian function to model the B^+ signal. All fits return a B^+ mass of 5279.0 ± 0.5 MeV in agreement with the PDG value.

The detector acceptance is calculated with a Monte Carlo simulation based on the NLO calculation. The $B^{\pm}$ decay is modeled with the EVTGEN Monte Carlo program. The detector response to the generated $B^{\pm}$ decay prongs is modeled with the CDF II detector simulation that in turn is based on the GEANT Monte Carlo program.

The differential cross section $d\sigma/dp_T$ is calculated as

$$\frac{d\sigma(B^+)}{dp_T} = \frac{N/2}{\Delta p_T \times \mathcal{L} \times \mathcal{A}_{\rm corr} \times BR} \tag{1}$$

where N is the number of $B^{\pm}$ mesons determined from the likelihood fit to the invariant mass distribution of the $J/\psi\ K^{\pm}$ candidates in each p_T bin. The factor 1/2 accounts for the fact that both B^+ and B^- mesons are used and assumes C invariance at production. Δp_T is the bin width and $\mathcal{A}_{\rm corr}$ is the geometric and kinematic acceptance that includes trigger and tracking efficiencies measured with the data. The integrated luminosity of the data set is $\mathcal{L} = 739 \pm 44$ pb^{-}1. The branching ratio $BR = (5.98 \pm 0.22) \times 10^{-5}$ is derived from the branching fractions $BR(B^{\pm} \to J/\psi\ K^{\pm}) = (1.008 \pm 0.035) \times 10^{-3}$ and $BR(J/\psi \to \mu^+\ \mu^-) = (5.93 \pm 0.06) \times 10^{-2}$.

The B^+ total cross section is $\sigma_{B^+}(p_T \geq 6.0$ GeV/c, $|y| < 1) = 2.78 \pm 0.24\ \mu$b, where the 8.6% error is the sum in quadrature of the 6% error on the integrated luminosity, the 3.7% uncertainty of the $B^+ \to J/\psi\ K^+$ and $J/\psi \to \mu^+\ \mu^-$ branching fractions, the 2.5% uncertainty of the acceptance calculation, and the 4.4% statistical error.

This analysis has been published on Phys. Rev. D **75**, 012010 (2007).

4.3 $b\bar{b}$ correlation

Another analysis in progress is the study of the so called $b\bar{b}$ correlation. This study is a new measurement of $\sigma_{b\bar{b}}$ that uses dimuons arising from from $b\bar{b}$ production. At the Tevatron, dimuon events result from decays of heavy quark pairs ($b\bar{b}$ and $c\bar{c}$), the Drell-Yan process, charmonium and bottomonium decays, and decays of π and K mesons. Background to dilepton events also comes from the misidentification of π or K mesons. We make use of the precision tracking provided by the CDF silicon microvertex detector to evaluate the fractions of leptons due to long-lived b- and c-hadron decays, and to the other background contributions.

The method used to determine the $b\bar{b}$ and $c\bar{c}$ content of the data is to fit the observed impact parameter distribution of the muon pairs with the expected impact parameter distributions of leptons from various sources. After data selection, the main sources of reconstructed muons are semileptonic decays of bottom and charmed hadrons, and prompt decays of onia and Drell-Yan production.

Herwig Monte Carlo simulations are used to model the impact parameter distributions for leptons from b- and c-hadron decays. The impact parameter distribution of leptons from prompt sources such as quarkonia decays and Drell-Yan production is derived using muons from $\Upsilon(1S)$ decays. In Fig. 3 we show the one-dimensional impact parameter distribution for muon pairs from different sources. Fig. 4 shows the breakdown of the result of the fit to the data with the various sources of dimuon events.

For muons with $p_T \geq 3$ GeV/c and $|\eta| \leq 0.7$, that are produced by b and $\bar{b}$ quarks with $p_T \geq 2$ GeV/c and $|y| \leq 1.3$, we measure $\sigma_{b\to\mu,\bar{b}\to\mu} = 1549 \pm 133$ pb. The NLO prediction is $\sigma_{b\to\mu,\bar{b}\to\mu} = 1293 \pm 201$ pb. The ratio of the data to the NLO prediction is 1.20 ± 0.21.

This analysis has been published on Phys. Rev. D**77**, 072004 (2008).

5 Search for dimuon resonances

This work repeats the study performed by the Frascati group in RUN I, published in G. Apollinari *et al.,* Phys. Rev. D **72**, 092003 (2005), that found an excess of events in the 7.2 GeV/c^2 region of the dimuon invariant mass distribution as shown in Fig. 5. We take advantage of a higher statistics data sample that corresponds to an integrated luminosity of 630 pb^{-1} collected with the

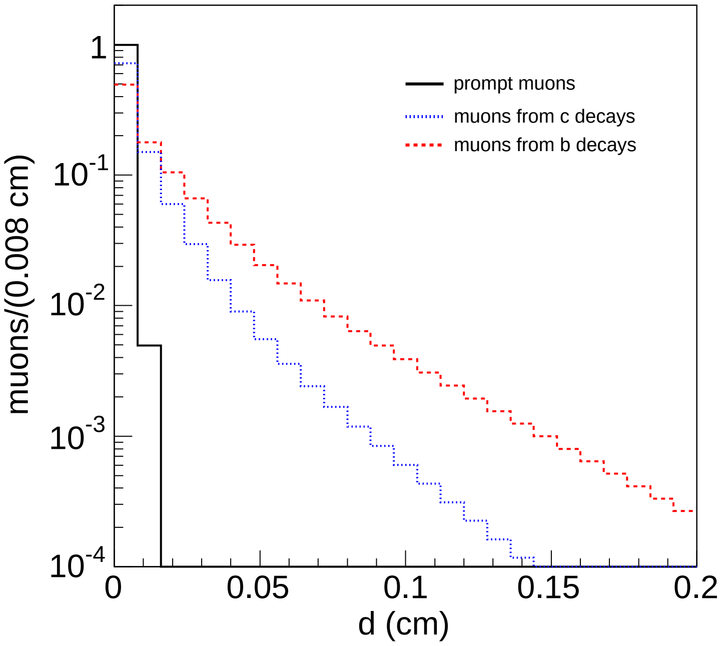

Figure 3: *Impact parameter distributions of muons coming from b- and c-hadron decays (simulation) and of prompt muons (data). Distributions are normalized to unit area.*

CDF II detector after may 2006. At that time, the CDF II trigger system has been upgraded and is capable of acquiring events containing muon pairs with invariant mass larger than 6 GeV/c^2 with a kinematical acceptance comparable to that of the Run I trigger system. As in G. Apollinari *et al.*, Phys. Rev. D **72**, we limit our search for narrow resonances to the mass region above 6.3 GeV/c^2 at which the kinematical acceptance becomes independent of the $\mathcal{E}$-candidate transverse momentum.

We use a fifth order polynomial to model the continuum in the invariant mass region $6-12$ GeV/c^2 and Gaussian functions to model the Υ contributions. The best fit returns 50286 ± 257 $\Upsilon(1S)$ mesons over a background of 13976 events in the region $9.3 \leq M_{\mu^+\mu^-} \leq 9.55$ GeV/c^2. To search for the existence of narrrow $\mathcal{E}$ states we add a Gaussian term to the likelihood function and fit the data in the $6-9.1$ GeV/c^2 mass interval. Fig. 5 shows the results of this fit where no excess is found.

This analysis has been submitted for publication to Phys. Rev. D.

6 Study of Multi-Muons events

This analysis extends the study which has used the dimuon data sample to measure the correlated $\sigma_{b\to\mu,\bar{b}\to\mu}$ cross section. The analysis shows that varying the dimuon selection criteria isolates a sizable, but unexpected background that contains muons with an anomalous impact parameter distribution. Further investigation shows that a smaller fraction of these events also has anomalously large track and muon multiplicities. We are unable to account for the size and properties of these events in terms of known SM processes, even in conjunction with possible detector mismeasurement

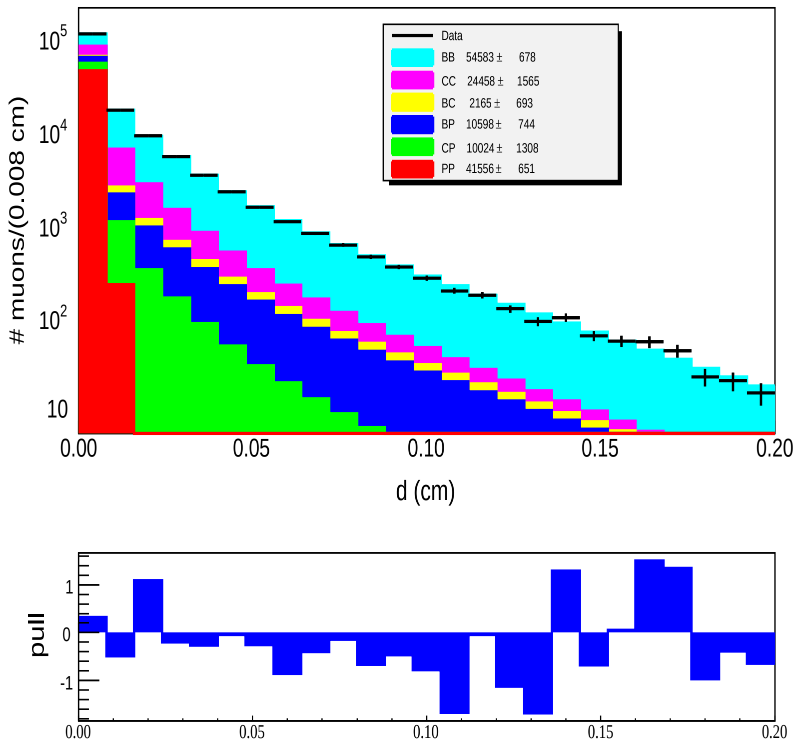

Figure 4: *For each contribution the impact parameter distribution of muon pairs is compared to the fit result (histogram).*

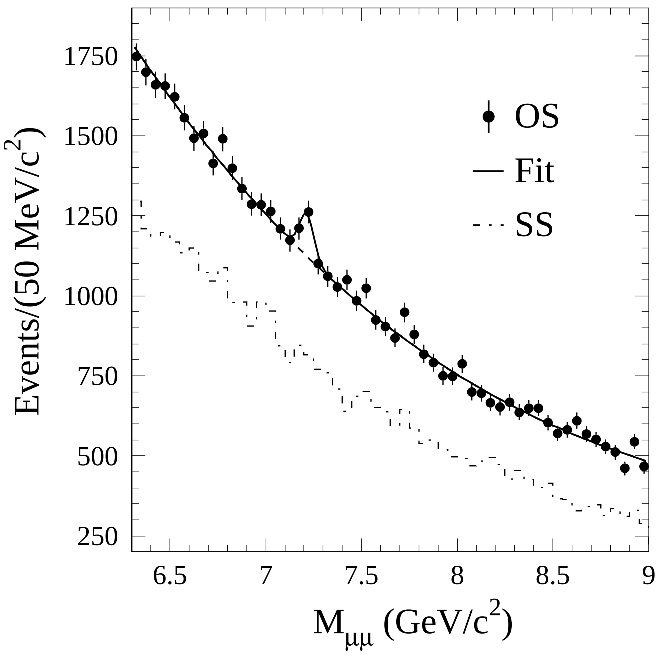

Figure 5: *Run I result of the dimuon resonance search.*

effects.

We use events containing two central ($|\eta| < 0.7$) muons, each with transverse momentum $p_T \geq 3$ GeV/c, and with invariant mass larger than 5 GeV/c^2. The value of $\sigma_{b\to\mu,\bar{b}\to\mu}$ is determined by fitting the impact parameter distribution of these primary muons with the expected shapes from all known sources. To ensure an accurate impact parameter determination, the $\sigma_{b\to\mu,\bar{b}\to\mu}$ analysis uses a subset of dimuon events in which each muon track is reconstructed in the SVX with hits in the two inner layers and in at least four of the inner six layers. The data are nicely described by a fit with contributions from the following QCD processes: semileptonic heavy flavor decays, prompt quarkonia decays, Drell-Yan production, and instrumental backgrounds from hadrons mimicking the muon signal. Using the fit result the study reports $\sigma_{b\to\mu,\bar{b}\to\mu} = 1549 \pm 133$ pb for muons with $p_T \geq 3$ GeV/c and $|\eta| \leq 0.7$. This result is in good agreement with theoretical expectations as well as with analogous measurements that identify b quarks via secondary vertex identification.

However, it is also substantially smaller than previous measurements of this cross section, and raises some concern about the composition of the initial dimuon sample prior to the SVX requirements. The tight SVX requirements used in the $\sigma_{b\to\mu,\bar{b}\to\mu}$ measurement select events in which both muons arise from parent particles that have decayed within a distance of $\simeq 1.5$ cm from the $p\bar{p}$ interaction primary vertex in the plane transverse to the beam line. Using Monte Carlo generated samples of events that are passed through the CDF detector simulation, we estimate that approximately 96% of the dimuon events contributed by known QCD processes satisfy this latter condition. Since the events selected are well described by known QCD processes, we can independently estimate the efficiency of the tight SVX requirements. Using control samples of data from various sources and the sample composition determined by the fit to the muon impact parameter distribution, we estimate that $(24.4 \pm 0.2)\%$ of the initial sample should survive the SVX tight requirements, whereas only $(19.30 \pm 0.04)\%$ actually do. This suggests the presence of an unexpected background that has been suppressed when making the tight SVX requirements. The size of this unexpected dimuon source can be determined by subtracting from the total number of dimuon events, prior to any SVX requirements, the expected contribution from the known QCD sources, which is estimated as the number of events surviving the tight SVX requirements divided by the efficiency of that selection. In a data set corresponding to an integrated luminosity of 742 pb^{-1}, 143743 dimuon events survive the tight SVX cuts. After dividing by the 24.4% efficiency, 589111 ± 4829 QCD events are expected in the initial dimuon sample, whereas 743006 are observed. The difference, 153895 ± 4829 events, is comparable in magnitude to the expected dimuon contribution from $b\bar{b}$ production, 221564 ± 11615. This estimate assumes the unexpected source of dimuon events is completely rejected by the tight SVX requirements and would explain all the observed discrepancies in the $\sigma_{b\bar{b}}$ measurements with respect to the theory when no silicon requirements are applied.

As shown in Fig. 6, muons due to ghost events have an impact parameter distribution that is completely different from that of muons due to QCD events.

Fig. 7 shows the two-dimensional distribution of the impact parameter of an initial muon versus that of all additional muons in a $\cos\theta \geq 0.8$ cone around its direction. The impact parameter distribution of the additional muons is found to be as anomalous as that of primary muons.

This analysis has been submitted for publication to Phys. Rev. D.

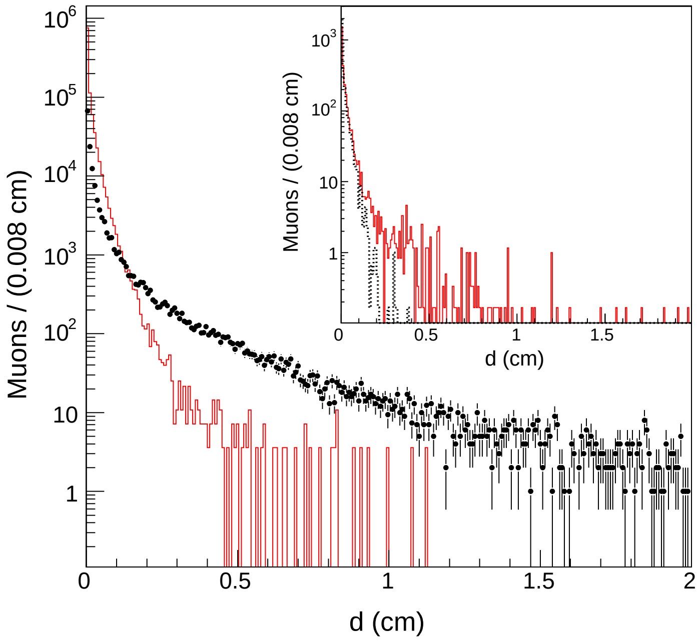

Figure 6: *Impact parameter distribution of muons contributed by ghost (●) and QCD (histogram) events. Muon tracks are selected with loose SVX requirements. The detector resolution is* $\simeq 30\ \mu m$*, whereas bins are 80* μm *wide. In the insert, we show the distribution of (histogram) simulated muons that pass the same analysis selection as the data and arise from the in-flight-decays of pions and kaons produced in a QCD heavy flavor simulation. The dashed histogram shows the impact parameter of the parent hadrons.*

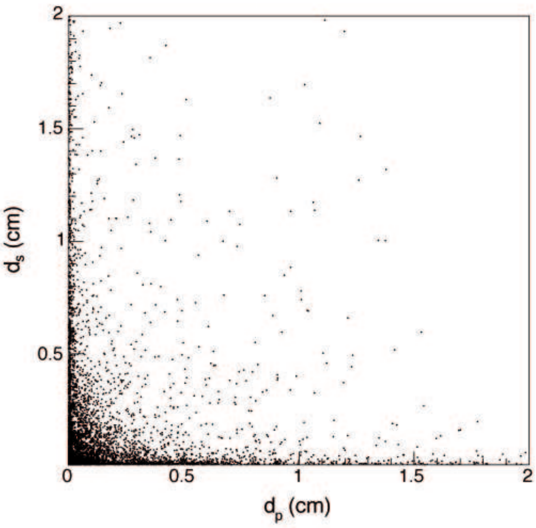

Figure 7: *Two-dimensional distribution of the impact parameter of an initial muon,* d_{0p}*, versus that,* d_{0s}*, of additional muons in ghost events. Muons are selected with loose SVX requirements.*

7 List of Conferences Talks

1. A. Annovi, "Quarkonium Production results from CDF", Presented at the VI Quarkonium Workshop, Nara, Japan, December 2nd-5th, 2008.

8 Publications 2008

1. T. Aaltonen *et al.* [CDF Coll.], arXiv:0812.4469.
2. T. Aaltonen *et al.* [CDF Coll.], arXiv:0812.4271.
3. T. Aaltonen *et al.* [CDF Coll.], arXiv:0812.4036.
4. T. Aaltonen *et al.* [CDF Coll.], arXiv:0812.3400.
5. T. Aaltonen *et al.* [CDF Coll.], arXiv:0811.2820.
6. T. Aaltonen *et al.* [CDF Coll.], arXiv:0811.2512.
7. T. Aaltonen *et al.* [CDF Coll.], arXiv:0811.1062.
8. T. Aaltonen *et al.* [CDF Coll.], arXiv:0811.0344.
9. T. Aaltonen *et al.* [CDF Coll.], arXiv:0811.0053.
10. P. Giromini *et al.*, arXiv:0810.5730.
11. T. Aaltonen *et al.* [CDF Coll.], arXiv:0810.5357.
12. T. Aaltonen *et al.* [CDF Coll.], Phys. Rev. D **79**, 052004 (2009).
13. T. Aaltonen *et al.* [CDF Coll.], Phys. Rev. D **79**, 032001 (2009).
14. T. Aaltonen *et al.* [CDF Coll.], Phys. Rev. Lett. **102**, 031801 (2009).
15. T. Aaltonen *et al.* [CDF Coll.], arXiv:0809.5007.
16. T. Aaltonen *et al.* [CDF Coll.], Phys. Rev. Lett. **102**, 041801 (2009).
17. T. Aaltonen *et al.* [CDF Coll.], arXiv:0809.4808.
18. T. Aaltonen *et al.* [CDF Coll.], Phys. Rev. Lett. **102**, 021802 (2009).
19. T. Aaltonen *et al.* [CDF Coll.], Phys. Rev. D **79**, 011101 (2009).
20. T. Aaltonen *et al.* [CDF Coll.], Phys. Rev. Lett. **101**, 252001 (2008).
21. T. Aaltonen *et al.* [CDF Coll.], arXiv:0809.0080.
22. T. Aaltonen *et al.* [CDF Coll.], Phys. Rev. Lett. **101**, 251801 (2008).
23. T. Aaltonen *et al.* [CDF Coll.], Phys. Rev. Lett. **102**, 042001 (2009).
24. T. Aaltonen *et al.* [CDF Coll.], Phys. Rev. Lett. **101**, 121801 (2008).

25. T. Aaltonen *et al.* [CDF Coll.], arXiv:0807.4652.

26. T. Aaltonen *et al.* [CDF Coll.], Phys. Rev. Lett. **101**, 251803 (2008).

27. T. Aaltonen *et al.* [CDF Coll.], Phys. Rev. D **79**, 031101 (2009).

28. T. Aaltonen *et al.* [CDF Coll.], Phys. Rev. Lett. **101**, 181602 (2008).

29. T. Aaltonen *et al.* [CDF Coll.], Phys. Rev. D **78**, 052006 (2008).

30. T. Aaltonen *et al.* [CDF Coll.], Phys. Rev. Lett. **101**, 202001 (2008).

31. T. Aaltonen *et al.* [CDF Coll.], Phys. Rev. D **78**, 072005 (2008).

32. T. Aaltonen *et al.* [CDF Coll.], Phys. Rev. Lett. **101**, 192002 (2008).

33. T. Aaltonen *et al.* [CDF Coll.], Phys. Rev. D **79**, 011104 (2009).

34. T. Aaltonen *et al.* [CDF Coll.], Phys. Rev. D **78**, 032015 (2008).

35. T. Aaltonen *et al.* [CDF Coll.], arXiv:0803.4264.

36. T. Aaltonen *et al.* [CDF Coll.], Phys. Rev. D **78**, 032008 (2008).

37. T. Aaltonen *et al.* [CDF Coll.], Phys. Rev. Lett. **101**, 071802 (2008).

38. T. Aaltonen *et al.* [CDF Coll.], Phys. Rev. D **77**, 092001 (2008).

39. T. Aaltonen *et al.* [CDF Coll.], Phys. Rev. Lett. **100**, 211801 (2008).

40. T. Aaltonen *et al.* [CDF Coll.], Phys. Rev. Lett. **100**, 201801 (2008).

41. T. Aaltonen *et al.* [CDF Coll.], Phys. Rev. D **77**, 072003 (2008).

42. T. Aaltonen *et al.* [CDF Coll.], Phys. Rev. Lett. **100**, 161803 (2008).

43. T. Aaltonen *et al.* [CDF Coll.], Phys. Rev. D **78**, 012008 (2008).

CMS

L. Benussi (Art. 23), M. Bertani, S. Bianco (Resp.), M.A. Caponero (Ass.)
S. Colafranceschi (Laur.), F.L. Fabbri (Ass.)
F. Felli (Ass.), M. Ferrini (Tecn., Osp.), M. Giardoni, T. Greci (Laur.)
B. Ortenzi (Tecn.), M. Pallotta (Ass.), A. Paolozzi (Ass.)
L. Passamonti (Tecn.), D. Piccolo (Osp.), C. Pucci (Dott.), G. Saviano (Ass.)

In collaboration with:
D. Pierluigi (Tecn.), B. Ponzio (Tecn.), A. Russo (Tecn.)

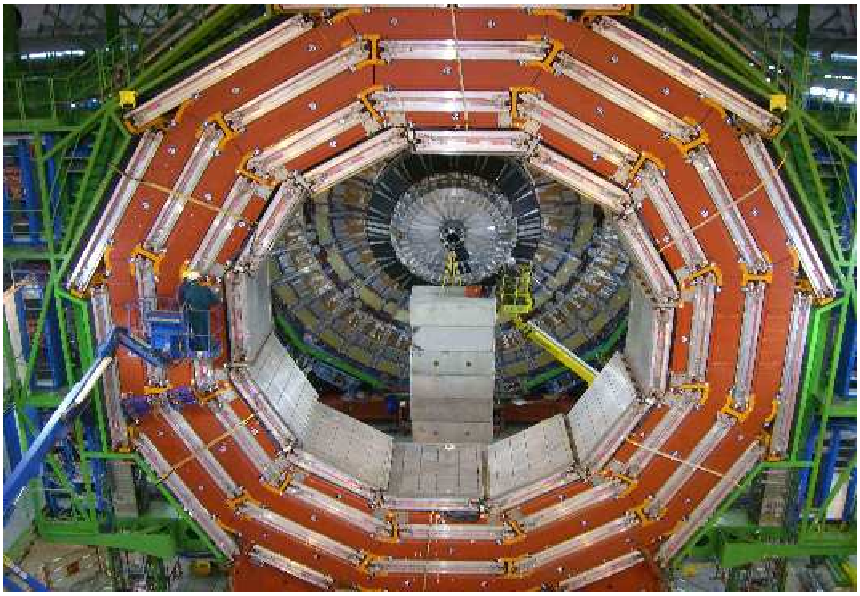

The Compact Muon Solenoid (CMS) experiment [1] will search for the missing block of Nature - the Higgs boson - and for new exotic elementary particles that are predicted by theory and by cosmological observations. The CMS detector uses Resistive Plate Chambers (RPC) as muon detectors, coupled to Drift Tubes in the barrel region, and to Cathode Strip Chambers in the endcaps. Resistive Plate Chambers (RPC) detectors are widely used in HEP experiments for muon detection and triggering at high-energy, high-luminosity hadron colliders, in astroparticle physics experiments for the detection of extended air showers, as well as in medical and imaging applications. While gain and efficiency stability are always a must, in the case of RPC detectors in high-rate experiments which use freon-based gas mixtures, utmost care has to be paid also for the possible presence of gas contaminants. RPC counters [3] are fast, efficient and economical charged particles detectors, well-suited for operation in high magnetic field. The elementary component is a gap, a gas volume enclosed between two resistive plates. Resistive plates are made of bakelite, coated with linseed oil for surface uniformity. Gas mix used is 96.2% $C_2H_2F_4$ / 3.5% Iso-C_4H_{10} / 0.3% SF_6, with a 45% relative humidity. Signal pulses are picked up by readout strips. In CMS, RPC counters are operated in avalanche mode to sustain high-rate operation, with the streamer suppressed by the addition of SF_6 gas in the mixture.

1 Status of the CMS experiment and the RPC muon detector

The RPC barrel system (5 wheels and 480 chambers) has been fully commissioned during the 2008 participating at the CMS global runs. About 370 millions of cosmic ray events have been taken during the 2008 and the RPC detector and trigger worked very well without any major problem. A large fraction of the cosmic data has been analyzed in real time using the DCS and the Data Quality Monitor in order to check online the quality of data. The two systems have been used to configure the detector and the trigger and to assure the quality of the data taken. At the same time the prompt analysis tool have been developed by RPC people to have a more detailed and complete offline data analysis. The first results obtained have shown a very good performances of the RPC detectors and trigger with an average efficiency of about 95%, obtained after having fixed few problems in the detector geometry description and cable maps.

The power system, installed in the 2007, has been fully tested and commissioned during the 2008 global runs showing a very stable functioning with a total failure of 11 channels over 1500 corresponding to less than 0,1%. The Detector Control System is working since the 2007 and has been intensively used during the 2008 showing a stable behaviour and also an user friendly graphical interface. All the DCS data have been stored in the online database (OMDS) and analyzed in real time with the WEB (Web Monitoring Based) tool, developed centrally by CMS and used by all the subdetectors. A subset of the OMDS data have been transferred to the offline database (ORCOFF) using the POPCON framework in order to analyze those data offline.

All the data taken by DCS and by XDAQ have been stored in OMDS and part (HV and Gas) of them has been transferred to ORCOFF after having been encapsulated in an object with an assigned interval of validity. When data are available in ORCOFF can be used in the event reconstruction, in the offline DQM and in any other data analysis. RPC people are using these data in the prompt analysis to correlate the detector performances with the environmental parameters and with the condition data.

All modules of the gas system (primary supply, mixer, purifier module I e II, humidifier, pump, pre-distribution and distribution) have been operational in closed loop mode since mid 2008. The clean mix fraction is about 10%. The system is integrated in DCS PVSS. Both IR analyzer for isobutane and O_2 + H_2O analyzer have been installed and are operational. The gas quality monitoring system (gas cromatograph and electrodes) are operational and routinely used to check the mix composition and presence of major pollutants. The gas system is stable and no currents increase have been observed due to closed loop mode. During year 2008 the activity at the scaled-down closed loop system in the ISR test area has continued for full characterization of purifiers.

2 Activity of the CMS Frascati group in 2008

The Frascati group has joined CMS in the RPC muon detectors at the end of year 2005. Frascati is responsible for the Gas Gain Monitoring system, RPC materials studies, and the test of the Closed Loop recirculation system at ISR for characterization of gas purifiers.

2.1 The CMS Closed Loop Gas System

Because of high costs and huge volumes of the freon-based gas mix used, CMS will use a recirculation (Closed Loop) gas system developed by the CERN gas group. The Closed Loop is a critical component of RPC. CMS has accumulated experience on its use and performances during the test at the Gamma Irradiation Facility at CERN in 2001 [4], and currently at the ISR where chambers are tested in CL prior to installation. At the GIF facility we observed substancial production of HF, linearly correlated with the signal current.

In the Closed Loop (CL) system, purifiers are the crucial component. Purifiers were determined after tests at the GIF in order to minimize the unknown contaminants which showed as spurious peaks besides the known gas mix components. Three filters were selected: 5A molecular sieve, Cu/Cu-Zn, Ni/Al_2O_3. A small scale CL system is currently in use at the ISR test station, where RPC chambers are tested at CERN prior to installation in the CMS detector.

A measurement campaign [5] on purifiers is in progress, using chemical, SEM/EDS (Scanning Electron Microscopy/Energy Dispersive Spectroscopy), XRD (x-ray Diffrattometry) analyses. Preliminary results show evidence of metal elements released by purifiers, and heavy HF production. During year 2008 the activity at the scaled-down closed loop system in the ISR test area has continued for full characterization of purifiers, with new sampling points for detection of gas pollutants produced in the system in correlation with RPC currents increase. The measurement cycle started in August 2008 and is currently in progress.

2.2 Gas Gain Monitoring System

The Gas Gain Monitoring (GGM) system of RPC detectors in CMS monitors the changes in working point due to gas variations, by means of monitoring of anodic charge in small RPC gaps in a cosmic ray telescope. The system is composed of three subsystem of RPC single gaps, readout by 45 cm x 45 cm pads in a cosmic ray telescope located in the SGX5 gas building. Each subsystem is flushed with a different gas. The Reference subsystem is flushed with fresh open loop gas mixture. The MonitorOut subsystem is flushed with CL gas downstream of CMS RPCs. The MonitorIn subsystem is flushed with CL gas upstream of CMS RPCs. Each subsystem is composed of three gaps, whose high voltage is set to the standard working point voltage at the efficiency knee, and to 200 V above and below the knee respectively. Each cosmic ray track therefore provides completely correlated pulses in the three subsystems, allowing one to study the differential response of gaps and by disentangling any effect due to changes in the gas mixture. In case a working point change is detected, an alarm condition is released and the gas quality monitoring system will verify what the change of work point is due to.

The system was located in the SGX5 gas room of CMS in December 2008 and operated before the January 2009 shutdown. During 2008 the GGM was operated at the scaled down closed loop gas system in the ISR test area. The large experience allowed one to determine both sensitivity to working point changes and cancellation algorithms for changes due to environmental variables. Results have been presented at RPC07 and IEEE08. At the end of 2008 the integration of GGM with the CMS DCS-based monitoring has started, with data exchange with PVSS and data save to the OMDS online database. A beta-release control panel was released in December 2008, completion of integration is planned for mid-2009.

3 Activity planned for 2009

The main activity in 2009 will be the participation to data taking shifts and operation of the RPC detector and the physics analysis.

A continuous series of cosmic ray runs is planned from March to June 2009, while collisions are planned to start in July 2009. The test at the scaled down Closed Loop system will continue at low-radiation environments, while a set of tests on new purifiers may be started in high-radiation environment at the GIF facility.

The Frascati group is actively working in the CMS Electroweak Analysis group and is involved in the study of the measurement of inclusive $Z \to \mu^+\mu^-$ cross section. This process is characterized by a clear signature in an almost free background environment and will be studied very soon after the arrival of the first colliding beams.

The work has been focused on the development of methods to select events and measure reconstruction and trigger efficiencies directly from data. An original method has been proposed which consists in five different categories of Z candidates according to the way the muons have been reconstructed (tracker track, standalone muon detector system, combined track+standalone muon) and trigger topologies.

A fit of Z production yield, reconstruction and trigger efficiency is then performed simultaneously on the five categories, thus allowing to extract all the needed information in a single step. This method has been showed to be very robust in handling also a low statistical sample as could be expected in case of few pb^{-1} of integrated luminosity collected.

This work has been presented in several CMS analysis meetings, it has been documented in an internal CMS Analysis note (CMS AN-2009/005) and has been reviewed and accepted by the CMS collaboration as a promising way to perform the analysis.

We expect to complete the analysis with a study of systematic effects and geometrical acceptance. Moreover an effort will be devoted in the next months to make the software tools ready for the start of LHC expected in the second half of year 2009. The analysis will be performed running the software through the GRID on the Tier-2 where the data will be saved, and the development of the tools is essential in order to be able to run in a fast and efficient way as soon as the data will be ready

4 List of Conference Talks

1. T. Greci for the CMS RPC Coll., "Material studies for the RPC muon detector of CMS". In: XCIV Congresso Nazionale SIF. Societa Italiana di Fisica- XCIV Congresso Nazionale. Genova. 22-27 settembre 2008. (vol. 1, pp. 6). Genova: Societa Italiana di Fisica (Italy).

2. S. Colafranceschi for the CMS RPC Coll., "Operational experience of the gas gain monitoring of the CMS RPC detector". In: XCIV Congresso Nazionale SIF. Societa Italiana di Fisica- XCIV Congresso Nazionale. Genova. 22-27 settembre 2008. (vol. 1, pp. 4). Genova: Societa Italiana di Fisica (Italy).

3. L. Benussi *et al.*, "Sensitivity and environmental response of the CMS RPC gas gain monitoring system". Report LNF-08/27(P); arXiv:0812.1710 [physics.ins-det], presented by L.

Benussi at RPC07, Mumbai (India) 2008, to appear on Nucl. Instr. and Methods.

4. L. Benussi *et al.*, "The CMS RPC gas gain monitoring system: an overview and preliminary results". Report LNF-08/29(P); arXiv:0812.1108, presented by S. Colafranceschi at IEEE08, Dresden (Germany) 2008, submitted to JINST.

5. S. Bianco *et al.*, "Materials, Filters and Gas analyses for CMS RPC detector in Closed Loop test setup", presented by G. Saviano at RPC07, Mumbai (India) 2008.

5 Theses, Preprints and CMS notes

1. T. Greci, "Studio preliminare dei materiali del rivelatore di muoni a RPC nell'esperimento CMS", Universitá di Roma "Sapienza", Facolá di Ingegneria, Corso di Laurea in Ingegneria Chimica, Relatore: F. Felli, Correlatore: G. Saviano, Tutor: S. Bianco.

2. Stefano Colafranceschi "Uso dei sensori in fibra ottica per applicazioni aerospaziali e per i rivelatori dell'esperimento CMS", Universitá di Roma "Sapienza", Scuola di Ingegneria Aerospaziale. Relatore: A. Paolozzi, Correlatori interni: F. Felli e G. Saviano, Correlatori esterni: S. Bianco e A. Sharma.

3. S. Bianco *et al.*, "An analysis of materials used in the RPC detector and in the closed loop gas system of CMS at the LHC", Report LNF-08/33(IR). Submitted to JINST.

4. S. Bianco et al., Material Studies for the RPC Muon Detector of CMS. Report LNF-08/34(IR).

5. D. Piccolo *et al.*, CMS Analysis Note AN-2009/005.

6 Papers

1. R. Adolphi *et al.* [CMS Coll.], JINST **3**, S08004 (2008).

References

1. CMS Coll. home page is /cms.cern.ch/.

2. R. Adolphi *et al.* [CMS Coll.], JINST **3**, S08004 (2008).

3. M. Abbrescia *et al.*, Nucl. Instr. & Meth. A **533**,102 (2004); M.Abbrescia et al., Nucl. Instr. & Meth. A **515**, 342 (2003).

4. M. Abbrescia *et al.*, "HF production in CMS Resistive Plate Chambers", submitted to Nucl. Instr. & Meth., presented by R. Guida at the RPC Conference, Seoul (Korea) 2005.

5. M. Abbrescia *et al.*, "Proposal for a systematic study of the CERN closed loop gas system used by the RPC muon detectors in CMS", Report LNF-06/26(IR).

6. M. Abbrescia *et al.*, "Gas analysis and monitoring systems for the RPC detector of CMS at LHC", presented by S. Bianco at the IEEE 2006, San Diego (USA); arXiv:physics/0701014.

KLOE / KLOE2

A. Antonelli, M. Antonelli, D. Babusci, G. Bencivenni, S. Bertolucci,
C. Bloise (Resp. Naz.), F. Bossi, P. Campana, G. Capon, T. Capussela (Ass. Ric.),
P. Ciambrone, E. De Lucia (Art. 23), P. de Simone, D. Domenici (Ass. Ric.),
M. Dreucci (Art. 2222), G. Felici, C. Gatti, S. Giovannella, F. Happacher (Art. 23),
M. Jacewicz (Bors. PD), J. Lee-Franzini (Ass.), M. Martini (Ass.), S. Miscetti,
M. Moulson, S. Müeller (Art. 23), F. Murtas, M. Palutan, V. Patera (Ass.),
P. Santangelo, B. Sciascia, A. Sciubba (Ass.), T. Spadaro,
O. Vasquez Doce (Art. 23), G. Venanzoni, R. Versaci (Ass.)

Technical Staff:
M. Anelli, M. Carletti, G. Fortugno, M. Iannarelli, R. Rosellini, F. Sborzacchi, E. Turri

1 Outline

During 2008 the KLOE Collaboration has continued to work on data analysis and progressed on the plans and the preparatory work for data-taking in year 2009-2010 as well as on the R&D activities for further detector upgrades.

On the Kaon sector, big efforts have been devoted to the analysis of the K_{e2} channel. The ratio $BR(K_{e2})/BR(K_{\mu 2})$ is sensitive to couplings beyond the Standard Model (SM) [1] that should enhance the elicity-suppressed K_{e2} mode well above SM prediction. In order to select the largest possible sample of K_{e2} decays, a completely new set of procedures, for the identification of the signal and the control samples, for the comparison and the correction of Monte Carlo data, for the evaluation of the systematics, has been devised and carefully studied. This is discussed in Sect. 2.1.

The KLOE results on $|V_{us}|$, obtained thanks to many, consistent, precision measurements summarized in Sect. 2.2, have been selected as one of the best achievements of year 2008, and presented to the INFN "Comitato di Valutazione", on July, 9.

Sect. 2.3 is devoted to the study of the quantum coherence of neutral Kaon pairs in the final state $\pi^+\pi^-\pi^+\pi^-$. Other branching ratio measurements, of the $K_S \to e^+e^-$, and the $K^\pm \to \pi^\pm\pi^+\pi^-$, are described in Sect. 2.4 and 2.5 respectively .

For the hadronic cross section, the analysis of $\pi\pi\gamma$ events with photons emitted at low polar angle ($|cos(\theta)| > cos(\pi/12)$), using Bhabha events as normalization, has been completed and published on PLB 672(2009)285. Independent results on the same topic are provided by the normalization of the $\pi\pi\gamma$ sample to the $\mu\mu\gamma$ events, by the study of the $\pi\pi\gamma$ final state with reconstructed photons at large angle, and by the analysis of off-peak data, taken at $\sqrt{s} = 1$ GeV. A status report is presented in Sect. 3.1.

For the η decays, the measurement of the BR($\eta \to \pi\pi$ e e) at the 4% precision level has been finalized, as described in Sect. 3.2, and work is in progress on the radiative $\pi\pi\ \gamma$ channel, reported in Sect. 3.3.

In June 2008 the plan for a new KLOE data taking, KLOE2, has been approved and funded. Test and revision of all the apparatus subsystems has started and the upgrade of the obsolete or inadequate components, including level-2 CPUs, online farm, data storage and the related software, has planned and realized to a great extent.

A tagger for $\gamma\gamma$ physics is being designed to be installed for the new data taking. The experimental setup consists of two stations to detect low, (160-230) MeV, and high, (435-490) MeV, energy electrons respectively. The first is located inside the KLOE detector, $\sim$ 1 m from the interaction region (IP), the second at the exit of the bending dipoles, $\sim$ 11 m from the IP. A report on the status of the project is given in Sect. 4.1.

R&D activities on the calorimeters to instrument the zone of the DAΦNE quadrupoles in the new interaction region are progressing and the realization of an entire module (1/12 of the whole azimuthal acceptance), $\sim$ 90 cm long, constituted by scintillating tiles and optically coupled fibers for signal transmission, as described in Sect. 4.2, is planned by the end of 2009.

Finally, Sect. 4.3 reports about the design and the test results on a prototype of the cylindrical triple-GEM chamber which is being studied for the KLOE tracking upgrade as a new inner tracker detector to be installed close to the beam pipe at the interaction region.

2 Results in kaon physics

2.1 SM test with $K^{\pm}_{e2}$ decays

Recently it has been pointed out that, in a SUSY framework, sizeable violations of lepton universality can be expected in K_{l2} decays [1)] from the couplings to a charged Higgs boson H^+. In a scenario which allows for violation of lepton flavor, the value of the ratio $R_K = \Gamma(K \to e\nu)/\Gamma(K \to \mu\nu)$, which in the SM is precisely determined, would be modified to:

$$R_K^{LFV} = R_K^{SM}\left[1 + \left(\frac{m_K^4}{m_{H^\pm}^4}\right)\left(\frac{m_\tau^2}{m_e^2}\right)|\Delta_{13}|^2 \tan^6\beta\right]. \tag{1}$$

With the lepton flavor violating term Δ_{13} of the order of $10^{-4} - 10^{-3}$, as expected from neutrino mixing, and moderately large values of $\tan\beta$ and $m_{H^\pm}$, SUSY contributions may enhance $R_{\rm K}$ up to a few percent. A measurement of the $K^\pm \to e^\pm\nu$ decay, K_{e2}, at the per cent accuracy is challenging, since one has to face a signal to background ratio which is of the same order of magnitude of $R_{\rm K}$. High background rejection has then to be achieved while keeping at the same time a good control of systematics.

For this measurement we decided to perform a "direct search" for K_{e2} and $K_{\mu2}$ decays without tagging, to keep the statistical uncertainty on the number of counts below 1%. The presence of a one-prong decay vertex in the drift chamber volume with a secondary charged decay track with relatively high momentum ($180 \div 270$ MeV) is required. A very good separation between K_{e2} events and the background, which is dominated by $K_{\mu2}$, is obtained by using the lepton mass squared, $M^2_{\rm lep}$, evaluated from the momenta of the kaon and the charged decay particle, assuming zero neutrino mass. Further background rejection comes by combining all of the calorimeter informations into a PID discriminating variable ($NNPid$ in the following).

The number of signal events is extracted from a likelihood fit to the two-dimensional $M^2_{\rm lep} - NNPid$ distribution, using MC shapes for signal and background. The number of signal events obtained from the fit is $N_{e2} \sim 13\,800 \pm 140$; the projection of the fit result on the $M^2_{\rm lep}$ axis for positive kaons is compared to data in fig.1. The number of $K_{\mu2}$ events in the same data set is extracted from a similar fit to the $M^2_{\rm lep}$ distribution, where no PID information is used. Using the number of observed K_{e2} and $K_{\mu2}$ events, we get as a final result

$$R_{\rm K} = (2.493 \pm 0.025 \pm 0.019) \times 10^{-5}, \tag{2}$$

with 1.3% total error. This value is compatible within errors with the SM prediction, $R_K^{SM} = (2.472 \pm 0.001) \times 10^{-5}$. Figure 2 shows the strong constraints on $\tan\beta$ and $m_{H^\pm}$ given by the KLOE $R_{\rm K}$ result. For a moderate value of $\Delta_{13} \approx 5 \times 10^{-4}$, the region $\tan\beta > 50$ is excluded for charged Higgs masses up to 1000 GeV/c^2 at 95% CL.

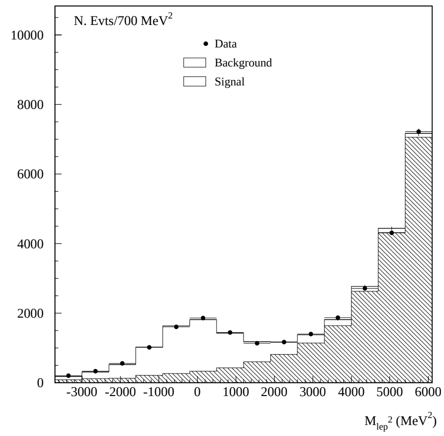

Figure 1: *Distribution of the squared lepton mass of the charged secondary track $M^2_{\rm lep}$: filled dots are data, open dots the result from the maximum-likelihood fit.*

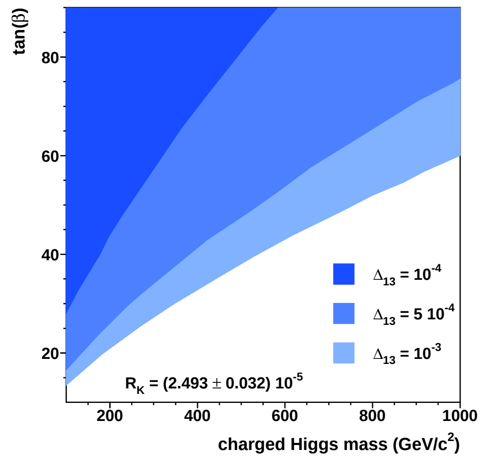

Figure 2: *Exclusion limits at 95% CL on* $\tan\beta$ *and the charged Higgs mass* $m_{H^\pm}$ *from* $R_{\rm K}$ *for different values of* Δ_{13}.

2.2 $V_{\rm us}$ and lepton universality with kaons

During the last years, we measured most of the decay branching ratios of K_S and K_L [2) 3)]. We published this year new measurements of $K^\pm$ semileptonic decay branching ratios [4)] and of the $K^\pm$ two-body decay branching ratio, BR($K^+ \to \pi^+\pi^0$) [5)], having published already in 2006 the BR($K^+ \to \mu\nu$) [6)]. We have also measured the K_L lifetime [7)] and we recently published a new measurement of the $K^\pm$ lifetime. Finally, the shape of the form factors in semileptonic decays have been measured for both K_{e3} [8)] and $K_{\mu3}$ decays [9)]. The above results provide the basis for the determination of the CKM parameter $V_{\rm us}$, and a test of the unitary of the quark flavor matrix. We also test the lepton universality in K_{l3} decays and place bounds on new physics using measurements of $V_{\rm us}$ from K_{l2} and K_{l3} decays. A well organized compendium of all of our data has been recently published, and presented in summer 2008 to the International Advisory Committee of the INFN as one of the major experimental results achieved during the year. We summarize here the main results.

Using our determinations of the kaon semileptonic decay rates, we obtained the values of $f_+(0)\,V_{us}$ for K_{Le3}, $K_{L\mu3}$, K_{Se3}, $K^\pm_{e3}$, and $K^\pm_{\mu3}$ decay modes. It is worth noting that the only external experimental input to this analysis is the K_S lifetime. The five different determinations have been averaged, taking into account all known correlations. We find

$$f_+(0)\,V_{us} = 0.2157 \pm 0.0006, \tag{3}$$

with $\chi^2/\mathrm{ndf} = 7.0/4(13\%)$.

Comparison of the values of $f_+(0)\,V_{us}$ for K_{e3} and $K_{\mu3}$ modes provides a test of lepton universality. Specifically,

$$r_{\mu e} = \frac{(f_+(0)\,V_{us})^2_{\mu3,exp}}{(f_+(0)\,V_{us})^2_{e3,exp}} = \frac{\Gamma_{\mu3}}{\Gamma_{e3}}\,\frac{I_{e3}(1+\delta_{Ke})^2}{I_{\mu3}(1+\delta_{K\mu})^2}, \tag{4}$$

where δ_{Kl} is a correction due to $SU(2)$ breaking and photon radiation. The ratio $r_{\mu e}$ is equal to the ratio g_μ^2/g_e^2, with g_ℓ the coupling strength at the $W \to \ell\nu$ vertex. In the SM, $r_{\mu e} = 1$. Averaging between charged and neutral modes, we find

$$r_{\mu e} = 1.000 \pm 0.008. \tag{5}$$

This has to be compared with the sensitivity obtained in $\pi \to \ell\nu$ decays, $(r_{\mu e})_\pi = 1.0042(33)$, and in τ leptonic decays, $(r_{\mu e})_\tau = 1.000(4)$ [10].

Lattice evaluations of $f_+(0)$ are rapidly improving in precision. For example, the RBC and UKQCD Collaborations have recently obtained $f_+(0) = 0.9644(49)$ from a lattice calculation with $2+1$ flavors of dynamical domain-wall fermions [11]. Using their value of $f_+(0)$, with our determination of $f_+(0)\,V_{us}$, with 2.8 per mill fractional accuracy, we obtain $V_{\mathrm{us}} = 0.2237(13)$.

The availability of precise lattice evaluations for the pion- and kaon-decay constants f_π and f_K allows to use the relation between $\Gamma(K_{\mu2})/\Gamma(\pi_{\mu2})$ and $|V_{\mathrm{us}}|^2 / |V_{\mathrm{ud}}|^2$, with the advantage that lattice-scale uncertainties and radiative corrections largely cancel out in the ratio [12]. From our measurements of $\mathrm{BR}(K_{\mu2})$ and $\tau_\pm$, and using $\Gamma(\pi_{\mu2})$ from [10], we evaluate:

$$V_{us}/V_{ud} \times f_K/f_\pi = 0.2766 \pm 0.0009. \tag{6}$$

Using the recent lattice determination of f_K/f_π from the HPQCD/UKQCD collaboration, $f_K/f_\pi = 1.189(7)$ [13], we finally obtain $V_{\mathrm{us}}/V_{\mathrm{ud}} = 0.2326 \pm 0.0015$.

To test the unitarity of the quark mixing matrix, we combine all the information from our measurements on $K_{\mu2}$, K_{e3}, $K_{\mu3}$, together with superallowed $0^+ \to 0^+$ nuclear β decays (fig.3). The best estimate of $|V_{\mathrm{us}}|^2$ and $|V_{\mathrm{ud}}|^2$ can be obtained from a fit to our results $V_{\mathrm{us}} = 0.2237(13)$ and $V_{\mathrm{us}}/V_{\mathrm{ud}} = 0.2326(15)$, together with $V_{\mathrm{ud}} = 0.97418(26)$ [14]. The fit gives $|V_{\mathrm{us}}|^2 = 0.0506(4)$ and $|V_{\mathrm{ud}}|^2 = 0.9490(5)$, with $\chi^2/\mathrm{ndf} = 2.34/1$ (13%) and a correlation coefficient of 3%. The values obtained confirm the unitarity of the CKM quark mixing matrix as applied to the first row. We find:

$$|V_{\mathrm{us}}|^2 + |V_{\mathrm{ud}}|^2 - 1 = -0.0004 \pm 0.0007 \quad (\sim 0.6\sigma). \tag{7}$$

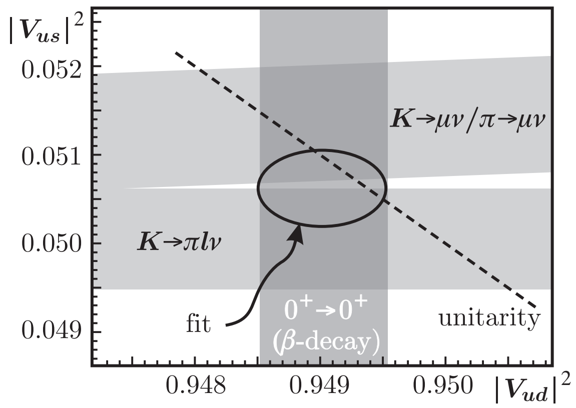

Figure 3: *KLOE results for* $|V_{\mathrm{us}}|^2$ *and* $|V_{\mathrm{us}}/V_{\mathrm{ud}}|^2$*, together with* $|V_{\mathrm{ud}}|^2$ *from* β*-decay measurements. The ellipse is the* 1σ *contour from the fit. The unitarity constraint is illustrated by the dashed line.*

2.3 Quantum interferometry

The neutral kaon pair from $\phi \to K^0\bar{K}^0$ are produced in a pure quantum state with $J^{PC} = 1^{--}$. The decay intensity to any two possible final states $f_1(t_1)$ and $f_2(t_2)$, integrated over all t_1 and t_2 for fixed $\Delta t = t_1 - t_2$, is expressed as:

$$\begin{aligned} I_{f_1, f_2}(\Delta t) \;\; = \;\; & \frac{1}{2\Gamma}|\langle\, f_1\,|K_S\rangle\langle\, f_2\,|K_S\rangle|^2 \times \Big[|\eta_1|^2 e^{-\Gamma_L \Delta t} + |\eta_2|^2 e^{-\Gamma_S \Delta t} \\ & - 2(1-\zeta)|\eta_1||\eta_2| e^{-(\Gamma_L+\Gamma_S)\Delta t/2} \cos(\Delta m \Delta t + \phi_2 - \phi_1)\Big], \end{aligned} \qquad (8)$$

where $\Delta t > 0$, and $\Gamma \equiv \Gamma_L + \Gamma_S$). The last term is due to interference between the decays to states f_1 and f_2 and ζ=0 in quantum mechanics. Fits to the Δt distribution provide measurements of the magnitudes and phases of the parameters $\eta_i = \langle\, f_i\,|K_L\rangle/\langle\, f_i\,|K_S\rangle$, as well as of the K_L-K_S mass difference Δm and the decay widths Γ_L and Γ_S.

Such fits also allow to test fundamental properties of quantum mechanics. For example, quantum-mechanical coherence can be tested by choosing $f_1 = f_2$. In this case, because of the antisymmetry of the initial state and the symmetry of the final state, there should be no events with $\Delta t = 0$. The analysis of the Δt distribution for $K_S K_L \to \pi^+\pi^-\pi^+\pi^-$ events on a statistics of $\sim$ 1500 pb^{-1} of data integrated during year 2004-2005 has been recently completed. The Δt distribution is fit with a function of the form of eq.8, including the experimental resolution and the peak from $K_L \to K_S$ regeneration in the beam pipe. Observation of $\zeta \neq 0$ would imply loss of quantum coherence. The value of ζ depends on the basis, $K^0 - \bar{K}^0$ or K_S-K_L used in the analysis. Using the $K^0 - \bar{K}^0$ basis we find

$$\zeta = (1.4 \pm 9.5_{\mathrm{stat}} \pm 3.8_{\mathrm{syst}}) \times 10^{-7} \qquad (9)$$

which improves by a factor of two with respect to the KLOE result published in 2006 [15], based on $\sim$ 400 pb^{-1} of data.

In the context of quantum gravity, CPT violation effects might occur in correlated neutral kaon states [16, 17], where the resulting loss of particle-antiparticle identity could induce a breakdown of state correlation imposed by Bose statistics. As a result, the initial state can be parametrized as:

$$|i\rangle = \frac{1}{\sqrt{2}}\left(|K^0,\vec{p}\rangle|\bar{K}^0,-\vec{p}\rangle - |\bar{K}^0,\vec{p}\rangle|K^0,-\vec{p}\rangle\right) + \frac{\omega}{\sqrt{2}}\left(|K^0,\vec{p}\rangle|\bar{K}^0,-\vec{p}\rangle + |\bar{K}^0,\vec{p}\rangle|K^0,-\vec{p}\rangle\right) \,, \quad (10)$$

where ω is a complex parameter describing a completely novel CPT violation phenomenon, not included in previous analyses. Its order of magnitude could be at most $|\omega| \sim \left[(m_K^2/m_{\rm Planck})/\Delta\Gamma\right]^{1/2} \sim 10^{-3}$ with $\Delta\Gamma = \Gamma_S - \Gamma_L$. Inserting the modified initial state in the expression of the $K_SK_L \rightarrow \pi^+\pi^-\pi^+\pi^-$ decay intensity, and fitting the Δt distribution as in the case of the previous analysis, we obtain the following results for the real and imaginary parts of ω:

$$\mathrm{Re}(\omega) = \left(-1.6^{+3.0}_{-2.1} \pm 0.4\right) \times 10^{-4}, \qquad \mathrm{Im}(\omega) = \left(-1.7^{+3.3}_{-3.0} \pm 1.2\right) \times 10^{-4}. \quad (11)$$

This can be translated into an upper limit on the absolute value, $|\omega| < 1.0 \times 10^{-3}$ at 95% CL, thus reaching the interesting Planck's scale region. Also in this case, the analysis of the full data sample allowed to improve by a factor of two with respect to the published results [15].

2.4 Direct search of $K_S \rightarrow e^+e^-$

This decay is a flavour-changing neutral current process, suppressed in the SM, with an amplitude dominated by the two photon intermediate state. Using ChPT to $\mathcal{O}(p^4)$, one obtains the prediction BR($K_S \rightarrow e^+e^-$) $\sim 2\times10^{-14}$ [18]. A value significantly higher could indicate new physics. Prior to KLOE, the best experimental limit on this decay was set by CPLEAR, BR($K_S \rightarrow e^+e^-$) $\leq 1.4 \times 10^{-7}$ at 90% CL [19].

We performed a search for the $K_S \rightarrow e^+e^-$ decay using 1.9 fb^{-1} of integrated luminosity. A MC background sample of comparable statistics and a large MC signal sample have been also used in the analysis. After K-crash tag, we search for the signal by requiring two tracks of opposite charge originating near the IP. The two tracks are required to have an invariant mass M_{ee}, evaluated in the electron hypothesis, in a $\sim$ 20 MeV window around the nominal K_S mass. This cut is particularly effective on $K_S \rightarrow \pi^+\pi^-$ events, which peak at $M_{ee} \sim 409$ MeV. After it the background is dominated by $K_S \rightarrow \pi^+\pi^-$ with at least one pion wrongly reconstructed, and by $\phi \rightarrow \pi^+\pi^-\pi^0$ events. The K_S events are strongly reduced by cutting on the track momentum in the K_S rest frame, which is expected to be $\sim$ 206 MeV for $K_S \rightarrow \pi^+\pi^-$ decays. To reject $\phi \rightarrow \pi^+\pi^-\pi^0$ events we use instead $|\vec{p}_{miss}| = |\vec{p}_\phi - \vec{p}_{K_S} - \vec{p}_{K_L}|$, where K_S and K_L momenta are evaluated from the charged tracks and from the K-crash tag, respectively. The value of $|\vec{p}_{miss}|$ peaks at zero for the signal, within the experimental resolution of few MeV. It spreads towards higher values for $\phi \rightarrow \pi^+\pi^-\pi^0$ events. The residual background, both from $K_S \rightarrow \pi^+\pi^-$ and $\phi \rightarrow \pi^+\pi^-\pi^0$ decays, is rejected identifying the two electrons by ToF, and by using the properties of the associated calorimetric cluster. The reliability of the MC background simulation is checked after each step of the selection on the invariant mass sidebands. At the end of the analysis chain, we don't count any event in the signal box; the background estimate is also compatible with zero. The upper limit on the number of signal events is therefore $N_{ee} = 2.3$ at 90% CL. The signal selection efficiency, after tagging, is $\sim$ 47%. Such performance in terms of exceptional background rejection ($> 10^8$)

with an acceptable signal efficiency, has been achieved largely thanks to the very good momentum resolution of our DC. To obtain un upper limit for the $BR(K_S \to e^+e^-)$, we normalize N_{ee} to the $K_S \to \pi^+\pi^-$ decays observed in the same data sample. Finally, we obtain:

$$\mathrm{BR}(K_S \to e^+e^-) \leq 9 \times 10^{-9} \quad \text{at } 90\% \text{ CL}, \tag{12}$$

which represents a factor of ~ 15 improvement with respect to the best previous limit. This result, submitted for publication at the end of 2008, has been recently published by Phys. Lett. B [20].

2.5 Measurement of $BR(K^\pm \to \pi^\pm\pi^+\pi^-)$

The measurement of the BR of this decay completes the KLOE program of precise and fully inclusive kaon dominant BR's measurements. The most recent result, $\mathrm{BR}(K^\pm \to \pi^\pm\pi^+\pi^-) = (5.56 \pm 0.20)\%$ [21], dates back to more than 30 years ago.

We plan to use two normalization samples given by the two tags, $K_{\mu 2}$ and $K_{\pi 2}$. The track of the tagged kaon is backward extrapolated to the interacion point, then the kinematic of the decay $\phi \to K^+K^-$ allows to define the path of the signal kaon (direction and momentum).

The decay products of the kaons have low momentum, less than 200 MeV/c, and curl up in the KLOE magnetic field (0.52 T); this increases the probability to reconstruct broken tracks and fake vertices. Selecting kaon decays before the inner wall of the drift chamber, the maximum number of tracks to be reconstructed is three instead of four, and the quality of the reconstruction improves.

We require at least two reconstructed tracks in the DC (pion candidates), and if their backward extrapolations give a vertex on the path of the signal kaon we evaluate the missing mass of the decay. Work is in progress to finalize the evaluation of the efficiency, and the associated systematic error, of the reconstruction procedure described above, using MC samples corrected to take into account tiny data-MC discrepancies in tracking.

Figure 4 shows the comparison between data and MC missing mass spectrum, that peaks in the pion mass region. Figure 5 shows the contributions to the MC missing mass distribution due to the signal selected sample and to the background; the ratio is $S/B \simeq 18.6$.

The good agreement between data and MC allows to perform event counting on the missing mass distribution with negligible systematic uncertainty.

3 Results in hadronic physics

3.1 The measurement of the hadronic cross section

During 2008, the analysis of the hadronic cross section measurement for the process $e^+e^- \to \pi^+\pi^-$ from KLOE data taken in year 2002 has been finalized [22]. The dipion contribution to the muon anomaly, $a_\mu^{\pi\pi}$, in the interval $0.592 < M_{\pi\pi} < 0.975$ GeV, has been measured with negligible statistical error and a 0.6% experimental systematic uncertainty. Radiative corrections increase the systematic uncertainty to 0.9%. Combining all errors we found:

$$a_\mu^{\pi\pi}(0.592 < M_{\pi\pi} < 0.975\,\mathrm{GeV}) = (387.2 \pm 3.3) \times 10^{-10}.$$

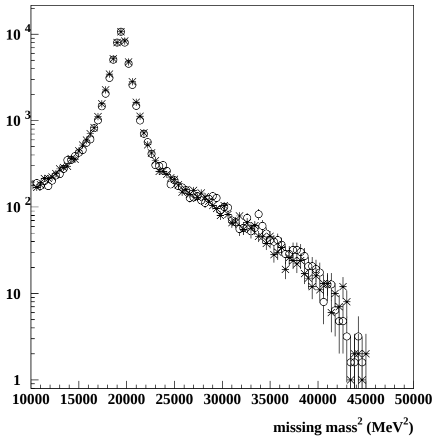

Figure 4: *$K\pi\pi$ missing mass distribution: empty dots are data, stars MC.*

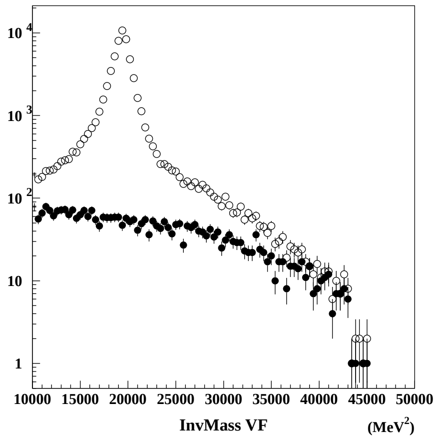

Figure 5: *MC $K\pi\pi$ missing mass distribution (empty dots), the backgrond contribution is superimposed (filled dots).*

This result represents an improvement of 30% on the systematic error with respect to our previous published value [23], and confirms the current disagreement between the standard model prediction for a_μ and the measured value, as shown in fig. 6, left. The spectrum of the pion form factor is also in very good agreement with recent results from SND and CMD2 experiments at Novosibirsk [24], as shown in fig. 6, right.

Independent analyses are in progress:

- to measure $\sigma_{\pi\pi(\gamma)}$ using detected photons emitted at large angle, improving knowledge of the FSR interference effects (in particular the $f_0(980)$ contribution);
- to measure the pion form factor directly from the ratio, bin-by-bin, of $\pi^+\pi^-\gamma$ to $\mu^+\mu^-\gamma$ spectra;
- to extract the pion form factor from data taken at $\sqrt{s} = 1$ GeV, off the ϕ resonance, where $\pi^+\pi^-\pi^0$ background is negligible.

We organized the PHIPSI08-Workshop at the Frascati laboratory, in April 2008, bringing together more than 120 physicists [27]. In this workshop our final result on dipion contribution to the muon anomaly was presented.

In addition, a meeting of the Working Group on Radiative Corrections and MC Generators for Low Energies, was held on April 10 at the LNF, with theorists and experimentalists discussing current status and developments on the calculations of radiative corrections and Monte Carlo generators for physics in the continuum at low energy.

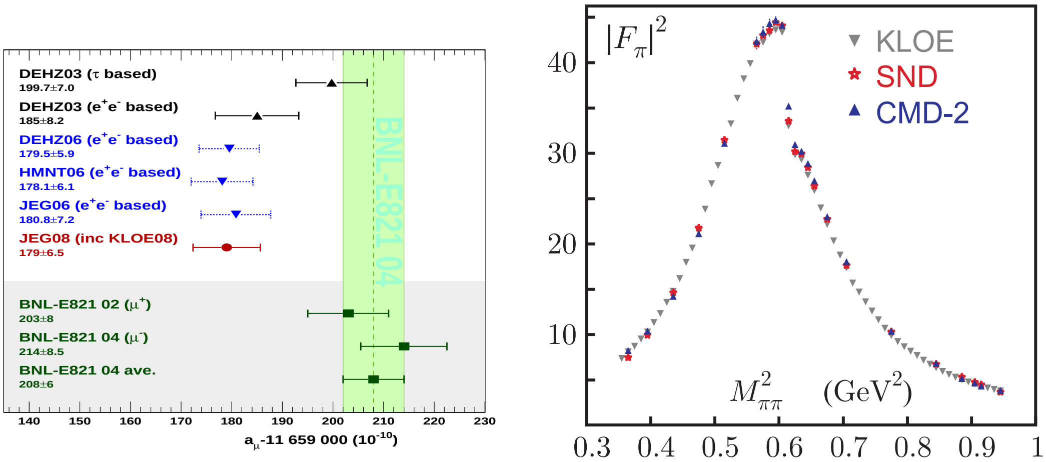

Figure 6: *Left: Comparison of the theoretical prediction for a_μ* [25] *with the BNL measurement* [26]*. Theoretical estimates from different groups are reported; the last (red) point includes the KLOE new measurement. Right: Pion form factor measured by KLOE, compared with CMD-2, SND.*

3.2 The measurement of the branching ratio and the search for a CP violating asymmetry in the $\eta \to \pi^+\pi^-e^+e^-$ decay

There are several theoretical reasons to study the $\eta \to \pi^+\pi^-e^+e^-$ decay. It allows to probe the structure of the η meson [28], to compare the predictions of the branching ratio value based on Vector Meson Dominance model, and ChPT [29, 30, 31, 32] and to study CP violation beyond the prediction of the Standard Model [33] measuring the angular asymmetry between pions and electrons decay planes.

The samples used in this analysis are: 1733 pb^{-1} from 2004-2005 data taking; 232 pb^{-1} from 2006 off-peak ($\sqrt{s} = 1000$ MeV) data taking; Montecarlo signal and background equivalent to 50 $\times$ 10^3 pb^{-1} and 3447 pb^{-1}, respectively. The signal MC has been produced using the PHOTOS package to account for FSR.

The events are required to have at least four tracks (two positive and two negative) coming from a cylinder around the Interaction Point (radius $R = 4$ cm, height $h = 20$ cm). For each charge, the two tracks with the highest momenta are selected. A cluster not associated to any track, having time compatible with the photon time of flight, energy of at least 250 MeV and in the polar-angle range ($23° - 157°$), is also required.

Background sources can be grouped into ϕ-decays and events in the continuum. The former is mainly due to $\phi \to \pi^+\pi^-\pi^0$ events (with π^0 Dalitz decay) and to $\phi \to \eta\gamma$ events either with $\eta \to \pi^+\pi^-\pi^0$ (with π^0 Dalitz decay) or with $\eta \to \pi^+\pi^-\gamma$ (with photon conversion on the beam pipe). The latter is due to $e^+e^- \to e^+e^-(\gamma)$ events with photon conversions, split tracks or interactions with some material in the region of DAΦNE quadrupoles inside KLOE. Because of poor MC statistics, this background has been studied using off-peak data taken at $\sqrt{s} = 1$ GeV, where ϕ decays are negligible. Backgrounds are rejected applying cuts on: 1- the momenta ((270 $<$ $|\vec{p}(\mathrm{p}^+_{Max})| + |\vec{p}(\mathrm{p}^-_{Max})| < 460$) MeV and ($450 < \sum_1^4 |\vec{p}_i| < 600$) MeV); 2- the invariant mass

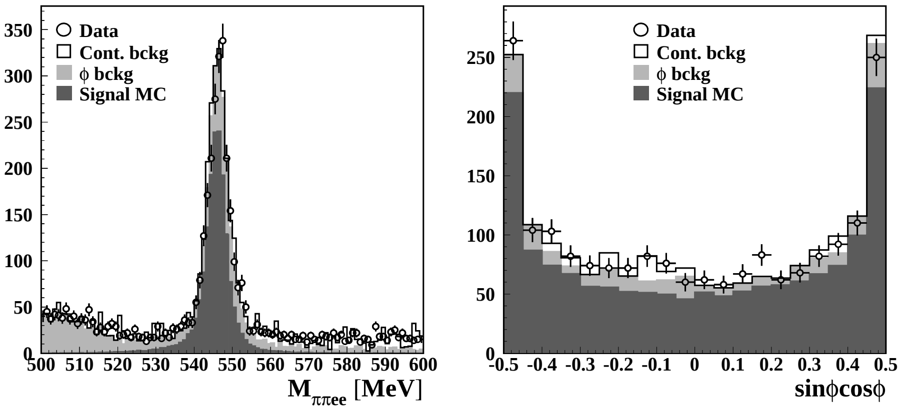

Figure 7: *Left: fit to the invariant mass of the four selected tracks. Right: distribution of the* $\sin\phi\cos\phi$ *variable in the signal region. Dots: data. The black histogram is the expected distribution, i.e. signal MC (dark grey),* ϕ *background (light grey) and background in the continuum (white).*

and the distance of the candidate electron tracks to reject photon conversions on the beam pipe ($M_{ee}(BP) < 15$ MeVs and $D_{ee}(BP) < 2.5$ cm); 3- the average polar angle of forward and backward particles identified as signal to reject background in the continuum ($\langle\cos\theta_f\rangle > 0.85$ and $\langle\cos\theta_b\rangle < -0.85$).

Background contribution is evaluated performing a fit to the data distribution of the $\pi^+\pi^-e^+e^-$ invariant mass after the cuts on the momenta using as input background shapes only. The fit is done on sidebands in order not to introduce correlations between signal and background ($[450, 520]$ MeV $\cup$ $[570, 650]$ MeV). The output of the fit ($\chi^2/dof = 32.5/30$, $P(\chi^2) = 0.35$) is shown in the left panel of Fig. 7. For the signal estimate we limit ourselves to the region $[535, 555]$ MeV and perform the event counting after background subtraction: we find 1555 (368) signal (background) events. The selection efficiency has been evaluated from MC.

The result obtained for the branching ratio is:

$$BR(\eta \to \pi^+\pi^-e^+e^-\gamma) = (26.8 \pm 0.9_{Stat.} \pm 0.7_{Syst.}) \times 10^{-5}. \tag{13}$$

The decay plane asymmetry is calculated starting from the momenta of the four particles and is expressed as function of the angle ϕ between the pion and the electron planes in the η rest frame. It has been evaluated for the events in the signal region after background subtraction. The value obtained is:

$$\mathcal{A}_\phi = (-0.6 \pm 2.5\ _{Stat.} \pm 1.8\ _{Syst.}) \times 10^{-2} \tag{14}$$

which is the first measurement of this asymmetry. The distribution of the $\sin\phi\cos\phi$ variable is shown in the right panel of Fig. 7.

The results are final and a paper has been submitted to PLB. The same four track final state is also under study to select the $\eta \to e^+e^-e^+e^-$, never observed before.

3.3 Radiative decay of eta meson, $\eta \to \pi^+\pi^-\gamma$

In the $\eta \to \pi^+\pi^-\gamma$ decay a significant contribution from chiral anomaly responsible for $\eta \to \gamma\gamma$ decay is expected [34]. Chiral anomaly describes the non-resonant coupling providing the distribution of the invariant mass of the pions ($m_{\pi\pi}$). The measurement of $m_{\pi\pi}$ is relevant to disentangle resonant contributions, e.g. from the ρ-meson. Several theoretical approaches have been developed to treat the contribution of the anomalies to the decay [35] [36] [37]. This decay has been measured in the 1970s with data samples of the order of 10^4 events [38] [39]. However, the theoretical papers which tried to combine the measurements found discrepancies in data treatment and problems with obtaining consistent results. Therefore, the results from experiments with large statistics are really needed to clarify the situation [40].

KLOE data contains about 3.5 $\times 10^6$ $\eta \to \pi^+\pi^-\gamma$ decays. With this statistics it is possible to investigate in detail the pion invariant mass distribution and the photon energy spectrum in order to disentangle non-resonant contributions and settle the inconsistencies of previous measurements. The measurement of the branching ratio of the $\eta \to \pi^+\pi^-\gamma$ decay will have an impact on the analysis of the rare η decays like $\eta \to \pi^+\pi^-e^+e^-$ and $\eta \to \pi^+\pi^-\mu^+\mu^-$ and, last but not least, the decay gives the opportunity to search for C violation signature in the left-right charge asymmetry.

The main background is the ϕ decay $\phi \to \pi^+\pi^-\pi^0$ (with ratio 200:1 to our signal) which mimics the event signature in the specific kinematical range when two photons (one coming from eta, γ_η, and the other, γ_ϕ, from ϕ decay) invariant mass is in the range of the π^0 reconstructed mass. In order to reduce background contribution, the following steps are made:

1. At least 2 neutral clusters [1] must be found and at least one of them with energy > 250 MeV (photon with maximum energy is assumed to originate from $\phi \to \eta\gamma$ decay). Two tracks (one positive and one negative) are selected on the basis of the distance of closest approach to the interaction point.

2. We improve the energy resolution on γ_ϕ using the constraints from the two-body kinematics of $\phi \to \eta\gamma$ decay, allowing to calculate photon energy from angular information only. Then, using event kinematics from $\phi \to \gamma\eta(\to \pi^+\pi^-\gamma)$ decay chain (with improved information about γ_ϕ) we calculate the γ_η momentum and use the opening angle (α) between this vector and the measured direction of each neutral cluster (if there are more than one) in order to select the cluster with minimum α as originating from the $\eta \to \pi^+\pi^-\gamma$ decay. Thereafter we require that selected γ_η has: $|E_\gamma - P_\gamma| < 10$ MeV and $\alpha < 0.2$ rad.

The selection efficiency for the signal and background contributions after each step is summarized in Table 1. The selection criteria allow to retain 50% of the signal while reducing signal-to-background ratio to 1:8. The efficiency distribution as a function of the energy of γ_η (fig.8, left) has a smooth behaviour in most of the kinematical range. The same figure (picture on the right-hand side) shows the distribution of the cosine of the angle β between γ_ϕ and γ_η, calculated in the π^0 rest frame, as the photons were coming from π^0 decay (background hypothesis). Background (mostly events from $\phi \to \pi^+\pi^-\pi^0$ decay) peaks strongly at $\cos\beta = -1$ while the signal is

[1] A cluster is defined neutral if it does not have any associated track and has a time compatible with the photon time of flight.

more uniformly distributed. Summing MC-predicted contributions from signal and background we obtain a very good agreement with the experimental data, so that cuts on the cosβ distribution can be well controlled by our simulation, allowing further background reduction with small systematic uncertainty. Studies are underway to finalize the selection procedure.

Table 1: Selection efficiency for signal and background of the part of the analysis procedure described in the text.

	Event signature		**Pre-selection**	
	efficiency	signal-to-bkg ratio	efficiency	signal-to-bkg ratio
SIGNAL	58%	1 : 100	50%	1 : 8
BACKGROUND	53%		3.5%	

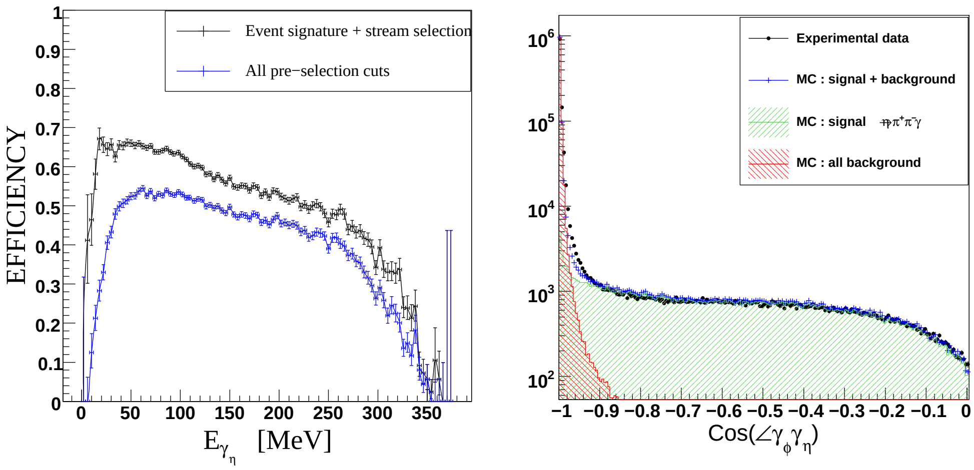

Figure 8: *The efficiency distribution as function of the energy of γ_η (left). Distribution of the cosine of the angle between γ_ϕ and γ_η calculated in the rest frame of π^0 (background hypothesis) (right).*

4 KLOE2

4.1 Studies for the $\gamma\gamma$ tagger

$\gamma\gamma$ physics [41] at the e^+e^- colliders gives access to states with $J^{PC} = 0^{\pm+}, 2^{\pm+}$, not directly coupled to the photon ($J^{PC} = 1^{--}$).

The cross section $\sigma(\gamma\gamma \to X)$ was studied at PETRA, CESR, LEP an at the B-factories over the years. In the low-energy region, $m_\pi \leq W_{\gamma\gamma} \leq 700$ MeV, measurements [42] are affected by large statistical and systematic uncertanties due to small detection efficiencies, large background contributions and particle identification ambiguities in the low-mass hadronic systems.

KLOE2 is the ideal place for precision measurements of low-mass hadronic systems with high statistics and well controlled systematic errors.

Many interesting channels can be investigated and both, the two-photon width of light pseudoscalar mesons, and the meson transition form factors [43] can be obtained. Search for σ meson is another interesting topic addressed by the $\gamma\gamma$ physics program.

The σ meson was suggested for the first time by the linear sigma model, describing pion-nucleon interaction. For many years, the experimental studies did not found any clear signal of this meson, whose existence and nature (i.e. quark substructure) remained controversial.

The situation has only recently changed. It has been shown [44] that the $\pi\pi$ scattering amplitude contains a pole with the quantum numbers of vacuum, a mass $M_\sigma = 441^{+16}_{-8}$ MeV and a width $\Gamma_\sigma = 544^{+25}_{-18}$ MeV. The σ has been looked for also in D decays by the E791 Collaboration at Fermilab [45]. From the $D \to 3\pi$ Dalitz plot analysis, E791 finds that almost 46% of the width is due to $D \to \sigma\pi$ with a $M_\sigma = 478 \pm 23 \pm 17$ MeV and $\Gamma_\sigma = 324 \pm 40 \pm 21$ MeV. BES [46] has looked for σ in $J/\psi \to \omega\pi^+\pi^-$, obtaining a mass value of $M_\sigma = 541 \pm 39$ MeV and a width of $\Gamma_\sigma = 252 \pm 42$ MeV.

It is worth to notice that the problem of assessing the existence and nature of the σ meson is not confined to low energy phenomenology. Just to mention a possible relevant physical scenario in which σ could play a role, consider the contamination of $B \to \sigma\pi$ in $B \to \rho\pi$ decays (possible because of the large σ width). This could sensibly affect the isospin analysis for the CKM-α angle extraction [47]. Similarly, recent studies of the γ angle through a Dalitz analysis of neutral D decays call for the σ resonance to fit data [48].

The only avalaible data at low energy come from Crystal Ball [42] and JADE [49] collaborations. Their precision does not allow to reach any firm conclusion on the presence of a resonance in the region of (400-500) MeV. KLOE2 data are very much awaited to clarify the situation.

To improve on the measurement of the $\gamma\gamma \to \pi\pi$ cross section, high statistics has to be complemented by a careful control of the systematics which cannot be obtained without strong reduction of background events.

The main source of background comes from ϕ decays. Studies currently underway on the KLOE data sample are using the off-peak data in order to evaluate the experimental capabilities leaving aside most of the background from ϕ decays. At KLOE2 we aim to analyze the on-peak sample performing background suppression with the information coming from a tagger system for efficient detection of scattered electrons.

Scattered electrons from $\gamma\gamma$ reaction deviate from the main orbit while propagating on the machine lattice. For the design of the tagging system we have performed MonteCarlo studies of the trajectories of scattered electrons, whose initial kinematical distribution is given by purpose-made $\gamma\gamma$ generators. The magnetic layout of DAΦNE has been fully treated.

The results show that the constraints coming from the DAΦNE structure do not prevent KLOE2 from obtaining a good coverage of the kinematic region of interest.

Satisfactory results have been shown using a tagger system composed by two stations located at ~ 1 m and ~ 11 m from the IP:

- a station to detect leptons at low energy (LET), located in the region between the two quadrupoles inside KLOE (QD0 and QF1). According to the tracking, the energy of the scattered leptons arriving on this detector is mostly in the interval (160-230) MeV;

- a station for leptons with high energy (HET), located at the exit of the first bending magnet (about 11 m from the IP). The energy of the scattered particles is in this case mostly in the range (425-490) MeV. The upper limit of the interval is determined by the minimum distance (3 cm) from the main orbit where we can place the detector without interfere with proper DAΦNE operations.

Scattered leptons on the LET detector pass through the first quadrupole, QD0 and, being off-energy, are deflected with respect to the main orbit. Energy distribution of these leptons is very broad, with tails reaching 50 MeV on one side and 450 MeV on the other. The measurement of the lepton energy requires a calorimeter, being the position of the exit point slightly correlated with the lepton momentum.

The HET detectors are located 11 m from the IP. The leptons propagate through the magnetic layout of the machine, and are selected by the B-fields according to their momenta. Only leptons within a cone of $\Delta\theta < 40$ mrad, with the axis on the flight direction of the incoming beam, are detected. A position detector in this case can measure the lepton momentum with good precision (fig.9).

A detector 7 cm long can tag leptons with energy between 430 and 475 MeV.

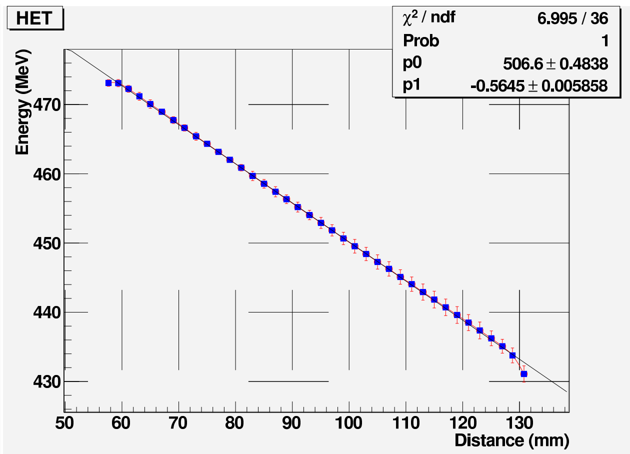

Figure 9: *Energy of the leptons on the HET as a function of the displacement from main orbit.*

When both scattered leptons are detected in the HET/LET taggers we can measure, independently from KLOE, the two-photon centre-of-mass energy $W_{\gamma\gamma}$ of the reaction $\gamma\gamma \to \pi^0\pi^0$.

With the realistic assumption of a 2 mm pitch for the HET and a LET resolution of $\sigma(E)/E = 5\%/\sqrt{E(GeV)}$, in case of coincidence HET $\otimes$ LET we obtain a resolution on $W_{\gamma\gamma}$ of σ_E =12.8 MeV, while in the case of coincidence LET $\otimes$ LET the resolution is σ_E =33.4 MeV.

On this basis, the design of the tagger detectors is being prepared. Tests for the choice of the crystals and the readout electronics have been carried out at the Frascati beam test facility. The Technical Design Report will be submitted for approval to the INFN by the end of March, 2009.

4.2 Studies for quadrupole instrumentation and calorimeters at low polar angle

The new DAΦNE interaction region, adopting the crab-waist scheme, has the two beam pipes already separated at ∼55 cm from the IP, well inside the KLOE detector, and before the focusing quadupoles QF1 (fig.10). For this reason the old instrumentation of the quadrupole zone, needed to veto photons from Kaon decay in the drift chamber, has to be replaced.

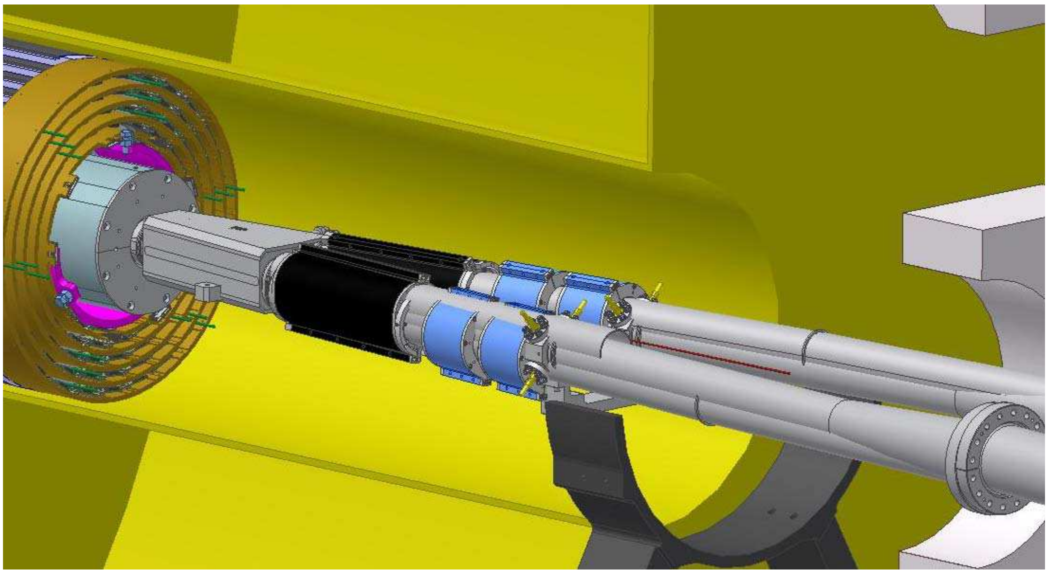

Figure 10: *DAΦNE beam pipe inside KLOE.*

The project, QCALT, requires the realization of a calorimeter composed by 12 + 12 modules of tungsten and scintillating tiles coupled with optical fibers for signal transmission to the Silicon-PhotoMultipliers. Each module, ∼ 90 cm long, is longitudinally divided into 18 tiles, and radially into 5 planes interspaced with tungsten, for a total of 5.7 radiation lengths (the maximum possible absorber in the available space). Electronics for power supply and readout cards, that are custom boards with pre-amplifier, HV distributor and controller, are being designed and realized by the LNF Electronics Service. The study of the tile-fiber and fiber-SiPM couplings is well advanced, as well as the design of the mechanical structure of the detector and its integration on the DAΦNE / KLOE central region.

We plan to realize an entire calorimeter module by the end of year 2009 to finalize the construction procedure and to measure at the LNF test beam the calorimeter performance with electrons of energy up to 500 MeV.

The group is also working on the R&D for a crystal (LYSO) calorimeter, CCALT, to detect low polar angle photons from the interaction region. An integrated plan to test the crystals for CCALT and for the LET station of the $\gamma\gamma$ tagger, is being followed. Test beams are being realized to study both, the crystal performance, and the response of the custom readout electronics.

4.3 R&D for the KLOE2 inner tracker

A fully cylindrical and dead-zone-free GEM detector has been designed as inner tracker for the upgrade of the KLOE detector. The proposed inner tracker, that opens the way for a new and competitive category of ultra-light, full sensitive vertex detectors for high energy physics experiments, will play a crucial role in the study of the K_S and η rare decays and in the measurement of the neutral kaon interferometry. Main requirements are: good spatial resolution, $\sigma(r\phi) = 200\ \mu m$ and $\sigma(z) = 500\ \mu m$ and very low material budget, 2% of X_0 for the whole detector. The inner tracker will be composed by five layers of cylindrical triple-GEM detectors (CGEM), covering the space from the beam pipe to the inner wall of the KLOE Drift Chamber (from 150 mm to 250 mm radius). Each CGEM is realized inserting one into the other five cylinders made of thin (50 μm) polyimide foils: the cathode, the three GEMs and the anode readout. In order to avoid support frames inside the sensitive volume, the cylindrical GEMs are mechanically stretched from their ends where annular fiberglass frames are glued. The final result is a very light detector: only 0.2% of X_0 per layer inside the active area. The readout will be performed with a XV pattern of readout strips engraved on the anode foil [50]. A full scale prototype (300 mm diameter, 360 mm length) of the first layer of the inner tracker has been successfully built and characterized under different experimental conditions. The results show that this technology can be successfully used for tracking improvement at KLOE2. A description of the construction procedure and the detector performance is given in the following section.

4.3.1 The CGEM prototype

In 2007 a CGEM prototype has been built with the same diameter of the innermost IT layer (300 mm) and a reduced length of 360 mm. For sake of simplicity the anode has been segmented only with longitudinal strips, with a pitch of 650 μm, providing the $r\phi$ coordinate. About 320 strips out of 1500 have been connected to FEE and readout.

Each CGEM is a Triple-GEM detector with a geometrical configuration of the gaps of 3/2/2/2 mm, respectively for drift/transfer1/transfer2/induction. The cathode is internal to the anode.

Three GEM foils are glued together at first, to obtain the single large foil needed to make a cylindrical electrode. We used an epoxy glue (Araldite), distributed along one edge of the GEM, on a 3 mm wide region. Then foil is rolled on an aluminum mould coated with a precision machined Teflon film providing a non-stick, low friction surface. The mould is then enveloped in a vacuum bag and vacuum is applied with a Venturi system, resulting in a uniform pressure of 0.8 Kg/cm^2 throughout the whole surface. At this step two fiberglass annular rings are also glued at the edges of the electrode, representing all the mechanical frames needed to support the detector. After the curing cycle of the glue the cylindrical electrode is extracted from the mould. Cathode and anode are obtained with the same procedure. At the end the five electrodes are inserted one into the other and the detector is sealed with epoxy on both sides [51].

The mechanical tension needed by the GEM foil in order to avoid oscillation and instability is given by hanging the protype and applying a traction along its axis. A detailed simulation has been performed with the ANSYS program in order to evaluate the static and dynamic behavior of the detector. In particular, we found that for a 100 N longitudinal traction the elongation is about

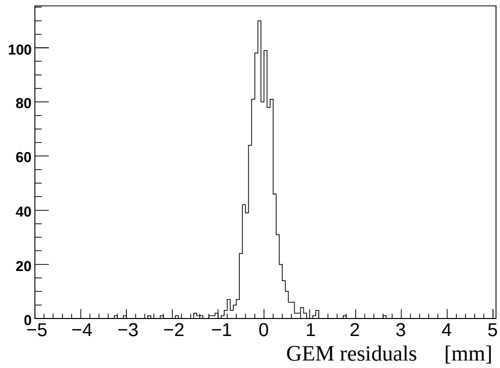

Figure 11: *Distribution of tracking residuals showing* σ_{res}= *250* μm*.*

0.03 mm, and the sagitta due the gravity is only 6 μm. We have experimentally verified that such a traction is enough to obtain a proper operation of the chamber.

The final IT detector will require GEM foils with an active area as large as 700x500 cm^2. The ST-DEM-PMT laboratory at CERN, where GEMs are produced, is planning a change of technology in order to realize such large area foils, leading to a different shape of the holes. We are both simulating the new GEM and building small prototypes in order to determine the operation parameters, such as gain, electron transparencies, charging-up, ion feedback.

The C-GEM prototype has first been tested in current mode with a 6 keV X-ray gun. A 10x10 cm^2 planar GEM has been placed in the same gas line and used as a reference in order to normalize the gain for changes of atmospheric variables. The gas gain has been measured up to a value of 2x10^4 and no discharge has been observed. The electron transparency has been measured as a function of the electric field, obtaining results in good agreement with expectations. Gain fluctuations throughout the 940 mm of circumference were within 9%, showing good uniformity on such a large surface.

Then, the prototype has been extensively tested with the 10 GeV pion beam at the T9 area of CERN PS. Here 128 channels have been equipped with the new GASTONE ASIC, which has been developed for the KLOE2 experiment, in order to fulfill low-power consumption and high integration requirements. It is composed of four different blocks: a charge sensitive preamplifier (20 mV/fC sensitivity), a shaper, a leading edge discriminator and a monostable circuit to stretch the digital signal waiting for the KLOE L1 trigger. While a version with 64 channels has been designed for the final readout card [52)], we mounted on the detector the first release of the ASIC, with 16 channels.

The detector was flushed with a Ar/CO_2= 70/30 gas mixture and operated at a gain of 2x10^4. Figure 11 shows the residuals of the clusters with respect to the reconstructed position of the track. The spatial resolution of the external tracker was σ_{trk}= 140 μm. Subtracting this contribution, the GEM spatial resolution is:

$$\sigma_{GEM} = \sqrt{\sigma^2_{res} - \sigma^2_{trk}} \simeq 200\ \mu\text{m} \tag{15}$$

in agreement with expections from a digital readout of 650 μm pitch strips.

The efficiency of the chamber has been measured for different track positions. In most of the region a very high efficiency of 99.6% has been obtained. Time distributions in normal regions of the chamber and in the junction zones of the foils have been studied. In the normal region a 13 ns RMS is obtained, in agreement with the performance of the gas mixture. In the gluing zone, representing less than 0.4% of the surface, the spectrum is much broader, with a 200 ns RMS. In particular, the signals are delayed up to 700 ns, suggesting a longer drift path to reach the anode. Such hypothesis has been confirmed by simulations with ANSYS and GARFIELD, showing a distortion of the field lines in the gluing regions due to space charge on the dielectric.

5 KLOE papers in year 2008

1. F. Ambrosino *et al.*, J. High Energy Phys. **02**, 09 (2008).
2. F. Ambrosino *et al.*, J. High Energy Phys. **01**, 073 (2008).
3. F. Ambrosino *et al.*, J. High Energy Phys. **0804**, 059 (2008).
4. F. Ambrosino *et al.*, J. High Energy Phys. **0805**, 006 (2008).
5. F. Ambrosino *et al.*, J. High Energy Phys. **0805**, 051 (2008).
6. F. Ambrosino *et al.*, Eur. Phys. J. C **55**, 539 (2008).
7. F. Ambrosino *et al.*, Phys. Lett. B **666**, 305 (2008).
8. F. Ambrosino *et al.*, Phys. Lett. B **669**, 223 (2008).
9. F. Bossi *et al.*, Riv. Nuovo Cim. **031**, 531 (2008).

6 Public notes in year 2008

1. A. De Santis and S. Giovannella, "Study of the $e^+e^- \to \omega\pi^0 \to \pi^+\pi^-\pi^0\pi^0$ process using KLOE data", KLOE Note 219, July 2008.
2. A. De Santis, S. Giovannella, and S. Miscetti, "Updates of the measurement of the $e^+e^- \to \omega\pi^0 \to \pi^0\pi^0\gamma$ cross section using 2001-2006 KLOE data", KLOE Note 220, July 2008.
3. S. Müeller *et al.*, "Measurement of $\sigma(\pi^+\pi^-\gamma)$ using initial state radiation and extraction of $\Delta a_\mu^{\pi\pi}$ for [0.35,0.95] GeV^2 with the KLOE experiment", KLOE Note 221, September 2008.

7 Contributions to Conferences and Seminars

1. C. Gatti, "K decays measurements with the KLOE detector", Les Rencontres de Physique de la Vallee d'Aoste, La Thuile, Italy, 24 Feb-1 Mar, 2008.
2. M. Testa , "Recent results from KLOE", 43rd Recontres de Moriond on Electroweak Interactions and Unified Theories, La Thuile, Italy, Mar 1-8, 2008.

3. F. Nguyen , “A precise new KLOE measurement of F(π) with ISR events and determination of $\pi\pi$ contribution to a_μ for [0.35,0.95] GeV^2”, PhiPSI08, Frascati, Italy, 7-10 Apr, 2008.
4. T. Spadaro, “K_{e2} measurements and lepton flavor universality”, Heavy Quarks and Leptons, Melbourne, Australia, June 5-9, 2008.
5. T. Capussela, “$\eta \to \pi\pi\pi$ Dalitz plot analysis”, FlaviaNet Workshop, Anacapri, June 12-14, 2008.
6. E. De Lucia, “Results on Vus”, FlaviaNet Workshop, Anacapri, June 12-14, 2008.
7. M. Martini, “$K_S \to \gamma\gamma$ and Ke3γ decays”, FlaviaNet Workshop, Anacapri, June 12-14, 2008.
8. R. Versaci, “KLOE study on $eta \to \pi\pi$ e e”, FlaviaNet Workshop, Anacapri, June 12-14, 2008.
9. M. Palutan, “CPT test from unitarity”, FlaviaNet Workshop, Anacapri, June 12-14, 2008.
10. T. Spadaro, “Precision test of the SM with leptonic and semileptonic kaon decays at KLOE”, BEACH 2008, University of South Carolina, Columbia, June 22-28, 2008.
11. M. Antonelli, “Vus and lepton universality from K decays with the KLOE detector”, PIC 2008, Perugia, Italy, June 25-28, 2008.
12. S. Mueller, “KLOE results on e^+e^- hadronic cross section”, QCD 2008, Montpellier, France, July 7-12, 2008.
13. M. Palutan, “Measurement of V_{us} from kaon decays with KLOE”, Meeting del Comitato di Valutazione Internazionale dell’INFN, Roma, July 9, 2008.
14. E. De Lucia , “Unitarity and universality with kaon physics at KLOE”, ICHEP 2008, Philadelphia, Pennsylvania, 30 Jul - 5 Aug, 2008.
15. B. Sciascia , “$K^{\pm}_{e2}$ search and lepton flavor violation at KLOE”, ICHEP 2008, Philadelphia, Pennsylvania, 30 Jul - 5 Aug, 2008.
16. T. Capussela, “Results from the KLOE collaboration: study of eta/etaprime meson”, Confinement 08, Mainz, Germany, Sep 1-6, 2008.
17. A. Sibidanov, “Measurements of Vus from Kaon decays at KLOE”, CKM 08, Rome, Italy, Sep 9-13, 2008.
18. T. Spadaro, “K_{l2} Review”, CKM 0, Rome, Italy, Sep 9-13, 2008.
19. V. Patera, “Future Experiments at DAFNE, the Frascati ϕ factory”, PANIC 08, Eilat, Israel, Nov 9-14, 2008.
20. F. Bossi, “The KLOE2 project”, Discrete 08, Valencia, Spain, Dec 11-16, 2008.
21. R. Versaci, “Study of $\eta \to \pi\pi$ e e at KLOE”, Discrete 08, Valencia, Spain, Dec 11-16, 2008.

References

1. A. Masiero, P. Paradisi, and R. Petronzio, Phys. Rev. D **74**, 011701 (2006).
2. F. Ambrosino *et al.* [KLOE Coll.], Phys. Lett. B **636**, 173 (2006).
3. F. Ambrosino *et al.* [KLOE Coll.], Phys. Lett. B **632**, 43 (2006).
4. F. Ambrosino *et al.* [KLOE Coll.], J. High Energy Phys. **02**, 098 (2008).
5. F. Ambrosino *et al.* [KLOE Coll.], Phys. Lett.B **666**, 305 (2008).
6. F. Ambrosino *et al.* [KLOE Coll.], Phys. Lett. B **632**, 76 (2006).
7. F. Ambrosino *et al.* [KLOE Coll.], Phys. Lett. B **626**, 15 (2005).
8. F. Ambrosino *et al.* [KLOE Coll.], Phys. Lett. B **636**, 166 (2006).
9. F. Ambrosino *et al.* [KLOE Coll.], J. High Energy Phys. **12**, 105 (2007).
10. W. M. Yao *et al.*, J. Phys. G **33**, 1 (2006).
11. P.A. Boyle *et al.* [RBC/UKQCD Coll.], arXiv:0710.5136.
12. W. Marciano, Phys. Rev. Lett. **93**, 231803 (2004).
13. E. Follana *et al.* [HPQCD/UKQCD Coll.], arXiv:0706.1726.
14. I.S. Towner and J.C. Hardy, arXiv:0710.3181.
15. F. Ambrosino *et al.* [KLOE Coll.], Phys. Lett. B **642**, 315 (2006).
16. J. Bernabeu, N. Mavromatos, J. Papavassiliou, Phys. Rev. Lett. **92**, 131601 (2004).
17. J. Bernabeu *et al.*, Nucl. Phys. B **744**, 180 (2006).
18. G. Ecker and A. Pich, Nucl. Phys. B **366**, 189 (1991).
19. A. Angelopoulos *et al.* [CPLEAR Coll.], Phys. Lett. **B**, 413 (1997) 232.
20. F. Ambrosino *et al.* [KLOE Coll.], Phys. Lett. B **672**, 203 (2009).
21. I.H. Chiang *et al.*, Phys. Rev. D **6**, 1254 (1972).
22. F. Ambrosino *et al.*, [KLOE Coll.] Phys. Lett. B **670**, 285 (2009).
23. A. Aloisio *et al.*, [KLOE Coll.] Phys. Lett. B **606**, 12 (2005).
24. R. R. Akhmetshin *et al.* [CMD-2 Coll.], Phys. Lett. B **648**, 28 (2007);
    M. N. Achasov *et al.* [SND Coll.], J. Exp. Theor. Phys. **103**, 380 (2006).
25. F. Jegerlehner and A. Nyffeler, arXiv:0902.3360.

26. G. W. Bennett *et al.* [Muon g-2 Coll.], Phys. Rev. Lett. **89**, 101804 (2002); Erratum *ibid.*, **89**, 129903 (2002).

27. Proc. of PhiPsi08 Conference, Frascati, Italy, 7-10 April 2008, Eds. C. Bini and G. Venanzoni, Nucl. Phys. B Proc. Suppl. **181-182**.

28. L. G. Landsberg, Phys. Rept. **128**, 301 (1985).

29. C. Jarlskog and H. Pilkuhn, Nucl. Phys. B **1**, 264 (1967).

30. A. Faessler, C. Fuchs, and M. I. Krivoruchenko, Phys. Rev. C **61**, 035206 (2000) .

31. C. Picciotto and S. Richardson, Phys. Rev. D **48**, 3395 (1993).

32. B. Borasoy and R. Nissler, arXiv:0705.0954.

33. D. N. Gao, Mod. Phys. Lett. A **17**, 1583 (2002).

34. S.L. Adler, Phys. Rev. **177**, 2426 (1969).

35. B.R. Holstein, Phys. Scripta T **99**, 55 (2002).

36. M. Benayoun *et al.*, Eur. Phys. J. C **31**, 525 (2003).

37. B. Borasoy and R. Nissler, Nucl. Phys. A **740**, 362 (2004).

38. P. Gormley, Phys. Rev. D **2** (1970) 501.

39. J. Layter, Phys. Rev. D **7**, 2565 (1973).

40. B. Borasoy and R. Nissler, arXiv:0705.0954.

41. see the review by M. R. Pennington, arXiv:hep-ph/0511146, and reference therein.

42. H. Marsiske et al. (Crystal Ball Collab.), Phys. Rev. D **41**, 3324 (1990).

43. F. Ambrosino *et al.*, Eur. Phys. J. C **50**, 729 (2007).

44. I. Caprini, G. Colangelo and H. Leutwyler, Phys. Rev. Lett. **96**, 132001 (2006).

45. E.M. Aitala *et al.*, [E791 Coll.], Phys. Rev. Lett. **86**, 770 (2001).

46. M. Ablikim *et al.*, [BES Coll.], Phys. Lett. B **598**, 149 (2004).

47. A. Deandrea and A.D. Polosa, Phys. Rev. Lett. **86**, 216 (2001); S. Gardner and U. Meissner, Phys. Rev. D **65**, 094004 (2002); I. Bigi, arXiv:hep-ph/0601167.

48. B. Aubert *et al.*, [BaBar Coll.], Phys. Rev. Lett. **95**, 121802 (2005).

49. T. Oest *et al.*, [JADE Coll.], Z. Phys. C **47**, 343 (1990).

50. D. Domenici, Frascati Physics Series Vol. XLVI (2007) pp. 1477-1484.

51. G. Bencivenni *et al.*, NSS Conference Record, IEEE Volume **6**, 4666-4670 (2007).

52. A. Balla *et al.*, in 8^{th} International Conference on Position Sensitive Detectors. 1-5 September 2008, Glasgow (UK).

LHCb

M. Anelli (Tecn.), G. Bencivenni, P. Campana, G. Capon, M. Carletti (Tecn.),
P. Ciambrone, E. Dané (Ass. Ric.), P. de Simone, A. Di Virgilio (Tecn.),
C. Forti, G. Lanfranchi, G. Mannocchi (Ass.), F. Murtas, M. Palutan,
M. Pistilli (Tecn.), M. Poli Lener (Ass. Ric.), R. Rosellini (Tecn.),
G. Sabatino (Dott.), M. Santoni (Tecn.), A. Saputi, A. Sarti (Art. 23),
A. Sciubba (Resp., Ass.), S. Valeri (Tecn.), A. Zossi (Tecn.)

In collaboration with:
LNF-SSCR: M. Arpaia, G. Bisogni, A. Cassará, A. Ceccarelli, E. Iacuessa, U. Martini;
LNF-SEA: A. Balla, G. Corradi, G. Felici, M. Gatta, G. Papalino, D. Tagnani
and A. Battisti

1 Introduction

The activities of the LHCb-LNF group on the **muon sub-detector** in year 2008 can be resumed as follows:

- the stations behind the calorimeters (M2-M5) have been commissioned for more of the 90% of the channels;
- MWPC and GEM detectors for M1 have been prepared and tested at CERN;
- the mechanics and the services (cables and gas pipes) of station M1 (between RICH2 and calorimeters) have been installed;
- the production of new chambers in the LNF-LHCb clean room has started, as well as the recovery of old ones at CERN, so to prepare a reserve of detectors for the running of the experiment;
- the activity of simulation and analysis of MonteCarlo sample has continued, in particular for the muon id, for the study of early physics with J/ψ, for the rare channel $B_s \rightarrow \mu\mu$ and for the measurement of the decay $B_s \rightarrow \phi\psi$.

Futhermore, the whole group has participated to the cosmic ray runs, to their analysis and to the preparation of the detector for the first collisions.

2 Commissioning of the Muon System

The LHCb muon trigger architecture relies on 1248 Trigger Sectors (TS) originated by 122,112 front-end channels. These physical channels are merged to generate 25,920 logical channels both in the chamber front-end and in the Intermediate Boards (IB) system. Logical channels are grouped in Trigger Sector in the Off Detector Electronics (ODE) system.

The last two item (IB and ODE systems) are under LNF responsibility and have been tested and installed on 2007; cabling was entrusted to LNF as well.

In 2008 the commissioning phase of stations M2 to M5 was almost completed.

Commissioning procedure followed four phases which required a lot of qualified manpower, mainly provided by Cagliari and Frascati:

- connectivity test with noise,
- pulse time alignment,
- optical link test to TRG and DAQ.

Connectivity: given the described detector and geometrical complexity, the system shows 12 different topologies. For each of them a different configuration of PVSS(mai definito prima) on-line processes has been set. The algorithm, communicating via ECS, sequentially masks all the front-end channels but one for which the threshold is properly set. All the related ODE channels are then read to verify right connectivity. Some tens of cables were found wrongly placed and more badly connectorized. Also some DIALOG board where replaced. During this phase we used as hardware tool a 192 channels DISPLAY board developed at Frascati which was a valuable aid in recognizing broken or mis-placed wires. Still a few noisy connections remains to be cured.

Timing: since the system is used for triggering purposes, the full detector efficiency must be exploited in the 25 ns bunch period length. This requires the about 26000 logical channels to be synchronized at the nanosecond level with the machine clock that is distributed by TFC via the TTCrx chip. To perform such alignment PDM sends a pulse to each physical channel; the answer is the histogramming provided by the SYNC chip inside the ODE. Unfortunately two effects complicate the procedure: the ringing of the too high pulse signal and a non linearity of TDC at the edges of his range. Nevertheless the system was substantially aligned with the pulse system even if the diagnostic took more time than previously planned. Some cable with swapped polarities were found or with one of the two LVDS lines broken; this required interventions on both signal and I2C cables. At the (this) moment 97% of the system is pulse aligned and the procedure is still going on.

Optical link: ODE data are sent to TRG and DAQ via optical link. To test the goodness of the communication Frascati developed a custom VME optical receiver board with Bit Error Rate (BER) measurement capability to fully qualify the ODE boards. The connections with the trigger were checked measuring the BER on test sequences sent by the ODE while the connection with the DAQ was tested by checking data correctness on the TELL1 readout system. A very few optical transmitter/receiver was replaced.

3 Tests with Cosmic Rays

During year 2008 data taking runs on cosmic rays have been regularly performed, to test the overall performances of the data acquisition and trigger systems after integration of most of the subdetectors. Moreover, the analysis of cosmic ray data is crucial for time and space alignment of the muon detector, since they represent the only sample of straight tracks available at the moment. In Frascati we focussed on the calibration of the time response of the muon chambers. As already reported before, since the muon system is used for triggering purposes, the time response of the stations has to be calibrated in order to give signals falling well within a 25 ns time coincidence window for a track generated at the interaction point. The average time of flight between two adjacent muon stations is 4 ns; on top of that one has also to account for obvious hardware delays which can vary on a channel by channel basis. So the trigger timing synchronization can only be fullfilled if a suitable set of delay constants are applied to each channel of the muon system. These constants have been first evaluated by pulsing the system with the PDM boards, and exploiting the histogramming capability of the SYNC chip to time align the channels belonging to the same ODE board. In parallel, a coarse correction to account for time of flight delay between the muon stations has been applied to each ODE board as a whole. Cosmic ray data allowed us to test the effectiveness of the previous time calibration, and to compute residual corrections to be applied to each channel of the apparatus. To this purpose, we analysed a statistics of 1.3 million events

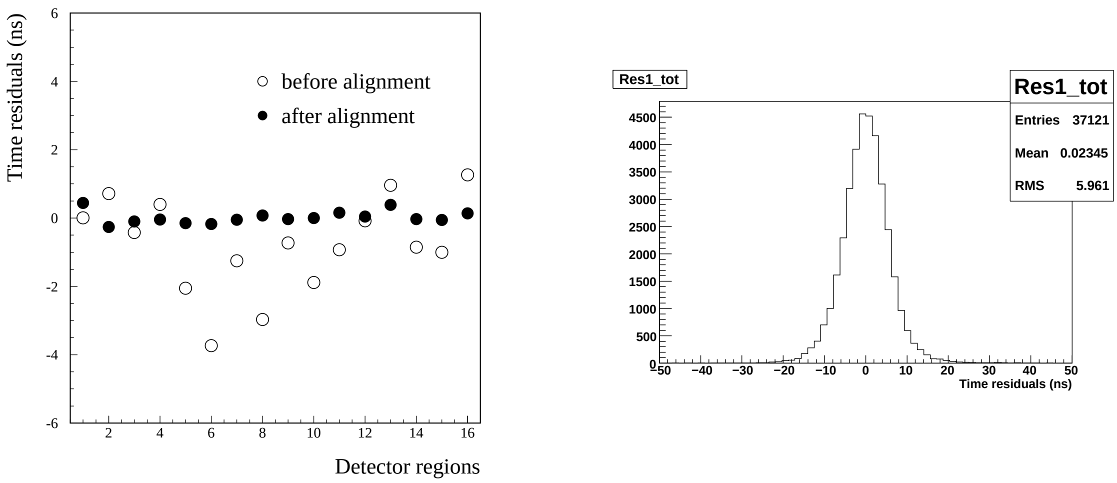

Figure 1: *Time residual averages for M2-M5 (left); time residuals of M2-M5 after alignment (right).*

collected in september 2008, from which we extracted a sample of 160 000 good-quality tracks traversing the detector in the forward direction, from M2 to M5 station. For each hit belonging to a track, a time residual has been evaluated, defined as the difference between the hit time and the average of the track hit times. The average of time residuals has been then evaluated for each channel separately, giving exactly the amount of delay needed to correct the time response of that particular channel. To test the performances of the time alignment algorithm, we divided the sample into two independent slices, and we followed a two steps procedure:

- we first evaluated the time offsets using only the first half of the cosmic tracks;
- we then used these time offsets to correct the time response of each channel in the second sample of tracks and we checked the effect on the time residuals.

The results are shown in figure 1, where the average time residuals have been computed for each of the 4 regions of stations M2 to M5 before and after the time alignment procedure. This demonstrates the feasibility of time alignment of the muon detector with precision of 1 ns using cosmic ray tracks.

Having subtracted the contribution due to the time misalignment (3 ns on average), one can assume that the width of the time residual spectrum gives a good approximation of the intrinsic resolution of the detector. and it indicates a time resolution of 6 ns, which is compatible with what expected given the present working point of the detector.

4 Preparation of GEM detectors

The innermost part (regions R1, $\sim$ 0.6 m^2 area) of the first muon station (M1) of the LHCb experiment will be equipped with a detector based on Gas Electron Multiplier (GEM) technology. The responsibility of the detector is shared between LNF and INFN Cagliari. In M1R1 region each detector is composed by two triple-GEM chambers logically OR-ed pad by pad (10$\times$25 mm^2 large). The detector is operated with an $Ar/CO_2/CF_4$(45/15/40) gas mixture at a gain of $\sim$4000.

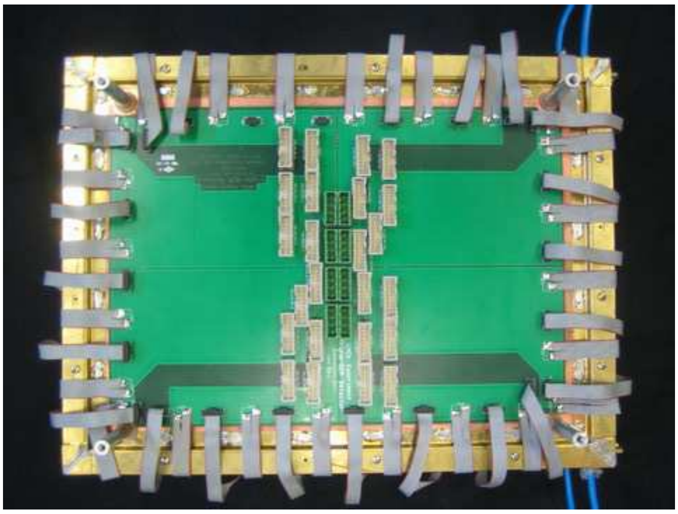

Figure 2: *A GEM detectors ready for installation.*

The construction of the chambers has been completed in December 2006 and the full integration of the detectors with the FEE, LV boards and HV filters, performed at CERN ended in 2007.

Tests and checks have been completed by the end of August 2007 and the detectors are ready for the installation (Fig. 2).

During 2008 we studied the detector integration in the tight space around the beam pipe, including cabling and gas piping. The installation of the gas pipes, the HV and LV, the LVDS and the I^{2}C cabling has be completed in july 2008.

The installation of detectors has been shifted to 2009, the commissioning phase will follow soon and will be concluded before the first LHC run.

5 Installation of the M1 Muon Station

A large effort has been put in the preparation of the mechanics of the M1 Station. This station, being inserted between the RICH2 and the Preshower detectors, has very little room (some 40 cm) for the installation and deserves special attention to the mechanical issues. Moreover, the station has to comply with as small as possible material budget (being in front of the calorimeters) and to face the presence of approximately 40% of the total amount of electronic channels of the whole Muon detector. The high electronics density on one hand requires air-cooling, on the other hand the large amount of cables (approximately 1,200) that must be movable together with the station, makes the whole project a real challenge. The layout of the station is shown in Fig. 3.

Figure 3: *Layout of the M1 station.*

An important item of the project has been the design of the moving system for the cable chain, its support, the mechanical system to attach the chambers to the wall, and the exact routing of all services (LV, Gas, HV, signal and control cables, Fig. 4). In particular, the cable chain and its suspension, has been conceived to sustain the approximately 2 t of cables hanging from the walls.

This task has been particularly difficult due to the limited space available and the constraints mentioned above. This work, together with the installation of the cables on the wall and inside the movable chain, has been completed in June 2008.

In parallel with this activities, the group has taken care of preparing the services needed to readout the system: the LV power modules, the HV system, the Off Detector Electronics boards, together with the optical links, the Service Boards, that have to provide the communications with the ECS Control System. These services have been almost entirely completed in 2008.

An important task undertaken at LNF has been the logistics of various material sent to CERN, both for the mechanics items and for the services (cables, connectors, etc...). In particular, all the HV cables of the muon system (including M1) have been produced and tested in the LNF-LHCb workshop. Due to the delayed startup of LHC, the activities to complete M1 resumed in November. Some cabling which was left behind, in particular on the side of the electronic racks, was completed, and at the end of the year the M1 station was ready for mounting the chambers

Figure 4: *The cable layout on the wall of the M1 station (left) and a detail of the cable chain moving system (right).*

on it. This work will last until the end of June 2009 and will be performed by teams of the LHCb INFN Sections.

While installing the M1 chambers, an important activity will be also the commissioning of the M1 Station, a work similar to the one performed for the M2-M5 one: connectivity tests, time alignment, determination of efficiency and time resolution.

6 Preparation and tests of spare chambers

In the second half of 2008, the LHCb-LNF group has started the preparation of the spare chambers for the experiment Fig. 5. Partly have been built brand new (and this task will continue in 2009), partly recovering chambers at CERN that had shown problems during the first tests (such as gas leaks, HV conditioning, etc...). The chambers have been tested against gas leaks, have been checked and trained with HV, equipped and tested with FEE electronics. Once this task will be completed, the spare chambers for the INFN regions (R2 of M4 and M5, R3 of M1 to M5, R4 of M1 and M5) will be approximately 60 (10% of the total production).

7 Software activities

The software activities in 2008 of the LHCb-LNF group were mainly focused in: finalizing the analyses started in 2007 using the full LHCb Monte Carlo production and preparing all the tools required for calibrating the Muon System with the first data.

Figure 5: *The preparation of a MWPC in the LNF-LHCb clean rooom.*

7.1 Analyses with the full LHCb Monte Carlo production

The Frascati group is involved in the preparation of the following analyses:

1. the measurement of the B_s mixing phase in the $B_s \to J/\psi(\mu\mu)\phi(KK)$ decay;
2. the search of the $B_s \to \mu^+\mu^-$ rare decay;
3. the measurement of the ratio of the cross section $\sigma(J/\psi(1S))/\sigma(\psi(2S))$;
4. the analysis of the 2-body hadronic decays, $B \to hh$.

The first two analyses are considered top priority for the LHCb collaboration since they are competitive with the Tevatron results already with 0.2 1/fb of integrated luminosity (which is what LHCb expects to collect in the 2009-2010 run). However, both analyses require a deep understanding of the detector behavior and rely on the calibration of many quantities (momentum scale, momentum resolution, particle ID, flavour tagging, proper time resolution) therefore they will be not the first measurement that will be performed.

Some earlier (and easiest) measurements have been foreseen at the beginning, like the measurement of $\sigma(J/\psi(1S))/\sigma(\psi(2S))$, where both $\psi(1S)$ and $\psi(2S)$ decays in muon pairs.

We underline the fact that these three measurements contains muons in the final state, making the Muon Detector one of the *main* LHCb detector for the first years. Analyses concerning hadronic channels in the final state ($B \to hh$) will be performed in a second phase of the experiment.

The potential of the LHCb experiment in these four measurements and the contribution of the Frascati group in each analysis is described below.

7.1.1 *Measurement of the mixing induced CP violation in $B_s \to J/\psi\phi$ channel*

The interference between B_s^0 decays to $J/\Psi\phi$ with or without $B_s^0 - \overline{B}_s^0$ oscillation gives rise to a CP violating phase $\Phi_{J/\Psi\phi}$. In the Standard Model this phase is predicted to be $\Phi_{J/\Psi\phi} = -2\beta_s = -0.0368 \pm 0.0017$ rad, where $\beta_{\rm s} = \arg\left(-V_{\rm ts}V_{\rm tb}^*/V_{\rm cs}V_{\rm cb}^*\right)$ is the smaller angle of the "b−s unitary triangle" of the CKM matrix. However New Physics (NP) could significantly modify this prediction if for example new particles contribute to the $B_s^0 - \overline{B}_s^0$ box diagram. The present experimental values come from CDF and D0 Collaborations: Their results have been combined by HFAG and the result is $-2\beta_{\rm s} = -0.77^{+0.29}_{-0.37}$ or $-2.36^{+0.37}_{-0.29}$. By the end of run 2, assuming 9 fb^{-1} for both CDF and DO and simple scaling with $1/\sqrt{\mathcal{L}_{\rm int}}$, the combined Tevatron sensitivity to $2\beta_s$ is expected to be ~ 0.13. The contribution of the Frascati group to this measurement has been to develop a

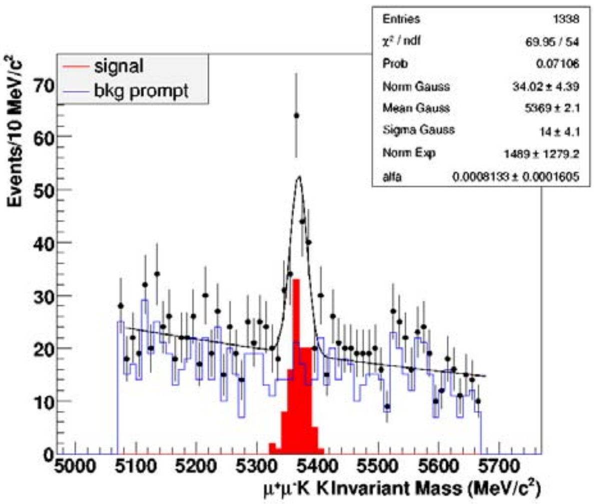

Figure 6: *Invariant mass of the* $\rm B_s^0 \to J/\psi\phi$ *candidates in the* $\rm J/\psi(\mu\mu)$ *inclusive sample. The solid histogram is pure signal.*

unified selection of the $\rm B_s^0 \to J/\psi\phi$ channel together with the two flavour specific control channels $\rm B^+ \to J/\psi K^+$ and $\rm B^0 \to J/\psi K^{*0}$with $\rm J/\psi \to \mu\mu$ in the final mode. The triple goal of this selection is maximizing the signal yield by maintaining the background at a reasonable level, minimizing the biases in proper time and angular acceptances and selecting the three channels in such a way that they share the same phase space.

This selection has been chosen as the *standard* selection for the $\rm B_s^0 \to J/\psi\phi$ analysis at LHCb. We found a yield of $\sim$ 156 000 events for $\rm B_s^0 \to J/\psi\phi$, $\sim$ 650 000 for $\rm B^0 \to J/\psi K^{*0}$ and $\sim$ 1 250 000 for $\rm B^+ \to J/\psi K^+$ modes after L0 trigger for 2 fb^{-1} integrated luminosity, with background mainly dominated by prompt modes (Fig. 6).

The statistical sensitivity expected at LHCb as a function of integrated luminosity is shown in Fig. 7. The systematic uncertainty is at present dominated by the knowledge of the proper time and angular acceptance which are known at 10% level.

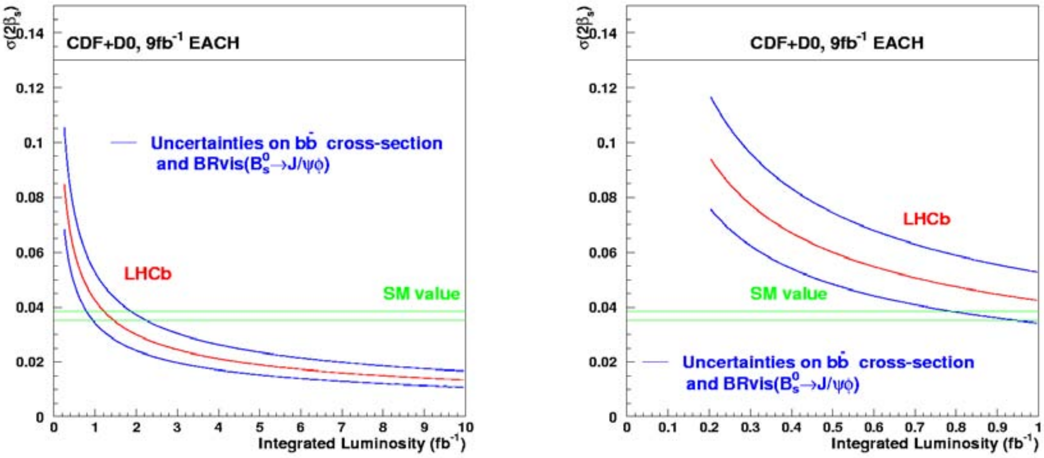

Figure 7: *Red line: Statistical uncertainty on 2 β_s versus the integrated luminosity. Blue line: uncertainties coming from the* $\mathrm{b\overline{b}}$ *cross-section and the visible branching ratio on* $\mathrm{B_s^0} \to \mathrm{J}/\psi(\mu\mu)\phi(\mathrm{KK})$*. The green band is the Standard Model value:* $2\beta_\mathrm{s} = 0.0368 \pm 0.0017$ *rad. Left: from zero to 10*$\,\mathrm{fb}^{-1}$*. Right; zoom on zero to 1*$\,\mathrm{fb}^{-1}$*.*

All these results are being finalized in a Road Map document which describes all the steps necessary to perform such a measurement with real data.

7.1.2 Search for the rare decay $B_s \to \mu^+\mu^-$

Due to its sensitivity to New Physics contributions, the Branching Ratio BR ($B_s \to \mu^+\mu^-$) is one of the most interesting measurements that the LHCb experiment can perform with the first data. The Standard Model predictions are $BR(\mathrm{B_s^0} \to \mu^+\mu^-) = (3.35 \pm 0.32) \times 10^{-9}$ while the current upper limit given by Tevatron is $BR < 47 \times 10^{-9}$ @ 90% CL, which is still one order of magnitude higher than predictions.

LHCb has the potential to exclude at 90% CL any value of the BR down to the SM value with only 0.5 fb^{-1} of integrated luminosity, corresponding to 1/4 of a nominal year (10^7 sec) running at 2×10^{32} cm^{-2} s^{-1}. The expected limit at the end of Tevatron, $\sim 2 \times 10^{-8}$, is overtaken with less than 0.1 fb^{-1}.

One of the crucial points of this analysis is the control of the background mainly coming from hadrons mistakenly identified as muons.

In LHCb the muons are identified by extrapolating well reconstructed tracks with $p > 3\,\mathrm{GeV}/c$ into the muon stations. The hits are searched within fields of interest (FOI) around the extrapolation point of the track in each muon station, considering the function of momentum for each station and region. Then a discriminant variable (DLL) is built based on the distribution of those hits inside the FOI and used to make an hypothesis test.

The responsibility of the Frascati group is to develop the MuonID algorithms and all the related tools for monitoring and calibrate the MuonID with data. We studied the MuonID performance for muons belonging to the phase space interesting for the $B_s \to \mu\mu$ analysis and all the possible sources of misID in that momentum range. In Figure 8 we show the MuonID efficiency and misID efficiency for six different samples: b-inclusive, $J/\psi \to \mu^+\mu^-$ and $B_s \to \mu^+\mu^-$ for muons and b-inclusive, $\Lambda \to \pi p$ and $B \to hh$ for hadrons. The two modes $J/\psi \to \mu^+\mu^-$ and $\Lambda \to \pi p$ are the *golden* calibration channels to extract the muonID performance from data, as explained later on.

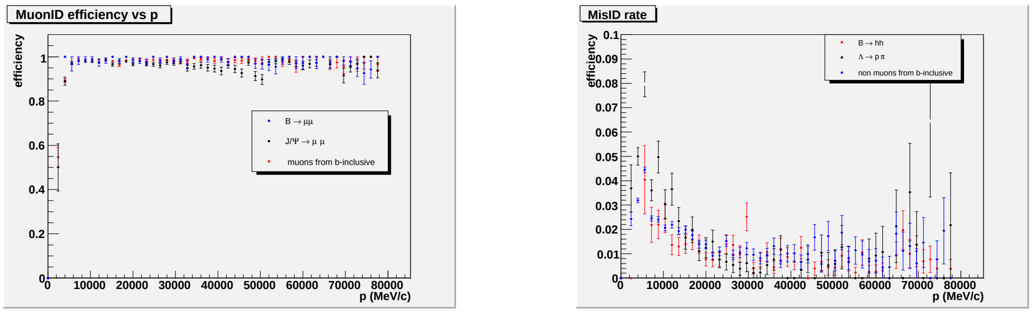

Figure 8: *MuonID efficiency versus p for b-inclusive, $J/\Psi \to \mu^+\mu^-$ and $B_s \to \mu^+\mu^-$ samples (right) and MisId rate versus p for b-inclusive, $\Lambda \to \pi p$ and $B \to hh$ samples (left).*

7.1.3 *Measurement of the ratio of the $\sigma(J/\psi)(1S)/\sigma(\psi(2S))$ at LHCb*

The measurement of the ratio of the $\sigma(J/\psi)(1S)/\sigma(\psi(2S))$ at a center-mass energy of 14 TeV is fundamental to understand the charmonium production mechanisms in the framework of the NRQCD theories.

The latest results by CDF and HERA-B in this sector still leave a lot of open problems. In fact while the introduction of Color Octet diagrams in the charmonium production allows to do prediction of cross sections in good agreement with the data, the same theories fail in the polarization prediction. Furthermore recent calculations at NLO and NNLO in the Color Singlet model clearly show that the amount of Color Octet contribution so far considered has been overestimated.

The theoretical uncertainty on the ψ(2S)/ψ(1S) ratio at the LHC is dominated by arbitrary assumptions made on the ψ(2S) production mechanisms and even a measure within 10% will be a good indication for the theorists.

The main experimental challenge of such a measure is to keep under control the efficiencies. However, selecting only events with $\mu\mu$ in the final state we would expect a partial cancellation of the trigger, reconstruction and MuonID efficiencies, with an efficiency ratio constant or slowly dependent on the kinematics and geometrical variables. How to extract these efficiency ratio from data is presently under study.

7.1.4 *Analysis of B→hh decays*

The effort to finalize the simultaneous analysis of B→hh decays, already pursued in CDF with success, was mainly directed to the completion of a road-map toward a realistic measurement with the first LHCb data. The key observables needed in such measurements and their extraction from real data, the strategies for addressing the systematics and the identification of control samples were carefully reviewed and documented.

The analysis proposed aims for the measurement of charge and CP asymmetries of 10 different B decay channels: $B_d \to \pi^+\pi^-$, $B_d \to K^+\pi^-$, $B_d \to \pi^+K^-$, $B_s \to K^+K^-$, $B_s \to \pi^+K^-$, $B_s \to K^+\pi^-$, $\Lambda_b \to K^+P^-$, $\Lambda_b \to P^+K^-$, $\Lambda_b \to \pi^+P^-$, $\Lambda_b \to P^+\pi^-$.

A simultaneous approach (common selection of all modes not making use of particle ID information) is pursued in order to reduce the systematics due to signal channels cross-feed and to use the kinematics and particle ID information in an optimized way directly in the unbinned maximum likelihood fit.

The mass and time distributions are fitted together with the sum of the PDFs of all the various signal channels and the background one extracting all the CP parameters.

As example the result of a fit to the mass distribution, obtained on MC DC06 events, of all the channels (using the pion mass hypothesis for both the charged tracks) is shown in figure 9: the individual channels contributions are shown as well as the cumulative distribution (histogram) and the PDF after the unbinned likelihood fit (blue curve). From this distribution is already possible to measure the charge asymmetry in Kπ modes. The sensitivities as well as the estimate of leading

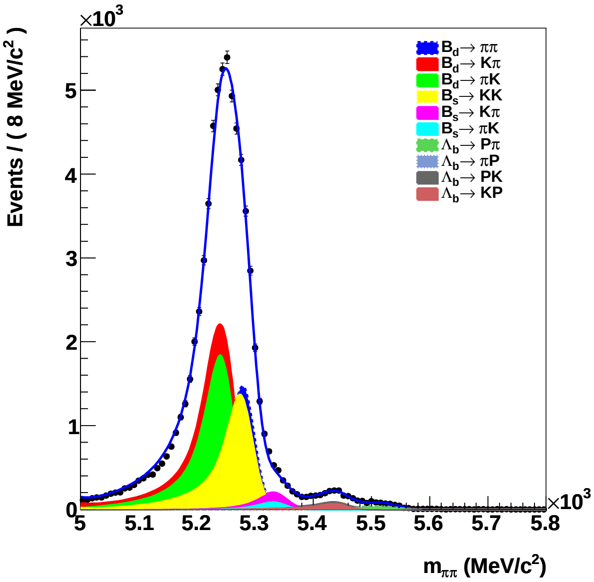

Figure 9: *Invariant mass distribution, in the $\pi\pi$ hypothesis, of the B→hh decay channels under study. The individual contributions are shown as well as the cumulative distribution (histogram) and the PDF after the unbinned likelihood fit (blue curve).*

contributions to the systematic errors are being re-evaluated with the latest reconstruction and simulation software, exploiting the full power of the simultaneous analysis approach.

7.2 Control samples for the Muon Detector monitoring and MuonID calibration

The two *golden* control samples for the calibration and monitoring of the muon detector are the prompt J/$\psi \to \mu\mu$ decay, which provides a clean sample of muons, and the $\Lambda(1115) \to p\pi$ decay which provides a clean and abundant sample of hadrons, decaying and not-decaying in flight, to be used for the evaluation of the misidentification probability. The selection procedure of these two calibration modes has been finalized and included in the official calibration stream of the collaboration.

7.2.1 Selection of the J/$\psi \to \mu\mu$ decay mode

The inclusive J/ψ cross section at LHC is $\sigma_{J/\psi} \sim 286\mu$b, where $\sim 266\mu$b comes from the prompt production $pp \to J/\psi X$ and 20μb from the b decay. Given the $BR(J/\psi \to \mu^+\mu^- = 6\%$, and the probability that both muons are within the LHCb acceptance, $p \sim 10\%$, we have an effective cross-section of $\sigma_{J/\psi \to \mu^+\mu^-} = 1.7\mu$b which corresponds to an yield of $N_{J/\psi \to \mu^+\mu^-} \sim 1.7 \times 10^6$ per pb^{-1}.

In LHCb we expect a prompt $J/\psi \to \mu\mu$ decay reconstructed and selected each 70k events. This corresponds to a rate of 7 Hz at $L \sim 10^{31}$ cm^{-1} s^{-1}.

The single muon trigger line has an efficiency of 90% on J/Ψ decays and of 0.012% on minimum bias (MB) events, thus we can expect a final rate of 2 Hz for $J/\Psi \to \mu\mu$ events for a total trigger rate of 2 kHz.

The $J/\psi \to \mu^+\mu^-$ has been selected by identifying with the Muon System one of the two muons and leaving the second one free for calibration purposes. The J/ψ candidates are selected by by requiring two *long* tracks of opposite charge, with some p, p_T cuts and track quality cuts, making a vertex, with an invariant mass ± 300 MeV/c^2 around the J/ψ nominal mass in the hypothesis of the muon mass. Moreover the two tracks are required to release in the electromagnetic calorimeter (ECAL) and hadronic calorimeter (HCAL) an energy compatible with a Minimum ionizing particle (MIP).

The $\Lambda(1115.7) \to p\pi$ is a quite abundant process at LHC. The prompt $pp \to \Lambda X, \overline{\Lambda} X$ processes have huge cross sections, $\sigma_{pp \to \Lambda X} \sim 11$ mb and $\sigma_{pp \to \overline{\Lambda} X} \sim 4.5$ mb. Given that the branching ratio (BR) of $\Lambda, \overline{\Lambda} \to p\pi$ is $BR(\Lambda \to p\pi) = (63.9 \pm 0.5)\%$ and assuming a total inelastic cross section for minimum bias events at $\sqrt{s} = 14$ TeV of $\sigma(pp) \sim 79$ mb, this means that we have a $\Lambda \to p\pi$ decay every 6 Minimum Bias events produced. The $\Lambda(\overline{\Lambda}) \to p\pi$ decay can be selected without any particle ID using only tight cuts in impact parameters, flight distance and invariant mass since the Λ is a very narrow resonance ($\sigma(M) \sim 1$ MeV) with a very long lifetime ($c\tau = 7.89$ cm).

The invariant mass distribution of the selected events in a minimum bias sample is shown in Figure 10. The statistics shown in the figure corresponds to few minutes of running at $L \sim 10^{31}$ cm^{-2} s^{-1}. The purity of the selected samples is above 95%.

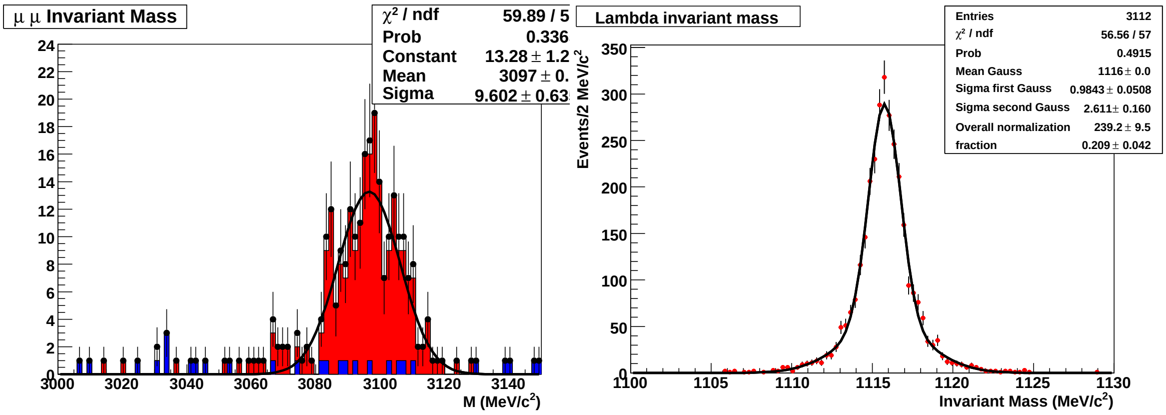

Figure 10: *Di-muon and $p\pi$ invariant masses extracted from a Minimum Bias sample.*

8 List of Conference Talks and Publications

1. G. Lanfranchi, "Il commissioning di LHCb" V Workshop sulla Fisica a LHC, Perugia, Italia, 30 gennaio-2 febbraio, 2008.

2. A. Sarti, "B-physics prospects at LHC", 19^{th} Hadron Collider Physics Symposium 2008 (HCP 2008) Galena, Illinois, USA, May 27-31, 2008.

3. G. Lanfranchi, "Search for New Physics in $B_s \to \phi\psi$ decay @ LHC", 5^{th} Inter. Workshop on the CKM Unitary Triangle Roma, Italy, September 9-12, 2008.

4. P. Campana, "L'upgrade di LHCb, Incontro sull'upgrade di ATLAS/CMS a SHLC", Sestri Levante, Italia, 13-14 Novembre, 2008.

5. LHCb Coll., JINST **3**, S08005 (2008).

6. M. Anelli *et al.*, Nucl. Instr. & Meth. A **593**, 319 (2008).

7. LHCb Coll., "Expression of interest for an LHCb upgrade", LHCb-2008-019.

8. A. Sarti, *et al.*, "Procedure for determination and settings of thresholds implemented in the LHCb Muon System", LHCb-2008-052.

NA62

A. Antonelli (Resp.), G. Maccarrone, M. Moulson,
M. Raggi (Ass. Ric.), T. Spadaro

In collaboration with the Servizio di Progettazione Apparati Sperimentali (SPAS):
C. Capoccia, A. Cecchetti, B. Dulach

the Servizio di Sviluppo e Costruzione Rivelatori (SSCR):
G. Bisogni, A. Franceschi

the Divisione Acceleratori, Servizio di Vuoto:
P. Chimenti, A. Clozza, V. Lollo

and the Servizio di Elettronica:
G. Corradi

1 The NA62 Experiment

The branching ratio (BR) for the decay $K^+ \to \pi^+\nu\bar{\nu}$ can be related to the value of the CKM matrix element V_{td} with minimal theoretical uncertainty, providing a sensitive probe of the flavor sector of the Standard Model. The measured value of the BR is $1.73^{+1.15}_{-1.05} \times 10^{-10}$ on the basis of seven detected events [1]. NA62, an experiment at the CERN SPS, was originally proposed as P326 with the goal of detecting $\sim$100 $K^+ \to \pi^+\nu\bar{\nu}$ decays with a S/B ratio of 10:1 [2]. The experimental layout is illustrated in Fig. 1.

The experiment will make use of a 75 GeV unseparated positive secondary beam. The total beam rate is 800 MHz, providing $\sim$ 50 MHz of K^+'s. The decay volume begins 102 m downstream of the production target. 10 MHz of kaon decays are observed in the 120-m long vacuum decay region. Ring-shaped large-angle photon vetoes are placed at 12 stations along the decay region and provide full coverage for decay photons with 8.5 mrad $< \theta <$ 50 mrad. The last 35 m of the decay region hosts a dipole spectrometer with four straw-tracker stations operated in vacuum. The NA48 liquid krypton calorimeter [3] is used to veto high-energy photons at small angle. Additional detectors further downstream extend the coverage of the photon veto system (e.g. for particles traveling in the beam pipe).

The experiment must be able to reject background from, e.g., $K^+ \to \pi^+\pi^0$ decays at the level of 10^{12}. Kinematic cuts on the K^+ and π^+ tracks provide a factor of 10^4 and ensure 40 GeV of electromagnetic energy in the photon vetoes; this energy must then be detected with an inefficiency

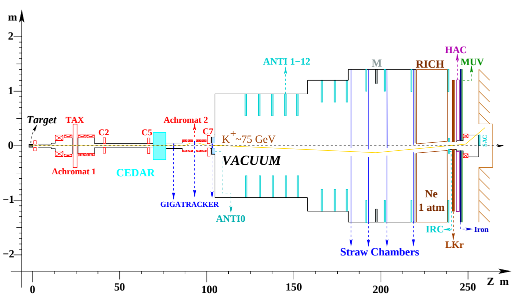

Figure 1: *The NA62 experimental layout.*

of $\leq 10^{-8}$. For the large-angle photon vetoes, the maximum tolerable detection inefficiency for photons with energies as low as 200 MeV is 10^{-4}. In addition, the large-angle vetoes (LAV) must have good energy and time resolution and must be compatible with operation in vacuum.

The principal involvement of the LNF NA62 group is in the design and construction of the LAV system. In 2008, the main responsibilities of the LNF NA62 group were

- Mechanical design of a prototype LAV station
- Design and construction of the vacuum vessel
- Development of tools and procedures for assembly of the station at LNF in 2009
- Vacuum testing and outgassing measurements for lead-glass detectors
- Development of the front-end electronics for the large-angle veto system
- Collaboration in analysis of NA62 data on $R_K \equiv \Gamma(K_{e2})/\Gamma(K_{\mu 2})$.

2 Large-Angle Photon Vetoes

2.1 Comparison of technologies

In 2007, the LNF NA62 group led the development and testing of prototype photon veto detectors, in order to guide the choice of technologies to be used in the experiment. Three possible technologies for the LAV system were considered. The first design, originally proposed for use in the (now canceled) CKM experiment at Fermilab, featured a modular structure consisting of alternate layers of 1-mm thick lead and 5-mm thick scintillating tile readout by wavelength-shifting fibers, providing a high sampling fraction and excellent light yield. A second option, adopted for the construction of the electromagnetic calorimeter for the KLOE experiment, featured a structure consisting of 1-mm diameter scintillating fibers embedded between 0.5-mm thick lead foils. The third solution makes use of lead-glass crystals obtained from the dismantled electromagnetic calorimeter of the OPAL experiment [4]. Prototype instruments based on each of the three technologies were obtained or constructed. Experimental tests conducted with the electron beam at the Frascati BTF demonstrated that all three technologies are suitable for use in the experiment [5]. The results obtained for the inefficiency with $E_{\rm thr} = 50$ MeV for all three prototypes are summarized in Fig. 2. The efficiency for detection of low-energy electrons is seen to be similar for all three technologies tested. Since there is a significant practical advantage to basing the NA62 LAV system on existing hardware, we decided to use the OPAL lead-glass modules.

2.2 Mechanical design for the LAV system

The 3800 modules from the central part of the OPAL electromagnetic calorimeter barrel [4] that recently became available for use in NA68 consist of blocks of SF57 lead glass with an asymmetric, truncated square-pyramid shape. The front and rear faces of the blocks measure about 10×10 cm^2 and 11×11 cm^2, respectively; the blocks are 37 cm long. The modules are read out at the back side by Hamamatsu R2238 76-mm PMTs, coupled via 4-cm cylindrical light guides of SF57.

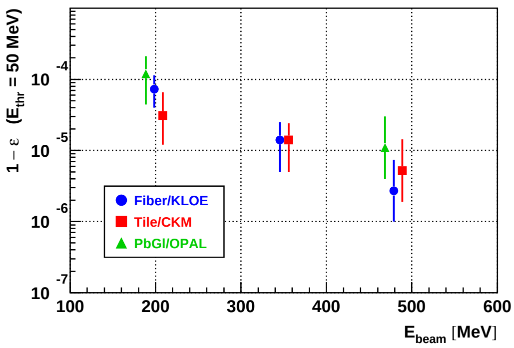

Figure 2: *Comparison of detection efficiencies for each of the three prototypes, for 203, 350, and 483 MeV electrons with $E_{thr} = 50$ MeV. Results obtained with the CKM tile prototype and OPAL lead-glass modules are preliminary.*

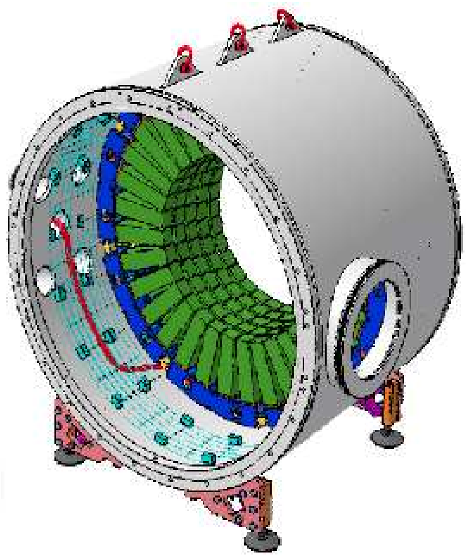

Figure 3: *Left: Design study of the prototype veto station making use of the OPAL lead-glass calorimeter elements. Right: Photograph of the vacuum vessel under construction.*

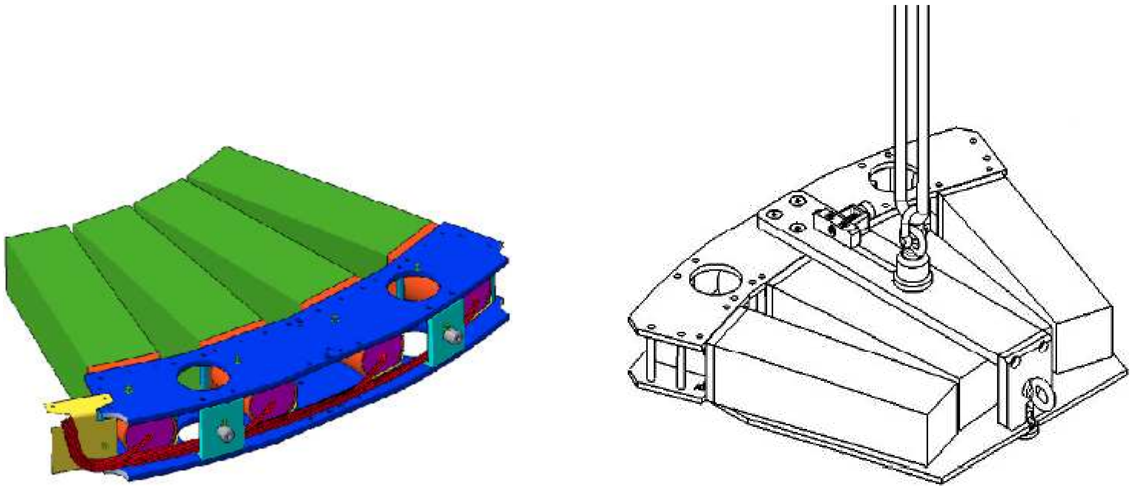

Figure 4: *Left: Support bracket for assembly of four lead-glass modules. Right: Lifting tool for use in manipulation of support brackets.*

During 2008, our group dedicated significant resources to the development of the mechanics for the incorporation of these modules into a veto station for use in the experiment.

The current design of the LAV system calls for the construction of 12 cylindrical stations of lead-glass blocks. The diameter of the stations increases with distance from the target, as does the number of blocks in each, from 160 to 250, for a total of about 2500 blocks. Each station consists of 5 rings of blocks, with the blocks staggered in azimuth in successive rings. The total depth of a station is 27 radiation lengths; this structure guarantees high efficiency, hermeticity, and uniformity of response. The overall design for the first prototype of such a station is illustrated in Fig. 3, left.

The principal elements of the mechanical design include the design of the vacuum vessel itself, the hardware associated with the vacuum vessel (i.e., access ports, feedthroughs, and hardware for cable routing, and the support structure for mounting the lead-glass blocks on the internal walls The LNF NA62 group has collaborated on the design of the vacuum vessel and associated hardware, as has borne the principal responsibility for the construction of the prototype, including the development of the tools and procedures necessary for its assembly.

2.2.1 Vacuum vessel

The vessel is made of steel, is 192 cm in diameter, and includes five flanges for HV and signal feedthroughs and for vacuum pumping, a large flange for access, and a mesh for cable routing. Construction on the prototype vessel was started in late 2008 at Fantini SpA (Anagni (FR)), a firm dealing in the manufacture of specialized industrial equipment, under the supervision of the LNF SPAS. A photo of the vessel is shown in Fig. 3, right. The vessel will be shipped to LNF in spring 2009 for the installation of the lead-glass detectors.

Table 1: *Examples of outgassing measurements.*

	Outgassing rate (mbar $\cdot$ l/s)
Complete module	$(2.2 \pm 1.4) \times 10^{-5}$
Unwrapped module	$(2.0 \pm 1.3) \times 10^{-5}$
OPAL wrapping	$(1.0 \pm 0.5) \times 10^{-6}$
PMT & mu-metal	$(2.1 \pm 1.7) \times 10^{-7}$
Bare crystal	$(2.0 \pm 2.9) \times 10^{-6}$

Figure 5: *Setup for leak test and outgassing rate measurements on vacuum vessel.*

2.2.2 Module support structures

The support brackets for the mounting of the lead-glass modules were developed at Pisa in 2008 and are now under construction. Four lead-glass modules are arranged on a single mounting bracket for installation in the vacuum vessel, as shown in Fig. 4, left. The LNF group is responsible for the development of procedures and tools for use in the installation of the four-module units and the overall assembly of the station. The tool for the manipulation of the four-module unit shown in Fig. 4, right, was designed by the LNF SPAS in collaboration with the NA62 group members. Procedures for installation and assembly are currently being finalized. A working space for assembly of the station has been set up in the new high bay next to the Gran Sasso building.

2.2.3 Vacuum tests and outgassing measurements

In the NA62 experiment, the interaction of the beam with residual gas in the decay region can produce a significant level of photon-free background to $K^+ \to \pi^+ \nu \bar{\nu}$ if the vacuum in the decay region is worse than a few 10^{-6} mbar. The measurement of the total outgassing rate of the LAV system and vacuum vessel into the decay volume is an essential parameter for the design of the pumping system of the experiment.

During 2008, a comprehensive series of measurements of outgassing rates of different components of the LAV system. The measurements were performed in close collaboration with the Servizio di Vuoto of the LNF Accelerator Division. Measurements were performed on components such as the wrapping materials for the lead-glass blocks, the PMT and mu-metal assemblies, fully wrapped blocks, and bare blocks. The measurement technique and setup are described in Ref. 6. Examples of outgassing measurements obtained are presented in Table 1. A complete vacuum test of the prototype vessel was performed at the Fantini SpA facility (Fig. 5). The vessel was found to be free of leaks and its outgassing rate was measured to be 1.2×10^{-5} mbar $\cdot$ l/s. These results are compatible with the operation of the detector in high vacuum.

2.2.4 Front-end electronics

The readout electronics are currently at a preliminary design stage; the design will have to be finalized over the course of the next two years. Monte Carlo simulations have shown that photons from $K^+ \to \pi^+\pi^0$ decay with a wide range of energies, from a few tens of MeV to several GeV, reach the veto stations. To be able to reject photons from $\pi^+\pi^0$ events with a maximum inefficiency of 10^{-4}, the detectors must simultaneously furnish time and energy measurements. The time resolution is dominated by the intrinsic contribution from the detectors. For the energy measurement, the biggest challenge in the design of the readout electronics is the need to accept signals over an extended dynamic range, from a few millivolts to tens of volts, and to provide charge measurements with a precision better than 10%.

To handle the analog signal from the detectors without saturating the elements of the front-end electronics, a multiscale system has been developed in collaboration with the Servizio di Elettronica. The signal levels correspond to attenuation factors of 1, 10, and 100. Each of these signals will be processed by a different acquisition channel, providing three measurements of the same signal at different amplitude scales. A photograph of the front-end card is shown in Fig. 6, top. A protection circuit after the attenuators will limit the amplitudes of the input signals to the digitizers to acceptable levels without introducing dead time. To measure the charge, a solution is under development based on the correlation between the signal amplitude and the duration during which the signal remains above a discriminator threshold. The energy can thus be measured via TDC time measurements only.

To study the potential of the time-over-threshold technique using cosmic-ray signals from actual detector elements, the group is using the front-end attenuator board described above, together with the NINO chip designed for time-of-flight measurements in the ALICE experiment. The test circuit is illustrated in Fig. 6, bottom. Elements of the readout system will be further tested in situ together with the first LAV ring in the fall of 2009. We expect to conduct a test of the final front-end electronics scheme and its integration with the data-acquisition system at CERN in 2010.

3 NA62 and the Measurement of R_K

Despite poor knowledge of the meson decay constants, ratios of leptonic decay rates of pseudoscalar mesons such as $R_K \equiv \Gamma(K_{e2})/\Gamma(K_{\mu 2})$ can be predicted with high accuracy within a given model, and have been considered to be stringent tests of the $V - A$ structure of the weak interaction and of lepton universality. By convention, the definition of R_K includes the contribution of inner

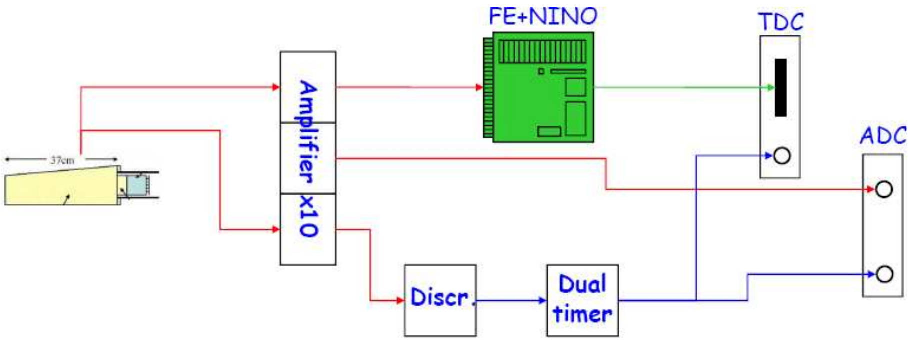

Figure 6: *Top: Photograph of front-end card with multiple attenuators, together with NINO board used for test measurements. Bottom: Schematic of electronics used to test the time-over-threshold measurement technique.*

bremsstrahlung (IB) to the radiative $K_{l2\gamma}$ width, while the structure-dependent processes are considered as background. The Standard Model prediction is [7]:

$$R_K^{\rm SM} = \left(\frac{m_e}{m_\mu}\right)^2 \left(\frac{M_K^2 - m_e^2}{M_K^2 - m_\mu^2}\right)^2 (1 + \delta R_{\rm QED}) = (2.477 \pm 0.001) \cdot 10^{-5} \tag{1}$$

where $\delta R_{\rm QED} = -3.6\%$ is a correction due to the contributions to the $K_{l2\gamma}$ width from IB and virtual photon processes. A recent theoretical study [8] points out that lepton-flavor violating effects arising in supersymmetric extensions of the Standard Model can induce sizable violations of $\mu - e$ universality, shifting the value of R_K by as much as a few percent, without contradicting any other presently known experimental constraints. The K_{e2} decay rate is particularly sensitive to new physics because the Standard Model contribution is helicity suppressed. The 2006 world average [9] is determined by experiments performed in the 1970s; the relative error on this average ($\delta R_K/R_K = 4.5\%$) is too large to allow tests of the Standard Model. Inclusion in the average of the recent preliminary results from the NA48/2 and KLOE collaborations leads to a new value of $R_K^{2007} = (2.457 \pm 0.032) \cdot 10^{-5}$ [10], with a precision of $\delta R_K/R_K = 1.3\%$.

During a run in 2007, NA62 collected more than 110 000 K_{e2} events, together with various smaller data samples to allow detailed systematic studies. The Frascati group contributed significantly to the success of this run. Group members participated in data taking for a significant fraction of the running period and provided on-call support for the hodoscope readout electronics. As run coordinators for five weeks of the 18-week run, LNF group members were directly responsible for the operational aspects of the experiment. The running period coordinated by LNF group members included K_{e2} data collection, the collection of samples for systematic studies, and the entire straw tracker beam test.

LNF group members are currently playing a central role in the analysis of the K_{e2} data. At the collaboration level, the analysis effort is being conducted by two independent groups to ensure redundancy and tighter systematic control. Frascati group members form the core of one of these two analysis groups. A preliminary result for R_K is expected during the first half of 2009.

4 List of Conference Talks

1. M. Moulson, "New directions in kaon physics," Ninth International Conference on Heavy Quarks & Leptons, Melbourne, Australia, Crete, June 2008.
2. T. Spadaro, "K_{e2} and lepton flavor violation searches with kaons," Ninth International Conference on Heavy Quarks & Leptons, Melbourne, Australia, Crete, June 2008.
3. M. Raggi, "A prototype large-angle photon veto detector for the NA62 experiment at CERN," Ninth International Conference on Applications of Nuclear Techniques, Crete, Greece, June 2008.
4. T. Spadaro, "K_{e2} and new physics searches with kaons," Fifth International Workshop on the CKM Unitarity Triangle, Rome, Italy, September 2008.
5. M. Raggi, "The NA62 rare kaon decay experiment photon veto system," Eighteenth International Conference on Particles and Nuclei, Eilat, Israel, November 2008.

References

1. A. Artamonov *et al.* [E949 Coll.], Phys. Rev. Lett. **101**, 191802 (2008).
2. G. Anelli *et al.*, CERN, Geneva, Tech. Rep. CERN/SPSC 2005-013 (2005).
3. V. Fanti *et al.* [NA48 Coll.], Nucl. Instr. & Meth. **A**574, 433 (2007).
4. K. Ahmet *et al.* [OPAL Coll.], Nucl. Instr. & Meth. **A**305, 275 (1991).
5. F. Ambrosino, *et al.*, in: 2007 IEEE Nuclear Science Symposium Conf. Record, Honolulu, 2007, pp. N05–6, arXiv:0711.3398.
6. A. Antonelli *et al.*, NA62 Note in preparation (2009).
7. V. Cirigliano, I. Rosell, Phys. Rev. Lett. **99**, 231801 (2007).
8. A. Masiero, P. Paradisi, R. Petronzio, Phys. Rev. D **74**, 011701 (2006).
9. Particle Data Group, W. M. Yao *et al.*, J. Phys. G **33**, 1 (2006).
10. [The FlaviaNet Kaon Working Group], arXiv:0801.1817.

P–ILC

A. Calcaterra (Resp.), L. Daniello (Tecn.), R. de Sangro, G. Finocchiaro,
P. Patteri, M. Piccolo, M. Rama

1 Introduction and motivation for this study

Silicon photomultipliers [1], often called "SiPM" in literature, are semiconductor photon detectors built from a square matrix of avalanche photodiodes (APD's) on a common silicon substrate. The side of each single APD square microcell can vary in length from 20 to 100 μm. Every microcell -or pixel- acts like a capacitor holding a given charge, and releases this entire charge when a photoelecton created in the cell reaches an active region inside the pixel, initiating a Geiger-like discharge. Pixel charges then build up again in a small time (25–250 ns). Although individual pixels are intrinsically digital, the SiPM behaves more like an analog device, because its signal is the sum of signals from all pixels discharged at the same time.

The PILC-LNF group started working in 2007 in the context of the "Proposal for ILC" initiative, with the intent to develop complete detectors of a size suitable for ILC calorimetry, and to study their performance with cosmic rays and beam tests.

2 New prototypes built in 2008 and Results at the Beam Test Facility

We exposed seven different assemblies of scintillator tiles coupled to different silicon photon detectors (PD) to the electron beam at the Frascati Beam Test Facility(BTF) [2] (≈ 500 MeV electrons, $(10\times5)\,\mathrm{mm}^2$ RMS transverse size). We cut and polished a total of 6 $(3\times3)\,\mathrm{cm}^2$ plastic scintillator tiles of 2 and 5 mm thickness, and wrapped them in aluminized mylar and black tape; we used as scintillators used Saint Gobain BC400 and Eljen Technology EJ212 which have almost identical characteristics, and a similar scintillator made in Vladimir (Russia). We also studied, as a reference, a CALICE tile made with the Vladimir scintillator and a 1 mm diameter Kuraray Y11 wavelength shifter fiber. We used photon detectors from Hamamatsu (see Tab. 1 for details). The PD was attached with optical glue directly to the middle of one *side* of the tile in all configurations except for the $(3\times3\,\mathrm{mm}^2)$, 3600 pixel Hamamatsu MPPC which was instead glued to the center of a *face*, and the CALICE tile, which has the MEPhI/Pulsar SiPM mechanically coupled, without glue or optical grease, to one end of the WS fiber.

Table 1: *Configurations under test. See text for the definitions of V_{brk}, V_{bias} and G.*

Config.	Scint. Type	PD (tot. area)	# of pxl	pxl size	V_{brk}(V)	V_{bias}(V)	G(10^6)
1	5 mm BC400	Hamam. (1 mm^2)	400	50μm	68.1	2.6	1.3
2	5 mm BC400	Hamam. (1 mm^2)	1,600	25μm	69.6	2.1	0.5
3	5 mm Vladimir	Hamam. (1 mm^2)	400	50μm	68.9	1.8	1.1
4	2 mm EJ212	Hamam. (1 mm^2)	400	50μm	69.0	1.6	2.2
5	2 mm EJ212	Hamam. (1 mm^2)	1,600	25μm	68.5	3.3	0.5
6	5 mm BC400	Hamam. (9 mm^2)	3,600	50μm	67.3	1.1	0.6
7	5 mm Vladimir	MEPhI (1 mm^2)	1,156	20μm	68.4	4.8	0.5

The PD's were read out with a low noise $\times 10$ amplifier based on the GALI-5 chip, an INFN-Pisa design built in Frascati. The seven tiles were then mounted in a test box, aligned to each other to ~ 1 mm in a fixed position.

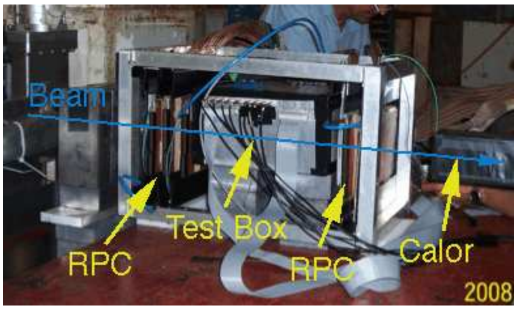

Figure 1: *Test beam set up.*

The box was equipped with a T-probe to monitor the operating temperature with a typical resolution of $\simeq 0.2$ °C. Temperature in the experimental hall was regulated to 23.4$\pm$ 0.5 °C, and the air inside the box was kept constant at 26.2$\pm$0.25 °C using a Peltier cell to extract some of the heat produced by the amplifiers.

To measure the impact point of the beam on the tile, we used an external tracker including 5 glass RPC [3], 3 of which were placed in front and 2 behind the test box on the beam line. The RPC were equipped with orthogonal planes of strips 8 mm wide, digitally read out, providing X-Y measurement in each plane with a point resolution of $\simeq$ 2.3 mm. As the beam at the Frascati BTF can provide a tunable number of particles per pulse (1-1000) [2], the test setup included a lead glass calorimeter module to measure the beam total energy on a pulse by pulse basis and allowing the selection of events containing any number of electrons (0,1,...n). A picture of the set up in the beam line is shown in Fig. 1. The response to 1 MIP of the tiles under test, in terms of number of fired pixels, is given in Fig. 2. All data shown were taken with the values for V_{bias} listed in Tab. 1, close to the corresponding gains, expressed in number of electrons (Q_{1pxl}/e).

3 Results from cosmic ray tests

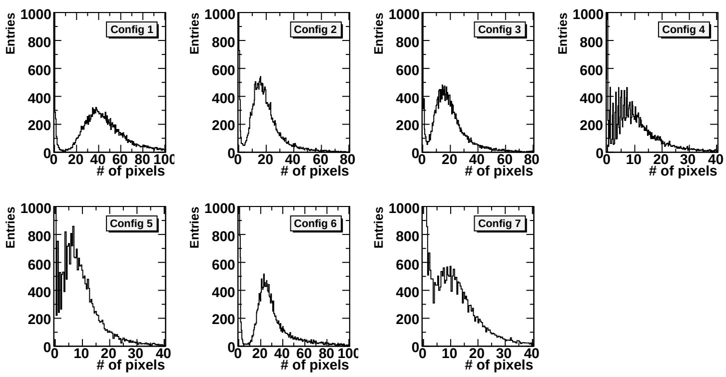

Figure 2: *Signal (number of pixels) collected by the 7 configurations in Tab. 1*

We have collected several million events containing exactly 1 MIP, and studied the performances of the various devices as a function of the beam particle impact point on the tiles. In Fig. 3 we show the amplitude of the PD signal (number of pixels), which is proportional to the amount of scintillation light collected, as a function of one coordinate, whereas in the four leftmost plots of Fig. 4 we show the efficiency in two dimensions. The efficiency is defined by the number of times a signal above 2 pixels is observed in the PD over the number of times a particle

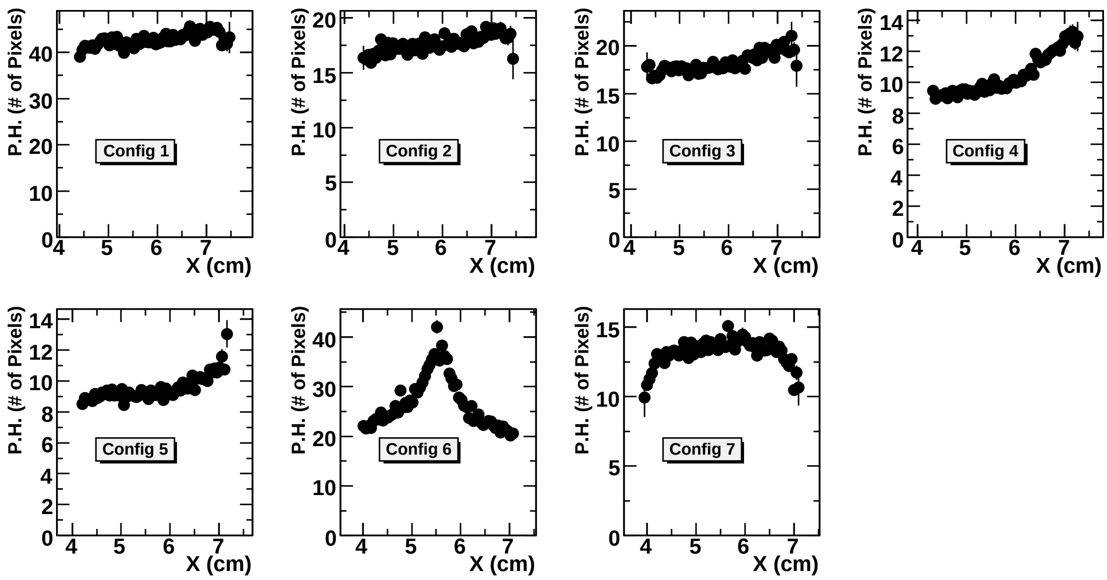

Figure 3: *Profile histograms of the signal (number of pixels) as a function of the MIP impact point of the tile, collected by the seven different test configurations of Tab. 1.*

has crossed the corresponding tile; the chosen threshold corresponds to about 1/8 to 1/4 of a MIP signal, depending on the configuration.

From Fig. 3, we can see that all tiles read out without using the fiber show a somewhat higher non-uniformity in light collection, but without loss of efficiency. The signal amplitude is maximal when the impinging particle is closest to the PD, and decreases with distance. This effect is not seen for the CALICE tile, where the light is collected by the fiber and where, on the other hand, a degradation of the light collection near the edges is observed. We estimate a rather high non-unifomity of $\simeq 35\%$ when the PD is attached to the face of the tile (config. 6), while config. 3 and 4 are more uniform ($\simeq 15\%$ and $\simeq 20\%$ respectively). The latter two values are small compared to the intrinsic fluctuations of a MIP energy deposit, therefore their effect on an energy measurement should also be small. In the four rightmost plots of Fig. 4 we show the X,Y distribution of the pulse height for configurations number 3,4,6 and 7. As one can see, the largest response variation is also restricted to a small region near the position of the PD, being quite uniform elsewhere. This means that only a small fraction of particles crossing a tile are affected by this non-uniformity. The difference in efficiency between the 5 mm and the 2 mm tile is evident from the two upper leftmost plots of Fig. 4 (config. 3 vs 4); nevertheless, an efficiency greater than $\simeq 90 - 95\%$ over a large portion of the tile is observed even with the thinner scintillator.

These preliminary results seem to suggest that direct read out of scintillator tiles with silicon PD for an ILC hadron calorimeter application is possible even using very thin tiles, and prompt for detailed Monte Carlo studies to estimate their performances in a detector.

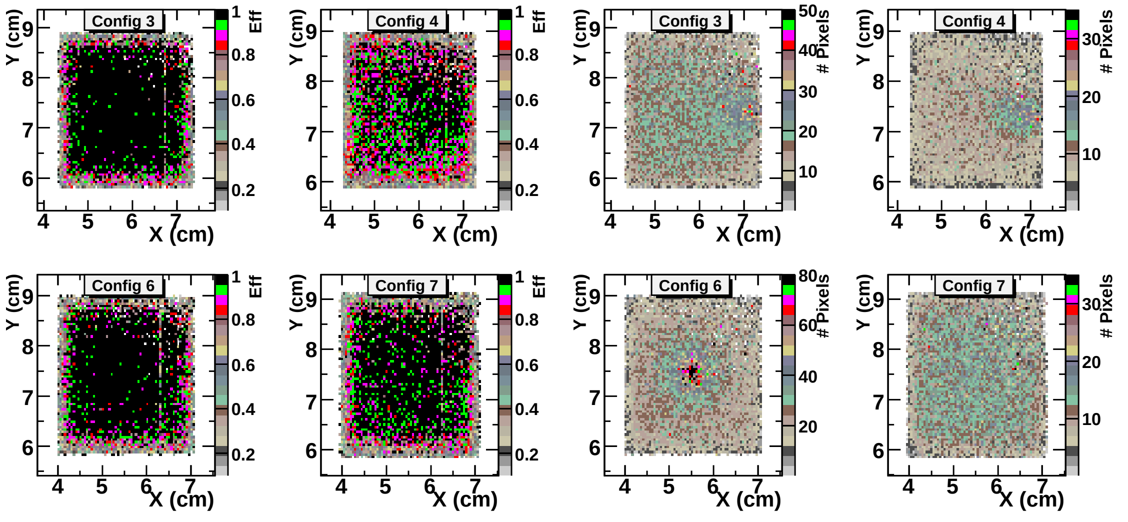

Figure 4: *The leftmost four plots show the efficiency as a function of the X,Y coordinates of the impact point on the tile for configurations number 3,4,6,7 of Tab. 1. The rightmost four plots show the pulse height in number of pixels as a function of X,Y.*

4 Results from cosmic ray data taking

The small temperature variations at the BTF are useful for the studies above, but a definite disadvantage when finding the dependence from T of the PD gain. To obtain this measurement, we continuously collect cosmic ray data using the same setup in a separate laboratory. We report here preliminary numbers for detectors 1 and 4 (see Fig. 5): the fitted values of the relative gain variation per degree of T are greater (resp.$-8\%/^\circ K$ and $-14\%/^\circ K$) than usually found in literature and moreover widely different for 2 supposedly identical PDs.

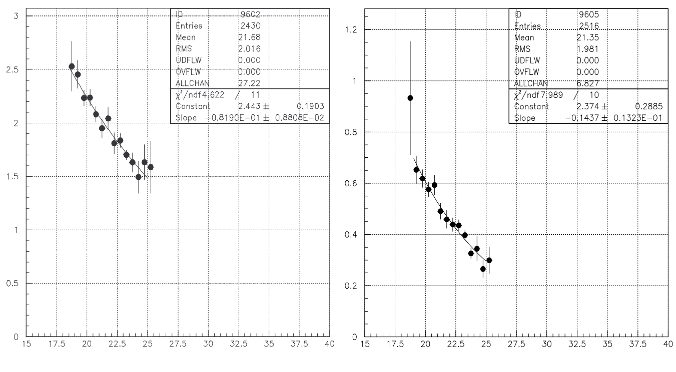

Figure 5: *The fitted T-coefficient ($\%/^\circ K$) for detectors 1 and 4 in Tab. 1.*

5 Foreseen activity in 2009

This R&D program will continue, both at the BTF and using cosmic rays, with the study of more PD types and configurations. The tunability of the number of particles in the beam, peculiar to the Frascati BTF, will also allow studies of the dynamic range of each tile-PD read out configuration. Future studies will also include measurements of the timing performances of PDs.

6 List of Conference Talks

1. R. de Sangro, "Study of Scintillation Tile Detectors readout via Silicon Photomultiplier Devices", presented at the 2008 International Linear Collider Workshop, Chicago (Il.)

7 Publications

1. A. Calcaterra *et al*, Nucl. Instr. & Meth. A **596**, 138 (2008).

References

1. A. Akindinov *et al.*, Nucl. Instr. & Meth. A **387**, 231 (1997); M. Danilov, arXiv:0812.1098.
2. A. Ghigo *et al.*, Nucl. Instr. & Meth. A **515**, 524 (2003).
3. A. Calcaterra *et al.*, IEEE Trans. Nucl. Sci. **53**, 341 (2006).

BENE_DTZ

F. Terranova

BENE-INFN is a study group closely related to the European initiative BENE (Beams for European Neutrino Experiments) and its follow-up in the 7th Framework Program of EU. It is aimed at developing novel sources for high intensity neutrino beams and is focused on the conceptual design of Superbeams, Beta Beams and Neutrino factories. In 2007, the outcome of the International Scoping Study for these future facilities has been delivered [1] and in 2008 activities toward a Conceptual Design Report have started. LNF contributed particularly on future applications of OPERA-like detectors [1], i.e. hybrid emulsion cloud chambers with and without magnetic field, as a far detector to exploit the $\nu_e \to \nu_\tau$ transitions ("silver channel") at the Neutrino Factories. LNF is also involved in the search of more innovative source based on laser-accelerated protons [2] to produce neutrinos in the GeV range. Further activities focused on the combination of accelerator data from Beta Beams with natural sources (atmospheric neutrinos) to improve the sensitivity to the neutrino mass hierarchy (sign of Δm^2_{32}) [3] and the study of the upgrades of the CERN acceleration complex to host a European high intensity ν source.

List of Conference Talks

1. F. Terranova "Neutrino factory e betabeam: potenzialitá e prospettive", VII Incontro di Fisica delle Alte Energie (IFAE), Bologna, 26-28 Marzo.
2. M. Maltoni and F. Terranova, "Neutrino Physics at and above GeV energies", session summary at the V Neutrino Oscillation Workshop (NOW2008) Conca Specchiulla, Otranto 6-13 Settembre.

References

1. T. Abe *et al.*, arXiv:0712.4129.
2. F. Terranova, H. Kiriyama, and F. Pegoraro, Opt. Commun. **281**, 4993 (2008).
3. A. Donini *et al.*, Eur. Phys. J. C **53**, 599 (2008).

LARES

G. Bellettini (Ass.), A. Boni (Dott.), C. Cantone (Bors.), S. Dell'Agnello (Resp.),
G.O. Delle Monache, M. Garattini (Dott.), N. Intaglietta (Tecn.), C. Lops (Dott.),
R. March (Ass.), M. Maiello (Dott.), M. Martini (Bors.),
L. Porcelli (Bors.), R. Tauraso (Ass.)

1 Introduction

We describe the INFN-LNF standard procedure (LNF-SCF-2008/01) for the optical Far Field Diffraction Pattern (FFDP) test of cube corner laser retroreflectors (CCRs) for space applications, when these CCRs are in air and in isothermal conditions around $(22 \pm 2)^{\circ}$C. This procedure was developed in 2007 and 2008, using prototype GLONASS CCRs lent to LNF by IPIE of Moscow and a GPS-2 flight model CCR array lent to LNF by the University of Maryland at College Park (all using Al-coated fused silica retroreflectors of 27 mm diameter). This was done in the context of the INFN experiment ETRUSCO[1]. The modeling of FFDP measurements is performed with a commercial software, CodeV by O.R.A. Inc., and it has been cross-checked against two independent software programs developed by other two members of the ILRS[2] "Signal Processing Working Group", D. Arnold and T. Otsubo, finding very good agreement among the three. In summer 2008 this procedure has been validated by performing the FFDP test of the LAGEOS "Sector", an engineering prototype on loan from NASA-GSFC, equipped with 37 uncoated, fused silica retroreflectors of 38 mm diameter. We report test results for the GLONASS and LAGEOS CCRs.

2 FFDP Test in Air and Isothermal Conditions

The basic "acceptance" test of the CCR optical performance is the measurement of the absolute angular size and shape of single-CCR FFDP with linearly polarized CW lasers. Our laser beam profiler (by Spiricon) uses a 2 MPixel CCD camera (by PtGrey), readout via Firewire or USB by a PC. FFDPs are acquired with the CCR in air and isothermal conditions. The absolute angular scale of the circuit is calibrated with the double-slit method to test the consistency of each CCR FFDP with its nominal dihedral angle offsets (DAO). The latter are related to the satellite velocity aberration, which is determined by its orbital altitude (velocity). The FFDP tests of LAGEOS Sector CCRs were done at the "Ex-Virgo" Optics Lab (SCF) of the LNF with a He-Ne laser of 633 nm (Nd:Yg laser of 532 nm) wavelength. We also measure the FFDP intensity relative to the Airy Peak, obtained with optical flats of known reflectivity, as an indicator of the CCR laser return.
FFDP measurements are modeled with CodeV, a software package by Optical Research Associates, Inc. (see http://www.opticalres.com/).
The INFN-LNF CCR FFDP test procedure has been developed in 2007/2008 with GLONASS prototypes and a GPS-2 flight model array lent to LNF by the University of Maryland at College Park,

[1]ETRUSCO (Extra Terrestrial Ranging to Unified Satellite Constellations) is dedicated to characterization and the improvement of the satellite laser ranging of GNSS constellations.

[2]International Laser Ranging Service.

all made by Al-coated fused silica retroreflectors with an hexagonal front face of approximately 27 mm diameter. In summer 2008 this procedure was applied to the FFDP test of the LAGEOS Sector.
While the optical specs of LAGEOS CCRs related to the velocity aberration effect are given in terms of a range of DAO values, for GLONASS CCRs they are given in terms of the (velocity-aberrated) angular distance between the two main peaks/lobes of the FFDP (about 50 μrad or about 5 arc-seconds).
For LAGEOS I (built in the US) and for LAGEOS II (built in Italy) CCR optical tests, including FFDPs and the so-called "range correction", were performed by NASA-GSFC. Now INFN-LNF developed FFDP testing capabilities also in Italy.

3 INFN-LNF Procedure for Optical Far Field Diffraction Pattern (FFDP) Tests of LAGEOS Cube Corner Retroreflectors (CCR)

LNF-SCF-2008/01 is the procedure for FFDP testing of the LAGEOS Sector prototype in STP conditions developed and validated in summer 2008. The laser wavelengths currently available are: 633 nm at the Optics Lab and 532 nm at the SCF Facility. FFDP modeling needed for these tests is done with the CodeV commercial software from O.R.A. Inc.
The procedure states that:

- "The shape of the Total FFDP contains the main quantitative information of the test"
- "The acceptance of the FFDP test is based on the comparison of the measured distance and the distance evaluated with CodeV, taking into account their respective uncertainties".

For DAOs above the specs range ("acceptance band") the FFPD maintains two distinctive, separated, main peaks/lobes of energy, preferentially located in the horizontal region. For DAOs at the lower bound of the "acceptance band" (0.75") a third additional peak of energy is present in the central region of the FFDP between the two main peaks/lobes with energy higher than the other two. If DAOs are below the specs range, only the third central peak remains. This is a very distinctive feature, which allows to detect DAOs below specs.
Failure of the test occurs for significant deviations from:

- The distance predicted by CodeV
- The configuration of two main peaks/lobes of energy with the appearance of a central 3rd peak of intensity much larger that the two horizontal peaks/lobes and up to the disappearance of the two horizontal peaks
- Any other major change of FFDP shape.

All the Sector CCRs are within DAO specifications, since the FFDP distance is always within specs and because no CCR showed a third central peak of significant intensity consistent with DAO<0.75".

4 The NASA-GSFC LAGEOS Sector and the GLONASS Prototypes

Three GLONASS CCR prototypes were lent to LNF by IPIE of Moscow for FFDP testing in air and in the SCF space facility. An engineering prototype of LAGEOS, the Sector, built around 1992, was sent to LNF by NASA-GSFC for FFDP testing in air and in the SCF. These loans were the result of a close cooperation of INFN-LNF with ILRS and other international partners, including the University of Maryland at College Park, NASA-GSFC and the Smithsonian Astronomical Observatory (SAO).

4.1 LAGEOS Sector FFDP Test in Air and Isothermal Conditions

The 37 Sector CCRs were tested at the Optics Lab with a He-Ne laser of 633 nm wavelength and at the SCF with a Nd:Yg laser of 532 nm, according to procedure LNF-SCF-2008/01. The measured Total FFDP angular distance and Total FFDP average intensity are shown in Fig. 1, compared to CodeV predictions.

4.2 FFDP Test of the GLONASS Prototypes in Air and Isothermal Conditions

The GLONASS FFDP tests reported in this section were carried out with the optical circuit of the SCF experimental apparatus, equipped with a 532 nm Nd:Yg laser. This was done in order to compare with the similar measurements performed by IPIE in Moscow at the same wavelength.

- The total FFDP of the GLONASS CCR with polished Al case measured by INFN-LNF and by IPIE are shown in Fig. 2-3, respectively. The peak distance measured by IPIE, about 50 μrad agrees with the one measured by INFN-LNF, 50 μrad. The two FFDP shapes are also consistent
- For the total FFDP of the GLONASS CCR with grey case, the peak distance measured by IPIE, about 50 μrad agrees with the one measured by INFN-LNF, 49 μrad. The two FFDP shapes are also consistent
- For the total FFDP of the GLONASS CCR with white case, the peak distance measured by IPIE, about 50 μrad agrees with the one measured by INFN-LNF, 44 μrad, within errors. The FFDP shapes are also consistent.

INFN-LNF measurements are consistent with IPIE measurements taken with procedure LNF-SCF-2008/01.

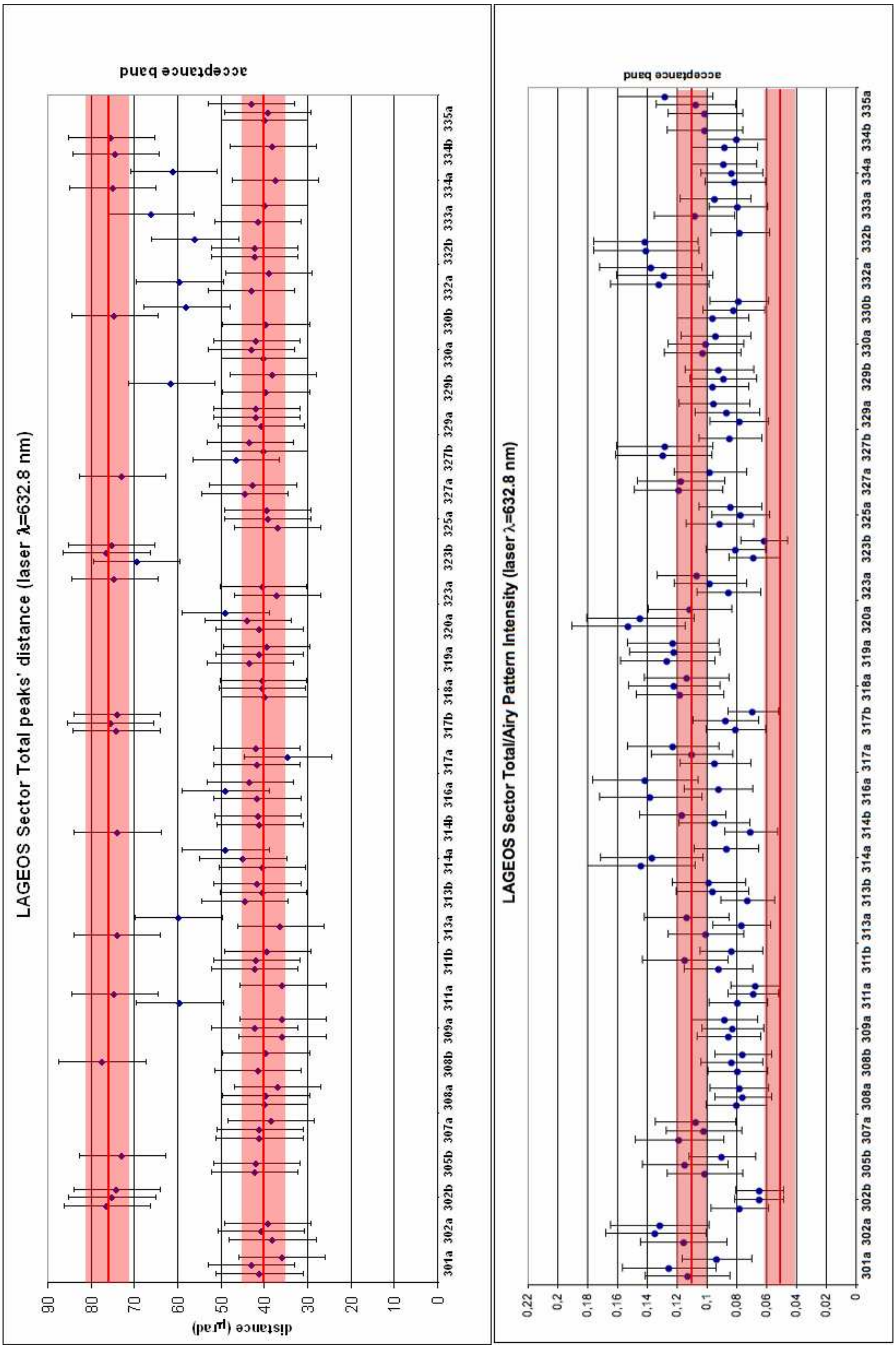

Figure 1: *LAGEOS Sector FFDP test at 633 nm: measured Total FFDP angular distance and Total FFDP average intensity compared to the CodeV predictions.*

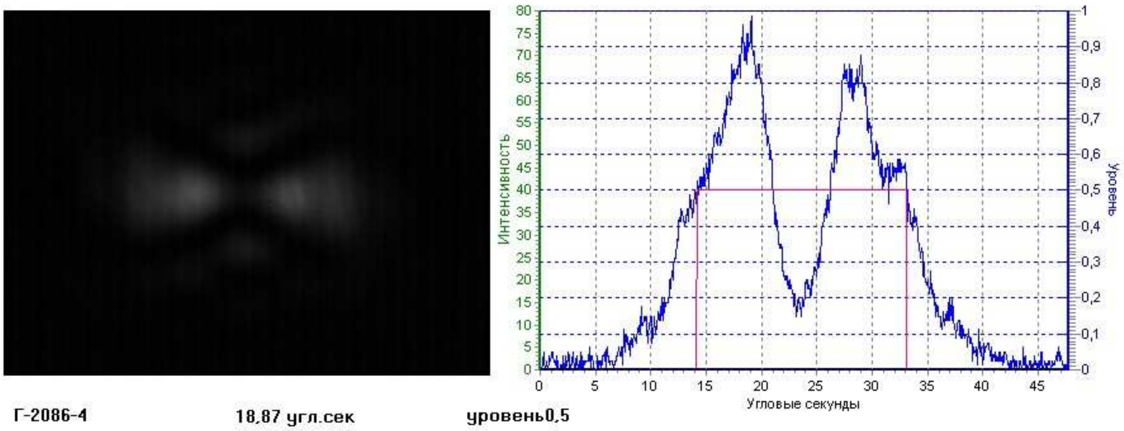

Figure 2: *Total FFDP angular distance measured by IPIE in arc-seconds.*

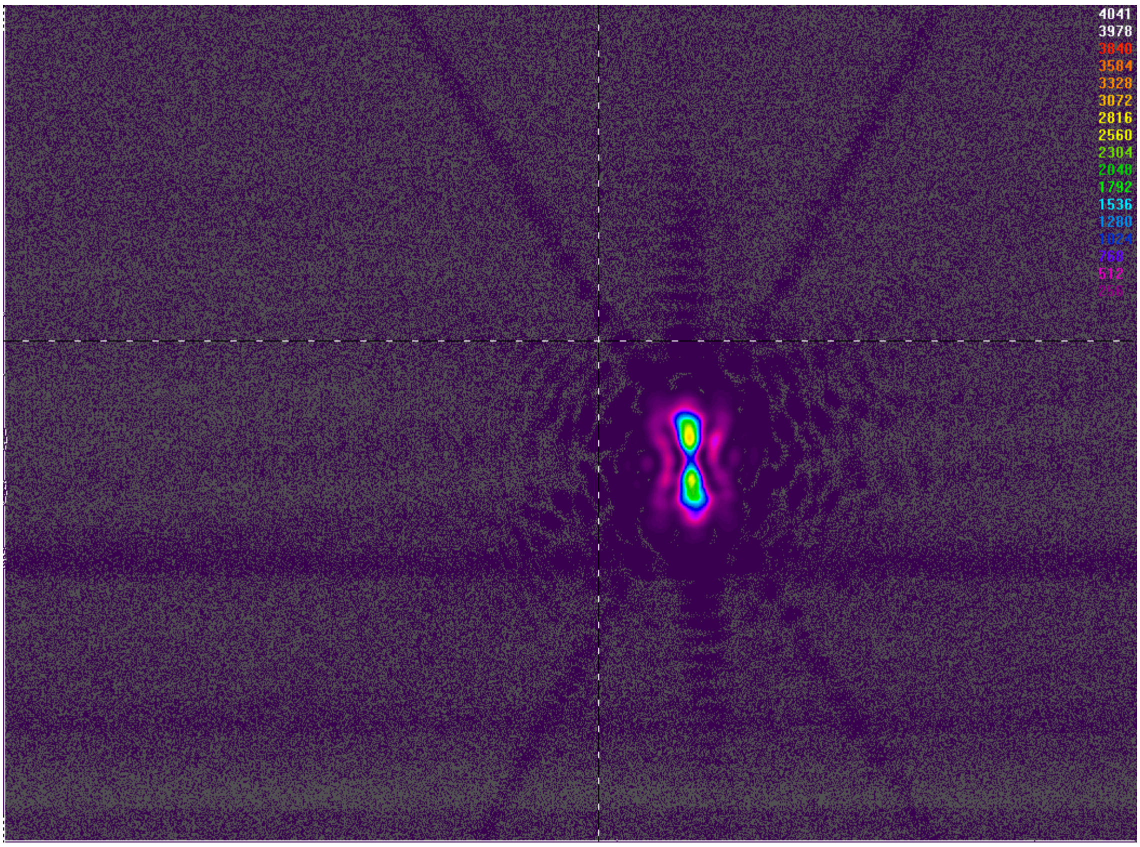

Figure 3: *Total FFDP measured by INFN-LNF.*

5 Talks by LARES-LNF Collaborators

1. S. Dell'Agnello, "Probing Gravity in the Solar System with Satellite and Lunar Laser Ranging", Rencontre de Physique de la Vallée d'Aoste, March 2008.
2. C. Lops, "Probing Gravity with LAGEOS and LARES", LNF Spring School, Frascati, May 2008.
3. M. Martini, "Probing Gravity with 2nd Generation Lunar Laser Ranging", LNF Spring School, Frascati, May 2008.
4. S. Dell'Agnello, "The INFN-LNF Satellite/lunar laser ranging Characterization Facility (SCF): Results on LAGEOS and GNSS".

References

1. A. Bosco *et al.* , Int. J. Mod. Phys. D, Vol. **16**, 2271 (2007).
2. S. Dell'Agnello *et al.*, Report LNF-07/8(IR).
3. D. G. Currie *et al.*, Reports LNF-06/28(IR); LNF-07/02(IR).

NEMO

Marco Cordelli, Agnese Martini, Luciano Trasatti (Resp.), Roberto Habel (Ass.)

1 Activity

The NEMO project aims at the construction of a kilometer cube detector for neutrino astronomy. During the year 2008 the NEMO group has continued work on the Phase 2 tower, which will be deployed in 2009. Meanwhile work is in progress on the properties of deep Mediterranean sea, and the group has produced several instruments to study the marine depths.

The LNF group has designed and built NERONE, an instrument to measure with great accuracy the water transparency using measurements performed at several distances from the source. During a cruise in September 2008 we obtained very good results with a deployment to 2500 m on the south coast of Sicily, proving the performance of the instrument. The LNF group is also developing the console software for the NEMO Phase 2 project.

The experiment includes INFN groups from: Bari, Bologna, Catania, Genova, LNS, Messina, Roma.

2 Publications

M. Cordelli, R. Habel, A. Martini, and L. Trasatti, Report LNF-08/25(IR).

OPERA

A. Cazes (Bors.), V. Chiarella, C. Di Troia (Ass.), B. Dulach, G. Felici,
A. Franceschi, F. Grianti (Ass.), A. Gambarara (Tecn.), N. Intaglietta (Tecn.)
A. Mengucci (Tecn.), T. Napolitano (Art. 23), M. Paniccia (Ass. Ric.), A. Paoloni,
M. Spinetti, F. Terranova (Resp.), T. Tonto (Tecn.), M. Ventura (Tecn.), L. Votano

In collaboration with

LNF-SEA: A. Balla, G. Corradi, U. Denni, A. Frani, M. Gatta, G. Papalino
LNF-SPAS: A. Cecchetti, S. Cerioni, D. Orecchini
LNF-SSCR: G. Catitti, A. Ceccarelli, A. Tiburzi
LNF Divisione Acceleratori: C. Fusco, F. Iungo, L. Pellegrino, C. Sanelli

1 The experiment

OPERA [1] has been designed to provide a very straightforward evidence for $\nu_\mu \to \nu_\tau$ oscillations in the parameter region indicated by Super-Kamiokande as the explanation of the zenith dependence of the atmospheric neutrino deficit. It is a long baseline experiment located at the Gran Sasso Laboratory (LNGS) and exploiting the CNGS neutrino beam from the CERN SPS. The detector is based on a massive lead/nuclear emulsion target. The target is made up of emulsion sheets interleaved with 1 mm lead plates and packed into removable "bricks" (56 plates per brick). The bricks are located in a vertical support structure making up a "wall". These bricks were produced in situ by a "brick assembly machine" (BAM) located near the OPERA experimental Hall; they are inserted into the wall support structure by a dedicated robot (BMS). Nuclear emulsions are used as high resolution tracking devices for the direct observation of the decay of the τ leptons produced in ν_τ charged current interactions. Electronic detectors positioned after each wall locate the events in the emulsions. They are made up of extruded plastic scintillator strips read out by wavelength-shifting fibers coupled with photodetectors at both ends. Magnetized iron spectrometers measure charge and momentum of muons. Each spectrometer consists of a dipolar magnet made of two iron walls interleaved with pairs of precision trackers. The particle trajectories are measured by these trackers, consisting of vertical drift tube planes. Resistive Plate Chambers (RPC) with inclined strips, called XPC, are combined with the precision trackers to provide unambiguous track reconstruction in space. Moreover, planes of RPC are inserted between the magnet iron plates. They allow a coarse tracking inside the magnet to identify muons and ease track matching between the precision trackers. They also provide a measurement of the tail of the hadronic energy leaking from the target and of the range of muons which stop in the iron. A block of 31 walls+scintillator planes, followed by one magnetic spectrometer constitutes a "super-module". OPERA is made up of two supermodules (SM) located in the Hall C of LNGS (see Fig. 1). In 2008 all the bricks have been produced (except a small amount produced in January 2009). Finally, the OPERA target is made of 150036 bricks corresponding to a target mass of 1.25 kton.
OPERA is able to observe the ν_τ signal with an impressively low background level. The direct and unambiguous observation of $\nu_\mu \to \nu_\tau$ appearance will constitute a milestone in the study of neutrino oscillations. Moreover, OPERA has some sensitivity to the sub-dominant $\nu_\mu \leftrightarrow \nu_e$

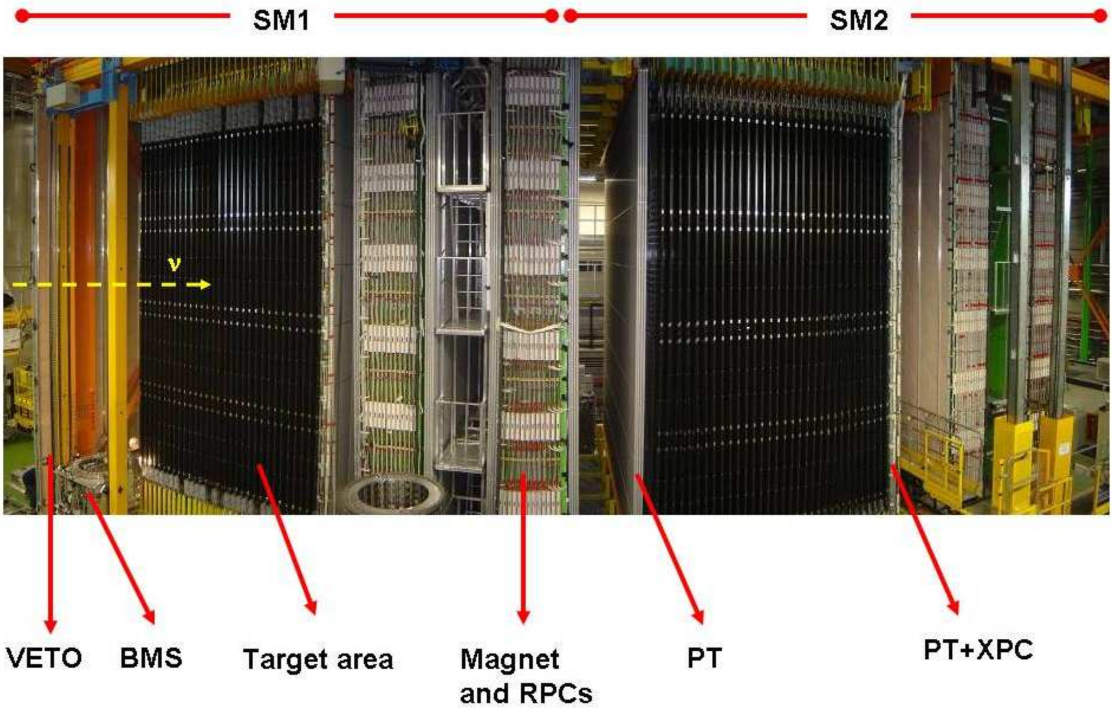

Figure 1: *A fish-eye view of the OPERA experiment. The upper red horizontal lines indicate the position of the two identical supermodules (SM1 and SM2). The "target area" is made up of planes of walls filled with lead-emulsion bricks interleaved with planes of plastic scintillators (TT): the black covers visible in the photograph are the end-caps of the TT. Arrows show also the position of the VETO planes, the drift tubes (PT) followed by the XPC, the magnets and the RPC installed among the magnet slabs. The Brick Manipulator System (BMS) is also visible. The direction of incoming neutrinos from CERN is indicated by the yellow arrow.*

oscillations in the region indicated by the atmospheric neutrino experiments. It has been shown [2] that the CNGS beam optimized for ν_τ appearance, will improve significantly (about a factor of three) the current limit of CHOOZ. Further results, concerning sterile neutrinos and non-standard interactions have been considered in [3, 4].
Opera is an international collaboration (Belgium, China, Croatia, France, Germany, Israel, Italy, Japan, Russia, Switzerland, Tunis and Turkey) and the INFN groups involved are Bari, Bologna, LNF, LNGS (Gran Sasso), Naples, Padova, Rome and Salerno. The Technical Coordinator (M. Spinetti), the Resource Coordinator (L. Votano), the Coordinator for detector operation and maintenance (A. Paoloni) and the Deputy Spokesperson of the Collaboration (F. Terranova) are LNF researchers.

2 Overview of the OPERA activities in 2008

During the 2007 high intensity run of CNGS a major failure has appeared in the beamline. It was traced back to the inappropriate shielding of the electronics for the control of the ventilation system. The data taking was, therefore, stopped the 22th of October. Further investigation showed that, due to a mistake in the design, many components have been located in areas where the neutron fluence was expected to be too high. In response to this, the CERN management and INFN setup a task force to re-design the shielding system, preventing radiation damage of the beamline components during the operation of CNGS at nominal intensity. The corresponding interventions were carried out during the 2007-2008 winter shutdown and the run was restarted the 16th of June. In the meanwhile, OPERA completed the production of all its bricks. In summer 2008, 97% of the bricks have been installed in the target. The production was stopped after an accident occurred in the firm producing the lead for the experiment [5] (JL Goslar, Germany). It has been resumed and completed in January 2009. During the 2008 the CNGS has accumulated 1.78 10^{19} protons on target. Correspondingly OPERA has observed 10100 events on-time with the beam and 1700 interactions in the target. This represents the first high statistics sample of OPERA. After the LHC accident, the run of CNGS continued until November the 9th having the CNGS as the only user of SPS. The maximum duty cycle reached at that time is 83%, comparable with nominal CNGS intensity. Fig.2 shows a charm candidate event (three prongs decay in flight of a charged meson) observed after emulsion scanning and occurred in the Opera target in summer 2008.

3 Activities in Frascati

The Frascati group has been responsible for the design and construction of the dipolar magnets and the general support structure for the subdetectors. It shares responsibility with INFN Padova and LNGS for the construction and running of the bakelite RPC planes. Frascati and Naples also designed and prototyped the wall support structures housing the lead/emulsion bricks and LNF was responsible for their production and installation. Moreover, the group contributes to software development and to analyses. LNF was highly involved in the construction and operation of the Brick Assembly Machine (BAM) and, since 2008, contributes to the emulsion scanning with two dedicated microscopes located in Frascati. Finally, since 2007 LNF follows the brick handling of

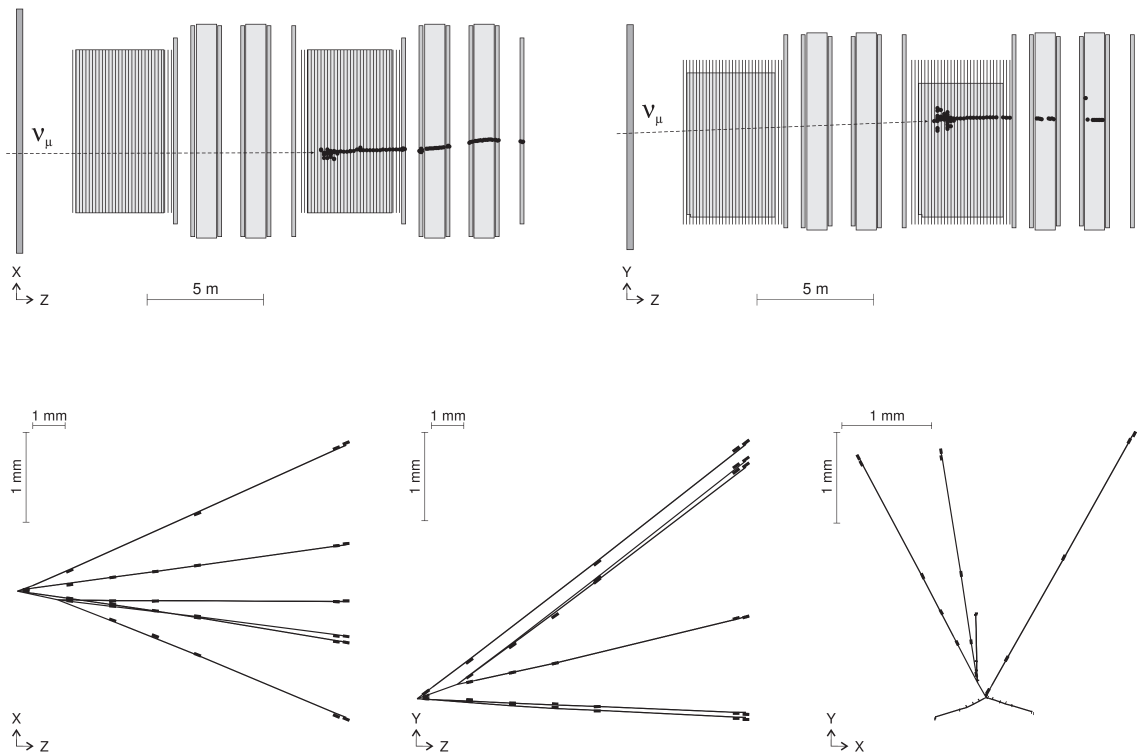

Figure 2: *A charm candidate in OPERA (three prong decay of a charged charmed meson).*

OPERA, i.e. the operation chain that goes from the extraction of the brick after an interaction has occurred up to the emulsion development.

3.1 OPERA General layout

The OPERA general support structure is a project by LNF-SPAS and external firms and it has been mounted in parallel with the electronic subdetectors and the brick walls between 2003 and 2006 [6]. The project has been completed in 2006 and, during 2007 and 2008, only auxiliary installations were added. The structure has been designed by LNF-SPAS; construction and mounting has been carried out by external firms under the supervision of LNF. In winter 2007, the filling with bricks of the first supermodule has been completed and the loading station feeding the BMS has been moved from SM1 to SM2. This operation required mechanical interventions, realignment and re-optimization of the BMS operations coordinated by LNF-SPAS and IN2P3-Annecy in collaboration with external firms. In 2008, the fences and the safety system has also been updated to fit the final position of the BMS and the loading/unloading stations.

3.2 Magnets

The OPERA magnets and their infrastructures have been commissioned in spring 2006 and were fully operative since the first CNGS run [7]. During the 2008 physics runs the magnets were operated continuously. The livetime in the presence of neutrino beam has been greater than 99% for both of them. Unwilled ramp-down have been reported only during two power cuts. A longer interruption occurred after the CNGS run, during a cosmic run with inverted polarity. The problem has been traced back to a defective card in one of the power supply and it has been solved during the winter shutdown. In 2008, the standalone OPERA cooling system has been interfaced with the water circuits of LNGS through a dedicated heat exchanger; it will act as a backup system in case of failure of the chiller and it will be commissioned in 2009. An automatic refill system for demineralized water was also installed in December 2008. The slow control was significantly improved thanks to the development of web interfaces to the database and the alarms. An automatic alerting system based on GPRS cards was commissioned in May 2008 and successfully employed during the run.

3.3 Resistive Plate Chambers

As mentioned above, for each of the two OPERA spectrometers 22 RPC planes have been installed. They are placed in the 2 cm gaps between the iron slabs of the magnet and equipped with horizontal and vertical readout strips. Two additional RPC layers with inclined read-out strips (called XPCs) are placed upstream the magnet along the beam direction. A short description of the read-out electronics can be found in [6]. The OPERA RPC are operated at 5.8 kV with the gas mixture $Ar/C_2H_2F_4/i\text{-}C_4H_{10}/SF_6=75.4/20.0/4.0/0.6$ [8]. Signals coming from horizontal and vertical strips are discriminated at 40 mV.

The XPC layers and 7 out of 22 RPC layers in each spectrometer are instrumented with dedicated Timing Boards (TBs). The Timing Boards are 16 channel positive discriminators, plugged on the read-out strip panels, performing the OR of the discriminated signal. Up to 14 TBs, corresponding to a whole RPC and one half XPC layer, are managed by one OPE board, performing

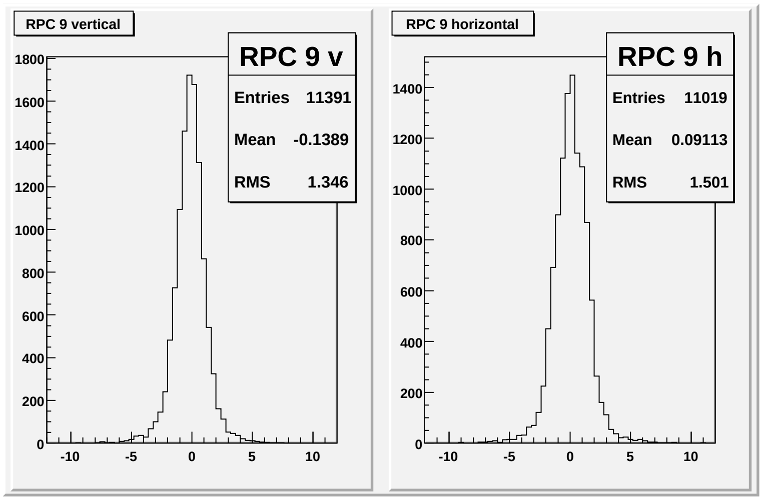

Figure 3: *Examples of tracking residuals of one RPC layer, for the bending projection (plot at left) and for the not-bending projection (plot at right).*

the global OR of the connected TBs; OR signals from OPE boards are used to generate the trigger signal for the drift tubes. The RPC signals are discriminated in the Timing Boards at 15 mV, well below the threshold employed for the RPC read-out. Each spectrometer is served by 153 timing boards and 11 OPE boards. Since the output signals from the Timing Boards are read out by means of TDCs, they can be used for time-of-flight measurements, exploiting the good time resolution obtainable with streamer operated RPC.

The full RPC system ran smoothly during the CNGS beam and the calibration runs, with almost no dead-time and with performances similar to those observed in the previous years [6), matching the required specifications.

Counting rates between 1 and 2 kHz/RPC layer have been observed with operating currents around 500 nA for each RPC row (3 chambers, corresponding to a sensitive area of 9 m^2). The operating currents are measured by means of precise custom nano-amperometers, designed by the LNF-SEA and described in [9)].

RPC layers showed average efficiencies around 95%, mostly limited by their geometrical acceptance (dead areas between the chambers). Typical cluster sizes are about 2.4 strips in the bending projection and 1.4 strips in the other projection. Tracking resolutions values around 1.4 cm have been observed for both projections, as shown in figure 3. The estimated time resolution is $\sim$3 ns for one entire layer [10)].

XPC layers show slightly worse performances because of the not-ideal adherence between the read-out strips and the chambers. Efficiencies about 90%, tracking resolutions better that 3 cm, 1.5 strips cluster sizes and $\sim$ 4 ns time resolutions have been measured.

The high statistics of the 2008 runs, with $\sim$ 40000 muons crossing each layer, has been used to improve the system alignment [11)]; systematics effects on the RPC performances related to the particles angular direction and primary ionization are also under study.

3.4 Wall support structure

The wall support structure ("wall") is made of thin stainless steel vertical bands welded to light horizontal trays where the bricks are positioned with a precision of one millimeter. The structure is suspended through rods and joints from the general support structure and tensioned from the bottom through a spring system. The walls were installed in parallel with the plastic scintillators. This project has been under the responsibility of LNF-SSCR and was successfully completed in 2006 [6]. In 2007 and 2008 only maintenance operations (see Sec. 3.7), fixing of damaged parts and alignment updates during the filling phase have been carried out.

3.5 Brick Assembly Machine

In 2007, the Brick Assembling Machine project had to face major difficulties during the startup of the mass production. In response to this, LNF increased substantially its involvement in this enterprise. The mechanical properties of the input material for the brick (mainly the new Ca-Pb alloy and the emulsions) have turned out to be significantly different with respect to early expectations. At the time of the commissioning and delivery at LNGS, the BAM piling stations were inadequate to handle these materials and the production rate was extremely slow. In 2007 all the 5 piling stations have been re-optimized by the firm in charge of the construction of the BAM (Tecnocut snc) in collaboration with INFN-Naples, LNGS and LNF-SSCR. Several changes have also been done in the system handling the lead boxes and, particularly, in the wrapping system after the lead-emulsion piling phase. In March 2007 the average production was 60 brick/day and it increased steadily up to 650-700 brick/day in October. Thanks to these efforts, OPERA was able to complete the first supermodule in November 2007. In 2008, the mean production rate was around 600 bricks/day with peak velocity exceeding 700 bricks/day. The mass production (97% of the target) has been completed in July 2008. The residual target, corresponding to about 4000 bricks were produced in January 2009. The produced bricks as a function of time up to January 2009 is shown in Fig.4. Until the completion of the OPERA target, LNF was also responsible for the organization and management of the production shifts, the maintenance of the BAM database and its interface with the OPERA central database.

3.6 The LNF scanning station

Emulsion layers are made of gel with interspersed AgBr crystals; in the case of OPERA, two such layers, each 40 μm thick are poured on a 200 μm plastic base. A particle crossing an emulsion layer ionises the medium, leaving a sequence of "sensitized" sites. After development, these sites are turned into silver grains, with a linear dimension of about 0.6 μm. About 30 grains every 100 μm are left by a minimum ionizing particle.

Nuclear emulsions are analyzed by means of optical microscopes: adjusting the focal plane of the objective lens through the whole emulsion thickness allows to obtain an optical tomography of each field of view, in order to reconstruct 3D tracks. A detailed description of the automatic microscopes developed for OPERA can be found in Ref. [12].

During 2006, two microscopes have been installed in Frascati. In 2007 one of this has been commissioned and aligned. The scanning laboratory (see Fig. 5) is now fully instrumented with the

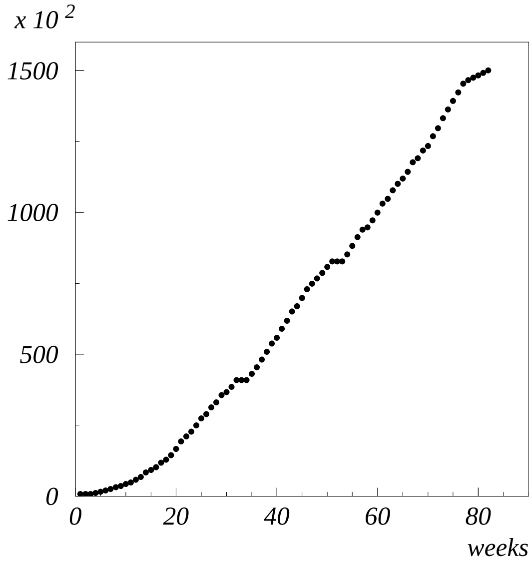

Figure 4: *Produced bricks as a function of time.*

handling system for the oil, the air conditioning and remote climate control station. The activities in 2008 have started with a revision of the scanning laboratory equipment. The air conditioning system has been set up in order to reliably keep the ambient temperature and humidity within the optimal range for nuclear emulsion storing, that is (20 ± 1)°C and (60 ± 5)% respectively. The scanning system, consisting of two Windows XP computers, controlling one microscope each, and a Windows Server computer devoted to host the DataBase for the local emulsion scanning data, has undergone a complete check of the hardware and software installations in order to outline the interventions needed to complete the system and make the scanning laboratory operative. The scanning software architecture has been completed with the installation of the missing tools, i.e. the local emulsion scanning data Oracle DataBase and the related packages for data publication on the global OPERA emulsion scanning data Oracle DataBase. Furthermore a supplementary Linux computer acting as remote controller of the scanning Windows computers and as emulsion data analysis workstation has been added to the scanning system infrastructure.

The commissioning of one of the two microscopes has been completed by the measurement of the scanning efficiency on nuclear emulsions which where exposed to pion beam at CERN in July 2007. The efficiency curve as function of the beam incident angle obtained is consistent with the OPERA European Scanning System efficiency measurements performed in the others European scanning laboratories. As final step towards the qualification of the LNF scanning laboratory, the scanning of one OPERA event brick previously analysed in the Naples scanning laboratory has been performed. The neutrino interaction vertex has been successfully localized and reconstructed in excellent agreement with the measurement performed in Naples. In November 2008 the LNF

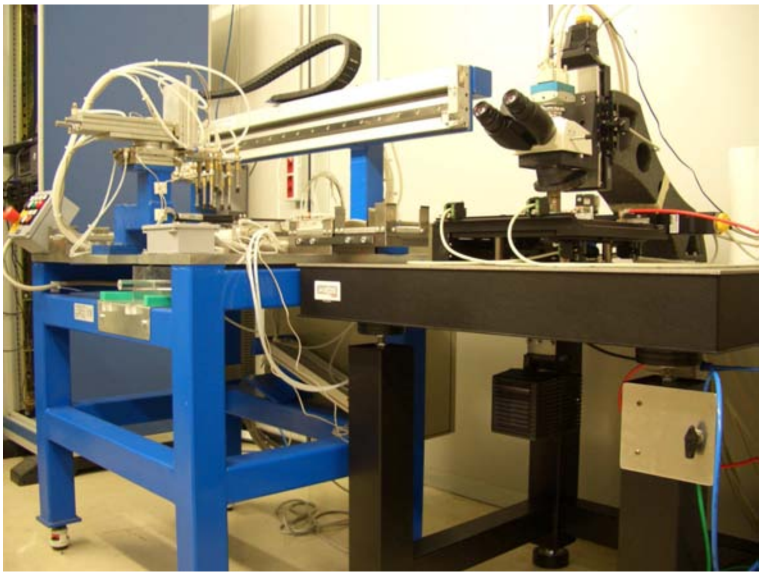

Figure 5: *The scanning laboratory at LNF.*

scanning laboratory has been assigned its first OPERA event brick to analyse, entering actively the European Scanning Laboratory team.

In Summer 2008 an automatic system for the emulsion plates loading on the microscope stage (Plate Changer) was installed in the LNF scanning laboratory. Since the Plate Changer works with a series of suction pad systems to handle the emulsion plates, the scanning laboratory has been instrumented with a 7 bar compressed air line supplied by a 300 l compressor. The Plate Changer is due to be installed on the actually working microscope: the electronic board, cables and interface board needed to connect the Plate Changer to the Windows computer controlling the microscope were ordered and installed. The commissioning of the Plate Changer is foreseen to be completed in spring 2009, on time for the 2009 OPERA Run.

Furthermore in 2009 we plan to complete the scanning system architecture with the commissioning of the second microscope and the substitution of the Linux computer with a new Linux machine with enhanced data storing capabilities. In parallel the scanning activity will proceed according to the brick extraction and assignment flow.

3.7 Brick handling

During nominal CNGS operation, about 20 neutrino interactions per day occur in the OPERA target and several candidate bricks are tagged as containing the corresponding primary vertex. These predictions are validated scanning preliminarily a pair of detachable emulsions ("changeable sheets", CS [13]). If confirmed, the corresponding brick is extracted, aligned using an X-ray machine and sent to the facilities located on surface for cosmic ray exposure (high precision alignment) and development. All the operations of CS and brick handling require dedicated tools and personnel running synchronously with the CNGS data taking. LNF is responsible of the coordination of these tasks and provides most of the tools for brick handling. In particular, in 2007 LNF-SPAS started the design of the unloading station and defined the procedure aimed at delivering the extracted bricks from the BMS to the X-ray marking area. The full operation chain started being operative by summer 2008. Some brick handling tasks have also been planned during the filling phase of the target: they included cleaning and maintenance of the walls, delivery of the temporary containers of the bricks ("drums") from the BAM to the BMS loading stations and the above-mentioned displacement of the stations after the completion of SM1 (see Sec.3.1). These tasks have been coordinated by LNF-SPAS and LNF-SSCR in collaboration with external firms until the completion of SM2 (June 2008). During the 2008 run, the brick handling system was able to keep pace with the CNGS extraction rate from CS extraction to cosmic exposure and development. Further improvements are foreseen in 2009, as an automatic rotating system for the bricks in the cosmic ray pit designed by LNF-SPAS. Moreover, the Opera Collaboration plans to replace about 17000 defective Changeable Sheets: such operation, coordinated by LNF, will be completed in spring 2009.

3.8 Software and analysis

In the last three years LNF has given major contributions to the online and offline software and analysis tools; LNF (A. Cazes) is currently responsible for the reconstruction of the electronic detector data, both at the level of single digit (calibration, alignment, etc...), in collaboration with the sub-detectors experts (INFN-Padova, Strasbourg, Hamburg), and at the level of the global event reconstruction. We provided crucial tools for the CNGS run: the online event display, the definition and implementation of the data format for the electronic detectors. Furthermore, we collaborated with the Lyon group to provide muon predictions extrapolated at the locations of the emulsion bricks [14]. In 2008 the brick finding strategy has been tested with a very large statistics: this allowed a further optimization of the pattern recognition and track finding strategy that acts as an input for the brick finding algorithms. Finally, LNF contributes to the development of the spectrometer slow control (SC) and the interface (through CORBA protocol) with the overall OPERA DAQ/SC system.

4 List of Conference Talks

1. A. Cazes, "Experience from OPERA", talk at X International Workshop on Neutrino Factories, Super beams and Beta beams, Valencia, 30 June - 5 July 2008.
2. A. Paoloni "Performances of the OPERA bakelite RPC", talk at the IX International Workshop on Resistive Plate Chambers and Related Detectors, Mumbai, India, 13 - 16 February 2008.
3. F. Terranova "Neutrino oscillation physics at Gran Sasso", talk at the Workshop "Neutrinos and Beams (NUBEAM08)" (Darjeeling, West Bengal, India, 5-7 Maggio)
4. F. Terranova "First results from OPERA", seminar at Dep. of Physics, Univ. of Roma Tre (17 June 2008).

References

1. M. Guler *et al.*, OPERA proposal, CERN/SPSC 2000-028, SPSC/P318, LNGS P25/2000.

2. M. Komatsu, P. Migliozzi, and F. Terranova, J. Phys. G **29**, 443 (2003); P. Migliozzi, and F. Terranova, Phys. Lett. B **563**, 73 (2003).

3. A. Donini, M. Maltoni, D. Meloni, P. Migliozzi, and F. Terranova, JHEP **0712**, 013 (2007).

4. M. Blennow, D. Meloni, T. Ohlsson, F. Terranova, and M. Westerberg, Eur. Phys. J. C **56**, 529 (2008).

5. A. Anokhina *et al.* [OPERA Coll.], JINST **3**, P07002 (2008).

6. See "LNF 2007 Annual Report", LNF-08/20 (IR), p. 103; "LNF 2006 Annual Report", LNF-07/10 (IR), p. 87; "LNF 2005 Annual report", LNF-06/10 (IR), p. 78; "LNF 2004 Annual Report", LNF-05/5 (IR), p. 70; "LNF 2003 Annual Report", LNF-04/08 (IR), p. 64.

7. A. Cazes *et al.*, JINST **2**, T03001 (2007).

8. A. Mengucci, A. Paoloni, M. Spinetti, and L. Votano, Nucl. Instr. & Meth. A **583**, 264 (2007).

9. M. Bazzi *et al.*, Nucl. Instr. & Meth. A **580**, 1441 (2007).

10. A. Paoloni *et al.*, OPERA Internal Note n.**90** (2008).

11. A. Paoloni, OPERA Internal Note n.**96** (2008).

12. N. Armenise *et al.*, Nucl. Instr. & Meth. A **551**, 261 (2005).

13. A. Anokhina *et al.* [OPERA Coll.], JINST **3**, P07005 (2008).

14. R. Acquafredda *et al.* [OPERA Coll.], New J. Phys. **8**, 303 (2006).

RAP

M. Iannarelli (Tecn.), R. Lenci (Tecn.), C. Ligi, A. Marini (Resp. Naz.), G. Mazzitelli,
G. Modestino, G. Pizzella (Ass), L. Quintieri (Art. 23), F. Ronga (Resp.), E. Turri (Tecn.)

1 Aim of the experiment

The primary scope of the experiment is to measure the longitudinal vibrations of cylindrical test masses, which are hit by electrons provided by the DAΦNE Beam Test Facility (BTF), in order to investigate if the particle energy loss conversion into mechanical energy depends on the conduction state of the bar.
The experiment was motivated by the fact that the gravitational wave antenna Nautilus detected high energy cosmic rays at a rate higher than expected when the bar was operated at T = 0.14 K, that is in the superconductive (s) state. On the contrary, the observed rate of high energy cosmic rays was in agreement with expectations when the bar was operated at T = 1.5 K, that is in the normal (n) state.
The experimental setup (*viz.* the beam, the test masses, the suspension system, the cryogenic and vacuum system, the mechanical structure hosting the cryostat, the readout, the data acquisition system) are described in [1, 2]. In particular, test masses made by pure niobium and by the same aluminum alloy (Al5056) used for Nautilus have been exposed to the BTF electron beam.
The amplitude of the fundamental longitudinal mode of the bar is the observed quantity. In the n state the amplitude (X) is proportional to the energy (W) released by the beam in the bar and to the ratio α/c_V, where α is the linear thermal expansion coefficient and c_V is the isochoric specific heat of the material [3]. This ratio is part of the definition of the Grüneisen parameter, which is a very slowly varying function of the temperature when the material is in the n state. Two scenarios are possible when the material is in the s state: a) Local $s-n$ transitions occur in tubular zones centered around the interacting particle tracks in the bulk [4, 5, 6] and b) Local transitions do not occur.

2 Activities in the year 2008

Two lines of activity were performed in the year: A) the systematic debug of the components of the dilution refrigerator, needed to cool the Al5056 bar at temperatures of the order of few tenths of kelvin and B) the completion of the analysis of the data taken in the year 2007 with the Al5056 bar above and below the transition temperature ($T_c \sim$0.84 K) among the two states of conduction.
The following results have been obtained:
1) The assessment that the amplitude of the oscillation induced by the interacting electrons depends on the state of conduction of the aluminum alloy. Fig. 1-(left) shows that the value of X/W is $b = 2.42\ 10^{-10}$ m/J for $T > T_c = 0.84$ K, that is in the n state. The same figure shows the onset of the superconducting effects at $T \leq T_c$. In the s state the amplitude becomes negative, indicating that a compression is generated in the bulk by the interacting particles, and its absolute values are greater then b.

2) The measured ratio of the amplitude in the s state to the amplitude in the n state is quantitatively consistent with the Nautilus observations on cosmic rays. Namely, Fig. 1-(right), which is related to the temperature interval $0.55 \le T \le 0.60$ K, the lowest observed temperatures, shows the averages of the normalized amplitude absolute values as a function of the released energy averages. The extrapolated value of the average at $\langle W \rangle = 10^{-8}$ J, which is the typical energy released by the cosmic rays in Nautilus, is $c = 8.3\ 10^{-10}$ m/J. Thus, a factor quantifying the Amplitude enhancement in the s state with respect to the n one is given by the ratio $c/b = 3.4$, which is consistent with the cosmic ray observations made by Nautilus in the s state [7].

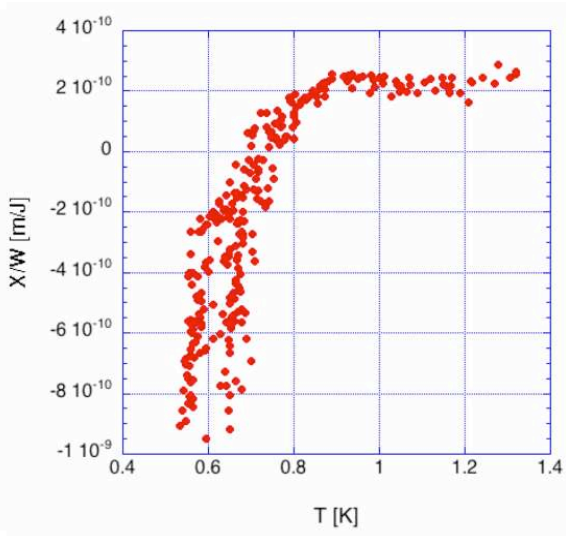

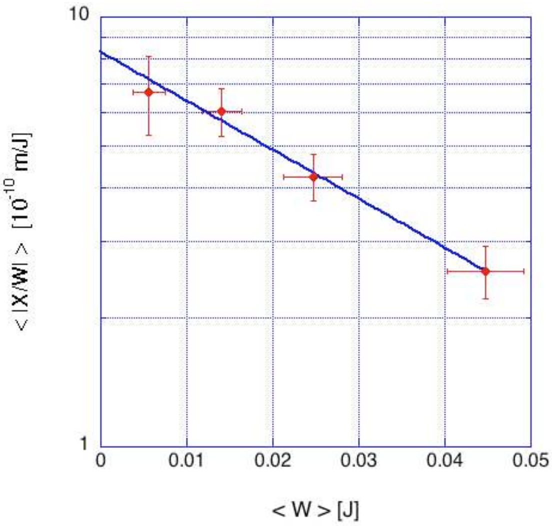

Figure 1: *Left - Amplitude* (X) *normalized to the energy* (W) *deposited in the bar per beam pulse vs. temperature* (T)*; Right - Averages of the absolute values of the normalized amplitudes* $(\langle |X/W| \rangle)$ *vs. the averages of the deposited energies (W) in the temperature interval* $0.55 \le T \le 0.60$ K.

3 Planned activities in the year 2009

Publication of the results on Al5056 (January) and runs with the bar at $T \le 0.3$ K (July).

4 List of Conference Talks

1. F. Ronga "Detection of high energy cosmic rays with the resonant detectors Nautilus and Explorer", CRIS 2008 - Malfa, Salina Island, (Italy), September 15-19.

2. C. Ligi "Rivelazione acustica di particelle in materiali massivi superconduttori", XCIV Congresso Società Italiana di Fisica - Genova (Italy), September 22-27.

References

1. B. Buonomo *et al.*, Astropart. Phys. **24**, 65 (2005).
2. C. Ligi, and S. M. Vinko, Report LNF–07/4(IR) (2007).
3. A.M. Grassi Strini, G. Strini, and G. Tagliaferri, J. Appl. Phys. **51**, 948 (1980).
4. A.M. Allega and N. Cabibbo, Lett. Nuovo Cim. **38**, 263 (1983).
5. C. Bernard, A. De Rujula, and B. Lautrup, Nucl. Phys. B **242**, 93 (1984).
6. N.K. Sherman, Phys. Rev. Lett. **8**, 438 (1962).
7. P. Astone *et al.*, Astropart. Phys. **30**, 200 (2008).

ROG

G. Giordano (Resp.), M. Iannarelli (Tecn.), R. Lenci (Tecn.), A. Marini, G. Modestino,
G.P. Murtas (Ass.), G. Pizzella (Ass.), F. Ronga (Resp.), E. Turri (Tecn.)

Collaboration with:
INFN Genova, University of Rome "Sapienza" and INFN Roma,
University of Rome "Tor Vergata" and INFN Roma 2, Geneva University

1 Introduction

The ROG group is currently operating two cryogenic gravitational wave (GW) bar detectors: EXPLORER (at CERN) and NAUTILUS (in Frascati). The main goal of this search is the direct detection of the GW's that could be emitted by astrophysical sources (such as Supernovae or Coalescent Binaries). Such detection would be of enormous interest for general relativity and astrophysics.

Both detectors consist of an aluminum cylindrical bar having a mass of $\simeq 2.3$ tons, with a capacitive resonant transducer mounted on one of the bar faces. They are contained in a vacuum cryostat, cooled at cryogenic temperatures ($\simeq 3$ K) to reduce thermal noise, and are isolated from seismic and acoustic disturbances.

The capacitive transducer is coupled to a very low noise superconducting amplifier (d.c. SQUID) whose output is acquired by a VME ADC board, sampled at 5 kHz.

A GW signal would excite the mechanical resonant modes of the bar-transducer system. When searching for impulsive signals, the data are filtered with an adaptive filter matched to a delta-like signal. This search for bursts is suitable for any transient GW which shows a nearly flat Fourier spectrum at the two resonance frequencies of each detector.

Both EXPLORER and NAUTILUS have been kept in continuous observational mode since 2003, with a duty cycle between 80 and 90%, mainly limited by the necessary periodic cryogenic operations.

The LNF group has major responsibilities in the maintenance and running of NAUTILUS (including the production of liquid Helium), in the maintenance, upgrading and running of the cosmic ray detectors, in the development of a new nearly quantum limited signal read-out, in the data acquisition and in many items of data analysis.

2 NAUTILUS and EXPLORER

The ultra-cryogenic detector NAUTILUS is operating at the INFN Frascati National Laboratory since December 1995. It is equipped with a cosmic ray detector based on a streamer tube assembly.

The present data taking started in 2003, with a new bar tuned at 935 Hz, where a pulsar, remnant of the SN1987A, is supposed to emit GW's, with a more sensitive readout chain (the same as for EXPLORER), and a new suspension cable, to provide a more stable position setting. At present, the temperature of the bar is 3.5 K and the resulting strain noise (the minimum detectable spectral density) is $\tilde{h} \simeq 1 \div 2 \cdot 10^{-21}\ /\sqrt{\mathrm{Hz}}$ around 935 Hz, and $\tilde{h} \leq 10^{-20}\ /\sqrt{\mathrm{Hz}}$ over about 30

Hz. The noise temperature is less than 2 mK, corresponding to an adimensional amplitude of GW bursts $h = 3.4 \cdot 10^{-19}$.

NAUTILUS is the only resonant detector capable of reaching a temperature as low as 0.1 K, being equipped with a ^{3}He-^{4}He dilution refrigerator. This ultra-cryogenic operational mode would result in a better sensitivity but also in a decrease of the duty cycle. Up to now, we decided to give the priority to the observational time and so we keep the standard operation at 3 K.

The EXPLORER antenna is located at CERN and is very similar to NAUTILUS, but can operate only down to 2.6 Kelvin. Also the duty cycle of EXPLORER is very high (of the order of 90%) and the noise temperature of the order of 2 mK, with a strain sensitivity $\tilde{h} \simeq 2 \div 3 \cdot 10^{-21}\ /\sqrt{\mathrm{Hz}}$ around the two resonances at 904 Hz and 927 Hz, and $\tilde{h} \leq 10^{-20}\ /\sqrt{\mathrm{Hz}}$ over about 30 Hz. Also EXPLORER is equipped with a cosmic ray detector, based on a set of long plastic scintillators.

The read-out systems installed in 2001 on EXPLORER and in 2003 on NAUTILUS, obtained a larger bandwidth and consequently improved the time resolution (now less than 10 ms), as it is also been checked with the events due to cosmic ray showers.

In the last years a continuos effort has been paied in improving the data analysis system already present and in testing independent algorithms and new methods. As a result of these, still going, efforts we were able to improve the accuracy in the reconstruction of both the amplitude and time characteristic of the signals. At the same time, we performed detailed studies of the detectors response to other class of signals than the simple delta-like burst previously considered. All this was done also with a particular eye on the perspective of performing joint analyses with the interferometric type of GW detectors.

2.1 EXPLORER-NAUTILUS coincidences

We continued to study all possible wide-band noises that can result in a candidate event and also, through simulations and software injections of signals, to find the event characteristics (e.g. length vs. amplitude) that an event due to a real excitation must have. All this was used to reduce the number of candidate events by putting vetos on periods or single events with understood instrumental noise excess, in addition to the usual vetos on events triggered by cosmic rays showers. We decided to maintain the same analysis conditions used in the past, namely a threshold at 19.5 in energy signal to noise ratio and a coincidence window fixed at 30 ms.

In 2006 we had a total overlap of 232.26 days of good data periods for both Explorer and Nautilus. The average number of accidentals, estimated as usual with relative shifts in time between the Explorer and Nautilus events, was 99.5, the true coincidences were 106.

2.2 IGEC-2 collaboration

The bar detectors distributed worldwide operated for a few years (1997-2000) as a network, giving for the first time significant upper limits to the yearly rate of GW burst events in the Galaxy. In 2003 and 2004 EXPLORER and NAUTILUS have been the only two detectors in data taking over long time periods. Since 2005 both Auriga at LNL and Allegro at the Louisiana State University restarted regular operation, so the former IGEC collaboration was restarted, under a new agreement (IGEC-2) between the 4 bar detectors.

The network of resonant bar detectors of gravitational waves resumed coordinated observations within the International Gravitational Event Collaboration (IGEC-2) with the analysis of 6 months of 2005, whose results were published in 2007. The joint analysis has continued with four detectors are taking part in this Collaboration: ALLEGRO, AURIGA, EXPLORER and NAUTILUS. We present here (the proper paper is under way) the results of the search for gravitational wave bursts over 14 months, November 16 2005 through December 31 2006. Table 1 shows the overlap times during the considered period. The implemented network data analysis is based on 5 time coincidence searches among the detectors, 1 fourfold and 4 threefold searches, later considering the logical OR of all of them.

Table 1: Mode of observation during analyzed period.

Configuration	**Time of operation (days)**
0 detector	0
1 detectors	0.981
2 detectors	21.942
3 detectors	144.101
4 detectors	243.976

The network amplitude sensitivity to bursts improved by a factor of 3 over the 1997-2000 IGEC observations; the wider sensitive band also allowed the analysis to be tuned over a larger class of waveforms. Given the higher single-detector duty factors, the analysis was tuned, through the use of suitable thresholds in signal-to-noise ratio, in such a way as to ensure the identification of any single candidate of gravitational waves with high statistical confidence. The false detection rate was as low as 1 per century. No candidates were found.

A second analysis was performed, leaving the thresholds at the level used by each group for the event extraction. This analysis could not provide candidates with a sufficient statistical significance, rather its aim was to provide anyhow possible candidates for further analysis, mainly in view of a possible data exchange with the interferometric detectors (LIGO and VIRGO) that were in operation at the same time. The results of this search is presented in tab.2.

Table 2: Results of the low-thresholds coincidence searches. (AL=Allegro, AU=Auriga, EX=Explorer, NA=Nautilus.)

Detectors	Coincidences	Accidentals
AL-AU-EX-NA	0	0.008
AL-AU-EX	3	3.93
AL-AU-NA	5	4.70
AL-EX-NA	7	9.45
AU-EX-NA	4	2.05

2.3 Other type of analyses

- Cosmic Rays - The study of the response of our detectors to cosmic ray showers [4] continues to demonstrate experimentally the actual capability to detect very small mechanical excitations of the bars. While the study of the timing characteristics of the larger events produced by the rare very high density showers allows us a real measure of the accuracy in the time reconstruction, the study of the much more numerous cases of low density showers, performed with a cumulative-type analysis, constitutes an independent cross-check of the amplitude response calibration.

- Search for monochromatic signals - The search for periodic gravitational wave signals is a stimulating challenge for data analists because of the considerable amount of computing time required.

Until a few years ago, in the case of a blind search, i.e. without any a priori knowledge about the source, a fully coherent analysis can not handle more than a few days of data because of the steep dependence of the size of the parameter space on the frequency resolution. Recently [3], it was possible to extend a search of this kind to about half a year of Nautilus data, obtaining a best upper limit of $3.4 \cdot 10^{-23}$ in a bandwidth of 1 Hz around 922.55 Hz.

The technique of using an incoherent analysis for a blind search, though in principle less sensitive than the coherent one, has the advantage of being much faster thus allowing the analysis of longer data periods, which in turn allows to improve the sensitivity of the search, and to enlarge the frequency range. This technique [2] allowed to analyze the Explorer data collected in 2005 with a bandwidth of 40 Hz, reaching a best upper limit of $3.1 \cdot 10^{-23}$ at 920.14 Hz, and an average of $\simeq 2 \cdot 10^{-22}$ in the full 885-925 Hz band.

- Search triggered by astrophysical events - The analysis of our detectors data at the time of a large number of Gamma-ray bursts allowed us to set upper limits on the amplitude of possible GW signals associated to them. This kind of study is continuing and actually has been extended to detailed analysis of the data collected in coincidence with some rare astrophysical events, like the giant flares happened 1998 and 2004, making use of the classical cross-correlation technique applied to the filtered data.

- Wavelet analysis - The search of GW performed with more than one detectors can be made with a method different from the usual one based on time coincidence between candidate events of each detector, that is by performing the cross-correlation between the data of two detectors. The technique developed inside the ROG group starts from the h-reconstructed data, conveniently whitened and performs their decomposition on a base of wavelet functions (this is in common with standard techniques used by other GW groups). The next step, that is the thresholding of the wavelet components in order to reduce the noise, is performed on an entropy based criterion, that appears more efficient than simply looking at the amplitude. Test of this technique are under way on real data taken by the detectors of the ROG group.

3 List of Conference Talks

1. G. Pizzella, "SN1987A: Revisiting the Data and the Correlation between Neutrino and Gravitational Detectors"; presented at Frontier Objects in Astrophysics and Particle Physics, Vulcano, Italy, 26-31 May 2008; arXiv:0810.3759.

2. F. Ronga, "Detection of high energy cosmic rays with the resonant gravitational wave detectors NAUTILUS and EXPLORER", presented at CRIS 2008 Conference, Malfa, Italy, 15-19 September 2008.

References

1. P. Astone *et al.*, Class. Quantum Grav. **25**, 114048 (2008).
2. P. Astone *et al.*, Class. Quantum Grav. **25**, 114028 (2008).
3. P. Astone *et al.*, Class. Quantum Grav. **25**, 184012 (2008).
4. P. Astone *et al.*, Astropart. Phys. **30**, 200 (2008).

WIZARD

G. Basini, F. Bongiorno (Ass.), L. Bongiorno (Bors.), G. Mazzenga (Tecn.), M. Ricci (Resp.)

Participant Institutions:

Italy: INFN Bari, LNF, Firenze, Napoli, Roma 2-Tor Vergata, Trieste;
CNR Ist. Fisica Applicata "Nello Carrara" Firenze;
ASI (Italian Space agency);
Electronic Engineering Department, University of Roma 2 "Tor Vergata";
Russia: MePhi Moscow;
FIAN Lebedev Moscow;
IOFFE St Petersburg;
TsSKB-Progress Samara;
Sweden: KTH Stockholm;
Germany: Siegen University;
USA: NASA Goddard Space Flight Center;
New Mexico State University.

1 Experimental Program and Scientific Objectives

The WIZARD experimental program is devoted to the extensive study of cosmic ray spectra (particles, antiparticles, isotopes, abundances and search for antimatter) in several energy ranges achievable through different instruments on board stratosferic balloons and long duration satellite missions. WIZARD is an International Collaboration between several Universities and Research Institutions from Russia, Sweden, Germany, USA togheter with the Space Agencies NASA, RSA (Russia), SNSB (Sweden), DLR (Germany) and ASI. The experimental activities have been and are carried out through three main programs:

- Stratospheric Balloon flights;
- Satellite missions NINA-1 and NINA-2;
- Satellite mission PAMELA.

We refer to previous editions of this report for the descrition of the activities related to the balloon flights and to the two NINA missions.

1.1 The satellite mission PAMELA

PAMELA is a cosmic ray space experiment installed on board a Russian satellite (Resurs-DK1) which has been successfully launched on June 15th, 2006 from the cosmodrome of Baikonur, Kazakhstan, by a Soyuz TM2 rocket. Fig. 1 shows the lift-off of the rocket.

The satellite is flying in a low altitude, elliptic orbit (350-610 km) with an inclination of 70.0 degrees. The PAMELA telescope consists of a magnetic spectrometer composed of a permanent

Figure 1: *Lift-off of the Soyuz rocket from the Baikonur cosmodrome.*

magnet coupled to a silicon tracker, an electromagnetic silicon-tungsten calorimeter, a time-of-flight system, an anticoincidence system, a shower tail catcher scintillator and a neutron detector [1, 2]. A sketch of the PAMELA instrument is shown in fig.2 and a photo of the completed Flight Model is shown in fig. 3.

The total height of PAMELA is $\sim$ 130 cm, the mass is 470 kg and the power consumption is 355 W.

The observational objectives of the PAMELA experiment are to measure the spectra of antiprotons, positrons and nuclei over an extended range of energies, to search for antimatter and for indirect signatures of dark matter and to study cosmic ray fluxes over a portion of the Solar cycle.

The main scientific goals can be schematically listed as follows:

a) measurement of the antiproton spectrum in the energy range 80 MeV-190 GeV;
b) measurement of the positron spectrum in the energy range 50 MeV-270 GeV;
c) measurement of the electron spectrum in the energy range 50 MeV-400 GeV;
d) measurement of the proton spectrum in the energy range 80 MeV-700 GeV;
e) measurement of the electron+positron spectrum up to 2 TeV;
f) measurement of light nuclei spectra (up to Z=6) at energies 100 MeV/n - 200 GeV/n;
g) search for antinuclei with a sensitivity better than 10^{-7} in the $\overline{\mathrm{He}}/\mathrm{He}$ ratio (95% C.L.).

Additional objectives are:
Long-term monitoring of the solar modulation of cosmic rays;

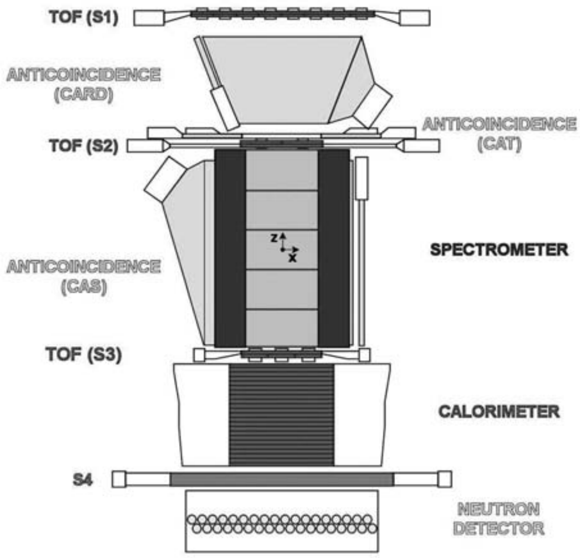

Figure 2: *Sketch of the flight detectors the PAMELA telescope.*

Measurements of Energetic Particles from the Sun;
High-energy Particles in the Earth magnetosphere and Jovian electrons.

After almost three years of operation, both the satellite and the PAMELA instrument have shown to be properly functioning and the overall performance of the detectors to be fairly good. Every day, an average of 14 GBytes of data are transmitted to the main Receiving Station NTsOMZ located in Moscow where quick-look and first control of the performances of the instrument are performed. Then, alla data are transferred through high-speed networks to CNAF, Bologna and to the participating institutions of the PAMELA International Collaboration for the full analysis

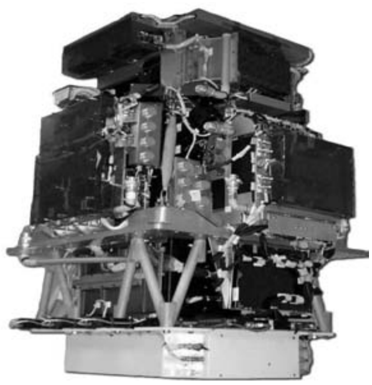

Figure 3: *The PAMELA Flight Model.*

of data. PAMELA, at present, has collected some 14 TByte of data corresponding to about 1.6 billion events.

Among the results so far obtained by the experiment, the most relevant are the anomalous spectrum of positrons and the antiproton to proton flux ratio studied up to the highest energies ever achieved so far (100 GeV) with the available statistics (see the list of publications for references). In particular, the positron result (Fig. 4) shows a significant distortion in the spectrum differently from what was expected according to the most credited models of propagation and acceleration of cosmic rays in the Galaxy. This effect could be an indication of production by dark matter particles or could be explained by the presence of an astrophysical source like, e.g., young nearby pulsars. Many articles, showing several possible interpretations and new models, have appeared after the first presentations at Conferences and publication of the PAMELA results. Work is in progress to push - thanks to the increasing statistics - the spectrum to higher energies (beyond 100 GeV) and to study the electron spectrum which is of most interest also due to the recent results obtained by the balloon experiment ATIC.

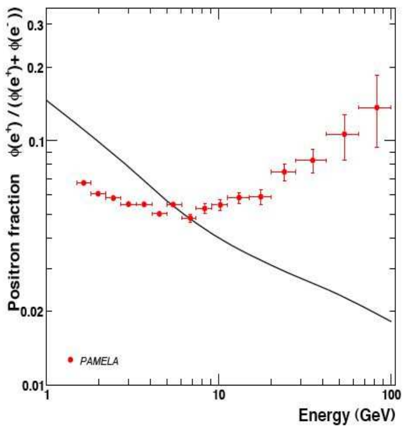

Figure 4: *The PAMELA positron fraction compared with theoretical model. The solid line shows a calculation by Moskalenko and Strong* [3] *for pure secondary production of positrons during the propagation of cosmic-rays in the Galaxy. One standard deviation error bars are shown. If not visible, they lie inside the data points.*

2 Activity of the LNF group during year 2008

The LNF WIZARD group has been fully involved in all the previous balloon and present satellite programs. During the year 2008 the LNF group has continued the activity in the analysis, quick-look and preparation and organization of next beam tests to be performed in 2009 at GSI Darmstadt for calibration with nuclei of the ground instruments of the Engineering Model.

3 A selection of 2008 publications

1. O. Adriani *et al.*, arXiv:0810.4995v1 (accepted by Nature).
2. M. Boezio *et al.*, Journal of Physics: Conference Series **110**, 062002 (2008).
3. V. Malvezzi *et al.*, Nucl. Instr. & Meth. A **588**, 250 (2008).
4. M. Casolino *et al.*, Nucl. Instr. & Meth. A **588**, 243 (2008).

References

1. M. Casolino *et al.*, Adv. Space Res. **42**, 455 (2008).
2. P. Papini *et al.*, Nucl. Instr. & Meth. A **588**, 259 (2008).
3. I.V. Moskalenko and A.W. Strong, Astrophys. J. **493**, 694 (1998).

AIACE

M. Aghasyan (Bors. PD), E. De Sanctis, M. Mirazita,
J. de Oliveira Echeimberg (Dott.), A. Orlandi (Tecn.), S. A. Pereira (Ass.),
W. Pesci (Tecn.), E. Polli, F. Ronchetti (Art. 23), P. Rossi (Resp. Naz.), A. Viticchié (Tech.)

1 Introduction

AIACE stands for Attività Italiana A CEbaf: it is the collaboration of the INFN groups of Frascati and Genova. They participate into the physics program carried on by the CLAS collaboration, at the 6 GeV Continuous Electron Beam Accelerator Facility (CEBAF) at the Jefferson Laboratory (JLab). The [CLAS Coll.] counts about 150 physicists from 36 Institutions from seven Countries. Its scientific program is focused on the precision study of the structure of the nucleon and the nature of the strong interaction.

CEBAF will increase its beam energy from currently 6 GeV to 12 GeV by 2014. This requires the upgrade of the CLAS detector, called CLAS12.

In the period covered by this report, the Frascati AIACE group has continued to work in the 6 GeV program and has started its partecipation to the 12 GeV one. Concerning the current activity with the 6 GeV beam, it has been focused on *a)* the study of the nucleon spin, *b)* the study of strangeness photoproduction and *c)* the study of exclusive reactions. As for the 12 GeV upgrade program, the group has centered its activity in the central detector project for CLAS12 and it has started the investigation of the construction of a RICH detector.

2 The 6 GeV program

2.1 The Spin of the Nucleon

The spin structure of the nucleon has been of particular interest since the EMC [1] measurements, subsequently confirmed by a number of other experiments [2, 3, 4, 5, 6, 7], implied that the helicity of the constituent quarks account for only a fraction of the nucleon spin. Possible interpretations of this result include significant polarization of either the strange sea (negatively polarized) or gluons (positively polarized) and the contribution of the orbital momentum of quarks. The semi-inclusive deep inelastic scattering (SIDIS) experiments, when a hadron is detected in coincidence with the scattered lepton provide access to spin-orbit correlations. Observables are spin azimuthal asymmetries, and in particular single spin azimuthal asymmetries (SSAs), of the detected hadron, which are due to the correlation between the quark transverse momentum and the spin of the quark/nucleon. Knowledge of SSAs provide access to a list of novel distribution functions, the Transverse Momentum Dependent distribution functions (TMDs) which contain information on the parton transverse momentum. Two fundamental mechanisms have been identified leading to Single Spin Asymmetries SSAs in hard processes; the Sivers mechanism [8, 9, 10, 11, 12], which generates an asymmetry in the distribution of quarks due to orbital motion of partons, and the Collins mechanism [11, 13], which generates an asymmetry during the hadronization of quarks. TMDs also contain unique information on the role of initial and final state interactions of active partons in hard scattering processes [10, 11, 12].

TMDs studies are one of the primary goal of experiments at JLab 12 GeV but their investigation has already started with the 6 GeV beam using unpolarized, longitudinally and transversely polarized target.

2.1.1 Beam Spin Asymmetries Measurement

During 2008 the beam-spin asymmetries in single neutral semi-inclusive pion electroproduction were measured using a 5.77 GeV electron beam and the CLAS detector. Scattering of longitudinally polarized electrons off a liquid-hydrogen target was studied over a wide kinematic region.

The cross section for single pion production by longitudinally polarized leptons scattering from unpolarized protons is given by:

$$\frac{d\sigma_{LU}}{dxdydzd\phi_h dP_T} \propto \lambda_e \sqrt{y^2+\gamma^2}\sqrt{(1-y-1/4\gamma^2)}\sin(\phi_h)F_{LU}^{\sin(\phi_h)} \tag{1}$$

The subscripts in σ_{LU} specify the beam and target polarizations, respectively (L stands for longitudinally polarized and U for unpolarized). The azimuthal angle ϕ is the angle between leptonic and hadronic plane according to the Trento convention [14]. The kinematic variables x, y, and z are defined as: $x(\equiv x_B) = Q^2/2(P_1q)$, $y = (P_1q)/(P_1k_1)$, $z = (P_1P)/(P_1q)$, where $Q^2 = -q^2$, $q = k_1 - k_2$ is the 4-momentum of the virtual photon, P_1 and P are the momenta of the target and the observed final-state hadron, and $\gamma^2 = 4M^2x^2y^2/Q^2$.

The ratio of polarized and unpolarized contributions defines the asymmetry, which is also the $\sin(\phi_h)$ moment of the normalized cross-section:

$$A_{LU}^{\sin(\phi_h)} = \frac{\sigma_{LU}}{\sigma_{UU}} \tag{2}$$

where

$$\frac{d^3\sigma_{UU}}{dxdydz} \propto (1-y+y^2/2)f_1(x)D_1(z). \tag{3}$$

is the unpolarized cross-section and $f_1(x)$ and $D_1(z)$ are the distribution and fragmentation functions, respectively.

The beam-spin asymmetries in single-pion production off the unpolarized target are higher-twist by their nature [15, 16]. The higher twist observables are important for understanding the long-range quark-gluon dynamics. Different contributions to the beam SSAs, discussed so far, provide information on different leading and sub-leading parton distribution and fragmentation functions, related both to Collins and Sivers production mechanisms. Higher-twist effects in hard processes arise from the quantum mechanical interference of amplitudes involving different partons in the interacting hadrons. At fixed and moderate values of the four momentum transfer Q^2 and at large values of x and z, the contribution of multiparton correlations or higher twist effects increases, eventually leading to a breakdown of the partonic description. Kinematical dependences of observables, thus, will provide tests of applicability of partonic description.

In CLAS we have measured the kinematic dependences of the π^0 beam-spin asymmetry from x_B, z and P_T. The asymmetry shows a strong enhancement at large values of z while no significant x_B-dependence is present within the measured range. There is also an indication that decrease of

A_{LU} at large P_T, expected from perturbative QCD, starts already at $P_T \sim 0.6$. Observed large BSA for π^0 indicates that major contribution in pion SSAs may be due to the Sivers mechanism. The obtained results provide very significant improvement in statistical errors compared with published HERMES data [17], providing important input for studies of higher twist effects.

The analysis note of this work is under the [CLAS Coll.] review and the publication of the paper is expected soon.

2.1.2 *Lambda Polarization in Semi-Inclusive Deep Inelastic Scattering*

Measurements of Λ polarization in Semi-Inclusive Deep Inelastic Scattering (SIDIS) provide an important probe of the strange sea in the nucleon [18, 19] and may shed light on the proton spin puzzle. The advantage of detecting Λ in the final state lies in the fact that the Λ is self-analyzing and that it can be used as a s quark polarimeter since the polarization of Λ is almost completely determined by polarization of its s quark. Measurements of Λ polarization have been made in deep-inelastic scattering experiments at CERN with $\sim$ 44 GeV ν and $\bar{\nu}$ [20, 21, 22], Fermilab with 470 GeV muons [23] and HERMES with 27.5 GeV positrons [24]. Non-negligible *positive* longitudinal polarization of Λ, measured with respect to the direction of the momentum transfer from the beam, has been observed in the target fragmentation region, $x_F = 2P_\Lambda/W < 0$ (being W the total CM energy and P_Λ is the CM Λ momentum). All these early experiments, however, suffered from a lack of statistics, and the results could not be considered conclusive.

During the reporting period the Frascati group has submitted to the [CLAS Coll.] a proposal to measure the Λ polarizaxion transfer in the $ep \to e\Lambda X$ semi-inclusive reaction using data collected at CLAS with 5.5 GeV beam off an unpolarized hydrogen target 5 cm long. This data set corresponds to an integrated luminosity of $2.1 \times 10^{39}\mathrm{cm}^{-2}$. The average beam polarization, frequently measured with a Møller polarimeter, was $P_B = 0.74 \pm 0.03$.

A preliminary analysis has been carried out showing that the beam spin asymmetry with the two helicities of the incoming electrons can provide a reliable way to extract the Λ polarization, relatively free of acceptance corrections and with small background contributions.

2.2 **Strangeness photoproduction**

An important key in the study of the structure of the nucleon is to understand its spectrum of excited states. Mapping out this spectrum will provide insight into the underlying degrees of freedom of the nucleon. However, due to the non-perturbative nature of QCD at these energies, this task is challenging. Recent symmetric quark model calculations predict more states than have been seen experimentally [25]. Because most of our present knowledge of baryon resonances comes from reactions involving pions in the initial and/or final states, a possible explanation could be that pionic coupling to the intermediate missing N^* or Δ^* states is weak. This suggests a search for these hadronic states in strangeness production reactions. Beyond different coupling constants (e.g. g_{KNY} vs $g_{\pi NN}$), the study of the exclusive production of $K\Lambda$ and $K\Sigma$ final states has the advantage that the higher masses of the kaon and hyperons, compared to their non-strange counterparts, kinematically favor a two-body decays mode for resonances with masses near 2 GeV, a situation that is experimentally advantageous.

The photoproduction data collected for the pentaquark search on a deuteron target (G10 experiment) have been used by the Frascati group to analyze the $\gamma n(p) \rightarrow K^+\Sigma^-(p)$ reaction in the invariant mass range from 1.54 to 2.76 GeV. The analysis has been completed and the differential cross section has been measured for tagged photons in the energy range 1.0-3.6 GeV and at kaon center-of-mass angles between 10^o and 140^o in 10^o step. In this exclusive measurement, K^+ and π^- and n from Σ^- decay (identified calculating the invariant mass of pion and neutron), are detected by CLAS [26] while the spectator proton is identified as missing particle, with the additional cut that the missing momentum should be less than 0.25 GeV/c (the proton doesn't partecipate to the reaction so its momentum is only due to the Fermi motion). After the channel identification and the background subtraction, a Monte Carlo simulation has been used to evaluate the event detection efficiency allowing the extraction of the corrected cross section.

The obtained differential cross section shows a relatively flat angular distribution, likely indicative of a s-channel production mechanism, at energies close to the threshold and up to photon energy of $\sim$ 1.8 GeV. For higher photon energies, instead, a clear forward peak starts to appear and becomes more prominent as the photon energy increases suggesting a strong t-channel photoproduction mechanism. Apart from the first photon energy bin, very close to the energy threshold, the size of these differential cross section is $\sim 1\mu$b sr^{-1} maximum.

The analysis note of this work is under the [CLAS Coll.] review and the publication of the paper is expected soon.

2.3 Single pion photoproduction reactions

The interplay between the nucleonic and partonic pictures of the strong interaction represents one of the major issues in contemporary nuclear physics. Although standard nuclear models are successful in describing the interactions between hadrons at large distances, and QCD accounts well for the quark interactions at short distances, the physics connecting the two regimes remains unclear. In fact, the classical nucleonic description must break down once the probing distances become comparable to those separating the quarks. The challenge is to study this transition region by looking for the onset of some experimentally accessible phenomena naturally predicted by perturbative QCD. Exclusive processes are essential probes to accomplish this aim.

The simplest signature of the partonic picture is the validity of the constituent counting rule (CCR) for high-energy exclusive reactions [27]. CCR predicts the energy dependence of the differential cross section at fixed center-of-mass angle for an exclusive two-body reaction at high energy and large momentum transfer as: $d\sigma/dt = h(\theta_{cm})/s^{n-2}$, where s (total energy in the center-of-mass frame) and t (momentum transfer squared) are the Mandelstam variables and n is the total number of elementary fields in the initial and final states, while $h(\theta_{cm})$ depends on details of the dynamics of the process.

The CCR scaling behavior has been investigate for the first time on the $\gamma n \rightarrow \pi^- p$ from a deuterium target at $\theta_{cm} = 50°, 70°$ and $90°$ [28]. The results at $\theta_{cm} = 70°, 90°$ exibit a global CCR scaling behaviour at the expected transverse momentum ($\sim 1.2\ GeV/c$), and in addition, an enhancement in the scaled differential cross section at $\theta_{cm} = 90°$ below the scaling region, and at center-of-mass energy ranging approximately from 1.8 GeV to 2.5 GeV. Furthermore, the scaled differential cross section drops by a factor of about 4 in a very narrow c.m. energy region (few hundreds of MeV) around 2.5 GeV. This sudden drop in the scaled differential cross section may shed light on the transition between the aforementioned physics pictures.

The aim of studying the $\gamma n \to \pi^- p$ using the G10 data, is to investigate this behavior in much finer photon energy bins and for a wide angular range and to study the angular dependence of the scaling behavior. The differential cross section has been extracted in the angular range between 50° and 115° (in 5° steps) and in the photon energy range between 0.8 and 3.6 GeV (in 50 MeV steps). The obtained results shown in Fig. 1 confirm the previous observation of a broad resonance structure around a center of mass energy of 2.1 GeV at $\theta_{cm}^{\pi^-} = 90°$ in the scaled differential cross section. They also show a center of mass angular dependence of the invariant mass of the observed new resonance structure. The scaling region is reached at backward angles (between 70 and 110 degrees) at transverse momenta of ~ 1.1 GeV/c, while in more forward angles higher photon energies need to reach the scaling region.

In the period covered by this report the paper has been reviewed by the [CLAS Coll.] and submitted to the Physical Review Letter journal.

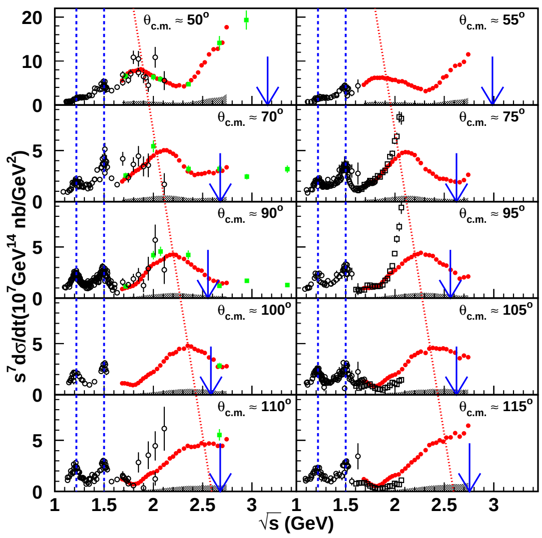

Figure 1: *Scaled differential cross section as a function of $\sqrt{s}$ for $\theta_{c.m.} = 50^0$ to 115^0 (red solid circles data from this experiment). The arrows indicate the location of $\sqrt{s}$ corresponding to a transverse momentum value of 1.1 GeV/c. The green solid squares are results from Ref.* [28]*. The black open circles and open squares are the world data collected from Refs.* [29] *and* [30]*, respectively. The blue dashed lines indicate the known resonances, and the red dotted lines illustrate the angular dependence feature of the broad enhancement structure discussed in the text.*

3 The 12 GeV program

The group will partecipate to the JLab 12 GeV program in Hall B. This requires an upgrade of the CLAS detector, called CLAS12 optimized for studying exclusive and semi-inclusive reactions to investigate the structure of nucleons and nuclei with the CEBAF 12-GeV upgrade. CLAS12 consists of a two-part detector : a forward spectrometer and a Central Detector. The Central Detector is essentially a recoil detector which will detect particles at large angles and lower energies. It consists of three sub-detectors: a Tracker, a Time-of-Flight scintillators array and a Neutron Detector.

During the reporting period the group has worked on the Neutron Detector. The physics motivation for having a neutron detector is to measure Deeply Virtual Compton Scattering (DVCS) on the neutron, with a deuterium target. The interest for this reaction is strong because it is the most sensitive to the Generalized Parton Distribution (GPD) E. The knowledge of the GPDs E and H (accessible through DVCS on the proton) can allow the extraction, via the Ji's sum rule, of the orbital angular momentum of the quarks. The minimal requirement in order to ensure the exclusivity of the nDVCS reaction is to fully detect (PID, angles and energy) the scattered electron and the photon, and to at least identify the neutron and measure its angles θ and ϕ. The electron and the photon will be emitted at small angles, and thus detected in the forward part of CLAS12, while based on GPD simulation, the neutron will be emitted predominantly with $\theta = 60^0$ in the lab frame. Detailed Monte Carlo studies have been undertaken to investigate different options for the construction of a neutron detector. In particular, efficiency, PID (γ/n separation, via TOF), and angular and momentum resolution have been evaluated for a spaghetti calorimeter (scintillating fibers embedded in lead) and a plastic scintillator detector.

Besides this, the group has also started the investigation of the construction of a RICH detector for the forward spectrometer of CLAS12. In the forward spectrometer the particle identification is made using low threshold gas Cerenkov counters (LTCC), high threshold gas Cerenkov counters (HTCC) and Time-of-Fligh scintillator counters. Neverthless, with this configuration in the $2.5 - 4$ GeV/c momentum region, the π/K separation relies only on the LTCC performance. Moreover, in the $4 - 8$ GeV/c momentum region it is not possible to separate protons from kaons. In general, this PID system is well matched to requirements of the main physics program at 12 GeV. However there are some physics measurements of high interest [31, 32, 33] which require a good kaon identification, that cannot be easily accessed without better PID. A RICH detector, to be installed in place of the low threshold Cherenkov counter, will significantly improve the CLAS12 particle identification overcoming the above limitations. A proximity focusing RICH similar to the one operating in Hall A at Jefferson Lab [34], may represent an adequate choice to fulfill our requirements. It will allow us a good separation of $\pi/K/p$ in the $3 - 5$ GeV/c energy region, and, in addition, replacing part or full LTCC will not have any impact on the baseline design of CLAS12.

During the reporting period simulations have been started to determine the best parameters and the main performances of the detector.

4 List of Publications

1. I. G. Aznauryan *et al.* [CLAS Coll.], Phys. Rev. C **78**, 045209 (2008).
2. A. Biselli *et al.* [CLAS Coll.], Phys. Rev. C **78**, 045204 (2008).
3. J. P. Santoro *et al.* [CLAS Coll.], Phys. Rev. C **78**, 025210 (2008).
4. P. Bosted *et al.* [CLAS Coll.], Phys. Rev. C **78**, 015202 (2008).
5. M. H. Wood, *et al.* [CLAS Coll.], Phys. Rev. C **78**, 015201 (2008).

6. R. Nasseripour, *et al.* [CLAS Coll.], Phys. Rev. C **77**, 065208 (2008).

7. F. X. Girod *et al.* [CLAS Coll.], Phys. Rev. Lett. **100**, 162002 (2008).

8. R. De Masi *et al.* [CLAS Coll.], Phys. Rev. C **77**, 042201 (2008).

9. D. G. Ireland *et al.* [CLAS Coll.], Phys. Rev. Lett. **100**, 052001 (2008).

10. K. Park *et al.* [CLAS Coll.], Phys. Rev. C **77**, 015208 (2008).

5 Presentation at Conferences, Workshops, Seminars

1. M. Mirazita, "Le GPDs: nuove distribuzioni partoniche nell'inclusivo", Workshop sulle prospettive di fisica adronica al Jlab - Genova (Italy), February 27-28, 2008.

2. P. Rossi, "Semi-Inclusive Deep Inelastic Scattering (SIDIS) studies @ CLAS and CLAS12", Workshop sulle prospettive di fisica adronica al Jlab - Genova (Italy), February 27-28, 2008.

3. S. Anefalos Pereira, "Measurement of the $\gamma n(p) \to K^+\sigma^-(p)$ at Jefferson Lab", 10th International Workshop on Meson Production, Properties and Interaction (MESON2008), Cracow (Poland), June 6-10, 2008.

4. P. Rossi, "Studies of Single-Spin Asymmetries with CLAS12", Workshop on Transversity Spin Physics, Beijing (China), June 30 - July 4, 2008.

5. M. Mirazita, "Update on the spaghetti-calorimeter studies", CLAS12 European Meeting, Paris (France), July 15-16, 2008.

6. M. Aghasyan, "Single Spin Asymmetries Measurements at CLAS", XCIV Congresso Nazionale Societa' Italiana di Fisica, Genoa (Italy), September 22-26, 2008.

7. S. Anefalos Pereira, "Measurement of the $\gamma n(p) \to K^+\sigma^-(p)$ at Jefferson Lab", XCIV Congresso Nazionale Societa' Italiana di Fisica, Genoa (Italy), September 22-26, 2008.

8. P. Rossi, "Fisica dello spin al JLab: presente e futuro", XCIV Congresso Nazionale Societa' Italiana di Fisica, Genoa (Italy), September 22-26, 2008.

9. M. Aghasyan, "Single Spin Asymmetries Measurements at CLAS", the 18th International Spin Physics Symposium, SPIN 2008, Charlottesville, VA (USA), October 6-10, 2008.

10. P. Rossi, "Deuteron Photodisintegration: experimental overview", International Workshop on High Density Nuclear Physics & QCD, Yerevan (Armenia), October 6-11, 2008.

11. M. Aghasyan, "Single Spin Asymmetries Measurements at CLAS", DNP08 Oakland, CA (USA), October 23-26, 2008.

12. M. Mirazita, "Semi-Inclusive Λ Polarization at CLAS", International Workshop on Strangeness Polarization in Semi-Inclusive and Exclusive Λ production, Trento (Italy), October 27-31, 2008.

References

1. J. Ashman *et al*, Phys. Lett. B **206**, 364 (1988).
2. D. Adams *et al*, Phys. Rev. D **56**, 5330 (1997).
3. K. Abe *et al*, Phys. Rev. D **58**, 112003 (1998).
4. P. Anthony *et al*, Phys. Lett. B **458**, 529 (1999).
5. K. Ackerstaff *et al*, Phys. Lett. B **464**, 123 (1999).
6. A. Airapetian *et al*, Phys. Rev. D **71**, 012003 (2005).
7. R. Fatemi *et al*, Phys. Rev. Lett. **91**, 222002 (2003).
8. D. W. Sivers, Phys. Rev. D **43**, 261 (1991).
9. M. Anselmino and F. Murgia, Phys. Lett. B **442**, 470 (1998).
10. S.J. Brodsky, D.S. Hwang, and I. Schmidt, Phys. Lett. B **530**, 99 (2002).
11. J.C. Collins, Phys. Lett. B **536**, 43 (2002).
12. X.D. Ji and F. Yuan, Phys. Lett. B **543**, 66 (2002).
13. P.J. Mulders and R.D. Tangerman, Nucl. Phys. B **461**, 197 (1996).
14. A. Bacchetta *et al.*, Phys. Rev. D **70**, 117504 (2004).
15. A. Afanasev and C.E. Carlson, (2003), arXiv:hep-ph/0308163.
16. F. Yuan, Phys. Lett. B **589**, 28 (2004).
17. A. Airapetian *et al.* [HERMES Coll.], arXiv:hep-ex/0612059.
18. J. Ellis, D. E. Kharzeev and A. Kotzinian, Z. Phys. C **69**, 467 (1996).
19. W. Melnitchouk and A. W. Thomas, Z. Phys. A**353**, 311 (1996).
20. P. Astier *et al.*, [NOMAD Coll.], Nucl. Phys. B **588**, 3 (2000);
    D. V. Naumov [NOMAD Coll.], AIP Conf. Proc. **570**, 489 (2001); arXiv:hep-ph/0101325.
21. S. Willocq et al, [WA59 Coll.], Z. Phys. C **53**, 207 (1992).
22. V. Ammosov et al, Nucl. Phys. B **162**, 208 (1980).
23. M. R. Adams *et al.* [E665 Coll.], Eur. Phys. J. C **17**, 263 (2000).
24. A. Airapetian *et al.* [HERMES Coll.], Phys. Rev. D **64**, 112005 (2001); S. Belostotski, IXth Workshop on High-Energy Spin Physics, Dubna, Russia, Aug 2 - 7, 2001.
25. S. Capstick and W. Roberts, Phys. Rev. D **58**, 74011 (1998).

26. B. Mecking et al., Nucl. Inst. & Meth. A **503/3**, 513 (2003).

27. S.J. Brodsky and G.R. Farrar, Phys. Rev. Lett. **31**, 1153 (1973); Phys. Rev. D **11**, 1309 (1975); V. Matveev *et al.*, Nuovo Cimento Lett. **7**, 719 (1973).

28. L. Y. Zhu *et al.*, Phys. Rev. Lett. **91**, 022003 (2003); L. Y. Zhu *et al.* Phys Rev. C **71**, 044603 (2005).

29. R.L. Anderson *et al.*, Phys. Rev. D **14**, 679 (1976);
the GWU CNS Database: *http://gwdac.phys.gwu.edu/analysis/pr_analysis.html*

30. H.J. Besch *et al.*, Z. Phys. C **16**, 1 (1982).

31. PR-09-008 "Studies of the Boer-Mulders Asymmetry in Koan Electroproduction with Hydrogen and Deuterium Targets";
http://www.jlab.org/exp_prog/PACpage/PAC34/agenda.pdf.

32. PR-09-009 "Studies of Spin-Orbit Correlations in Kaon Electroproduction in DIS with polarized hydrogen and deuterium Targets";
http://www.jlab.org/exp_prog/PACpage/PAC34/agenda.pdf.

33. PR-09-007 "Studies of partonic distributions using semi-inclusive production of kaons";
http://www.jlab.org/exp_prog/PACpage/PAC34/agenda.pdf.

34. F. Garibaldi *et al.*., Nucl. Inst. & Meth. A **502**, 117 (2003); M. Iodice *et al.*, Nucl. Inst. & Meth. A **553**, 231 (2005).

ALICE

N. Bianchi (Resp.), G.P. Capitani, A. Casanova (Ass.), G. Conesa (Ass.),
L. Cunqueiro (Ass.), P. Di Nezza, A. Fantoni, D. Hasch (Art. 23), V. Muccifora,
A. Orlandi (Tecn.), W. Pesci (Tecn.), F. Ronchetti (Ass.),
A.R. Reolon, R. Vieira (Laur.), A. Viticchié (Tecn.)

1 Introduction

ALICE is an experiment at CERN which involves about 1000 physicists from more than 100 Institutions from several Countries. Italy participates with 12 groups and more than 150 physicists. The Frascati group is participating to the electromagnetic calorimeter project (EMCal), which will complete the ALICE detector capabilities for measuring the entire range of physics observables in heavy ion interactions. Jet quenching, the interaction of energetic partons with dense matter, has been shown at RHIC to provide a broad range of unique and sensitive probes of the hot QCD medium. Jet quenching will play an important role in the LHC heavy ion physics program. The EMCal enables ALICE to explore the physics of jet quenching in detail, over the large kinematic range provided by the LHC. The EMCal will provide fast triggers (level 0 and 1) for photons, electrons, and jets. The EMCal also measures the neutral energy component of jets, enabling full jet reconstruction in all collision systems, from proton.proton to Pb.Pb. The combination of the EMCal, the excellent ALICE charged tracking capabilities, and the modest ALICE magnetic field strength, is a preferred configuration for jet reconstruction in the high background environment of heavy ion collisions, allowing detailed optimization of background rejection while preserving the crucial jet quenching signals at moderate transverse momentum.

2 The EMCal Project

The EMCal is a large Pb-scintillator sampling calorimeter with cylindrical geometry, located adjacent to the ALICE magnet coil at a radius of ~ 4.5 meters from the beam line. Its coverage in phase space is $-0.7 < \eta < 0.7$ and $\Delta\phi = 107°$, positioned approximately opposite in azimuth to the high precision but low acceptance ALICE Photon Spectrometer (PHOS) calorimeter.

The EMCal is segmented into 12672 projective towers. The chosen technology is a layered Pb-scintillator sampling calorimeter with a longitudinal pitch of 1.44 mm Pb and 1.76 mm scintillator. Wavelength shifting readout fibers are configured in a Shashlik geometry and are coupled to an Avalanche Photodiode (APD) sensor. The EMCal is composed by 11 Super Modules which represent the basic structural unit of the detector. Each full size super module is assembled from 12x24=288 modules arranged in 24 strip modules 12x1 modules each. Each module contains a 2x2=4 independent towers built up from 76 alternating layers of 1.44 mm Pb (Pure Pb-standard mill spec.) and 77 layers of 1.76 mm polystyrene base, injection molded scintillator (BASF143E + 1.5%pTP + 0.04%POPOP) with an intrinsic light output of 50% Anthracene. White, acid free, bond paper serves as a diffuse reflector on the scintillator surfaces and, in addition, provides the required degree of static friction between the calorimeter layers. The scintillator edges are treated with a TiO_2 loaded reflector to improve the transverse optical uniformity within a single tower. All modules in the calorimeter are mechanically and dimensionally identical. The front face dimensions of the towers are 6x6 cm^2 resulting in individual tower acceptance of $\Delta\eta x\Delta\phi \sim 0.014x0.014$.

The Pb-scintillator stack in a module is secured in place by the static friction between individual layers under the load of an internal pressure of 1.5kg/cm^2. The module is closed by a skin of 150 μm thick stainless steel on all four transverse surfaces. Flanges are welded to the ends of the stainless steel skin (straps) to permit secure attachment to the front and rear plates of the module. This thin stainless skin plus the optical treatment of the scintillator edges is the only inert material between the active tower volumes. The internal pressure in the module is stabilized against thermal effects, mechanical relaxation and long term flow of the Pb and/or polystyrene by a customized array of 5 non-linear spring sets (Belleville washers) per module. In this way, each module is a self supporting unit with a stable mechanical lifetime of more than 20 years with a large safety factor on the final compressing force. This compressed module design allows the detector to be completely supported from its rear surface.

3 Experimental activity of the LNF group in 2008

3.1 Module Production

The EMCal modules massive assembly at LNF is carried on using two production lines where the assembly takes place with very high mechanical accuracy. Each line is composed by a stacking fixture and two kits of pressure sensors used to apply and measure the internal load of the modules. Each module is of trapezoidal shape (required by the ALICE tapered geometry) with an overall tapering angle in the η direction of 1.5 deg.

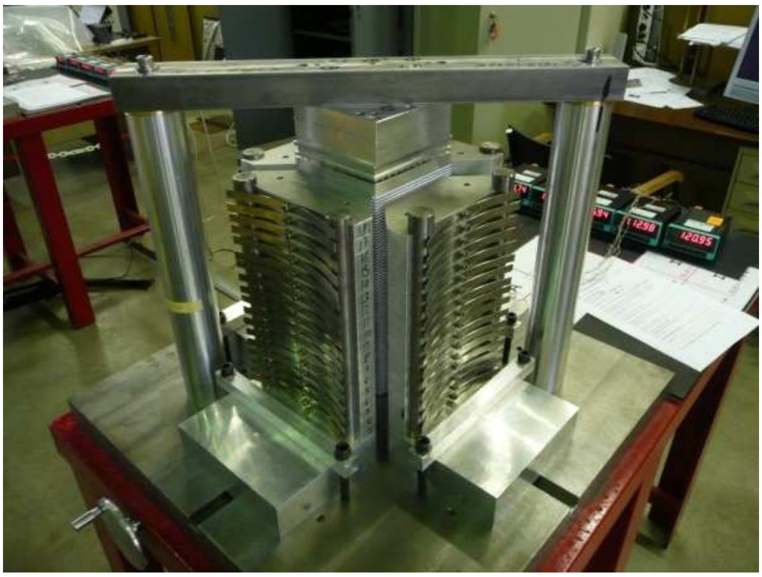

Figure 1: *Stacking fixture for EMCal modules.*

In order to guarantee the module mechanical stability the lead-scintillator sandwich is closed into containing structure made of two aluminum plates (so called front and back plates) connected by stainless steel foils (straps) kept under tension by the Bellville washers resident into the module itself. All the lead and scintillator tiles composing the sandwich have a square matrix of trough holes to allow the WLS fibers to run inside the module.

Each line has a regime production cycle of 1 module/day. A newly produced module goes through a pre compression phase (high load $\sim$ 550 kgf) to flatten out the sandwich components (lead tiles). The module then is finalized by applying a layer of black sticker on its sides for light insulation. The four stainless steel lateral straps are then installed to maintain the module internal nominal load at 200 kgf overall once it will leave the fixture. At this point the pressurized modules are kept into a temperature controlled environment which reproduces the conditions of the ALICE cavern (21 C).

In this environment, WLS fibers are inserted into the four optically isolated elements of the modules (towers). Each tower is read out by a bundle of 36 fibers which run inside the module and ends with a terminator for the coupling with the optoelectronic chain (light guide + APD + CSP package). Each module is also provided with a white paper diffuser placed at the center of the 4 towers to allow for gain monitoring of the APDs. In Frascati, a total of 146 modules have been produced in 2008 (1/2 of the first EU SuperModule)

Figure 2: *Modules aligned and ready for the StripModule making. The LED light diffuser is visible at the center of the installed fiber bundles that run into the module depth. The M5 studs are also visible and ready to be locked into the StrongBack.*

3.2 Strip module production

Sets of 12 modules are aligned and blocked along the non tapered sides using a flat pinned iron plane in order to form the so called StripModule units. The mechanical stability of the unit is given by the insertion of an aluminum back cover (StrongBack) on the top of the aligned modules fixed to the modules by 48 M5 studs (4 per module). The contact lines between the StrongBack and the module plates are sealed with black silicon to ensure light insulation. The StrongBack has 48 through trough holes allowing for the fiber terminators to stand out from the cover. On the standing fiber terminators the light guide + APD + Charge Sensitive Preamplifier packages are installed using of plastic manifolds. The cover has also 12, 6-mm large, through holes opened in correspondence of the position of the light diffuser in the center of each module. A set of 12 fibers is installed into these holes, combed and fixed to the StrongBack using silicon spots. The fiber terminator is accessible once the StrongBack is closed in order to allow the fibers excitation with a LED driver for gain monitoring purposes. In 2008, a total of 12 StripModules have been produced at the LNF.

Figure 3: *StripModule unit with the light guides + APD packages mounted and cabled into the readout cards (T-cards) and the LED driver fibers installed.*

3.3 Fiber Polishing and aluminization

The LNF group provides fiber bundles for the optical readout for all the EMCal SuperModules assembled in Europe. The fibers are bundled in groups of roughly 300, cut, ice-polished and aluminized (using a thin film deposition sputtering chamber built for this purpose) at one end to maximize light collection since the readout happens only on one side of the fiber. The processed fibers are then re-bundled in groups of 36, glued and polished to allow the insertion into the EMCAL modules. In 2008 about 1200 bundles (1 bundle = 36 fibers of length 37mm) have been produced and installed into the first EU EMCal SuperModule. Each fiber bundle, to be inserted by the operator, is built of two sub bundles to match the different path lengths between central and peripheral fibers in the towers.

4 EMCal beam test at CERN

During a period of five weeks in autumn 2007 the first ALICE EMCal modules constructed according to final design were tested in the CERN SPS (H6 beam line with energy range 5-100 GeV) and PS (T10 beam line with energy range 0.5-6.5 GeV). The test utilized a stacked 4×4 array of EMCal modules (8×8 towers). All towers were instrumented with the full electronics chain with shapers and APD gains operated as planned in ALICE. A LED calibration system was installed in order to monitor time-dependent gain changes. The readout of the front end electronics used the full ALICE DAQ readout chain. The goals of the test beam measurements were:

- To determine the intrinsic energy resolution and the position resolution using electron beams.
- To investigate the linearity and uniformity of the response; in particular across towers and module boundaries and for tilted or recessed modules.
- To determine the light yield (signal) per unit of deposited electromagnetic energy.
- To study the effect of shorter shaping times as planned for the final design.
- To study the energy dependence of the response to electrons and hadrons to determine the particle identification capabilities of the EMCal by shower shape analysis.
- To develop and investigate the performance of monitoring and calibration tools (gain stability, time dependencies) using electron beams, MIPs from hadron beams, and LED events.
- To develop and test ALICE standard software for readout, calibration, and analysis.

In order to reach the design EMCal energy resolution for high energy electromagnetic showers, a tower-by-tower relative energy calibration of about 1% has to be obtained and maintained in the offline analysis. In addition, since analog tower energy sums provide the basis of the L0 and L1 high energy shower trigger input to the ALICE trigger decision, the EMCal should operate with APD gains adjusted to match online relative tower energy calibrations to better than about 5%.

Figure 4: *From the left: sputtering chamber in operation. Middle: Aluminized fibers. Right: Bundles of 36 fibers (16 inner + 20 outer) in the gluing fixture.*

A LED calibration system has been successfully tested to track and adjust for the temperature dependence of the APD gains during operation. The LED triggers where collected for all the towers in parallel with the beam particle events. The variation of the LED signal amplitude with time and temperature was studied in order to test the system for calibration purposes. The temperature coefficients obtained from the correlation of the LED peak amplitude with the measured temperature were used to correct for the time dependence of the APD gain. An overall inter-calibration procedure was carried out for all towers by normalizing the hadron MIP amplitudes in each tower, to one of the central towers. An alternative inter-calibration map was also considered by using the information given by the electron beam peak in each tower. An absolute calibration for each tower was obtained by comparing the nominal electron beam energy with the corresponding peak in the energy spectrum, as obtained by a sum over a 3×3 tower cluster.

An important goal of the test beam measurements was to extract the average light yield. This quantity determines the overall APD+shaper gain required to match the desired dynamic range in ALICE to that of the input signal to the digitization ALTRO chip. Due to the large number of individual towers planned for the final design of the EMCal, it is also important to estimate the tower-to-tower dispersion of the light yield. As a preliminary result, the average light yield was found to be (4.3 ± 1.4) photoelectrons/MeV.

By combining data taken at the CERN-PS and SPS a wide energy range of 0.5 GeV to 100 GeV has been explored. No systematic variation of the resolution depending on the position was observed. The resolution obtained at the different positions was combined and the average values as a function of the incident beam momentum are displayed in Fig. 5. For the SPS data, the momentum spread of the incident beam of typically 1.3% was subtracted in quadrature. A fit to

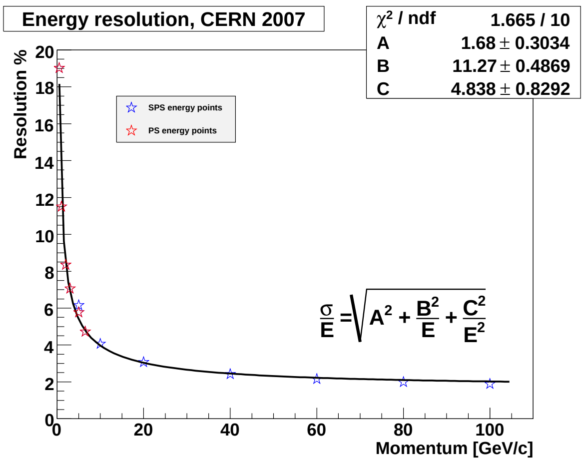

Figure 5: *Energy resolution for electrons as function of the incident beam momentum. The beam energy spread was subtracted from the measured result.*

the energy resolution as function of the incident energy is also shown in Fig. 5. The fit is made with the conventional constant, $\sqrt{E}$, and linear E terms, added in quadrature. The results on resolution are in agreement with the requirements needed for the EMCal physics.

The linearity of the energy response was also investigated and a very good linearity is observed, despite possible deviations from unity for the ratio of measured to incident beam energy were expected at high energies due to leakage. Only at very low energies (below 5 GeV), due to threshold effects the reconstructed energy is systematically lower than the incident one. A very good uniformity of the energy response of different modules was found with a RMS better than 1 GeV, for 80 GeV incoming electrons. Ongoing analysis are investigating the position resolution as well as the response of the EMCal to hadrons by shower shape studies.

5 Offline

5.1 Prompt photons

We studied the capability of the EMCal to measure direct prompt photons. A full simulation of proton-proton collisions at 14 TeV and PbPb collisions, quenched, at 5.5 ATeV was made with full material transport in the detectors of ALICE. Events with prompt photons and with high energy π^0, main background source of photons in the event, were generated. The combination of shower shape analysis in EMCal and isolation cuts combining EMCal and tracking detectors shows that we will able to measure the prompt photon spectrum with low contamination level for energies of the prompt photon larger than 15-20 GeV, with good statistics up to 100 GeV in a standard year of data taking, in both pp and Pb-Pb collisions at LHC. PYTHIA generator predicts the production of fragmentation photons, a priori background for prompt photon studies. The analysis shows that fragmentation photons are isolated like the prompt photons only when they carry most of the jet energy. Moreover, if we isolate charged hadrons like pions, we will select pions which will be a jet themselves. In fact, the correlation of isolated fragmentation photons and charged pions with their opposite jets showed the same behavior as the correlation for prompt photons. This result suggests another way to calibrate jets or calculate the jet fragmentation function without having to reconstruct the jet with standard jet algorithms, what right now would be only possible with g-jet events. More detailed studies are needed with full detector reconstruction or other generators.

5.2 Jet quenching

Jet quenching is usually explained by a modification of the partonic radiative energy loss in the dense medium. A Monte Carlo simulator, to consider the QCD branching process in the final state with full energy and momentum conservation, has been developed in Frascati. In spite of the fact that a probabilistic interpretation of radiation in a medium requires phenomenological assumptions, the practical advantages of a Monte Carlo are numerous. First, it allows the access to other observables different from the limited single inclusive measurements, such as different jet shapes, jet multiplicities, multi-particle intra-jet correlations etc. Moreover, such an implementation makes it possible to explore new physical mechanisms in jet development, such as the interplay of the multi-gluon radiation with the medium length, effects of the color flow and reconnections, effects of recoil with the medium, etc. QPYTHIA is a Monte Carlo with medium modified final state radiation, where medium effects enter as an additive correction to the standard, vacuum splitting functions. In our approach, the inelastic energy loss and the angular broadening of the shower are dynamically related through a single parameter, the transport coefficient $\hat{q}$. The longitudinal evolution of the shower is implemented by considering the formation time of the radiated gluons.

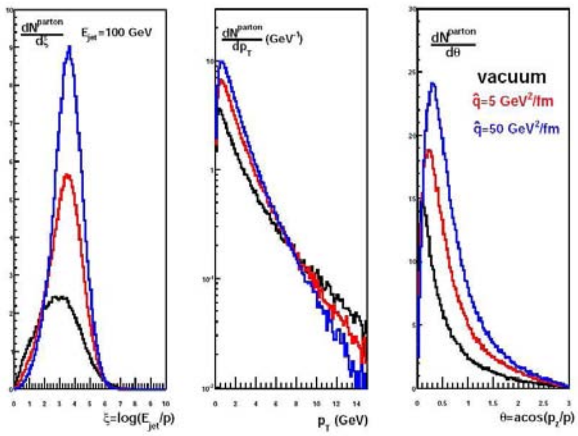

Figure 6: *QPYTHIA prediction for a jet of initial energy of 100 GeV and for different transport coefficients, namely the suppression/enhancement of high/low energy particles (left) , the broadening of the jet transverse momentum with respect to the jet axis and the suppression of high pT particles (middle) as well as the broadening on the jet polar angle (right).*

5.3 Software code Development

The analysis presented above needs large amount of data to produce significant results, not only with real data but also with simulations. An analysis frame adapted to run on the GRID (where real data and simulation will be stored) and to perform analysis with the calorimeters information combining them with the tracking system has been evolving along 2008 and will continue evolving. The code developed has been released to be fully available for the ALICE collaboration. EMCAL calorimeter simulation and reconstruction code has also been modified to match the last decisions about the hardware and the electronics.

6 Conferences and Papers in 2008

6.1 Conference Talks

1. G. Conesa, "High pT direct photon measurement and correlations with hadron-jet in ALICE", ALICE Physics Week, Prague, 4-7 March 2008.
2. G. Conesa, "High pT direct photon measurement and correlation with hadrons and jets in ALICE", Workshop on High pT Physics at LHC, Tokaj, 16-19 March 2008.
3. G. Conesa, "Measurement of hard probes in heavy ion collisions at LHC with ALICE: Jets and photons", Workshop on Strings and Strong Interactions, 18-19 September 2008.
4. G. Conesa, "Review on direct photon measurement and jet correlations with EMCal", IV Convegno Nazionale sulla Fisica di ALICE, Palau 28-30 September 2008.
5. L. Cunqueiro, "A MonteCarlo for jet quenching: medium studies in ALICE", IV Convegno Nazionale sulla Fisica di ALICE, Palau 28-30 September 2008.

6. L. Cunqueiro, "Jets in heavy ion collisions", Seminars at USP and at CPCTR, Brasil, 16-19 December 2009.
7. V. Muccifora, "Accessing characteristics for hadronization from nuclear attenuation", Workshop on Parton Fragmentation in Vacuum and in Medium, ECT* Trento, 25-29 February 2008.
8. F. Ronchetti, "The ALICE Electromagnetic Calorimeter Project", XLVI Winter Meeting, Bormio, 21-26 January 2008.
9. F. Ronchetti, "The ALICE Electromagnetic Calorimeter Project", XIII International Conference on Calorimetry in HEP, Pavia, 26-30 May 2008.
10. V. Muccifora (Organizer) Workshop on Nuclear Medium effect on the quark and gluon structure of the Hadrons, ECT* Trento, 3-7 June 2008.

6.2 Publications

1. ALICE Coll., JINST **0803**, S08002 (2008).
2. ALICE Coll., ALICE Electromagnetic Calorimeter TDR, CERN-LHCC-2008-014.
3. G. Conesa *et al.*, Eur. Phys. J. C **613**, 57 (2008).
4. L. Cunqueiro *et al.*, Eur. Phys. J. C **53**, 585 (2008).
5. L. Cunqueiro *et al.*, JHEP **02**, 048 (2008).
6. L. Cunqueiro *et al.*, arXiv: 0809.4433.
7. V. Muccifora *et al.*, "Parton Propagation in QCD matter", Il Nuovo Cimento, submitted.
8. V. Muccifora *et al.*, arXiv:0804.2021.

FINUDA

L. Benussi (Art. 23), M. Bertani (Resp.), S. Bianco, M. A. Caponero (Ass.), F. L. Fabbri (Ass.)
P. Gianotti, M. Giardoni, V. Lucherini (Resp. Naz.), E. Pace, M. Pallotta (Ass.), A.R. Reolon,
S. Tomassini, L. Passamonti (Tecn.), D. Pierluigi (Tecn.), F. Pompili (Art. 23), A. Russo (Tecn.)

1 Introduction

FINUDA is the experiment devoted to hypernuclear physics studies at DAΦNE. Hypernuclei are nuclear systems in which one or more nucleons are replaced by a hyperon. This feature adds explicit strangeness to the nuclear system allowing to study, in a more general environment, the baryon-baryon interaction. FINUDA produces hypernuclei via the reaction:

$$K^- + ^A Z \rightarrow ^A_\Lambda Z + \pi^- \quad (1)$$

stopping K^- from $\phi(1020)$ decay almost at rest into thin ($\sim$ 0.2 g cm^{-2}) nuclear targets. The spectroscopy of the hypernuclear levels produced is performed by measuring the momentum of the outgoing π^-. The products of the sub-sequent decay of the Λ bound to the nucleus can be detected by FINUDA, allowing to investigate simultaneously the decay mechanisms of hypernuclei.

The hypernuclear research program includes also Neutron-rich hypernuclei, systems with a large N/Z ratio, which could give more information on baryon-baryon interaction, and on the importance of the ΛNN force related to the "coherent $\Lambda - \Sigma$ coupling" in connection with nuclear astrophysics implications [1]. The unique combination of the clean K^- source (DAΦNE) and the very transparent and complete detector optimized for the study of the interactions of Kaons in thin nuclear targets (FINUDA) has allowed the study of new items, not foreseen in the original proposal, such as a study of the ^{7}Li(K$^+$, K^0) reaction close to threshold [2] and topics related to the possible existence of Deeply Bound Kaon States (DBKS). The interest in such an item was triggered by a theoretical suggestion by Akaishi and Yamazaki [3] about possible aggregates of few nucleons strongly bound by a K^- and with a narrow width. These systems should have a density even ten times larger than the usual nuclear matter one, with a potential great impact on the comprehension of the origin and structure of the neutron stars.

The FINUDA Collaboration consists of about 60 physicists coming from LNF, several INFN sections and Italian universities (Bari, Brescia, Pavia, Torino, Trieste) plus foreign researchers from Canada, the University of Victoria, Vancouver; from Japan, the KEK laboratory of Tsukuba, RIKEN and the University ok Tokyo; from South Korea, the Seoul National University, from Russia, the Joint Institute for Nuclear Research of Dubna and from Iran, the S. Beheshty University of Teheran.

2 FINUDA Activity in 2008

The main effort of the LNF FINUDA group in 2008 has been devoted to the analysis of the whole set of data corresponding to a total integrated luminosity of about 1.2 fb^{-1} and to the preparation of a proposal for a new data taking at DAΦNE [4].

Lets recall that in the first (engineering+data) data taking (December 2003-March 2004), a total of 220 pb^{-1} (190 for physics) were collected with a set of eight targets: 2 ^{6}Li, ^{7}Li, 3 ^{12}C, ^{27}Al and ^{51}V. No measurements on medium A targets were performed before and FINUDA showed that reaction (1) has a reasonable capture rate for p-shell nuclei only, and the analysis was focused mostly on light Hypernuclei.

The targets installed for the 2006-2007 data taking were: 2 ^{6}Li, 2 ^{7}Li, 2 ^{9}Be, D_2O, ^{13}C, and 966 pb^{-1} were collected.

3 Study of the Hypernuclear Weak Decay

A Λ-hupernucleus normally decays electromagnetically to its ground state before undergoing a weak decay to an ordinary nucleus. The dominant decay modes of a bound Λ-hypernucleus are the following:

- Mesonic Weak Decay (MWD) in which the Λ decays as in free space:
  $\Lambda \to p + \pi^-$ or $\Lambda \to n + \pi^0$. Due to the empirical $\Delta I = 1/2$ rule in the strangeness-changing non-leptonic weak decay, in the free space the branching fraction of $\Lambda \to p + \pi^-$ decay is approximately twice larger than that of $\Lambda \to n + \pi^0$. But in the nuclear matter the decay of the Λ may not follow the same rule. Moreover, the final state nucleon produced in the MWD has a very low momentum (< 100MeV/c), therefore the process is Pauli-blocked (the Fermi momentum for a nucleon is 270 MeV/c) and much suppressed in all but the lightest nuclei. The primary decay channel therefore would be the following:

- Non-Mesonic Weak Decay(NMWD) which takes place through the interaction of the Λ with neighboring nucleons: $\Lambda + p \to n + p$ or $\Lambda + n \to n + n$. The momentum of the outgoing nucleons is 417 MeV/c and the decay has much larger phase space compared to the MWD and is not Pauli-blocked.

  Another non-mesonic channel is the so called “two-nucleon-induced-decay“ $\Lambda NN \to NNN$ which has not been experimentally established yet.

The hypernuclear NMWD is the most spectacular example of nuclear medium modification and it gives information on the four baryon weak process $\Lambda N \to NN$, with possible hints also on the ΛNN interaction. Nevertheless the process of NMWD of hypernuclei has been scarcely studied on the experimental side for a few decades due to experimental difficulties.

FINUDA is suited to perform high resolution spectroscopy of the emitted charged particles: 260-280 MeV/c π^-'s for production of the ground state, π^-'s from MWD with momentum lower than 130 MeV/c, protons from NMWD with momentum lower than 600 MeV/c. FINUDA has measured MWD and NMWD for p-shell Λ-hypernuclei formed in the ^{6}Li, ^{7}Li, ^{9}Be, ^{12}C, ^{13}C and D_2O targets.

3.1 Mesonic Weak Decays

MWD was studied in events in which a high momentum π^-, tagging the formation of ground or low lying excited states, was detected in coincidence with a low momentum π^-. MWD of $^{7}_{\Lambda}$Li,

$^9{}_\Lambda$Be, $^{11}{}_\Lambda$B (from ^{12}C targets), and $^{15}{}_\Lambda$N (from ^{16}O targets) has been investigated.

The π^- momentum resolution is $\Delta p/p \simeq$1% FWHM at 270 MeV/c and $\simeq$6% FWHM at 110 MeV/c. The acceptance function for low momentum π^-'s was evaluated with simulated tracks. Background from quasi-free Λ production and decay was simulated and subtracted from the $^1 1_\Lambda$B and $^{15}_{\Lambda}$ N spectra.

Kinetic energy spectra were evaluated and compared with theoretical predictions of decay strength functions [5] and a good agreement is found. Decay rates and decay amplitudes were calculated, using, for each hypernucleus, known $\Gamma_{tot}/\Gamma_\Lambda$ or a linear fit to the measured value from the available A=4-12 Λ-hypernuclei. Fig.1 shows the FINUDA results on the $\Gamma_{\pi^-}/\Gamma_\Lambda$ as a function of A compared with previous data [6, 7] and with theoretical calculations [5].

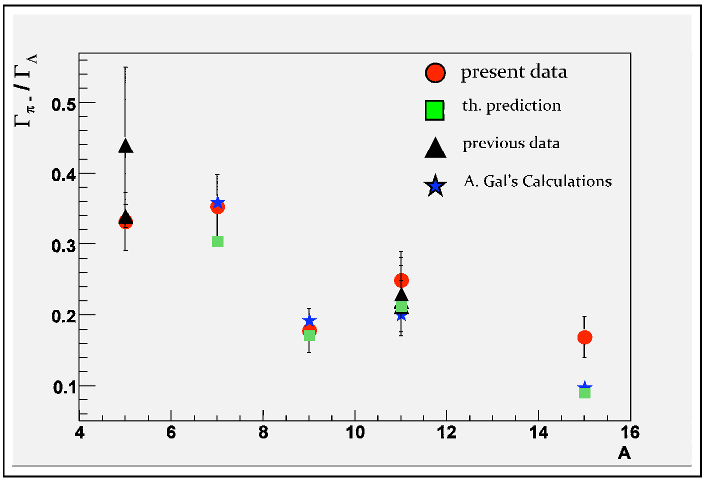

Figure 1: *FINUDA measurements of* $\Gamma_{\pi^-}/\Gamma_\Lambda$ *as a function of A, compared with existing data and theoretical calculations.*

3.2 Non Mesonic Weak Decays

NMWD was studied [8, 9] by selecting events with a π^- from the hypernucleus formation in coincidence with a proton from its decay. Kinetic energy spectra of the decaying protons were obtained featuring a detector threshold as low as 15 MeV, and a resolution $\Delta T/T \simeq 1.5\%$ FWHM at 80 MeV. The background due to the absorbtion of K^- on a (np) cluster of the target nucleus was simulated and subtracted, as described in [8]. Acceptance corrections were applied. All the spectra, shown in Fig2, show a similar shape, *i.e.* a peak around 80 MeV, corresponding to about half the Q-value for the free $\Lambda p \to np$ weak reaction, with a low energy rise due to the final state interactions (FSI) and/or to the "two nucleon induced weak decays" (Λnp). FINUDA estimates [9] a contribution due to (Λnp) as large as 40% to the spectra.

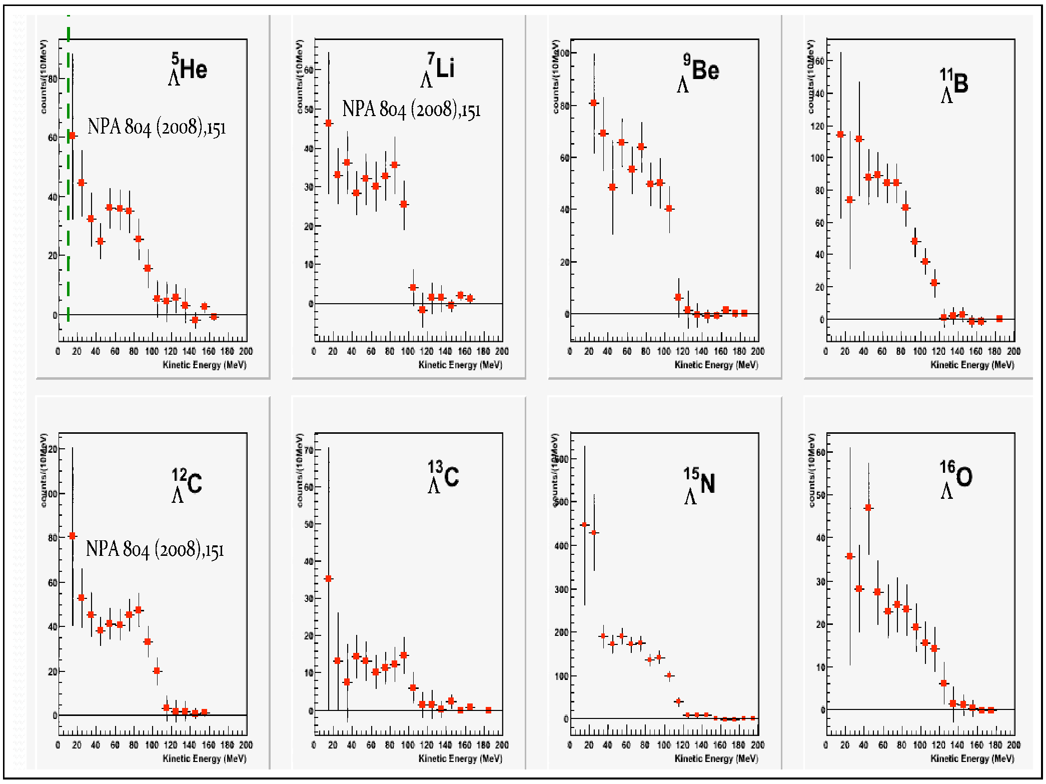

Figure 2: *Proton energy spectra from hypernuclaes NMWD after background subtraction.*

4 Nuclear bound kaonic systems

The detector characteristics have turned out to be excellent to give clear results on a topic that has became of extreme interest in the last years. In fact, the existence of kaon-nucleon bound systems is highly debated. The main features of $\bar{K}N$ and $\bar{K}A$ interactions don't foresee clearly detectable levels since the expected binding energies are around 10-30 MeV, and the widths of 80-100 MeV exclude the possibility of an experimental observation. Nevertheless, a different approach of recent theoretical works by Akaishi and Yamazaki [3)] shows the possibility that $\bar{K}N$ interaction, under certain conditions, could became strongly attractive allowing the formation of kaon-multinucleon systems with a binding energy varying from 86 MeV to 113 MeV, depending on the target nucleus, and with widths of 20-40 MeV. These Authors also suggest that the presence of a K^- inside the nucleus should enhance the binding energy of the system increasing the density several times that of the ordinary nuclei. These aggregates should be formed with higher probabilities when the kaon interacts with light nuclei.

The first paper published by FINUDA on the evidence of a Deeply Bound K$^-$-Nuclear States observed in the (K^-pp) system [10)] presented the first observations in agreement wih Akaishi-Yamazaki model, but in the following years several criticisms raised [12)] in that it was claimed that the data could be simply explained by FSI effects. A way to disprove this interpretation would be the observation of the same signal in different targets, where the FSI effect should act differently, more sizeably in heavier nuclear media, but the results on the new data are in agreement with the first result. The problem has also been attacked in a different way (resorting to inclusive spectra), in order to cross-check possible biasing effects and the results are still in agreement with the first statement that the signal on Λp events is generated by a kaon-nuclear bound system.

4.1 K^--multinucleon absorption

In the FINUDA paper [14] the invariant mass spectrum of the (Λd) system following the capture of K^-_{stop} in ^{6}Li was shown. The presence of such a system produced in light nuclei would be a nice confirmation of a genuine bond, since in this case the FSI contribution should be largely reduced as compared to systems decaying in nucleons.

Thanks to the excellent (dE/dx) particle identification in FINUDA, it has been possible to clearly detect tritons. Correlated Λt pairs [11] from K^-_{stop}A absorption reaction in light nuclei ^{6,7}Li and ^{9}Be have been found. Regardless of A, the Λt pairs are preferentially emitted in opposite directions. Reaction modeling predominantly assigns to the $K^-_{stop}A \rightarrow$ Λt (N)A' direct reactions the emission of the Λt pairs whose yeald is found to range from 10^{-3} to $10^{-4}/K^-_{stop}$.

5 Activity planned for 2009

The Collaboration has presented a proposal [4] to re-install the apparatus in IP of DAΦNE in order to take additional data up to 3 fb^{-1} in order to clarify many interesting aspect both in hypernuclear physics and in the kaon-nucleons absorbtion mechanisms. The time-window proposed by FINUDA is after the actual SIDDARTHA run and before KLOE roll-in but the LNF Scientific committee did not recommend the installation of FINUDA after the completion of SIDDARTHA but recommended indeed the prompt installation of KLOE (36° meeting of the committee). Therefore the main plan of the group for the year 2009 is to complete the analysis of the data both in the hypernuclear sector and in the study of nuclear bound states.

6 List of 2008 FINUDA publications

1. M. Agnello *et al.*, Nucl. Phys. A **804**, 151-161 (2008).
2. M. Agnello *et al.*, "Mesonic and Non-Mesonic Weak Decay of Hypernuclei with FINUDA", Proc Int. Conf. PANIC 2008 (2008).
3. M. Agnello *et al.*, Phys. Lett. B **669**, 229-234 (2008).
4. FINUDA Coll., "Proposal for a new FINUDA Data taking", February 2008.

7 List of Conference Talks

V. Lucherini, "Recent results from FINUDA", Sendai International Symposium on Strangeness in Nuclear and Hadronic Systems, Sendai, 15-18 Dicembre 2008.

References

1. Y. Yamamoto *et al.*, Nucl. Phys. A **691**, 432c (2001).
2. M. Agnello *et al.*, Phys. Lett. B **649**, 25 (2007); M. Agnello *et al.*,“ Study of the (K^+,K^0) reaction on medium light nuclei close to threshold”, Frascati Physics Series Vol. XLVI (2007);
3. Y. Akaishi, T. Yamazaki, Phys. Rev. C **65**, 044005 (2002); T. Yamazaki and Y. Akaishi, Nucl. Phys. B **535**, 70 (2002); Y. Akaishi *et al.*, arXiv:nucl-th/0501040.
4. FINUDA Coll., “Proposal for a new FINUDA Data taking”, February 2008;
5. T. Motoba and K. Itonaga, Progr. Theor. Phys. Suppl. **117**, 477 (1994).
6. S. Kameokada *et al.*, Nucl. Phys. A **754**, 173c (2005).
7. Y. Sato *et al.*, Phys Rev. C **71**,025203 (2005).
8. M. Agnello *et al.*, Nucl. Phys. A **804**, 151-161 (2008).
9. M. Agnello *et al.*,“Mesonic and Non-Mesonic Weak Decay of Hypernuclei with FINUDA”, Proc. Int. Conf. PANIC 2008, (2008).
10. M. Agnello *et al.*, Nucl. Phys A **775**, 35 (2006).
11. M. Agnello *et al.*, Phys. Lett. B **669**, 229-234 (2008).
12. V. Magas *et al.*, Phys. Rev. C **74**, 0205206 (2006).
13. M. Agnello *et al.*, Phys. Lett. B **640**, 145 (2006).
14. M. Agnello *et al.* [FINUDA Coll.], Phys. Lett. B **654**, 80 (2007).

GRAAL

D. Babusci, P. Levi Sandri (Resp.), D. Pietreanu (Ass. Ric.)

1 Introduction

The Graal experiment has aimed at a more detailed knowledge of the baryon spectrum via the precise measurement of cross sections and polarisation observables in photo-induced reactions on the nucleon.

The use of the electromagnetic probe and of it's polarisation, coupled to large acceptance detectors with cylindrical symmetry and high efficiency in the detection of all final state particles, is the technique chosen in many laboratories to perform the ambitious program of a full determination of the scattering amplitude of a given photonuclear reaction. Such determination requires, for each reaction channel, the measurement of the cross section, of the three single polarisation observables and of four appropriately chosen double polarisation observables.

The Graal esperiment is performed in collaboration between INFN sections of Roma2, LNF, Catania-LNS-Messina, ISS-Romaf and Torino, LPSC-Grenoble and INR-Moscow.

2 The Graal Beam and the Lagranγe apparatus

The Graal facility provides a polarised and tagged photon beam by the backward Compton scattering of laser light on the high energy electrons circulating in the ESRF storage ring [1]. Using the UV line (350 nm) of an Ar-Ion laser we have produced a gamma-ray beam with an energy from 550 to 1550 MeV. Its polarisation is 0.98 at the maximum photon energy and the energy resolution has been measured to be 16 MeV (FWHM).

The Lagranγe detector is formed by a central part surrounding the target and a forward part. Particles leaving the target at angles from 25° to 155° are detected by two cylindrical wire chambers with cathode readout, a barrel made of 32 strips of plastic scintillator parallel to the beam axis, used to determine the ΔE/Δx of charged particles, and the BGO *Rugby Ball* made of 480 crystals of BGO scintillator.

The BGO ball is made of crystals of pyramidal shape with trapezoidal basis which are 21 radiation lengths long (24 cm). This calorimeter has an excellent energy resolution for photons [2], a good response to protons [3], a high detection efficiency for neutrons [4] and is very stable in time due to a continuous monitoring and to the calibration slow control system [5].

Particles moving at angles smaller than 25° encounter two plane wire chambers, (xy and uv) two walls of plastic scintillator bars, 3 cm thick, located at 3 m from the target point, that provide a measurement of the time-of-flight for charged particles (700 ps FWHM resolution) followed by a shower wall made by a sandwich of four layers of lead and plastic scintillators, 4 cm thick, that provides a full coverage of the solid angle for photon detection (with 95 percent efficiency) and a 20 percent efficiency for neutron detection [6].

The beam intensity is continuously monitored by a flux monitor, composed by three thin plastic scintillators and by a lead/scintillating fibre detector that measures energy and flux [7].

3 2008 activity

During the year 2008 the Graal experiment has collected data to improve the upper bound to the anysotropy of the speed of light and, in parallel, has continued the data collection for the meson photoproduction off the deuteron and has started and concluded an experiment to detect η-mesic nuclei. Data analysis was concluded for many final state channels, and the relevant papers are being submitted.

At the end of 2008 the Graal experiment was completely dismounted. Many parts of the apparatus are being moved to the B1 S-photon beamline of the ELSA stretcher in Bonn where the experimental studies initiated at GRAAL will be continued and extended to higher energies. In particular, the new Bonn experiment will profit from the BGO *Rugby Ball* calorimeter, the liquid H2/D2 target system, the scintillator barrel and the beam monitors.

4 Graal Pubblications in 2008

1. J. Ajaka *et al.*, Phys. Lett. B **651**, 108 (2007).
2. O. Bartalini *et al.*, Phys. Atom. Nucl. **71**, 75 (2008).
3. J. Ajaka *et al.*, Phys. Rev. Lett. **100**, 052003 (2008).
4. A. Fantini *et al.*, Phys. Rev. C **78**, 015203 (2008).
5. A. Ignatov *et al.*, Prog. Part. Nucl. Phys. **61**, 253 (2008).

References

1. J. P. Bocquet *et al.*, Nucl. Phys. A **622**, 110c (1997).
2. P. Levi Sandri *et al.* Nucl. Inst. & Meth. A **370**, 396 (1996).
3. A. Zucchiatti *et al.*, Nucl. Inst. & Meth. A **321**, 219 (1992).
4. O. Bartalini *et al.*, to be published in Nucl. Instr. & Meth. A.
5. F. Ghio *et al.*, Nucl. Inst. & Meth. A **404**, 71 (1998).
6. V. Kouznetsov *et al.*, Nucl. Instr. & Meth. A **487**, 396 (2002).
7. V. Bellini *et al.*, Nucl. Inst.& Meth. A **386**, 254 (1997).

HERMES

E. Avetisyan (Ass.), N. Bianchi, E. De Sanctis, P. Di Nezza,
A. Fantoni (Resp. Naz.), C. Hadjidakis (Ass. Ric.), D. Hasch (Art.23),
A. Orlandi (Tecn.), W. Pesci (Tecn.), E. Polli, A.R. Reolon, A. Viticchié (Tecn.)

1 Introduction

HERMES (HERa MEasurement of Spin) is an experiment at DESY mainly dedicated to study the spin structure of the nucleon, using the longitudinally polarised positron/electron beam of 27.5 GeV and a longitudinally/transversely/null polarised gas target internal to the HERA storage ring. HERMES has taken data from 1995 to 2007, till the HERA shutdown, obtaining successful results in all fields. A lot of analyses are still going on, i.e. the exclusive production of mesons and reall photons with positron and electron beams, and the nuclear effects. HERMES is still a large collaboration, of about 180 physicists from 31 Institutions from 12 Countries. Italy participates with 4 groups and more than 30 physicists from Bari, Ferrara, Frascati and Rome. The Frascati group mantained the same responsibilities from the past, being involved in the management (A. Fantoni as a Deputy Spokesperson), in the Editorial Board (P. Di Nezza and D. Hasch), in the analysis groups and in many Drafting Committees.

2 Data analysis and physics results of the LNF group in 2008

2.1 Technical software

LNF members were main responsible for Particle Identification (PID). In particular they worked on the maintenance and code development of the PID library function, on the PID calibration, on the new data productions of 2004, 2005, 2006, 2007 and 2008 on the flux corrections to PID for different physics analysis.
The LNF group acted also as HERMES Linux administrator and represented HERMES on DESY Linux user meeting, where user requirements and future strategy for Linux support were discussed.

2.2 Transverse momentum broadening of hadron production in semi-inclusive deep inelastic scattering on nuclei

The first direct measurement of the dependence on target nuclear mass of the average squared transverse momentum $\langle p_t^2 \rangle$ of π^+, π^-, and K^+ mesons from deep inelastic lepton scattering has been obtained as a function of several kinematic variables. QCD predicts a relationship between energy loss and the broadening of hadron transverse momentum p_t distributions. As the relationship between these two quantities is completely independent of the dynamics of the initial scattering process, it holds equally well in "cold" nuclear matter and in finite-length "hot" matter, produced, *e.g.,* in ultra-relativistic heavy ion collisions or high energy proton-nucleus interactions. Thus the understanding of this broadening in the "cold" nuclear medium provides precious information for the interpretation of such high-energy processes. The average squared transverse momentum was clearly observed to increase with atomic mass number. The effect increases as a function of Q^2 and x and remains constant as a function of both the virtual photon energy ν and the fractional hadron energy z, except that it vanishes as z approaches unity. The result is summarized in Fig. 1, where the p_t-broadening for π^+, π^-, and K^+ mesons is shown as a function of atomic mass number A.

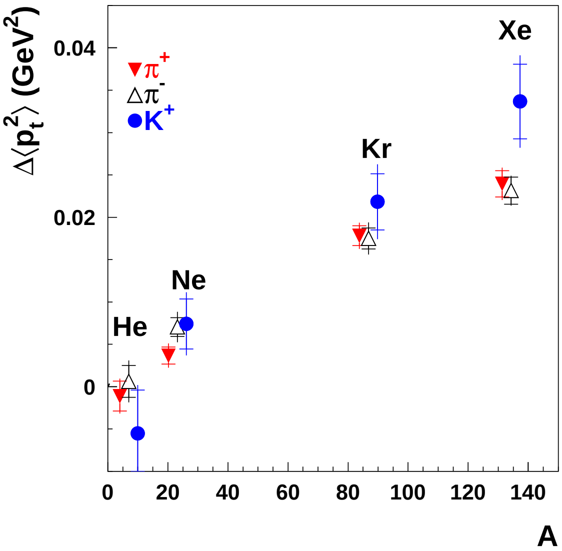

Figure 1: *The p_t-broadening for π^+, π^-, and K^+ mesons as a function of atomic mass number A. The inner error bars represent the statistical uncertainties; the total bars represent the total uncertainty, obtained by adding statistical and systematic uncertainties in quadrature.*

2.3 Nuclear DVCS

HERMES performed studies of DVCS on nuclear targets: $eA \to e'\gamma A$ using H, He, N, Ne, Kr and Xe. Nuclear targets provide a laboratory where, compared to the nucleon, additional information can be obtained on GPDs by observing how they become modified in the nuclear environment. Moreover, it has been argued that GPDs of nuclei provide access to the spatial distribution of energy, pressure, angular momentum and shear forces in nuclei in terms of the fundamental degrees of freedom in QCD. Therefore, studies of nuclear GPDs offer a new opportunity to address the problem of the origin of nuclear forces. For DVCS on nuclei, various observables were estimated theoretically for coherent scattering from the whole nucleus. In these estimates, the binding energy is assumed to be negligibly small compared to the virtuality of the exchanged photon, and nuclear GPDs are expressed in terms of slightly modified nucleon GPDs. These models predict an enhancement of DVCS beam–charge and beam–spin asymmetries for spin–0 and spin–1/2 nuclei compared to the free proton. For incoherent scattering where the nucleus breaks up, the description of the process is approximated by that on free nucleons.

In experimental studies of DVCS on nuclear targets, the important issue of the interplay between the coherent and incoherent contributions to the measured cross section has to be taken into account. The two contributions have a very distinct dependence on the momentum transfer t: the coherent contribution has a fast t-dependence proportional to the nuclear form factor squared; the incoherent contribution has a slow t-dependence proportional to the nucleon form factor squared. At small values of the momentum transfer t, nuclear break-up is unlikely and the DVCS process is predominantly coherent. At large t, the target nucleus break-up and DVCS takes place on individual uncorrelated nucleons. The rapid t–dependence of coherent scattering on the nucleus which is exploited for the separation of coherent and incoherent contributions.

For H, Kr and Xe, where data with both electron and positron beam are available, a 'combined analysis' has been performed which exploits the dependence on the beam charge of the beam-spin asymmetry of the interference term. Such, the squared DVCS and interference beam-spin asymmetry can be separated.

The A–dependence of the beam–charge and beam–spin asymmetry amplitudes is presented separately for the coherent– and incoherent–enriched samples in Fig. 2. The asymmetry amplitude $A_{\mathrm{C}}^{\cos\phi}$ is consistent with zero for the coherent–enriched sample for all three targets, while it is about 0.1 for the incoherent–enriched sample without showing any dependence on the target mass within uncertainties.

The beam–spin asymmetry amplitude shown in Fig. 2 (right panel) has values of about -0.2 for both the coherent– and incoherent–enriched samples without showing any dependence on A within uncertainties.

This behaviour supports the simplified model approximation where binding effects are neglected and the nucleus is viewed as a collective of quasi–free nucleons. In this picture, both beam-charge and beam-spin asymmetry are essentially independent on the nuclear mass.

It is interesting to compare these amplitudes for nuclear targets to the amplitudes from a free proton. This ratio is found to be 0.91 ± 0.19 for the coherent–enriched sample and 0.93 ± 0.23 for the incoherent–enriched sample, both of which are compatible with unity.

Model calculations for nuclear DVCS, which essentially all base on the above approximation of the nucleus as a collective of quasi–free nucleons, predict an enhancement of the asymmetries by the effect from the neutron contribution compared to the free proton asymmetries for spin–0 and spin–1/2 nuclei. The predicted value for the ratio of nuclear–to–hydrogen beam–charge and beam–spin asymmetries ranges between about 1.1 for ^{4} and about 2 for ^{20}Ne and ^{76}Kr. The data do not support this predicted enhancement for spin–0 and spin–1/2 nuclei.

For incoherent scattering, the asymmetry amplitude for nuclei is anticipated to be similar to the amplitude for hydrogen, since scattering on the protons inside the nuclei should dominate due to the fact that the Bethe–Heitler process on the neutron is suppressed.

Neglecting the neutron contribution, the asymmetry amplitude ratio for incoherent scattering is predicted to be unity. Any deviation from unity would result from the neutron contribution. The measured ratio of the nuclear–to–hydrogen beam–spin asymmetry agrees with the expected suppression of the neutron contribution in incoherent scattering on nuclei.

3 Outlook

The data taking with Recoil Detector has been successfull, new precision data on hard exclusive reactions have been collected and are under study, providing results on the exciting and new field of hard exclusive production of mesons and real photons with positron and electron beams. DVCS can be directly measured and the background rejected; pre-recoil results will be refined once the background processes are measured.

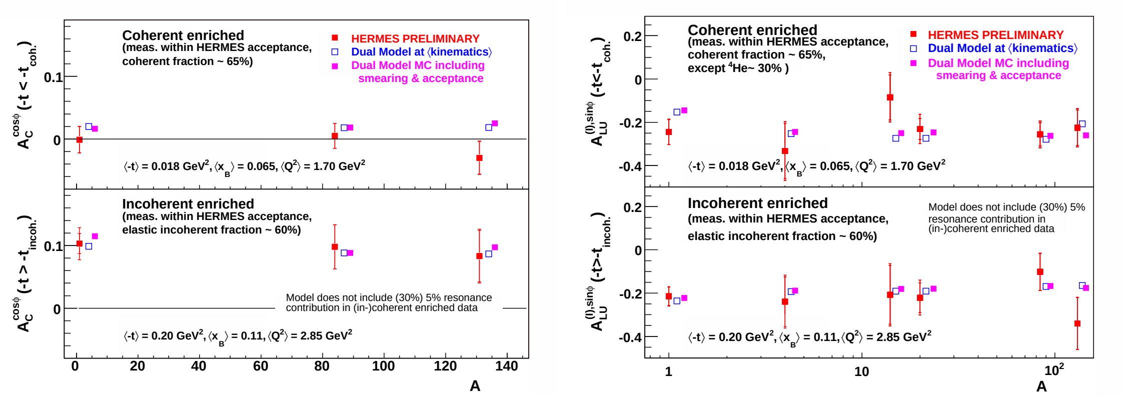

Figure 2: *Left: A–dependence of the beam–charge asymmetry amplitude for the coherent–enriched (upper panel) and incoherent–enriched (lower panel) data samples for H, Kr and Xe targets. Right: A–dependence of the beam–spin asymmetry amplitudes for the coherent–enriched (upper panel) and incoherent–enriched (lower panel) data samples. In all cases the inner bar represents the statistical uncertainty and the outer bar the quadratic sum of statistical and systematic uncertainties.*

The analysis of data with a transversely polarized hydrogen target has been completed and the paper is under completion, providing a demonstration of a new tool for studying the transverse structure of the nucleon.
The ongoing physics analysis and the phenomenological investigations will be completed.

4 Conferences

4.1 List of Conference Talks

1. P. Di Nezza, "Space-time evolution of the hadronization process", XLVI International Winter Meeting on Nuclear Physics, Bormio, Italy, January 2008.

2. P. Di Nezza, "Hadron production in DIS: experimental overview", Nuclear Medium Effects on the Quark and Gluon Structure of the Hadrons, ECT*, Trento, Italy, June 2008.

3. A. Fantoni, "Spin Physics at HERMES: recent results", International Workshop on Hadron Structure and Spectroscopy (IWHSS08) Torino, Italy, March-April 2008.

4. D. Hasch, "Transversity and friends from HERMES", International Workshop on Hadron Structure and Spectroscopy (IWHSS08) Torino, Italy, March-April 2008.

5. D. Hasch, "Towards a 3D immaging of hadrons", 4th Electron Ion Collider Workshop "A new Experimental Quest to Study QCD, Hadron Structure, and Nuclear Matter" Hampton (USA), May 2008.

6. D. Hasch, "HERMES measurements of nuclear DVCS", Nuclear Medium Effects on the Quark and Gluon Structure of the Hadrons, ECT*, Trento, Italy, June 2008.

7. D. Hasch, "GPD overview", International Workshop on Transverse Spin Physics, Beijing, China, June-July 2008.
8. D. Hasch, "Spin structure of the nucleon from the HERMES point of view", Ringberg Workshop "New Trends in HERA Physics 2008", Tegernsee, Germany, October 2008.
9. D. Hasch, "Spin Physics - experimental overview", 18th International Conference on Particles and Nuclei (PANIC 08), Eilat, Israel, November 2008.

4.2 Conference organization and advisory, Projects, Seminars, Lectures, Editors

1. N. Bianchi, Editor of The European Physical Journal A.
2. E. De Sanctis, Member of HERMES Nominating Committee.
3. P. Di Nezza, Member of HERMES Editorial Board.
4. A. Fantoni, Organizer of the Workshop "Nuclear Medium Effects on the Quark and Gluon Structure of Hadrons", ECT*, Trento, Italy, June 2008.
5. A. Fantoni, Member of the Planning Committee.
6. D. Hasch, Member of HERMES Editorial Board.
7. D. Hasch, Member of the committee for the DESY thesis award
8. D. Hasch, Organizer of the Second International Workshop on Transverse Polarisation Phenomena on Hard Processes (Transversity 2008), Ferrara (Italy), May 2008.

5 Publications

1. A. Airapetian *et al.*, Phys. Lett. B **659**, 486 (2008).
2. A. Airapetian *et al.*, JHEP **06**, 017 (2008).
3. A. Airapetian *et al.*, Phys. Lett. B **666**, 446 (2008).
4. A. Airapetian *et al.*, JHEP **06**, 066 (2008).
5. A. Airapetian *et al.*, "Spin Density Matrix Elements in Exclusive ρ^0 Electroduction on ^1H and ^2H Targets at 27.6 GeV Beam Energy", DESY-08-23
6. P. Di Nezza, "Space-time evolution of the hadronization process" Proc. of XLVI International Winter Meeting on Nuclear Physics Universita' degli studi di Milano, Supplemento n.129, 2008.
7. D. Hasch, "GPD overview", RBRC proceedings of the International Workshop on Transverse Spin Physics, Beijing, China, June-July 2008.
8. D. Hasch, "Spin structure of the nucleon from the HERMES point of view", Proceedings of the Ringberg Workshop "New Trends in HERA Physics 2008", Tegernsee, Germany, October 2008.

$\overline{\text{P}}$ANDA - $\overline{\text{p}}$ Annihilation at Darmstadt

B. Dulach, P. Gianotti (Resp. Naz.), M. Giardoni, C. Guaraldo, M. Iliescu (Art. 23),
V. Lucherini, D. Orecchini (Tecn.), E. Pace, L. Passamonti (Tecn.), D. Pierluigi, (Tecn.),
D. Pietreanu (Ass. Ric.), A. Russo (Tecn.), D. Sirghi (Art. 2222)

1 Introduction

$\overline{\text{P}}$ANDA is one of the biggest future experiments in hadron and nuclear physics that will be carried out at the new Facility for Antiproton and Ion Research (FAIR) at Darmstadt, Germany. It is dedicated to study annihilations of antiprotons on nucleons and nuclei up to a maximum center-of-mass energy in $\overline{\text{p}}$p of 5.5 GeV. Presently, the $\overline{\text{P}}$ANDA collaboration consists of 400 physicists from 17 countries spread all over the world. The Italian groups involved are: Torino, University, Politecnico and INFN, Trieste, University and INFN, Genova INFN, Pavia, University and INFN, Ferrara, University and INFN, Frascati INFN laboratory, Catania, University and INFN. The LNF group is involved in the design and construction of the central tracker of the $\overline{\text{P}}$ANDA detector.

2 $\overline{\text{P}}$ANDA experiment

A new facility for hadronic physics is under construction in Germany. It consists of a major upgrade of the presently running GSI accelerator complex of Darmstadt [1]. An intense, high momentum

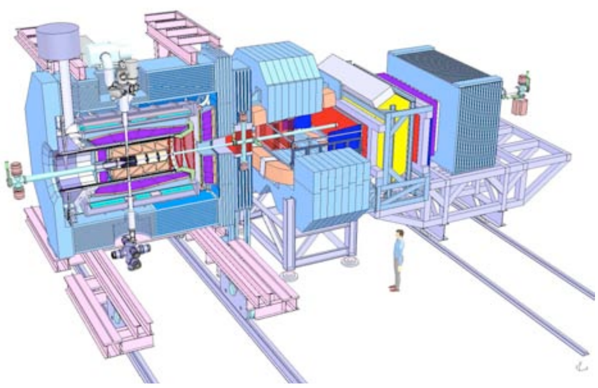

Figure 1: *A schematic view of the $\overline{\text{P}}$ANDA detector.*

resolution antiproton beam, with momenta between 1.5 and 15 GeV/c, will be available at the High Energy Storage Ring (HESR), and the experimental activity will be carried out using a general purpose detector $\overline{\text{P}}$ANDA that will be build surrounding an internal target station installed in one of the two straight sections of the storage ring. Fig. 1 shows a schematic drawing of the $\overline{\text{P}}$ANDA detector. It is designed as a large acceptance multi-purpose detector consisting of two

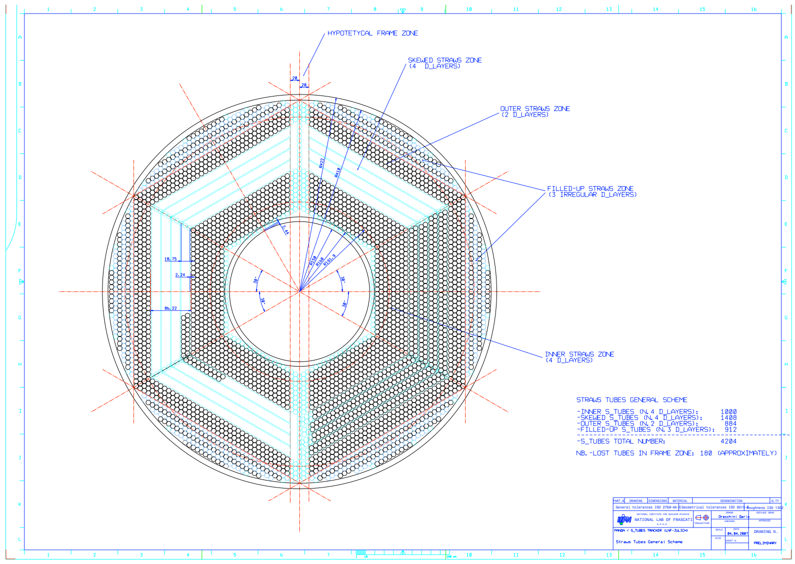

Figure 2: *The layout of the STT. Details are in the text.*

distinct parts: a solenoidal spectrometer, surrounding the interaction target region, and a forward spectrometer to cover the solid angle between 5 and 22 degrees.

3 The $\overline{\text{P}}$ANDA Central Tracker

The $\overline{\text{P}}$ANDA Central Tracker has to satisfy the following requirements:

- almost full solid angle coverage;
- momentum resolution $\delta p/p \sim 1.5\%$;
- low material budget $X/X_0 \sim$ few %;
- good spatial resolution $\sigma_{r,\phi} = 150\ \mu$m, $\sigma_z =$ few mm.

This detector will be placed around the Micro Vertex Detector (MVD) at a radial distance from the interaction point between 15 and 42 cm. Along the beam axis the allowed space is 150 cm. Presently, for this detector, two options are under discussion: a Straw Tube Tracker (STT) and a Time Projection Chamber (TPC). The LNF $\overline{\text{P}}$ANDA group, having experience in straw tubes, is involved in the realization of the STT.

3.1 Straw tube detector layout

The overall $\overline{\text{P}}$ANDA tracking volume will be divided in two half by the target pipe, therefore the detector will consist of two identical semi-chambers. In the hypothesis of a straw tube tracker, each one will be made of aluminized mylar straw tubes, diameter 10 mm, length 1500 mm, thickness 30 μm, arranged in planar double layers. Inside a double layer the tubes are glued together and

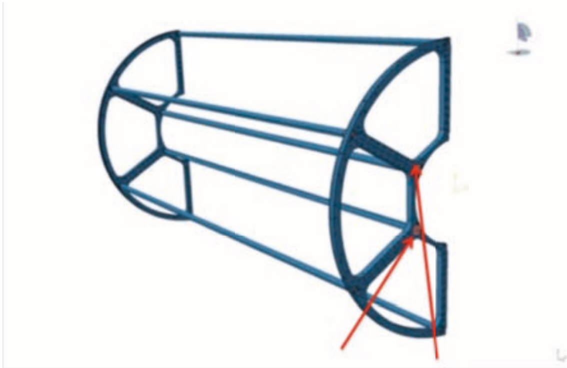

Figure 3: *Layout of the STT mechanical structure. The arrowsindicated removable elements (see text for more details)*

operated with an Ar+CO_2 (90+10) gas mixture with an over-pressure of 1 bar. This solution will help to avoid strong support structures and will keep the detector design modular and simple. To measure also particle z coordinate, some layers will be mounted with a skew angle $\pm$ 3° with respect to the beam axis.

Figure 2 shows the layout for the STT. There are 4 internal double-layers parallel to the beam axis, then 4 double-layers mounted with an opposite skew angle, and finally 2 other layers parallel to the beam axis. To fill up the cylindrical volume, the remaining region houses smaller tube layers.

One basic advantage of the proposed solution is that each double-layer is an independent object that can be treated separately from the others.

In order to support the straw tube double-layers, and to precisely position them, an external mechanical structure is necessary.

4 Activity of the LNF $\overline{\text{P}}$ANDA group

The activity of the LNF $\overline{\text{P}}$ANDA group during 2008 has been devoted to the design of this mechanical structure. The structure of this support is very light, and, in the hypothesis of using Aluminum for the realization, we will have the following numbers:

- density 2.7 g/cm^3 ;
- Youngs modulus: 70 GPa;
- radiation Length (X_o): 9 cm;
- thermal expansion: 24 ppm/°C;

with a total weight of 8.2 kg. The two internal rods (signed with the arrows in fig.3) are needed only during the straw double-layers mounting phase, and then could be removed. To check the

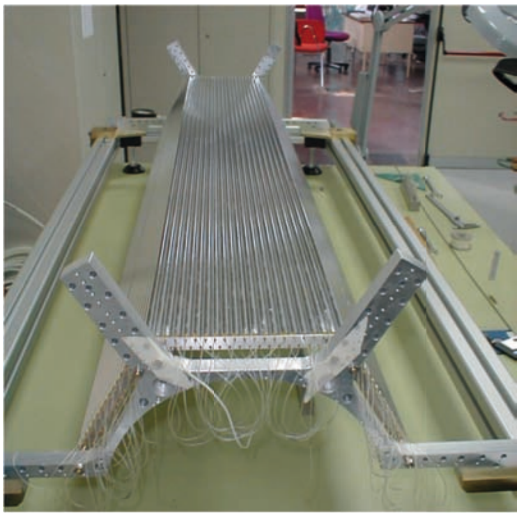

Figure 4: *Prototype of the Straw Tube Tracker.*

mounting procedure of straw tube double-layers a first prototype of the mechanical structure flanges has been build at the LNF mechanical workshop, and mounted on dummy supports. On these flanges 4 axial double-layers and 2 skewed ones can be mounted. Fig. 4 is a picture taken during the mounting phase.

For 2009 tests with cosmic rays and beams are foreseen for the STT prototype. The group will also continue the design activity approaching the problems related with the integration of the STT with the other components of the $\overline{\text{P}}$ANDA detector. Furthermore a Technical Design Report for the STT will be prepared.

5 Conference presentations

1. P. Gianotti, "Physics with antiprotons at FAIR", invited talk at the XLVI International Winter Meeting on Nuclear Physics, Bormio (Italy) 26-30 January, 2008.

2. P. Gianotti, "Baryon Form Factors at FAIR", invited talk at the International Workshop on e^+e^- collisions from ϕ to ψ (PHIPSI08), Frascati (Italy) 7-10 April, 2008.

References

1. http://www.gsi.de/fair/

2. http://www-panda.gsi.de/auto/_home.htm

SIDDHARTA

M. Bazzi (Art. 23), M. Bragadireanu (Bors. UE), C. Curceanu Petrascu (Co-Resp. Naz.), A. D'Uffizi (Bors.), C. Guaraldo (Co-Resp. Naz.), M. Iliescu (Art. 2222), P. Levi Sandri, V. Lucherini, F. Lucibello (Tecn.), S. Okada (Bors. PD), D. Pietreanu (Ass. Ric.), M. Poli Lener (Art. 2222), A. Rizzo (Bors.), A. Romero Vidal (Bors PD), A. Scordo (Dott.), D. Sirghi (Art. 2222), F. Sirghi (Bors. UE), D. Tagnani (Bors.), O. Vazquez Doce (Art. 23)

1 The SIDDHARTA scientific program

The objective of the SIDDHARTA (Silicon Drift Detector for Hadronic Atom Research by Timing Application) experiment is to continue, to deepen and enlarge the successful scientific line, initiated by the DEAR experiment in performing precision measurements of X-ray transitions in exotic (kaonic) atoms at DAΦNE.

The few eV precise determination of the shift and width of the $1s$ level with respect to the purely electromagnetic calculated values, in kaonic hydrogen and kaonic deuterium, generated by the presence of the strong interaction, through the measurement of the X-ray transitions to this level, will allow the first precise experimental determination of the isospin dependent antikaon-nucleon scattering lengths.

The shift ϵ and the width Γ of the $1s$ state of kaonic hydrogen are related to the real and imaginary part of the complex s-wave scattering length, a_{K^-p}, through the Deser formula (in the isospin limit):

$$\epsilon + i\Gamma/2 = 2\alpha^3\mu^2 a_{K^-p} = (412 \text{ eV fm}^{-1}) \cdot \mathrm{a_{K^-p}} \tag{1}$$

where α is the fine structure constant and μ the reduced mass of the K^-p system. In the isospin limit, i.e. in the absence of the electromagnetic interaction and at $m_d = m_u$, a_{K^-p} can be expressed directly in terms of the scattering lengths for isospin I=0 and I=1:

$$a_{K^-p} = \frac{1}{2}(a_0 + a_1) \tag{2}$$

A similar relation applies to the case of kaonic deuterium and to the corresponding scattering length a_{K^-d}:

$$\epsilon + i\Gamma/2 = 2\alpha^3\mu^2 a_{K^-d} = (601 \text{ eV fm}^{-1}) \cdot \mathrm{a_{K^-d}} \tag{3}$$

An accurate determination of the K^-N isospin dependent scattering lengths will place strong constraints on the low-energy K^-N dynamics, which, in turn, constraints the SU(3) description of chiral symmetry breaking in systems containing the strange quark.

The DEAR measurement on kaonic hydrogen, performed in 2002 (Phys. Rev. Lett 94 (2005), 212302):

$$\epsilon = -193 \pm 37(stat.) \pm 6(syst.) \text{ eV} \tag{4}$$

$$\Gamma = 249 \pm 111(stat.) \pm 39(syst.) \text{ eV}. \tag{5}$$

has already triggered an increased activity of the theoretical groups working in the low-energy kaon-nucleon interaction field, as well as in more general non-perturbative QCD.

The SIDDHARTA experiment aims to improve the precision obtained by DEAR by an order of magnitude and to perform the first measurement ever of kaonic deuterium. SIDDHARTA plans as well to perform accurate measurements on kaonic helium transitions to the 2p level (L-series). Other measurements (as sigmonic atoms or the precise determination of the charged kaon mass) are as well considered in the scientific program.

2 The SIDDHARTA setup

SIDDHARTA represents a new phase in the study of kaonic atoms at DAΦNE. The DEAR precision was limited by a signal/background ratio of about 1/70. To significantly improve this ratio, a breakthrough is necessary. An accurate study of the background sources present at DAΦNE was redone. The background includes two main sources:

- synchronous background: coming together with the kaons – related to K^- interactions in the setup materials and also to the ϕ-decay processes; it can be defined as hadronic background;
- asynchronous background: final products of electromagnetic showers in the machine pipe and in the setup materials originating from particles lost from primary circulating beams either due to the interaction of particles in the same bunch (Touschek effect) or due to the interaction with the residual gas.

Accurate studies performed by DEAR showed that the main background source in DAΦNE is of the second type, which shows the way to reduce it. A fast trigger correlated to a kaon entering into the target would cut the main part of the asynchronous background.

X rays were detected by DEAR using CCDs (Charge-Coupled Devices), which are excellent X-ray detectors, with very good energy resolution (about 140 eV FWHM at 6 keV), but having the drawback of being non-triggerable devices (since the read-out time per device is at the level of 10 s). A recently developed device, which preserves all good features of CCDs (energy resolution, stability and linearity), but additionally is triggerable - i.e. fast (at the level of 1μs), was implemented. This new detector is a large area Silicon Drift Detector (SDD), specially designed for spectroscopic application. The development of the new 1 cm^2 SDD device, together with readout electronics and very stable power supplies, was partially performed under the Joint Research Activity JRA10 of the I3 project"Study of strongly interacting matter (HadronPhysics)" within FP6 of the EU.

The trigger in SIDDHARTA will be given by a system of scintillators which will recognize a kaon entering the target making use of the back-to-back production mechanism of the charged kaons at DAΦNE from ϕ decay of the type:

$$\phi \rightarrow K^+K^-. \tag{6}$$

Successful tests of SDD detectors were performed in 2003-2007 at the Beam Test Facility of Frascati (BTF), The results of these tests showed, in DEAR-like conditions, a trigger rejection factor of 5 x 10^{-5} - which will allow to SIDDHARTA to perform few eV precision measurements.

The SIDDHARTA setup contains 144 SDD chips of 1 cm^2 each, placed around a cylindrical target, containing high density cryogrenic gaseous hydrogen (deuterium). The SDDs are grouped in units od 3 detectors, read individually, Fig. 1; units of 18 SDDs are then realized, Fig. 2. The target is made of kapton, 75 μm thick, reinforced with aluminium grid, see Figure 3.

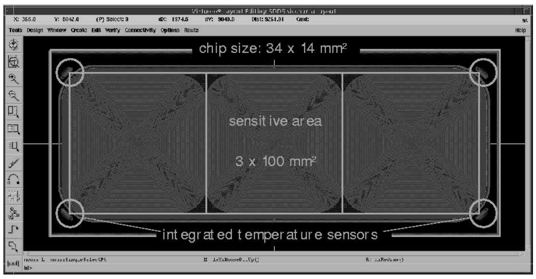

Figure 1: *SDD layout on the readout side: 3 SDD cells, read independently, each of 1 cm^2 area, monolithically integrated on one chip.*

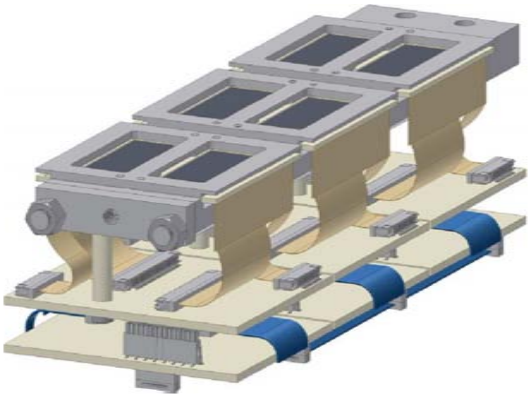

Figure 2: *An 18 cm^2 SDD unit, containing 18 SDD individual chips.*

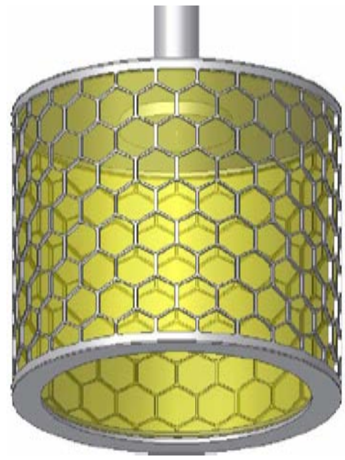

Figure 3: *The SIDDHARTA target cell, done in kapton, reinforced with an aluminium grid. It will contain about 3 liters of cryogenic and high density hydrogen (deuterium) gas.*

8 SDD 18 cm^2 units will be placed all around the target cell, as shown in Figure 4. The SIDDHARTA setup was installed on DAΦNE in summer 2008 - as discussed in the next section.

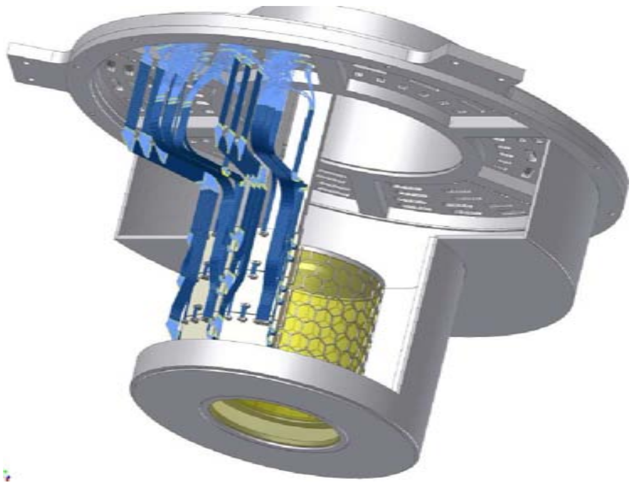

Figure 4: *The SIDDHARTA target cell surrounded by SDD units (detail).*

3 Activities in 2008

In what follows, we present the main 2008 SIDDHARTA activities performed at LNF.

3.1 Installation of SIDDHARTA setup on DAΦNE

The SIDDHARTA setup was installed on the DAΦNE collider in 2008: the trigger system, composed by 2 scintillators one above, one below the beam pipe - measuring the back-to-back charged kaons and giving the trigger to the SDD detectors, was installed in early Spring 2008, Figure 5, was tested and optimized in collaboration with DAΦNE team; the full setup was installed in September 2008, Figure 6.

The installation of the setup was followed by a period of debud and tests; a lead shielding was as well installed: a layer of 5 cm of lead below and around the setup, in order to shield the SDD detectors from the high background.

3.2 First SIDDHARTA measurements

After the setup debug, in the period November - December 2008 the degrader optimization was performed (degrader has to be optimized taking into account the boost of the ϕ-particles; the optimization is done in a range of 100 μm) - by measuring the kaonic helium transitions to the 2p level; this measurement is easier than the kaonic hydrogen one (being the yield of transitions much bigger) and, in the same time, represents a measurement interesting in itself, worthy to be published.

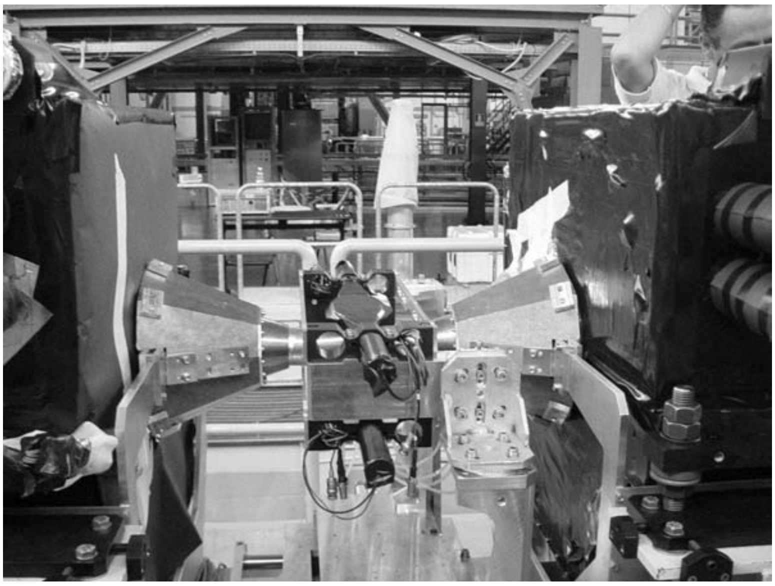

Figure 5: *The SIDDHARTA trigger system installed at DAΦNE.*

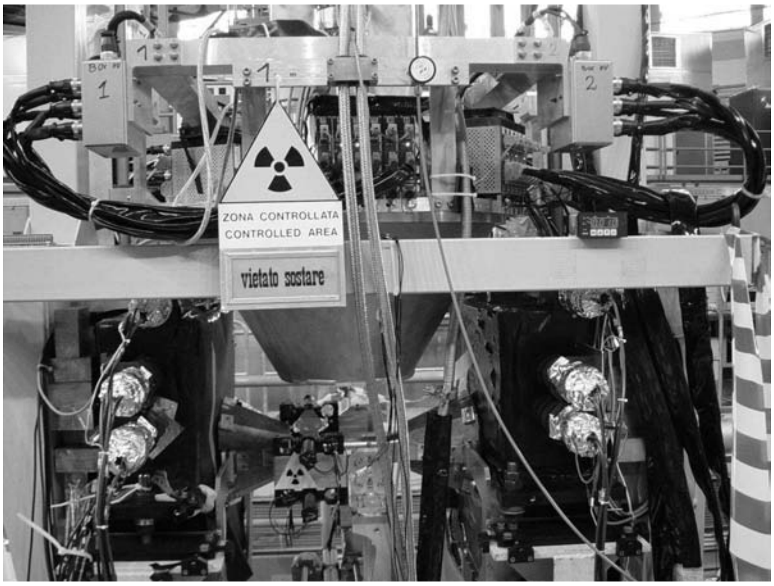

Figure 6: *The SIDDHARTA full setup installed at DAΦNE.*

A typical preliminary example of the obtained spectra is given in Figure 7: in the upper histogram the spectrum obtained without trigger signal is shown, while in the lower part the same spectrum with trigger signal is given. The trigger rejection factor was estimated to be at the level of 7 x 10^{-5}, perfectly in agreement with what expected. The L-lines transitions in kaonic helium are clearly visible; this is the first measurement performed in gaseous helium; data are going to be published.

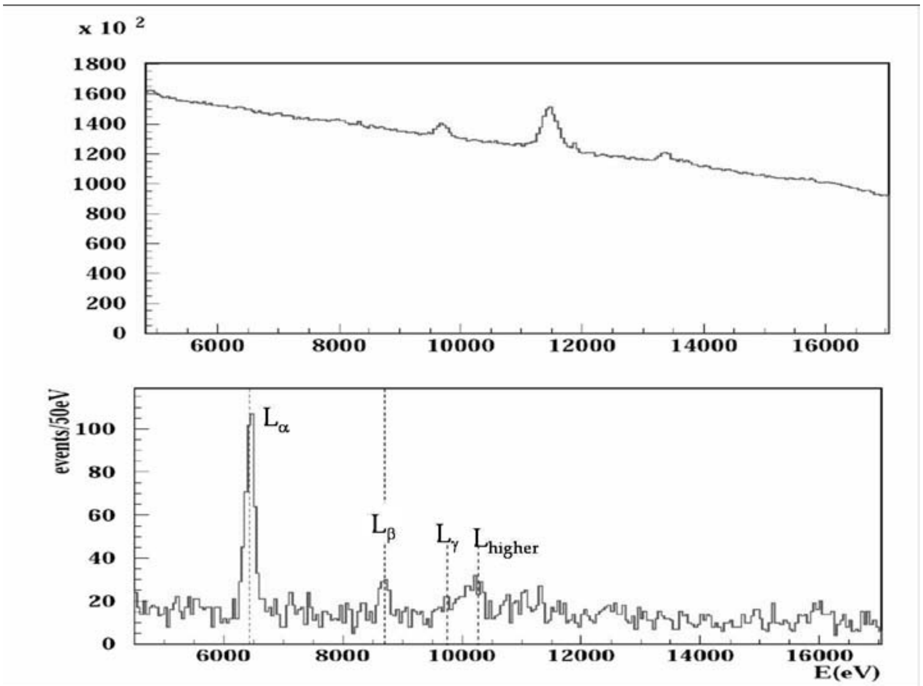

Figure 7: *Kaonic helium preliminary measurement - upper spectrum: measured without trigger, the visible lines are coming from gold transitions (gold is present in infinitesimal amount in the readout electronics); lower spectrum - the triggered spectrum: kaonic helium transitions to the 2p level, the L-series, are clearly visible.*

4 Activities in 2009

The LNF group main activities in SIDDHARTA for 2009 are the following ones:

- finalize analyses of kaonic helium data and publish them;
- measurement of kaonic hydrogen;
- measurement of kaonic deuterium;
- data analyses and Monte Carlo simulations.

5 Publications 2008

5.1 List of Conference Talks

1. C. Curceanu (Petrascu), “Kaonic atoms and nuclei measurements at the DAΦNE accelerator”, talk at the 14th International QCD Conference, QCD08, 7-12 July 2008, Montpellier, France

2. C. Curceanu, “AMADEUS experiment”, talk at the Vienna FOPI meeting, 24 April 2008, Vienna, Austria

3. A. Scordo, “Kaonic atoms measurement at DAΦNE: the SIDDHARTA experimet”, talk at the XIII Frascati Spring School ”Bruno Touschek” in Nuclear, Subnuclear and Astroparticle Physics, May 12th-16th, 2008, Frascati, Italy.

4. O. Vazquez Doce, “The AMADEUS experiment: search for kaonic clusters at DAΦNE”, talk at the XIII Frascati Spring School ”Bruno Touschek” in Nuclear, Subnuclear and Astroparticle Physics, May 12th-16th, 2008, Frascati, Italy.

5. O. Vazquez Doce, “The AMADEUS experiment: search for kaonic clusters at DAΦNE”, talk at the 10th International Workshop on Meson Production, Properties and Interaction (MESON2008), 6-10 June 2008, Kracow, Poland

6. O. Vazquez Doce, “KLOE data analyses in the search for kaonic clusters and AMADEUS experiment”, talk at the International Conference on Exotic Atoms EXA08, 15-18 September 2008, Vienna, Austria

7. C. Curceanu (Petrascu), “Kaonic atoms measurements at the DAΦNE accelerator”, talk at the International Conference on Exotic Atoms EXA08, 15-18 September 2008, Vienna, Austria

8. O. Vazquez Doce, “The AMADEUS experiment: deeply bound kaonic nuclear states at DAΦNE”, talk at the XCIV Congresso Nazionale Societa’ Italiana di Fisica, 22-27 September 2008, Genova, Italy

9. A. Romero Vidal, “Kaonic atoms measurements at DAΦNE: the SIDDHARTA experiment”, talk at the XCIV Congresso Nazionale Societa’ Italiana di Fisica, 22-27 September 2008, Genova, Italy

10. O. Vazquez Doce, “Preliminary results from KLOE data analyses in the search for kaonic clusters”, talk at the Vienna FOPI meeting, 24 April 2008, Vienna, Austria

11. O. Vazquez Doce, “The AMADEUS experiment: study of the kaonic clusters at DAΦNE”, talk at the XLVI International Winter Meeting on Nuclear Physics, January 2008, Bormio, Italy

5.2 Papers and Proceedings

1. C. Curceanu *et al.*, Modern Phys. Lett. A **23**, 2524 (2008).

2. M. Bazzi *et al.*, Few-Body systems **44**, 79 (2008).

3. R.S. Hayano *et al.*, Modern Phys. Lett. **A23**, 2505 (2008).

4. M. Bazzi *et al.*, "New precision measurements of the strong interaction in kaonic hydrogen", Proceedings of the International Conference on Muon Catalized Fusion and related Topics, Dubna, JINR 2008, p. 218

5. J. Marton *et al.*, "Low-energy kaon-nucleon interaction studies with x-ray spectroscopy", Proceedings of the XLVI Winter meeting on nuclear physics, Bormio 2008, Ricerca Scientifica ed Educazione Permanente N. 129, 2008, p. 121.

6. J. Marton *et al.*, "New X-ray detectors for exotic atom research", Proceedings SORMA-west, Symposium on Radiation measurements and applications, Berkeley, USA, 2008, IEEE, in press

7. J. Zmeskal *et al.*, "Kaonic Atoms at DAΦNE - the SIDDHARTA Experiment", Proceedings of the 10th International Workshop on Meson Production, Properties and Interaction, 6-10 June 2008, Krakow, Poland, in press in International Journal of Modern Physics.

8. E. Widmann *et al.*, "Kaonic Atoms at DAΦNE - the SIDDHARTA Experiment", Proceedings of PANIC08 - in press.

9. C. Curceanu *et al.*, "Kaonic atoms measurements at the DAΦNE accelerator", Proceedings of the EXA08 International Conference, 15-18 Sept. 2008, Vienna, in press in Hyperfine Interactions.

10. C. Curceanu *et al.*, "Kaonic atoms and nuclei measurements at the DAΦNE accelerator", Proceedings of the 14th International QCD Conference, Montpellier, France, in press in Elsevier publication series.

VIP

S. Bartalucci, S. Bertolucci, C. Curceanu Petrascu (Resp. Naz.),
C. Guaraldo, M. Iliescu (Art. 2222), F. Lucibello (Tecn.),
D. Pietreanu (Ass. Ric.), A. Romero Vidal (Bors. PD), D. Sirghi (Art. 2222),
F. Sirghi (Bors. UE), L. Sperandio (Ass.), O. Vazquez Doce (Art. 23)

1 The VIP scientific case and the experimental method

The Pauli exclusion principle (PEP), which plays a fundamental role in our understanding of many physical and chemical phenomena, from the periodic table of elements, to the electric conductivity in metals, to the degeneracy pressure (which makes white dwarfs and neutron stars stable), is a consequence of the spin-statistics connection. Although the principle has been spectacularly confirmed by the number and accuracy of its predictions, its foundation lies deep in the structure of quantum field theory and has defied all attempts to produce a simple proof. Given its basic standing in quantum theory, it seems appropriate to carry out precise tests of the PEP validity and, indeed, mainly in the last 15-20 years, several experiments have been performed to search for possible small violations. The indistinguishability and the symmetrization (or antisymmetrization) of the wave-function should be then checked independently for each particle, and accurate tests were and are being done.

The VIP (VIolation of the Pauli Exclusion Principle) experiment, an international Collaboration among 6 Institutions of 4 countries, has the goal to improve the limit on the probability of the violation of the PEP for electrons, (P $< 1.7 \times 10^{-26}$ established by E. Ramberg e G. A. Snow: *Experimental limit on a small violation of the Pauli principle*, Phys. Lett. **B 238** (1990) 438) by three-four orders of magnitude (P $< 10^{-(29 \div 30)}$), exploring a region where new theories might allow for a possible PEP violation.

The experimental method consists in the introduction of new electrons into a copper strip, by circulating a current, and in the search for X-rays resulting from the forbidden radiative transition that occurs if one of the new electrons is captured by a copper atom and cascades down to the 1s state already filled by two electrons with opposite spins. The energy of this transition would differ from the normal K_α transition by about 300 eV (7.729 keV instead of 8.040 keV) providing an unambiguous signal of the PEP violation. The measurement alternates periods without current in the copper strip, in order to evaluate the X-ray background in conditions where no PEP violating transitions are expected to occur, with periods in which current flows in the conductor, thus providing "fresh" electrons, which might possibly violate PEP. The rather straightforward analysis consists on the evaluation of the statistical significance of the normalized subtraction of the two spectra in the region of interest.

The experiment is being performed at the LNGS underground Laboratories, where the X-ray background, generated by cosmic rays and natural radioactivity, is reduced.

2 The VIP experimental setup

The VIP setup was built in 2005, starting from the DEAR setup, reutilizing the CCD (Charge Coupled Devices) X-ray detectors, and consists of a copper cylinder, 4.5 cm in radius, 50 μm thick, 8.8 cm high, surrounded by 16 equally spaced CCDs of type 55.

The CCDs are at a distance of 2.3 cm from the copper cylinder, grouped in units of two chips vertically positioned. The setup is enclosed in a vacuum chamber, and the CCDs are cooled to about 165 K by the use of a cryogenic system. A schematic drawing of the VIP setup is shown in Fig. 1.

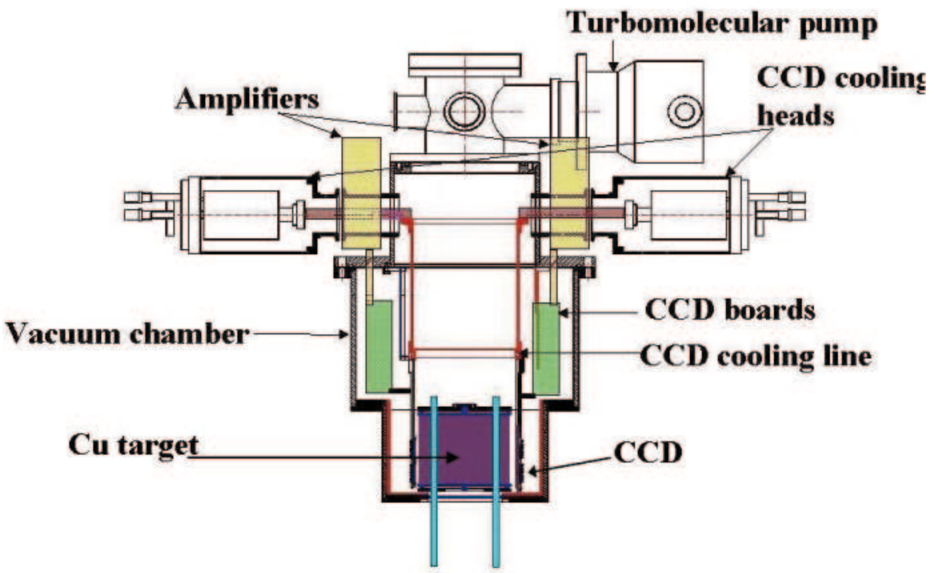

Figure 1: *The VIP setup. All elements af the setup are identified in the figure.*

The DAQ alternates periods in which a 40 A current is circulated inside the copper target with periods without current, referred as background.

VIP was installed and is taking data at the LNGS Laboratory since Spring 2006; see Figure 2 - during installation, and Figure 3 - VIP setup installed at LNGS.

3 Activities in 2008

3.1 VIP data taking and analyses results

During 2008 the VIP experiment was in data taking, alternating periods of "signal" (I=40 A) with periods without signal (I=0 A). Data analyses were performed (energy calibration, sum of spectra, subtraction of background) and the probability of violation of PEP for electrons obtained (upper limit).

A new result, improving the previously published VIP result (S. Bartalucci *et al.*, Phys. Lett. B **641**, 18 (2006)) by about an order of magnitude was obtained:

$$\frac{\beta^2}{2} < 5.7 \times 10^{-29} \tag{1}$$

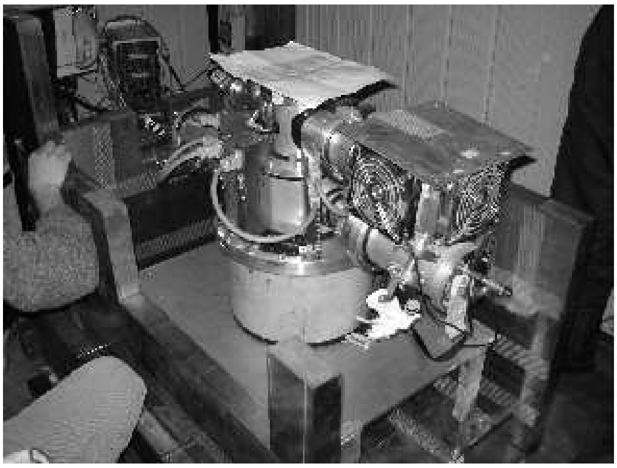

Figure 2: *The VIP setup during the installation at LNGS.*

Figure 3: *The VIP setup installed at LNGS.*

in the work performed by L. Sperandio in her Ph. D. thesis.

We have thus improved the limit obtained by Ramberg and Snow by a factor about 300, representing the new world's best limit at present.

3.2 Organization of the SpinStat2008 International Workshop

An international workshop dedicated to the spin-statistics connection and related symettries, *"Theoretical and experimental aspects of the spin-statistics connection and related symmetries"*, was organized in the period 21-25 October 2008 at Trieste:

http://www.ts.infn.it/eventi/spinstat2008/index.php

Catalina Curceanu from LNF-INFN was the co-chair, together with Edoardo Milotti from Univ. Trieste and INGN Trieste, of the Workshop.

More than 60 theoretical and experimental physicists attended, as well as a number of philosophers of science; an article published in CERN Courier January/Februaty 2009 item, was dedicated to this Workshop (title of the paper: "The Pauli principle faces testing times").

3.3 The VIP upgrade

In parallel to the actual VIP data taking, we are planning to perform a dedicated study for a possible VIP-upgrade, by replacing the CCD detectors with triggerale Silicon Drift Detectors and include a veto system (scintillators or crystals) surrounding the Copper target and SDD detectors, such as to further reduce the background. In 2008 we planned and started a series of test measurements in laboratory - data analyses are undergoing.

4 Activities in 2009

In 2009 the VIP setup will continue the data taking at LNGS, alternating periods of DAQ with current with periods of DAQ without current, at least until Spring. Periodical energy calibrations, using an X-ray tube which activates foils of Ti and Zr placed inside the setup, will be performed.

The data analyses will go on in parallel with the DAQ.

The feasibility of the upgrading of VIP by using new X-ray triggerable detectors (Silicon Drift Detectors) and the veto system will proceed, with the aim to arrive at the (new) setup definition and to start its construction.

5 Publications

5.1 List of Conference Talks

1. A. Romero Vidal, "New limit for the violation of the Pauli exclusion principle for electrons", talk at the XIII LNF Spring School in Nuclear, Subnuclear and Astroparticle Physics, INFN National Laboratories in Frascati, Italy, 12-16 of May, 2008.

2. D. Pietreanu, "Update on the VIP experiment", talk at the fourth International Workshop DICE2008, Castello Pasquini, Castiglioncello (Tuscany), 22-26 September 2008.

3. D. Pietreanu, "VIP experiment: new experimental limit on Pauli Exclusion Principlefor electrons", talk at the 10th International Workshop on Meson Production, Properties and Interaction, 6-10 June 2008, Krakow, Poland.

4. D. Pietreanu, "VIP experiment: the experimental limit on Pauli Exclusion Principle for electrons", talk at the Theoretical andexperimental aspects of the spin-statistics connection andrelated symmetries, 21-25 Octover 2008, Trieste, Italy.

5. C. Curceanu, "New experimental limit on the Pauli Exclusion principle violation by electrons (the VIP experiment)", talk at the Symposium on Prospects in the Physics of Discrete Symmetries, DISCRETE08, 11-16 December 2008, IFIC, Valencia, Spain

6. C. Curceanu, "New experimental limit on the Pauli Exclusion principle violation by electrons (the VIP experiment)", seminar given on 29 July 2008, at the Bicocca Univ. Milano, Italy.

5.2 Papers and Proceedings

1. L. Sperandio, “New experimental limit on the Pauli Exclusion Principle biolation by electrons from the VIP experiment”, Ph. D. thesis, 5 March 2008 - Tor Vergata University, Roma.

2. C. Curceanu *et al.*, “New experimental limit on the Pauli Exclusion principle violation by electrons (the VIP experiment)”, Proc. of the Symposium on Prospects in the Physics of Discrete Symmetries, DISCRETE08, 11-16 December 2008, IFIC, Valencia, Spain, to be published in Journal of Physics.

3. D. Pietreanu *et al.*, “VIP experiment: the experimental limit on Pauli Exclusion Principle for electrons”, Proc. of the Theoretical andexperimental aspects of the spin-statistics connection andrelated symmetries, 21-25 Octover 2008, Trieste, Italy, to be published in Foundations of Physics.

4. D. Pietreanu *et al.*, “VIP experiment: new experimental limit on Pauli Exclusion Principlefor electrons”, Proc. of the 10th International Workshop on Meson Production, Properties and Interaction, 6-10 June 2008, Krakow, Poland, to be published in International Journal of Modern Physics.

5. D. Pietreanu *et al.*, “Update on the VIP experiment”, Proc. of the at the fourth International Workshop DICE2008, Castello Pasquini, Castiglioncello (Tuscany), 22-26 September 2008, to be published in Journal of Physics.

4 – Theory and Phenomenology

FA51: Astroparticle Physics

D. Aristizabal Sierra (Bors.), E. Nardi (Resp.)

1 Description of the 2008 activity

During 2008 the research activities of the IS FA51-LNF focused on several different topics:

- A long and detailed study of higher order contributions to the charged fermion mass operators, in models based on the GUT-flavor symmetry $SU(5) \times U(1)$, was concluded and published in ref. [1]. Among various interesting results, it was found that in these models b-τ Yukawa unification is generally preserved, while for the two lighter families, the mass degeneracies for the leptons and quarks belonging to the same $SU(5)$ representation is always lifted, in agreement with observations.

- In ref. [2] we have investigated the possible effects on the leptogenesis mechanism of the presence of a new scale, possibly related to the breaking of a flavor symmetry. This scale is assumed to lie in-between the lepton number breaking scale and the electroweak scale. Interesting new effects have been found, among which the possibility of generating the baryon asymmetry through a lepton number conserving (but lepton flavor violating) CP asymmetry. Thus, the Cosmic baryon asymmetry could arise exclusively as a result of lepton flavor dynamics. In addition, we have also found that the presence of a flavor symmetry breaking scale allows to lower the leptogenesis scale down to a few TeV.

- Ref. [3] is a comprehensive review article on leptogenesis, that was published in Physics Reports.

- The generation of neutrino masses in leptoquarks models was investigated in ref. [4]. Special attention was put in identifying possible signatures of these models at the LHC.

- In ref. [5] novel signals of Higgs decays in supersymmetric models without R-parity were analyzed, and it was suggested that in the context of these models the Higgs may be efficiently observed at the LHC through its decay -via two neutralinos- into final states containing missing energy and isolated charged leptons.

- Neutrino masses generated through radiative 1-loop corrections within the so-called radiative seesaw model might be experimentally tested. In ref. [6] a throughout study of this scheme was carried out. Possible new collider signatures and lepton flavor violating signals, in connection with constraints from dark matter, were highlighted.

- In ref. [7] the $e^{\pm}$ cosmic rays excesses recently reported by PAMELA and ATIC where analyzed and interpreted in terms of decaying dark matter. It was found that this interpretation is compatible with all constraints, and testable by dedicated HESS observations of the Galactic Ridge. ATIC data indicate a DM mass of about 2 TeV, and it was shown that this mass naturally implies the observed DM abundance relative to ordinary matter $\Omega_{DM}/\Omega_{\rm matter} \sim 5$, of this type naturally occur in technicolor models.

if DM is a quasi-stable composite particle with a baryon-like matter asymmetry. Candidates of this type naturally occur in technicolor models.

- Purely Flavored Leptogenesis is a scenario that was first discovered in ref. [2], in which leptogenesis proceeds solely because of flavor effects, being the total lepton number violating CP asymmetry in the decays of the heavy seesaw singlet neutrinos vanishing. We are presently concluding the study of this scenario, that has the nice feature of allowing for leptogenesis at the TeV scale. Preliminary results have been already reported in ref. [8].

Talks at Conferences

1. E. Nardi, "Recent Issues in Leptogenesis", Invited talk at the International Workshop: Low Energy Precision Electroweak Physics in the LHC Era, 12-22 October, 2008; Institute for Nuclear Theory, University of Washington Seattle (USA).
`www.int.washington.edu/talks/WorkShops/int_08_3/People/Nardi_E/Nardi.pdf`
2. E. Nardi, "Leptogenesis", Invited talk at the International Workshop Neutrino Frontiers 2008, 23-26 October 2008, University of Minnesota, Minneapolis (USA).
`www.ftpi.umn.edu/neutrinos08`
3. D. Aristizabal Sierra, "Implications of an additional scale on leptogenesis". Talk at DISCRETE '08: Symposium on Prospects in the Physics of Discrete Symmetries, 11-16 December 2008, Valencia (Spain).

References

1. L. F. Duque, D. A. Gutierrez, E. Nardi, and J. Norena, Phys. Rev. D **78**, 035003 (2008).
2. D. Aristizabal Sierra, M. Losada, and E. Nardi, Phys. Lett. B **659**, 328 (2008).
3. S. Davidson, E. Nardi, and Y. Nir, Phys. Rept. **466**, 105-177 (2008).
4. D. Aristizabal Sierra, M. Hirsch, and S. G. Kovalenko, Phys. Rev. D **77**, 055011 (2008).
5. D. Aristizabal Sierra, W. Porod, D. Restrepo, and C. E. Yaguna, Phys. Rev. D **78**, 015015 (2008).
6. D. Aristizabal Sierra, J. Kubo, D. Restrepo, D. Suematsu, and O. Zapata, Phys. Rev. D **79**, 013011 (2009).
7. E. Nardi, F. Sannino, and A. Strumia, JCAP **0901**, 043 (2009).
8. D. Aristizabal Sierra, L. A. Muñoz, and E. Nardi, "Implications of an Additional Scale on Leptogenesis", Invited talk at DISCRETE '08, to appear in Journal of Physics: Conference Series.

LF21: Phenomenology of elementary particle interactions at colliders

O. Cata (Bors. PD), V. Del Duca (Ass.), J. Kamenik (Bors. PD) G. Isidori (Resp.),
O. Leitner (Bors. PD), F. Mescia (Art. 23), S. Pacetti (Bors. PD),
G. Pancheri (Ass., Resp. Naz.), O. Shekhovtsova (Bors. PD)

1 Summary of the project

The research topics investigated by this project can be divided into the following areas:

- Flavour physics, precision tests and physics beyond the Standard Model (G. Isidori, J. Kamenik, F. Mescia).
- Light flavour spectroscopy and τ-physics (G. Isidori, O. Leitner)
- Hadronic Form Factors and meson spectroscopy (S. Pacetti)
- Hadronic cross-sections (G. Pancheri, O. Shekhovtsova)
- Theoretical and phenomenological aspects of QCD at colliders (V. Del Duca)

The activity of the phenomenology group at Frascati can be seen in detail on our public web page [`www.lnf.infn.it/theory/pheno2.html`]. In the following we shall briefly describe all the different projects undertaken by the above participants.

2 Flavour physics, precision tests, and physics beyond the Standard Model

One of the strategies to obtain additional clues about the nature of New Physics (NP) is by means of precision tests of the Standard Model (SM) at low energies. These are particularly interesting in: i) electroweak processes calculable with high precision, where even tiny deviations from the SM can be detected; ii) processes which are not mediated by tree-level SM amplitudes, where the relative effect of NP contributions can be enhanced. Up to now there is no clear evidence for deviations from the SM in both type of processes, and this leads to significant constraints in building realistic extensions of the SM. For instance, realistic models must possesses a highly non-generic flavour structure. These constraints are particularlysevere for NP models with new degrees of freedom around the TeV scale, as required by a natural stabilisation the $SU(2)_L \times U(1)_Y \to U(1)_Q$ spontaneous symmetry breaking [1, 2, 3]. The attempt to clarify this problem, both at the phenomenological level (with the help of precision data on rare decays) and at a more fundamental level (with the help of new symmetry principles), is one of the main activity of our group.

A closely related subject –which is also one of the primary research objectives of our group– is a better understanding of the SM itself, fixing his fundamental couplings (quark masses, CKM angles, non-perturbative condensates, . . .) by means of precise calculations within the framework of effective field theories and Lattice QCD.

Within this general scenario, last year we have performed a series of works on:

Precision constraints in Supersymmetry extestions of the SM.

Motivated by recent progress in consistently and rigorously calculating electroweak precision observables and flavour related observables, we have updated our previous analyses of the Constrained Minimal Supersymmetric Standard Model (CMSSM), taking into account electroweak precision data, flavour physics observables and the abundance of Cold Dark Matter [4].

Higsless models.

One or more heavy spin-1 fields may replace the Higgs boson in keeping perturbative unitarity up to a few TeV. By means of general description of spin-1 fields in the electroweka chiral Lagrangian, we have analysed if and how the sole exchange of these fields can also account for the ElectroWeak Precision Tests. This turns out to be impossible in the models where the heavy vectors are gauge fields of some hidden broken symmetry. However, generic composite model hints to apositive solution [5].

Signatures of minimal flavour violating new physics at large $\tan\beta$*.*

Minimal Flavor Violation (MFV) is an attractive approach to solve the flavour problem assuming that the Yukawa couplings are the only irreducible sources of flavour symmetry breaking also beyond the SM [6]. This ansatz allows also a successful Leptogenesis [7]. We have reviewed and updated the constraints on dimension-six effective operators in models respecting the MFV hypothesis, both in the one-Higgs doublet case and in the two-Higgs doublet scenario with large tan beta [8]. The constraints were derived mainly from flavour changing neutral currents (FCNCs) and helicity suppressed observables measured at the kaon and B meson factories. In particular, the recently measured semileptonic decay $B \to D\tau\nu$ was found to give competitive bounds on charged Higgs parameters in MFV models at large $\tan\beta$, [9] mainly because the associated theoretical uncertainties can be brought under control [10]. We have also discussed the implications of the derived bounds in view of improved measurements in exclusive and inclusive observables in $b \to s$ and $s \to d$ transitions.

Signatures of new physics in the flavour changing neutral current top processes.

The upcoming LHC can be considered a top "factory" giving us an unique possibility to study possible new physics signatures in unprecedented ways. Many scenarios of new physics (NP) allow top quark flavour changing neutral current (FCNC) decays. Using the most general model independent Lagrangian we have investigated [11] possible experimental signals of new physics in $t \to c(u)\ell^+\ell^-$ FCNC top decays. We found that a measurement of two possible angular asymmetries might give important and interesting information on the structure of NP contributions. It is particularly interesting to use these observables to discriminate among variety on NP scenarios.

Spectator effects in heavy meson decay widths.

Controlling the power corrections in the spectra of inclusive semileptonic heavy to light decays has been and still is an important obstacle when aiming at the reliable extraction of the corresponding CKM parameters, especially $|V_{ub}|$. The relevant $1/m_b^3$ corrections involve the matrix elements of dimension-6 four-quark operators of the flavour structure $\Delta B = 0$ and also enter the lifetime differences of hadrons containing one valence b-quark. They can be computed on the lattice, where however, control over the chiral extrapolation is essential in order to reduce the systematic uncertainties. Therefore, in Ref. [12] we have provided the chiral corrections associated with the bag parameters computed in the static heavy quark limit of heavy meson chiral perturbation theory (HMχPT). Performing also a rough phenomenological estimate in the limit of three light quarks we have found that the chiral logarithmic corrections alone cannot easily reconcile the experimental results on the lifetime ratios of B-mesons with theory predictions.

Lattice QCD.

Weak decays of hadrons observed in experiment are quite promising to discover physics beyond the SM. Theoretical uncertainties, however depends on our knowledge of QCD at low energy. At this regime, QCD is non-perturbative and considerable efforts are devoted to taming this uncertainty by QCD simulation (Lattice QCD).This approach has already shown promising results to study weak decays of hadrons and will be very powerful also in the LHC era. Nowadays, thanks to improved computing power (MareNostrum and PC-clusters) and to better theoretical approaches on lattice action formulation, first principle QCD calculations are becoming feasible. Working together with European Twisted Mass QCD Collaboration (ETMC), we have studied the $N_F = 2$ setup, where only two quarks (heavy up and down) are added to sea of gluons, for several phenomenological quantities. [13] In this $N_F = 2$ setup, strange effects on sea are neglected and make these approximations not suited for phenomenology. However, a project of generating $N_F = 2 + 1 + 1$ configurations, where both strange and charm quarks are considered on sea, shows reliable and under study.

3 Light flavour spectroscopy and τ-physics

Theoretical description of Scalar Meson.

We have discussed the effect of the instanton induced, six-fermion effective lagrangian on the decays of the lightest scalar mesons in the diquark-antidiquark picture. The addition allows for a remarkably good description of scalar meson decays. The same effective lagrangian produces a mixing of the lightest scalars with the positive parity $q\bar{q}$ states. Comparing with previous work where the $q\bar{q}$ mesons are identified with the nonet at 1200-1700 MeV, we find that the mixing required to fit the mass spectrum is in good agreement with the instanton coupling obtained from light scalar decays [14].

Tau decay

A way to explain the puzzling difference between the pion form factor as measured in e^+eannihilations and in τ decays is discussed. We show that isospin symmetry breaking, beside the already identified effects, produces also a full mixing between the ρ^0, ω and ϕ mesons which generates an isospin 0 component inside the ρ^0 meson. This effect, not accounted for in current treatments of the problem, seems able to account for the apparent mismatch between e^+e and τ data below the ϕ mass [15, 16].

Scalar mesons effects in D decays

We propose a model for $D^+ \to \pi^+\pi^-\pi^+$ decays following experimental results which indicate that the two-pion interaction in the S-wave is dominated by the scalar resonances $f_0(600)/\sigma$ and $f_0(980)$ [17]. The weak decay amplitude for $D^+ \to R\pi^+$, where R is a resonance that subsequently decays into $\pi^+\pi^-$, is constructed in a factorization approach. In the S-wave, we implement the strong decay $R \to \pi^-\pi^+$ by means of a scalar form factor. This provides a unitary description of the pion-pion interaction in the entire kinematically allowed mass range $m^2_{\pi\pi}$ from threshold to about 3 GeV^2. In order to reproduce the experimental Dalitz plot for $D^+ \to \pi^+\pi^-\pi^+$, we include contributions beyond the S-wave. For the P-wave, dominated by the $\rho^0(770)$, we use a Breit-Wigner description. Higher waves are accounted for by using the usual isobar prescription for the $f_2(1270)$ and $\rho^0(1450)$. The major achievement is a good reproduction of the experimental $m^2_{\pi\pi}$ distribution, and of the partial as well as the total $D^+ \to \pi^+\pi^-\pi^+$ branching ratios [18].

4 Hadronic form factors

Pointlike Baryons? [19]

A peculiar feature, observed in the *BABAR* data on $e^+e^- \to \mathcal{B}\overline{\mathcal{B}}$ cross sections ($\mathcal{B}$ stands for baryon), is the non-vanishing cross section at threshold for all these processes. This is the expectation due to the Coulomb enhancement factor acting on a charged fermion pair. Remarkably, in the case of $e^+e^- \to p\overline{p}$ it is found that Coulomb final state interactions largely dominate the cross section at threshold and it turns out a form factor $|G^p(4M_p^2)| \simeq 1$, as a pointlike fermion. A similar phenomena occurs in the $e^+e^- \to \Lambda_c\overline{\Lambda_c}$, recently measured by Belle. In the case of neutral strange baryons the non-vanishing cross section at threshold is interpreted as a remnant of quark pair Coulomb interaction before the hadronization, taking into account the asymmetry between attractive and repulsive Coulomb factors. Besides strange baryon cross sections are successfully compared to U-spin invariance relationships.

A practical guide to unravel time-like transition form factors [20]

We have defined a general procedure which, combining: the description of the transition form factors (tff) in terms of vector meson propagators, the quark-counting rule (QcR) asymptotic power law, and the analyticity requirement by means of dispersion relations, provides a parameterization for the tff's valid in the whole q^2-real axis. The experimental and theoretical constraints, that individually concern only certain energy regions, have been "propagated" to all values of q^2.

The application of this procedure is twofold. By assuming as known the quark structure of the mesons under consideration, we can look for vector resonances, i.e. excited states of the $\phi(1020)$, $\omega(782)$ and $\rho^0(770)$, which couple with the studied final state. By exploiting the fact that this procedure is strongly dependent on the quark structure of the final mesons, we may test how well different hypotheses about this structure agree with data. We have analysed this procedure in detail in the $\phi\eta$ channel, where the parameters of resonances belonging to the ϕ-family have been determined in agreement with other analyses.

By way of example, an application to the $\phi\eta$ channel is reported, see fig. 1. In the case of vertices like $H\gamma M_I$, where H is an heavy $c\bar{c}$ and $b\bar{b}$ vector meson, the lack of data, mainly in conversion decay and cross section, precludes every possibility of having good descriptions of the corresponding tff's. On the other hand, the study of the $\gamma\gamma^* M_I$ coupling looks more promising. Some mechanisms of the procedure must be modified, in particular the expressions to extract the tff's from decay rates and cross sections, and the power law for the asymptotic behavior, because in this case the hadronic helicity is conserved.

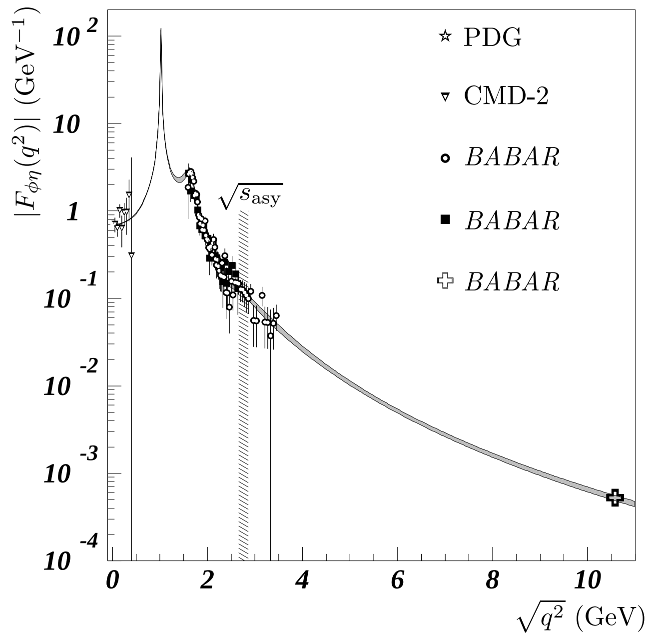

Figure 1: *Reconstructed* $|F_{\phi\eta}(q^2)|$ *tff shown in a wide rage of* q^2.

5 Hadronic cross-sections

Hadronic cross-sections were studied in two different type of processes and different energy ranges, namely at DAΦNE, and at high energy colliders in reactions of the type $A + B \to X$ where A, B could be a proton or an antiproton or a photon, with emphasis on the role played by soft gluons on the saturation of the Froissart bound.

Final State Radiation effects at DAPHNE

The problem of the final state radiation (FSR) is one of the main problems in the measurement of the the hadronic cross section at DAFNE. It is related with a fact that the FSR process is an irreducible background in radiative return measurements of the hadronic cross section and spoils the factorization of the cross section. In any experimental setup the process of FSR cannot be excluded from the analysis. The KLOE experiment has developed two different analysis strategies: the first one is with the photon emitted at small angle ($\theta_\gamma < 15°$) and the other one is for the photon reconstructed at large angle ($60° < \theta_\gamma < 120°$), being for both $50° < \theta_\pi < 130°$. In the case of the small angle kinematics the FSR contribution can be safely neglected, while for the large angle analysis it becomes relevant (upto 40% of ISR).

From another side the FSR process is interesting in itself. In fact, a detailed experimental study of FSR allow us to get information about pion-photon interaction at low energies. In the region below 2 GeV the pQCD is not applicable to describe FSR and calculation of the cross section relies on the low energy pion–photon interaction model. Thus the measured FSR cross section gives an unique possibility to get very interesting information on the dynamics of interacting mesons and photons, to test the pion–photon interaction models and extract their parameters [21].

We have proposed to consider together the charged ($\pi^+\pi^-\gamma$) and neutral ($\pi^0\pi^0\gamma$) final channels. The measured cross section in the neutral channel together with the measured asymmetries and cross section in the charged channel, allows to extract information on pion-photon interaction and test effective models for FSR.

The developed computer code FASTERD (FinAL STatE Radiation at DAΦNE) is a Monte Carlo event generator written in FORTRAN that simulates both processes, where the hard photon can be emitted by the leptons [22]. To test the accuracy of the program we compared the numerical results with the analytical prediction and with the results of the MC program PHOKHARA runnig the last one at the leading order approximation (only one photon is radiated). The results of the PHOKHARA program coincides with the FASTERD prediction better than 1%.

An important feature of FASTERD is a possibility to estimate the double resonance contribution. At the first sight in the energy region about $s \approx m_\phi^2$ it is enough to include only the $\gamma^* \to \phi \to \rho\pi \to \pi\pi\gamma$ mechanism. However, at $s = m_\phi^2$ our simulation gives the $\sigma(\phi \to ((f_0+\sigma)\gamma+\rho^0\pi^0) \to \pi^0\pi^0\gamma) = 0.451 \pm 0.001$ nb whereas $\sigma((\rho/\rho') \to \omega\pi^0 \to \pi^0\pi^0\gamma) = 0.529 \pm 0.012$ nb (in agreement with KLOE results).

Total cross-sections and the Froissart bound

LHC will soon measure the total hadronic cross-section, adding one more point to a long quest in the understanding of hadronic collisions. As yet, there is no first principle calculation to predict the value of the total cross-section at any given energy, but it is possible to obtain QCD and QCD inspired descriptions, which, together with a certain degree of parameter fitting, can give some insight on the underlying dynamics. Since quite some time, a model was developed within this group, in which the rise with energy is driven by the increasing number of low x (fractional momenta) gluons. In such model high energy saturation is obtained through soft gluon emission, with integration of the soft gluon momenta extended down to zero, and with an appropriate ansatz for the behaviour of the strong coupling constant in this region. This model, inspired by the Bloch-Nordsieck (BN) theorem for soft photons and thus called the BN model, was applied to make predictions for the total proton-proton cross-section at LHC [23, 24, 25, 26]. Subsequently the model has been applied to photo-production. The predictions of the BN model were considered both in the present accelerator energy ranges [27] as well as extended to very high energies, like the ones reachable though cosmic ray experiments, as shown in Fig. 2.

This work has been presented at various meetings, including the Warsaw meeting on Linear Collider Physics, Diffraction 2008 [28] and is presently under submission [29]. This work is

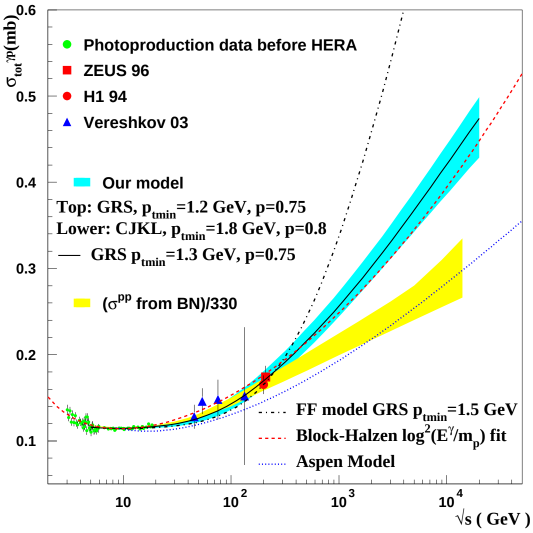

Figure 2: *The Bloch-Nordsieck model results for γp total cross-sections are compared with data and other model predictions.*

done in collaboration with researchers from University of Perugia, University of Granada and the Center for Technology and Science, Bangalore, India.

6 Theoretical and phenomenological aspects of QCD at colliders

Higgs Boson Production in Hadronic Collisions

At the LHC, the Higgs boson will be produced mostly via gluon fusion, with the Higgs boson interacting with the gluons via a top-quark loop. This production mode is known at next-to-leading-order (NLO) accuracy in the strong coupling constant α_S for finite values of the top-quark mass m_t, and at next-to-next-to-leading-order (NNLO) accuracy in the limit $m_t \to \infty$. The latter, though, generates spurious logarithms $\ln(\hat{s}/m_H^2)$, which are not present when the full m_t dependence is taken into account. Higgs production via gluon fusion has been considered for finite values of m_t in the limit of high parton centre-of-mass energy $\hat{s}$ [30], which allows us to improve upon the NNLO calculation mentioned above. Furthermore, multiple hard radiation emitted in the process can be resummed using a high-energy factorisation of the scattering amplitude [31].

Higher-Order Corrections to Scattering Cross Sections at high Q^2

In the quest to discover New Physics signals, typically covered by the huge SM backgrounds, the precise experimental measurements at the Tevatron and at the LHC require theoretical calculations which are at least as precise. In some instances, like in the inclusive production of the Higgs boson via gluon fusion mentioned above, the desired accuracy is achieved only at NNLO in α_S. Thus, a general algorithm to compute jet cross sections at NNLO is being implemented [32]

Scattering amplitudes in the maximally supersymmetric $N = 4$ super-Yang-Mills theory

In the context of the maximally supersymmetric N = 4 super-Yang-Mills theory, we have analysed in the high-energy limit the question of the validity of a guess (the Bern-Dixon-Smirnov ansatz) on the exponentiation of a scattering amplitude at any number of loops and legs. The ansatz is believed to be valid for four-point [33)]and five-point amplitudes at any number of loops, but it is known to fail for two-loop amplitudes with six or more legs. However, the ansatz-violating contribution is known only numerically. This piece of information has proven insufficient, so far, to learn the correct form of the exponentiation, if any. We have established that the simplest high-energy limit is not detailed enough to probe the ansatz-violating contribution. Accordingly, we have lain down the conditions for more sophisticated high-energy limits to probe the ansatz violation [34)].

7 List of Conference Talks

1. F. Mescia, "Theory Review of Kaon Physics", Conference on Flavor Physics and CP Violation, Taipei, Taiwain May 5^{th} - 9^{th} 2008.

2. F. Mescia, "Precision Tests from Kaon Decays", Incontri di Fisica delle Alte Energie, Bologna, Italy, March 26^{th} - 28^{st} 2008.

3. F. Mescia, "Flavour Physics in the LHC era", Nadal Meeting at UB, Barcelona, Spain, December 16^{th} - 18^{st} 2008.

4. J. F. Kamenik, "$\Delta F = 1$ Constraints on Minimal Flavour Violation", Rencontres de Moriond EW 2008, La Thuile, Italy, 1-8 Mar 2008.

5. J. F. Kamenik, "Theory of the decays $B \to D\tau\nu$", Incontri di Fisica del B, Cagliari, Italy, 4-5 Apr 2008.

6. J. F. Kamenik, "Low energy signals of MFV at large $\tan\beta$", Planck 08, Barcelona, Spain, 19-23 May 2008.

7. J. F. Kamenik, "Constraining Minimal Flavor Violation at Large $\tan\beta$", B physics workshop Capri 2008, Anacapri, Italy, 16-18 Jun 2008.

8. J. F. Kamenik, "Review of B-Physics Theory", Euroflavour 2008, Durham, UK, 22-26 Sep 2008.

9. G. Isidori, "Lepton Flavor Violation in charged leptons", Neutrino Oscillations in Venice, Venezia, 17 Apr 2008.

10. G. Isidori, "Standard Higgs, Susy Higgs or no Higgs at all", Congresso Italiano di Fisica Teorica, Sestri Levante, 4 June 2008.

11. G. Isidori, "The Higgs Puzzle: Standard Model vs. Supersymmetry", Munich Colloquium, Munich, 27 October 2008.

12. G. Isidori, “The breaking of flavour and CP symmetries”, Symmetries in the Universe, Kloister Irsee, Germany, June 2008.

13. G. Isidori, “B Physics in the LHC era”, UK meeting on Particle Physics Phenomenology, Durham, February 2008.

14. S. Pacetti, “Charmed Particles Production in $e^+e^- \to c\overline{c}$ at 10.6 GeV”, Workshop on parton fragmentation processes in the vacuum and in the medium, February 25-29, 2008, ECT* Trento, Italy.

15. S. Pacetti, “Initial state radiation at *BABAR*, Workshop on parton fragmentation processes in the vacuum and in the medium”, February 25-29, 2008, ECT* Trento, Italy.

16. S. Pacetti, “Mesoni leggeri e fattori di forma del nucleone a *BABAR*”, Mini-Workshop sulle prospettive di fisica adronica al Jefferson Lab e in altri laboratori, February 27-28, 2008, Genova, Italy.

17. S. Pacetti, “Unexpected features of $e^+e^- \to$ baryon-antibaryon cross sections near threshold and analysis of G_E^p/G_M^p”, Hadron Structure and QCD: from LOW to HIGH energies, June 30-July 4, 2008, Gatchina, Russia.

18. G. Pancheri, “Total photon-photon cross-sections”, ECFA 2008, Warsaw June 2008.

19. G. Pancheri, “QCD Issues and total cross-section at the photon collider, LC08, e^+e^- physics at the TeV scale”, September 2008, Frascati.

20. G. Pancheri, “Zero momentum gluons and the total pp and p anti-p cross-section”, Poster session at ICHEP08, Philadelphia july 2008.

21. V. Del Duca, “Higgs production in association with jets at the LHC”, Epiphany Conference, Krakow, Poland 2008.

22. V. Del Duca, “MSYM amplitudes in the high-energy limit”, Workshop Gauge Theory and String Theory, Zurich, Switzerland 2008.

References

1. M. Antonelli *et al.* [FlaviaNet Working Group on Kaon Decays], arXiv:0801.1817.

2. M. Artuso *et al.*, Eur. Phys. J. C **57**, 309 (2008).

3. M. Raidal *et al.*, Eur. Phys. J. C **57**, 13 (2008).

4. O. Buchmueller *et al.*, JHEP **0809**, 117 (2008).

5. R. Barbieri, G. Isidori, V. S. Rychkov, and E. Trincherini, Phys. Rev. D **78**, 036012 (2008).

6. G. Isidori, Int. J. Mod. Phys. A **22**, 5841 (2008).

7. V. Cirigliano, A. De Simone, G. Isidori, I. Masina, and A. Riotto, JCAP **0801**, 004 (2008).

8. T. Hurth, G. Isidori, J. F. Kamenik, and F. Mescia Nucl. Phys. B **808**, 326 (2009).

9. J. F. Kamenik and F. Mescia, Phys. Rev. D **78**, 014003 (2008).

10. J. O. Eeg, S. Fajfer, and J. F. Kamenik, Phys. Rev. D **78**, 074008 (2008).

11. J. Drobnak, S. Fajfer, and J. F. Kamenik, arXiv:0812.0294, accepted for publication at JHEP.

12. D. Becirevic, S. Fajfer, and J. F. Kamenik, Phys. Lett. B **671**, 66 (2009).

13. P. Dimopoulos *et al.*, PoS **LATTICE2008**, 271 (2008), arXiv:0810.2443.

14. G. 't Hooft, G. Isidori, L. Maiani, A. D. Polosa, and V. Riquer, Phys. Lett. B **662**, 424 (2008).

15. M. Benayoun, P. David, L. Del Buono, O. Leitner, and H. B. O'Connell, Eur. Phys. J. C **55**, 199 (2008).

16. M. Benayoun, P. David, L. Del Buono, O. Leitner, and H. B. O'Connell, Nucl. Phys. Proc. Suppl. **181-182**, 161 (2008).

17. D. R. Boito, J. P. Dedonder, B. El-Bennich, O. Leitner, and B. Loiseau, arXiv:0812.3843.

18. B. El-Bennich, O. Leitner, J. P. Dedonder, and B. Loiseau, arXiv:0810.5771.

19. R. Baldini, S. Pacetti, and A. Zallo, arXiv:0812.3283.

20. S. Pacetti, Eur. Phys. J. A **38**, 331 (2008).

21. G. Pancheri, O. Shekhovtsova, and G. Venanzoni, J. Exp. Theor. Phys. **106**, 470-480 (2008).

22. O. Shekhovtsova, G. Venanzoni, and G. Pancheri, arXiv:0901.4440, to be published in Computing Journal of Physics.

23. A. Achilli, R.M. Godbole, I. Grau, G. Pancheri, and Y.N. Srivastava, Phys. Lett. B **659**, 137 (2008).

24. A. Achilli, R.M. Godbole, I. Grau, G. Pancheri, and Y.N. Srivastava, "LHC predictions for total cross-sections from the eikonal mini-jet model and the Froissart bound", Proc. XLII Rencontres de Moriond, Eds. E. Auge', B. Pietrzyk and J. Tran Than Van, La Thuile, March 2007, pag. 321 (World Scientific, Singapore, 2008).

25. A. Achilli, R.M. Godbole, I. Grau, G. Pancheri, and Y.N. Srivastava, To appear in the proceedings of 34th International Conference on High Energy Physics (ICHEP 2008), Philadelphia, Pennsylvania, 30 Jul - 5 Aug 2008; arXiv:0810.3411.

26. A. Achilli, R.M. Godbole, I. Grau, G. Pancheri, and Y.N. Srivastava, Fizika B **17**,143-150 (2008); arXiv:0807.3826.

27. R.M. Godbole, I. Grau, G. Pancheri, and Y.N. Srivastava, Nucl. Phys. Proc. Suppl. **184**, 85-90 (2008).

28. R.M. Godbole, I. Grau, G. Pancheri, and Y.N. Srivastava, To be published in the Proceedings of Diifraction 2008; arXiv:0812.4705.

29. R.M. Godbole, I. Grau, G. Pancheri and Y.N. Srivastava, arXiv:0812.1065, submitted to EPJC.

30. S. Marzani, R. D. Ball, V. Del Duca, S. Forte, and A. Vicini, Nucl. Phys. B **800**, 127 (2008).

31. J. R. Andersen, V. Del Duca, and C. D. White, JHEP **0902**, 015 (2009).

32. U. Aglietti, V. Del Duca, C. Duhr, G. Somogyi, and Z. Trocsanyi, JHEP **0809**, 107 (2008).

33. V. Del Duca and E. W. N. Glover, JHEP **0805**, 056 (2008).

34. V. Del Duca, C. Duhr, and E. W. N. Glover, JHEP **0812**, 097 (2008).

LF61: Low-dimensional systems and spin-Hall effect

S. Bellucci (Resp. Naz.), M. Benfatto, M. Cini (Ass.), F. Corrente (Dott.),
K. Hatada (Borsista PD), K. Hayakawa (Borsista PD), G. Iovane (Ass.),
C. Natoli (Ass.), P. Onorato (Borsista PD), F. Palumbo (Ass.), R. Pastore (Ass.),
E. Perfetto (Borsista PD), N. Pugno (Ass.), G. Stefanucci (Ass.)

1 External collaborating Institutions:

Univ. Roma La Sapienza, Univ. Roma Tor Vergata, IHEP-Protvino (Russia), Univ. Pune, India, Burnham Institute (La Jolla, CA, USA), ILL (Grenoble, France).

2 Research Activity

In the last decade enormous attention has been devoted toward control and engineering of spin degree of freedom in nanostructures, usually referred to as spintronics. In fact physicists are trying to exploit the spin of the electron rather than its charge, in order to create a remarkable new generation of spintronic devices that are able to control the electron spin in submicrometric devices. Since the pioneering work of Datta and Das, in which they proposed a spin transistor based on the spin-orbit interaction (SOI), there has been a great deal of theoretical and experimental work concerning the possibility of controlling the electron spin by means of an electric field with or without the help of magnetic field and magnetic material. Our research activity on the crossover from the ballistic to the resonant tunneling transport for an ideal one-dimensional quantum ring with spin-orbit interaction, has pursued the objective of proposing a device which works in the regime of resonant tunneling and is able to handle a single electron. Also, in dealing with the ballistic spin rotator based on a Π nanojunction with spin-orbit interaction, we showed that a large class of unitary transformations can be attained with already one Π nanojunction or a few Π nanojunctions in series. By choosing appropriate parameters the spin transformations can be made unitary, which corresponds to lossless gates.

We also proposed an all-electrical nanostructure where a spin accumulation, an observable signature of the spin Hall effect, and a spin current are induced in the probes attached to a quantum-coherent ballistic onedimensional T junction when unpolarized charge current is injected through its longitudinal lead. Our proposal is essentially based on the Rashba SOI and on the presence of one lead where the SOI vanishes. Tuning of the Rashba SOI in the semiconductor heterostructure hosting the junction generates quasiperiodic oscillations of the predicted spin current due to spin-sensitive quantum-interference effects caused by the difference in the interferometric phase accumulated by opposite spin states.

We have developed a generalization of the multiple-scattering formalism to deal with Auger-photoelectron coincidence spectroscopy (APECS) in the solid state. We have merged the exact atomic treatment of the angular correlations between the two electrons and the single-particle approach, on which the multiple-scattering description of condensed matter relies. This allows the recovering, even in extended systems, of the entangled form of the electron-pair wave function characterizing the coincidence angular diffraction pattern. We have then performed numerical calculations for the Ge(100) $L_3M_{45}M_{45}$ APECS and compared the results with previous experiments. We found that, in the given geometry, the diffraction patterns in coincidence with different directions of the photoelectron keep little memory of the atomic anisotropy. We speculated on the conditions to be fulfilled in order to enhance the atomic-orbital sensitivity in APECS through solid-state diffraction effects.

We have continued our work on a rigorous derivation of a real space full-potential multiple-scattering theory (FP-MST), valid both for continuum and bound states, for the calculation of core-level synchrotron radiation spectroscopy as applied to many interdisciplinary problems in condensed matter physics. In particular this approach provides a straightforward solution to the problem of calculating scattering states for the 3-dimensional Schrodinger equation in extended systems without any approximation for the geometrical shape of the scattering potential.

We recently proposed an exact bosonization procedure which generates a Hamiltonian of composite bosons interacting among themselves and with fermionic quasiparticles. The interaction among composites whose mixing is allowed by symmetries is strong, but a simple condensate cannot have a significant mixing with other composites. We determine the conditions of no mixing, study their effects and compare the results with the Random Phase Approximation and the BCS theory.

One of us (N. Pugno) was also involved in works on super-adhesive or super-strong materials, specifically in nano and bio science and technology.

We organized so far nine Schools and Workshops on nanoscale science and technology, aiming to assess the current state of the art and stimulate research networking, held under the patronage of INFN and other institutions from both the public and private sectors:

- 1. N&N2000, S. Margherita di Pula (Cagliari), Italy, September 24 - October 4, 2000, http://www.lnf.infn.it/conference/nn2000/default.html
- 2. N&N2001, Frascati (Roma), Italy, October 17 - 27, 2001, http://www.lnf.infn.it/conference/nn2001/Welcome.html
- 3. N&N2002, Frascati (Roma), Italy, September 23 - 28, 2002, http://www.lnf.infn.it/conference/nn2002/
- 4. N&N2003, Frascati (Roma), Italy, September 15 - 19, 2003, http://www.lnf.infn.it/conference/nn2003/
- 5. N&N2004, Frascati (Roma), Italy, October 14 - 20, 2004, http://www.lnf.infn.it/conference/nn2004/
- 6. N&N2005, Monteporzio Catone (Roma), Italy, November 14 - 16, 2005, http://www.lnf.infn.it/conference/nn2005/
- 7. N&N2006, Monteporzio Catone (Roma), Italy, November 6 - 9, 2006, http://www.lnf.infn.it/conference/nn2006/
- 8. N&N2007, Frascati (Roma), Italy, October 15 - 16, 2007, http://www.lnf.infn.it/conference/nn2007/

- 8. N&N2008 Frascati (Roma), Italy, October 20-23, 2008,
  http://www.lnf.infn.it/conference/nn2008/

We published the Proceedings of the School and Workshop n SAM2006, with the title: Nanoparticles and Nanodevices in Biological Applications. The INFN Lectures - Vol I, S. Bellucci (ed.), Lecture Notes in Nanoscale Science and Technology Vol. 4, Springer-Verlag Berlin Heidelberg, 2009, XII, 198 p., ISBN: 978-3-540-70943-5, <http://www.springer.com/series/7544.

3 Awards received by LNF Authors in the Year 2008

Primo Premio Corrente Fabio, "Polarizzazione delle correnti di spin in nanostrutture a bassa dimensionalitá." Italian Physical Society Congresso SIF, Pisa September 2008.

4 List of Conference Talks

1. C. Natoli, "An Overview of multiple scattering theory Type", Workshop on X-ray Spectroscopies: theory and experiment Place: Lausanne, January 30 - February 1, 2008.

2. S. Bellucci, "Electronic transport in carbon nanotubes: Luttinger Liquids and correlated superconductivity", Computational Challenges and Tools for nanotubes (CCTN08), 28 June 2008, Le Corum, Montpellier, France.

3. E. Perfetto, "Electron Correlations in Carbon Nanotubes and Graphite from Auger Spectroscopy", School and Workshop on Nanoscience and Nanotechnology 2008, Frascati, October 20, 2008.

4. M. Cini, "W=0 mechanism of superconductivity in Carbon Nanotubes", School and Workshop on Nanoscience and Nanotechnology 2008, Frascati, October 20, 2008.

5. G. Stefanucci, "Ultrafast manipulation and engineering of spin currents and densities in Quantum Dot devices", School and Workshop on Nanoscience and Nanotechnology 2008, Frascati, October 22, 2008.

6. M. Cini, "Models of superconductivity by repulsive interactions and quantum transport phenomena in nanoscopic systems", School and Workshop on Nanoscience and Nanotechnology 2008, Frascati, October 23, 2008.

7. P. Onorato, "Nanojunctions as logical gates for spintronics", Presented at the XCIV Congresso Nazionale SIF, Genova, 22-27 September 2008.

8. P. Onorato, "Physics of nanostructures and semiclassical approach for teaching the quantum theory of summing over the paths", Presented at the XCIV Congresso Nazionale SIF Genova, 22-27 September 2008.

9. N. Pugno, "Smart flexible nanovectors", 1st International Conference on Drug Design and Discovery, February 4-7, 2008, Dubai, UAE.

10. N. Pugno, “Gecko-inspired suit could have you climbing the wall”, 3rd Int. Conf. Smart Materials, Structures; Systems, CIMTEC2008, June 8-13, 2008, Acireale, Italy.
11. N. Pugno, “The role of defects in the strength of the megacable”, 2nd International Conference on Space Elevator and CNT Tether Design, December 6-7, 2008, Luxembourg, Luxembourg.

References

1. F. Da Pieve *et al.*, Phys. Rev. B **78**, 035122 (2008).
2. K. Hatada, K. Hayakawa, M. Benfatto, and C. Natoli J. Phys.: Condens. Matter **21**, 104206 (2009).
3. V.M. Biryukov and S. Bellucci, Nucl. Instr. & Meth. B **266**, 235 (2008).
4. S. Bellucci and P. Onorato, Phys. Rev. B **78**, 235312 (2008).
5. S. Bellucci and P. Onorato, Phys. Rev. B **77**, 165305 (2008).
6. S. Bellucci and P. Onorato, Phys. Rev. B **77**, 075303 (2008).
7. S. Bellucci, F. Carillo, and P. Onorato, Eur. Phys. J. B **66**, 509 (2008).
8. M. Cini, E. Perfetto, G. Stefanucci, and S. Ugenti, J. Phys.: Condens. Matter **20**, 474209 (2008).
9. S. Bellucci and P. Onorato, J. Phys.: Condens. Matter **20**, 474214 (2008).
10. S. Bellucci, F. Corrente, and P. Onorato, Nuovo Cimento della Società Italiana di Fisica B **122**, 665 (2008).
11. F.Palumbo, arXiv:0812.3825.
12. N. Pugno and A. Carpinteri, Philosophical Magazine Letters **88**, 397 (2008).
13. N. Pugno and E. Lepore, Journal of Adhesion **89** 949 (2008).
14. N. Pugno, A. Carpinteri, P.P. Delsanto, F. Bosia, and A. Gliozzi, Phys. Rev. E **78**, 046103-1 (2008).
15. P.P. Delsanto, A. Gliozzi, C. Bruno, N. Pugno, and A. Carpinteri, CHAOS, Solitons and Fractals (2008) ISSN: 0960-0779.
16. N. Pugno, CHAOS, Solitons and Fractals **38**, 1369 (2008).
17. A. Carpinteri, A. Kashtanov, N. Pugno, and Y. Petrov Int. J. of Fracture **150**, 227 (2008).
18. N. Pugno and E. Lepore, Biosystems **94**, 218 (2008).
19. A. Carpinteri and N. Pugno, Int. J. of Fracture **150**, 221 (2008).
20. N. Pugno, The Open Med. Chem. Journal **2**, 62 (2008).

21. N. Pugno, P. Cornetti, and A. Carpinteri, Journal of Adhesion **84**, 439 (2008).

22. A. Carpinteri, N. Pugno, and A. Sapora, CHAOS, Solitons and Fractals (2008) ISSN:0960-0779.

23. N. Pugno, A. Carpinteri, and P. P. Delsanto, CHAOS, Solitons and Fractals (2008) ISSN: 0960-0779.

24. E. Lepore *et al.* Journal of Nanomaterials, **1194524**, 1 (2008).

25. N. Pugno, Journal of Nanomaterials **156724**, 1 (2008).

26. N. Pugno, Scripta Materialia **58**, 73 (2008).

27. A. Borghi, E. Gualtieri, L. Calabri, N. Pugno, and S. Valeri, Tribology Letters (2008) ISSN: 1023-8883.

28. N. Pugno, Cancer Therapy **6**, 965 (2008).

29. N. Pugno, Nano Today **3**, 35 (2008).

30. N. Pugno and A. Carpinteri, Int. J. of Fracture **149**, 113 (2008).

31. N. Pugno, Acta Astronautica **63**, 687 (2008).

32. F. Bosia, N. Pugno, G. Lacidogna, and A. Carpinteri, Int. J. of Solids and Structures, pp. 5856-5866 (2008) ISSN: 0020-7683.

33. N. Pugno, F. Bosia, and A. Carpinteri, Small **4**, 1044 (2008).

34. A. Carpinteri and N. Pugno, Journal of the British Interplanetary Society **61**, 290 (2008).

35. P. P. Delsanto, C. A. Condat, N. Pugno, A. Gliozzi, and M. Griffa, Journal of Theoretical Biology **250**, 16 (2008).

36. N. Pugno, Materials Today **11**, 40 (2008).

37. N. Pugno, Carpinteri A, Ippolito M, A. Mattoni, and L. Colombo, Engineering Fracture Mechanics **75**, 1794 (2008).

38. A. Carpinteri, P. Cornetti, N. Pugno, A. Sapora, and D. Taylor, Engineering Fracture Mechanics **75**, 1736 (2008).

39. N. Pugno, Journal of Physics: Condensed Matter **20**, 474205-+7 (2008).

40. L. Calabri, N. Pugno, C. Valeri, and S. Valeri, Journal of Physics: Condensed Matter **20** , 474208-+7 (2008).

41. C. Portesi, E. Monticone, G.B. Picotto, Pugno N. and A. Carpinteri, Journal of Physics: Condensed Matter **20**, 474210-+8 (2008).

42. M. Pavese, S. Musso, S. Bianco, M. Giorcelli, and N. Pugno, Journal of Physics: Condensed Matter **20**, 474206-+7 (2008).

43. A. Carpinteri and N. Pugno, Journal of Physics: Condensed Matter **20**, 474213-+8 (2008).

44. N. Pugno, Journal of the Mechanical Behavior of Materials **18**, 265 (2008).

MI12: Gauge and String Theories

S. Bellucci (Resp.), S. Ferrara (Ass.), E. Latini (Dott.), S. Krivonos (Osp.),
A. Marrani (Bors. PD), V. Ohanyan (Osp.), A. Shcherbakov (Bors. PD),
A. Saharian (Oosp.), A. Sutulin (Osp.), A. Yeranyan (Bors. PD)

1 Research Activity

The topics covered are current issues in the theory of elementary particle interactions and of the theory of the gravitational force. Most of on-going research is on several aspects of extremal black holes, on their underlying supersymmetry in superstring effective theories, and their behaviour near the horizon, where a flow equation for the scalar fields (attractor mechanism) determines the Bekenstein-Hawking entropy in terms of topological properties of the theory (Ferrara, Kallosh, Strominger). In the study of black-hole evolution toward the horizon, scalar fields get fixed in terms of the electric and magnetic charges, giving rise to the study of "attractor varieties", which are of mathematical interest in algebraic geometry (Moore). An interesting outcome is the discovery of moduli spaces for non-BPS N=2 attractors, and their classification in terms of coset spaces in the case of special geometries based on symmetric homogeneous manifolds. This investigation has also been performed for all NN>2-extended supergravities, in which also 1/N-BPS attractors exhibit a related moduli space. The interconnection of moduli spaces of black holes and strings in 4, 5 and 6 dimensions has also been studied. Another line of research is the structure of N = 6 supergravity in 4D anti de Sitter space and its holographic connection to 3D Cher-Simons Yang-Mills theories.

The main research activity is on the following topics: 1) Study of BPS and non-BPS black hole attractors and their interpretation in the "fake supergravity"; 2) Study of the classes of perturbative quantum corrections to the N=2 Attractor Equations encompassed by modifications of the holomorphic prepotential; 3) Relation between the black brane potential and the entropy function for intersecting branes and their attractors; 4) Structure of N = 6 gauged supergravity at D = 4 and its dual theory with N = 2 supersymmetry; 5) Attractors and extremal black holes in 4-dimensional asymptotically non-flat backgrounds.

Active collaborations include: JINR-Dubna, Russia Tomsk Univ. Russia Univ. Hannover, Germany Turin Polytechnic, Italy CERN, Switzerland Annecy, LAPTH, France Valencia U., Spain

Prof. Ferrara, a distinguished member of the group, received several awards in 2008: 1) 2008 recipient of an "Advanced Research Grant" from ERC (European Research Council) in Frontier Research; 2) Recipient of the 2008 Amaldi Medal, European Prize awarded by the The Italian Society of General Relativity and Gravitational Physics (SIGRAV); 3) Miller Visiting Professor Award (Fall 2008), awarded by the Miller Institute for Basic Research in Science, University of California, Berkeley; 4) Gold Medal delivered by the Accademia dei Lincei, Rome, in the occasion of the 2008 Avogadro Lecture (Conferenza Lincea).

We published the Proceedings of the School SAM2006, with the title: Supersymmetric Mechanics - Vol. 3: Attractors and Black Holes in Supersymmetric Gravity, Stefano Bellucci Editor, Springer Lecture Notes in Physics 755, November 2008, ISBN: 3540795227, ISBN-13: 9783540795223, 373 pages.

We participated as a main node to the Project MRTN-CT-2004-005104 Constituents, Fundamental Forces and Symmetries of the Universe (Short title: ForcesUniverse), a Marie Curie Research Training Network supported by the European Community's Sixth Framework Programme and coordinated by Dieter Luest. The network contract was completed on 1st November 2008 after a period of 48 months.

Within this network a School was organized at CERN in Geneva, January 21 - 25, 2008, http://www.unine.ch/phys/string/rtn-school/08/index.php and a Workshop was organized at Varna, September 11 - 17, 2008, http://theo.inrne.bas.bg/ dobrev/FU-4.htm with talks by A. Shcherbakov and A. Yeranyan.

Another important and related event has been String phenomenology in Frascati 4-8 June 2007, with invited talks by S. Ferrara and S. Bellucci on N>2 attractors and N=2 attractors respectively.

We coordinate an INTAS project "Extended supersymmetry, strings and noncommutativity in field theory", involving a consortium of 12 international Institutions, with duration of 30 months starting Nov. 2006, until October 2009.

2 List of Conference Talks

1. S. Ferrara, Frascati LNF workshop on "Strings and Strong Interactions", September 2008.
2. S. Ferrara, International school of Subnuclear Physics, 45th Course on "Searching for the totally unexpected in the LHC era", Erice, Italy, August 2008.
3. S. Ferrara, UCLA Conference on "Symmetry in Mathematics and Physics", January 2008.
4. S. Ferrara, Meeting of the INFN Networks MI12, PI14, TS11 and TV12, "Theories of the fundamental interactions", Villa Mondragone, Monte Porzio Catone (Rome), June 2008.
5. A. Shcherbakov,"$N = 4$ Superconformal Mechanics and Black Holes", 4-th EU RTN Workshop, Constituents, Fundamental Forces and Symmetries of the Universe, Varna (Bulgaria), 12 September 2008.
6. A. Shcherbakov, "Supersymmetric and conformal aspects of the attractor mechanism", talk at the University of Torino, 29 April 2008.
7. A. Shcherbakov, "Black Holes, Geometry and Quantum Corrections", International School of Subnuclear Physics 46th Course, Erice (Italy), 29 Aug - 7 Sep 2008.
8. A. Yeranyan, "The STU Black Holes and Beyond", 4-th EU RTN Workshop, Constituents, Fundamental Forces and Symmetries of the Universe, Varna (Bulgaria), 12 September 2008.
9. A. Yeranyan, "Generalized potential for black hole attractors", International School of Subnuclear Physics 46th Course, Erice (Italy), 29 Aug - 7 Sep 2008.

References

1. S. Bellucci, S. Krivonos, A. Shcherbakov, and A. Sutulin, Phys. Rev. D **78**, 125001 (2008).
2. S. Bellucci, S. Krivonos, O. Lechtenfeld, and A. Shcherbakov. Phys. Rev. D **77** 045026 (2008).

3. S. Bellucci, S. Ferrara, A. Marrani, and A. Yeranyan. Phys. Rev. D **77**, 085027 (2008).
4. S. Bellucci, D. O'Reilly, Phys. Lett. B **666**, 193 (2008).
5. S. Bellucci, S. Krivonos, and A. Sutulin, Nucl. Phys. B **805**, 24 (2008).
6. S. Ferrara and A. Marrani, Nucl. Phys. B **788**, 63 (2008).
7. S. Bellucci, S. Ferrara, and A. Marrani, Fortsch. Phys. **56**, 761 (2008).
8. G. Iovane, S. Bellucci, and E. Benedetto, Chaos, Solitons Fractals **37**, 49 (2008).
9. S. Bellucci and A. A. Saharian, Phys. Rev. D **77**, 124010 (2008).
10. S. Bellucci, V. Ohanyan. Phys. Lett. A **372**, 5765 (2008).
11. S. Bellucci, S. Ferrara, R. Kallosh, and A. Marrani, Lect. Notes Phys. **755**, 115 (2008).
12. S. Bellucci, S. Ferrara, A. Marrani, and A. Shcherbakov, JHEP **0802**, 088 (2008).
13. S. Bellucci, S. Ferrara, A. Marrani, and A. Yeranyan, Entropy **10**, 507 (2008); arXiv:0807.3503.
14. S. Ferrara, A.Gnecchi, and A. Marrani, Phys. Rev. D **78**, 065003 (2008).
15. S. Ferrara, K. Hayakawa, and A. Marrani, Fortsch. Physik, **54**, 956 (2008).
16. F. Bastianelli, O. Corradini, and E. Latini, JHEP **0811**, 054 (2008).

PI11: Quantum Field Theory and Statistical Mechanics

F. Palumbo (Resp. Loc.)

Recently a new bosonization method has been used to derive, at zero fermion density, an effective action for relativistic field theories whose partition function is dominated by fermionic composites, chiral mesons in the case of QCD. This approach shares two important features with variational methods: the restriction to the subspace of the composites, and the determination of their structure functions by a variational calculation. But unlike standard variational methods it treats excited states on the same footing as the ground state.

I show that this bosonization method is an approximation of an exact procedure in which composites are introduced in the presence of fermionic states with the quantum numbers of the constituents (quasiparticles), satisfying a compositeness condition which avoids double counting. This procedure consists in an independent Bogoliubov transformation at each time slice. The time dependent parameters of the transformation are then associated to composite fields. In this way states of nonvanishing fermion (baryon) number (neglected in the bosonization approach) are retained. By the exact procedure I derive an effective action for QCD at finite temperature and baryon density. I test the result on a four-fermion interaction model [1)].

We study generalized Bogoliubov transformations in the formalism of the transfer matrix of relativistic field theories regularized on a lattice. We derive the conditions these transformations must satisfy to factorize the transfer matrix into two terms which propagate fermions and antifermions separately, and we solve the relative equations under some conditions. We relate these equations to the saddle point approximation of the bosonization method outlined above and to the Foldy–Wouthuysen transformations which separate positive from negative energy states in the Dirac Hamiltonian [2)] .

References

1. F. Palumbo, Phys. Rev. D **78**, 014514 (2008).
2. S. Caracciolo, F. Palumbo, and G.Viola, Annals of Phys. **324**, 584 (2009).

RM31: Phases of Strong Interactions

Maria Paola Lombardo

1 Main Collaborations

Albert Deuzeman, Elisabetta Pallante (Rijksuniversiteit Groningen, NL), Claudia Ratti, Jacobus J.M. Verbaasrchot (SUNY at Stonybrook, USA), Karl Jansen DESY Zeuthen, DE), Michael Muller-Preussker, Marcus Petschlies (Humboldt–Universitaet Berlin, DE), Owe Philipsen, Lars Zeidlewicz (Westfaelische Wilhelms-Universitaet Muenster, DE), Kim Splittorff (NBI, Copenhagen, DK).

2 Scientific Activity

The general goal of these studies is to understand the phase diagram of the strong interactions, and to make contact with the ongoing and upcoming experiments.

During 2008 my collaborators and I have addressed the following issues

1. *High temperature QCD with improved Wilson fermions*
2. *QCD at low temperature and high density, model study* 3.
3. *Analysis of the sign problem at nonzero density*
4. *QCD with a large number of flavors*

The first line of research aims at understanding of the thermodynamical region to be explored at the LHC. The main 2008 result is the full clarification of the lattice phase diagram of Wilson fermion with a twisted mass term. The second and third projects focus on the challenging domain of lower temperatures, and moderately high densities, ranging from those currently explored at RHIC to the future GSI scans which will be performed by the FAIR experiment. We have completed our study of the glueball spectrum in cold and dense matter, and we have started an investigation of the technical problems still hampering realistic simulations of QCD in this regime. Finally, *QCD with a large number of flavors* opens a window towards new physics beyond the standard model, in particular concerning the role of near conformal dynamics in Technicolor inspired theories. We have confirmed the existence of a conformal window for QCD with N_f fundamental fermions for $N_f > N_f^*$, with $8 < N_f^* < 12$

My work has been co–supported by MIUR via PRIN06 *Fasi di QCD* , by the EU I3 *Hadron Physics*, by the International Graduate School Bielefeld-Orsay and by the US National Science Foundation.

3 Professional Service for the LNF

Spring School 2008: Member of the Local Organising Committee; the School was partially supported by my PRIN grant; *Strings&Strong Interactions*: Main Organiser; The meeting was partially supported by my PRIN grant; *Proceedings of Hadron07, Frascati Physics Series*: Co-Editor; *LNF*

General Seminar : Committee appointed member; *LNF Theory Seminars*: I have invited and supported via my PRIN grant four (out of ten total) speakers during 2008; I have contributed to the technical document *Computing at the LNF*; I have proposed a Visitor Program at the LNF, approval pending; I am the Coordinator of the LNF-Cosenza node for the Lattice Network of the I3 Hadron Physics2.

4 Community Service

Lattice 2009, The XXVII International Symposium on Lattice Field Theory : Member of the International Advisory Committee; *Quark Matter 2009, the 21st International Conference on Ultra-Relativistic Nucleus- Nucleus Collisions* Member of the International Advisory Committee; *Extreme QCD, Workshop on QCD in Extreme Conditions* Member of the International advisory Committee; *Workshop on Tools for QCD at finite density, Bielefeld, November 2009* : Member of the Local Organising Committee.

5 Main Invited Talks

Lattice and phase diagram in QCD,, invited review at Sixth International Conference on Perspective in Hadron Physics, Trieste ICTP 12–16 May 2008, published in AIP Conf. Proc. 1056 71 (1008),
QCD at finite temperature and density on the lattice invited lectures at Dubna International Advanced School of Theoretical Physics, Dubna Russia, 14-26 July 2008,
Phase Diagram of QCD: Lattice Results, invited review at VIII International Workshop Relativistic Aspects of Nuclear Physics, Rio de Janeiro, Brazil, 3-6 November 2008
QCD at Non-Zero Density : Lattice Results, invited review at Quark Matter 2008: 20th International Conference on Ultra-Relativistic Nucleus Nucleus Collisions (QM 2008), Jaipur, India, 4-10 Feb 2008, published in J. Phys. G **35**, 104019 (2008)

Finite Temperature Field Theory, invited essay for *The Nature Description in Quantum Field Theory*, Springer, 2009, I. Licata and A. Sakaji (eds).
In addition, seminars at Niels Bohr Istitute CPH, TorVergata University, RomaI University, Bielefeld University and invited topical talks at ExtremeQCD, Raleigh, TIFR, INT Seattle.

References

1. M. P. Lombardo, AIP Conf. Proc. **1056**, 71 (2008).
2. A. Deuzeman, E. Pallante, M. P. Lombardo, and E. Pallante, PoS **LATTICE2008**, 060 (2008).
3. A. Deuzeman, M. P. Lombardo, and E. Pallante, PoS **LATTICE2008**, 060 (2008).
4. E. M. Ilgenfritz *et al.*, PoS **LATTICE2008**, 060 (2008).
5. M. P. Lombardo, J. Phys. G **35**, 104019 (2008).
6. M. P. Lombardo, M. L. Paciello, S. Petrarca, and B. Taglienti, Eur. Phys. J. C **58**, 69 (2008).
7. A. Deuzeman, M. P. Lombardo, and E. Pallante, Phys. Lett. B **670**, 41 (2008).
8. M. D'Elia, F. Di Renzo, and M. P. Lombardo, AIP Conf. Proc. **964**, 342 (2007).
9. C. Davies *et al.*, arXiv: 0803.2368.

5 – Technological and Interdisciplinary Research

3+L
(Time Resolved Positron Light Emission)

A. Bocci (Art. 23), A. Clozza, A. Drago (Resp. Naz.), A. Grilli (Tecn.),
A. Marcelli, R. Sorchetti (Tecn.), A. Raco (Tecn.)

1 Introduction

To improve the diagnostics of the e^+ ring of the DAΦNE collider, a novel beam diagnostics experiment: the 3+L (Time Resolved Positron Light Emission) has been proposed and funded by the V Committee of the Istituto Nazionale di Fisica Nucleare [1,2]. The main goal of the proposal is to perform a bunch-by-bunch and turn-by-turn longitudinal and transverse beam diagnostics of the e^+ beam at DAΦNE in order to investigate bunch instabilities and to improve collider performances. Instrumentations have been assembled and tested in 2008 and is now in operation in the DAΦNE hall where a compact optical system collects the IR synchrotron radiation emission from one of the bending magnet of the e^+ ring and focus the radiation on compact fast IR photo-detectors to perform real-time bunch diagnostics. During the year preliminary measurements of the e^+ bunches were performed.

2 2008 Activity

The 3+L instrumentation collects the IR light extracted by a bending magnet with a critical energy of 273 eV positioned at DAΦNE after IP2, one of the two interaction regions of DAΦNE. It consists of a compact front-end with an HV chamber that hosts a gold-coated plane mirror. The mirror collects and deflects the synchrotron radiation emission through a ZnSe window that transmits radiation in the range 0.6 to 12 μm (800-17000 cm^{-1}). We designed a compact optical system composed by 5 mirrors working in air that have been installed and aligned after the ZnSe window in the DAΦNE hall. The optical system allows focusing radiation on a small spot of about 0.1 mm^2. A schematic optical layout of the 3+L exit port and of the optical system is showed in Fig. 1.

The mirrors were mounted on the optical table showed in Fig. 1 together with the ideal path of the light outlined with a red line. Looking at the optical layout, all mirrors are plane mirrors except one spherical mirror. To maintain the layout compact, the 4th plane mirror has a centre hole to allow radiation focused by the 5^{th} spherical mirror to have its focus behind the 4^{th} mirror. Detectors placed behind the 4^{th} mirror are mounted on a xyz micrometer stage to align them to the light spot. A first characterization of the optical system has been performed with a commercial CCD camera used to monitor the spot size along the optical path near the focus. In Fig. 2 is showed the contour plot of the focal spot. The estimated FWHM of the visible spot is of $\approx$ 750x150 μm^2(HxV).

The size is a bit larger then both ray tracing simulations performed with ZEMAX and wave optics simulations performed with the SRW package software [3] that however returned a spot dimension of about 100 x 55 μm^2(HxV) calculated at 10 μm.
A determination of the source power at IR wavelengths has been also performed using a calibrated NIST power meter. Data have been collected with a Melles Griot 13 PEM 001/J power meter and

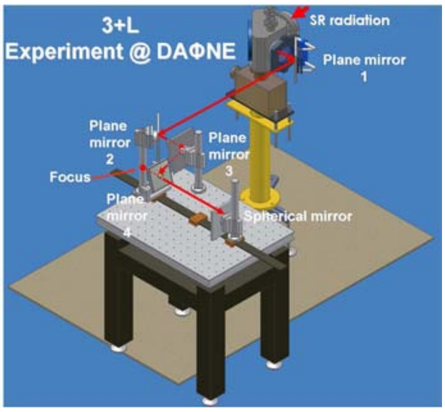

Figure 1: *View of the optical layout of the 3+L experiment with the front end, the optical table and the mirrors. The ideal path of the IR light focused on a small spot is also indicated with a red line.*

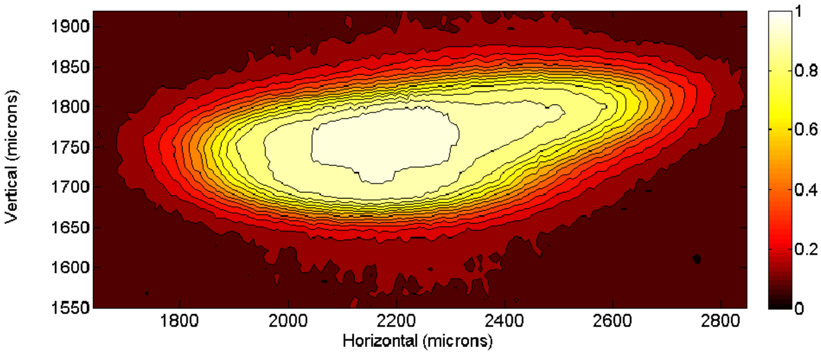

Figure 2: *Contour plot of the focal spot of the optical system measured with a CCD at visible wavelengths.*

with filters in the range 5-20 μm. The estimated power at the focus of the optical system is 2.2 mW at 500 mA of beam current in the range 5-20 μm. The power allows obtaining a good S/N ratio with the fast IR detectors used for acquisitions. Calculations of the power emitted by the bending magnet in the same wavelength range returned a value of 3.2 mW comparable with experimental data obtained with the power meter at the focus of the optical system. A PC installed in the DAΦNE hall allows the remote control of the experiment. In particular a PCI-COM bridge RS-232 board controls the motors and the xyz stage. Two webcams and a camera monitor the detector position and the positioning of the mirrors. A scope model Tektronics TDS 820 with 6 GHz of bandwidth is available and connected to the PC by a USB-GPIB interface for data collection. A power supply connected to the PC by a GPIB I/O controller is used to supply amplifiers and detectors. Dedicated software packages have been developed under the LabVIEW platform for data acquisition, to control the supply of the detectors and the amplifiers, and to move the xyz stage. In 2008, during the DAΦNE operations different fast IR photon detectors were tested at the focus of the optical system. In particular, measurements were carried out using fast PVMI 3-stages detectors of the VIGO System S.A optimized at 10 μm of wavelength. [4]. These IR photodiodes based on HgCdTe multilayer heterostructures grown by MOCVD on (211) and (111) GaAs substrates work at room temperature. They can also be cooled at low temperatures ($\approx$ 205 K) with a three stages Peltier cooler achieving a response time of the order of 100 ps or lower. A first preliminary characterization of the e^+ beam with these latter detectors has been performed. As an example, in Fig. 3 3 we show the signal of few e^+ bunches acquired when a beam current of 650 mA was circulating in the e^+ ring. As showed in the picture, the time resolution of the set-up allows the separation of the emission of single bunches of the e^+ beam and addresses the possibility of a real time longitudinal bunch-bunch diagnostics. A measurement of a single bunch acquired with the 3+L experimental set-up is reported in Fig. 4

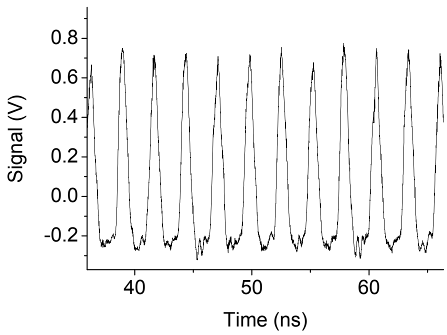

Figure 3: *The signal of few e^+ bunches. The bandwidth of the experimental set-up allows the separation of consecutive bunches.*

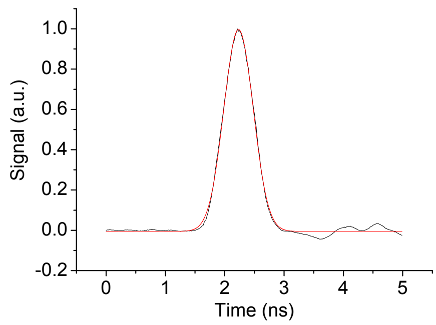

Figure 4: *The shape of a e^+ bunch (black curve) and its Gaussian fit (red curve) at IR wavelengths.*

From these experiments we may obtain bunch parameters and information regarding the characteristics of the detectors and of the electronics. Data show that the bunch profile is Gaussian with a length $\sigma \approx 240$ ps. The rise time and the fall time of the detector is of $\approx$400 ps. The comparison of the data obtained with IR detectors at the same bunch current with those

obtained with the streak camera at visible wavelengths [5] shows that the σ at IR wavelengths is between 3 and 4 times higher. At present the experimental set-up is still slower with respect to the streak camera but improved results are expected in 2009 with optimized electronics and improved detectors.
Within the framework of the Scientific and Technological Co-operation Agreement between the Italian Republic and the People's Republic of China supported by Italian Ministry of Foreign Affairs, in order to compare the data collected at DAΦNE using the same diagnostics technique, we performed similar experiments at the IR port of the Hefei Light Source (HLS), the dedicated synchrotron radiation facility of the Hefei National Synchrotron Radiation Laboratory (NSRL). Measurements of the bunch lengths of the electron beam at different beam current have been performed and compared with data of the diagnostics beamline operational at HLS. The instrumentation allows measurements of the longitudinal dimensions of the electron beam with both a fast visible photodiode and a streak camera.

3 Planned activity in 2009

In 2009 we plan to install and test new IR detectors and an optimized electronics trying to improve the actual longitudinal diagnostics. A prototype of an imaging device has been also assembled and first tests are planned in spring. The device is a fast photon array detector composed by 2x32 pixels working at mid-IR wavelengths. Each element has 50x50 μm^2 area and a measured time response of about 1 ns. A fast dedicated electronics composed by 64 channels has been built in order to amplify the signals of the array. A fast digital electronics will be also used in order to acquire and store the signals of the 64 channels. The array may allow performing real time imaging of the DAΦNE IR synchrotron source and a turn-by-turn and a bunch-by-bunch diagnostics of the transverse dimensions of the $^+$ beam. With such new diagnostics would be possible the investigation of beam instabilities possibly trying to correlate them with bunch positions along the train. This real-time diagnostics could improve DAΦNE performances and may be help achieving a higher e^+ current and higher collider luminosity.

4 Acknowledgments

We gratefully acknowledge Jozeph Piotrowski of Vigo System S.A. for many fruitful discussions and his continuous support to the research. A.B. acknowledges in particular the Italian Ministry of Foreign Affair for the financial support.

5 List of Conference Talks

1. A. Bocci, "Beam diagnostics at DAΦNE with fast uncooled IR detectors", BIW'08, 4-8 May 2008, Lake Tahoe, California.

6 References

1. A. Bocci *et al.*, "Beam diagnostics at DAΦNE with fast uncooled IR detectors", Proc. BIW'08, http://www.als.lbl.gov/biw08/papers-final/WECOTC03.pdf (2008).

2. A. Bocci *et al.*, "Beam Diagnostics with IR Light Emitted by positron at DAΦNE", Proc. EPAC'08, 1056 (2008).

3. O. Chubar and P. Elleaume, Proc. EPAC'98, 1177 (2008).

4. J. Piotrowski and A. Piotrowski, Proc. SPIE **B**5957, 117 (2005).

5. A. Ghigo *et al.*, Proc. EPAC'02, 1494 (2002).

ALTCRISS

M.A. Franceschi, G. Mazzenga (Tecn.), T. Napolitano, M. Ricci (Resp.), B. Spataro

Participant Institutions:

Italy: INFN LNF, Firenze, Roma 2-Tor Vergata, Trieste; University of Genova
Germany: SIS (Darmstadt)
Russia: MePhi, IBMP, RKK "Energia" (Moscow)
Sweden: KTH (Stockholm)
ESA European Astronaut Center

1 Introduction

The ALTCRISS experiment (Alteino Long Term monitoring of Cosmic Rays on the International Space Station) - previously named SI-RAD - is a continuation of the activities carried out for the experiments SIEYE1 and SIEYE2 on board the Russian Space Station MIR and for the experiments SIEYE3/ALTEINO on board the International Space Station (ISS) in the years 1995-2002 [1) 2) 3) 4) 5)].

The experimental task of the ALTCRISS experiment (approved by ESA) is to develop a detector to be placed on the external part of the ISS. The detector will be used to monitor cosmic rays and radiation environment in Low Earth Orbit. Long (Solar modulation) and short (coronal mass ejections, orbit dependence) of the particle flux and the dose absorbed by the astronauts will be monitored. In addition, data will be compared with measurements taken inside the ISS with ALTEA (see below) and ALTEINO detectors to validate radiation transport and dose estimation codes. At the same time, the investigation, with a more sophisticated instrument, of the "Light Flashes" phenomenon [6)], will be conducted to improve and refine the results obtained with the previous SIEYE experiments.

To meet these goals, a precursor mission in space with a high performance cosmic ray detector, LAZIO/SIRAD [7)], has been accomplished to measure and identify all particles traversing the detector separating nuclei from electrons/positrons, in the energy range $\sim$ 10 to $\sim$ $100 MeV$. LAZIO/SIRAD has been launched in April 2005 on a Soyuz rocket and placed aboard the ISS by the italian astronaut Roberto Vittori. We refer to the previous Annual Report LNF 2005 for details on this mission [8)].

Moreover, in July 2006, the ALTEA experiment [9)], launched with the Space Shuttle Discovery, has been placed on board the ISS by the Swedish astronaut Christoph Fuglesang and has started taking data one month later.

The preparation of the next ALTCRISS extended mission is advancing towards the completion of the full flight instrument consisting of a 16-plane tower of double-sided silicon detectors (8x8 cm^2 area) equipped with trigger and anticoincidence counters. The total weight is about 15 kg and the total power consumption should not exceed 30 W. The hardware set-up is accomplished through three steps by the construction of a laboratory prototype model, an engineering model and the final flight, space qualified model.

The activity in 2008 has been focused on the development of the following systems of the engineering model:

- Trigger system.
- Development of Silicon Photomultiplier (SI-PM) technology for space applications and test of different SI-PM configurations.
- Completion and test of a highly integrated silicon board (16 cm x 16 cm).
- Production and test of a low-power, low-mass Digital Processing Unit (DPU).

For the year 2009, the planned activity includes the completion of the engineering ALTCRISS unit and the set-up of the flight configuration equipped with autotrigger capabilities for heavy nuclei and a trigger for crossing protons and nuclei. The interface with the ISS Space Station will be realized with an intermediate CPU to manage the telecommands from ground and the download of the data. Beam tests at the LNF-BTF, GSI/Darmstadt and other facilities are also planned together with the continuation of the R&D on the SI-PM technology.

2 Activity of the LNF group

The LNF group has taken the responsibility of the design, construction and test of the mechanical structures and interfaces of the three models of the detector also contributing to the integration of the mechanical support for the DAQ. This activity is carried out with the support and the participation of the LNF Service of Development and Costruction of Detectors (SSCR). The activity in 2008 has been mainly devoted to the completion of the mechanical support of the engineering model and to the interfaces of the front-end and DAQ with the detector. These systems are being developed for the final space-qualified flight configuration in the year 2009. The LNF group participates as well in the beam test activities at the above mentioned facilities having the responsibility of the beam trigger counters and of the general arrangement and set-up.

3 Selection of recent publications

1. M. Casolino *et al.*, Nuovo Cim. **31C**, 77 (2008).
2. V. Zaconte *et al.*, Nucl. Instr. & Meth. B **266**, 2070 (2008).
3. D. Badoni *et al.*, Nuovo Cim. **30C**, 503 (2007).
4. M. Casolino *et al.*, Adv. Space Res. **40**, 1746 (2007).

References

1. V. Bidoli *et al.*, Journal of Physics G: Nuclear and Particle Physics **27**, 2051 (2001).
2. S. Avdeev *et al.*, Acta Astronautica, **50**, 511 (2002).

3. M. Casolino *et al.*, Nucl. Phys. B **113**, 88 (2002).
4. V. Bidoli *et al.*, Nature **422**, 680 (2003).
5. P. Maponi *et al.*, Nuovo Cim. B **116**, 1173 (2001).
6. G. Horneck, Nucl. Tracks Radiat. Meas. **20**, 185 (1992).
7. F. Altamura *et al.*, "Preliminary results from the LAZIO-Sirad experiment on board the International Space Station", Proc. XXIX ICRC, Pune (2005), SH35 p.101.
8. LNF 2005 Annual Report, Report LNF-06/10 (IR).
9. L. Narici *et al.*, Adv. Space Res. **31**, 141 (2003).

CGBT

Francesco Scaramuzzi (Resp., Ass.)

1 Activity

This acronym, which means "Caricamento Gassoso a Bassa Temperatura" (in English: "Low Temperature Gas Loading"), refers to an experiment that is being built and performed at the LNF of INFN. It is well known that the most diffused idea in the research field known with the name of Cold Fusion is based on the hypothesis that it is possible to have nuclear fusion reactions between deuterium nuclei when they are embedded in the crystal lattice of palladium. The reaction is supposed to take place with the production of a nucleus of ^{4}He and an excess energy of 24 MeV. The thesis accepted (not by everyone) is that the 24 MeV are transformed in heat of the lattice of palladium, so that the ^{4}He nucleus stays, unbroken, as the only nuclear ash of the process. Thus, being able to put in evidence the production of both these elements (heat and helium) is the most convincing proof of this idea. This has been done in many cases, but reproducibility is not perfectly achieved. This is also the scope of this experiment.

It is common knowledge that a necessary condition for the reaction to take place is that the amount of deuterium absorbed in the palladium lattice be above a threshold value, which is about 1 (intended as the atomic ratio between deuterium and palladium). In order to satisfy this condition, in most of the experiments in the literature the electrolysis of heavy water with a palladium cathode has been used. In the CGBT experiment a different approach is followed, i.e., the direct contact between deuterium gas and a palladium sample. Since it is known that the equilibrium amount of deuterium in the palladium lattice is a decreasing function of temperature, it was decided to study this reaction at low temperature (typically 150 K). This experiment was started at ENEA Frascati years ago, with a quite promising preliminary result [1].

Then, it has been rebuilt at the LNF of INFN. During the year 2008 the measurements of absorption of deuterium on palladium have suffered for an interruption, due to the necessity of a revision of the experimental set-up. The revision is by now complete, and the measurements should start again in 2009.

Nevertheless, during 2008 measurements of the electric resistance of a thin palladium sample while loading deuterium were performed. An interesting anomaly was noted, presumably connected with the presence of an electric potential on the palladium sample. The data are presently scarce, but there is the hope to enrich them in 2009.

The set-up of the system aimed at the measure of traces of ^{4}He in D_2 is also (rather slowly) proceeding.

References

1. F. Scaramuzzi, Journal of Alloys and Compounds, **385**, 19-27 (2004).

CUP: Positron Channeling at the DAΦNE BTF Facility

S.B. Dabagov (Resp. Naz., Art. 23), L. Quintieri (Art. 23), C. Natoli

Collaboration: Italy INFN - LNF, Frascati
Russia RAS P.N. Lebedev Physical Institute, Moscow
Germany MAMI, Mainz
Denmark Aarhus University, Aarhus

The CUP experiment is a first important step of a more ambitious project that investigates the feasibility to create new powerful sources of high-frequency monochromatic electromagnetic radiation: crystal undulator and γ-laser based on channeling of positrons in crystals. In this report the main goal of the CUP experiment and the first measurements at the DAΦNE BTF facility will be presented.

1 The CUP experiment

The final objective of the CUP experiment (**C**rystal **U**ndulator for **P**ositrons) is to study the features of radiation emitted by positron channeling in a crystal. For our investigation the positron beam of the DAΦNE Beam Test Facility, the transfer line of which is presented by Fig. 1, will be used.

As known, the BTF facility provides electrons and positrons with energy ranging from 20 to 800 MeV (750 MeV for positrons). Working around the nominal DAΦNE energy of about 500 MeV, we expect to identify in a silicon monocrystal the radiation at (110) channeling of positrons having a peak at a photon energy of 1 MeV. The DAΦNE –BTF is the unique European Facility that at present time is able to deliver positron beams in the energy range of interest for the CUP experiment. In fact, according to well accepted channeling radiation theories a strong photon peak with energy from 20 KeV up to 1.5 MeV should appear for the (100) plane of a single crystal at a positron beam energy of about 600 MeV. At BTF this peak could be detected and its intensity

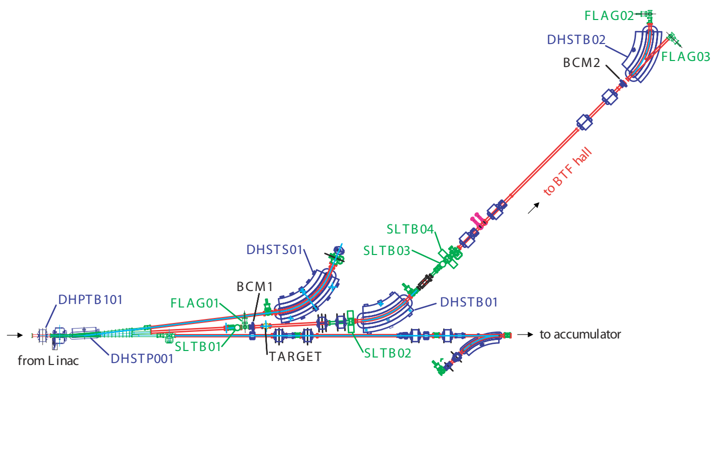

Figure 1: *Transfer line of the DAΦNE Beam Test Facility*

should be investigated as a function of several parameters (crystal thickness, angle of incidence of impinging beam, etc). Unfortunately, the high background around the crystal in the experimental hall of the DAΦNE BTF has represented a strong limit to detectability of the signals we are looking for. Anyway important upgrade on the shielding structure along the BTF transfer line (part of which had been implemented soon after our measurement tests) and the use of suitable magnets to redirect the positrons at the transfer line exit could solve most of the problems we have met. These technical solutions are discussed in the following.

2 The DAΦNE BTF Facility

The DAΦNE Beam Test Facility is an electron/positron transfer line, by which the beam accelerated from the Linac, is transported to an experimental hall where the beam tests as well as the experiments can be performed. The facility can provide e-/e+ beam in a wide range of intensity: from single particle per bunch up to 10^{10} particles per pulse. The BTF is operating since 2002: during these years, tens of high energy physics experiments from all over Europe have been hosted. The main applications of the facility are: high energy detector calibration, low energy calorimetry, low energy electromagnetic interaction studies, detector efficiency and aging measurements, tests of beam diagnostic devices.

3 Experimental Setup and First Measurements at BTF

The aim of the first measurements at the DAΦNE BTF was to identify and investigate the intense radiation at (110) channeling of 500 MeV positrons in a plane silicon single crystal, for which a peak at a photon energy of 1 MeV is expected.

In Fig. 2 the experimental-setup used for the BTF measurements campaign has been shown. The beam spot diameter at the target position was approximately 10 mm with a maximum angular divergence of 1 mrad according to the Linac specications.

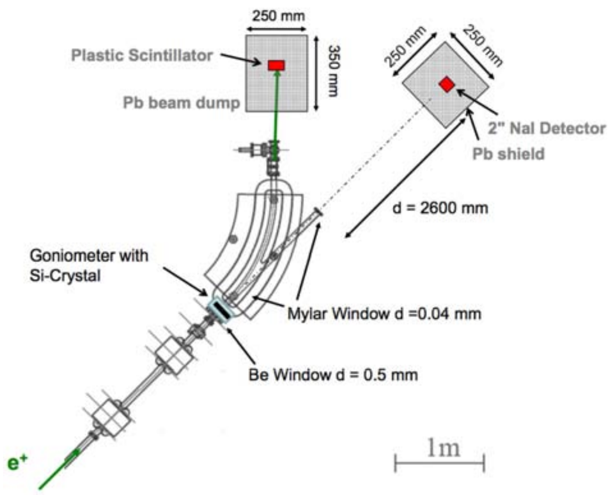

Figure 2: *The end part of the DAΦNE BTF and the experimental setup for CUP.*

As a first step, positrons of 508 MeV have been sent to impinge on a plane silicon single crystal target for testing the efficiency of positron channeling. When particles are channeled inside a crystal, the particle flux after the crystal results structured in peaks in correspondence of the direction of the planar channels (main channeling directions). Due to the fact that the critical angle for positron of high energy (800 MeV) on silicon crystal is about $\psi_c = 0.27$ mrad and consequently much smaller than the best BTF beam divergence[1], we expect for a substantial broadening and lowering of the peaks with respect to the background (i.e a deteriorated peaks to background ratio than expected from theoretical previsions). The calculation were done for a beam energy of 600 MeV which is somewhat higher as the experimental beam energy of 500 MeV. A detector distance from the Si target of 2.5 m has been assumed, as well as a beam spot size at the Si crystal of $\sigma_x = \sigma_y = 5$ mm, and a beam divergence of $\sigma'_x = \sigma'_y = 2$ mrad (Fig. 3). At a primary occupation in the channeling state of 4.3%, and a loss of 50% due to dechanneling (dechanneling length of 240 μm assumed), a number of 1.0×10^{-4} channeling radiation photons per positron and 0.1 MeV energy bin is expected at the maximum for a detector aperture of 20 mm diameter. This number is a factor of 3 larger in comparison to the bremsstrahlung background of 3.5×10^{-5} per positron and 0.1 MeV energy bin. Even if an about 60% increase by bremsstrahlung production in the 500 μm thick beryllium window, which closes the beam tube, is taken into account, the shoulder at 1.5 MeV should easily be observable with a 2"×2" NaI detector.

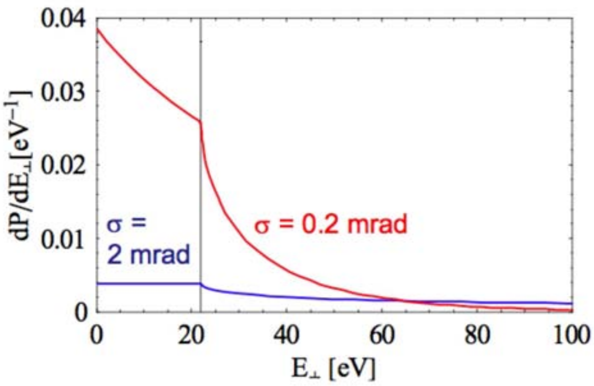

Figure 3: *Initial occupation probabilities as function of the transverse energy. Bound states in the potential well are located below U_0 = 22 eV. Curves are shown for two angular divergences σ of the positron beam as indicated. Integrals between 0 $0 \leq E \leq 0.5\, U_0$ are 0.043 and 0.38 for $\sigma = 2$ mrad and $\sigma = 0.2$ mrad, respectively.*

Measurements were performed at beam energy of 508 MeV at varying repetition rates. A goniometer, capable of aligning the target crystal by varying the rotational angles, as showed in Fig. 4, was mounted in an air gap between the beam line and the final 45° bending magnet. The beam line is terminated with a 0.5 mm beryllium window and the magnet is sealed with 0.04 mm mylar windows. Approximately 1m behind the magnet a beam dump was erected with lead bricks. A small plastic scintillator was put inside in order to do the measurement of the relative beam pulse intensity. In a straight line, 2.6 m apart from the mylar output window a 2"×2" NaI detector was mounted within a lead shield. The background level was determined by looking at the NaI signal normalized over the beam intensity for various congurations. A large background signal was detected even without a target and it did not change signicantly with an aluminium target (d = 3 mm) in place. The shielding of the detector in the beam direction with 100 mm

[1]The beam divergence can be tuned by means of a slit system.

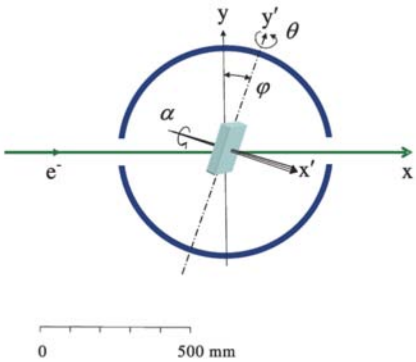

Figure 4: *Target setup and definition of angles.*

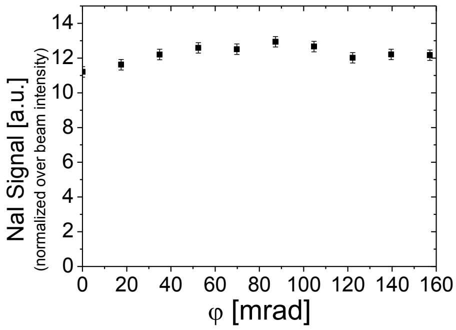

Figure 5: *Scan overt the azimuthal angle ϕ of a Si single crystal. A number of 10000 beam pulses were accumulated per data point. The error bars show the variance of the normalized radiation signal over a scan range of 157 mrad.*

of lead attenuated the signal about a factor of 4. This suggests that most of the background is a result of bremsstrahlung produced in the beam line. However, a smaller part may be attributed to neutrons from the beam dump nearby.

Due to the large background and the high beam divergence, the scanning over the azimuthal angle ϕ of the Si crystal did not allow to individuate any positron peak contrarily to what we are expected for (see Fig. 5).

4 Activity in 2009

As a conclusion, the most important thing we learnt from this measurement campaign was that it is mandatory to reduce the background level by at least one order of magnitude if we want to detect positron planar channeling. The latter requires upgrading of the BTF transfer line by multiple shielding. In addition, a possible solution could consists in installing a magnetic chicane in the straight line after the last 45° bending magnet as shown in Fig. 6.

It should deflect the beam after the target into a dump. The detection device for recording the channeling radiation would be mounted after the last magnet in a straight line from the target chamber (as reference take in mind that we follow the particle motion). This setup offers several advantages:

- it is comparatively inexpensive;
- full advantage can be taken of the existing and optimized beam- line to produce an adequate beam spot in the target chamber;
- with the slit systems the emittance can be reduced, the momentum spread of the linac positron beam be handled and, in turn, hopefully a high quality positron beam be generated with the required beam divergence of 0.2 mrad at a spot size of lesst than 10 mm diameter;

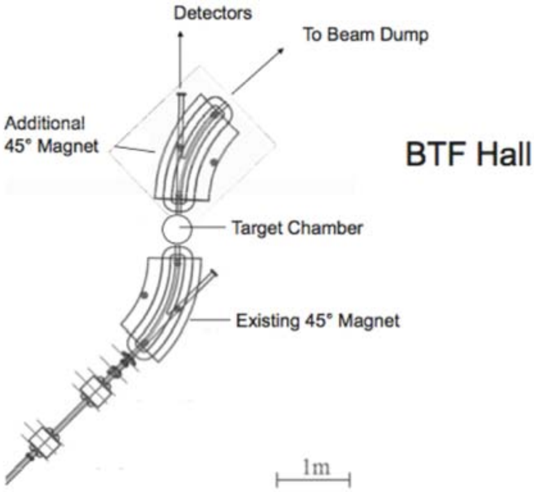

Figure 6: *Proposed scheme of chicane solution for separation of positron beam and channeling radiation.*

- the intensity can be adapted to make counter experiments feasible. Because the detector has in this geometry not anymore a direct line of sight into the region of the background producing slit systems, the background should be strongly reduced. Furthermore, it is also of great importance that the detectors could be shielded sufficiently well from the radiation produced in the beam dump.

The results of the first test we have done in BTF proved that we have high background due to which it is difficult to resolve positron channeling and channeling radiation peaks. In 2009 we are going to continue our experiment with upgraded layout and exploiting the advantages of the multiple shielding along the transfer line that is going to reduce of at least an order of magnitude the background level in the experimental hall. Multiple advantages can also be derived by a magnetic chicane that is going to be installed at the end of the BTF transfer line.

5 Conferences, Seminars

1. S.B. Dabagov, L. Quintieri, and BTF Team, "CUP: First Experience at BTF Frascati. Background and Suppression", Oral report to the PECU meeting, January 18, 2008, Frankfurt, Germany.

2. L. Quintieri, B. Buonomo, S.B. Dabagov, and G. Mazzitelli, "Positron Channeling Experiments at the DAΦNE BTF Facility: the CUP Experiment", Poster report to the 51st Workshop INFN ELOISATRON: the 3rd International Conference on Charged and Neutral Particles Channeling Phenomena - CHANNELING 2008, October 25 - November 1, 2008, Erice, Italy.

3. S.B. Dabagov, Director of the 51st INFN ELOISATRON Workshop: the 3rd International Conference on Charged and Neutral Particles Channeling Phenomena - CHANNELING 2008, October 25 - November 1, 2008, Erice, Italy.

References

1. S.B. Dabagov and N.K. Zhevago, La Rivista del Nuovo Cimento **31**, 491 (9) (2008).

2. A. Babaev *et al.*, Report LNF-08/22 (IR), October 2 (2008).

3. S.B. Dabagov, M. Ferrario, L. Palumbo, and L. Serafini, “Channeling projects at LNF: From crystal undulators to capillary waveguides, in *The Physics and Applications of High Brightness Electron Beams*, Eds.: L. Palumbo, J. Rosenzweig, and L. Serafini, World Scientific Publishing, (2007) p. 602.

4. L. Quintieri, B. Buonomo, S.B. Dabagov, G. Mazzitelli, and P. Valente, Proc. SPIE **6634** (2007) 66340U1-7.

5. A. Babaev, and S.B. Dabagov, Report LNF-07/23 (IR).

6. S.B. Dabagov, M. Ferrario, L. Palumbo, and L. Serafini, Int. J. of Modern Physics A **22**, 4280 (2007).

ETRUSCO

A. Boni (Dott.), C. Cantone (AR), S. Dell'Agnello, G.O. Delle Monache, M. Garattini (Dott.), N. Intaglietta (Tecn.), C. Lops (Dott.), M. Maiello (Dott.), M. Martini (Bors.)

1 Introduction

We created a new experimental apparatus (the SCF) and a new test procedure (the SCF-Test) to characterize and model the detailed thermal behaviour and the optical performance of laser retro-reflectors in space for industrial and scientific applications. One of the primary goals of this innovative tool is to provide critical capabilities in a timely fashion for the advent of the European GNSS[1], GALILEO: (i) validation of the functionality of GNSS laser retro-reflector payloads; (ii) optimization of their design in order to maximize the efficiency of Satellite Laser Ranging (SLR) observations by the International Laser Ranging Service (ILRS) and, therefore, improve the positioning of GNSS satellites, both in terms of absolute precision and of long-term stability. The SCF-Test was developed in the context of the ETRUSCO experiment of INFN (approved in Summer 2006) at INFN-LNF, Frascati (Italy), a large-scale infrastructure of the European Research Framework Programme (FP). This research has been funded by INFN and it was carried out at two dedicated LNF facilities, in collaboration with Italian and American partners. Since a comprehensive and non-invasive space characterization like the SCF-Test has never been performed before, the results reported in this paper are important to understand the SLR performance on current and future GNSS, as well as the fundamental physics reach of 2nd generation Lunar Laser Ranging (LLR). We identified the SCF-Test as a missing industry standard for space applications and as a missing critical service/functionality for GALILEO. We propose its adoption as a tool for the simulation and testing of GALILEO SLR and of 2nd generation LLR for the International Lunar Network (ILN) and for NASAs manned landings. We report the SCF-Test of the 3^{rd} existing flight model of Laser Retro-reflector Array (LRA) for the GPS, the "GPS3".

2 SCF-Test of the GPS3 LRA Flight Model in Air/Isothermal conditions at 632.8nm

We performed the FFDP test of each single CCR in air and isothermal conditions at 632.8 nm in the Optics Lab. The procedure is described in ref. [6)]. Figure 1 shows the FFDPs of 4 CCRs mounted with different relative orientations. For 12 CCRs, like the third in Fig. 1, the two peaks are close to each other and almost blend into one. In the presence of thermal perturbations, "blended" peaks will separate into two peaks; this has been demonstrated by the SCF-Test.

Fig. 2 shows the distance between the two peaks of the 20 CCRs whose FFDP has two cleanly separated peaks. The CodeV prediction assumes a 50 μrad central value of the GPS velocity aberration and an uncertainty of 5 μrad related to the inaccurate knowledge of the FFDP circuit.

[1]Global Navigation Satellite System.

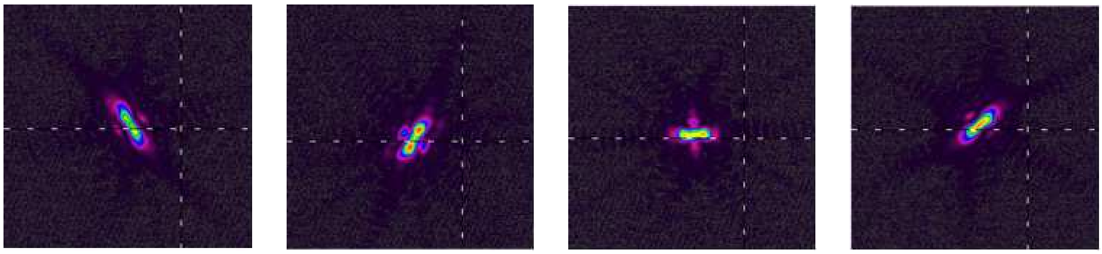

Figure 1: *FFDPs of flight GPS3 retroreflectors in air, $T = 22°C$ and $\lambda = 632.8$ nm.*

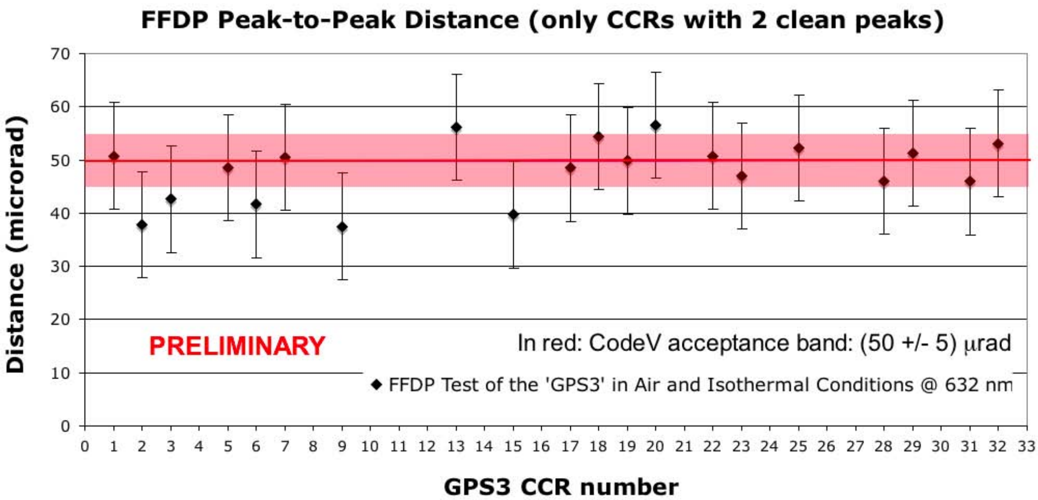

Figure 2: *Peaks distance of the GPS3 retroreflectors with two separate peaks.*

3 SCF-Test of the GPS3 LRA Flight Model at 532 nm

We performed the SCF-Test of four CCRs at 532 nm.

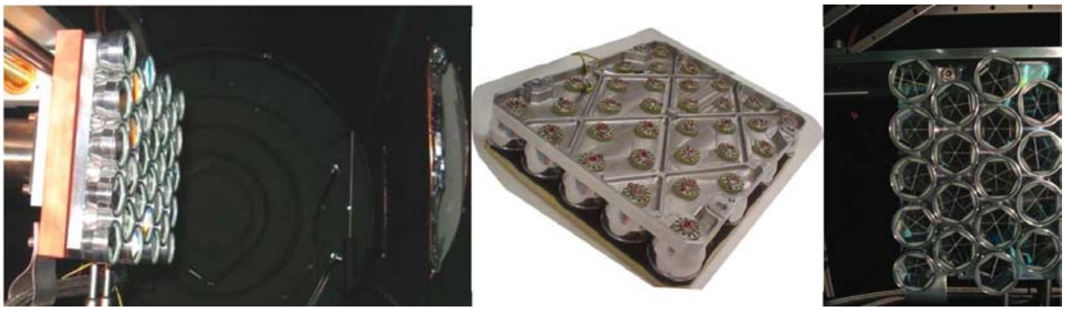

Figure 3: *GPS3 in the SCF on the Cu thermal control plate and roto-translation system (left); GPS3 Al back plate with PT100s (center); CCRs with staggered orientations (right).*

The SCF-Test was done whit in representative space conditions inside the SCF (vacuum $= 10^{-6}$ mbar, cold inner black shield at $\sim 80\,K$); the GPS3 temperature was controlled with a custom copper plate (Fig. 3, left) in thermal contact with the array Al base plate (Fig. 3, center), via indium washers in order not to damage the array base plate. The copper plate is, in turn, thermally controlled with a fluid driven by an external chiller. The temperature of the array Al back plate is measured via PT100 probes (Fig. 3, center); during the test it was set to (19 ± 1)°C. Once the CCRs and the array base plate were stable in the SCF, we turned on the SS[2] beam, normally incident with respect the CCRs surface, for about 8000 sec. The solar constant had a slightly reduced value of $(0.92 \pm 0.02) \times AM0$ due to technical reasons. The temperature of the CCR in the heating phase was measured with the IR camera (a plot of the heating phase is shown in Fig. 4, left). In this phase we recorded a τ_{CCR} of 700 sec. Then we rotated the CCR by 90° in a few seconds to record its FFDP at ~ 7 hz rate through the optical window of the SCF (Fig. 3 left, GPS3 in front the window). During FFDP data taking the SS was turned off. We recorded FFDPs at 7 Hz for a little less than 2 hours and towards the end of this time we took single shots every 5 min because the FFDP had become stable (cool down phase is shown in Fig. 4, right).

Four CCRs were SCF-Tested; here we present the FFDP variations vs time for one of them, whose "hot" (right after the rotation) and "cold" (at the end of cool down) FFDPs are shown in Fig. 5.

The heating of the CCR causes a thermal gradient inside itself, hence an index of refraction gradient (dn/dT, n=index of refraction, T=temperature), which influences its optical performance: distance between peaks and intensity. At the end of the heating phase the two peaks are farther and weaker. If this configuration occurred in orbit the CCR would retro-reflect most of the energy to the wrong angle and the signal that a CCR in such thermal/optical conditions at GNSS altitudes would return to ILRS stations would be severely and maybe unacceptably reduced compared to the nominal, expected value. At the end of the cool down, the CCR regains its thermal homogeneity, hence its optical properties. The degradation of the optical performance caused by a thermal gra-

[2]Sun Simulator.

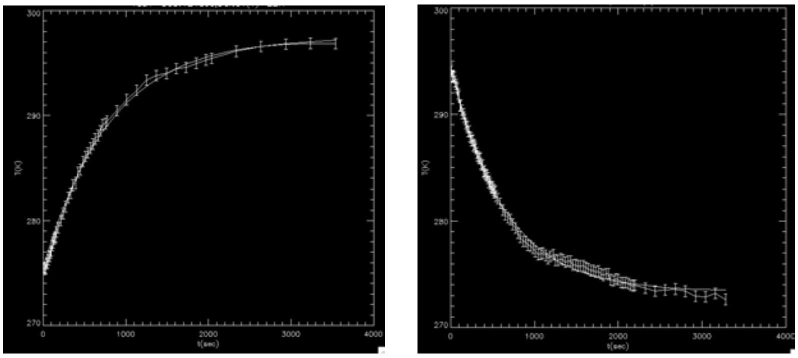

Heating phase Cooling phase

Figure 4: *Heating and cooling phases of a CCR of the array. Data are taken with the IR camera.* τ_{CCR} *for both of them is 700 sec.*

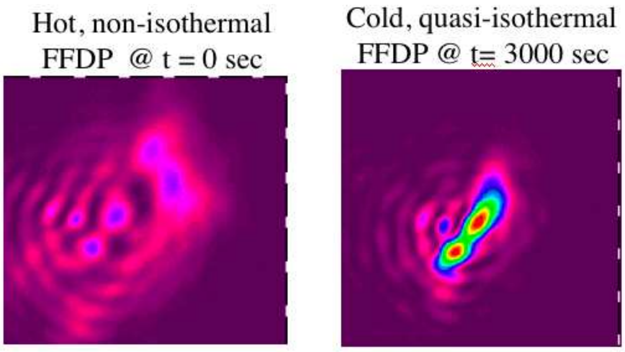

"Hot" FFDP "Cold" FFDP

Figure 5: *Hot FFDP (left), at the end of CCR heating by the SS at normal incidence, and cold FFDP (left), at the end of cool-down, after 3000sec that SS has been turned off.*

dient is common among CCRs, but what makes it significantly worse for the GPS and GLONASS CCRs is the aluminum coating on the three reflecting back surfaces and the complicated mounting system which prevents a good heat dissipation.

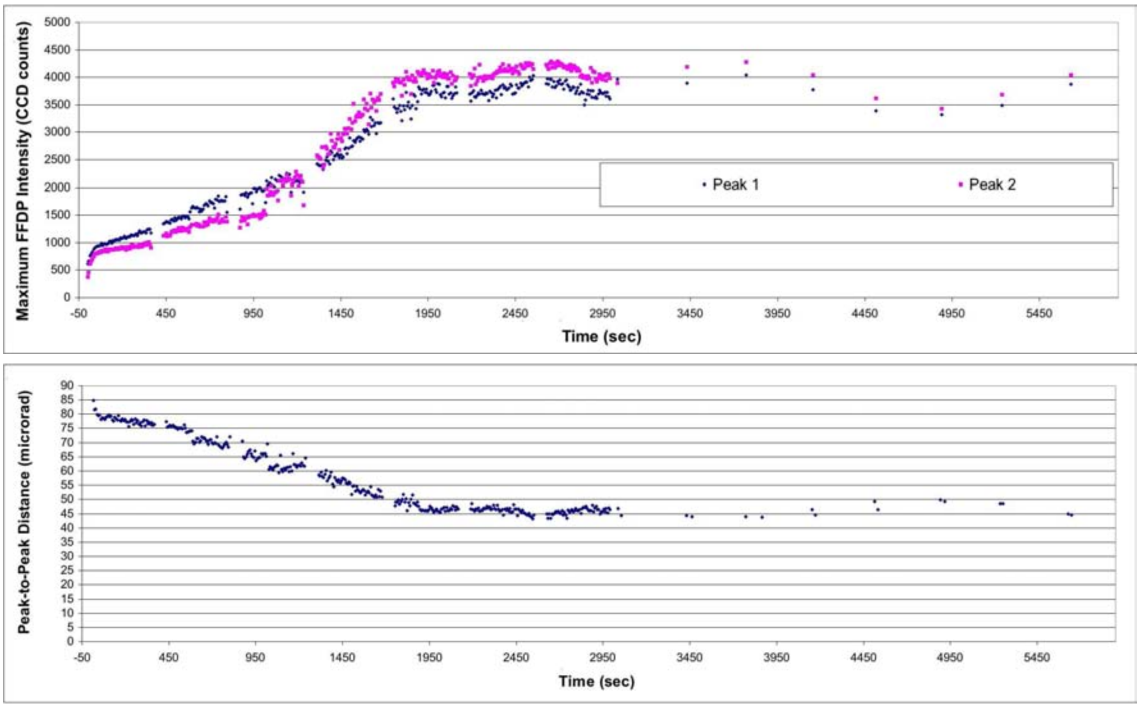

Figure 6: *CCR FFDP peaks intensity (top) and distance (bottom) vs time.*

The FFDP behaviour vs time is shown in Fig. 6. The data clearly indicate the presence of, at least, two significantly different time constants in both plots of Fig. 6: a fast rise/decay (of the order of a couple of minutes), probably due to the fast cooling down of the Al paint in the back of the three CCR faces, followed by much slower recovery of the nominal performance, probably due to the stabilization of the CCR mounting components. This second effect is much more severe, because it lasts much longer.

The oscillation of the FFDP peak heights in Fig. 6 (top) for times above 2000 sec is due to a few degree instability of thermal control system. This technical issue has now been solved, but it shows that small bulk temperature changes, directly influence the LRA optical performance (a 20% effect).

These data show that the optical performance are significantly degraded for this geometric and thermal configuration. The degradation of the initial “hot” FFDP is worse than for the GLONASS prototype, probably because the GPS3 is an older and less optimized payload. However ILRS stations tracking GNSS satellites are located, in the FFDP plane, at a fixed velocity aberration of about $20 \div 25\ \mu rad$; at that distance the reduction in intensity between the hot and cold conditions is a factor of ~ 7, like for the SCF-Test of the most recent GLONASS CCR.

Based on their nominal specifications (number of cubes, their size, Al-coating, etc) and assuming isothermal conditions, the GPS LRAs are known to provide a LIDAR optical cross section about a factor 5 lower than the 100 million m^2 required by ILRS for GNSS altitudes [3]. Thermal perturbations like those measured with our SCF-Test represent a dramatic degradation of this cross section. This is not "a 20% effect".

SCF-Tests help predict the SLR signal strength of the GPS3 in orbit. This requires correcting the data for the residual instrumental effects, differences between the SCF and orbital configurations, computing the optical cross section and correcting that for the (distance) reduction. Since GALILEO is higher than GPS/Glonass/Compass, greater care must be taken to make the return pattern uniform when the satellite moves across the sky and to avoid degradations due to on-board thermal effects. Our ultimate goals is to provide data useful to optimize the LRA design and boost the signal strength to allow for daylight ranging by the majority of ILRS stations; this in turn will allow SRL-only orbits to be computed more frequently than weekly, as it was done during the important tracking campaign of GIOVE-A in 2006 (see [4]).

References

1. M.R. Pearlman, J.J. Degnan, and J.M. Bosworth, Advances in Space Research **30**, 135 (2002). See also: http://ilrs.gsfc.nasa.gov

2. http://ilrs.gsfc.nasa.gov/docs/retroreflector_specification_070416.pdf. The document describes the rationale for LRAs on GNSS.

3. http://ilrs.gsfc.nasa.gov/docs/ILRSRetroreflectorStandards_200812.pdf. This document reports the up-to-date ILRS Standard for Retroreflector Arrays at GNSS Altitudes. The ILRS has established a standard for the effective cross section (or active area times gain) to provide sufficient return signal strength.

4. GIOVEs Track, M. Falcone *et al.*, GPS World, page 34, November 2006; www.gpsworld.com

5. A. Bosco *et al.*, Int. J. Mod. Phys. D **16**, 2271 (2007).

6. A. Boni *et al.*, Report LNF-08/26(IR), 2008.

FAST

D. Alesini, M. Bellaveglia (Art. 2222), A. Drago, L. Ficcadenti (Art. 23), A. Gallo (Resp.),
G. Gatti (Art. 23), A. Ghigo, M. Serio, A. Stella, F. Tazzioli (Ass.), C. Vicario (Art. 23)

1 FAST and the recent synchronization issues

The "Femtosecond Active Timing and Synchronization" (FAST) experiment supported by the INFN, V National Committee, is an R&D program to obtain general synchronization in the femtosecond scale among laser pulses, RF fields and LINAC electron bunches in the complex constituted by the SPARC FEL facility and the FLAME laser, both situated in the same experimental area of the LNF. Timing and Synchronization in the femtosecond scale is becoming a crucial item for a large variety of applications:

- Laser seeding of FEL process;
- Pump and probe measurements with different sources (FEL, LASER, e-bunches);
- Wakefield Laser-plasma Acceleration of externally injected electron bunches;
- Thomson scattering of counter-propagating short laser pulses and electron bunches

The high brillance beams required to drive the FEL process are characterized by minimum transverse emittance ($\epsilon \approx 1\mu$m) and short bunches ($\sigma_z \approx 1$mm). One necessary condition to minimize the transverse emittance is to precisely synchronize the laser pulse on the photocathode with the accelerating RF field in the RF gun. The required synchronization is <1 ps (SPARC working point). A very efficient way to compress the bunch and reduce its length is to adopt the RF compression scheme. The bunch is injected into the 1st TW accelerating section of the linac at an optimal phase. Because of the velocity difference between the wave and the not fully relativistic bunch, there is a slippage between them, and the bunch shortens by rotating in the longitudinal phase space (the head is less accelerated than the tail). Optimization of the compression factor requires $<$ 500 fs synchronization between bunch arrival time and RF field in the RF compressor (SPARC). These specifications have been already achieved by the SPARC synchronization system, which is based on a distribution of electrical reference signals through a coaxial cable network. However, in the near future more severe synchronization specifications need to be achieved in order to cope with the requests of a family of new experiments where the SPARC beam will interact with the FLAME laser, which is presently under installation in a dedicated building close to the SPARC experimental area. In particular, the SPARC beam will be injected in a plasma wave generated by the FLAME laser colliding with a proper target to perform a wakefield laser-plasma acceleration experiment. This technique requires a synchronization between the SPARC electron bunch and the plasma wave (synchronous with the FLAME laser) at $<$ 100 fs level. The FAST collaboration is aimed at studying and implementing upgrades of the existing SPARC synchronization system to cope with the most demanding specifications of future experiments. During year 2008 the FAST work program for the LNF component of the collaboration consisted in the following points:

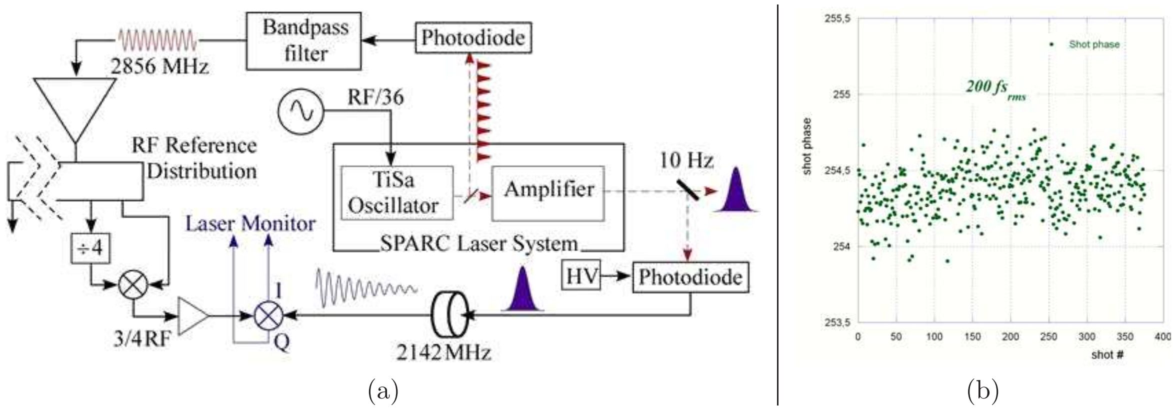

Figure 1: *Laser driven configuration @SPARC: (a) schematics of the setup and (b) acquired phase values with statistics.*

- first tests of a laser-driven synchronization architecture at SPARC, to improve the relative phase jitter between the photocathode laser and the RF reference clock;
- first measurements of the phase stability of the laser FLAME laser oscillator performed at the factory site;
- upgrade of the existing resonant arrival time monitor for the SPARC photocathode laser toward a final resolution in the ≈ 100 fs scale;
- Construction of 2 resonant Bunch Arrival Monitor RF cavities, resonating at 3/4 RF frequency (2142MHz) to be mounted on the SPARC beam pipe for on-line synchronization measurements.

2 Laser driven configuration @SPARC

At SPARC the time jitter of the photocathode laser has been identified as the major source affecting the facility synchronization. In the present configuration the reference signal is generated by a commercial microwave synthesized oscillator tuned at the linac frequency of 2856 MHz. The photocathode laser repetition rate is locked to this reference, but due to some limitation in the performances of the electro-mechanical locking system, the jitter relative to the reference can not be reduced below 400fs. A different architecture of the timing system, as sketched in figure 1a, has been tested to overcome this limitation. In this case the timing reference signal is extracted directly from the laser oscillator with a fast photodiode and a bandpass filter, and the linac low-level RF system is driven by this new reference tone. This makes virtually jitter-free (in relative terms) the laser system. The result of the test is reported in figure 1b, which shows a reduction of the laser pulse after the amplifier from > 400 to ≈ 200fs. The measured residual jitter, according to our interpretation, is mainly due to the presence of a digital ECL prescaler board (a frequency divider-by-4) in the set-up, while the laser amplifier and the resolution of the phase noise equipment are expected to give a lower contribution. The test will be repeated with a better set-up

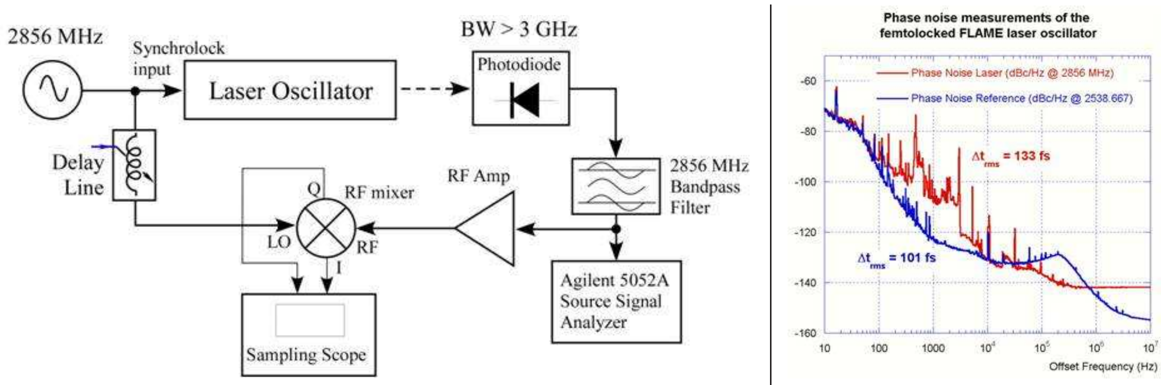

(a) (b)

Figure 2: *Flame oscillator measurement @Amplitude Technologies: (a) schematics of the setup and (b) acquired phase noise spectra with statistics.*

excluding the prescaler, and the laser driven synchronization architecture will be implemented to exploit the relative jitter reduction in the operation of SPARC.

3 FLAME oscillator characterization

The FLAME laser is going to be a very important client of the SPARC synchronization system in order to make the experiments involving the FLAME photons and the SPARC electrons possible. In order to have a first estimate of the time jitter of the FLAME laser, we have measured at the factory site the phase noise spectrum of the FLAME oscillator locked to an RF reference. The measurement set up is shown in figure 2a and the obtained measurements are reported in figure 2b. The absolute phase noise of the locked laser and of the RF reference, integrated in the 10 Hz $\div$10 MHz range, are $\approx$ 130fs and $\approx$ 100fs, respectively. The residual phase noise of the laser oscillator integrated outside the lock bandwidth is $<$ 100fs, which can be considered a promising starting point, being already substantially better than the phase noise measured on the SPARC photocathode laser.

4 SPARC photocathode laser time-of-arrival monitor

The time-of-arrival monitor of the SPARC laser photocathode is a very useful diagnostic tool in use during operation. It is based on a resonant pulse stretching method, which means that a sample of the UV photocathode laser pulse is converted in an electric short pulse exciting a resonant cavity tuned at 3/4 the linac RF frequency (2142 MHz). The cavity filters the input pulse transforming it in a long-lasting (few μs) exponentially decaying sine wave, suitable for standard phase detection by means of a microwave mixers. The quality of the photodiode converting the laser into a current pulse is crucial for the quality of the measurement. In order to get the highest possible peak pulse voltage and reduce the RF amplification downstream the cavity, high voltage vacuum photodiodes have been used. Our measurement set-up has been upgraded purchasing a pair of new photodiodes (Photek PD025) operated

(a)

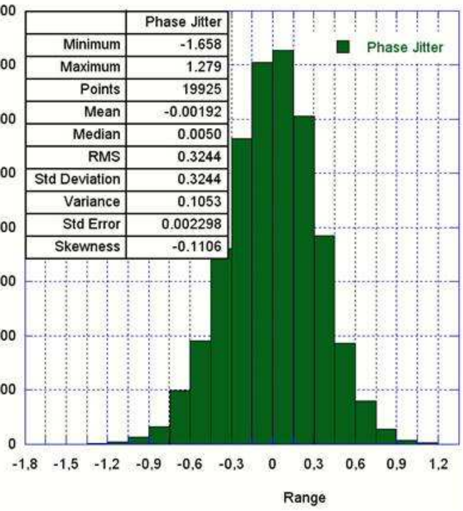

(b)

Figure 3: *Amplified UV laser pulse time-of-arrival measurement: (a) high voltage photo diode picture and (b) acquired arrival time values with statistics.*

with their $5kV$ high voltage power supplies. By controlling the bias level of the photodiodes it is possible to limit their saturation, drastically reducing the AM-to-PM conversion which might severely affect precise synchronization measurements. Under these conditions we use the new photodiodes to monitor continuously the laser time of arrival on the photocathode. A picture of the PD025 photodiodes is shown in figure 3a, while a typical acquisition of ≈ 20000 shots is reported in figure 3b. The standard deviation of the reported sample is $0.324°$ (measured at 2142MHz), corresponding to ≈ 430fs.

5 Resonant cavity bunch-arrival-monitor

The resonant pulse stretching method can be effectively used to monitor the arrival time of the electron bunches at some selected positions along the linac. To do that, precisely tuned cavities have to be placed along the beam trajectory on the linac beam pipe. The electron bunch directly excite cavity field free oscillations that are sampled and carried outside by 2 antennas connected to vacuum coaxial feedthroughs. Two resonant Bunch Arrival Monitors (BAM) cavities have been designed and built, and are now ready for installation on the SPARC linac beam pipes. A sketch of the mechanical 3D model of the BAM cavity and a picture of the manufactured device are reported in figures 4a and 4b, respectively. The BAM cavities are pill-box like, and their characteristics are reported in figure 4c.

The BAM cavities are equipped with two tuning ports. The larger port will accommodate a fixed tuning plunger to coarsely tune the cell, while the smaller port will host a remotely controlled tuner plunger to finely correct the cavity natural resonant frequency of the fundamental mode to <10kHz respect to the reference 3/4 RF to limit the detected phase slippage during the measurement time slot.

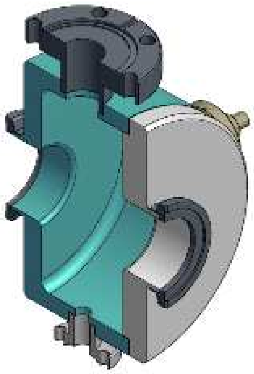

(a)

(b)

Opearting mode	TM010
Frequency	$f_0 = 2142MHz$
Unloaded Q factor	$Q_0 = 16000$
R/Q factor	$R/Q = 40\Omega$
Antenna ext. Q fact.	$Q_{ext} = 30000$
Loaded Q factor	$Q_L = 7500$
Decay time	$\tau_d = 1\mu s$
Output peak voltage @$1nC$ bunch charge	$V_{pk} \approx 2V$

(c)

Figure 4: *Amplified UV laser pulse time-of-arrival measurement: (a) high voltage photo diode picture and (b) acquired arrival time values with statistics.*

The coupling of the antennas is designed to produce large detectable signals ($\approx 2V$ for 1nC bunches) which will eventually require no extra RF front-end amplification before being demodulated. The use of BAMs on the SPARC linac will allow monitoring directly the electron bunch synchronization and, by differentially comparing the measurements of 2 different BAMs, finally qualifying the ultimate resolution attainable by the pulse resonant stretching method which is fully based on electrical microwave techniques.

References

1. M. Ferrario *et al.*, "Recent Results and Future Perspectives of the SPARC Project", Proc. of EPAC08, Genoa, Italy.
2. D. Alesini *et al.*, Proc. of EPAC 2006, Edinburgh, Scotland.
3. A. Gallo *et al.*, "Performances of the SPARC Laser and RF Synchronization Systems", Proc. of EPAC08, Genoa, Italy.

FLUKA2

M. Carboni, C. D'Ambrosio (Ass.), M. Pelliccioni (Resp., Ass.),
V. Patera (Ass.), A. Patriarca (Ass.)

1 Activity

During the 2008 the LNF FLUKA2 group has partecipated to the optimization of the FLUKA code for hadron therapy applications. A particular effort has been devoted to the introduction of the radiobiological effects of the released dose by carbon ions, focusing mainly on the following items:

1. Computing of a radiobiological data-base of the alpha and beta parameters that describe the survival probability of the CHO (Chinese hamster ovary) cells, assuming a liner-quadratic relationship of the logarithm of the survival probability with respect to the delivered dose. This work has been accomplished in collaboration with the group of INFN of Torino, using the LEM (Local Effect Model) as radiobiological model.

2. Studies of the possible cpu optimization: tracking parameters, physical process cuts, insertion of variance minimization tecniques, with a total gain in cpu time ranging from 3 to 6, depending on the geometry of the problem (mainly on the size of the treatment region).

3. Verification of the Dual Radiation Action for the description of the radiobiological effect induced by mixed field (beams not composed by pure carbon ions). That is particularly relevant because, due to the fragmentation process, the carbon ion beams produce a sizeable fraction of lighter ions in the tumor region. To study this effect a code that compute the radiobiological damage of each single track, based on the LEM, has been inserted in FLUKA.

Moreover, in collaboration with the ICRP, the calculation of the fluence-to-effective dose conversion coefficients for mono-energetic neutrons of energy up to 10 GeV has been restarted with the new neutron library of the FLUKA code and the new blood compositions recently adopted by the ICRP.

At last, the FLUKA code has been widely engaged to study the radiation problems of the CNAO (i.e. beam stopper of the extraction beam lines).

2 List of Publications

1. G. Battistoni *et al.*, Nuovo Cimento C **31**, 69 (2008).

GIAF

L. Ficcadenti (Art. 23), D. Alesini, R. Boni, A. Gallo, F. Marcellini,
M. Migliorati, A. Mostacci, B. Spataro (Resp.), M. Ferrario,
V. Fusco (Art.23), M. Esposito (Ass.), L. Palumbo, J. Rosenzweig

1 Aim of the experiment

The aim of GIAF group is related to the design, realization and measurements of a hybrid standing wave (SW) traveling wave (TW) gun operating at 2.856 GHz. The structure is a 1.6-cell cavity in the standing wave part operating on a π- mode, followed by a 5-cell cavity in the traveling wave part operating on a $2\pi/3$-mode. The hybrid section has been designed with the HFSS and SUPERFISH codes. The copper prototype of the structure has been successfully characterized. In addition an intense activity on the innovative technological methods to make cavities resonators are in progress, too.

2 2008 Activity

2.1 LNF copper prototype

The picture of the copper prototype realized at LNF is reported in Fig. 1, the design of the structure, the cavity dimensions and parameters is reported on [1, 2, 3, 4, 5].

The device is assembled using four copper rods. In the half cell of the SW part has been introduced a little probe to measure the quality factor of the π-mode.

Figure 1: *Copper prototype.*

The reflection coefficient measured from the input port and the transmission coefficient between the small half SW cell probe and the input port are reported in Figs. 2 and 3 respectively. The unloaded quality factor of the operating π-mode is 12600.

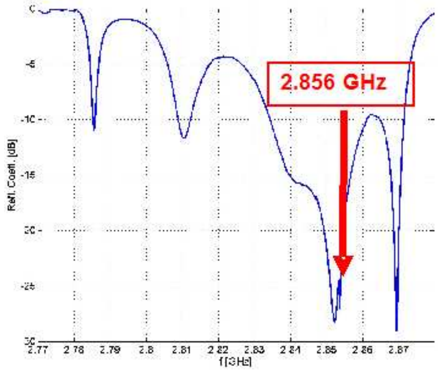

Figure 2: *Input port reflection coefficient.*

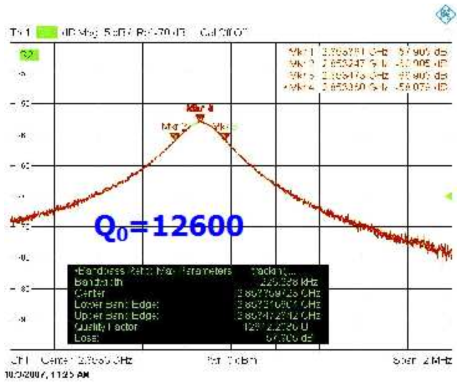

Figure 3: *Trasmission coefficient between the input port and the small lateral probe.*

The measured longitudinal electric field on axis, compared with the one of the HFSS simulation is reported in Fig. 4, where it is possible to see a very good agreement in amplitude and phase with the simulation results.

2.2 Technological activity

The Electroforming is a galvanoplastic procedure to obtain R.F. (radio-frequency) devices through a metal deposition on a core. The standard procedure to obtain an electroformed structure, is to prepare an Al core on wich Cu is deposited. At the end of the deposition a Sodium Hydroxide chemical etching eliminates the inner Al core (Fig. 5). Additional experimental studies are in progress.

2.3 Coupler

The first tentative to obtain an Electroformed Coupler gave rather good results. Anyway the shape of the connection between waveguide and central cell has to be modified. For this reason a second

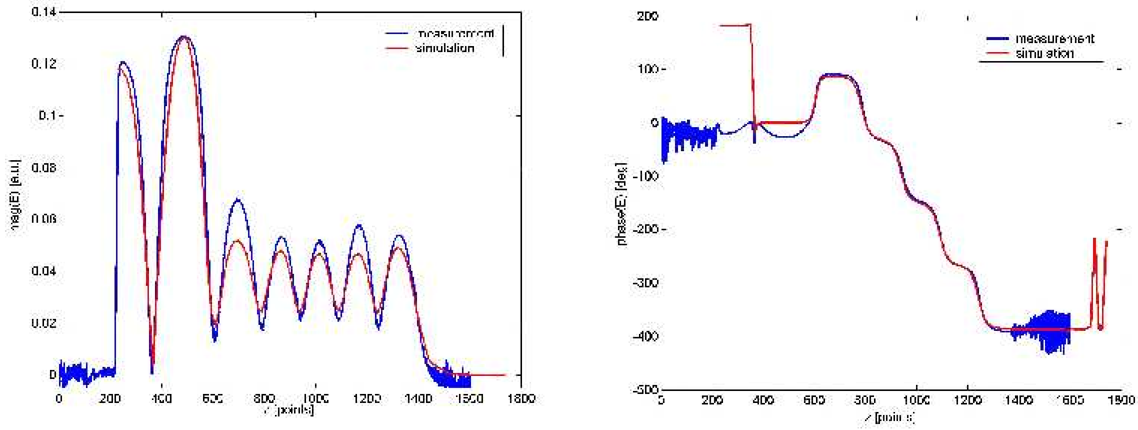

Figure 4: *Amplitude and phase of the on axis longitudinal electric field.*

Figure 5: *An aluminium structure (or core) ready to be treated in order to deposit copper on it by electroforming.*

Al core is going to be completed. Then it will be sent to our Galvanotechnic Company for the Cu deposition. A couple of months will be necessary to have it back.

2.3.1 Other materials

Presently some other materials, in addition to the Copper, are under study: essentially Molybdenum and alloy Copper Zirconium. Regarding Molybdenum some electroformed multicell structures with Mo irises have already been made with good results (see 2007 report). These prototypes were made only to check the procedure. For these special materials the Electroforming technique could be used as a way to encapsulate the components of the multicell structures, making something like a cold brazing of the multicell elements, as well as the end flanges. The above procedure will have the advantage to avoid the high thermal stress of these metals during the brazing. In particular this is valid for the Cu/Zr because it loses its RF properties above a 300 °C treatment. Finally the way to obtain electroformed multicell structures with the presence of two tuners per cell will be considered as soon as a proper tuner structure designed for this procedure will be tested

3 Activity 2009

The next steps will be the realization at LNF of the final model of the copper hybrid section. The design has been completed and includes the vacuum pumping, the cooling systems etc so on. Measurements at room temperature will be carried out at LNF while the high power tests will be made at Los Angeles UCLA. Additional activities on the innovative methods to realize the cavity resonators are in progress, too.

References

1. D. Alesini *et al.*, "The Design of a Hybrid Photoinjector for High Brightness Beam Applications", EPAC 2006, Edimnburgh, Scotland.

2. B. D. O'Shea *et al.*, "Measurement of the UCLA/URLS/INFN Hybrid gun", Albuquerque, New Mexico, USA.

3. B. O'Shea *et al.*, "RF Design of the UCLA/INFN Hybrid SW/TW Photoinjector", http://pbpl.physics.ucla.edu, 12^{th} Advanced Accelerator Concepts Workshop (AAC 2006), Lake Geneva, Wisconsin, Jul 2006.

4. J. Rosenzweig *et al.*, "Beam Dynamics in a Hybrid Standing Wave-Travelling Wave Photoinjector", 12^{th} Advanced Accelerator Concepts Workshop (AAC 2006), Lake Geneva, Wisconsin, Jul 2006.

5. A. Fukasawa *et al.*, "A hybrid standing wave traveling-wave photoinjector", FEL08, Gyeongiu, Korea, 24-29 August 2008.

GRANITA

G. Celentano (Ass.), U. Gambardella (Resp.)

1 Purposes of the project

The *GRANITA* experiment is devoted to study the use of heat pipe for cryogenic cooling. This is kind of cooling, in between the liquid bath cooling and thermal conduction, is required under specific circumstancies such as environment incompatibility between cooler and operating conditions (e.g. strong magnetic fields, vacuum, etc.) and/or when there are large distances from the cooler to the device and the conductive cooling, i.e. by means of long metallic shortcuts, became heavy and inefficient. This project has been largely reduced by the scientific commission, thus it was limited to the realization and test of one prototype of heat pipe sized for the available cryogenic equipment i.e. an existing vacuum chamber and cryocooler. Two INFN sections are involved: Genova (group leader), and LNF, in collaboration with CRIS-Ansaldo (Finmecanica Group), Naples.

2 The experiment

The Frascati group, made of LNF and ENEA Frascati researchers, in 2008 designed the heat pipe circuit, the heat exchangers, and its assembling in the test facility. For the fabrication and design also Ansaldo-CRIS, Naples was involved. The heat pipe principle is based on the fluid free circulation in a closed circuit, induced by hydraulic pressure only, between two heat exchangers: an upper one connected with the cryogenic source and a lower one connected to the device to be cooled. In Fig. 1a) the cross section view of the conceptual design of the heat pipe circuit is shown. The key features of the design are reported in Tab. 1, where hydrogen was taken into account as working fluid. We considered a working temperature of 20 K, but changing the working fluid we could work at 27 K (with neon), 4 K (with helium), 77 K (with nitrogen). Of course for each gas an optimized circuit should be designed. This means setting the pipe size, its length and heat exchangers dimensions, in order to get the best performance. With the dimensions in Tab. 1, a power of 27 W at low temperature for hydrogen gas is estimated.

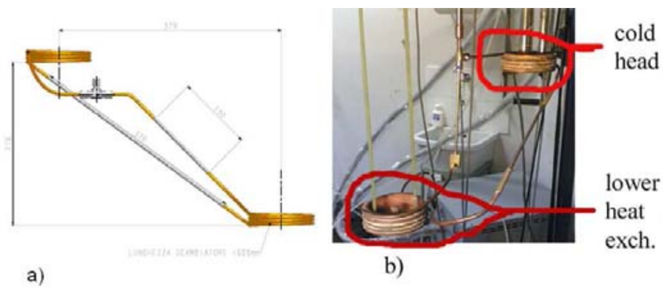

Figure 1: *View of the conceptual design of the heat pipe circuit (a). Picture of the assembled heat exchangers below the cold head of the cryocooler (b).*

Table 1: *Main design parameters.*

Laplace constant [m]	2.52×10^{-3}
Pipe diameter [m]	4.00×10^{-3}
External pipe connection diameter [m]	1.00×10^{-2}
Pipe length [m]	3.73
Length to be filled with liquid [m]	0.85
Length to be filled by gas [m]	2.89
Pipe section [m^2]	1.26×10^{-5}
Pipe volume [m^3]	4.69×10^{-5}
Liquid volume [m^3]	1.06×10^{-5}
Gas volume [m^3]	3.63×10^{-5}
Bottom heat exchanger length [m]	1.00
Upper heat exchanger length [m]	1.00
Maximum gap [m]	0.274
Δ T [K] hypoteses	9.0

This number comes from a heat exchange coefficient of 250 W $m^{-2}K^{-1}$ and the hydrostatic pressure of the liquid hydrogen column height into the circuit. The experimental setup is shown in Fig. 1b), where the two heat exchangers are indicated. Both exchangers were provided with thermometers and heaters. The upper one sets the working temperature of the cryocooler, which can go down to 4.0 K, by means of a thermal regulator (Oxford ITC503). The heater on the lower exchanger will be operated to reveal the maximum heat value not affecting the fluid circulation.

The first cooldown tests were performed at a constant pressure of 2 atm, using the high pressure bottle to provide make-up gas as it gets denser and denser. In this way we avoid to work with high pressure (150 atm) required to put in the circuit the necessary amount of H_2 gas. We observed that the upper heat exchanger cools down below 20 K in less than 2 hours, while the lower one keeps the constant room temperature for more than 4 hours. Only after the fluid circulation begun, and we started to record a temperature decrease on the lower heat exchanger. Unfortunately we did not put good thermal shields on the heat pipe, and consequently we were not able to reach a temperature in the bottom heat exchanger to keep liquid H_2, i.e. the operating condition was out of the heat pipe design. We just produced liquid on the top exchanger which dropped down but the input radiation heat power on the bottom was too high did not allow to fill up the exchanger with liquid. However we were able to trigger the natural convection of liquid/gas phases. After these tests we recently assembled the thermal shield which should allow condensation of LH_2 in the bottom exchanger. With this improvement we hope to measure shortly the efficiency of the heat pipe with hydrogen and neon at least.

IMAGEM
(Imaging with Triple GEM Detectors)

B. Buonomo (Art. 23), G. Corradi (Tecn.), G. Mazzitelli, F. Murtas (Resp.),
M. Pistilli (Tecn.), L. Quintieri (Art. 23), D. Tagnani (Tecn.)

1 Introduction

The main tasks of this R&D is the development of different detectors basted on GEM technologies essentially for beam diagnostic. The use of GEM foils for detector construction started in Frascati on 2002 with the R&D for LHCb muon chambers M1R1. Ever since several triple GEM chambers have been built for different applications. The results obtained in several beam tests show high performances: high rate capability (> 50 MHz/cm^2), good time resolution (~ 4 ns), good space resolution $O(200\mu\text{m})$, and good aging resistance after 2C/cm^2 of integrated charge. The IMAGEM R&D is devoted not only to the detectors but also to the readout electronics and power supply.

2 Track Luminometer for Dafne Upgrade

In the mainframe of Dafne Upgrade, for the luminosity measurement in e^+e^- collision using the Crab Waist mode , four semi anular detectors for Bhabha events detection have been designed and built. A new GEM foil have been designed as shown in the Figure 1(left) with 32 pads on the anode with a total detector diameter of 20 cm.

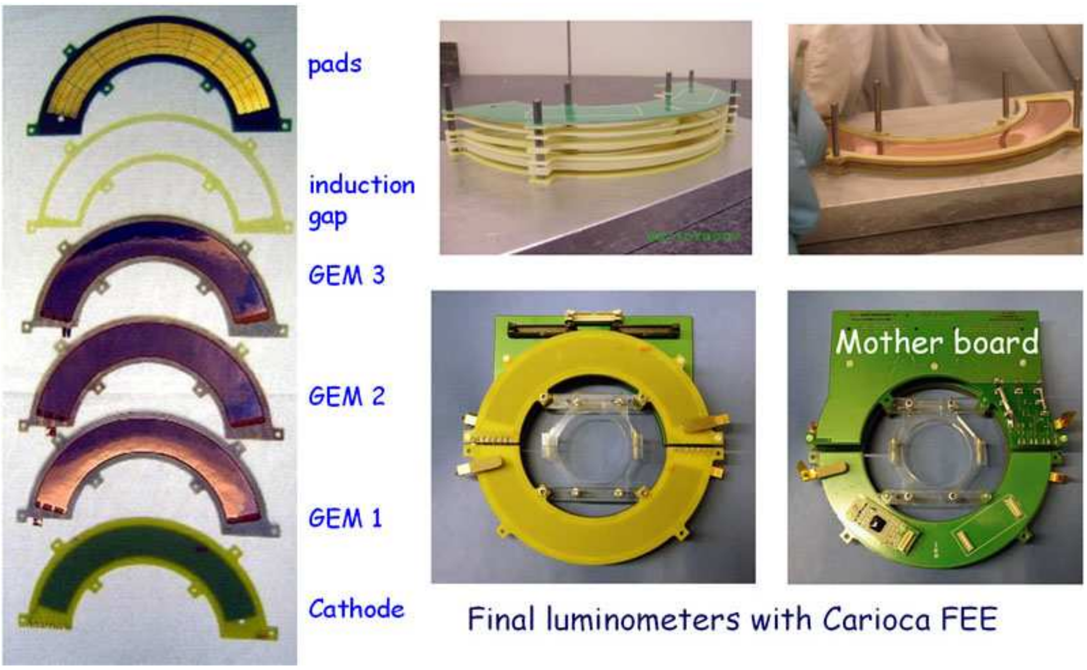

Figure 1: *Assembilng the GEM track Luminometer.*

The pad dimensions are $6 \times 24(32)$ mm^2 depending on the ring radius. On the back side of the anode PCB two small connectors for the front end has been foreseen. These cards have been designed and realized in Frascati using the chip Carioca GEM developed at CERN for the LHCb muon chamber M1R1. The Fig. 1(right) shows the Carioca Card assembled on the back side of the detector. A mother board for the LV and HV power supply is successively plugged on them. The same mother board houses the connectors for LVDS signals coming out from the Carioca cards. The detectors have been installed at the beginning of 2008 near Sidhartha experiment at 18 cm from interaction point of Dafne. They are run for few months furnishing information on machine background (about 700 KHz on the whole detector when a beam current of 500 mA is circulating inside Dafne). In coincidence with the scintillator tail calorimeter placed behind the GEM track luminometer the impact point of electrons and positrons have been measured together with collinearity of the bhabha event (see fig 2).

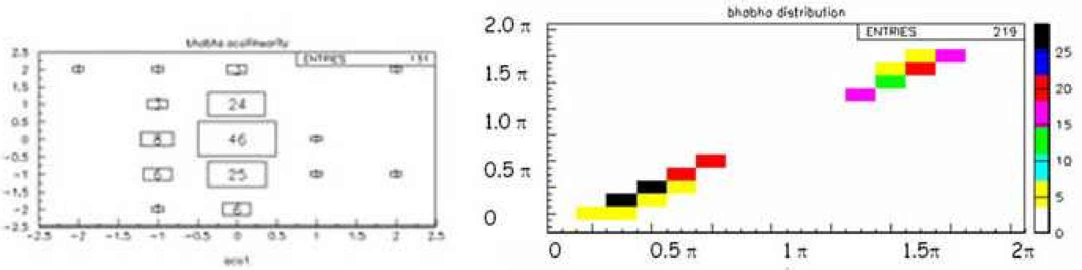

Figure 2: *Collinearity of Bhabha events measured by the GEM track Luminometer.*

The hit cluster size was below 1.2 and the space resolution of the O(1 cm) was in agreement with the pad dimension. The events taken during four months of data taking has shown low noise even if the detectors were close to the beam pipe. Due to the high sensitivity of Siddhartha experiment built around the same interaction region, the installation of a further lead protection just around the beam pipe to screening from the machine background, has required a removal of the GEM detector, preventing the run follow up.

3 TPG: a Time Projection Chamber with a triple GEM readout

A compact time projection chamber (TPC) has been designed, built and tested, for beam monitoring at the Dafne Beam Test Facility (BTF). The Facility provides electron and positron beams in a wide range of intensity, from single particle up to 10^{10} particles per pulse, and energy, from a few tens of MeV up to 800 MeV. The large range of operation of the facility requires the implementation of different detectors, for real-time beam monitoring. The main idea in developing this detector is to place a standard triple GEM detector parallel to the beam and to use it as a time projection chamber, by enlarging the drift gap. In this way the depth of the material crossed by the particle is particularly small and the beam position measurement could be more precise, in the coordinate along the drift O(100 μm), by measuring the time of arrival of the electron clusters. Moreover, a very compact detector can be realized, using standard $10{\times}10$ cm^2 GEM foils and a drift gap of 4 cm. The 128 readout channels organized in a matrix of 8×16 pads allow to obtain a good resolution O(1 mm) also in the other two coordinates. Thanks to a small material budget crossed by the particle and the 3D reconstruction of the particles track, it's use for ion beam monitor in adrotherapy is very promising and under study.

4 Monitor for high intensity neutron flux

In 2008 some beam tests have been done at FNG (Neutron Gun Facility) at ENEA Frascati for the measurements of high neutron flux produced by strong nuclear reaction Deuterium-Deuterium e Deuterium-Tritium. Neutron of 2.4 MeV e 14 MeV are produced by this two reactions. A prototype 10×10 cm^2 made of a triple GEM with a cathode of alluminum and polietilene has been placed in front of the gun at few centimeter. The neutrons impinging on polietilene are converted in proton that release its final energy inside the gas producing electrons. The 64 readout pads organized in a matrix 16×4 allow to create an intensity image of the neutron source. The total counting rate has been compared with the measurement done with a liquid scintillator NE213 detector placed 10 meter far from the neutron source showing a good linearity up to 12 MHz/cm^2 (the maximum flux for FNG). As shown in Fig. 3 the detector efficiency is not high (4×10^{-4}) but in any case is not necessary for this type of measurement.

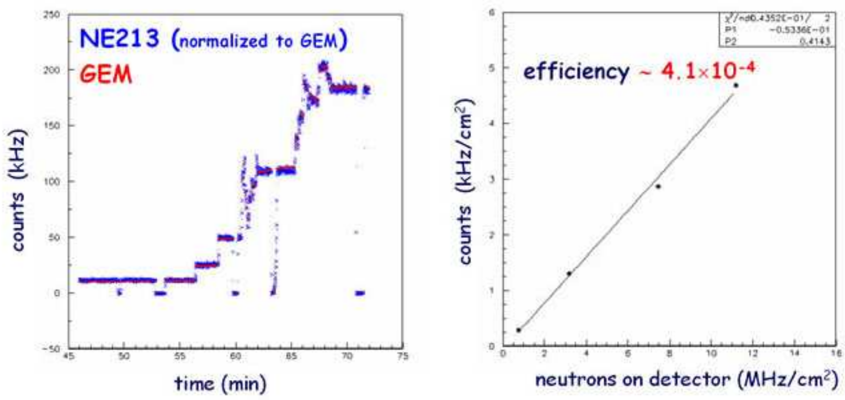

Figure 3: *The flux measurement compared with NE213 and the linearity up to* $12\ MHz/cm^2$.

Thanks to the strength signal released by the proton inside the gas the low gain settings of the chamber allow to have a good rejection to the photons produced by the radioactivation of material around the gun. At present a second prototype is under construction with 128 channels, more compact and able to measure at the same time the DD and DT component of the neutron flux.

5 High Voltage System for triple GEM detector

A novel High Voltage System for triple GEM detectors has been designed and realized in Frascati in the LHCb framework. The system element is built with seven floating power supply, with a maximum of 1200 V each, and controlled via CANbus, for voltage settings and monitoring. Several HV modules can be installed in a nano-ammeter mainframe already developed in Frascati, realizing a HV crate able to supply up to 24 triple GEM chambers with a 1 nA resolution monitoring system.

Figure 4: *A single HV GEM Module (on the left) and the 4 HVGEM system (on the right).*

A single HVGEM module has been used for several months supplying the detectors placed near the interaction region at Dafne, in radioactive hostile environment, showing good performances and reliability. A system with 4 modules has been realized and used for supply the four GEM track luminometers (see Fig 4) A the moment about 40 modules have produced up to now; some of them have been requested by groups working on GEM detectors.

6 Future

Other groups of INFN, ENEA and CERN are interested in use of these triple GEM detectors. Recently two monitors have been requested at CERN SPS for a crystal channeling collimation experiment. They will be installed before and after the bending crystal, just on the face tank that will contain the protractor, at few cm from the proton beam.

Any other information can been found on the web site

`http://www.lnf.infn.it/esperimenti/imagem/`

7 List of Conference Talks

1. A. Ferrari, "A GEM based Neutron Flux Monitor for diagnostics in Fusion Reactors", IEEE 2008, Dresden, Germany.

2. F. Murtas, "Beam Diagnostics with GEM detectors", Invited Seminar at IHEP Beijing 26-5-2008.

References

1. F. Sauli, Nucl. Instr. & Meth. A **386** 531 (1997).

2. M. Alfonsi *et al.*, "The Triple-GEM detector for the M1R1 muon station at LHCb", N14-182, 2005 IEEE NSS Conference, Puerto Rico.

3. A. Corradi, F. Murtas, and D. Tagnani, Nucl. Instr. & Meth. A **572**, 96 (2007).

KLONE
(KLOe calorimeter Neutron Efficiency)

S. Bertolucci, G. Corradi (Tecn.), M. Iliescu (Art. 2222), A. Lucá (Laur.)
M. Martini(Ass. Ric.), S. Miscetti (Resp. Naz.), I. Sarra (Laur.), B. Sciascia (Art. 23),
F. Sirghi (Bors. PD), D. Tagnani (Tecn.)

1 Measurement of detection efficiency to neutrons of 21, 46 and 174 MeV energy

As shown in the 2006 and 2007 LNF activity report, the detection efficiency of heterogeneous calorimeters with high sampling to low energy neutrons is much larger than what expected if the signal was due only to the equivalent scintillator thickness in the calorimeter. The measurements with the lead-scintillating fiber KLOE calorimeter prototype has been carried out at the "The Svedberg Laboratory" (TSL) high energy neutron facility. A first measurement with a neutron beam at 174 MeV was carried out in October 2006 while a second one at lower energies (21 and 46 MeV) took place in the same experimental facility in June 2007. In October 2008 a third measurement has been carried out to better understand neutron background and to measure the efficiency of different version of Pb-scifi calorimeters.

The standard prototype is composed of ~ 200 layers of 1 mm diameter blue scifi glued inside grooved lead layers of 0.5 mm thickness. The readout consists of four planes for the first 16.8 cm calorimeter thickness. Each plane is subdivided in 3 columns along the horizontal coordinate originating cells of 4.2×4.2 cm^2 area. The calorimeter was positioned with fibers running vertically, the lower (upper) end is called side A (B). We use the discriminated signals of the calorimeter analog sums, SA and SB, to make the trigger as $SA \cdot SB$. A reference counter for efficiency, of transversal dimensions 10×20 cm^2, was built with a 5 cm thick bulk of NE110 organic scintillator. When running with the beam, the scintillator was positioned with its longest dimension along the horizontal coordinate. To trigger on the scintillator, the PM signals, $S1$ and $S2$, were discriminated and a coincidence, $S1 \cdot S2$, formed. The neutron beam was shaped by a cylindrical collimator of 2 cm diameter at 3 m distance from the neutron source. We positioned the calorimeter from 5 to 6 m distance from the source to grant full beam acceptance. Neutron flux rate of 20 kHz/cm^2 were required to make negligible the probability of double neutrons/triggered event. Beam intensity was monitored by a calibrated beam Ionization Chamber (ICM) positioned just in front of the collimator exit. The trigger signal was phase locked with the cyclotron RF replica.

The preliminary detector efficiency to the overall neutron spectrum, ϵ_D, is determined as the ratio of the counted detector rate with the neutron beam rate estimated by the ICM assuming full acceptance and no background contamination. A good agreement with the thumb rule of 1%/cm of scintillator thickness is observed. While the scintillator covers a small solid angle, the calorimeter coverage is much more extended and we carefully analized data to quantify the eventual presence of halo neutrons surrounding the beam core. As reported in 2007 activity report, the contribution for the halo is obtained fitting the TOF distribution of data using signal shape from Monte Carlo and a flat distribution to simulate halo.

In Fig.1, we report the neutron detection efficiency after correcting for the halo fraction obtained from fitting procedure. We also report our previous results measured in different conditions.

For the 2008 test beam, we also prepared a dedicated beam position monitor to study the presence of the halo. We realized two identical counters composed by 16 tiles of BC404 $(1 \times 0.5 \times 20)$ cm^3. Light from the tiles was transported by WLS fibers to multi-anodes PMs on both fiber ends. When running with neutron beam, the two detectors were placed orthogonally to measure its transversal dimensions. Data analysis from this detector has not yet been completed.

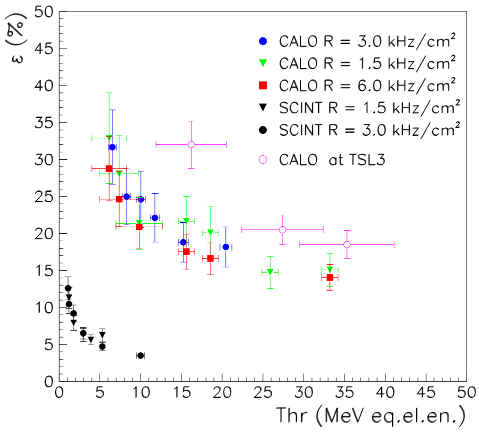

Figure 1: *Calorimeter detection efficiency. Comparison between different test beams and reference counter.*

These results show that at 174 MeV, with the lowest trigger threshold of 15 MeV, the neutron detection efficiency of the calorimeter is 33 %. This corresponds to a sizeable enhancement with respect to the expected 8% based on the equivalent amount of scintillator only. Unfortunately in this last test, was not possible to lower the threshold down to 15 MeV. This is probably due to the "aging" of the system and to the deterioration of optical contact between PM's and guides caused to transportation.

FLUKA has been used for a detailed simulation of the calorimeter structure and of the TSL experimental beam-line. The primary reason for the observed efficiency enhancement appears to be the huge inelastic production of neutrons on the lead planes. The high sampling frequency of the calorimeter appears also to be a crucial point in the efficiency enhancement. Results obtained by Monte Carlo are in reasonable agreement with data after taking into account halo correction. Detailed simulation of the entire system are in progress.

In the last test beam of October 2008, we measured the efficiency of other two similar calorimeters. Following the prediction of FLUKA simulation for the efficiency enhancement, we prepared a small lead-scifi detector with a larger quantity of absorbing material in the composition. This increases the inelastic production of secondary neutrons but decreases the sampling frequency of the calorimeter. This measurement is important to understand the best tuning between active and absorbing material in this kind of detector in order to maximize efficiency. We prepared also another prototype with the same composition and size of the KLONE detector but with one side equipped with hamamatsu multi-anode PMs. With this solution, we have a finest granularity given by the pitch dimension of 1 cm^2 which can provide detailed study of the neutron interaction topology.

Results of the first two test beams have been shown at various international conference [1, 2, 3] while the work on the last data are still in progress [4] together with the analysis of the other two new calorimeters used.

References

1. M. Anelli *et al.*, Nucl. Instr. & Meth. A **581**, 368 (2007).
2. M. Anelli *et al.*, Transaction of Nuclear Science **55**, 1409 (2008).
3. M. Anelli *et al.*, Nucl. Instr. & Meth. A **598**, 244 (2009).
4. A. Lucá, master thesis, `www.lnf.infn.it/kloe/klone`.

MicroX

S.B. Dabagov (Resp. Naz., Art. 23), G. Cappuccio (Ass.), G. Cibin (Osp.), A. Esposito, V. Guglielmotti (Osp.), D. Hampai (Ass.), A. Marcelli, V. Sessa (Osp.)

Participant Institutions:

Italy: INFN LNF, Milano Bicocca
Dipartimento di Energetica, "Sapienza" University , Rome
CNR ISMN, Istituto Studio Materiali Nanostrutturati, Rome
Politecnico, Milan
University "Tor Vergata", Rome
Russia: RAS P.N. Lebedev Physical Institute, Moscow
Institute for Röntgen Optics, Moscow
Bielorussia: Institute of Applied Physics Problems, Minsk
EAU: Unisantis S.A., Dubai

The aim of MicroX project is to study and, successfully, to realize a pototype of multi-functional X-ray microscopy unit based on polycapillary optics in combination with compound refractive lens. During the first two years of the project, a microscope prototype that can make μXRF mapping and X-ray imaging with high resolution simultaneously was realized on the base of various types of polycapillary optical structures. Moreover, we have developed a unified theory of X-ray propagation in ultra narrow guides (see MicroX 2007 annual report).

1 Activity in 2008

In second year of the MicroX project, we continued to study new options for X-ray microscopy that were based on the confocal geometry for two polycapillary optical elements (lenses and half lenses). In 2008, the first prototype of a transmission imaging microscope was realized at LNF INFN. The microscope is composed by an X-ray source (Oxford, 50W, CuK_α), a half lens and two detectors, one of which is a scintillator and another one is a CCD.

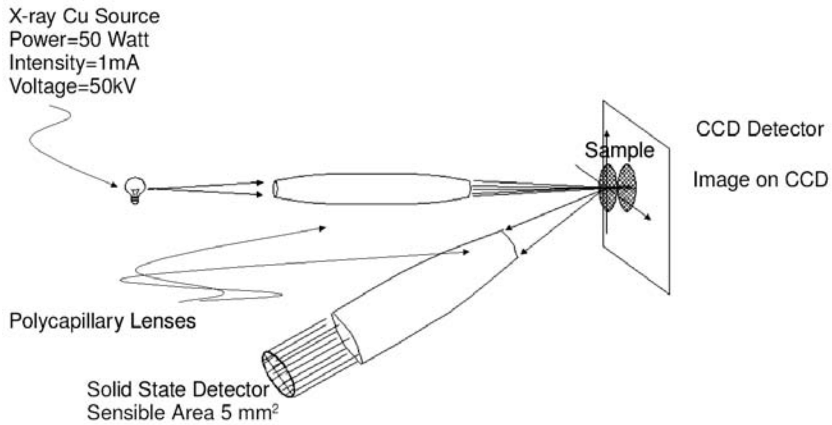

Figure 1: *Scheme of the experimental setup. The polycapillary optics are in the confocal mode, while a laser prophilometer is used in order to monitor and control the sample position.*

The new prototype version allows a special confocal scheme for micro X-ray fluorescence measurements that enables us to obtain not only elemental mapping of the sample but simultaneously its own X-ray imaging. Polycapillary optics (fabricated by Unisantis S.A.) with a full lens shape was used to focus the divergent beam from the X-ray Cu tube onto the sample. A second polycapillary lens inserted between the sample and the detector makes possible to implement the μXRF unit with a prototype of X-ray projection microscope. This type of configuration, called "confocal geometry", allowed detection of the sample X-ray fluorescence with a nominal focal spot size of less than 100x100 μm^2. In recent years a lot of reported works has shown the advantages of this optical configuration to simultaneously perform micro-fluorescence mapping and imaging. To obtain the confocal configuration we used two full lenses in combination providing both the smallest focal spot and the highest transmission. The first lens is characterized by a focal spot of $\sim$ 90 μm and 50% transmission; the second has a spot of $\sim$100 μm and 42% transmission. The prototype scheme is shown in Fig. 1.

A real mapping of μXRF spectroscopy was obtained on standard sample of ferric oxide Fe_2O_3. The standard monophasic minerals of Fe_2O_3 were prepared in a 1000 class clean room at Dipartimento di Scienze e Tecnologie per l'Ambiente, University of Milano Bicocca. So, to eliminate of two close measurements overlapping, we have scanned a 4x4 mm^2 sample by the remote system with a step movement of 200x200 μm^2. Fig. 2 shows the XRF image result (so called elemental mapping): the red colour corresponds to iron (in intensity scale of gray), while the white bright pixels - to manganese (contamination is probably present, so we are designing a glow box for performing measurements in a helium atmosphere). The microscopic image of that mapping is presented by Fig. 3.

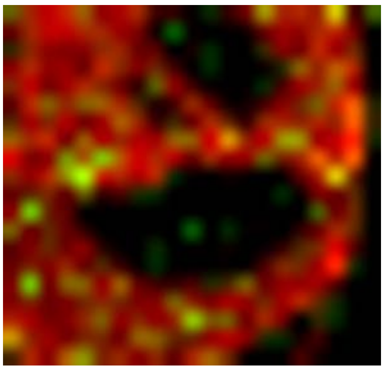

Figure 2: *μXRF mapping spectrum ferrum oxide sample, deposited on a silicon wafer. The gray pixels represent iron (in red scale), while the yellow bright spots are a manganese trace. The measured area is 4x4 mm^2 with a step size of 200x200 μm^2.*

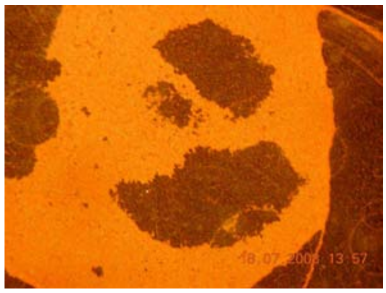

Figure 3: *The microscopic image of the sample presented in Fig. 2.*

Thus, we can conclude that for the year 2008 a new prototype for μXRF analysis has been developed. We have confirmed that polycapillary lenses in the confocal scheme are the ideal candidates to overcome some of the main problems of laboratory X-ray instruments including the portable units; this combination can deliver high photon flux on a sample.

2 Activity in 2009

We have shown first results both for X-ray imaging and for XRF spectroscopy. For the imaging, the simple use of a polycapillary half lens helps us to get a spatial resolution of about 6 μm, which is the limit of our detector resolution. In order to increase the resolution, in 2009 we are planning to combine a full polycapillary lens with a compound reflective lens manufactured by the group of IAPP, Minsk (Fig. 4).

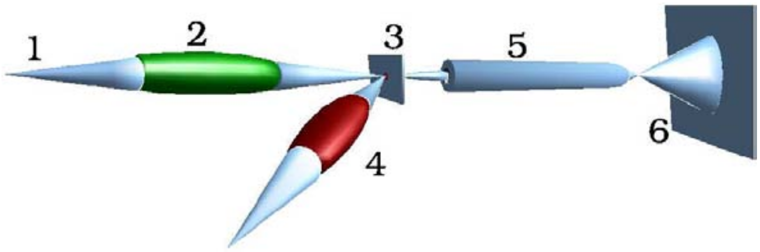

Figure 4: *Scheme of a X-Microscope prototype based on two polycapillary optical units (2, 4) for μXRF analysis and a compound refractive lens (5) for x-imaging. 1 - X-ray source; 3 - sample; 6 - CCD camera.*

In second case we have shown that a confocal optical scheme used with a low power conventional tube and high resolution SDD detector becomes a powerful instrument for X-ray fluorescence analysis of micro-size samples (about 100x100 μm spot). The latter is suitable for a portable experimental setup. In order to decrease the X-ray spot dimensions, we would like to substitute present polycapillary lenses with the last generation ones; these lenses will provide the focal spots of a few microns in diameter.

In 2009, we would like to combine our experimental setups to design a new compact and portable layout for simultaneous elemental and imaging analysis.

3 Conferences, Seminars

1. S.B. Dabagov, "Features of X-Ray Nanofocusing", Invited lecture to the 2nd International Symposium on X-ray Imaging, March 24-28, 2008, Huangshan, China.

2. D. Hampai *et al.*, "X-Ray Microfocusing by Capillary Optics", Oral report to the 2nd International Symposium on X-ray Imaging, March 24-28, 2008, Huangshan, China.

3. S.B. Dabagov, "On Features of Extreme X-Ray Focusing", Oral report to the European Conference on X-Ray Spectrometry - EXRS 2008, June 16-20, 2008, Chavtat-Dubrovnik, Croatia.

4. S.B. Dabagov, "On Extreme X-Ray NanoFocusing", Invited talk to SPIE 2008 - the Annual Meeting of SPIE, August 10-14, 2008, San Diego, USA.

5. D. Hampai, S.B. Dabagov, G. Cappuccio, G. Cibin, and V. Sessa, “X-Ray Microfocusing by Polycapillary Optics”, Oral report to SPIE 2008 - the Annual Meeting of SPIE, August 10-14, 2008, San Diego, USA.

6. S.B. Dabagov, “On Extreme X-Ray Focusing: from Micro- down to Nano-guiding”, Plenary lecture at the VI Int Symposium X-Ray Structure Analysis, October 5-10, 2008, Krasnodar-Tuapse, Russia.

7. D. Hampai *et al.*, “X-ray Microfocusing by Polycapillary Optics”, Oral report to the 51st Workshop INFN ELOISATRON: the 3rd International Conference on Charged and Neutral Particles Channeling Phenomena, CHANNELING 2008, October 25 - November 1, 2008, Erice, Italy.

8. S.B. Dabagov, Director of the 51st INFN ELOISATRON Workshop: the 3rd International Conference on Charged and Neutral Particles Channeling Phenomena, CHANNELING 2008, October 25 - November 1, 2008, Erice, Italy.

References

1. D. Hampai *et al.*, Optics Letters **33**, 2743 (2008).

2. D. Hampai *et al.*, Proc. SPIE **7077**, 70770U-1-9 (2008).

3. S.B. Dabagov and H. Uberall, Nucl. Instr. & Meth. B **266**, 3881(2008).

4. D. Hampai, S.B. Dabagov, G. Cappuccio, G. Cibin, and V. Sessa, Spectrochimica Acta B (2008) (to be published).

5. S.B. Dabagov, Spectrochimica Acta B (2008) (to be published).

NANOPAD
(NANO Palladium Absorbing Deuterium)

F. Celani (Resp.), Antonio Spallone (Ass.), E. Righi (Ass.), G. Trenta (Ass), A. Marmigi (Laur.), V. Andreassi, G. Cappuccio (Ass.), D. Hampai (Ass.), A. Marcelli

Collaboration with: INFN-University of Perugia
External Collaborations with: ISCMNS (International Society of Condensed Matter Nuclear Science, Rome), STMicroelectronics (Cornaredo and Catania sites), CSM SpA (Centro Sviluppo Materiali, Castel Romano), ORIM SpA (Macerata), Pirelli Labs. (Milan), Osaka University.

1 Argument and location of the experiments; International organization of all theoretical and experimental activities

The NANOPAD (nano-Palladium absorbing Deuterium) experiment is devoted to study the anomalies (of thermal and/or nuclear origin) that sometimes are detected in Deuterium-Metal systems, especially when the D/Metal ratio is quite large (at least locally) and the system is forced to some *non-equilibrium condition.*

See the Activity Reports of previous years of DIAFF, FREETHAI, FREEDOM experiments for further details.

The experiment is located, mainly, at Frascati National Laboratories. Some tests are also performed at Perugia INFN and University sites (Hydrogen, Deuterium absorption on Pd and Pd alloy) by a very high resolution and stability Sievert apparatus. Some of the materials for the experiment are prepared at: ORIM SpA (Macerata), STMicroelectronics (Cornaredo and Catania), Centro Sviluppo Materiali (Castel Romano).

Some of the reproducibility tests with the "new" nano-coated Pd wires (see later for details), after agreement with the scientific management of our Institute, are in progress at:

a) R&D Laboratory linked to Los Alamos National Laboratories (USA);

b) R&D Laboratory linked to a very big Company in USA;

c) R&D Laboratory linked to a big Company in Italy.

From over 6 years such kind of studies, both theoretical and experimental, are organised in the framework of the "Condensed Matter Nuclear Science". It was founded, since 2003, a Scientific International Society (the "ISCMNS"), registered according to the U.K. laws. Among others, F. Celani was elected, on October 2007 and in charge from January 2008 for three years, as Vice-President and Chairman of Executive Committee.

2 Experimental Activities on 2008

Main activities during 2008 at LNF were:

a) Further development/refining of the true differential, high pressure (0-100 bar) and temperature (350 °C), reactor made in SS and insulated from environment (thermal power loss of

Figure 1: *The twin chamber differential reactor developed at INFN-LNF. Pressure: up to 100 bar. Temperature: up to 320 °C. Useful volume of the crucibles: 15 cm^3.*

15 W at 320 °C measured inside the 12 cm^3 crucible SS chamber and 60 bar pressure of Deuterium gas, see Fig.1);

b) Developing/improving the preparation of nanoparticles based on nanometric (mean diameter of holes is, nominally, 5.8nm) gamma Alumina “filled” with soluble salts of Pd and Sr;

c) Reassembling of the previous (2005) large volume (over 3 l) pressurised (max 10 bar at RT) SS reactor in order to study ***Pd nano-coated*** thin and long ***wires*** under different gas, pressures and current flowing or voltage drop (the so-called “electromigration effect”).

Such last activity, together with the continuous developing of innovative procedures to deposit, and stabilize, nano-materials at the surfaces of thin (diameter of 50 and 100 μm) and long (50–100cm) Pd wires were the main tasks performed on 2008. The results obtained were recognised as so innovative (from the scientific point of view) and important (for possible practical applications) that, after the presentation of the experimental results at the International Congress (ICCF14) held at Washington on 9-16 August 2008, were recognised worldwide: even an INTERNET Scientific Forum, aimed to discuss in deep our results, was organised by Researchers, Technicians, Industrials and Politicians in USA since August 20, 2008. At the end of the discussions (lasted over 5 months), the people involved agree that our experimental set-up was free from trivial mistakes and that it can be the starting point for technological applications.

2.1 Experiments with nano-coated Pd wires

The experiment was conceived in order to evaluate, in a way as easy as possible, the following specific aspects of experimentations in CMNS studies:

a) Evaluate the role of electromigration, by itself, to generate "anomalous effects in Palladium-Deuterium systems;

b) Evaluate the effect of nano-Palladium, not stabilised (i.e. without the addition of materials that would reduce the self-sintering effects), for the generation of anomalous effects and the stability over time;

c) Evaluate the role of stabilizing materials of nano-Palladium. As reference, Prof. Yoshiaki Arata (Osaka University, Japan) that pioneered such studies, used powders of nano-Pd embedded in a ZrO_2 matrix;

d) Evaluate the role of pressure of Deuterium;

e) Evaluate the role of temperature, especially in the region of 400-550 °C where the aimed technological applications of such "anomalous effects will be at high thermodynamic efficiencies (Carnots cycle) because high temperature of the warm source (e.g. about 820K providing, in principle, an efficiency as high as 63%).

In order to fulfil such results we improved our previous procedure to coat Pd wires, long (50-200cm) and thin (50-100 μm), with nano-materials based on: specific time pattern, high temperature profiles (up to over 800 °C), complex chemical solution (soluble salts of Pd, nanomaterials and anti-sintering agents). The composition of the chemical solution and the procedure of deposition, developed in several years of try and analyze process by our experimental Group, are one of the key points of our success worldwide. As pointed out before, several International R&D Laboratories requested our nano-coated Palladium wires for their experiments. The main result, up to now, was a power gain of over 5 W at a Pd wire temperature of over 450 °C. Such power gain, considering the amount of Pd wire involved (only 14 mg), is equivalent to a power gain of over 400 W/g of Pd.

The main experiment made was shown at the ICCF14 Conference (Invited Paper); the paper was accepted for publication by World Scientific (Condensed Matter Nuclear Science series). The paper is allowable also as preprint of our Institute at the address:
`www.lnf.infn.it/sis/preprint/pdf/getfile.php?filename=LNF-09-1(P).pdf`

In Table 1, extracted from the preprint, are reported some of the experiments performed.

Analyzing the results shown on Table 1, it can be easily understood the role played by the nano-coating material to improve the over-all power gain and stabilize the system for long time operations.

The future work will be devoted to increase the power gain by: increasing the Deuterium pressure (now at about 6bar), reducing the geometrical dimensions of the chamber (to reduce heat dissipation), increasing the length of the wire (now long only 65 cm). Anyway, several technological problems (mainly contaminations coming out from the ancillary materials adopted for the construction of the reactor) are expected: the high temperature will be not anymore only in a short volume very close to the Pd wire (and insulated from the reactor wall by tick glassy foam insulators) but in all the chamber (the goal is about 100cm^3, i.e. about 1/30 in respect to that showed at ICCF14) and in the electrical/mechanical feed-troughs.

Table 1: Summary of the main 3-wire braid experiments Pd (99.9% purity) by J/M, Φ=50 μm, l=60-65 cm, S=0.94-1.02 cm^2, weight=14-15.3 mg; coating weight 1 mg.

Date	Pd wire treatments	Gas type, Pressure) (bar	Input Power (W)	Excess power (W)	Notes
10 Jun 08	nano-coated Air 800 °C	He, 5.2	–	No excess power (blank test)	Wire prepared on 5 May 08 and used in previous experiments
12 Jun 08	nano-coated Air 800 °C	He, 1.2	–	No excess power (blank test)	Same wire
13 Jun 08	nano-coated Air 800 °C	D2, 5.2	52	5.2 (370 W/g Pd)	Same wire
19 Jun 08	nano-coated Air 800 °C	D2, 1.5	48	3.1	Wire operative for 50 days. Wire broken after 2 hours of experiments with H_2
30 Jun 08	nano-coated 800 °C Air	H2, 5.2	41.6	1.4	New wire. Wire broken after 1 day with H_2
02 Jul 08	Virgin	D2, 5.2	–		Broken at loading
03 Jul 08	Air 800 °C no nano-coating	D2, 5.2	50 55	3.3 4.0	Broken after 4 days

3 List of Publications

1. F. Celani *et al.*, “Deuteron electromigration in thin Pd wires coated with nano-particles: evidence for ultra-fast Deuterium loading and anomalous, large thermal effects”, Invited Paper at ICCF14 (International Conference on Cold Fusion ♯14), Washington D.C. August 9-15, 2008. Publishing by World Scientific, Condensed Matter Nuclear Science series.

2. F. Celani *et al.*, “Studio della velocitá limite di diffusione dell’idrogeno dentro fili sottili di palladio, in ambiente gassoso, tramite rivestimento superficiale di nanoparticelle”, Contributed paper at XCIV National Congress of Italian Physical Society, pg. 225, of Proceedings. Genova, September 22-27, 2008.

3. F. Celani *et al.*, “Studio di possibili anomalie termiche, in fili sotttili di palladio, ricoperti da particelle nanometriche, immersi in atmosfere gassose di idrogeno o deuterio e sottoposti a cicli termici provocati da alte correnti di elettromigrazione”, Contributed paper at XCIV National Congress of Italian Physical Society, pg. 225-226, of Proceedings.Genova, September 22-27, 2008.

4. A. Marmigi, “Progettazione e realizzazione di sistemi HW/SW di acquisizione dati in un esperimento di Fisica Nucleare nella Materia Condensata”, Master of Science, thesis in Engineering; final marks: 110/100 Magna cum Laude. University of Rome, Tor Vergata, February 27, 2008. Tutors: Dr. Francesco Celani, Prof. Arnaldo D’Amico (Univ. Roma).

5. F. Celani *et al.*, “High temperature deuterium absorption in palladium nano-particles”, Invited Paper at ICCF 13 (July 2007), published as Conference Proceeding on December 2008 by: “Center MATI”, Moscow; pg. 181-201, ISBN: 978-5-93271-428-7. Ed. by Yury Bazhutov.

NEXT
(Nanotube Emission Sources for X-ray Tubes)

S. Bellucci (Resp. Naz.), R. Baldini (Tecn.), Balasubramanian C. (Osp.),
P. Borin (Dott.), G. De Bellis (Art. 2222), G. Giannini (Art. 2222),
A. Grilli (Tecn.), M. Leone (Art. 2222), A. Marcelli, F. Micciulla (Art. 2222),
R. Pastore (Ass.), A. Petrucci (Art. 2222), A. Raco (Tecn.), I. Sacco (Laur.)

1 External collaborating Institutions:

Univ. Roma La Sapienza, ISPESL Monte Porzio Catone, Univ. Pune India, Burnham Institute La Jolla CA USA, CIRIMAT Toulouse France, Univ. Salerno, IMT Bucharest Romania).

2 Relevant results achieved:

We made progress with respect to the earlier results published in the article "Study of field emission of multiwalled C nanotubes synthesized by arc discharge", S. Bellucci et al. J. Phys.: Condens. Matter 19 (2007) 395014 (7pp), where we studied CNT grown by arc discharge and their field emission and imaging on small distances, .e. less than 2 mm. In the research carried out in 2008 and currently submitted for publication, we extended the study in two directions: comparison with nanotubes of commercial origin obtained by chemical vapor deposition (CVD), of two kinds: SWNT up to 90% and SWNT up to 50% (+ 40% of MWNT); substantial increase, by about one order of magnitude, of the distance between the electrodes, up to 16 mm. The first point has interest as we want to succeed in reaching large distances between the electrodes for having an optimal imaging of issued electrons and their emitters, without having to go to high voltages that are technologically disadvantageous. The second one indicates, through the carried out comparison, that the nanotubes obtained at LNF are rich enough in single wall ones, so as to compete with the commercial samples that are made of approximately have half single and half multi wall nanotubes. This is confirmed also by the following study.

We applied Raman spectroscopy to the study of carbon nanotubes and use a Multi Lorentzian Fit to analyze the Raman bands. We report experimental evidences of unexpected presence of single wall CNTs in a carbon mixture grown by arc discharge without intentionally added catalysts at the Laboratori Nazionali di Frascati. The investigation by micro-Raman spectroscopy allowed us to estimate the radius distribution by an accurate analysis of the radial breathing modes of the spectra with the help of a fitting program.

We also carried out a comparative study of the electric field emission behaviour of vertically aligned few-layer graphene and carbon nanotubes evaluated in a parallel plate type setup. Few-layer graphene was synthesized in the absence of any metallic catalyst by microwave plasma enhanced chemical vapour deposition with gas mixtures of methane and hydrogen. The deposit consists of nanostructures that are several micrometers wide, highly crystalline stacks of four to six atomic layers of graphene, aligned vertically to the substrate surface in a high density network. The electric field emission of few-layer graphene was compared to the emission of single-walled carbon nanotubes, as grown multi-walled carbon nanotubes and processed multi-walled carbon nanotubes in the form of buckypaper. The field emission of few-layer graphene is found to be comparable to buckypaper, since both materials are characterized by turn-on fields as low as 2 V/m and field amplification factors up to several thousands. As grown single-walled and multi-walled carbon nanotubes reveal remarkable better field emission behaviour when compared to few-layer graphene, with turn-on fields below 1 V/m and field amplification factors up to several times the value for few-layer graphene.

We continued the study of the electrical, mechanical and thermal properties of nanocomposite materials based on carbon nanotubes and epoxy resins, for the realization of screening protective devices for sensitive electronic equipment against the effect of electromagnetic interference.

We participate as a partner (the INFN unit) to the EU FP7 Project CATHERINE, Carbon nAnotube Technology for High-speed nExt-geneRation nano-InterconNEcts, Grant Agreement number: 216215, Funding Scheme: Collaborative Project - Small or medium-scale focused research project (STREP). CATHERINE has a duration of 36 months and started its activities on 1st January 2008. The consortium binds together five Universities, three Research Organizations, one Large Industry, one SMEs and one Service Company. The partners are located in 6 EU Member States (Italy, The Netherlands, Sweden, France, Romania, Latvia).

We considered the application of nanoparticles, carbon nanotubes, nanofibers, buckypaper, graphene etc., to biology and medicine, in view of the possible realization of nanodevices for diagnostics and therapy ("theranostics"). We characterized the cellular toxicity of carbon nanotubes. A relevant national project we participate to as a partner (the INFN unit) since 1 January 2008 is the two-year project financed by the Italian Ministry of Health, "Innovative Methodologies for risk assessment in the occupational exposure to nanomaterials", coordinated by the Italian Institute for Occupational Health and Prevention (ISPESL).

3 List of Conference Talks

1. S. Bellucci, "Carbon nanotubes based epoxy nanocomposites", International Conference on Nanotechnology Opportunities and Challenges ICON008 (June 17-19, 2008), Jeddah (Saudi Arabia), 18 June 2008.

2. S. Bellucci, "Carbon nanotube based composites: electrical and mechanical properties", Tutorial Lecture at the School on Nanoscience and Nanotechnology 2008, INFN-Laboratori Nazionali di Frascati, Frascati (Italy), 21 October 2008.

3. S. Bellucci, "Introduction to Nanotechnolog", Invited Lecture at the Technical High School "E. Kant", Roma (Italy) 12 February 2008.

4. S. Bellucci, "Electronic transport, screening and correlated superconductivity in carbon nanotubes.", Invited seminar at the Univ. of Calabria, Arcavacata di Rende (Cosenza, Italy), 14 February 2008.

5. S. Bellucci, "Nanocomposites for Electronic Protection. Nanoscience and Nanotechnology 2008", INFN-Laboratori Nazionali di Frascati, Frascati (Italy), 22 October 2008.

References

1. S. Bellucci, C. Balasubramanian, G. De Bellis, F. Micciulla, and G. Rinaldi, Macromolecular Symposia **263**, 21(2008).

2. S. Bellucci *et al.*, Journal of Physics: Condensed Matter **20**, 474211 (2008).

3. R. Ramoni *et al.*, Journal of Physics: Condensed Matter **20**, 474201 (2008).

4. I. Venditti *et al.*, Journal of Physics: Condensed Matter **20**, 474202 (2008).

NUVOLA
(Study of the Vacuum Chamber Surface Electronic Properties Influencing Electron Cloud Phenomena)

A. Balerna, M. Boscolo, R. Cimino (Resp.), M. Commisso (Ass. Ric.), A. Drago, T. Demma (Art. 23), S. Guiducci, C. Milardi, C. Vaccarezza, M. Zobov
INFN-LNF
P. Barone, A. Bonanno , D. Grosso, M. Minniti,
P. Riccardi, A. Oliva, F. Xu,
Calabria University

The existence of electron cloud effect (ECE) has been clearly established experimentally at several accelerators [1, 2, 3, 6]. It may cause detrimental effects to the performance of modern storage rings, which make use of intense and positively charged bunched beams and/or vacuum chambers of small transverse dimensions. The need to clarify and reduce these effects has brought the creation of Nuvola experiment.
Nuvola project started in 2007 and during this year we continued experimental and theoretical works and here we report our findings.

We continued to study the behaviour of Secondary Electron Yields as a function of material and material status. In Frascati laboratory, we investigated the scrubbing (reduction of SEY), due to the fact that the electrons produced during electron cloud formation hit the vacuum chamber walls modifying its surface properties, hence its Secondary Yield. Up to now surface scrubbing induced by electron bombardment has been studied as a function of dose (number of the impinging electrons per unit area on sample surface) for fixed incident energies of 300-500 eV.

These various experiments showed that, in case of LHC Cu beam screen material, an impinging electron dose between 10^{-6} C·mm^2 and 10^{-2} C· mm^2 is sufficient to reduce the SEY of such as received surface from its initial value (about 2.1) to its final value (about 1.15). These experimental findings allowed to obtain an estimate of the time (hence the commissioning effort for LHC) needed to reduce the SEY to less than 1.3, at which value operational parameters are predicted to be obtained without any limitation due to e-cloud detrimental effects. Such studies are not complete and other accurate experiments are required to study the scrubbing dependence as a function of e-cloud electron energy, since this parameter is missing. In the case of LHC, infact, simulations predict that e-cloud is formed by electrons with very low energies (< 50 eV). For this reason and given the peculiar behaviour observed by our group for low energy electrons, we decided to study this dependence accurately. In this context, some findings have been presented in the conferences of EPAC08 [3, 6] and MULCOPIM08 [2], where we report some of the experimental results obtained bombarding surfaces of the real Cu sample used in Large Hadron Collider (LHC) beam screen, with electron beams in a wide range of energies between 10-500 eV. These results, showed in Fig. 1 A), clearly indicate for the first time that the efficiency of scrubbing depend on the energy of the irradiating beams, being lower for low energy electrons compared to the high energy ones. Our finding could have significant implications to machine commissioning procedure. In addition, these issues strengthen the uselfulness of measuring the actual energy of electrons forming the cloud, encouraging us to continue the tests on the home made retarding field analyzer analyser mentioned in the previous annual reports. A detaliled description of the detector and of its potentialities was presented at the conference EPAC08 [4].

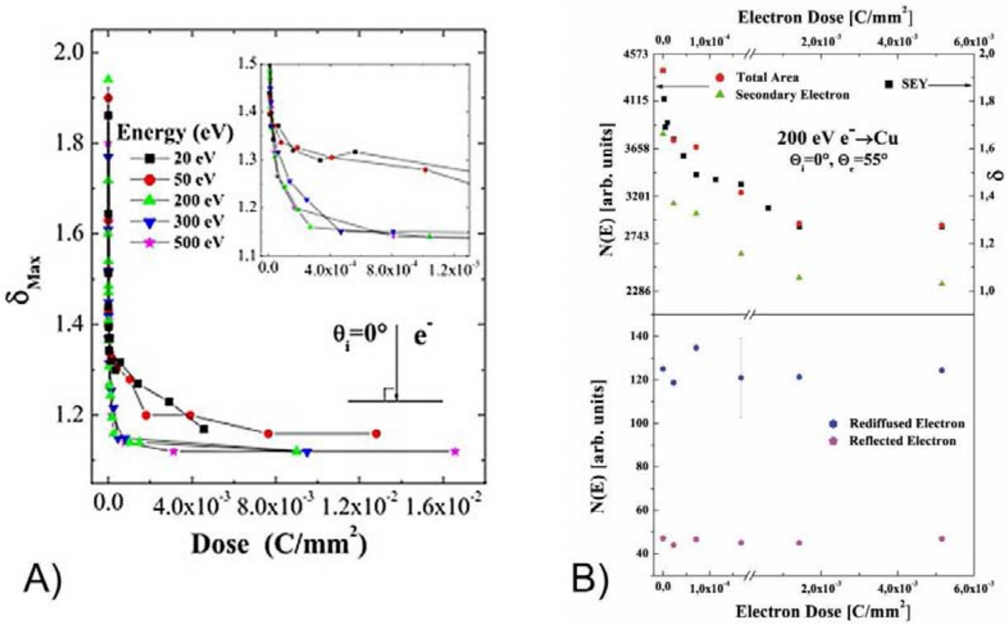

Figure 1: A) δ_{max} *versus dose for different impinging electron energies at normal incidence.* B) *Top: SEY, Secondaries intensity and spectra total area as a function of electron dose bombardmet. Bottom: Reflected and rediffused intensity as a function of electron dose bombardment, after background subtraction.*

In parallel to those activities, in the Surface Science laboratory of the university of Cosenza we focused also on the scrubbing process by measuring the variation of energy distribution curves (EDC) of electrons emitted with bombarding electron dose. Some results were presented in the conference EPAC08 [5], and published on international journal [1]where we analyzed experiments of electron bombardment on representative samples of LHC as a function of an incident dose of 200 eV. In this context, dose dependent energy distribution curves of emitted electrons were measured and analyzed by separation into three energy regions conventionally termed elastically reflected, rediffused and true secondary electrons. We observe that these three contributions to SEY behave differently as a function of bombarding dose, as shown in Fig. 1 B). New preliminary angle resolved measurements performed conditioning samples with an incident dose of 50 eV show a similar behaviour to the case of 200 eV, and we are trying to study the case at lower energies. In fact, the comparison between EDC curves and SEY measurements done in Frascati laboratory suggests the need to perform further experiments by bombarding surfaces with electrons of energy lower than 50 eV, when the contribution of the reflected in EDC increases with respect to secondaries and becoming the dominating component at low (< 20 eV) primary energies. In close collaboration with Anka, we are participating in the development of a diagnostic tool to be used in various rings (like Diamond and Anka) to characterize heat load problems observed but not expected in superconducting Wigglers [7]. Theoretical work, mainly done by T. Demma, is continuing to assess the effects of e-cloud on DAΦNE and to compare simulations carried out with different codes (ECLOUD and POSINST, PEI-M, and HeadTail) with the experimental observations done at our accelerator [6]. We are also continuing in the construction of two XUV beamlines from a DAΦNE Bending Magnet [8]. When ready we will be the only laboratory in the word to be able to analyse SEY variation after electron and photon scrubbing on the same samples. This is a situation which does occur in real accelerators, but has never been studied in a laboratory experiment.

1 List of Conference Talks

1. R. Cimino, "Surface science for e-cloud characterization", Presented at Mini-Workshop on a Cold Vacuum Chamber for Diagnostics 2008, January 2008, Karlsruhe, Germany.
2. R. Cimino, M. Commisso, and V. Baglin, "Surface Studies on the Effect of Electron Bombardment on Secondary Emission Yield and on its Efficiency to Mitigate E-Cloud Formation in Accelerators", Presented at the MULCOPIM 08, Valencia.
3. R. Cimino, "Review of INFN SEY measurements and progress on electron energy analysers", Presented at ECM'08 Workshop at CERN, Geneva (Swiss).
4. T. Demma, A. Drago, S. Guiducci, M. Zobov, and K. Ohmi, "Preliminary simulation results for e-cloud induced instability at DAΦNE", Presented at LCWS08 and ILC08, University of Illinois at Chicago, Chicago (USA).
5.) T. Demma, "E-cloud instability simulation for DAΦNE", Presented at ECM'08 Workshop at CERN, Geneva (Swiss).
6. S. Casalbuoni *et al.*, "Design of a vacuum chamber for diagnostics", Presented at SRI 08, Canada.

References

1. M. Comisso *et al.*, Journal of Physics: Conference series **100**, 092013 (2008).
2. R. Cimino, M. Commisso, and V. Baglin, "Surface Studies on the Effect of Electron Bombardment on Secondary Emission Yield and on its Efficiency to Mitigate E-Cloud Formation in Accelerators", Proc. of MULCOPIM 08, (in press).
3. R. Cimino *et al.*, "Electron Energy Dependence of Scrubbing Efficiency to Mitigate E-Cloud Formation in Accelerators," Proc. of the EPAC 08 Conference, (in press).
4. M. Commisso *et al.*, "A Retarding Field Detector to Measure the Actual Energy of Electron Partecipating in E-Cloud Formation in Accelerators", proc. of EPAC 08, (in press).
5. D. Grosso *et al.*, "Scrubbing Process of Cu Surfaces Induced by Electron Bombardment," Proc. of EPAC 08, (in press).
6. T. Demma, R. Cimino, S. Guiducci, C. Vaccarezza, and M. Zobov, "Electron Cloud Simulations for DAΦNE", Proc. of EPAC 08, (in press).
7. S. Casalbuoni *et al.*, "Design of a vacuum chamber for diagnostics", Proc. of EPAC 08, (in press).
8. A. Balerna *et al.*,"DAΦNE - Light Laboratory and Activity", this Annual Report.

PRESS-MAG-O

M. Cestelli Guidi (Art. 23), G. Della Ventura (Ass.), D. Di Castro (Ass.),
D. Di Gioacchino (Resp. Naz.), A. Marcelli, A. Mottana (Ass.),
M. Piccinini (Ass. Ric.), P. Postorino (Ass.), S. Zhang (Osp.)

1 The PRESS-MAG-O project

The PRESS-MAG-O experiment, one of the 2005 highlights of the INFN Vth Committee, is devoted to the investigation of new materials and new phenomena in condensed matter under extreme conditions. Because of its uniqueness a large collaboration is involved in the project e.g., scientists and technicians of the 'LNF-INFN', scientists of the High-pressure Raman Spectroscopy group of the Department of Physics of the "La Sapienza" University and of the Department of Geological Science of the Roma Tre University. The project is based on the R&D of a cryostat and of the instrumentation necessary to perform concurrent ac magnetic measurements and magneto-optic experiments on samples under high pressure, high DC magnetic field and in a wide temperature range ($\sim$ 4K - Room Temperature). The system has been also designed to perform experiments with IR synchrotron radiation (IRSR). In 2008 the main activities of the collaboration are summarized below:
a) set up of the cooling procedure of the cryostat;
b) design of the optical components necessary to focus the IRSR beam inside the cryostat in order to fit the small aperture of the diamond anvil cell (DAC). The order of the optical system has been emitted at the end of the year;
c) cabling of the ac exciting coils of the insert including wires of the SQUID gradiometer and of thermometers. After a technical evaluation and a.c. magnetic test of the exiting coils we decided to replace the Cu-Be DAC-holder with a sapphire one. This new holder will improve performances avoiding the large reduction of the exciting magnetic signal due to the Focault losses. The delivery of the device is expected in the first weeks of 2009;
d) experiments of ac high harmonic susceptibility on correlated systems such as the superconductor $NdAsFeO_{0.6}F_{0.4}$ has been also performed using an ac gradiometer working at ambient pressure. The data represent the magnetic reference of the future experiments vs. pressure to be performed on other materials inside the PRESS-MAG-O apparatus.

In the last months of the year we started set up of the new l aboratory area inside the LNF dedicated to the PRESS-MAG-O apparatus. A technical support to the new laboratory has been also approved.

2 The know-how of the project

To realize the different components of this large apparatus important know-how have been carried out. The construction of the PRESS-MAG-O project required a large effort and relevant: advancements on materials and technological processes [1]. Among the many we may underline: 1) the construction of a compact a-magnetic steel cryostat hosting a superconducting split magnet made with a unique vacuum vessel and three low temperature shields, a cold finger and two windows for

optical experiments;
2) the construction of a DAC in Cu-Be with two (brilliant cut) diamonds IIA type and two 400μm conic holed push-diamond made by $SiC - \delta$ cylinders;
3) the manufacture of an original superconducting miniaturized micro-SQUID gradiometer with two photolithography coils to fit in the DAC cell;
4) the design and the construction of a vertical sample-holder insert with four degree of freedom ($x - y - z - \Theta$) to align the hole of the DAC cell to the beam;
5) the design and the manufacture of a large and complex DAC holder made in sapphire;
6) the set up of an external heating system based on a commercial laser of 3 W in collaboration with the Solid State Laser Laboratory team of the ENEA Frascati who provided the experimental laser system;
7) the design of optical systems to focus IR/VIS radiation inside the DAC and to collect the transmitted radiation to the detector;
8) the construction of a stable a.c. power supply (1 Hz-5 KHz, up to 2A) to perform experiments in a variable frequency range and vs. temperature.

3 The cryostat

The heart of the system is a *"cold finger static cryostat"* that allows concurrent magneto-optic and magneto-dynamic measurements. In cooperation with Rivoira S.p.a. we performed the first cooling tests to set up the standard procedure. After the tests we evaluated that the pre-cooling requires about two days, but because the cryostat exhibits a large thermal inertia, in stable conditions the system may remain at low temperature for more than five days without He refilling. Performances are fully compatible with the requirements of magnetic and IR optical experiments with IRSR at the SINBAD beamline at DAϕNE. Unfortunately during a cooling test a vacuum leak at low temperature (at about $T = 77$ K) appeared. The leak is present only at low temperature and after several cooling cycles and different attempts to fix the problem the cryostat has been send to the factory also for an upgrade that have been considered after the first tests. The improvements of the cryostat will allow optimization of the operation and improve vacuum safety and cryogenic operations. External cryogenic pipes among shield will be also implemented to reduce liquid nitrogen losses and speed up the cooling procedure. Moreover, after the cryogenic tests, we designed a cone-insert with a small tube located at the bottom of the cryostat to allow, after the LN2 pre-cooling, pumping the residual LN2 before the LHe cooling procedure start. In addition, to improve cooling of cryogenic shields and to additionally reduce the cooling time we considered the addition of a by-pass for the He cold vapors. Finally additional Pt thermometers will be inserted inside the cryostat and in the internal shields to better monitor of the pre-cooling procedure. Regarding the optical lines (see Figure 1), the design of the IR/VIS reflective concentrators (Figure 2) is started. The optical system when ready will be able to concentrate the $2 - 50\,\mu$m laser light and/or the IR synchrotron radiation in a small spot ($\sim 250\,\mu$m of diameter) matching the small aperture of the diamond cell.

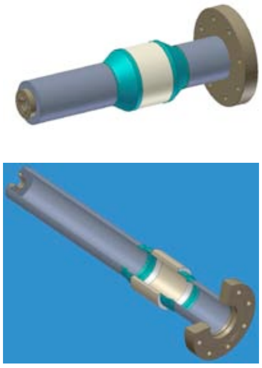

Figure 1: *The PRESS-MAG-O optic line.*

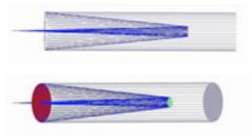

Figure 2: *The optical layout of the IR reflective concentrator.*

4 The PRESS-MAG-O insert

The *'PRESS-MAG-O insert'* is a complex object composed by three main sections:
1) the first section is a $x - y - z - \Theta$ micro-positioning system that will allow the alignment of the aperture of the DAC cell to the IR beam. At the bottom of the section we found the *sapphire holder* with the split coils around the DAC cell volume (Figure 3). An additional lateral slot allows the precise introduction inside the DAC cell of the slider with the chip gradiometer.
2) The second section is a tube placed around the first one and with *Cu-Be springs* to guarantee the thermal contact. This component allows cooling the *insert* with the bottom cold finger made by a *'SQUID'* system and a Nb_3Sn magnetic shield.
3) The third section is the load-lock system. It completes the *'PRESS-MAG-O insert'* and allows to remove the *'insert'* from the top flange of the cryostat without having to break vacuum and maintaining the superconducting magnet on.
Always in 2008 in cooperation with the 'LNF Research Division Electronic Service' (Figure 4) it has been designed and realized the power supply and the controller of the a.c. magnetic field excitation. The power supply delivers a maximum of 400 mAin the frequency range (10 Hz - 2 kHz) allowing the achievement inside the DAC of a magnetic field up to 5 Gauss.

Figure 3: *A photo of the manufactured sapphire sample holder.*

Figure 4: *The PRESS-MAG-O a.c. power supply.*

5 a.c. magnetic susceptibility experiments on new iron-based superconductors

Regarding future magnetic measurements on superconductors under pressure that are one of the goal of the experiment, the recent discovery of the high T_c superconductivity in quaternary compounds doped with flourine, e.g., $RFeAsO_{1-x}F_x$ (R=La, Ce, Nd, Sm, Gd) stmulated the magnetic characterization of these systems. Infact, these iron-based superconductors which consist of alternating layers of RO and FeAs are very sensitivity to the pressure. In $RFeAsO_{1-x}F_x$ compounds the RO layer contains a slight positive charge, which is balanced by a negative charge on FeAs layers. Replacing O with F increases the number of mobile carriers and increasing T_c. Pressure may have a similar effect because it pushes adjacent layers closed together, increasing the number of mobile carriers in the FeAs layers. We measured multi-harmonic a.c. susceptibility in $NdFeAsO_{0.6}F_{0.4}$, at room pressure. These samples provided by Rome Sapienza University and Heifen University. Preliminary data of the flux dynamic in $NdFeAsO_{0.6}F_{0.4}$ have been presented at the International Conference on "FeAs High Tc Superconducting Multilayer and Related Phenomena" held in Roma in December 2008 (see Figure 5) [2]. Additional analysis are in progress.

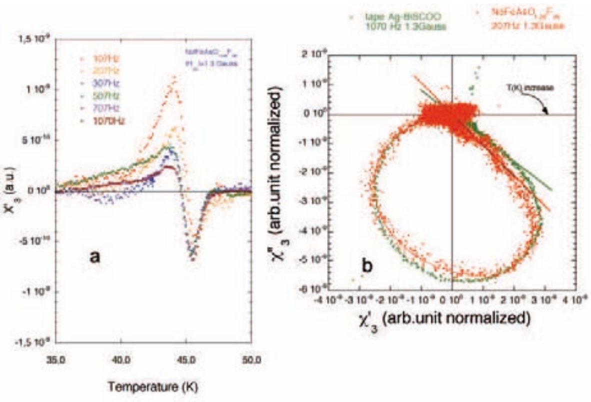

Figure 5: *(a) a.c. third harmonic components of the $NdFeAsO_{0.6}F_{0.4}$ sample vs. temperature at different frequencies; (b) high harmonic, χ_3'- χ_3'', cole-cole plots comparison beetwen $NdFeAsO_{0.6}F_{0.4}$ and BiSCOO2223 tapes showing a clear 2D flux dynamic behavior.*

6 Acknowledgements

A sincere thank is due to Rosa Maria Montereali for her contribution to experiments performed in CRE ENEA and E. Santini of the University La Sapienza for fruitful discussions.

References

1. D. Di Gioacchino *et al.*, J. of Phys. and Chem. of Solids **69**, 2213 (2008).
2. D. Di Gioacchino *et al.*, "Flux dynamics in $NdFeAsO_{0.6}F_{0.4}$", contribution presented at the Inter. Conf. on FeAs High T_c Superconducting Multilayers and Related Phenomena, Proc. of Stripes 2008, Rome, December 9-13 2008; Journal of Superconductivity (2009) in press.

CATHERINE
(Carbon nAnotube Technology for High-speed nExt-geneRation nano-InterconNEcts)

S. Bellucci (Resp. Naz.), R. Baldini (Tecn.), G. De Bellis (Art. 2222),
G. Giannini (Art. 2222), M. Leone (Art. 2222), F. Micciulla (Art. 2222),
P. Onorato (Art. 2222), A. Petrucci (Art. 2222), I. Sacco (Laur.)

1 External collaborating Institutions:

Univ. Roma La Sapienza and Consorzio Sapienza Innovazione, Technische Universiteit Delft and Philips Electronics Nederland B.V. The Netherlands, Université Paul Sabatier Toulouse France, Univ. Salerno, IMT Bucharest Romania, Latvijas Universitates Cietvielu Fizikas Instituts, Swedish Defence Research Agency and Smoltek AB Sweden).

We participate as a partner (the INFN unit) to the EU FP7 Project CATHERINE, Carbon nAnotube Technology for High-speed nExt-geneRation nano-InterconNEcts, Grant Agreement number: 216215, Funding Scheme: Collaborative Project - Small or medium-scale focused research project (STREP). CATHERINE has a duration of 36 months and started its activities on 1st January 2008. The consortium binds together five Universities, three Research Organizations, one Large Industry, one SMEs and one Service Company. The partners are located in 6 EU Member States (Italy, The Netherlands, Sweden, France, Romania, Latvia).

2 Project objectives:

The final objectives of CATHERINE are: 1. Development of cost-effective and reliable technological process for the realization of high-performance next-generation interconnects; 2. Development of a multi-scale simulation tool for the prediction of the multifunctional performance of the interconnect and for the EMC analysis; 3. Development of electromagnetic and multifunctional test procedures and experimental characterization methods; 4. Manufacturing and testing of proof-of-concept samples of nano-interconnects at laboratory level.

3 Relevant results achieved:

One of the tasks is finalized to the development of simulation models describing the growth mechanism of carbon nanostructures inside porous alumina templates. The scope of the simulations is to predict that a specific typology of carbon nanotube could grow inside a specific template having defined periodicity and hole dimensions. This simulation support is necessary for understanding the basic mechanism of growth, and to achieve tight control of the fabrication process. During 2008, in collaboration with Latvijas Universitates Cietvielu Fizikas Instituts, we developed both atomistic and continuum models, constructing atomistic models of SWCNT ropes and isolated MWCNT that could fit into a porous alumina with a hole diameter 20-20.5 nm. Periodic 1D models were for atomistic calculations, with the minimum period along the z axis h = 6.32 nm, which follows from noticeable difference in a periodicity of nano-tubes with armchair and zigzag chiralities. The developed atomistic structures contained $\sim 140{,}000$. The activity of constructing an atomistic 1D periodic model of a hexagonal fragment of amorphous alumina membrane containing > 20 nm diameter pore was also started. This diameter was estimated to be around ~ 20.6-20.7 nm since some gap should exist between CNTs and the wall of the pore. The total energies of configurations, including a SWCNT bundle and an MWCNT, were also computed using a continuum model in the large length limit. Our analysis indicates that pure energy considerations in the large length limit are not sufficient to determine the most favourable configuration, the role of nucleation and substrate-nanotube interaction should be additionally investigated.

Another task we contributed to is the electronic/electrical properties modelling. This task is focused on the modelling of the transport mechanisms and of the conducting properties of single- and multi-walled CNTs, in particular, using Luttinger liquid theory. The effects of the number of channels per shell contributing to conduction and of the variation of the mean-free path has been studied considering the presence of several concentrically nested SW CNTs. Theoretical aspects related to the realization of low-resistance CNT/metal contacts have been analysed.

Our experimental activity aims to fabricate perfectly aligned carbon nanotube arrays with optimised geometric characteristics, thorugh growing nanotubes by catalyzed chemical vapor deposition (CCVD) inside catalytic nano-ordered anodic aluminium oxide (AAO) nanostructures (membranes and templates) with controlled nano geometrical characteristics. In order to optimize the physical parameters of the CCVD of carbon nanotubes in the pores of alumina template structures and waiting for optimization of porous alumina on silicon wafer by other partners, we performed carbon nanotubes syntheses by using commercially available Whatman alumina membranes. One side of the alumina membrane was covered with Nickel by a precise control sputtering system. Nickel catalyst was nano-structured at the temperature of 700 °C, under a 100 sccm flow of hydrogen during 30 min. Afterwards the hydrogen flow meter was switched off, and when the final temperature was reached 100 sccm of methane was filled in the CCVD reactor for 30 min. In order to avoid the oxidation of carbon nano-tubes, the cooling of the CCVD reactor down to the room temperature was performed under 500 sccm of Argon. Two different temperatures were tested, 850°C and 800°C. Scanning Electron Microscope characterization of the samples synthesized by us shows the formation of a lot of carbon nano-tubes in Ni sputtered alumina membrane, with the synthesis quality yet to be optimized, once a more perfect membrane will become available. We also are carrying out field emission measurements during optimization of CNT growth.

Within the conference Nanoscience and Nanotechnology - N&N2008, held in Frascati, we organised on 22nd October 2008 a special session Carbon Nano-tube Technology for High-speed Nano-interconnects, open to all N&N2008 participants and devoted to CATHERINE progresses. During the session, which was attended by 30 persons, the following presentations were given: 1) CATHERINE: Carbon nAnotube Technology for High-speed nExt-geneRation nano-InterconNEcts, M.S. Sarto (SAPIENZA-CNIS); 2) Elaboration of nano-porous alumina templates for carbon nanotubes growth, L. Arurault (UPS Toulouse); 3) 2D periodic models of Ni(111)/CNT interconnects (bundles): ab initio calculations, Y. Zhukovskii (LU-CFI, Latvia); 4) Simulations of properties of CNT/Ni(111) interconnects using the effective media approach, Y.N. Shunin, Y.F. Zhukovskii, and S. Bellucci (LU-CFI and INFN).

4 List of Conference Talks

1. S. Bellucci, "Carbon nanotubes based devices for next-generation nano-interconnects, flat panels, electromagnetic screening", 4th Inter. Baltic Sea Region Conference on Functional materials and nanotechnologies 2008, Riga (Latvia), 1-4 April, 2008.

2. S. Bellucci, "Carbon Nanotube based Devices", Pre-conference Tutorials (June 14-16, 2008), Inter. Conference on Nanotechnology Opportunities and Challenges ICON008, Jeddah (Saudi Arabia), 16 June 2008.

3. S. Bellucci, "CNT for nanointerconnects, flat panels and e.m. screening", Invited seminar at Turin Politechnical University POLITO, Turin (Italy), 5 March 2008.

References

1. Yu. N. Shunin, Yu. F. Zhukovskii, and S. Bellucci, Computer Modeling and New Technologies (Latvia), 2008, 12, p. 66-77.

INNOVATIVE METHODOLOGIES FOR RISK ASSESSMENT IN THE OCCUPATIONAL EXPOSURE TO NANOMATERIALS

S. Bellucci (Resp. Naz.), R. Baldini (Tecn.), Balasubramanian C. (Osp.),
G.A. Carru (Ass.), G. De Bellis (Art. 2222), M. Chiaretti (Ass.),
G. Giannini (Art. 2222), F. Micciulla (Art. 2222), A. Tiberia (Laur.)

1 External collaborating Institutions

Universitá Roma La Sapienza, Policlinico Umberto I University Hospital Roma, ISPESL Monte Porzio Catone, Univ. Roma Tor Vergata, Univ. Parma, Fondazione Salvatore Maugeri Pavia, Agenzia Regionale Prevenzione e Ambiente Regione Puglia.

We participate as a partner (the INFN unit) since 1 January 2008 to the project financed by the Italian Ministry of Health, "Innovative Methodologies for risk assessment in the occupational exposure to nanomaterials", coordinated by the Italian Institute for Occupational Health and Prevention (ISPESL). The project will run for two years.

2 Relevant results achieved:

We investigated, in collaboration with Univ. Sapienza Roma Faculty of Medicine and Policlinico Umberto I University Hospital, the effects in vitro on three different cellular clone culture administrations. Commercially available Carbon nanotube (Cnts) were produced by the CVD method, yielding samples with over 90% carbon content, and with metal contaminants, i.e. mostly iron, amounting to less than 0.2%. The Cnts considered here are MWCnt having diameter 110-170 nm and length 5-9 micron, as shown by TEM and SEM microphotographs.

TEM: Transmission electron microscopy is a microscopy technique whereby a beam of electrons is transmitted through an ultra thin specimen, interacting with the specimen as it passes through it. An image is formed from the electrons transmitted through the specimen, magnified and focused by an objective lens and appears on an imaging screen, a fluorescent screen in most TEMs, plus a monitor, or on a layer of photographic film, or to be detected by a sensor such as a CCD camera.

The scanning electron microscope (SEM) is a type of electron microscope that creates various images by focusing a high energy beam of electrons onto the surface of a sample and detecting signals from the interaction of the incident electrons with the sample's surface. The type of signals gathered in a SEM vary and can include secondary electrons, characteristic X-rays, and back scattered electrons. In a SEM, these signals come not only from the primary beam impinging upon the sample, but from other interactions within the sample near the surface. The SEM is capable of producing high-resolution images of a sample surface in its primary use mode, secondary electron imaging.

3 In vitro tests

Cnts were placed in bidistilled water and dispersed by sonication (90 min), in order to get homogeneous suspensions. After centrifugation at 14000 rpm to remove larger agglomerates, the resulting suspension was used for cell count assay. Cell culture. The human colorectal cancer cell line Caco-2 and the human breast adenocarcinoma cell line MCF-7 were obtained from European Collection of Cell Cultures (ECACC). Primary human arterial smooth muscle cells (hSMCs) were isolated from a thyroid artery by a collagenase type II digestion and used for experiments from passages 4 to 8. SMCs were identified by positive ($>95\%$) staining with a monoclonal antibody to muscle specific alpha-actin. All cells were seeded into 25 cm^2 flasks (Falcon; Becton Dickinson Laboratoryware; Franklin Lakes NJ, USA) in Dulbecco modified Eagle medium (DMEM) supplemented with 10% Fetal Calf Serum (FCS) and antibiotics (Penicillin 100 IU/ml, Streptomycin 100 μg/ml, Gentamycin 200 μg/ml) (standard medium). The cultures were kept at 37 Celsius degrees in an atmosphere of 5% CO2 in air. The medium was changed every 3th day. At confluence, the cells were subcultured after removal with 0.05% trypsin-0.01% EDTA. Cell viability was assessed with the Trypan Blue (Sigma Chemical Co., St. Louis MO, USA) dye exclusion method.

4 Cell proliferation assay

Caco-2 cells, MCF-7 cells and hSMCs were seeded in 6-well culture plates Falcon, Becton Dickinson Laboratoryware) at a concentration of 1×105 cells/well in a standard medium. The following day, the cells were refed with standard medium containing Cnts at concentrations ranging from 0.001 mg/ml to 0.1 mg/ml. The plates were incubated for 24, and 72 hours at 37 Celsius degrees in an atmosphere of 5% CO2 in air. The cells were then detached from wells by trypsinization and centrifuged, and cell pellets were resuspended in PBS. Cell count was performed by a particle count and size analyzer (Beckman Coulter, Inc.), and by a Thoma haemocytometer. Two replicate wells were used for each data point, and every experiment was performed three times.

5 Statistical analysis

Data were expressed as mean standard deviation (SD). Data were statistically analyzed with the analysis of variance (ANOVA) followed by the Bonferroni post-test. Differences were considered significant at the level of $p < 0.05$. Statistical analysis was performed by using GraphPad Instat software (GraphPad Software, Inc.; San Diego, CA, USA).

6 Results

In our in vitro study, three different cell types were exposed in culture to various concentrations of Cnts, in order to estimate their cytotoxic effects. Interestingly, the three cell types gave different responses to the treatment with Cnts. The breast adenocarcinoma cells, MCF-7, showed a well evident inhibition of the proliferation, when treated with Cnts at all concentrations used, for both 24 and 72 hours of incubation. Particularly, after the first 24 hours of treatment, at a Cnts concentration of 0.1 mg/ml, there was a significant decrease in the cell number, as compared with the number of cells present in culture at time 0. This result indicates that Cnts early exert a strong cytotoxic action on these cells. After 72 hours the cell count assay demonstrated that all cellular samples proliferated, but at the highest Cnts concentrations the number of cells was significantly lower than the control. These results are consistent with the findings of other authors who demonstrated the toxicity and the hazardous effects of carbon-based nanomaterials on a variety of cultured cells, although there exist many different morphologies of Cnts, which can also be chemically or functionally modified. In our experiments, hSMCs showed a significant inhibition of cell proliferation with respect to control only after 72 hours of treatment with Cnts at the concentrations of 0.1 mg/ml and 0.01 mg/ml; at the lowest concentration tested, there was no inhibition of the cell growth. After 24 hours of treatment hSMCs did not show any significant variation in the proliferation pattern in all conditions studied. Our results are in accordance with other studiesperformed on rat aortic smooth muscle cells treated with SWCnts (single-walled Cnts) that demonstrated the lack of growth inhibition at the end of the 1st day of cell culture, whereas there was a significant dose-dependent decrease in cell proliferation from day 2.5 to day 3.5 for concentrations from 0 to 0.1 mg/ml. In human colorectal cancer cell line Caco-2, the treatment with Cnts did not produce any modification of cell growth as compared with the control. The surprising result seems to be consistent with other studies in which various kinds of Cnts (SWCnts and MWCnts) did not determine any acute toxicity on cell viability and apoptosis in two cell types, i.e. the rat alveolar macrophage cell line NR8383 and the human lung epithelial cell line A549. Moreover, the Cnts treatment in both cell lines did not induce the release of inflammatory mediators, but it produced a dose- and time-dependent increase of the intracellular reactive oxygen species (ROS). In conclusion, our in vitro studies showed that the anti-proliferative response to Cnts may differ, depending on the cell line and tissue types used. It is necessary that other effects of Cnts on various cell types, such as cytokine release and ROS production, be studied, in order to explain the true hazard of these nanomaterials.

7 List of Conference Talks

1. S. Bellucci, “Nanotechnology for Biological and Medical Applications”, Postgraduate Course on Occupational Health and Safety in the Workplace, International Training Centre of the International Labour Organization (ILO), Torino (Italy), 5 March 2008.
2. S. Bellucci, “Toxicology of carbon nanotubes: in vitro and in vivo results”, Talk given at MeMoMat, Univ. ”Sapienza” Rome (Italy), 27 May 2008.
3. M. Chiaretti, “Buckypaper toxicology and effects on metabolism and immunological modification in vitro and in vivo”, Talk given at Nanoscience and Nanotechnology, LNF, Italy, 23 October 2008.
4. S. Bellucci, “Carbon nanotubes buckypaper toxicity: in vitro and in vivo effects on the metabolism and immunological modifications” , Presented at National Nanomedicine Conference NNC, Genova, Italy, 28 November 2008.

References

1. M Chiaretti *et al.*, J. Phys.: Condens. Matter **20**, 474203 (2008).
2. M. De Nicola *et al.*, J. Phys.: Condens. Matter **20**, 474204 (2008).
3. A. Di Sotto, M. Chiaretti, A. Carru, S. Bellucci, and G. Mazzanti, “Multi-Walled Carbon Nanotubes: lack of mutagenic activity in the bacterial reverse mutation assay”, Toxicology Letters, 2009 (in press).
4. B. M. Rotoli *et al.*, Toxicology Letters **178**, 95 (2008).

6 – Accelerator Physics

DAΦNE

The DAΦNE Team
D. Alesini, M.E. Biagini, C. Biscari, R. Boni, M. Boscolo, F. Bossi, B. Buonomo (Art. 23),
A. Clozza, G. Delle Monache, T. Demma (Art. 23), E. Di Pasquale, G. Di Pirro, A. Drago,
A. Gallo, A Ghigo, S. Guiducci, C. Ligi, F. Marcellini, C. Marchetti, G. Mazzitelli,
C. Milardi, F. Murtas, L. Pellegrino, M. Preger, L. Quintieri (Art. 23), P. Raimondi (Resp.),
R. Ricci, U. Rotundo (Art. 23), C. Sanelli (Resp.), M. Serio, F. Sgamma, B. Spataro,
A. Stecchi, A. Stella, S. Tommasini, C. Vaccarezza, M. Zobov

The DAΦNE Technical Staff
G. Baldini, P. Baldini, A. Battisti, A. Beatrici, M. Belli, B. Bolli, L. Cacciotti, G. Ceccarelli,
R. Ceccarelli, A. Cecchinelli, S. Ceravolo, R. Clementi, O. Coiro,
S. De Biase, I. De Cesaris, M. De Giorgi, N. De Sanctis, R. Di Raddo, M. Di Virgilio,
A. Donkerlo, G. Ermini, G. Fontana, U. Frasacco, C. Fusco, F. Galletti, E. Gaspari, M. Giabbai,
O. Giacinti, E. Grossi, F. Iungo, V. Lollo, V. Luppino, M. Marchetti, C. Marini,
M. Martinelli, A. Mazzenga, C. Mencarelli, M. Monteduro, A. Palleschi, M. Paris,
E. Passarelli, V. Pavan, S. Pella, D. Pellegrini, R. Pieri, G. Piermarini,
S. Quaglia, F. Ronci, M. Rondinelli, F. Rubeo, M. Sardone, M. Scampati, G. Sensolini,
R. Sorchetti, A. Sorgi, M. Sperati, A. Sprecacenere, P. Tiseo, R. Tonus, T. Tranquilli,
M. Troiani, V. Valtriani, R. Zarlenga, A. Zolla

1 Introduction

DAΦNE is an "electron-positron meson factory" operating at Frascati since 1997. Factories are storage ring colliders designed to work at the energies of the meson resonances, where the production cross section peaks, to deliver a high rate of events to high resolution experiments. The collider luminosity (the number of events per unit time of the reaction under investigation divided by its cross section weighted by the acceptance of the detector) is very high, about two orders of magnitude larger than that obtained at the same energy in colliders of the previous generation. One of the key-points to get a substantial luminosity increase is the use of separated vacuum chambers for the two beams merging only in the interaction regions (IRs). When sharing the same ring the two N-bunch trains cross in 2N points and the maximum obtained luminosity is limited by the electromagnetic beam-beam interaction. The unwanted effects of this interaction can be reduced with a very strong focussing (called "low-β") at each of the crossing points, obtained by means of quadrupole doublets or triplets. At the same time these magnetic structures take up much room and excite chromatic aberrations which must be corrected elsewhere in the ring. A large number of bunches can be stored only with twice the number of low-β points and due to the compactness of the DAΦNE machine only two of these regions can be realized, and therefore only a single electron bunch and a single positron one could be stored in a single ring.

This limitation does not hold for the double ring option, consisting in two separate rings crossing at two low-β points. The number of bunches that can be stored in such a collider is limited only by the geometry of the IR's. DAΦNE is an accelerator complex consisting of a double-ring collider, a linear accelerator (LINAC), an intermediate damping ring to make injection easier and faster and 180 m of transfer lines connecting these machines. The beam accelerated by the Linac can also be switched into a laboratory called "BEAM Test Facility (BTF)", for dedicated experiments and calibration of detectors. The accelerator complex has been designed to fit into the existing ADONE buildings (ADONE was the 3 GeV center of mass electron-positron collider in operation at LNF from 1969 to 1993). In the DAΦNE collider the two beam trajectories cross at the interaction point (IP) with an horizontal angle that has been recently increased from ≈30 mrad to ≈ 50 mrad. A positron bunch leaving the IP after crossing an electron one will reach the following electron bunch at a distance of half the longitudinal separation between bunches from the IP. Due to the horizontal angle between the trajectories of the two beams, the distance in the horizontal direction between the two bunches is equal to the horizontal angle times half the longitudinal distance between the bunches in each beam. The beam-beam interaction can be harmful to the beam stability even if the distance in the horizontal direction between bunches of opposite charge is of the order of few bunch widths at points where the β function is high and this sets a lower limit on the bunch longitudinal separation and therefore on the number of bunches which can be stored in the collider. However, the so called *crab waist collision scheme* (CW) recently implemented in the machine alleviates this problem, as it will be exhaustively explained in the following of this report. By design the minimum bunch separation at DAΦNE has been set to $\approx 80\ cm$, and therefore the maximum number of bunches that can be stored in each ring is 120. This number determines the frequency of the radiofrequency cavity which replaces at each turn the energy lost in synchrotron radiation, which must be 120 times the ring revolution frequency. The luminosity of the collider can therefore be up to 120 times larger than that obtainable in a single ring with the same size and optical functions. Crossing at an angle could in principle be a limitation to the maximum single bunch luminosity. In order to make the beam-beam interaction less sensitive to this parameter and similar to the case of single ring colliders where the bunches cross head-on, the shape of the bunches at the IP is made very flat (typical ranges of r.m.s. sizes are $15 \div 30$ mm in the longitudinal direction, $0.2 \div 1.5$ mm in the horizontal and $2.5 \div 10\ \mu$m in the vertical one). The double ring scheme with many bunches has also some relevant challanges: the total current in the ring reaches extremely high values (5 A in the DAΦNE design, ≈ 2 A in the DAΦNE operation so far) and the high power emitted as synchrotron radiation (≈ 50 kW) needs to be absorbed by a complicated structure of vacuum chambers and pumping systems in order to reach the very low residual gas pressure levels necessary to avoid beam loss. In addition, the number of possible oscillation modes of the beam increases with the number of bunches, calling for sophisticated bunch-to-bunch feedback systems.

The double annular structure of the DAΦNE collider as it is now after the recent modifications to implement the crab waist scheme is shown schematically in Fig. 1. Both rings lay in the same horizontal plane and each one consists of a long external arc and a short internal one, as briefly described in section 3. Starting from the IP the two beams share the same vacuum chamber while traveling in a common permanent magnet defocusing quadrupole (QD) which increase the divergence of the two beam trajectories to ≈ 75 mrad. Shortly after the QD, at a distance of ≈ 82 cm from the IP, the common vacuum chamber splits in two separated ones connected to

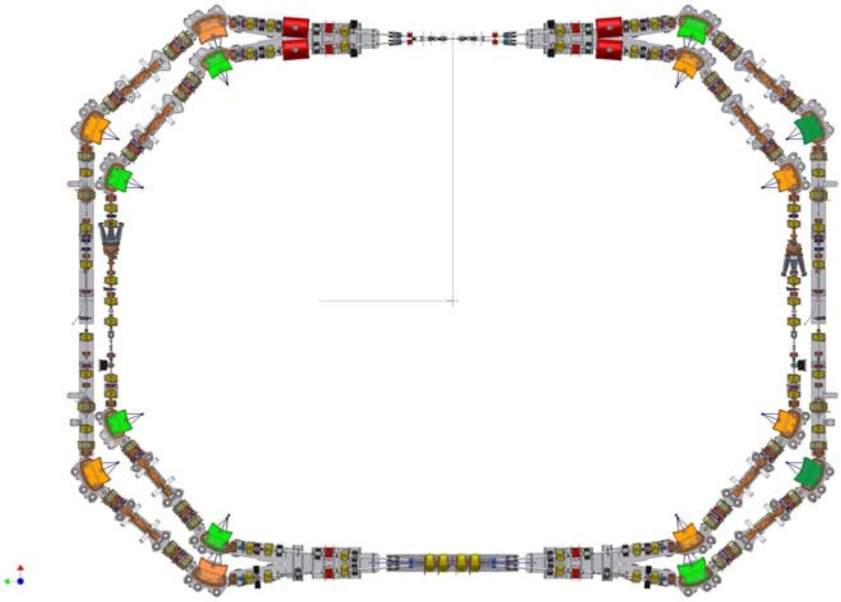

Figure 1: *The DAΦNE Main Rings.*

the vacuum chambers of the long and short arcs. Two individual permanent magnet quadrupoles (QFs) are placed just after the chamber separation. Together with the previous QD they constitute the low-β doublets focusing the beams in the IP. The long and short arcs consist of two "almost achromatic" bends (deflecting the beam by $\approx$ 85.4 degrees in the short arc and $\approx$ 94.6 degrees in the long one) similar to those frequently used in synchrotron radiation sources, with a long straight section in between. Each bend consists of two dipoles, three quadrupoles, two sextupoles and a wiggler. This structure is used for the first time in an electron-positron collider and it has been designed for the particular requirements of DAΦNE: the amount of synchrotron radiation power emitted in the wigglers is the same as in the bending magnets and the wigglers can be used to change the transverse size of the beams. The increase of emitted power doubles the damping rates for betatron and synchrotron oscillations, thus making the beam dynamics more stable, while the possibility of changing the beam sizes makes the beam-beam interaction parameters more flexible.

The straight section in the long arc houses the kickers used to store into the rings the bunches coming from the injection system, while in the short straight arc there are the radiofrequency cavity and the equipment for the feedback systems which are used to damp longitudinal and transverse instabilities.

The most delicate part of the whole structure are the IR's, which has been deeply modified during 2007 to implement the novel crab waist collision scheme as reported in details in the following of this paper. Before the last major modifications, the IRs have undergone many others readjustments during the years to optimize the performances of the machine while operating for different detectors. In principle the collider could host two experiments in parallel, but only one at a time has been installed so far. Three detectors have taken data until 2007, namely KLOE, DEAR and FINUDA, while SIDDHARTA, a renewed version of the DEAR detector, started its operation last March 2008. Siddharta started with a preliminary set-up and then started collecting data with the final set-up last September 2008.

KLOE has been in place on the first IP from 1999 to 2006, while DEAR and FINUDA have alternatively run on the second one. The detectors of KLOE and FINUDA are surrounded by large superconducting solenoid magnets for the momentum analysis of the decay particles and their magnetic fields represent a strong perturbation on the beam dynamics. This perturbation tends to induce an effect called "beam coupling", consisting in the transfer of the betatron oscillations from the horizontal plane to the vertical one. If the coupling is not properly corrected, it would give a significant increase of the vertical beam size and a corresponding reduction of luminosity. For this reason two superconducting solenoid magnets placed on both sides of the detector with half its field integral and of opposite direction have been turned on while running KLOE and FINUDA in such a way that the overall field integral in the IR's vanishes. However, this was not sufficient to obtain full compensation of the beam coupling induced by the main solenoids. In the case of KLOE the low-β at the IP was originally designed with two quadrupole triplets. Due to the flat shape of the beam at the IP, the low-β is realized only in the vertical plane. The quadrupoles cannot be of the conventional electromagnetic type for two reasons: the first is that the iron of the joke would degrade the flatness of the magnetic field in the detector and the second is that the overall transverse size of a conventional quadrupole is at least twice its useful aperture. Therefore quadrupoles realized with permanent magnets have been built, which exhibit an excellent field quality, very small transverse size and are fully transparent to external fields. The region of space around the IP occupied by machine elements, which is unavailable for the detection of decaying particles by the experiment consists in two cones with the vertex at the IP and a half aperture of only 9 degrees. In order to obtain a good compensation of the above mentioned coupling effects induced by the KLOE and FINUDA solenoids, the quadrupoles have been rotated around their longitudinal axis (by angles between 10 and 20 degrees in the KLOE case) and have been provided with actuators to finely adjust their rotation.

The structure of the FINUDA IR is quite similar to the KLOE one. Since its superconducting solenoid magnet has half the length (but twice the field) of the KLOE one, the low-β focusing at the IP was obtained by means of two permanent magnet quadrupole doublets inside the detector and completed with two other conventional doublets outside.

The DEAR experiment, which was installed on the IR opposite to KLOE, took data during the years 2002-2003. It does not need magnetic field and therefore only conventional quadrupoles were used for the low-β. FINUDA rolled-in at DEAR's place in the second half of 2003 and took data until spring 2004. It was then removed from IP2 in order to run the KLOE experiment with only one low-β section at IP1, and rolled-in back in 2006 for a second data taking run ended in June 2007. After that the detector has been rolled-out again, and presently there are no detectors installed in IR2. The two chambers are vertically separated so that the two beams do not suffer from parasitic interactions in the whole IR2. A summary of the peak luminosity during these runs is shown in Fig. 2.

Two synchrotron radiation lines, one from a bending dipole and the other from the wiggler are routinely operated by the DAΦNE-LIGHT group in a parasitic mode, providing to users radiation from the infrared to soft X-rays. However, DAΦNE provides also some dedicated runs for the

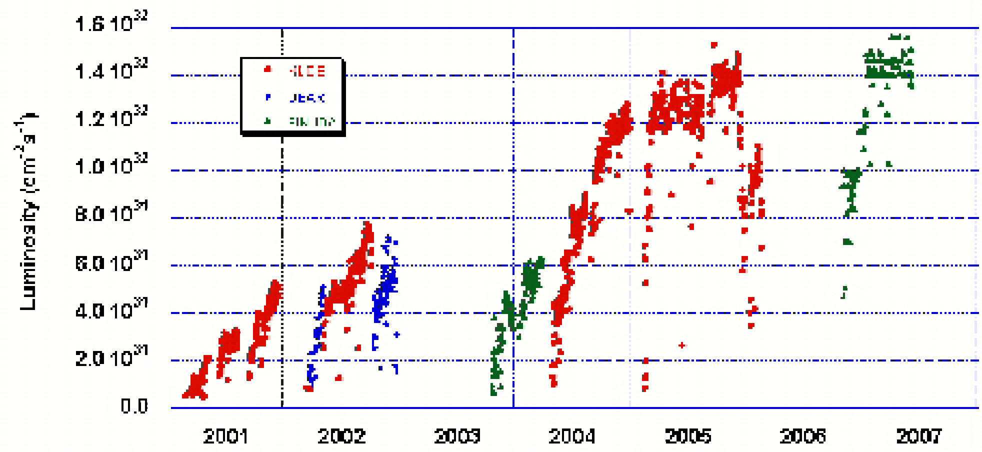

Figure 2: *Peak luminosity at DAΦNE.*

synchrotron light during which Siddharta works in a parasitic mode, allowing, when needed, longer data taking to the synchrotron light users.

The vacuum chambers of the arcs have been designed to stand the nominal level of radiation power emitted by the beams (up to 50 kW per ring). They consist of 10 m long aluminum structures built in a single piece: its cross section exhibits a central region around the beam and two external ones, called the antechambers, connected to the central one by means of a narrow slot. In this way the synchrotron radiation hits the vacuum chamber walls far from the beam and the desorbed gas particles can be easily pumped away. The chambers contain water cooled copper absorbers placed where the radiation flux is maximum: each absorber has a sputter ion pump below and a titanium sublimation pump above.

The single cell copper radiofrequency cavities, one in each ring, resonate at 368 MHz with a maximum accelerating voltage larger than 250 kV. Particular care has been taken in damping the high order modes (HOMs) which could induce longitudinal and transverse instabilities in the multibunch structure of the beams. This has been obtained by means of external waveguides strongly coupled to the cavity HOM fields and terminated on 50 Ω loads to dissipate the energy delivered to the HOMs by the beams. Sophisticated longitudinal and transverse feedback systems have, however, been built to damp the residual coupled-bunch instabilities and reach beam currents up to 2 A in operation. These systems are based on digital signal processing techniques, and act individually on each bunch.

The correct superposition of the beams at the IP is of course critical for the luminosity of the ring. For this reason, 46 beam position monitors are available in each ring and 31 small dipoles can be used to steer the beam and correct orbit distortions caused by alignment errors or current errors in the magnetic elements by means of dedicated software algorithms implemented in the Control System of the collider. Additional beam diagnostics are two synchrotron radiation outputs, from which the transverse and longitudinal size of the beam can be measured, total beam current monitors and strip-line pickups used to measure the charge of each bunch.

In a low energy electron-positron collider, such as DAΦNE, the lifetime of the stored current is mainly limited by the Touschek effect, namely the particle loss due to the scattering of the particles inside the bunches. In the present typical operating conditions the Touschek lifetime is of the order of 1000 s. It is therefore necessary to have a powerful injection system, capable of refilling the beam without dumping the already stored one. In addition, flexibility of operation requires that any bunch pattern can be stored among the 120 available buckets. The injection system of DAΦNE is therefore designed to deliver a large rate of particles in a single bunch at the working energy of the collider.

It consists of a linear accelerator with a total accelerating voltage of 800 MV. In the positron mode, electrons are accelerated to $\approx$ 250 MeV before hitting a tungsten target (called positron converter) where positrons are generated by bremsstrahlung and pair production with an efficiency of $\approx$1%. The positrons exit from the target with an energy of few MeV and are then accelerated by the second section of the LINAC to their final energy of $\approx$ 0.51 GeV. The positrons are then driven along a transfer line and injected into a small storage ring, called Accumulator, at frequency of 50 Hz. Up to 15 positron pulses are stacked into a single bucket of the Accumulator, then injection stops and the bunch damps down to its equilibrium beam size and energy spread, which are much smaller than the LINAC ones. Damping takes $\approx$ 0.1 s and then the beam is extracted from the Accumulator and injected into the positron main ring at an overall repetition rate of 2 Hz. A powerful and flexible timing system allows the storage of any desired bunch pattern in the collider. In the electron mode, a magnetic chicane deviates the particle trajectory around the positron converter and electrons are directly accelerated to 0.51 GeV and injected into the Accumulator in the opposite direction with respect to positron operation. They are then extracted like in the positron case and injected into the electron main ring through the second transfer line.

The Accumulator ring has been introduced in the accelerator complex to increase the injection efficiency, especially for the positrons that are produced in the LINAC at 50 Hz rate in 10 ns pulses with a charge of $\approx$ 0.5 nC. Since the design charge of the main ring at the maximum luminosity is $\approx$ 1.5 μC and the longitudinal acceptance of the main rings is only 2 ns, the number of 50 Hz pulses necessary to fill the ring is of the order of 10^4. In order to avoid saturation it is therefore necessary that at each injection pulse a fraction smaller than 10^{-4} of the already stored beam is lost, and this is not easy to achieve. The Accumulator instead works with a lower frequency RF cavity and therefore with a larger longitudinal acceptance. In this way the full charge coming from the LINAC can be stored in a single RF bucket. In a complete injection cycle, that has a duration of 500 ms, up to 15 LINAC pulse can be stored in a single Accumulator RF bucket, and after being damped to the ring equilibrium emittances and energy spread, the whole stacked charge can be stored into a single RF bucket of the main ring. In this way the nominal single bunch charge can be stored with only one pulse from the Accumulator, reducing to 120 the number of injection pulses (at 2 Hz) into each main ring. As an additional benefit, the transverse beam size and energy spread of the beam coming from the Accumulator are at least one order of magnitude smaller than those of the LINAC beam, and this strongly reduces the aperture requirements of the main ring and, as a consequence, the overall cost of the collider.

2 The crab waist collision scheme at DAΦNE

In high luminosity colliders with standard collision schemes the key requirements to increase the luminosity are: the very small vertical beta function β_y at the IP, the high beam intensity I, the small vertical emittance ϵ_y and the large horizontal beam size σ_x and horizontal emittance ϵ_x required to minimize beam-beam effects. However, β_y can not be smaller than the bunch length σ_z without incurring in the hour-glass effect and it is very difficult to shorten the bunch in a high current ring without exciting instabilities. Moreover, high current implies high beam power losses, beam instabilities and a remarkable enhancement of the wall-plug power.

In the CW scheme of beam-beam collisions a substantial luminosity increase can be achieved without bunch length reduction and with moderate beam currents. In this novel approach the hour-glass effect is avoided by shortening the length of the two-beams overlap spot by means of an increase of the crossing angle and a reduction of the horizontal beam size at the IP, as sketched in Fig. 3. The potential luminosity improvements have pushed several accelerator teams to study and consider the implementation of this scheme on their machines. In particular, the upgrade of DAΦNE is aimed at increasing its luminosity up to 10^{33} cm^{-2}s^{-1} to be compared with $1.6{\cdot}10^{32}$ cm^{-2}s^{-1} obtained during the last DAΦNE run for the FINUDA experiment. Besides, the physics and the accelerator communities are discussing a new project of a Super B-factory with luminosity as high as 10^{36} cm^{-2}s^{-1}, i.e. by about two orders of magnitude higher with respect to that achieved at the existing B-factories at SLAC and KEK. The first CW collisions at DAΦNE started at the beginning of 2008 and the machine tuning with this new scheme went on for the whole year 2008. Results are discussed in section 4, here we describe the CW principle together with beam-beam simulations.

In addition to preventing the hourglass effect, the CW scheme of beam-beam collisions combines several other potentially advantageous ideas. The first one is large Piwinski angle. For collisions under a crossing angle θ the luminosity L and the horizontal ξ_x and vertical ξ_y tune shifts scale as:

$$L \propto \frac{N\xi_y}{\beta_y} \propto \frac{1}{\sqrt{\beta_y}} \tag{1}$$

$$\xi_y \propto \frac{N\sqrt{\beta_y}}{\sigma_z\theta}; \tag{2}$$

$$\xi_x \propto \frac{N}{(\sigma_z\theta)^2} \tag{3}$$

The Piwinski angle ϕ is a collision parameter defined as:

$$\phi = \frac{\sigma_z}{\sigma_x}\tan\left(\frac{\theta}{2}\right) \approx \frac{\sigma_z}{\sigma_x}\frac{\theta}{2} \tag{4}$$

with N being the number of particles per bunch. Here we consider the case of flat beams, small horizontal crossing angle $\theta << 1$ and large Piwinski angle $\phi >> 1$.

In the CW scheme described here, the Piwinski angle is increased by decreasing the horizontal beam size and increasing the crossing angle. In such a case, if it were possible to increase N

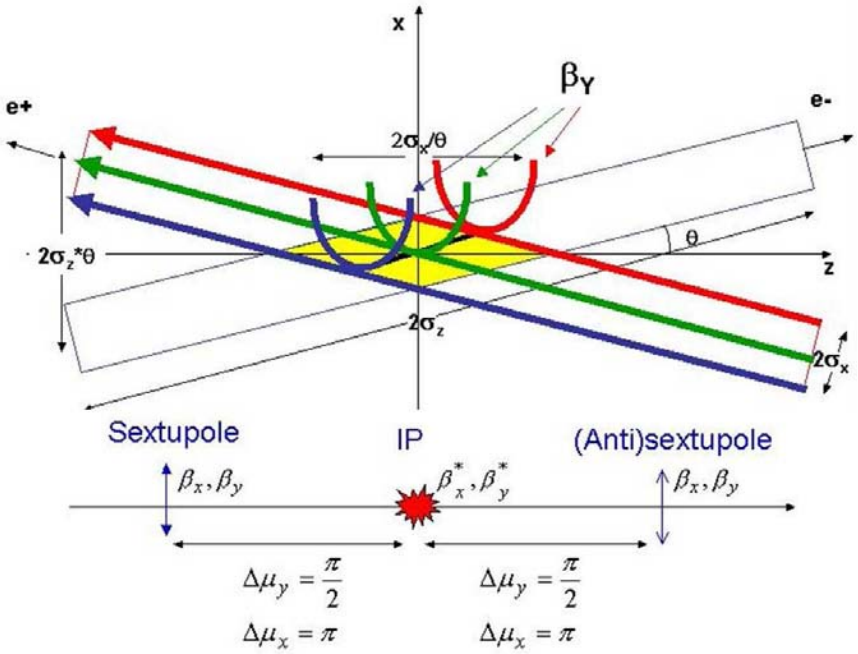

Figure 3: *Crab waist scheme*

proportionally to $\sigma_z\theta$, the vertical tune shift ξ_y would remain constant, while the luminosity would grow proportionally to $\sigma_z\theta$. Moreover, the horizontal tune shift ξ_x would drop like $1/\sigma_z\theta$. However, the most important effect is that the length of the overlap area of the colliding bunches is reduced, as it is proportional to σ_x/θ(see Fig. 3). Then, the vertical beta function β_y can be made comparable to the overlap area size (i.e. much smaller than the bunch length):

$$\beta_y \approx \sigma_x/\theta << \sigma_z \tag{5}$$

We get several advantages in this case:

- Small spot size at the IP, i.e. higher luminosity L.
- Reduction of the vertical tune shift ξ_y.
- Suppression of synchrobetatron resonances.

There are also additional advantages in such a collision scheme: there is no need to decrease the bunch length to increase the luminosity as proposed in standard upgrade plans for B- and Φ-factories. This will certainly help solving the problems of HOM heating, coherent synchrotron radiation of short bunches, excessive power consumption etc. Moreover, parasitic collisions (PC) become negligible since with higher crossing angle and smaller horizontal beam size the beam separation at the PC is large in terms of σ_x.

However, large Piwinski angle itself introduces new beam-beam resonances which may strongly limit the maximum achievable tune shifts. At this point the crab waist transformation enters

Table 1: Beam parameters for KLOE (2006) and SIDDHARTA (2008) runs used for beam-beam simulations.

PARAMETERS	KLOE Run	SIDDHARTA Run
L [$cm^{-2}s^{-1}$]	$1.5{\cdot}10^{32}$	$> 10^{33}$
$N_{bunches}$	110	110
$N_{part}/bunch$	$2.65 \cdot 10^{10}$	$2.65 \cdot 10^{10}$
I_{bunch} [mA]	13	13
ϵ_x [10^{-9} m·rad]	300	200
ϵ_y [10^{-9} m·rad]	1.5	1
σ_x [μm]	700	200
σ_y [μm]	15 ($blow-up$)	2.4
σ_z [mm]	25	20
β_x^* [m]	1.5	0.2
β_y^* [mm]	18	6
θ [mrad]	2×16	2×25

the game boosting the luminosity, mainly because of the suppression of betatron (and synchro-betatron) resonances arising (in collisions without CW) through the vertical motion modulation by the horizontal oscillations. The CW vertical beta function rotation is provided by sextupole magnets placed on both sides of the IP in phase with the IP in the horizontal plane and at $\pi/2$ in the vertical one (see Fig. 3). A numerical example of the resonance suppression is shown in Fig. 4.

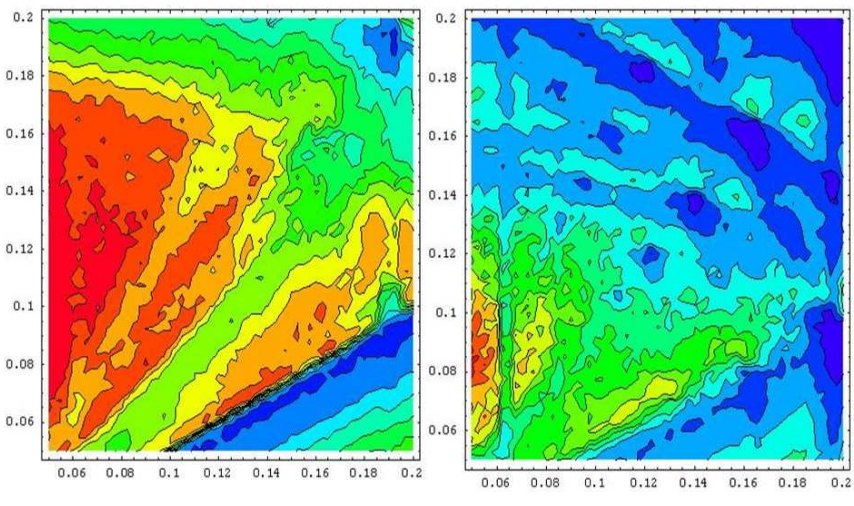

Figure 4: *Luminosity tune scan (ν_x and ν_y from 0.05 to 0.20). CW sextupoles on (left), CW sextupoles off (right). Chromatic scale is from blue (low luminosities) to red (high lumonosities)*

In order to estimate the achievable luminosity in DAΦNE with the CW scheme and to investigate distribution tails arising from beam-beam collisions, which may affect the beam lifetime, simulations with the code LIFETRAC have been performed. The beam parameters used for the simulations are summarized in Table 1. For comparison, the parameters used during the last DAΦNE run with the KLOE detector (2005-2006) are also shown. As discussed above, in order to realize the CW scheme in DAΦNE, the Piwinski angle ϕ should be increased and the beam collision area reduced: this is achieved by increasing the crossing angle θ by a factor 1.5 and reducing the horizontal beam size σ_x. In this scheme the horizontal emittance ϵ_x is reduced by a factor 1.5, and the horizontal beta function β_x lowered from 1.5 to 0.2 m. Since the beam collision length decreases proportionally to σ_x/θ, the vertical beta function β_y can be also reduced by a factor 3, from 1.8 cm to 0.6 cm. All other parameters are similar to those already achieved at DAΦNE.

Using the parameters of Table 1 and taking into account the finite crossing angle and the hourglass effect, a luminosity in excess of 1.0×10^{33} cm^{-2}s^{-1} is predicted with the beam current values already achieved during the KLOE run, which corresponds to an improvement of a factor of ≈ 6 with respect to the highest value ever measured at DAΦNE of 1.6×10^{32} cm^{-2}s^{-1}. The only parameter that seems to be critical for a low energy machine is the high vertical tune shift: $\xi_y = 0.08$, to be compared with the value of 0.03 so far obtained at DAΦNE.

In order to check whether these tune shifts -and luminosities- are achievable luminosity tune scan simulations have been performed. Fig. 4 shows 2D luminosity contour plots in the tune plane for the CW collisions with the crabbing sextupoles on (left) and off (right), for comparison. The color scale of the plot goes from blue (low luminosities) to red (high luminosities). For each plot ten contour lines between the maximum and minimum luminosities are drawn. The two plots of Fig. 4 show that the area of the high luminosity region is much wider when crabbing sextupoles are turned on in the simulations, while many betatron resonances appear when they are turned off. The absolute luminosity values are higher in the CW collisions: a peak luminosity of $L_{max} = 2.97\times10^{33}$ cm^{-2} s^{-1} is foreseen against L_{max} =1.74×10^{33} cm^{-2} s^{-1} in the case without CW. It should be noted that the worst luminosity value obtained with CW (L_{min} =2.5×10^{32} cm^{-2} s^{-1}) is still higher than the present luminosity record at DAΦNE. Without CW the lowest luminosity value drops by an order of magnitude, down to L_{min} =2.71×10^{31} cm^{-2} s^{-1}.

Many beam-beam simulations have been performed to validate experimental results during the CW test this year 2008. To summarize, strong-strong simulations agree within 20% with experimental results. Much lower luminosity is achieved with crab sextupoles off, as discussed in the following section 4. Moreover, stronger blowup, a sharp lifetime reduction is observed for bunch currents greater than 8-10 mA. This is in accordance with beam-beam simulations taking into account the realitic DAΦNE nonlinear lattice.

3 Hardware upgrades for the CW test at DAΦNE

During the summer shutdown of 2007 DAΦNE has been upgraded to allow the CW collision scheme test with the SIDDHARTA run. Other machine parts not directly related to the new collision scheme, such as injection kickers and shielded bellows, have been also upgraded or renewed. The general layout of DAΦNE upgrade has been already shown in Fig. 1, while drawings of the upgraded (top) and old (bottom) IR1 are reported in Fig. 5.

The major upgrades on the machine are summarized as:

- new IR1 geometry for the CW test;

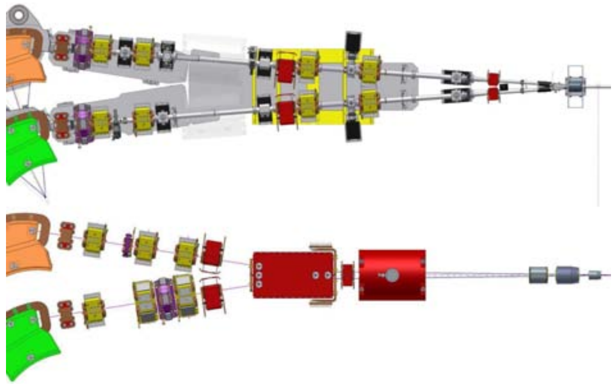

Figure 5: *DAΦNE IR1 after (top) and before (bottom) the crab waist upgrade.*

- new IR2 geometry with two completely separated vacuum chambers with half moon profile (opposite ring crossing section, called *RCR*);
- new shielded bellows;
- the four e^+ e^- transverse feedbacks have been upgraded;
- solenoid windings in the two long IR and RCR sections of the e^+ ring;
- new calorimeter for luminosity measurement and tuning;
- new longitudinal position of the two IRs horizontal collimators;
- new injection kickers.

The need of a new IR2 geometry is essentially due to have a very small β_y (6 mm) and a large crossing angle (25 mrad per beam). splitter dipoles that have been in use at DAΦNE before, so they have been removed. Splitter magnets installed in the original design have been removed thanks to the large crossing angle in the CW scheme. Defocusing and focusing quadrupoles (QD, QF) on both sides of the IP have been placed to obtain the required low-β structure. Further trajectory separation is provided by two small dipole correctors upstream and downstream the quadrupole doublets, while other three quadrupoles are used to match the betatron functions in the arcs. The low-β section quadrupoles near the IP are of permanent magnet (PM) type. The QDs are located near the IP where the beams share a common vacuum chamber, while the QFs are positioned where the chambers are splitted and each one acts on a single beam. Therefore a total of two QDs and four QFs is required to get the two doublets around IP1. Four corrector dipoles provide a deflection of 9.5 mrad to match the inlet and outlet arc chamber flanges. CW sextupoles are placed at $\sim$ 9.3 m far from the IP1. Bending dipoles facing the IRs have been rotated and their field adjusted according to requirements. They have been powered with independent supplies to match these requirements. The new layout allows to reinstall the solenoid compensators for the future KLOE run. In fact, the KLOE detector back roll-in is foreseen this fall 2009.

Figure 6: *New RCR section.*

Most vacuum chambers and pumps have been reused. However, for the SIDDHARTA experiment a new aluminium alloy (AL6082T6) chamber with two thin windows (0.3 mm ± 0.02 thickness) in the top and bottom sides has been designed and built. Electromagentic simulations have shown the presence of trapped modes which add resonant contributions to the beam coupling impedance in the Y-chamber junctions, the regions where the two separate ring pipes merge in the common vacuum chamber near the IP. In the worst possible scenario, that occurs when a beam spectrum line at a frequency equal to a multiple to the bunch repetition rate is in full coupling, the joule loss does not exceed 200 W. To keep this effect under control the Y-chambers have been equipped with cooling pipes. This additional cooling circuit allows to remove the beam induced HOM heating and, if necessary, to reduce it by detuning the mode frequencies with respect to the dangerous beam spectrum lines.

Similar modifications were made in the second interaction region (IR2), where the beams will not experience a low β insertion and will be vertically separated in order to avoid parasitic collisions. A new design of the central IR2 beam pipe, where the two beams are vertically separated, is shown in Fig. 6. The two vacuum chambers are completely separated and their cross section has an half moon profile.

In order to keep the beam coupling impedance low, the total number of bellows has been reduced to the minimum strictly needed to compensate the thermal strain and mechanical misalignment. In each crossing region only 4 bellows per beam are used. The technology of copper-beryllium strips has been adopted optimizing the cost and the shielding performance. The working axial stroke is ± 7 mm and the radial offset ± 3 mm.

The four e^+ e^- transverse feedbacks have been upgraded by adopting the new iGP (Integrated Gigasample Processor) feedback units. Beyond its ordinary stabilization function, this system allows to build a variety of diagnostic tols ranging from the single bunch tune to the single turn beam position measurement, useful in the injection kickers optimization.

Solenoid windings with a field $B_{sol} \approx 45$ Gauss have been added in long straight sections to counteract positron beam instability due to electron cloud. They allowed the increase of the maximum stored e^+ current. Solenoids have been effective especially in the first commissioning phase, in fact they reduce the transverse instability rise-time boosting the action of the transverse feedbacks.

In order to ensure a fast, accurate and absolute measurement of the luminosity and to fully understand the background conditions, the new interaction region has been equipped with three different luminosity monitors (Fig. 7): a Bhabha calorimeter, a Bhabha GEM tracker and a gamma Bremsstrahlung proportional counter. Three different processes are used to measure the luminosity at DAΦNE:

- the Bhabha elastic scattering $e^+e^- \to e^+e^-$: it has a very clean signature (two back-to-back tracks); the available angle is limited due to the presence of the low-β quadrupoles, however, in the actual polar angle range covered by our calorimeters, $18 \div 27$ degrees, the expected rate ($\sim$ 440 Hz at a luminosity of 10^{32} cm^{-2} s^{-1} is high enough and the backgrounds low enough to allow an online clean measurement;
- the very high rate of the radiative Bhabha process $e^+e^- \to e^+e^-\gamma$: it has the advantage that 95% of the signal in contained in a cone of 1.7 mrad aperture, but it suffers heavily from beam losses due to interactions with the residual gas in the beam-pipe, Touschek effect, and particles at low angles generated close to IR;
- the resonant decay $e^+e^- \to \Phi \to K^+K^-$: a rate of about 25 Hz at 10^{32} is expected in the SIDDHARTA experiment monitor at ≈ 90 deg.

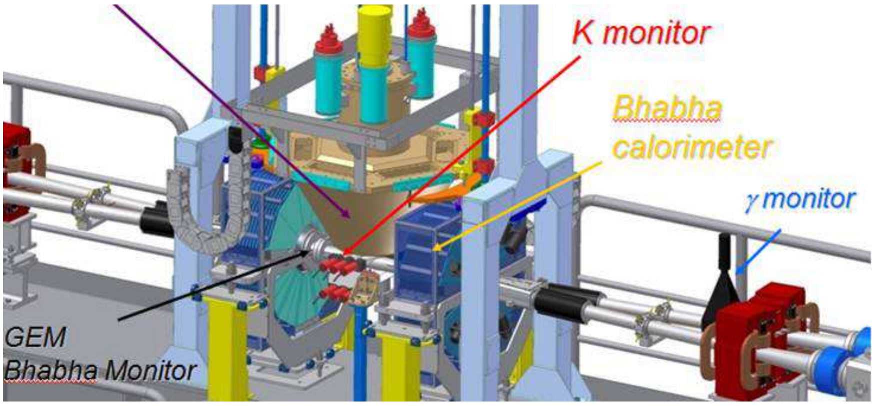

Figure 7: *Overview of the upgraded DAΦNE IR1 showing the various luminosity detectors.*

The main Bhabha monitor consists of a 4-modules sandwich calorimeter, made of lead and scintillator. Four modules of calorimeters surround the final permanent quadrupole magnets, located at a distance of 32.5 cm on both sides of the IR, as shown in Fig. 7. They cover an acceptance of $18 \div 27$ degrees in polar angle, and are segmented in azimuthal angle in five sectors, 30 degrees wide.

Two gamma monitor detectors are located 170 cm away from the IR, collecting the photons radiated by electron or positron beam. The detectors replace the gamma monitors previously installed in DAΦNE and are now made of four $PbWO_4$ crystals (squared section of 30×30 mm^2 and 110 mm high) assembled together along z, in order to have a 30 mm face towards the photon beam, and a total depth of 120 mm corresponding to about 13 X_0. Thanks to the high rate, those detectors are mainly used as a fast feedback for the optimization of machine luminosity versus background, more than providing a measurement of the luminosity, since the relative contribution of background is changing with the machine conditions. However, on the short time scale and as relative luminosity monitors, those counters have demonstrated to be extremely useful. All systems showed very good performance and fully achieved the design parameters. A total systematic uncertainty on the luminosity measurement of 11% can be estimated. Detectors have been fully implemented in the machine controls, and data are available for the community on word wide web DAΦNE accelerator page.

The two IRs horizontal collimators have been moved to a different longitudinal position, according to the new lattice. Dedicated simulations of Touschek scattering have been performed to determine their proper position along the rings. The IR1 collimator has been placed at 8 m upstream the IP. On the other hand, the collimator that was upstream IP2 has been moved downstream at a position with low β_x and high horizontal dispersion. Simulations predicted for these two positions high efficiency of the collimators in rejecting scattered particles. Measurements during operation confirmed these expectations.

New injection kickers have been designed, built and installed. The design is based on a tapered strip inside a rectangular vacuum chamber cross section in order to simultaneously improve the deflecting field quality obtaining a uniform horizontal deflection as a function of the horizontal coordinate, reduce the beam coupling impedance by means of the tapered transition between the beam pipe and the kicker structure, have a uniform beam pipe cross section between the dipole region and the kickers region. This also reduces the total beam coupling impedance of the machine and obtain a better matching between the generator and the kicker structure at high frequency. This can avoid multiple reflections of the deflecting pulse in the kicker structure that can perturb the stored bunches. Moreover it allows extracting all the power released to the HOM of the structure by the beam.

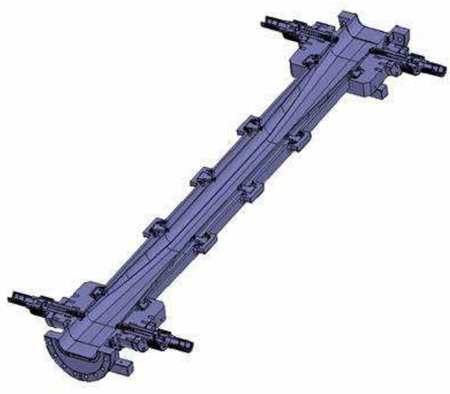

Figure 8: *CAD drawings of the strip line kickers.*

The new kickers allow to obtain a short pulse ($\approx$ 6 ns) by driving the stripline kickers with novel HV fast pulsers which are now available on the market. Special 50 kV feed-throughs have been integrated in the device after being successfully tested on the bench.

The strip line kickers (see the CAD drawing in Fig. 8) for beam injection in DAΦNE storage

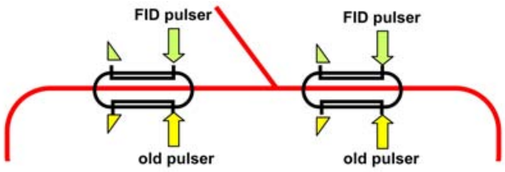

Figure 9: *Scheme of the "hybrid" configuration.*

rings have been installed since November '07. In the past year 2008 they worked properly and never gave problems. For great part of the operation time, they worked with the old long pulse generators, already used with the previous kicker, in both the rings. As a matter of fact, the final version of the FID fast pulse generators has shown very poor reliability, even after repair and substitution of damaged parts with upgraded ones. For this reason we never had the possibility to use, at the same time, the four FID pulsers on the 2 kickers of the positron ring as scheduled for 2008.

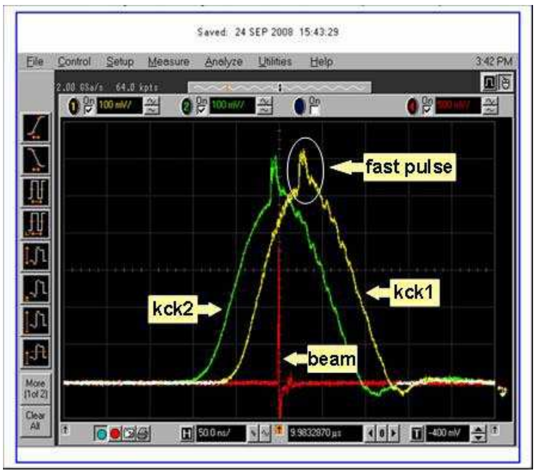

Figure 10: *Combined pulses coming from the old and the FID fast generators observed at the scope.*

Nevertheless, different "hybrid" configurations were successfully tested, where FID pulsers were used together with the old pulsers, even on the same kicker, connecting to each stripline a different kind of kicker. This scheme and the combined pulses coming from the old and the FID fast generators observed at the scope are illustrated in Fig. 9 and in Fig. 10, respectively. The new stripline kicker has been also used as an additional kicker for the horizontal feedback. Both the kickers of the positron ring have, at present, one stripline connected with the old pulser for beam injection and the remaining stripline connected to the amplifiers of the feedback system. Thanks to this configuration we are able to inject the beam and to improve the feedback performance at the same time.

Table 2: Present DAΦNE luminosity performances with the CW scheme and low-β parameters compared to the KLOE and FUNUDA runs. SIDDHARTA data taking does not profit of the fast injection rate system, that would increase $L_{\int logged}$.

	SIDDHARTA March 08÷Feb 09	KLOE May 04÷Nov 05	FINUDA Nov 06÷Jun 07
L_{peak} [cm^{-2}s^{-1}]	4.05	1.5	1.6
$L^{MAX}_{\int day}$ $[pb^{-1}]$	14.98	9.8	9.4
$L^{MAX}_{\int hour}$ $[pb^{-1}]$	1.033	0.44	0.5
$I^{-\ MAX}_{coll}$ $[A]$	1.4	1.4	1.5
$I^{+\ MAX}_{coll}$ $[A]$	1.1	1.2	1.1
$n_{bunches}$	105	111	106
$L_{\int logged}$ $[fb^{-1}]$	1.2	2.0	0.966
β^*_x $[m]$	0.26	1.5	2.0
β^*_y $[m]$	0.009	0.018	0.019
ϵ_x $[10^{-6}\ m \cdot rad]$	0.26	0.34	0.34
ξ_y	0.0245	0.0291	0.0361

4 Test and commissioning with the Crab Waist collisions scheme

The commissioning of the upgraded machine started in November 2007. At the end of the year the ring vacuum was almost recovered, the beams were stored in the upgraded rings, all the sub-systems (injection, RF, feedback and diagnostics, ...) went rapidily to regime operation. The first collisions in the CW scheme have been obtained in February 2008, with the first experimental confirmation of the potentiality of the new configuration in terms of specific luminosity growth and reduction of the beam-beam disruption effects. At the beginning of this run the machine operation was limited by effects such as positron beam instabilities, short lifetimes of both beams, vacuum in e^- RF cavity and detector background. The DAΦNE team has been working on all these aspects to increase the machine performance and to fulfill successfully the test of the CW scheme.

The beam current routinely stored for 105 colliding bunches exceeds 1 A and 2 A for the e^+ and e^- beam, respectively.

The maximum peak luminosity up to February 2008 is of 4.05$\cdot$ 10^{32} cm^{-2}s^{-1} obtained with $I^- = 1.43$ A and $I^+ = 1.11$ A with 105 bunches, that corresponds to a 150% larger value than what obtained during the FINUDA run in 2007.

The best hourly integrated luminosity compatible with the SIDDHARTA data taking is 0.79 pb^{-1}. Moreover, in high rate inection regime the best hourly integrated luminosity is 1.033 pb^{-1}. The maximum integrated luminosity per day is $\approx$ 15 pb^{-1} in moderate injection rate regime. Luminosity is significantly higher than during the previous 2003–2004 FINUDA run, as shown in Table 2.

The peak luminosity measured by the FINUDA detector has been increased by a factor ≈ 2.5; correspondingly the maximum daily integrated luminosity has been increased by a factor ≈ 1.6.

Integrated luminosity for SIDDHARTA in Table 2 refers to the period going from March

14th 2008 to February 25th 2009; we notice that the $L_{\int logged}$ could be larger if the machine could inject in the fast injection rate regime. In fact, fast injection is not compatible with the Siddharta operations. The maximum number of pulses injected in the accumulator has been increased from 15 to 17 to speed up the injection in the main rings. The stored current in the accumulator increased by $\sim 13\%$. This has been possible executing in parallel the procedure commands. The injection switch time was 150 s for the system upgrade and now is 40 s.

Moreover, specific luminosity with the CW scheme is $\sim 3 \div 4$ times larger than before the upgrade and the beam-beam tune shift exhibits a fairly linear behaviour as a function of current per bunch in the opposite colliding beam.

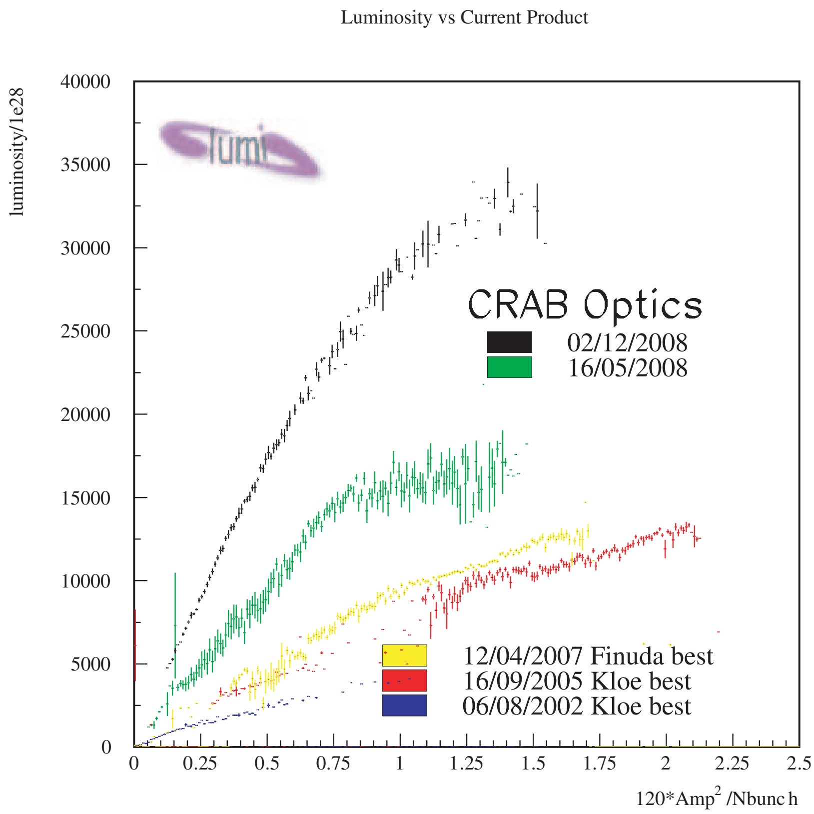

Figure 11: *Specific luminosity versus colliding currents showing the increase obtained in few months of commissioning.*

DAΦNE luminosity as a function of the colliding bunches compared to past runs is reported in Fig 11. Blue and red dots refer to the two KLOE runs, with the initial triplet low-β IR quadrupoles and with the new IR doublet, respectively. Yellow dots refer to the FINUDA run; in green is the luminosity with the CW scheme at the beginning of the test, in May 2008 while in black is a typical day in December 2008 with a peak luminosity reaching $\approx 3.5\times10^{32}$ cm^{-2}s^{-1}.

A similar plot is shown in Fig. 12 where now only one typical day of the last KLOE and FINUDA run is shown, together with a good day of machine operation with the CW scheme (December 28th 2008) where both the average (in green) and the peak (in black) luminosities are shown. As a comparison, the luminosity with the crab sextupoles switched off is shown in blue dots.

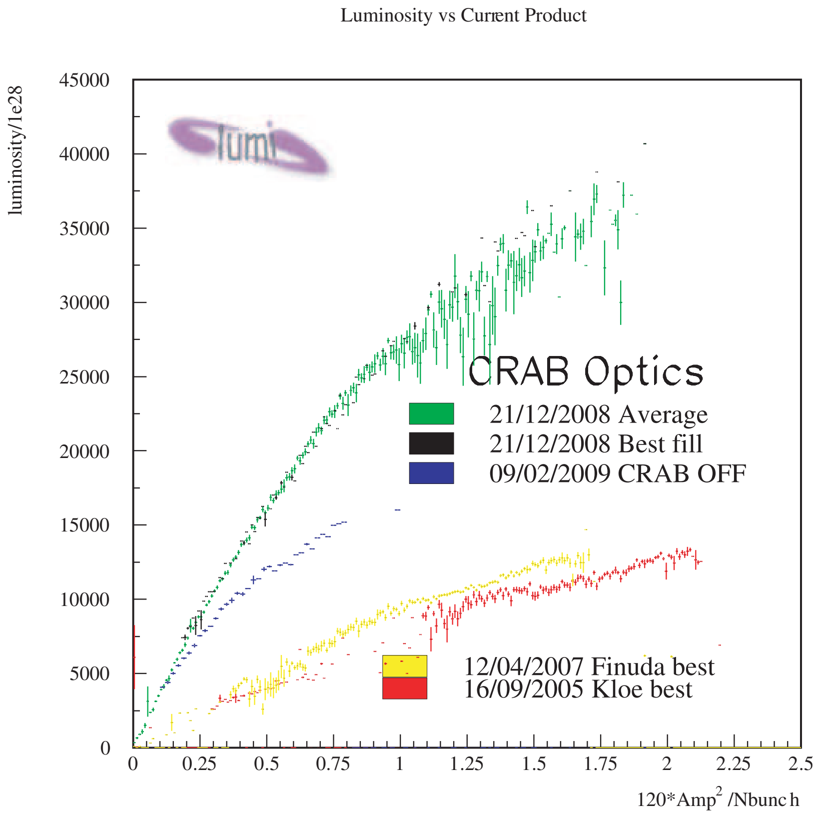

Figure 12: *Specific luminosity versus colliding currents for different runs, effect of crab sextupoles is evident.*

A comparison of the specific luminosity with crab sextupoles switched on and off with the CW scheme is shown in Fig. 13.

During the machine tuning both the luminosity value and the signal to noise ratio (S/N), i.e. luminosity to backgrounds ratio, have to be maximized at the same time. A lot of effort has been spent in minimizing the backgrounds induced in the SIDDHARTA detector. It it has been progressively reduced, mainly by tuning the collider optics and adjusting the collimators, as happened in the past runs. Fortunately SIDDHARTA is a small gas detector, so shieldings around it could be added fairly easily. Different shapes of shieldings have been tested and optimized until a satisfactory setup has been found with a better S/N than that obtained during the DEAR run.

The machine lifetime and backgrounds are dominated by Touschek effect which is, as expected, more important in the CW scheme than the standard collision scheme. In fact, beam sizes are smaller, especially at the IR. Touschek simulations are in agreement with measured lifetime and backgrounds. A lot of effort has been put in machine tuning to enhance the Touschek lifetime, essentially by increasing dynamic aperture with sextupoles tuning and by orbit optimization.

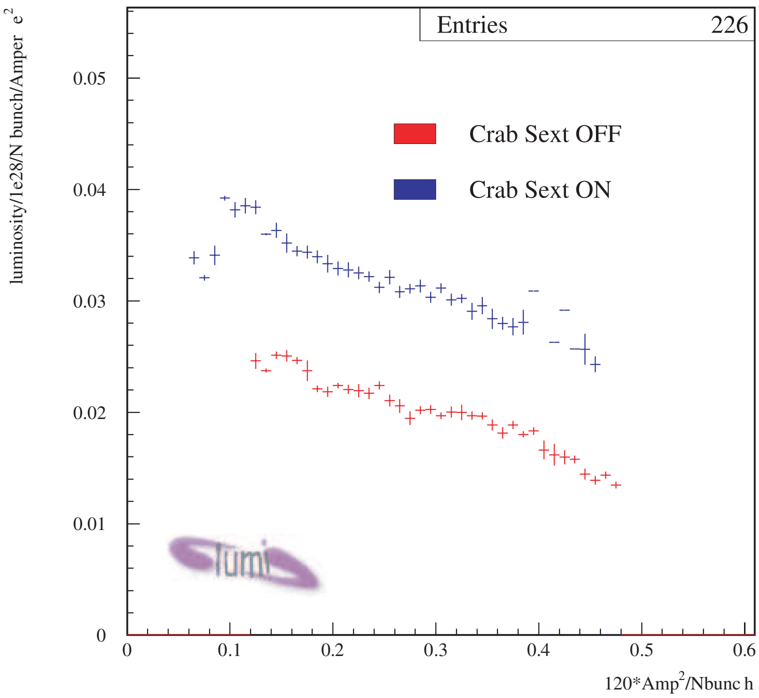

Figure 13: *Specific Luminosity with Crab sextupoles on and off in* 10^{28} $cm^{-2}s^{-1}A^{-2}$ *unit and 95 bunches.*

The rings optics commissioning with the CW scheme can be summarized as follows: fixing misalignment errors in some elements, correction of transverse betatron coupling mainly by rotating the permanent focusing quadrupoles in the IR, minimization of the vertical dispersion, addition of two electromagnetic quadrupoles around the IP in order to meet the phase advance requirements imposed by the CW collision scheme, establishment of the procedure for the CW sextupoles alignment in single beam operation mode in order to have betatron tunes, coupling and background constant when they were switched on.

During the second half of year 2008 a lot of work has been done on the positron horizontal instability. Measuring by diagnostic inside the feedback system the instability growth rates in many different machine conditions and for different beam currents. As a conclusion of the measurements analysis the decision to double the e^+ horizontal feedback system has been taken. In this way, the instability has been completely under control. The positron beam current has overcome 1.16 A. However, a real improvement in the machine has been obtained by pointing out and mitigating a 50 Hz noise propagating through the ground system and affecting some beam instrumentation, the e^+ longitudinal and transverse feedbacks and the RF system. So, this noise produced longitudinal instability at high current on the e^+ beam and transverse size blow-up, spurious phase modulation of the RF voltage at line frequencies (50 Hz and multiples), disturbances entered through the feedback system stabilizing the beam barycentric coherent oscillation mode. This noise produced unstable beams.

5 Present Status and Future Plans

The SIDDHARTA run should be completed before summer 2009, while delivering data to the experiment machine performances are optimized both adiabatically and with dedicated machine studies.

The roll-in of KLOE after the SIDDHARTA run has been approved and the detector should roll back in next fall 2009. The new KLOE run is expected to start by the end of 2009. The DAΦNE and the KLOE teams are working together to prepare the next run. In particular, all the different aspects of the new IR design are under study, like the new low-β quadrupoles, the material and shape of the new IR vacuum chamber, the masks and shieldings to prevent background contamination in the physics events, the IR stay-clear, IR parameters and new lattice.

6 Publications

1. M. Boscolo *et al.*, "Crab Waist Scheme Luminosity and Background Diagnostic at DAΦNE", Proc. of BIW08, Lake Tahoe, Ca, USA.

2. C. Milardi *et al.*, "DAΦNE Setup and Operation with the Crab-Waist Collision Scheme", Proc. of EPAC08, Genoa, Italy, p. 2599.

3. P. Raimondi *et al.*, "Crab Waist Collisions in DAΦNE and Super-B Design", Proc. of EPAC08, Genoa, Italy, p. 1898.

4. M. Boscolo *et al.*, "Luminosity Measurement at DAΦNE for Crab Waist Scheme", Proc. of EPAC08, Genoa, Italy, p. 1203.

5. F. Marcellini *et al.*, "Coupling Impedance of DAΦNE Upgraded Vacuum Chamber", Proc. of EPAC08, Genoa, Italy, p. 1661.

6. S. Tomassini, F. Marcellini, P. Raimondi, and G. Sensolini, "A new RF Shielded Bellows for DAΦNE Upgrade", Proc. of EPAC08, Genoa, Italy, p. 1706.

7. A. Drago, D. Teytelman, and M. Tobiyama, "Commissioning of the IGP Feedback System at DAΦNE", Proc. of EPAC08, Genoa, Italy, p. 3251.

8. T. Demma, R. Cimino, S. Guiducci, and M. Zobov, "Electron Cloud Simulations for DAΦNE", Proc. of EPAC08, Genoa, Italy, p. 1604.

9. A. Bocci *et al.*, "Beam Diagnostics with IR Light emitted by positron at DAΦNE", Proc. of EPAC08, Genoa, Italy, p. 1056.

10. M. Preger and S. Tomassini, "Beam Trajectory Inside the Modified Dipoles for the DAΦNE Upgrade", DAΦNE Techn. Note L-39, 11/03/2008.

11. M. Esposito *et al.*, "Alignment Operations for the DAΦNE Ugrade", DAΦNE Techn. Note ME-20, 20/11/2008.

The DAΦNE Beam Test Facitily (BTF)

The BTF Staff: B. Buonomo (Art. 23), G. Mazzitelli (Resp.),
L. Quintieri (Art. 23), P. Valente (Osp.)

The DAΦNE Operation Staff: G. Baldini, A. Beatrici, M. Belli, B. Bolli, G. Ceccarelli,
R. Ceccarelli, A. Cecchinelli, S. Ceravolo, R. Clementi, O. Coiro, S. De Biase,
M. De Giorgi, M. Di Virgilio, G. Ermini, G. Fontana, C. Fusco, O. Giacinti, E. Grossi,
F. Iungo, C. Marini, M. Martinelli, C. Mencarelli, E. Passarelli, V. Pavan, D. Pellegrini,
G. Piermarini, S. Quaglia, M. Sardone, M. Scampati, G. Sensolini, A. Sorgi,
M. Sperati, A. Sprecacenere, R. Tonus, T. Tranquilli, M. Troiani, R. Zarlenga

The LNF Technical Staff:
A. Donkerlo, R. U. Frasacco, F. Galletti

BTF Committee
P. Di Nezza - LNF, F. Gatti - INFN, Genova, C. Matteuzzi (Chairperson) - INFN, Milano,
G. Mazzitelli (Resp.) - LNF, A. Passeri - INFN, Roma III, P. Valente - INFN, Roma

1 Description of the DAΦNE BTF 2008 Activities

The DAΦNE Beam Test Facility (BTF) successfully operated for the 6th year. A total of 200 days have been allocated to user experimental groups, 20% less than the average of previous years, essentially due to less detector testing activities in the community for the starting-up of LHC experiments. Still, the facility has been full operational during the entire period in which DAΦNE main rings have been running.

Table 1: Allocated days of operation during last 5 years.

2008	200 days
2007	224 days
2006	244 days
2005	364 days
2004	282 days

During the last 5 years, the users accessing the BTF were mainly coming from INFN ($\sim$ 65%) and other Italian research institutions ($\sim$ 15%), while the remaining ($\sim$ 20%) was mainly coming from European countries partially supported by TARI (Transnational Access to Research Infrastructure in the 6th Framework Programme) and also from industries. The BTF has now the permission of the radio-protection Italian Agency to deliver almost the full DAΦNE LINAC beam in the experimental hall. This opens the possibility to host a new class of tests and experiments. Since the beginning of year 2008, we have then started operations also in very high intensity mode (10^{10} electro/seconds). The DAΦNE main experiment operation is in any case strongly limiting the duty cycle to less than 40%, due to the continuous injection in the main rings. This has

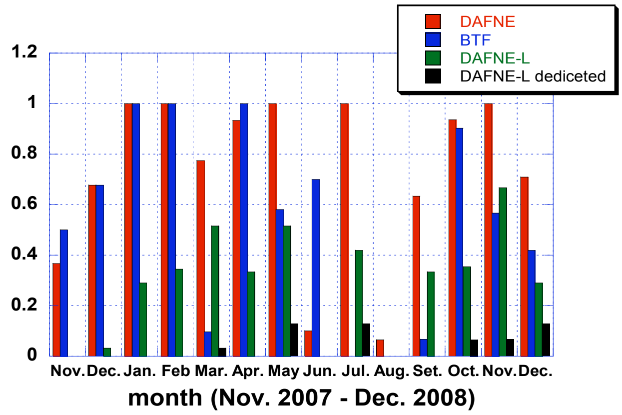

Figure 1: *2008 run: user access to the facility (blue) in percentage of the mouth days. DAΦNE main experiment operation (red), DAΦNE light source parasitic (green) and dedicated (black) operation.*

convinced us to allocate future requests for high intensity beam mainly during a period dedicated to BTF users. On the other hand, the standard operations with the target attenuator (1 to 10^4 particles/spill, 49 spills per seconds) have been very stable, with a typical duty cycle of 80%. Due to problems in the LINAC system, during all 2008 the positrons current of the primary beam impinging the attenuator target have been largely different from the electrons one (up to a factor 5). This causes a large difference in the beam intensity detected by the hosted experiments, when the primary beam is switched (about every 20 minute during SIDDHARTA operations), when one is not changing the collimators settings correspondingly. The slit system settings can be indeed changed automatically, also including a feedback system adjusting the collimators aperture on the basis of the beam intensity measured by the WCM monitors upstream of the attenuating target, but this needs some modifications in the DAΦNE control system.

2 Advancement in the Feasibility Study of a Photo-Neutron Source at the DAΦNE BTF Facility

During 2008 we have also continued the study for the feasibility of a neutron source by photo-production on target in BTF [1]. This is motivated essentially by the general increasing interest of the BTF scientific community, as well as: by the interest of testing detectors at low neutron fluxes and low energy, the opportunity of generating the know-how needed for next generation of high energy source (see FEL) and the possibility to have a new European facility in ISO standard. The project has been presented and approved by the INFN CSN5, and now is going in an executive phase, during which we foresee to make some preliminary tests in fall 2009.

The results of the simulations allowed us to define the optimized target, the shielding and assembly setup.

Table 2: Ta and W: Nuclear and Mechanical Properties.

Properties	Ta	W
density(g/cm3)	16.69	19.25
Z	73	74
P.M (g mol-1)	180.95	183.84
Moliere radius [cm]	1.073	0.9327
Rad Length [cm]	0.4094	0.3504
K (thermal cond)[W/mK]	57.5	173
E(young) [GPa]	186	411
Poisson Ratio	0.34	0.28
α [μ/mK]	6.3	4.5
T(melting point) [k]	3290	3695

2.1 Description of the Calculations results

In order to maximize the photo-neutron production, the material to be used for the target, on which the electron beam impinges, is typically a high Z material. Detailed Monte Carlo simulation (by Fluka code [2]) have been done for comparing the neutron yield obtainable essentially with tantalum and tungsten as suitable material for the target. In table 2, the main nuclear and mechanical properties of tantalum and tungsten have been reported.

The possibility to use Uranium has been also considered: in terms of neutron yield by photo-production, the advantage should consist in increasing of about 1.5 times the neutron yield respect to tungsten [3]. The gain of neutron yield due to the contribution of photo-fissions has to be estimated, but anyway, the manage of Uranium could cause important radiation safety issues, for which our laboratory at present time is not properly equipped. This is the reason for which we have abandoned for the moment the idea of using Uranium as material of which the target should be made.

Table 3: Comparison between a Ta and W cylindrical target of R=L=10 X_0: n_{yield} is the neutron yield produced per primary electron; E_{dep} is the total energy deposited in target by primary electron; n_{out} gives the neutron fluence leaving the target; $n_{out} \cdot S$ is the number of electrons exiting the target (integrated on all the energy spectrum and solid angle); ph_{out} indicares the photon fluence leaving the target; $ph_{out} \cdot S$ is the total number of photon exiting the target (S being the lateral surface of the target.)

Parameter	W	Ta
n_{yield}[n/pr]	1.985E-01	1.938E-01
E_{dep}[GeV/cm3]	4.438E-01	4.425E-01
n_{out}[n/cm2/pr]	1.9713E-03	1.366E-03
$n_{out} \cdot S$[n/pr]	0.3035	0.2886801
ph_{out}[ph/cm2/pr]	0.1768	0.128
$ph_{out} \cdot S$[ph/pr]	27.213	27.123

Several calculations have been done to compare in more deep details the difference between tantalum and tungsten. As we can see in the table 3, there are not so big differences in terms of neutron yield between an optimized target made of W with respect to the one made of Ta[1], so that the choice between the two cases can be essentially done on the basis of thermo-mechanical and price considerations.

Tungsten is less expensive and has a better thermal conductivity with respect to tantalum. Considering that the maximum beam power that can be transported in BTF hall is about 40 W, the estimated maximum temperature reached in the target, during a reasonable operation time (es. about half an hour of full power on the target), should be around 400 K. This suggests that the target cooling could be not needed, even if this depends on the operational duty cycle and it will be considered if necessary.

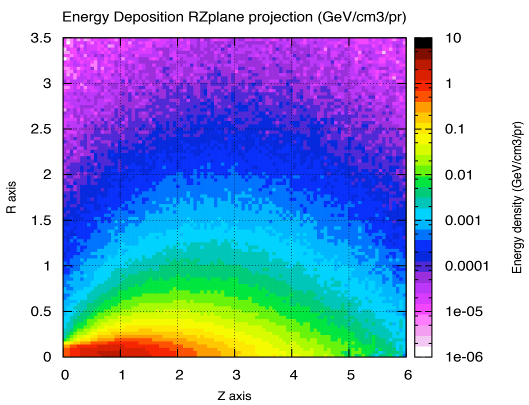

Figure 2: *Energy Deposition profile in ZR plane.*

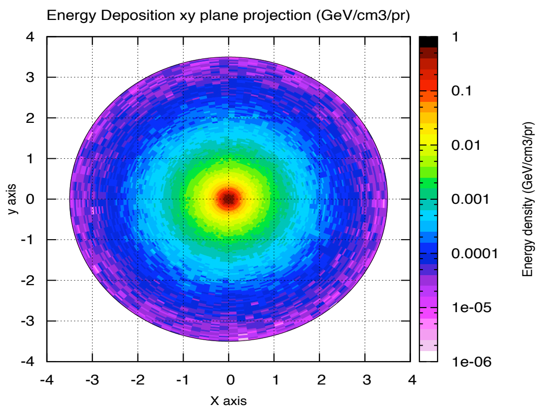

Figure 3: *Energy Deposition profile in XY plane.*

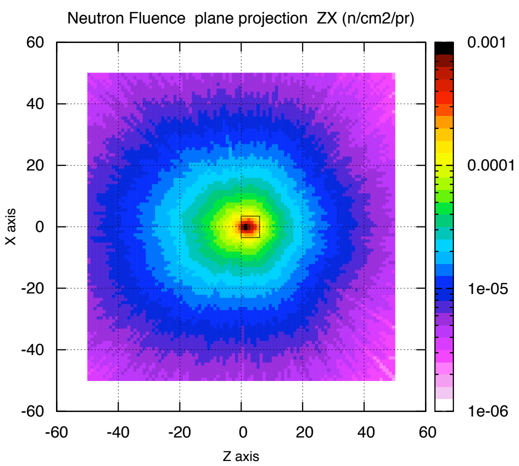

Figure 4: *Fluence [n/cm^2/pr] projection on xz plane (z being the beam direction.)*

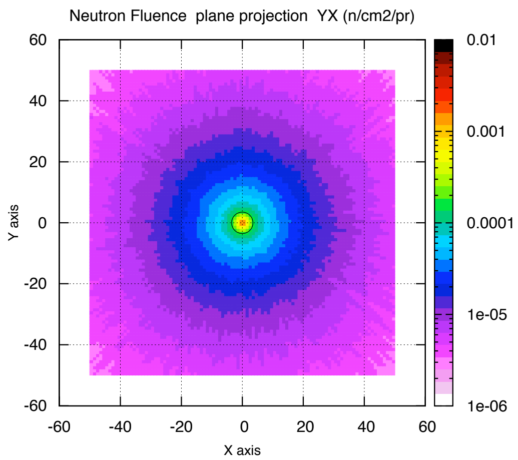

Figure 5: *Fluence [n/cm^2/pr] projection on xy plane (z being the beam direction.)*

[1]The energy spectrum is almost the same in the two cases as shown in the technical report [1]).

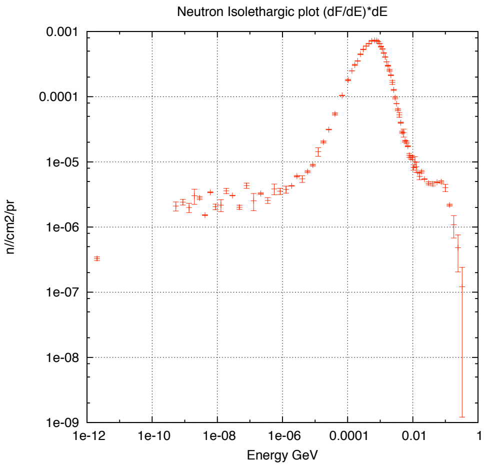

Figure 6: *Isolethargic Neutron Fluence from W Target.*

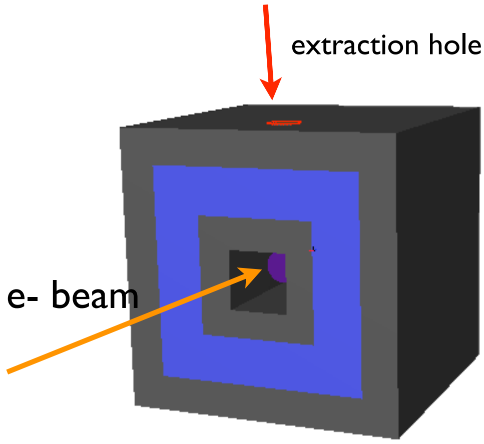

Figure 7: *Monte Carlo Model of all the assembly.*

Tungsten has almost the same heat capacity but thermal conductivity three times higher than that of Tantalum, and consequently it has a better thermal diffusivity and so it seems to be more effective in heat exchange with respect to tantalum (the diffusivity[2], being the ratio [k/C/ρ], indicates the ability of a body to conduct heat and for tungsten is almost 4 times greater than the one of tantalum).

After having fixed the material, many cases have been simulated in order to tune the optimum value of the cylinder height and diameter in such a way to maximize the neutron fluxes exiting the target and minimize (as possible) the photon ones.

At the end we designed the optimum target for neutron photoproduction at the DAΦNE BTF: it is a cylinder made of tungsten with 3.5 cm of radius and 6 cm of height.

In the pictures 2 and 3, we reported the energy deposition in the target and in 4 and 5 pictures , the neutron fluences around it, respectively. The energy spectrum of neutron produce for photo-absorbtion in the optimized W optimized target has been estimated, too, and is reported in figure 6. The number of neutrons produced per primary electron impinging on the W target is 2.2E-1. This means that if we consider a primary beam flux of $5 \cdot 10^{11}$ e-/s (corresponding to the maximum beam power transportable in BTF), about $8 \cdot 10^{8}$ n/s neutrons have been estimated to enter a spherical detector of 12.5 inch (corresponding to the largest Bonner sphere available in our laboratory) located at 1m from the upper shield surface.

As we can see in figures 4 and 5 the neutron fluence is pretty well isotropic. On the contrary the photon fluence is strongly anisotropic (the photon rate in a narrow solid angle around the beam direction is more than 2 order of magnitude higher than that around 90 degrees). This explains why we have designed two extractions line in the plane xy perpendicular to the z beam axis: we want to locate the neutron detectors in places where the photon background is minimum.

The estimated neutron and photon fluences at 1m from the target, at different polar angles

[2]k is the thermal conductivity, C the heat capacity and ρ is the density.

Start	End	User	beam (days)	dose	Min. Energy	Max. Energy	Particle	Min. Mult.	Max. Mult.
01-02	01-20	LUMI	19	0.0	250.0	500.0	Electron	1.0	1000.0
01-21	01-27	FOPI-test	7	999.9	50.0	500.0	Electron	1.0	1000.0
01-28	02-10	LUMI	14	0.0	500.0	500.0	Electron	1.0	1.0
02-18	03-02	P326gamma	14	0.0	500.0	500.0	Electron	1.0	1.0
03-31	04-06	CUP	7	0.0	300.0	500.0	Positron	1.0	1000.0
04-07	04-20	P326gamma	14	0.0	50.0	500.0	Electron	1.0	100.0
04-21	05-04	SHARPS	14	0.0	500.0	500.0	Electron	1.0	1000.0
04-28	05-04	P-ILC	7	0.0	500.0	500.0	Electron	1.0	1000.0
05-05	05-18	K2CAL	14	0.0	25.0	500.0	Electron	1.0	100.0
06-09	06-15	P-ILC	7	0.0	500.0	500.0	Electron	1.0	1000.0
06-16	06-22	P326gamma	7	0.0	50.0	500.0	Electron	10.0	100.0
06-17	06-17	RAD-LEN	1	30.0	500.0	500.0	Electron	1.0	1000.0
06-23	06-29	COMANCHE	7	999.9	500.0	500.0	Electron	1.0	10.0
09-29	10-12	TPG	14	0.0	500.0	500.0	Electron	1.0	1000.0
10-13	10-17	COMANCHE	5	999.9	500.0	500.0	Electron	1.0	5.0
10-20	11-02	TPG	14	0.0	500.0	500.0	Electron	1.0	1000.0
11-13	11-14	RAD-LEN	2	0.0	500.0	500.0	Electron	1.0	1000.0
11-17	11-26	C-SHAPE	10	20.0	25.0	500.0	Electron	1.0	1000.0
11-27	11-28	RAD-LEN	2	0.0	500.0	500.0	Electron	1.0	1000.0
11-30	12-09	P-ILC	10	0.0	500.0	500.0	Electron	1.0	1000.0
12-10	12-16	SHARPS	7	0.0	500.0	500.0	Electron	1.0	1000.0
12-17	12-19	COMANCHE	3	0.0	500.0	500.0	Electron	1.0	10.0

Figure 8: *User 2008 beam Request.*

with respect to the beam impinging direction, have allowed to reconstruct the photonic and neutronic field around the target and, consequently, design a popper shield around it. The shield is made of essentially 2 layer of lead (7.5 cm each) with a layer of polyethylene (10 cm) in between. In figure 7 the 3D the model used for the Mont Carlo simulations has been reported. The Shield has 3 holes: one for the beam inlet and the other two, in the transversal plane respect to the beam direction, in the horizzontal and vertical direction respectively.

3 BTF Support

Since the beginning of 2008 a secretariat has been assigned to BTF as support for the administrative issues connected to users access, safety etc. The documentation for accessing the facility, operations and safety manuals are also available on the BTF web site:

`http://www.lnf.infn.it/acceleratori/btf/access/`

A dedicated e-mail address (btfsupport@lnf.infn.it) is also available to the users for any administrative question.

4 Conference Communications of BTF activities during 2008

G. Mazzitelli *et al.*, 37Th LNF Scientific meeting, 2 December 2008, LNF Frascati Roma.

G. Mazzitelli *et al.*, Channeling 2008, 25 Octobber 2008, Erice, Italy.

G. Mazzitelli *et al.*, CNS5, 17 September 2008, Apertura sigla n@BTF, Ferrara, Italy.

B. Buonomo *et al.*, BIW 2008, 4-8 May 2008, Lake Taohe, California, USA.

G. Mazzitelli *et al.*, invited talk, 26 May 2008, Beijing University, Beijing, Cina.

G. Mazzitelli *et al.*, BTF activities presentation, 19 May 2008, Roma, Italy.

B. Buonomo *et al.*, EPAC, 23-27 June 2008, Genova, Italy.

4.1 Poster Session

L. Quintieri *et al.*, "Positron Channeling Experiments at the DAΦNE BTF Facility: the CUP Experiment", Channeling 2008, 25 Octobber 2008, Erice, Italy.

5 Technical Reports and articles during 2008

L. Quintieri *et al.*, "Feasibility Study of a Neutron Source at the DAΦNE BTF Facility", Report LNF-08-24(NT).

L. Quintieri *et al.*, "Design of the Radiation Shielding Around the DAΦNE BTF Target", Report LNF-08/23(NT).

References

1. L. Quintieri *et al.*, "Feasibility Study of a Neutron Source at the DAΦNE BTF", Report LNF-08-24(NT).
2. A. Fasso *et al.*, "A multi-particle transport code", Report CERN-2005-10 (2005), INFN/TC-05/11, SLAC-R-773.
3. W.P. Swanson, "Calculation of Neutron Yields Released by Electrons Incident on Selected Materials", Report SLAC-PUB-2042 November 1977.

DAΦNE-Light Laboratory and Activity

A. Balerna (Resp.), P. Calvani (Ass.), C. Castellano (Ass. Ric.),
M. Cestelli Guidi (Art. 23), R. Cimino, M. Commisso (Ass. Ric.), A. De Sio (Osp.),
L. Gambicorti (Osp.), A. Grilli (Tecn.), D. Hampai (Ass. Ric.), S. Ning (Ass.),
A. Nucara (Ass.), E. Pace (Ass.), M. Piccinini (Ass. Ric.), M. Pietropaoli (Tecn.),
A. Raco (Tecn.), V. Sciarra (Tecn.), V. Tullio (Tecn.), G. Viviani (Art. 15)

1 Summary

During 2008 on the IR and soft X-ray beamlines, new experiments were performed by Italian and European users in parasitic mode, during the SIDDHARTA runs, but also using 15 dedicated days for some specific experiments from March 2008 up to the end of July when the DAΦNE shutdown started and then from the middle of October up to the end of December 2008. In particular, 13 EU teams within the Integrated Infrastructure Initiatives for Transnational Access to Research Infrastructure (TARI) and 9 Italian teams with the submission of their scientific proposals to the Synchrotron Radiation Scientific Committee got access to the synchrotron radiation facility.

Experimental activities were also related to the organization and improvement of the existing soft X-ray and IR beamlines, to the reorganization of the UV beamline but also to the realization of two new XUV beamlines. Concerning the synchrotron infrared beamline (SINBAD), its instrumentation has been implemented in 2008 and now includes a diamond anvil cell for measuring the IR properties of samples at high-pressure up to 30 GPa. The focal plane array (FPA) detector ,installed in 2007, has been used for many interesting experiments including the first infrared imaging of single cells of rat glioma very important in the determination of the biodistribution of collagens (triple helical proteins) types within healthy and dystrophic connective tissues (Fig. 1).

X-ray fluorescence measurements were performed testing the silicon drift detector (SDD) installed in the experimental chamber of the soft x-ray beamline and, using the new cryostat ,EXAFS spectra at 77 K were taken at the Al and Mg K-edges. Concerning the x-ray beam alignment a relevant improvement was given by the installed fluorescent target and the double wire beam monitor that will be fully tested in 2009 (Fig. 2).

The upgrade of the UV branch-line with a new experimental area went on and the clean room has been equipped with a new VUV monochromator (120-300 nm) coupled to an HV experimental chamber designed to perform any kind of optical experiments like reflectivity, absorption, scattering and detector calibrations (Fig. 3) that will be commissioned in 2009.

Concerning the new XUV laboratory its construction has been continued and the low energy beamline (LEB) will probably be commisioned and will start delivering photons in the energy range 35 eV- 200 eV in 2009.

Among the many initiatives of 2008 mention should be given to the appoval of the European project E.LI.S.A. (European LIght Source Activities- FP7) for research cooperation involving the world largest network of synchrotron and FEL facilities throughout Europe that will start in 2009. Mention should also be given to the organization in October 2008 at the Frascati National

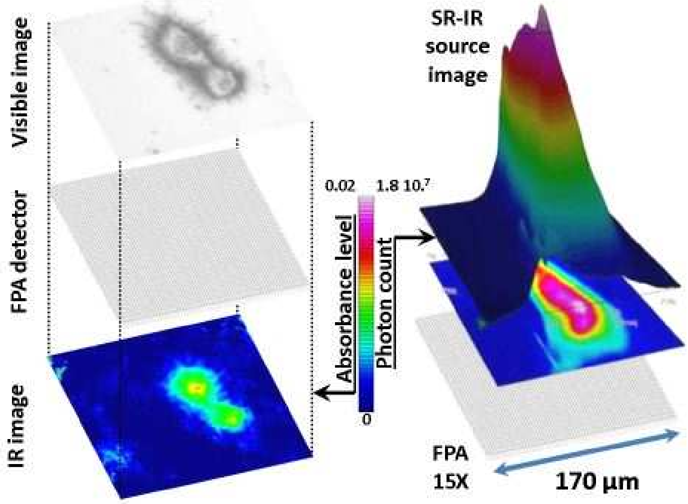

Figure 1: *Left panel: Visible image and infrared spectral mapping on a single cell of rat glioma giving the biodistribution of collagen types within healthy and dystrophic connective tissues. Right panel: Reconstruction of the IR DAΦNE source illuminating a FPA detector. Both FTIR images are in false colors and the intensity is associated to the integer of the spectrum in the spectral range 4000-850 cm^{-1}.*

Laboratory of the workshop *WUTA08* on Ultraviolet Techniques and Application which has seen the presence of many interested scientists.

2 Activity

2.1 SINBAD - IR beamline

SINBAD is the Synchrotron Infrared Beamline At DAΦNE, a facility that gives access to users for IR spectroscopy experiments since 2002. The beamline is equipped with two experimental stations which can be used also with conventional sources. Biomedical, chemical and material science research activity is performed in different conditions of temperature and pressure, and high resolution IR imaging of biological tissues and cells is taken with an Infrared microscope equipped with a 64x64-element focal plane array detector.

The beamline instrumentation has been implemented in 2008 and now includes a diamond anvil cell for measuring the IR properties of samples at high-pressure up to 30 GPa. The toroidal mirror focusing the radiation in the second interferometer has been bought and will be installed in the vacuum chamber in the second half of 2009, connecting definitively both experimental stations to the beamline. In 2008 experiments with synchrotron radiation have been performed in parasitic mode during SIDDHARTA runs and with 15 dedicated days for specific experiments.

The scientific activity at SINBAD was associated to experiments performed by Italian teams that submitted scientific proposals approved by the LNF Synchrotron Radiation Scientific Committee and by European scientists who got access within the EU framework of TARI I3 program.

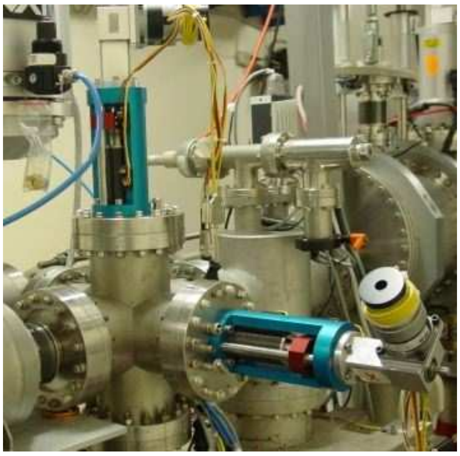

Figure 2: *Double wire beam monitor installed at the soft X-ray beamline.*

In 2008, 15 experimental teams (9 TARI + 6 Italians) were hosted and 27 experimental weeks were assigned. Italian projects included the participation of graduates and PhD students who had access to the IR beamline performing experiments together with the SINBAD staff. Measurements at SINBAD were performed also within the framework of the 5th INFN Committee with the experiment called *3+L* to test high speed infrared detectors to be used for DAΦNE beams diagnostics. Some of the 2008 scientific highlights achieved with the experimental activity are here summarized:

1. *Observation of Charge-Density-Wave Excitations in Manganites.* The optical conductivity of LaCa, NdSr, and BiSr manganites with commensurate charge order (CO) has been first observed in the Far infrared and sub-THz region. Below the ordering temperature TCO well-defined peaks are observed, associated with side bands. They are assigned to pinned phasons, and to combinations of phasons and amplitudons, respectively. In $La_{1+n/8}Ca_{n/8}MnO_3$with n = 5, 6, one can thus determine the electron-phonon coupling, the effective mass of the CO system, and its contribution to the dielectric constant. Their values support a description of the CO in LaCa manganites in terms of a CDW approach. In $Bi_{0.5}Sr_{0.5}MnO_3$, where TCO$\geq$ 500 K and the coupling is stronger, only the combination bands are clearly detected.

2. *Stain Effects Studied by Time-Resolved Infrared Imaging* Pattern formation in evaporating colloidal droplets is an important phenomenon that is commonly observed i n several solute-solvent systems; this is also an emerging technique for obtaining fine patterning through controlled conditions of drying. After evaporation of the solvent a ring-like pattern remains on the solid substrate under the condition of contact line pinning. A new analytical technique, time-resolved infrared imaging, has been used to investigate the formation of patterned structures with droplet drying, which is a typical time-dependent phenomenon. This technique was coupled with optical imaging to follow the evolution of the droplet shape and dimension in correspondence with the chemical images. The main advantage of the technique is represented by the possibility to have simultaneous spatial and time resolved information; the method was applied to a water-methylene blue system that has been studied during drying.

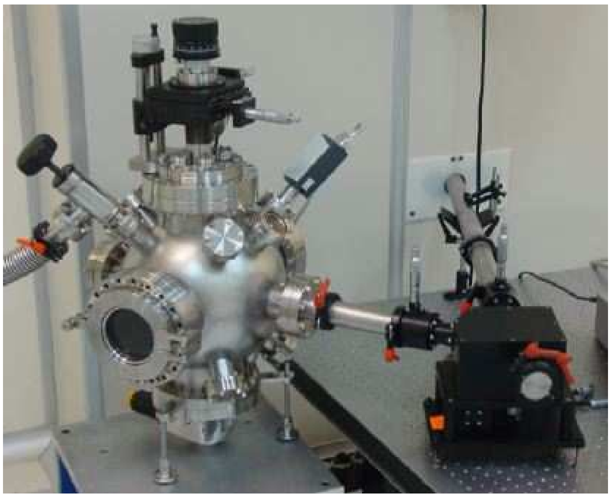

Figure 3: *The new VUV monochromator directly connected to the beam line and to the HV experimental chamber.*

The droplet profile change was monitored, in terms of water and methylene blue variation with time and space, at the droplet edge. The analysis has allowed a detailed reconstruction of the evaporating droplet profile with a micrometer scale resolution and of the change in concentration of the dye as a function of evaporating time. A uniform ring-like pattern, after evaporation in controlled relative humidity, was observed (Fig. 4). The data are consistent with a constant evaporation model, whose conditions are realized when a constant evaporation is achieved along the entire droplet. The technique has allowed elucidating the evaporation phenomenon close to the contact line in a dye solute-solvent system, which is very difficult to study with other techniques.

3. *FT-IR spectro-imaging of connective tissue alterations in muscular dystrophy.* Abnormal formation and organization of collagens network is commonly observed in several pathologies such as myopathies, and more particularly in muscular dystrophies. However, only a few analytical methods are able to provide information about collagen types biodistribution and assembly. The goal of this project was to map the distribution of collagen types within healthy and dystrophic connective tissues. Spectral imaging on a given tissue area allowed to reconstruct the chemical image of the tissue analyzed (Fig. 1). To our knowledge, this is the first infrared imaging of single cell performed with synchrotron radiation at resolution. The reason is that, to map the whole cell simultaneously with a Focal Plane Array detector, a very homogeneous, broad and intense source is needed. A broad source is usually not very bright, unless working at very high beam current like those circulating in the DAΦNE storage ring. It is quite interesting to note that the cell presented is a C6 rat glioma line made grow on silicon substrate for 24 hours and further cryofixed without addition of chemicals. Only cell contents and extracellular matrix produced by the cell during growth remain on the substrate after washing with saline buffer.

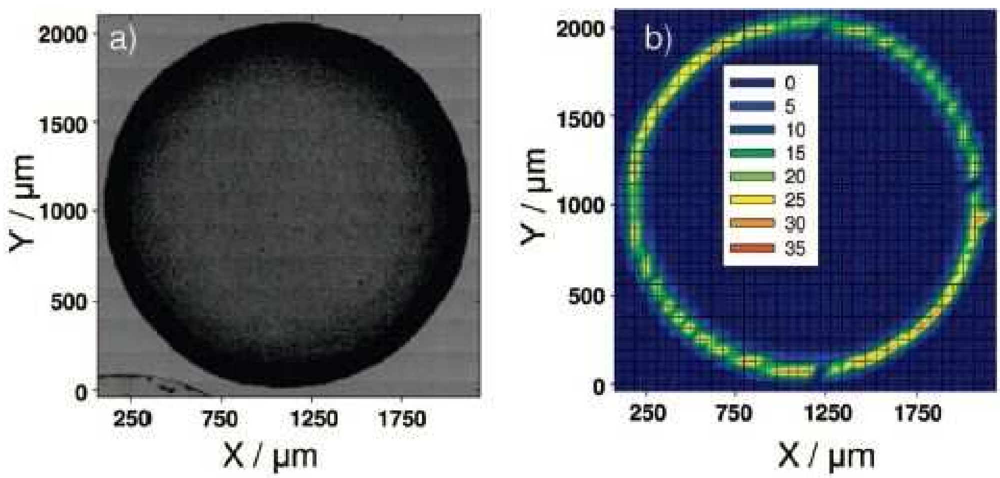

Figure 4: *Optical image (a) and infrared chemical image (methylene blue) (b) taken at the end of the evaporation process of a water droplet with methylene blue. The false colour scale represents the change of i ntegrated absorbance of the1600 cm^{-1}) band of methylene blue.*

2.2 DXR1 - Soft X-ray Beamline

The DAΦNE soft X-ray beamline, DXR-1, is mainly dedicated to soft X-ray absorption spectroscopy. The X-ray source of this beamline is one of the 6-poles equivalent planar wiggler devices installed on the DAΦNE electron ring (0.51 GeV) for the vertical beam compaction. The 6 wiggler poles and the high storage ring current (higher then 1 Ampere) give a useful X-ray flux for measurements well beyond ten times the critical energy. The useful soft X-ray energy range is 900 eV - 3000eV where the lower limit is given by the Beryl crystals used in the double-crystal monochromator and the higher limit is given by the wiggler working conditions.

During 2008 tests were performed on many of the important elements installed in 2007 like the SDD detector and the He cryostat for sample cooling (Fig. 5). All the allignments of the input and output slits and of the new support of the experimental chamber are now under remote control and are working quite well. In 2009 the final tests of the double wire beam monitor must be performed and new software must be developed to allow the aquisition of absorption spectra in fluorescence and total yield mode.

The scientific activity at the soft X-ray beamline included the use of 12 dedicated beam time days starting from May, after making some tests in April to check the beam stability and availabe flux, distributed between 4 experiments performed by Italian teams and 4 by European scientists that achieved the access within TARI program. The EU funded experimental runs related to the feasibility of the experimental proposal, accounted for a total of 4 experimental weeks with 8 dedicated beamtime days. Several Italian scientists coming from other Italian Institutions used the beamline with dedicated and parasitic beamtime for about 4 weeks (2 dedicated days). The LNF staff performed some tests using the SDD detector and the cryostat (2 IR dedicated days).

Some of the 2008 scientific highlights achieved by the performed experimental activities are

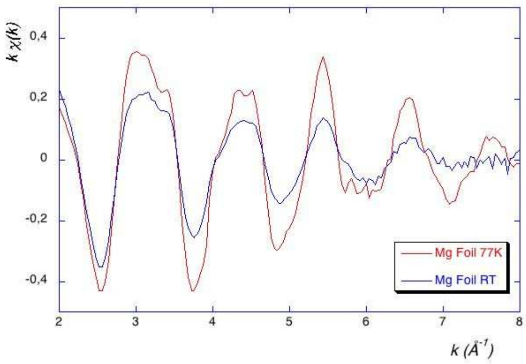

Figure 5: *Temperature induced Debye-Waller effect on the EXAFS (Extended X ray Absorption Fine Structure) signal of a magnesium foil at the Mg K-edge measured at the DAΦNE-L soft x-ray beamline.*

here summarized:

1. *Electronic structure of magnesium sulphate with and without amino-acid doping studied by infrared and X-ray absorption spectroscopy (TARI 68)* Epsomite or heptahydrite or $MgSO_4$ - $7H_2O$, hydrated magnesium sulfate, is one of only a few water soluble sulfate minerals. Among numerous magnesium salts, $MgSO_4$ is the most commonly used in the field of medicine and agriculture. $MgSO_4$ is often used in clinics for the treatment of pre-eclampsia (pregnancy-induced hypertension) and sometimes used as a tocolytic medication to slow uterine contractions during preterm labor. These salts are very important both in basic than in applied science, so the aim of the proposal was to understand the how their electronic structure changes as a function of the water content with and without amino-acids doping. This study is quite important because amino-acids are the building blocks of proteins. The authors of this experimental proposal succeeded in the crystallization of some of the $MgSO_4$ salts and of the amino acids doped $MgSO_4$ salts using solution growth methods. These crystals were characterized also by other techniques like X-ray diffraction, and optical measurements including IR by using laboratory sources at room temperature. The interesting results of the investigations performed at the DAΦNE-Light soft X-ray beam line using X-ray absorption near-edge structure (XANES) at the sulfur K-edge were likely to provide a selective investigation of the local atomic environment about the S atoms in the different systems studied. The amino acids included in the study at different percentages were: serine, L-alanine, L-glutamic and glycine.

2. *Characterization of $CuGaS_2$ and Mn-doped $CuInS_2$ and $AgInS_2$ by x-ray absorption near edge structure spectroscopy (TARI 88)* Semiconductors are of great scientific and technological interest in the realization of several electronic and optoelectronic devices. $CuGaS_2$, $CuInS_2$ and $AgInS_2$ belong to I-III-VI2 compound semiconductors [I = Cu & Ag; III = Al, Ga & In; VI = S, Se & Te] which crystallize with a tetragonal chalcopyrite-structure. These compound semiconductors have been extensively studied because of their wide range of direct

band gap over the infrared to ultraviolet spectral region and have attracted much interest, because of their potential applications in optoelectronic devices such as solar cells, optical parametric oscillators, light emission diodes laser diodes and non-linear optical devices. The t raditional approach for integrating magnetic and semiconducting phenomena is to substitute magnetic ions to nonmagnetic semiconductors, creating Diluted Magnetic Semiconductors (DMS). The presence of magnetic ions as dopants leads to a number of unusual electronic and optical properties, which offers a variety of unique device applications and luminescence properties. The major objective of this experimental proposal was to perform near-edge x-ray absorption spectroscopy at S K-edges in order to study how the electronic structure of Mn-doped compounds changes at different Mn percentages. X-ray absorption near-edge fine structure (XANES) spectra at S K-edge have been collected at the DAΦNE-L soft x-ray beamline to selectively investigate the local atomic environment around the S atoms. Many different spectra have been measured and the differences as a function of the dopant contributions are also clearly visible.

2.3 DXR2 -UV branch Line

The synchrotron radiation (SR) photon beam from a wiggler installed on the DAFNE storage ring is split by a grazing incidence Au-coated mirror ($\theta_i = 40$ mrad, cut-off energy about 800 eV), in order to provide the X-ray and UV beamlines. The reflected UV radiation travels through the UV beamline and ends in a 38 mm diameter sapphire window. The experimental apparatus installed at the exit window of the beamline is partially refurbishing and partially under construction.

The optical layout of the whole apparatus, that is shown in (Fig. 6), has been designed in collaboration with the Istituto Nazionale di Ottica Applicata at Firenze and it will allow measurements in a very wide spectral range from 120 nm up to 650 nm (2-10 eV).

The first experimental area (EXP1) is irradiated by monochromatic VIS-UV SR in the wavelength range 180-650 nm after exiting the beamline and being collected by two focusing mirrors (M1 and M2) and dispersed by a Czerny-Turner monochromator. This instrumentation was already available in a small hutch (A1) and has been refurbished and aligned. This light channel has been also provided by a 500 Watt Hg/Xe VIS-UV radiation source in order to perform experiments even when SR is off. This source is optically coupled to the entrance slit of the monochromator (the M2/M3 arrangement can be pulled up opening the optical path between the lamp and the monochromator) through a double-mirror system that is under development.

In order to extend the spectral coverage to shorter wavelengths, a MgF_2 entrance window has been substituted for the sapphire one and the optical system will be included in a high-vacuum (HV) chamber that has been designed and commissioned to an external mechanical workshop. This HV chamber will allow the SR beam propagation in vacuum. M1 will be remotely controlled and aligned by a two-axes manipulator that replaces a manual stage previously available. On the back of M2 has been arranged a divergent mirror (M3) having a focal distance 2 m long. A roto-translational manipulator having 3 axes and 2 rotational stages will allow the remotely controlled alignment of M2/M3 mirrors and following the beam in order to fix its position on the entrance slit of the monochromator. Thus, M3 replace M2 by a simple rotation in front of the VUV SR beam that after impinging on M1 and M3 is sent to the experimental areas EXP2 and EXP3 that

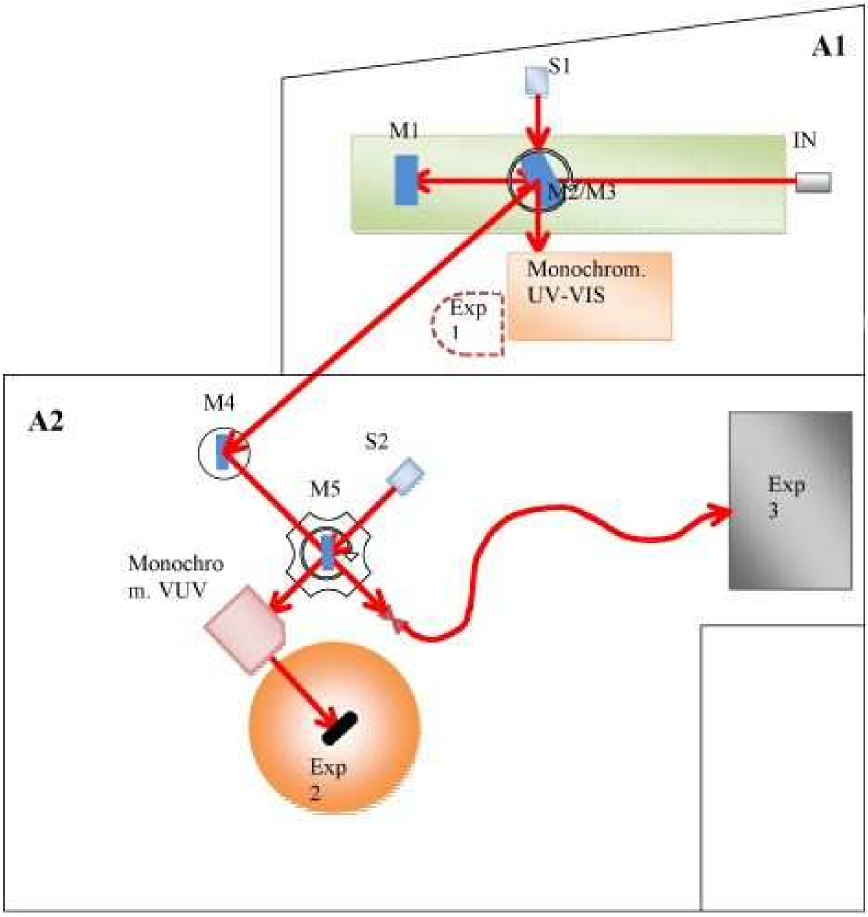

Figure 6: *Schematic layout of the experimental apparatus at the exit of the VIS-UV beamline.*

are located in a clean room (A2, class 10000). SR having wavelengths ranging between 120 nm and 650 nm is folded and focused by the M4 mirror onto another rotating mirror, M5. M5 can select the operational mode by sending radiation to a specific apparatus: a VUV monochromator (120-300 nm) that is coupled to an HV experimental chamber (EXP2) or to and UV-grade optical fiber that bring SR to an optical bench (EXP3) where the beam can be used filtered or not for testing and calibration measurements of optical components and detectors or to irradiate any kind of material sample.

The EXP2 HV chamber has been designed in order to perform any kind of optical experiments: reflectivity, absorption, scattering, detector calibration, etc. A rotational stage, moving also along the z-axis can put any sample in the center of the chamber and in front of the focused SR beam. Another rotational stage, entering from the bottom, moves a C-shaped arm that can support a photon detector in order to measure the incident SR beam intensity or the reflected, diffused or scattered radiation at any angle from the incident beam direction. By rotating M5, a 150 Watt D2 VUV radiation source can also be selected and put in line when SR is off, thus allowing a full-time use of the facility.

The instrumentation of this apparatus will be fully remotely controlled by a specifically designed software developed in house. I/O peripherals and interfaces as well as data acquisition instrumentation has been acquired in order to have a remote control of any experimental step and to facilitate the users. The just described experimental apparatus has been designed and developed mostly during 2008. All the instrumentation has been already acquired. Only the HV chamber hosting the front-end optical system is still under construction. Therefore, the experimental setup will be completed when this important component will be delivered to our laboratory (expected March 2009). In the meantime, testing of vacuum components, testing of the remotely controlled movements, testing of the radiation sources, and testing of the delivered optical systems have been carried out. Wavelength calibration of the two monochromators has been performed and the remote control and data acquisition will be completed in March 2009.

The EXP1 area is now available for VIS-UV experiments; testing experiments on carbon nanotube UV detectors and on the VIS-UV optical properties of nanodiamond powders have been carried out in the last months of 2008 and a poster have been presented to the WUTA08 Italian workshop in October 2008.

2.4 New XUV beamlines

In 2008, the construction of the new XUV laboratory has continued, based both on the detailed plans approved by the Synchrotron Radiation Scientific Committee and on the available resources. This new laboratory should host two bending magnet (BM) beamlines covering the photon energy range from 30 eV to 1000 eV: one will cover the low energy part of this interval (30-200 eV) and is called LEB (Low Energy Beamline), the other will cover the range from 100 to 1000 eV and is called HEB (High Energy Beamline). All the optical and vacuum components of the LEB beamline were purchased and mounted during 2008.

Figure 7: *Picture of the entire LEB Beamline as installed i n 2008 in the DAΦNE XUV laboratory.*

In figure 7 a panoramic picture is reported, were a series of photos have been collated to give an ensamble overview of the entire hardware built in the XUV laboratory. On the blue stand there is the sperical grating monochromator (SGM); moving backwards there are the pipes connecting the focussing mirror (LB2) and the first optical element in the DAΦNE hall; moving forward there is the last refocussing optic (LT3).

All the system is in vacuum contact to the main ring and is all in UHV but the connecting pipes from the ring to the laboratory, which are NEG coated chambers (LHC type) and need to be backed removing the present lead safety screen. Unfortunately this operation could not be accomplished during the last part of 2008 due to the nearly continuous operation of the accelerator. In figure 7 ion gauges and pneumatic valves along the whole beamline are also visible. Safety protocol and control systems have been established (with the aid of the Control Service of the Research Division) and will be completed and tested as soon as possible. In the course of 2009 we plan to finally commission the entire LEB beamline and start to deliver photons from 35 eV to 200 eV to interested users. Fig. 8 shows an artistic view of this second high energy beamline. In parallel the optical elements and UHV vacuum chambers needed for the construction of the HEB, have been defined, and for most of them all the procedures needed for their purchasing have been completed; they will be delivered,tested and installed in our laboratory during 2009.

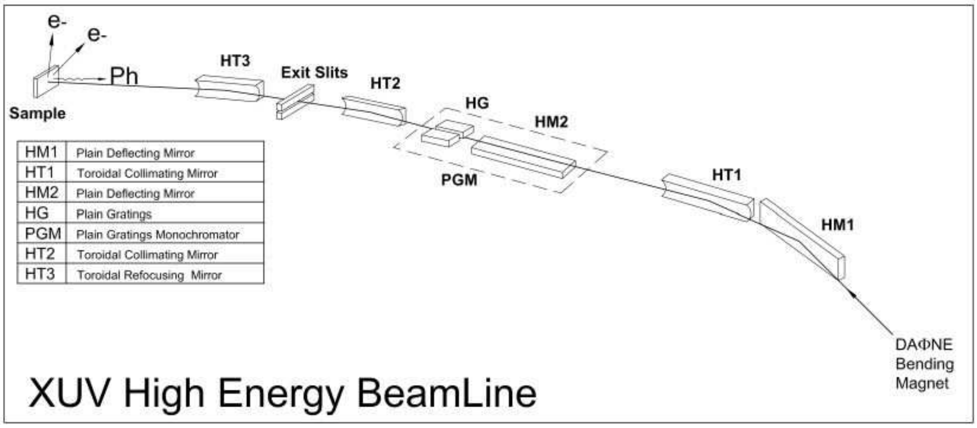

Figure 8: *Artistic view of the XUV-HEB optical lay out. All the optical elements are described in the text.*

The HM1 and HT1 mirrors are both hosted in the pre-optic chamber in the DAFNE building (see annual report 2007). These mirrors are used to deflect the emitted BM radiation, into the tunnel conducting to the XUV-laboratory maintaining the angle of incidence on each optical element to be 3^o in order to get a high photon reflectivity up to 1000 eV. The toroidal mirror HT1 is at 3.6 m from the source and collimates into a parallel beam 6 x10 mrad^2 (vertical x horizontal acceptance) of the total solid angle emitted by the stored electrons. After this the beam travels into the laboratory entering in a slit-less PGM (plain grating monochromator) which consists of a deflecting plane mirror HM2 and 2 interchangeable plain gratings (PG1 with 800 l/mm and PG2 with 1200 l/mm) which are optimized for 60-250 eV and 200-1000 eV energy ranges respectively. The monochromatized beam is then focussed both vertically and horizontally into the exit slits by the HT2 mirror. Finally HT3 is used to refocus the spot emerging from the slits at the sample position.

The performances of such HEB beamline have been calculated and will need careful testing and experimental verification. During 2009 we plan to mount the entire HEB beamline and to start testing all the components to be ready to deliver photons from 60 eV to 1000 eV to interested users from 2010.

References

1. C. Petibois and M. Cestelli Guidi, Anal. Bioanal. Chem. **391**, 1599 (2008).
2. A. Nucara *et al.*, Phys. Rev. Lett. **101**, 066407 (2008).
3. P. Innocenzi *et al.*, J. of Phys. Chem. A **112**, 6512 (2008).
4. D. Di Gioacchino *et al.*, J. of Phys. and Chem. of Solids **69**, 2213 (2008).
5. A. Nucara *et al.*, Phys. Rev. B **77**, 064431 (2008).
6. P. Innocenzi *et al.*, Journal of Sol-Gel Science and Technology **48**, 253 (2008).
7. G. Della Ventura, F. Bellatreccia, and M. Piccinini, American Mineralogist **93**, 1538 (2008).
8. I. Ascone *et al.*, Inorg. Chem. **47**, 8629 (2008).
9. W.M. Kwiatek, M. Podgorczyk, C. Paluszkiewicz, A. Balerna, and A Kisiel, Acta Physica Polonica A **114**, 463 (2008).
10. L. Reale *et al.*, Microscopy Research and Technique **71**, 459 (2008).

GILDA
(General Purpose Italian Beamline for Diffraction and Absorption at ESRF)

A. Balerna, A. Grilli (Tecn.), S. Mobilio (Resp.),
A. Raco (Tecn.), V. Sciarra (Tecn.), V. Tullio (Tecn.)

1 Introduction

GILDA (General Purpose Italian BeamLine for Diffraction and Absorption), is the Italian CRG beamline, built to provide the Italian scientific community with an easy access to the European Synchrotron Radiation Facility to perform experiments with a high energy and brilliance X-ray photon beam. GILDA was proposed, designed, constructed and commissioned by a collaboration between LNF and a large number of University groups; it is operative since autumn 1994. Today GILDA is funded by the Italian public research Institutes: Consiglio Nazionale delle Ricerche (CNR) and Istituto Nazionale di Fisica Nucleare (INFN). Experimental stations for X-ray Absorption Spectroscopy, Anomalous X-ray Scattering and X-ray Diffraction (XRD) are present on the GILDA beamline.
The LNF group is involved in the technical maintenance and update of the beamline, with particular emphasis to the electronic and software controls of all the instrumentation and to the apparatus for X-ray diffraction.

2 Summary of the Activity on the GILDA beamline during 2007

The main technical activity during 2007 were: the installation of a new LINUX based VME in the absorption hutch; the implementation of a very high signal/noise ratio acquisition system on 200 μm-tick optical fiber; a mechanical system for optimize the measure of spectra in grazing incidence, without the use of the REFLEXAFS chamber; an on-fly XAS data analysis software package; a liquid nitrogen cryostat for diffraction experiments; the recording and data analysis of full Debye scattering via the radial distribution function formalism.
4000 hours of the 5300 delivered by ESRF were used for user's experiments; a total of 45 experiments were performed, 33 of Italian users and 12 of European users.
Among the relevant studies performed, we mention the study on Indium-Barium cerate for fuel cell, the test of diamond detectors for X-ray applications, the study of Fe implanted in InGaP alloys, which produce a semi-insulating material, the binding site of Zn in respiratory enzymes, the study on exchange bias magnetic materials, on negative thermal expansion materials like CuCl, the analysis of pigments in decorated archaeological pottery.

3 Activity on the GILDA beamline during 2008

During 2008 many technical works were performed on the instrumentation both to keep the very good beamline efficiency at an internationally competitive level and to upgrade its characteristics. Namely:

1. The recently acquired fluorescence detector based on a Laue diffracting crystal was successfully tested at the K edges of Cr, Mn and Fe. A resolution of 140 eV was achieved, with an excellent rejection of the elastic scattering.
2. A new motorized sample holder was designed, realized and tested; the new holder allows the alignment of the sample at grazing incidence with high accuracy; it can be cooled down to 120K.
3. A software programme for a complete quantitative data analysis of the ReflEXAFS spectra was developed and successfully tested on standards compounds.
4. A new limit switch system was installed on the safety beam shutter of the optical hutch; the new system allows a rapid change of the beamline configuration from the low energy one with mirrors to the high energy one without mirrors, and viceversa.
5. A standard criterium for the use of the beamline with or without the mirrors was defined; Pd mirrors are used in the spectral range 6-18 keV, the Pt ones to extend the range up to 26 keV; the mirror are not used above 26 keV.
6. The first nanocluster samples have been successfully produced using the sputtering source at the LNF.

4 Beamtime use during 2008 and scientific outcomes

During 2008 ESRF delivered beam for about 5300 hours; about 4000 hours were used for user's experiments,the remaining for in-house research, beamline improvements, maintenance and alignment. Totally 37 experiments were performed, 25 of Italian users and 12 of European users.
Studies and results to be mentioned are the followings:

1. *Exchange bias and structural disorder in the nanogranular Ni/NiO system produced by ball milling and hydrogen reduction.* The exchange bias effect has been studied in Ni/NiO nanogranular samples prepared by mechanical milling and partial hydrogen reduction of NiO; the Ni weight fraction varied between 4 and 6 per cent. In this procedure, coarse-grained NiO powder has been ball milled in air for 20 h and subsequently subjected to annealing in H2 (at a temperature ranging between 200 and 300 C) to induce the formation of metallic Ni. The structural properties of the samples have been studied by x-ray diffraction, electron microscopy, and extended x-ray absorption fine structure. The magnetic properties have been extensively investigated by carrying out hysteresis loops and magnetization measurements in the 5300 K temperature range, in zero-field-cooling and field-cooling conditions. The results indicate that both in the as-milled NiO powder and in the hydrogenated samples, the NiO phase is composed of nanocrystallites (having a mean size of 20 nm, structurally and magnetically ordered) and of highly disordered regions. The samples with low Ni content (up to 15 per cent) can be modelled as a collection of Ni nanoparticles (mean size of 10 nm) dispersed in the NiO phase; with increasing Ni content, the Ni nanoparticles slightly increase in size and tend to arrange in agglomerates. In the Ni/NiO samples, the exchange field depends on the Ni amount, being maximum (600 Oe), at T=5 K, in the sample with 15

per cent Ni. However, exchange bias is observed also in the as-milled NiO powder, despite the absence of metallic Ni. In all the samples, the exchange bias effect vanishes at 200 K. We propose a mechanism for the phenomenon based on the key role of the disordered NiO component, showing a glassy magnetic character. The exchange bias effect is originated by the exchange interaction between the Ni ferromagnetic moments and the spins of the disordered NiO component (in the as-milled NiO powder, the existence of ferromagnetic moments has been connected to chemical inhomogeneities of the NiO phase). The thermal dependence of the exchange bias effect reflects the variation of the anisotropy of the NiO disordered component with temperature.

2. *Atomic structure of Mn-rich nanocolumns probed by x-ray absorption spectroscopy.* Extended x-ray-absorption fine-structure (EXAFS) technique was used to investigate the structure of Mn-rich self-organized nanocolumns grown by low temperature molecular beam epitaxy. The EXAFS analysis has shown that Mn-rich nanocolumns exhibit a complex local structure that cannot be described by a simple substitutional model. Additional interatomic distances had to be considered in the EXAFS model which are in excellent agreement with the structure of a Ge3Mn building block tetrahedron of Ge3Mn5.

3. *Diamond solid state ionization chambers for x-ray absorption spectroscopy applications.* The photoresponse of a diamond detector has been compared with a standard ionization chamber in x-ray absorption spectroscopy applications. A photoconductive device based on a nitrogen-doped single crystal diamond has been tested by synchrotron radiation. Time stability and linearity have been studied by x rays at 10 keV to assess its performances. Finally, extended x-ray absorption fine structure at the Fe K-edge was carried on a standard iron target using both the diamond device and the IC. Spectroscopical results have been compared including references to literature.

4. *Temperature dependence of the structural parameters of gold nanoparticles investigated with EXAFS.* The L3 edge of Au nanoparticles, having sizes ranging from 2.4 to 5.0 nm, have been investigated by x-ray absorption fine structure spectroscopy in the temperature range of 20300 K. Data were recorded at the European Synchrotron Radiation Facility with a very good signal to noise ratio. To achieve a very high accuracy in the determination of the first shell distance, a very careful data analysis was performed also taking into account the presence of asymmetry effects. In all samples, the temperature dependence of the first neighbor distance results is different from that of the macrocrystalline counterpart. In the largest size samples, a reduction of the thermal expansion was found, whereas in the smallest ones, the presence of a crossover from an initial thermal expansion to a thermal contraction was observed. Calculations based on a simple model show that localization effects that increase as the nanoparticle size decreases can explain the reported thermal effects.

5 2009 - GILDA Forseen Activity

During the 2009 the activity foresees the followings:

1. a standard vacuum and safety control system, compatible with those in use at the ESRF, will be implemented on the beamline;
2. the motor control system based on the new ICEPAP cards developed at the ESRF will be implemented;
3. the nanocluster sputtering source now operative at the LNF will be used to produce magnetic clusters to be investigated at the ESRF.

6 Publications

1. T. Comaschi, A. Balerna, and S. Mobilio, Phys. Rev. B **77**, 075432 (2008).

NTA-CLIC
(CLIC Test Facility 3)

D. Alesini, C. Biscari, B. Buonomo (Art. 23), M. Castellano, A. Ghigo (Resp.),
F. Marcellini, M.A. Preger, M. Serio, A. Stella, C. Vicario (Art. 23)

1 Introduction

The Compact Linear Collider Test Facility (CTF3) project aims to study the feasibility of an electron-positron linear collider, with c.m. energy up to 3 TeV, based on two-beam acceleration scheme. Acceleration gradient of 100 MeV/m, provided by high power 12 GHz radio-frequency generated by a powerful electron drive beam, has to be demonstrated. The INFN Frascati Laboratory (LNF) designed the two rings of the drive beam recombination system in the framework of CTF3-CLIC international collaboration. The first ring, named Delay Loop, was realized under LNF fully responsibility, installed in 2005 in the existing building at CERN and commissioned in 2006. INFN was in charge of the construction of the RF deflectors, the vacuum chambers and diagnostics of the second ring (Combiner Ring), installed in 2006 and completed in 2007. In 2008 the commissioning of the ring continued sharing the machine time with the installation of the CLIC experimental area.

2 LNF Group Contribution in year 2008

In 2008 the LNF group has been involved in the Combiner Ring commissioning and contributed to the multiplication of the electron beam current by injecting up to four train of bunches with the interleaving bunches technique. Vertical beam instability, observed at high current, was measured and studied. The trapped RF parasitic mode, responsible for the instability, was recognized in the injection RF deflectors. New RF deflectors have been studied, and realized during the first months of the year, with special loops inserted in the cavities of the deflector structure, to extract the parasitic dangerous mode and damp it on an external load. The new RF deflectors have been realized in aluminum, instead of copper; the RF cavities are machined in half-cells, clamped and welded on the external side. This technique permits to avoid brazing procedure and limit the total cost. After the low power tests the RF deflectors were installed in the Combiner Ring and tested at the nominal power: no multi-pacting effect has been observed during the test. The commissioning of the Combiner Ring restarted with the new RF deflectors and the vertical instability disappears. The multiplication of the current of factor 4, bypassing the delay Loop, has been proved with no significant losses achieving current of 14A on 280 nsec pulse-length.

3 Foreseen activity of the LNF group during year 2008

In 2009 the foreseen activities include the commissioning of the Delay Loop and Combiner Ring together to achieve the CTF3 nominal current and the participation to the CLIC Test Facility scientific program.

4 References

http://accelconf.web.cern.ch/AccelConf/e08/papers/wepp125.pdf
http://accelconf.web.cern.ch/AccelConf/e08/papers/tupd014.pdf
http://accelconf.web.cern.ch/AccelConf/e08/papers/mopp010.pdf
http://accelconf.web.cern.ch/AccelConf/e08/papers/mopp011.pdf

NTA-DISCORAP

G. Celentano (Ass.), A. Della Corte (Ass.), U. Gambardella (Resp.)

1 General program

The DISCORAP (DIpoli Super COnduttori RApidamente Pulsati) program comes out from the new requirement of developing fast ramped superconducting dipoles for the SIS 300 of the FAIR accelerator complex at GSI, Darmstadt, Germany. The four years program includes the development of a fully working bent dipole 3.8 m long in its horizontal cryostat. The dipole peak field is 4.5 tesla with ramping rate of 1 tesla/sec [1]. Among other requirements it has to keep dissipations at reasonable levels as well as to generate low harmonic contents [2]. Three INFN sections are involved: Genova (group leader), Milano LASA, and LNF, in cooperation with Ansaldo Superconduttori Genova, Italy, and LUVATA, Finland. The Frascati group, made of *LNF* and *ENEA* Frascati researchers, in 2008 took care of wire characterizations, analyzing NbTi superconducting wires for low losses applications previously developed in the framework of other projects, and the design of horizontal cryostat [3]. In Nov. 2008 we also had a two days Technical Design Report in Genova. The TDR was reviewed by an international group of experts, from CERN, LBNL and ITER, aimed to examine the whole design and the tests in progress before starting the construction of the dipole.

2 Resume of the Frascati group activity

Our activity on NbTi wire characterization is always present in the projects, as we are refining further techniques to increase the capability of measuring the transverse resistivity too. In fact, after the magnetization losses, the coupling losses among the superconducting filaments, are one of the dominant losses for the dipole, being $\sim 1/4$ of the total losses. This study was initially carried out with VSM measurements at different ramp rates. In Figure 1 are shown the M(H) curves for wire type SC356, a NbTi wire with a 2.5 μm filament size manufactured by Supercon Inc., designed for the SSC project [4]. These cycles were limited to 4.0 T $\pm$ 0.5 T and performed at different ramp rates, ranging from 0.3 mHz to 8.3 mHz, within the limits of our equipment. The area within the cycle represents the total losses, *i.e.* the irreversible and eddy current losses.

In order to have the same information with different techniqes we also set up the ac magnetic susceptibility option in the magnetometer. In fact the out of phase susceptibility signal χ" coming from the voltage picked up around the sample, under sinusoidal excitation at a given frequency, is straight related to the ac losses. The technique, previously developed at INFN Genova, consists in analyzing the χ" signal as a function of the frequency.

We ara also in charge of the design and procurement of the horizontal cryostat for the bended dipole. The cryostat, although it is not designed to be used in the SIS 300, will have specific features as the machine cryostats. Our design is based on the latest dipole design (LHC, RICH, etc.) including plastic supports for the cold mass. However the marked bending of our dipole, which

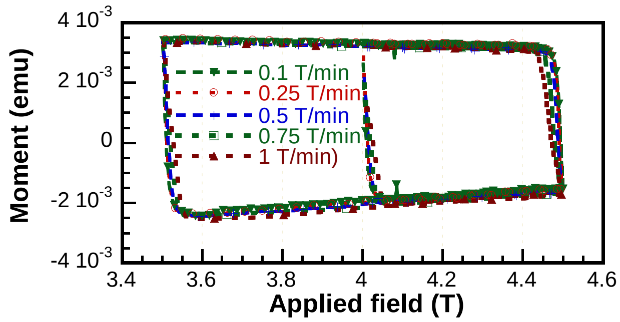

Figure 1: *M(H) 1 T cycles for SC356 wire at different ramp rates.*

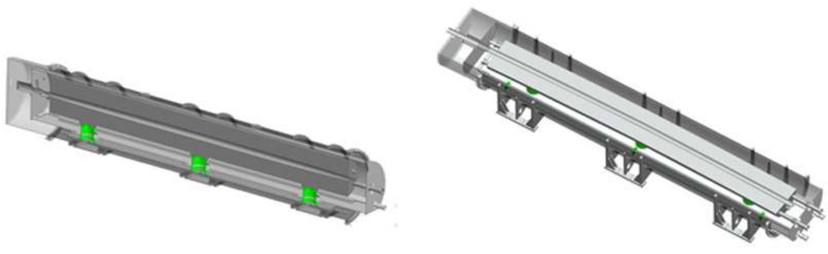

Figure 2: *Vertical and horizontal 3D cross sections of the cryostat with the cold mass. The curvature of the magnet follows the central beam tube.*

loose the straight symmetry, made the design difficult. In fact, in spite of the straight geometry of the outer shell, the mechanical analyses revealed new problems on the mechanical stability of the dipole, which have to be supported by the cryostat pillars and structure. In Fig. 2 are reported two cross sections of the cryostat, vertical and horizontal, with the cold mass supported by three plastic POSTs (green color in the Fig. 2). As we cannot afford specific development for the POSTs we adopted the LHC POSTs as they are, i.e. not optimised for our design. We performed full mechanical stress analyses on the 6 ton cold mass within the cryostat, either static and dynamic, setting the special supports needed for the transport of the whole assemby from Italy to GSI. We found that in static conditions the compressive stress on the plastic supports are largely below the critical ones, as expected from using LHC POSTs designed for 25 ton magnets, but also the unexpected shear stresses, related mainly to the bending of the cold mass, are lower than the critical ones.

References

1. P. Fabbricatore *et al.*, IEEE Appl. Supercon. **18**, 232 (2008).
2. M. Sorbi *et al.*, IEEE Appl. Supercon. **18**, 138 (2008).
3. G. Volpini *et al.*, IEEE Appl. Supercon. **18**, 997 (2008).
4. http://indico.cern.ch/getFile.py/access?contribId=41&sessionId=8&resId=1&materialId=paper&confId=28832

NTA-ILC

D. Alesini, M. E. Biagini, R. Boni, R. Cimino, T. Demma (Art. 23), G. Di Pirro,
A. Ghigo, S. Guiducci (Resp.), F. Marcellini, S. Pella (Tecn.), P. Raimondi,
G. Sensolini (Tecn.), A. Stecchi, C. Vaccarezza

1 Introduction

The INFN has contributed to the project design and R&D for the International Linear Collider (ILC) with a qualified participation to the GDE (Global Design Effort). The INFN activity is focused on the superconducting accelerator technology and on the Damping Rings (DR). The groups participating in the collaboration are: LNF, LNL, Milano (LASA), Pisa, Roma Tor Vergata. The INFN groups actively contributed to the preparation of the "Reference Design Report" (RDR) [1] with the cost estimate, presented at the 9th ACFA ILC Physics & Detector Workshop & GDE Meeting (IHEP, Beijing 4-7 February 2007). The LNF activity is focused on damping rings. The possibility of making experimental observations at DAΦNE offers a great opportunity to test simulation studies and prototypes. The DR activity is fully integrated at the European level with the coordination of the DR work package of the EUROTeV design study.

2 Year 2008 Activities

The next phase of the ILC Global Design Effort should produce a technical design of the accelerator in sufficient detail that project approval can be sought in a timescale when LHC results justify the project. In this phase the GDE activity will be focused on the crucial R&D issues that allow to reduce the cost and improve the performance of the accelerator. For the Damping Rings these issues are: mitigation of the e-cloud instability, fast kickers and low emittance tuning. The first two issues are the objective of R&D at DAΦNE, which is considered as a DR test facility together with CesrTA and KEK-ATF. In 2008 fast kickers with pulse rise/fall times of less than 6 ns and maximum voltage of 45 kV have been tested with beam at DAΦNE [2, 3, 4, 5]. A pulse duration according to the design and a high injection efficiency have been measured but the fast pulsers have shown poor reliability. After long interactions with the producers, it has been decided to use a different type of pulser with reduced voltage (20 KV) that should be more reliable. The injection optics of the DAΦNE ring has been modified in order to accept injection at a lower voltage. A new ultra fast kicker, with pulse duration suitable for the 3 ns bunch distance, has been designed and is under construction. This kicker, designed to get a low beam impedance, will be tested at KEK-ATF2, the beam delivery international test facility.

The e-cloud instability is the most crucial DR beam dynamics issue since it could produce a limitation of the maximum stored current or a growth of the vertical beam emittance for the positron DR. Studies on the e-cloud instability in the DAΦNE positron ring, and in particular in the wigglers, are in progress. Simulation studies have been performed to understand the dependency of the instability on the various machine parameters [6, 7]. These studies have shown a good agreement between simulations and experimental data and have reproduced the growth time and the main oscillation mode of the instability as observed by the diagnostic tools of the transverse feedback system [8, 9]. Recently, on the DAΦNE positron ring a second feedback to contrast the e-cloud instability has been installed. The damping time of a single feedback has been halved, achieving a value of 4.3 μs, corresponding to 13 machine turns and the maximum stored current has been increased from 0.8 A to 1.1 A [9]. This result is very interesting since for the DR it is required a feedback system with a damping time of a few machine turns.

Toward the end of 2008 the design of the optical structure for a short DR, with a length of 3.2 km (instead of the present 6.4 km), based on the SuperB arc cell, has started. It will be used for the study of the Minimal Machine, i.e. the minimal configuration of the accelerator that allows to achieve the design performance.

3 Plans for Year 2009

The LNF activity will continue to focus on damping rings and in particular on fast kickers and e-cloud studies. The new fast kickers are operating on DAΦNE and will be tested for continuous operation. The new ultra fast kicker, with pulse duration suitable for the 3 ns bunch distance, will be tested at KEK-ATF2. Another kicker will be installed on the DAΦNE positron ring to be used as the backend of the second horizontal feedback system. The comparison between simulations and experimental observations at DAΦNE will continue in order to improve the comprehension and mitigate the electron cloud instability. LNF will be involved in the project of modelling and reducing the DR vacuum chamber impedance providing the drawings of the low impedance bellows developed for the DAΦNE upgrade. The optimization of the optical structure and dynamic aperture for a short DR, proposed for the Minimal Machine, will continue in 2009. The R&D on fast feedback systems will continue with special attention to the effect of the feedback on the vertical beam emittance. The effect of wigglers on beam dynamics is a relevant issue for the ILC DR, which need a wiggler section nearly 200 m long to achieve the nominal damping time. In 2007 a modification of the poles of the DAΦNE wigglers has been studied to reduce the nonlinear components of the magnetic field on the beam trajectory and to improve the dynamic aperture [10]. This modification has been realized and will be tested with beam measurement within 2009.

4 References

1. N. Phinney *et al.*, International Linear Collider Reference Design Report, August 07, ILC-Report-2007-001; Report LNF - 07 / 9(NT).

2. D. Alesini *et al.*, Design and Tests of New Fast Kickers for the DAΦNE Collider and the ILC Damping Rings. Proc. of EPAC06, Edimburgh, Scotland, 1502, (2006).

3. F. Marcellini, "Fast kickers status", Presented at EUROTeV Annual meeting, LNF, Frascati, January 23-25 2008; (http://ilcagenda.linearcollider.org/conferenceDisplay.py?confId=2410.)

4. F. Marcellini, "Fast kickers status", Presented at Final EUROTeV Scientific Workshop, Uppsala University, Sweden, 26-28 August 2008; (http://www5.tsl.uu.se/EUROTeV2008/.)

5. F. Marcellini, "Fast kickers tests and bellows impedance at DAΦNE", Presented at LCWS08 - ILC Linear Collider Workshop, Chicago, 15-20 Nov. 2008;
(http://www.linearcollider.org/lcws08/.)

6. T. Demma *et al.*, "Electron Cloud Simulations for DAΦNE", Proc. of EPAC08, Genova, Italy, June 23-27, (2008).

7. T. Demma, "Electron Cloud Studies at DAΦNE", Presented at Final EUROTeV Scientific Workshop, Uppsala University, Sweden, 26-28 August 2008;
(`http://www5.tsl.uu.se/EUROTeV2008/.`)

8. T. Demma, Preliminary simulation results for e-cloud induced instability at DAΦNE. Presented at LCWS08 - ILC Linear Collider Workshop, Chicago, 15-20 Nov. 2008.

9. A. Drago, "Fast feedbacks for diagnostics and mitigation of e-cloud instability", Presented at LCWS08 - ILC Linear Collider Workshop, Chicago, 15-20 Nov. 2008.

10. S. Bettoni *et al.*, "Reduction of the Non-Linearities in the DAΦNE Main Rings Wigglers", Proc. of PAC07, Albuquerque, New Mexico, 1463, (2007).

NTA PLASMONX

C. Benedetti, P. Londrillo, S. Rambaldi, G. Turchetti
Sezione INFN Bologna

R. Bonifacio, M. Castellano, A. Clozza, L. Cultrera, G. Di Pirro, A. Drago, M. Esposito, M. Ferrario, D. Filippetto, A. Gallo, G. Gatti, P. Gaudio, A. Ghigo, A. La Monaca, M. Migliorati, D. Nanni, L. Palumbo, M. Richetta, C. Sanelli, F. Tazzioli, A. Tenore, F. Terra, S. Tomassini, C. Vaccarezza, C. Vicario
Laboratori Nazionali di Frascati

A. L. Bacci, F. Broggi, M.M. Cola, A. Flacco, C. Maroli, M. Passoni, V. Petrillo, N. Piovella, R. Pozzoli, M. Romé, A. R. Rossi, L. Serafini
Sezione INFN Milano

D. Batani, A. Galassi, G. Lucchini, R. Jafer, R. Redaelli, R. Benocci, T. Desai
Sezione INFN Milano Bicocca

U. De Angelis, S. De Nicola, R. Fedele, G. Fiore, C. Nappi
Sezione INFN Napoli

S. Betti, C.A. Cecchetti, A. Giulietti, D. Giulietti, A. Gamucci, L.A. Gizzi, P. Koester, L. Labate, T. Levato, A. Macchi, P. Tomassini, M. Vaselli
Sezione INFN and CNR Pisa

1 Summary

The 2008 has been a very fruitful year for the NTA-PLASMONX project. The laser laboratory has been completed and equipped, the laser FLAME assembled and tested at Amplitude Technologies laboratories, the first Laser-Plasma Acceleration experiment (full Italian!) successfully performed in Pisa, new experimental results useful for the project main goals obtained at European laser facilities and at BNL, the design of the e-beam and interaction chamber for the Thomson Scattering based X-ray source completed. Moreover the theoretical and simulation groups have fully supported the experimental activity and anticipated the future scenario of the LPA experiments and X-ray innovative sources that will be carried out in the very next future at LNF. All that will be shortly presented in the following.

2 FLAME

During 2008, construction of the FLAME laser system was carried out at Amplitude Technologies, following requirements and specifications defined during the tender procedure. Several visits of the FLAME team were carried out at Amplitude, including a session for measurements on timing and synchronization, a preliminary acceptance test and a final acceptance test. Final tests included full system energy measurements, survey of the pulse duration optimization procedure, pulse duration measurer nents, including the control-command interface (see Figure 1).

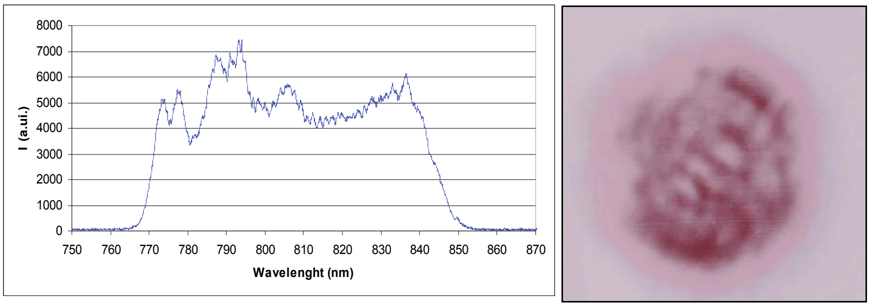

Figure 1: *Left: Spectrum of the laser pulse after amplification showing a bandwidth exceeding 70 nm. Right: Single shot 7 J burn pattern.*

The main parameters of the system measured during the final acceptance test at the factory, during full energy operation at 10 Hz rep. rate are: 5.6 J (energy after compression); 23 fs (pulse duration); 250 TW (peak power), $< 10^{10}$ (ASE contrast); $< 10^{-8}$ (pre-pulse contrast). The average energy (before compression) was measured to be 7.07 J.

3 FLAME laboratory

During 2008 the construction of the FLAME building was completed as shown in the Figure 2 and the design of the entire laboratory layout was carried out including all main subsystems and components: clean room for hosting the laser system, beam transport to the FLAME underground target area and to the SPARC bunker, electricity and ethernet networks, water cooling and air conditioning. Detailed design of the FLAME target area for the planned test experiment on self-injection was also carried out. Procurement for the construction of the beam transport vacuum line and for the set up of the test experiment was started, including the main mirrors, the focusing off-axis parabola and the main experimental diagnostics (see Figure 3).

Figure 2: *FLAME building at LNF completed on 23rd June 2008.*

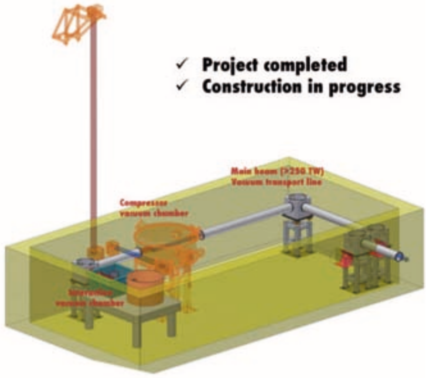

Figure 3: *Design of the layout of the underground target area of the FLAME laboratory, with the main compressor chamber, the vacuum transport line and the target chamber for laser-only experiments.*

4 Laser-Plasma Acceleration Experiment at ILIL-CNR/PISA: First Results from the Plasmon-X Project

4.1 The experimental set up

In the experiment, the main pulse was focused onto a gas-jet target using an F/6 off-axis parabola. The gas-jet target was irradiated at full laser energy varying the gas backing pressure, (i.e. the pressure in the pipe before the fast valve controlling the nozzle) to change the value of the maximum density of the neutral gas. Two gases were used in our experiment, namely He or N_2.

Characterisation of the neutral gas was carried out using optical interferometry. The use of two gases He and N_2, enabled us to explore targets characterised by dfferent physical properties mainly related to the atomic number, and, in particular, to the ionization properties under irradiation of ultrashort, intense laser pulses. The gas-jet nozzle was characterised by a 4 mm long, 1.2 mm wide slit and was mounted on a micrometric motorized support in order to move the interaction point along the three cartesian axes (position scan). During the pulsed operation, the gas flows out of the slit at supersonic speed in order to produce steep interfaces between gas and vacuum. The vacuum in the chamber before the shot is maintained at a pressure below $\approx 10^{-4}$ Torr by a turbo-molecular pump connected to the chamber by a gate-valve.

A full scan of the position of the focal plane along the laser propagation axis and with respect to the top of the nozzle was performed to find the best conditions for acceleration. An important feature consistently observed throughout the experiment is that electron acceleration in our experimental conditions was always found to occur when the focal plane (waist) was located in the proximity of the near edge of the nozzle, typically at ≈ 0.6 mm from the top of the nozzle. A full scan in pressure was also performed, showing that at higher pressure more stable, but less collimated electron bunches are produced. Several diagnostics were used to study the laser-target interaction and the accelerated electrons as shown schematically in Fig. 4. Thomson scattering and Nomarski interferometry were set up perpendicularly to the main laser pulse propagation axis to study and characterize ionisation and basic laser-plasma interaction issues. A second group of diagnostics including scintillators coupled to photomultipliers, a phosphor screen (LANEX), an electron spectrometer based upon permanent magnets and dose sensitive, radiochromic film stacks (SHEEBA), enabled indirect and direct detection and characterization of the electron bunches accelerated during the laser-gas interaction.

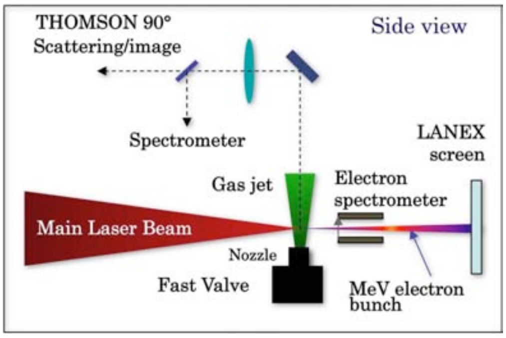

Figure 4: *Design of the layout of the underground target area of the FLAME laboratory, with the main compressor chamber, the vacuum transport line and the target chamber for laser-only experiments.*

4.2 Thomson scattering

Thomson scattering diagnostic was used throughout the experiment to monitor interaction conditions and to identify the basic plasma parameters (see Figure 5). In the classical picture of Thomson scattering, the electrons oscillate in the laser field and, in turn, emit radiation.

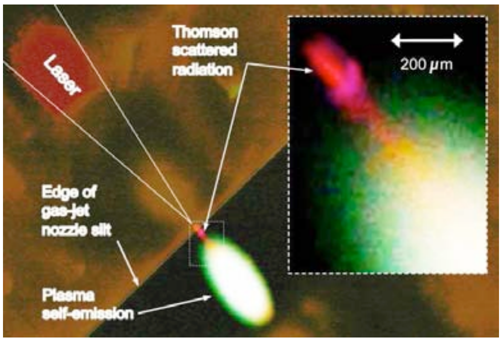

Figure 5: *Typical top-view image of the gas-jet nozzle obtained by the Thomson scattering diagnostic channel showing the main features of the interaction. The waist of the laser beam is placed on the edge of the gas-jet where Thomson scattering radiation is clearly visible (red in colour image). Beyond that point, the laser beam expands and the emission visible in the image is dominated by white light plasma self-emission. The insert in the top-right side of the image shows the magnified region of interaction.*

The properties of this scattered radiation are thus related to the properties of the medium and provide combined information on the laser intensity and electron density. Since in our case, knowledge on the plasma density can be derived independently from the plasma interferometry, we can use Thomson scattering to derive information on the laser intensity. In our experimental set up an F/10 achromatic doublet was used to produce a 10X magnied image of the interaction region. The image of Fig. 5 shows an overview of the emission produced along the entire laser propagation axis. The waist of the laser beam is placed on the edge of the gas-jet (dashed line in the image) and Thomson scattering radiation is clearly visible as a $\approx 200\,\mu$m long channel-like structure.

A spectral analysis of the accelerated electrons was carried out using a magnetic spectrometer coupled with the LANEX screen (see Figure 6). The spectrometer, based upon permanent NeFeB magnets generating a quasi-uniform magnetic eld ($B_{Max} \approx 0.45$ T), was placed at a distance of 44 mm in front of the LANEX screen. The magnetic field amplitude was mapped in the region of interest using a millimeter-sized Hall magnetic probe. A 2 mm thick Pb foil with a 0.5 mm slit width was placed in front of the magnet, with the slit direction parallel to the magnetic field, in order to limit the transverse momentum of electrons accepted by the electron spectrometer and consequently to increase the resolution of the spectrometer (see Figure 7).

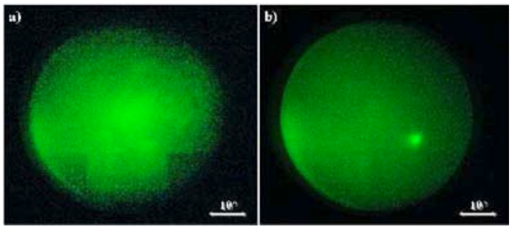

Figure 6: *Typical outputs of LANEX in detection conguration. a) non collimated laser-accelerated electrons in case of N_2 gas at 50 bar. b) collimated laser-accelerated electron bunch in case of He gas at 50 bar.*

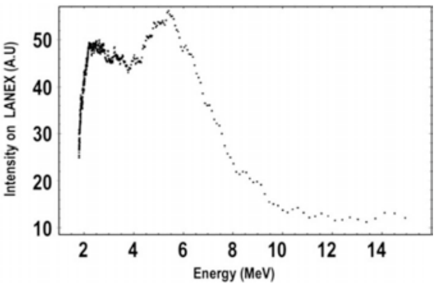

Figure 7: *Electron spectrum obtained with the magnetic spectrometer showing quasi monoenergetic peak between 5 and 6 MeV. The spectrum was obtained from irradiation of a N_2 gas-jet at a backing pressure of 45 bar.*

Numerical modeling based upon particle tracing in the mapped magnetic eld was implemented to describe the performance of the spectrometer in order to obtain the dispersion curve and the intrinsic resolution of both the imaging acquisition system and the LANEX screen. The code also account for errors introduced by beam pointing instability and space-charge effects along propagation. The results obtained by the magnetic spectrometer were confirmed by independent measurements carried out using an energy spectrometer consisting of sandwiched Radiochromic films (RCF). A sample spectrum obtained with the magnetic spectrometer with N_2 gas-jet is displayed in Fig. 7. According to this spectrum, electrons up to 10 MeV were detected, with an overall spectral distribution characterized by a broad peak with a maximum between 5 and 6 MeV. In some shots, narrower spectral components were found, thought with a poor reproducibility. These results confirm that, in spite of the very low laser intensity compared with most of the experiments available in literature, the electrons accelerated in our experimental conditions are well in the multi-MeV region, with evidence of mono-energetic components emerging clearly from the broad energy spectrum.

4.3 Efficient electron acceleration with 10 TW laser pulses and possible medical applications

In order to improve the characteristics of an electron bunch coming from ultra-intense laser-plasma interaction, an experiment was performed at the SLIC laboratory of CEA Centre in Saclay (France) with a 10 TW Ti:Sa laser system delivering pulses with duration of 65 fs (FWHM) at a wavelength of 800 nm, accounting for a laser strength parameter $a_0 \leq 2$. The experiment, carried out jointly by the ILIL group of CNR, Pisa with the host PHI (Physique a Haute Intensite) group, plus a group from LULI (Ecole Polytechnique, France) and a group from ITU (Institute for Transuranium Elements, Karlsruhe, Germany), allowed the best interaction conditions between the laser pulse and a supersonic gaseous target to be found, and stable and reproducible electron bunches with energy in the range 10-45 MeV to be accelerated (Fig. 8). This task is very important in the context of the comprehension of the mechanisms involved in the laser-plasma interaction and acceleration process (with particular attention to the propagation process) in order to produce high-energy electron bunches. Improvements in the comprehension of such phenomena will be in turn exploited in the frame of the project PLASMONX at ILIL and the Laser Facility that will be soon operating at LNF.

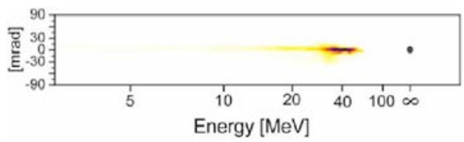

Figure 8: *Representative calibrated image from the magnetic spectrometer. Accelerated electrons show a mono-kinetic component with energy as high as 40 MeV.*

Several advanced diagnostics have been employed to monitor the interaction and the accelerated electron bunches. The photo-activation of nuclear material $^{1}97$Au driven by the high-energy electrons bremsstrahlung (Fig. 9) in a suitable converter has also been employed to get the number of particles in the bunch with a high degree of accuracy. The total number of electrons with energy greater than 3 MeV was found to be (3.15 ± 0.13) x 10^{10} per laser shot, evinced consistently from all the employed diagnostics. The presented efficient electron source contributes to indicate laser driven electron accelerators, provided them stability and reliability, as a suitable source for medical uses, in particular for Intra-Operative Radiation Therapy (IORT) of tumors. The main properties

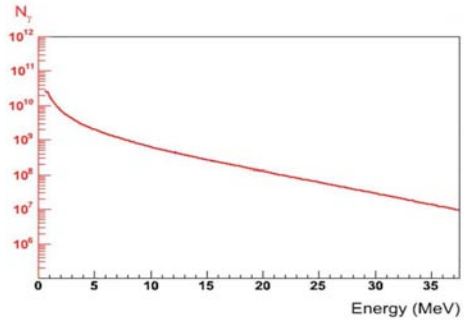

Figure 9: *Spectrum of the bremsstrahlung gamma yield obtained after interaction of the accelerated electrons in a tantalum converter. The number of electrons found after comparison with Monte Carlo tracking code is (3.15 ± 0.13)* $\times 10^{10}$ *per laser shot.*

of commercial RF Hospital accelerated electron bunches for IORT treatment and those of this laser driven accelerator are comparable in terms of bunch charge and electron energy. However, although the dose delivered for each shot is also comparable, the electron bunch duration is about six orders of magnitude lower in the case of the laser-plasma accelerator: few picoseconds versus few microseconds. Thus, the peak current is approximately a million times higher. The radiobiological effects of such difference are still unknown. The new ultrashort laser-plasma electron source thus opens an exciting field of basic bio-medical research.

4.4 Theory and simulations for self-injection experiments

We present some theoretical/numerical studies on electron acceleration (self-injection configuration) with the parameters of the FLAME laser, considering half of the maximum nominal power (P = 150 TW instead of 300 TW), in view of the first LPA experiments which will be carried out during 2009 for the commissioning of the laser system. In order to check the predictions of the scaling laws we have performed several 2D/3D simulations for the 1.2 mm gas-jet. Two-dimensional simulations to study the production of GeV electrons (propagation lengths of ≈ 6 mm are required) are underway. All the simulations have been carried out with the fully self-consistent, relativistic, parallelized PIC code ALaDyn. We acknowledge the support of the CINECA computing center for the 3D runs (grant: Simulazioni PIC 3D per l'accelerazione laser-plasma).

- Case 1: We consider $w_0 = 8.9\ \mu$m ($I \approx 1.2 \times 10^{20}$ W/cm^2) and $n_e = 10^{19}$ cm^{-3} (Lgas-jet = 1.2 mm). In Figure 10 (left, center) we show the electron density (XY cut) and the electron energy spectrum. Already inside the plasma (0.7 mm from the beginning of the gas-jet) we observe a monochromatic peak E = (160 ± 5) MeV (FWHM) with a charge of 0.45 nC. Unfortunately we observe also a significant erosion of the laser-pulse front (causing an anticipate dephasing not predicted from the scaling laws) which limits the energy gain for the electrons (160 instead of 400 MeV). This phenomenon has been observed in several 2D simulations when the plasma density is higher than 10^{19} cm^{-3} and the laser is intense. In Figure 10 (right plot) we plot the transverse (x -px) phase space for the monochromatic bunch. The r.m.s. amplitudes of the bunch are ≈ 0.8 μm (transverse) and ≈ 2.5 μm (longitudinal), while the normalized emittances are ≈ 5 mm mrad. The (high) value of the emittance is related to the large transverse momentum of the trapped particles and seems to be an unavoidable feature of the bubble regime, however, working at lower laser intensities can give some advantage in this respect.

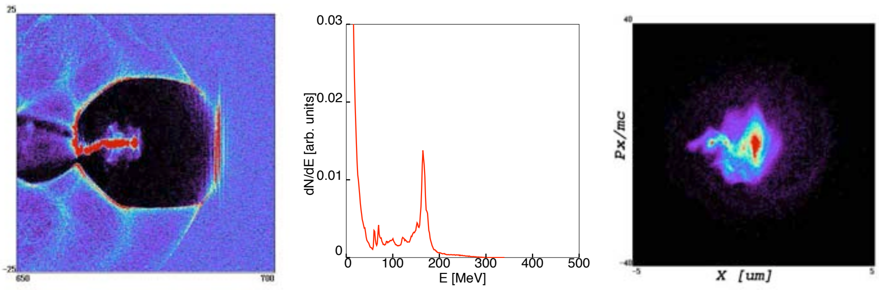

Figure 10: *Case 1:* w_0 *= 8.9* μm *(I ≈ 1.2* 10^{20} *W/cm*^{2}*) and* $n_e = 10^{19}$ *cm*$^{-3}$ *(Lgas-jet = 1.2 mm). (left, center) the electron density (XY cut) and the electron energy spectrum. (right plot) the transverse (x-px) phase space for the monochromatic bunch.*

- Case 2: We consider $w_0 \approx 12$ μm (I ≈ 6×10^{19} W/cm^2) and $n_e = 6 \times 10^{18}$ cm^{-3} (Lgas-jet = 1.2 mm). The predicted maximum energy is ≈ 440 MeV and the dephasing length is longer than the gas-jet length so we dont expect a monochromatic beam at the end of the simulation. In Figure 11 we plot the electron spectrum at the exit of the gas-jet and we find a broad peak with an energy of E = (420 ± 40) MeV (FWHM), the corresponding charge is 0.4 nC. Both values are in agreement with theory. The r.m.s. amplitudes of the bunch are ≈ 0.5 μm (transverse) and ≈ 1 μm (longitudinal), the normalized emittances are ≈ 2.5 mm mrad.

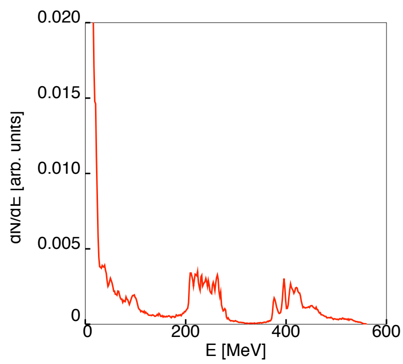

Figure 11: *Case 2:* $w_0 \approx 12$ μm *I* ≈ 6×10^{19} *W/cm*^{2}*)* $n_e = 6 \times 10^{18}$ *cm*$^{-3}$ *(Lgas-jet = 1.2 mm).*

4.5 External Injection: a route for multi GeV high-quality e-beams

4.5.1 Goals and acceleration scheme

The aim for the external-injection studies were the search of an innovative scheme for the generation of multi-GeV beams with promisingly good slice quality and acceptable projected emittances. High-gradient acceleration requires relatively high plasma densities (10^{17}-10^{18}) cm^{-3} that are linked to electron plasma waves in the range (30-100) μm. Since beam-quality requirements are tight, injected beam length is one of the crucial parameters of the scheme and for a 100 μm long wave beam monocromaticity requires injected bunches having lengths not exceeding 2-3 μm rms, a challenging result for current RF-photoinjector technology. Other critical issues are emittance preservation that has been achieved by using an adiabatic injection scheme (i.e. injection in the wake of an adiabatically focusing laser pulse), acceleration length elongation (that should be extended up to 20 Reyleigh lengths via pulse guiding), detailed Langmuir wave phase control that has been obtained via appropriate plasma profile tailoring and jitter of the injection phase. Another issues are nonlinear dynamics of the laser pulse that may undergo self-focusing or phase-modulation and pulse erosion.

4.5.2 Simulation tools

Simulations were performed with the **QFluid** code [P. Tomassini, 2005-2008] that solves in the quasistatic approximation nonlinear equations of fluid response to ponderomotive forces of the laser pulse and beam-loading effects. The **QFluid** code works in a 2D cylindrical space and it has been tested with ALaDyn. The code does not take into account for laser pulse nonlinear dynamics and erosion. While pulse erosion in 10cm should be negligible since the pulse strength a_0 reduces by less the 4% [1D PIC results], detailed self-consistent simulations should be performed for studying pulse nonlinearities.

4.6 Simulation results

A 25 pC, 5 μm and 2.5 μm of rms transverse and longitudinal sizes, energy of 150 MeV and transverse normalized emittance of 1 mm·mrad electron bunch is injected in the second bucket of the Langmuir wave excited by a Ti:Sa pulse delivering 7 J of energy in 30 fs. The laser pulse with initial waist size of 130 μm and minimum size of 32.5 μm is guided by a matched channel profile. The plasma is 9.88 cm long and its density profile has a positive and varying slope with starting and ending densities of 1.5×10^{17} cm^{-3} and 2.5×10^{17} cm^{-3}, respectively. At the final simulation step (see Figure 12) a 2.2GeV electron beam with global energy spread and emittance of 4% rms and 1.5 mm·mrad, respectively, is produced.

Slice analysis with slice thickness of 250 nm reveals the potentialities of the bunch as a driver in X-FEL. While slice emittance is in the range (1.2-1.4) mm.mrad the slice energy spread is in the range (0.02-0.1)% for slices 8-13, with a local current of about 1kA.

5 Ion Laser-Plasma Acceleration

Ion acceleration from solid targets irradiated by high-intensity pulses is a burgeoning area of research, currently attracting a phenomenal amount of experimental and theoretical attention

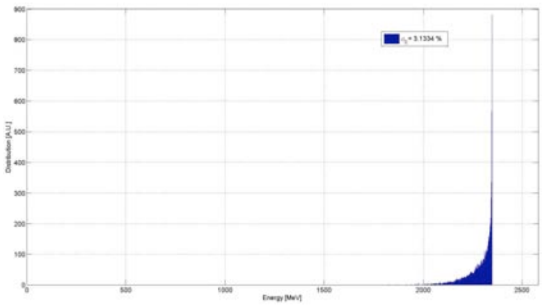

Figure 12: *Energy distribution of the produced e-bunch.*

worldwide. Key to this interest are the ultra-compact spatial scale of the accelerator and the fact that the properties of laser-driven ion beams are, under several respects, markedly different from those of "conventional" accelerator beams. In particular, the spatial quality of laser-driven beams is exceptionally high, and their duration at the source is - down in the ps scale - orders of magnitude shorter than other available sources. In view of such properties laser-driven ion beams have the potential to be employed in a number of innovative applications in the scientific, technological and medical areas, where proton beams with energies greater than 100 MeV are of interest. The FLAME laser could be ideally suited to perform experimental campaigns aimed at improving our basic understanding in this area, towards the achievement of "true" ion beams for applications. In this context, within the PLASMONX project a working group devoted to this subject has been established. A research program has been identified, with the following specific goals:

1. Study and development of dedicated beam diagnostic in order to characterize the quality, the control and the reproducibility of the ion beams, with methods and techniques which are typical of the accelerators physics and technology.

2. Theoretical and experimental investigation of the acceleration mechanisms of ions in the interaction of the ultrashort superintense FLAME laser pulses with solid targets, aimed at the improvement and optimization of the beam properties.

5.1 Theoretical and experimental activity on the TS-source

i) The design of the laser-beam interaction chamber and the devoted e-beam:

   A complete design of the interaction chamber, with the focussing solenoid, the bending dipole for the dumping of the beam, the screening of the interaction region and the laser path is presented in Fig. 13. The technical design of the e-beams devoted to the TS based source and the LPA of the external injected electrons has been completed (see Fig. 14).

ii) The development of a procedure of optimization of the X-rays photon flux by means of a genetic algorithm:

   In the framework of the maximization of the photon flux of the X radiation produced by the TS source, the genetic code ALGEN has been developed with the aim of optimizing the beam line. The beam line used is similar to that adopted in previous simulations for the

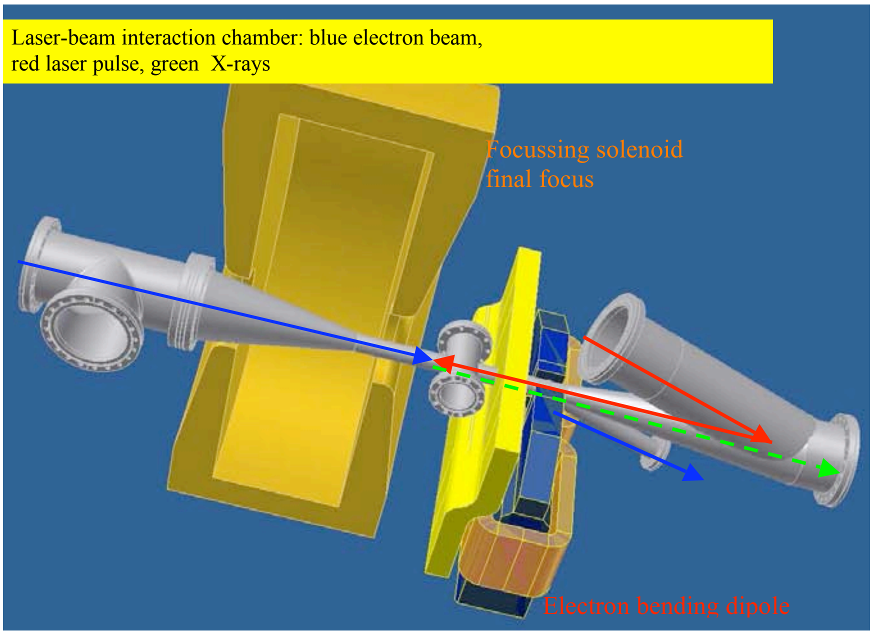

Figure 13: *Interaction chamber for Thomson Scattering based source.*

SPARC/PLASMONX experiment. The bunch has total charge of 1 nC and is extracted from the cathode with a laser pulse of 30 ps. The optimization plays with the following parameters: the gradient of the electric field of the gun $\mathrm{d}E_g/\mathrm{d}z$, the injection phase in the gun Φ_g, the maximum magnetic field of the gun B_g, the gradients of the accelerating structures $\mathrm{d}E_n/\mathrm{d}z$, the injection phase in the structures Φ_n, the maximum magnetic fields B_n, the position of the solenoids zn, and injection phase and position of the forth harmonic cavity Φ_{IVH} and z_{IVH}.

iii) The temporal structure of the X-ray electric field, the field phase and the impact that these characteristics can have on the phase contrast imaging have been considered. For the application to the phase contrast imaging it is very important to determinate the degree of spatial coherence of the radiation. In fact, the electrons of the beam have initial positions and velocities randomly distributed. The inherent randomness of the source will reflect itself on all parameters and measured quantities of the process.

iv) The participation to the measurements of imaging at the TS-source at ATF (BNL, Brookhaven) and the application of these tools to them:

Cooperation with the BNL group working at ATF has been initiated, with the participation of members of the PlasmonX experiment to the measurements made along 2008 on the TS source of Brookhaven. The measurements regard the use of the phase contrast technique for the imaging of wires of various materials and dimensions. A measure of the X rays spot with the traces of the wires has been performed. The X-intensities as given by a phase contrast simulation for a pet wire of dimension of 200 micron have been afterwards evaluated.

v) The investigation of other possible X radiation schemes (All Optical Thomson Source, AOFEL):

Other possible X radiation schemes (All Optical Thomson Source, AOFEL) have been invesigated. In particular we have studied the generation of low emittance high current monoenergetic beams from plasma waves driven by ultra-short laser pulses, in view of achieving beam brightness of interest for FEL applications. The aim is to show the feasibility of generating nC charged beams carrying peak currents much higher than those attainable with photoinjectors, together with comparable emittances and energy spread, compatibly with typical FEL requirements. We have focused on the regime based on a LWFA plasma driving scheme on a gas jet modulated in areas of different densities with sharp density gradients, because it seems more promising in terms of beam emittance. Simulations carried out using VORPAL show, in fact, that in the first regime, using a properly density modulated gas jet, it is possible to generate beams at energies of about 30 MeV with peak currents of 20 kA, slice transverse emittances as low as 0.3 mm.mrad and energy spread around 0.4 %. This beams break the barrier of 1018 A/(mm·mrad)^2 in brightness, a value definitely above the ultimate performances of photo-injectors, therefore opening a new range of opportunities for FEL applications.

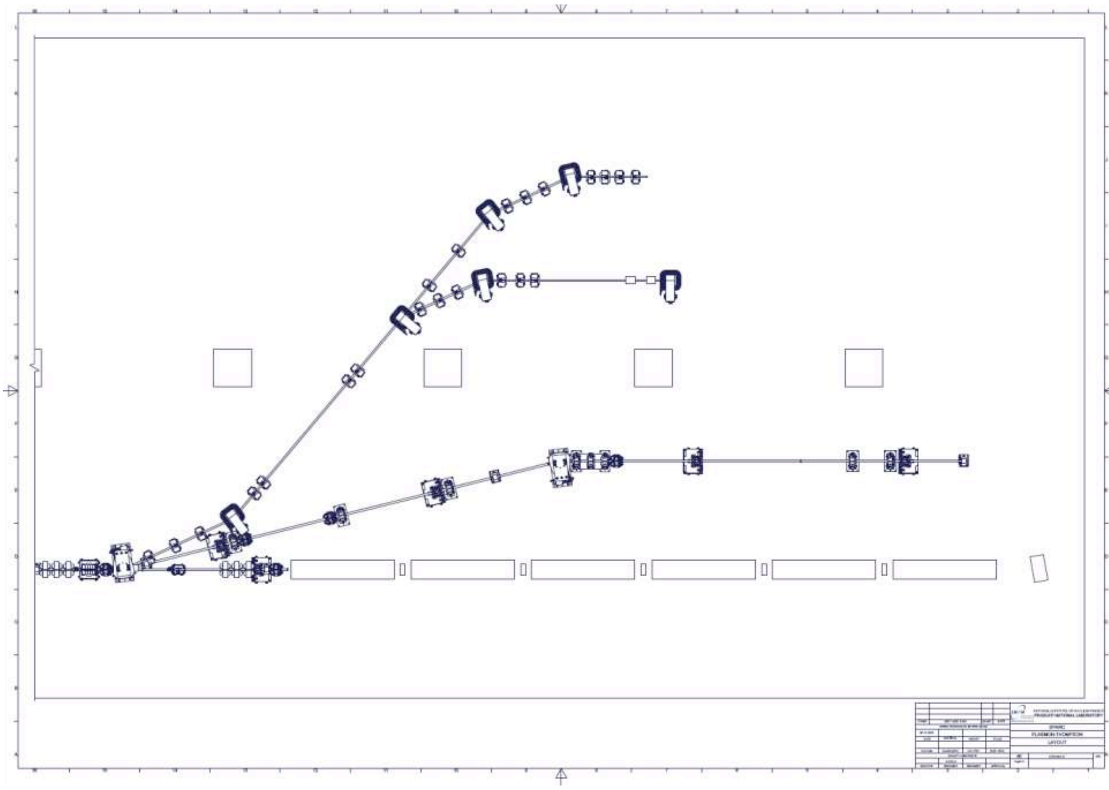

Figure 14: *The technical design of the e-beams devoted to the TS based source and the LPA of the external injected electrons.*

6 References

1. A. Giulietti *et al.*, Phys. Rev. Lett. **101**, 105002 (2008).
2. C. Benedetti, A. Sgattoni, G. Turchetti, and P. Londrillo, IEEE Trans. on Plasma Science, **36**, 1790 (2008).
3. L. A. Gizzi *et al.*, “An integrated approach to ultraintense laser sciences: the plasmon-x project”, Europ. Phys. Journal - Special Topics 2009, in press.
4. A. Gamucci *et al.*, IEEE Trans. Plasma Sci. **36**, 1699 (2008).
5. C. Benedetti *et al.*, IEEE Trans. Plasma Sci. **36**, 1790 (2008).
6. C. Benedetti, A. Sgattoni, and P. Tomassini, “ALaDyn: a high accuracy code for the laser-plasma interaction”, Proc. of EPAC08, Genova, Italy (2008).
7. C. Benedetti *et al.*, “PIC simulations of the production of high-quality electron beams via laser-plasma interaction”, accepted for publication on Nucl. Instr. & Meth. A.
8. A. Bacci, C. Maroli, V. Petrillo, A. Rossi, and L.Serafini, Nucl. Instr. & Meth. in Phys. Res. B **263**, 488 (2007).
9. A. Cedola, I. Bukreeva, S. Lagomarisino, C. Maroli, and V. Petrillo, “Theoretical consideration for X-rays phase contrast mammography by Thomson Source“, to be published on Nucl. Instr. & Meth. in Phys. Res. A.
10. P. Tomassini *et al.*, IEEE Trans. on Plasma Science **36**, 1782 (2007).
11. V. Petrillo, L. Serafini, and P. Tomassini, Phys. Rev. Spec. Top. Accel. Beams **11**, 070703 (2008).

NTA-SUPERB

M.E. Biagini (Resp.), R. Boni, M. Boscolo, T. Demma (Art. 23), A. Drago,
S. Guiducci, G. Mazzitelli, P. Raimondi, G. Sensolini (Tecn.),
S. Tommasini, M. Zobov

1 Introduction

SuperB is an asymmetric (7 GeV HER, 4 GeV LER) e^+e^- collider at the center of mass B pairs production energy (10.58 GeV), to be built in the Tor Vergata University campus (Rome, Italy), with a design peak luminosity of 10^{36} cm^2 s^{-1}. A collider like SuperB will open a unique window on this physics because it allows a high statistics study of the current hints of new aggregations of quarks and gluons. Besides the physics one can study in running at the (4S) resonance, the following alternative energies are of interest: (3S) (at least 0.3 ab^{-1}) and a high luminosity scan between 4-5 GeV (5 MeV steps of 0.2 fb^{-1} each would require a total of 40 fb^{-1}). While this is not huge statistics, this scan is only feasible with SuperB. The only possible competitor, BES-III, is not planning to scan above 4 GeV, since their data sample would, in any case, be lower than that of the B Factories alone. Finally, the search for exotic particles among the decay products of the "bottomonia" can probe regions of the parameters space of non-minimal supersymmetric models that cannot be otherwise explored directly, for instance at LHC. These studies are particularly efficient when producing (nS) mesons with n<4. The superiority of SuperB with respect to the planned upgrade of KEKB lies both in the ten times higher statistics, which broadens the range of cross sections the experiment is sensitive to, but also in the flexibility to change center of mass energy. A Technical Design Report (TDR) will be started in Spring 2009 to define the accelerator design and to clarify R&D activities before to proceed with construction. In the following section the work performed at LNF on the design of the accelerator will be briefly described. LNF contribution is essential for the design and construction of SuperB. This activity at LNF has been funded by the INFN NTA commission for 33.6 kEuro in 2008.

2 Design strategy

The construction and operation of modern multi-bunch e^+e^- colliders have brought about many advances in accelerator physics in the area of high currents, complex interaction regions, high beam-beam tune shifts, high power RF systems, controlled beam instabilities, rapid injection rates, and reliable uptimes (90%). The SuperB design is based on a novel collision scheme, the so called "large Piwinski angle and crab waist" [1, 2], which will allow to reach unprecedented luminosity with low beam currents and reduced background at affordable operating costs. A polarized electron beam will allow for producing polarized leptons, opening an entirely new realm of exploration in lepton flavor physics. The principle of operation of this scheme has been tested in 2008 at the upgraded DAΦNE Φ-Factory in Frascati with very successful results [3] (see also the DAΦNE section in this report). Figure 1 shows the SuperB beam cross sections at the IP with unequal emittances but equal beam-beam tune shifts in the crab waist collision scheme.

A Conceptual Design Report (CDR) [4] was issued in May 2007, with about 200 pages dedi-

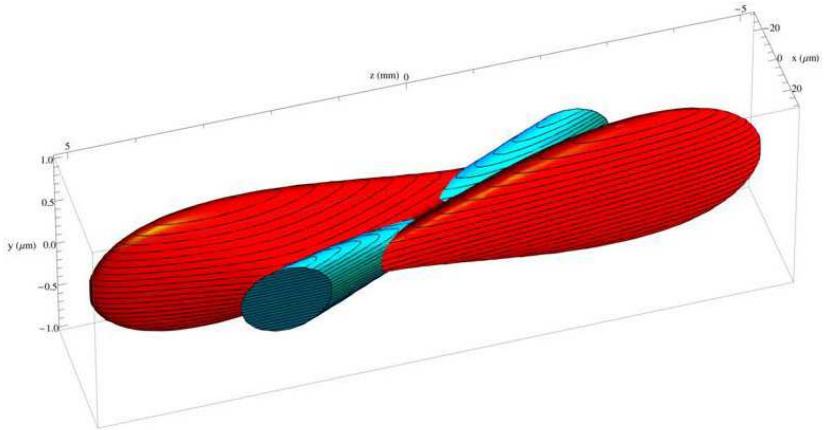

Figure 1: *Beam cross sections (1 rms sigma) at the IP crab waist (LER red, HER blue).*

cated to the accelerator design. This report discusses site requirements, crab waist compensation, parameters optimization in order to save power, IP quadrupole design, Touschek backgrounds, spin rotator scheme, and project costs. The ring lattices have been modified to produce very small horizontal (a few nm-rad) and vertical emittances (a few pm-rad). Crab waist sextupoles near the interaction region introduce a left-right longitudinal waist position variation in each beam allowing a vertical beta function which is much smaller than the bunch lengths. SuperB consists of two rings of different energy (electrons in HER, 7 GeV, positrons in LER, 4 GeV) colliding in one Interaction Region (IR) at a large (60 mrad total) horizontal angle. Spin rotator sections in the HER will provide helicity of a polarized electron beam. The two rings each have two arcs and two long straight sections. One straight is for the IR, the other is for diagnostics, RF, and injection. The crab waist scheme, with a couple of sextupoles per ring in a dispersive section near the IR, and appropriate betatron phase with respect to the IP, will create a longitudinal waist shift over the width of the beam, so providing suppression of betatron and synchrobetatron resonances arising from the crossing angle geometry. A possible layout at Tor Vergata University near Rome is shown in Figure 2.

The injection system needed for the SuperB is similar to that for PEP-II. A preliminary design is shown in Figure 3. Since the beam lifetimes are of the order of 10-30 minutes, continuous injection is needed

3 Year 2008 activity

3.1 Lattice studies

The optimization of the ring lattices, performed in 2008 after the CDR completion, aimed to minimize the intrinsic emittance so that nominal values can be obtained even without wigglers and the ring circumference is shortened, better fitting the proposed construction site. When increasing the horizontal phase advance x in the SuperB arc cell, the intrinsic emittance naturally decreases. The damping time increases by 30% but the RF power decreases, with a net operational costs

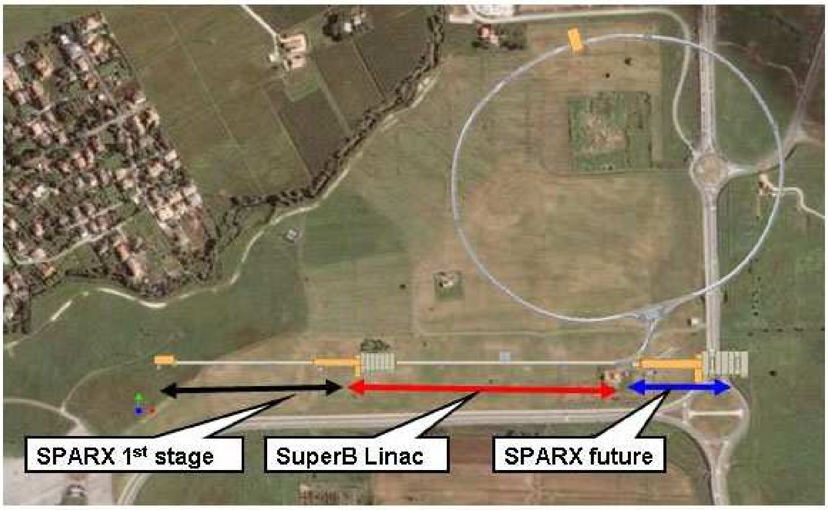

Figure 2: *Possible SuperB location at Tor Vergata University with a ring circumference of 1800 m and an injector located adjacent to the future SPARX FEL.*

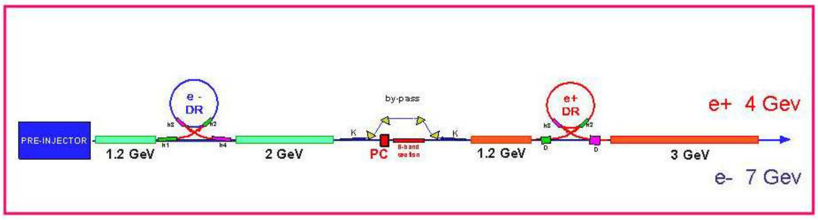

Figure 3: *Schematic of the SuperB injector.*

saving. Beam-beam simulations have studied the degree to which an increase in the damping time affects the luminosity and beam-beam induced tails: an increase by a factor of 2.5 does not lead to any substantial luminosity degradation. In the new lattice the longitudinal damping times are of the order of 20 msec in both rings, about 1.3 times larger than the CDR values and still below the threshold of beam tail growth. Moreover the design emittances can be reached without the insertion of wiggler magnets.

LER and HER lattices are very similar, and based on the reuse of most PEP-II (SLAC) hardware. The arcs have an alternating sequence of two different cells: a x = cell, that provides the best dynamic aperture and a x = 0.72 cell that has a much smaller intrinsic emittance and provides a phase slippage for the sextupoles pairs, in such a way that one arc corrects all the phases of the chromaticity. As a consequence, the chromatic functions Wx and Wy are lower than 20 and the second order dispersion is almost zero everywhere except in the Interaction Region (IR). With this arrangement, the number of arcs can be reduced to 4, with two 40 m long "empty" wiggler sections for the upgrade scenario. The increase of the phase advance, together with future wigglers installation, will provide the required emittance and damping time for the upgrade parameters. With 14 cells in each arc a horizontal emittance of 1.6 nm in HER and 2.8 nm in LER are obtained, the LER lattice having still room for further reduction.

Dynamic aperture (DA) studies are being carried out with the Acceleraticum code [5] which allows for both the optimization of DA and the choice of a good machine working point (WP) at the same time. The code uses the “best sextupole pair” method to find the optimal sextupoles configuration. An example of sextupoles optimization and scan of the DA as a function of tunes for the HER is shown in Fig. 4, where in red are ”good” DA regions, with a different WP (black dot) preferred to the nominal one (cross). Optimization of HER and LER DA is still in progress.

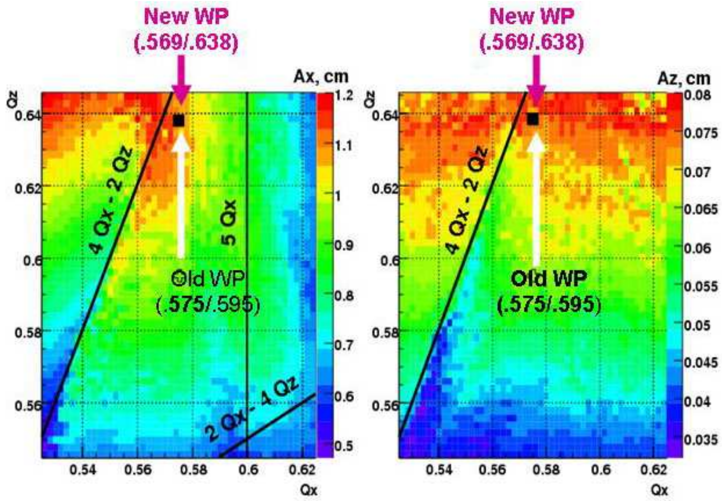

Figure 4: *Dynamic aperture with crab waist for the HER versus horizontal and vertical tune used to find the optimum tune plane locations. Red is better and blue is worse DA.*

3.2 Interaction region design

The Interaction Region (see Figure 5) is designed to be similar to that of the ILC and to leave about the same longitudinal free space for the detector as that presently used by BABAR or BELLE, but with superconducting quadrupole doublets QD0/QF1 as close to the interaction region as possible [6,7]. The total Final Focus (FF) length is about 160 m and the final doublet is at 0.4 m from the IP. A plot of the optical functions in the incoming half of the FF region is presented in Figure 6. The choice for a finite crossing angle at the IP greatly simplifies the IR design, naturally separating the beams at the parasitic collisions. The resulting vertical beta is about 0.2-0.3 mm and the horizontal 35 mm. These beta values are much closer to a linear collider design than a traditional circular collider. The beams enter the interaction point nearly straight to minimize synchrotron radiation and lost particle backgrounds. The beams are bent more while exiting the IR to avoid parasitic collisions and the resulting beam-beam effects.

The mechanical constraints are too tight for a conventional septum magnet, a novel concept to compensate the cross-talk among the two QD0’s core and fringe fields has then been studied [7], and 3D finite-elements simulations show field errors well under ten parts per million. This design strongly reduces the rate of off-energy particle losses near the IP, thus reducing the background

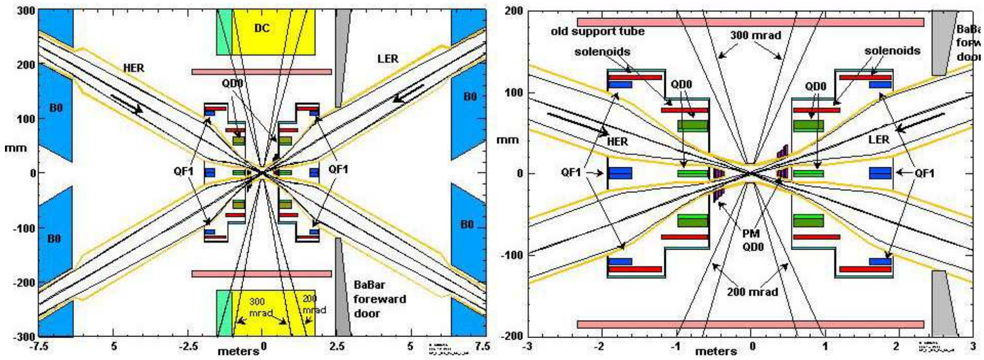

Figure 5: *IR for two asymmetric beams (left) and close up of the IP zone (right).*

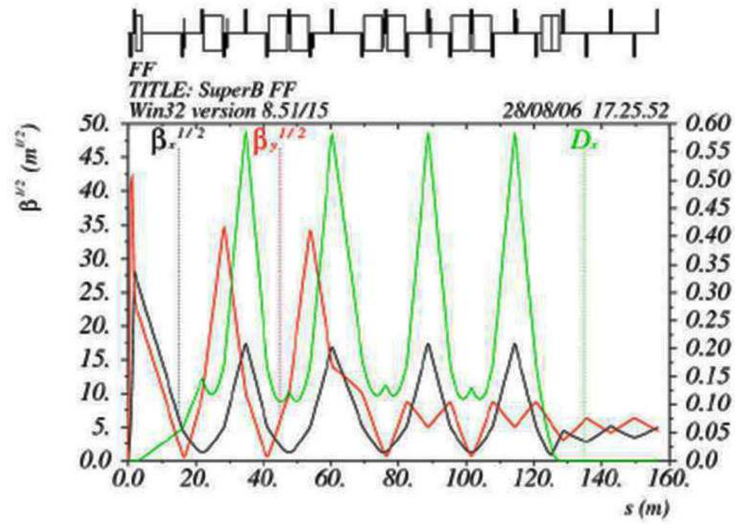

Figure 6: *Optical functions for half Final Focus.*

rates seen in the detector with respect to a conventional design with a shared QD0. An additional small D-quadrupole will provide the necessary focusing to the HER beam.

3.3 Polarization scheme

At SuperB energies, Sokolov-Ternov polarization takes too long and polarized electrons will be injected. The injector will have the necessary spin handling, and polarized sources with the required intensity exist (e.g. the SLC gun). At the IP, the desired polarization is longitudinal; this can be provided in principle either by 90 deg spin rotators up and downstream of the IP or by a Siberian Snake (180 deg rotator) diametrically opposite in the ring, thus avoiding the need for spin rotators matched to the critical IR optics. The rotators or Snake(s) can be designed either using solenoids or vertical dipoles together with horizontal dipoles. The overall spin matching in SuperB will be less critical than in facilities like HERA or LEP because of the short beam lifetime. This causes frequent injection of freshly polarized beam, thus reducing the effect of depolarization in the ring, so that maintaining above 90% of the injecting polarization is an achievable goal, provided rotators are spin-matched across the whole energy spread of the beam. It is still important to avoid integer spin tunes (and their synchrotron sidebands) as the spin orientation will move away from longitudinal at the IP for such values. Solenoid spin rotators tend to be more compact than pure dipole rotators, however for first-order spin matching they need to be anti-symmetric about the IP, leading to a horizontal "dog leg" in the IR layout causing a distortion of the ring geometry. The orbital coupling introduced by the solenoids is compensated by inserting a plane twister between two half-solenoids [8]. A pure dipole spin rotator has been designed that avoids this, i.e. its dipoles become part of the overall 360 deg bending, however, the vertical bends will raise the minimum vertical emittance achievable [9]. Figure 7 shows the HER half IR optical functions, with the spin rotator inserted [10].

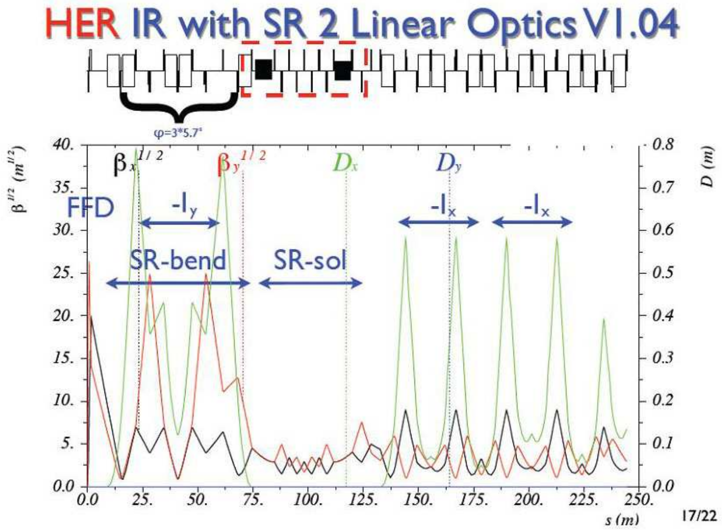

Figure 7: *HER half IR optical functions, with the spin rotator inserted.*

4 Year 2009 activity

In 2009 the work on the Technical Design Report will start. An international accelerator team will be formed for this scope, and work will be focused on the description of each accelerator subsystem, so to have a ready-to-build accelerator document for the end of year 2010. There will be three general SuperB meetings in June, October and December 2009.

5 Summary

After the completion of the CDR accelerator studies have continued in order to optimize the rings performances while simplifying their designs, and including unique features as the polarization scheme of the electron beam. In 2008 the SuperB accelerator design has been scrutinized by an International Review Committee (IRC) and by a Machine Advisory Committe (MAC). The IRC, established in 2007 to review the project, and formed by 8 international experts chaired by J. Dainton (Daresbury, UK), has closed its works in April 2008, with a very positive statement, namely: "We recommend strongly that work towards the realisation of a SuperB, taken to be an asymmetric e^+e^- collider with luminosity at least 10^{36} cm^2 s^{-1}, continues. The SuperB concept is at an important stage. The significance of the physics programme at such a machine continues to be developed, increasing in both scope and importance. It motivates an even more concerted effort to meet many technical challenges, in particular concerned with the design of storage rings which meet the physics specification. So far there has been no showstopper; rather there has emerged a number of innovative and noteworthy developments at the cutting-edge of contemporary technique in accelerator physics and of detector technology." The Machine Advisory Committe (MAC) for the accelerator, chaired by J. Dorfan (SLAC) and formed by 10 international accelerator experts from US and EU, has met for the first time in July 2008. The outcome from this first look at the accelerator design was highly positive, namely: "SuperB is a very exciting project: the committee is exhilarated by the challenge. Physics requirement of 10^{36} cm^2 s^{-1} or 75 ab^{-1}/5yr is very demanding; the requirement of polarization potentially adds complexity. The design is imaginative and ambitious: the committee endorses the design approach, which offers flexibility to either raise the luminosity or compensate for surprises". The MAC has issued a list of topics which will require further attention and study in order to fully validate the design. Work in the second half of 2008 has been focused on these topics. The next MAC review will take place at LNF the last week of April 2009. In 2008 the SuperB project has also been presented to the CERN Strategy Group, to be included in the list of the European projects. Final decision will probably take place in Fall 2009.

An ICFA Advanced Beam Dynamics Workshop dedicated to the SuperB accelerator took place in Novosibirsk (Russia) on April 14-17 2008. A general SuperB project Meeting ahs been organized on Elba island, Italy, on May 31- June 3 2008.

6 Publications in 2008

1. M.E. Biagini for the SuperB Coll., "The SuperB Factory project", Presented at CARE-HHH-APD Mini-Workshop IR'07 "Interaction Regions for the LHC Upgrade, DAΦNE and SuperB", (IR'07), W. Scandale, (ed.), F. Zimmermann, (ed.); CERN-2008-006; CARE-CONF-08-001-HHH, 2008.

2. M.E. Biagini for the SuperB Coll., "SuperB Accelerator Overview and Lattice", Presented at ICFA08 Workshop, Novosibirsk, Russia, Apr. 14-16, 2008.

3. A. Drago, "Trends in fast feedback R&D", Presented at ICFA08 Workshop, Novosibirsk, Russia, Apr. 14-16, 2008.

4. E. Paoloni, S. Bettoni, M.E. Biagini, and P. Raimondi, "Design of the QD0 for SuperB Interaction Region", Presented at ICFA08 Workshop, Novosibirsk, Russia, Apr. 14-16, 2008.

5. M. Boscolo, “Touschek effect: DAΦNE, DAΦNE crab waist and SuperB”, Presented at ICFA08 Workshop, Novosibirsk, Russia, Apr. 14-16, 2008.

6. M.E. Biagini *et al.*, J. Phys. Conf. Ser. **110** 112001 (2008).

7. M.K. Sullivan *et al.*, “An Improved Design for a SuperB Interaction Region”, Proc. of 11th European Particle Accelerator Conference (EPAC 08), Genova, Italy, June 2008.

8. E. Paoloni, S. Bettoni, M.E. Biagini, and P. Raimondi, “Magnetic design studies for the final focus quadrupoles of the SuperB large crossing angle collision scheme”, Proc. of 11th European Particle Accelerator Conference (EPAC 08), Genova, Italy, June 2008.

9. M. E. Biagini *et al.*, “New Low Emittance Lattices for the SuperB Accelerator Project”, Proc. of 11th European Particle Accelerator Conference (EPAC 08), Genova, Italy, June 2008.

10. M. E. Biagini *et al.*, “Design of a 10^{36} cm^{-2} s^{-1} SuperB Factory”, Proc. of 11th European Particle Accelerator Conference (EPAC 08), Genova, Italy, June 2008.

11. P. Raimondi, M. Zobov, and D. Shatilov, “Suppression of beam-beam resonances in crab waist collisions”, Proc. of 11th European Particle Accelerator Conference (EPAC 08), Genova, Italy, June 2008.

12. M.E. Biagini for the SuperB collaboration, ICFA Beam Dyn. Newslett. **46** 193, (2008).

7 References

1 P. Raimondi, “SuperB design directions”, Proc. of Particle Accelerators Conference, Albuquerque, June 2007.

2 P. Raimondi, D. Shatilov, and M. Zobov, Report LNF-07/003 (IR).

3 P. Raimondi *et al.*, “DAΦNE crab waist beam tests”, Proc. of 11th European Particle Accelerator Conference (EPAC 08), Genova, Italy, June 2008.

4 SuperB Conceptual Design Report, Report INFN/AE-07/2, SLACR-856, LAL 07-15, arXiv:0709.0451.

5 P. Piminov, Master’s Thesis, BINP, Russia (2000).

6 M. Sullivan *et al.*, “SuperB interaction region design”, Proc. of 11th European Particle Accelerator Conference (EPAC 08), Genova, Italy, June 2008.

7 E. Paoloni *et al.*, “IR SC quadrupole design for SuperB”, Proc. of 11th European Particle Accelerator Conference (EPAC 08), Genova, Italy, June 2008.

8 A. Zholents and P. Litvinenko, Report BINP Report 81-60, Novosibirsk, Russia.

9 I. Koop, Proc. of 40th ICFA Advanced Beam Dynamics Workshop, BINP, Russia, 2008.

10 W. Wittmer, SLAC, private communication.

NTA TTF

L. Cacciotti (Tecn), M. Castellano (Resp), E. Chiadroni (Art. 23), A. Clozza,
G. Di Pirro, R. Sorchetti (Tecn)

1 Introduction

The TESLA Test Facility (TTF) is an international effort, based at Desy (Hamburg), aiming at the development of the technologies required for a Superconducting e+e- Linear Collider. High gradient superconducting RF cavities, with their high power coupling and tuning device, and low cost cryostats were the main goal of the project, but also the production of a high power, long pulse electron beam from a RF gun was required. This involved the development of new photocathode, an adequate laser source and new beam diagnostics. In addition to prove the possibility of producing and accelerating the kind of beam required for the future superconducting Lineal Collider, TTF has also demonstrated that this beam was of enough good quality to be successfully used for the production of UV coherent radiation with the Self Amplified Spontaneous Emission (SASE) Free Electron Laser process. TTF is now transformed in FLASH (Free-electron LASer in Hamburg), becoming a test bench not only for the Linear Collider, but also for the European X-ray FEL Facility. INFN contribution comes from LNF, LNL, Sezione di Milano and Sezione di Roma2.

2 Activity 2008

This scientific activity was completed in 2008 with two shift periods dedicated to the ODR experiment. In these two presences at Desy, as well as in the shorter ones required to present the results, the complete control of the optical system was transferred to Desy people. As already illustrated in the 2007 Report, in the long linac shutdown of the second half of the year we installed a new ODR screen, shown in Fig. 1, composed by two parts, one of which carried a shield with larger cuts just in front of the screen. It was intended for screening the ODR from the synchrotron radiation background.

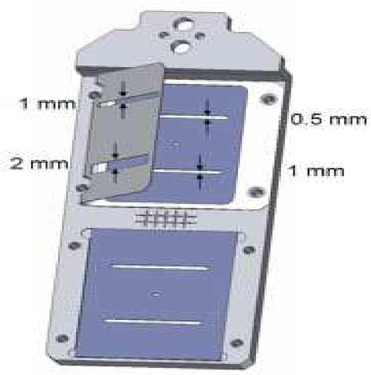

Figure 1: *Sketch of the new screen together with its shielding mask.*

In January 2008, at the restart of the Linac operation after the shutdown, the beam energy was almost the nominal 1 GeV, and a much better transport in the by-pass was possible, allowing the passage of the beam through the .5 mm slit. The presence of a very strong dark current from the gun that could not be cured in a short time prevented any possible measurement of ODR for the impossibility to perform a significant background subtraction. We were thus forced to use the screen with the shield, with a very good result in terms of background suppression and the first operation of a new instrument that we named ODRI (Optical Diffraction Radiation Interferometer). Indeed the 1 mm cut in the shield in front of the .5 mm slit in the ODR screen is not large enough to completely prevent the emission of forward ODR at the energy near 1 GeV. This forward radiation has a phase difference of with respect to the standard backward one, to which must be added the phase difference originating from the velocity and path difference between the electrons and the radiation at a given angle. What we measure as radiation angular distribution is the result of the two amplitudes interference. This new instrument offers a number of advantages with respect to the simple ODR from a slit: the number and amplitude of interference fringes are increased, the equivalence of beam size and beam position in modifying the fringes structure is no more valid, and last but not least, the synchrotron radiation background is almost eliminated. A paper with the complete description of the experiment and the ODRI theory is in preparation. In Fig. 2 the picture of a typical ODRI far field radiation is shown, while in Fig. 3 the central profile is compared to the theory assuming beam size and divergence measured directly. In Fig. 4 we present a comparison between the results obtained with beam size of 78 and 90 microns, demonstrating the sensitivity of the technique.

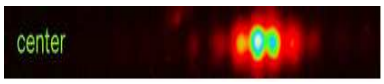

Figure 2: *A typical ODRI image.*

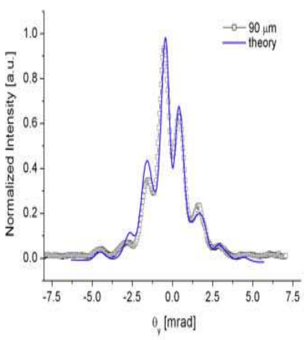

Figure 3: *Central profile and comparison with the theory.*

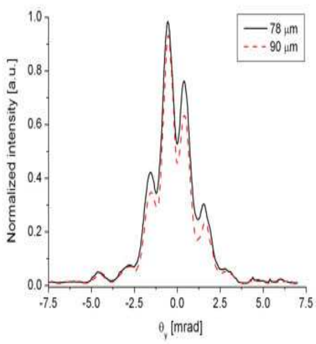

Figure 4: *Comparison of ODRI for two slightly different beam sizes.*

3 Publications

1. A. Lumpkin, C.-Y. Yao, E.Chiadroni, M. Castellano, and A. Cianchi, "Considerations on ODR beam size monitoring for gamma = 1000 beams". Proc. of 2008 Beam Instrumentation Workshop, Lake Tahoe, California.
2. E. Chiadroni, M. Castellano, A. Cianchi, K. Honkavaara, and G. Kube, "New Experimental Results with Optical Diffraction Radiation Diagnostics". Proc. of the 11th Particle Accelerator Conference (EPAC08), Genova, Italia.
3. E. Chiadroni, M. Castellano, A. Cianchi, K. Honkavaara, and G. Kube, "New Experimental Results with Optical Diffraction Radiation Diagnostics". Proc. of the Conference on Charged and Neutral Particles Channeling Phenomena, Channeling08, Erice, Sicily.
4. M. Castellano, E. Chiadroni, and A. Cianchi, "Diffraction Radiation as a diagnostics Tool at FLASH". Proc. of the International Conference on Charged and Neutral Particles Channeling Phenomena, Channeling08, Erice, Sicily.

SPARC–SPARX

D. Alesini, M. Bellaveglia (Art. 2222), R. Boni, M. Boscolo, M. Castellano,
E. Chiadroni (Art. 23), A. Clozza, L. Cultrera (Art. 23), G. Di Pirro, A. Drago,
A. Esposito, M. Ferrario (Resp.), L. Ficcadenti (Art. 23), D. Filippetto (Art. 23),
V. Fusco (Art. 23), G. Gatti (Art. 23), A. Gallo, A. Ghigo, M. Migliorati (Ass.),
A. Mostacci (Ass.), L. Palumbo (Ass., Resp. Naz.), L. Pellegrino, R. Ricci,
F. Sgamma, B. Spataro, F. Tazzioli (Ass.), S. Tomassini, C. Vaccarezza,
M. Vescovi (Ass.), C. Vicario (Art. 23)
INFN - LNF

L. Catani, A. Cianchi, D. Di Giovenale, B. Marchetti, S. Tazzari
INFN - Roma2

A. Bacci, I. Boscolo, F. Broggi, S. Cialdi, D. Giove,
C. Maroli, V. Petrillo, A. R. Rossi, L. Serafini
INFN - Milano

M. Mattioli
INFN - Roma

A. Perrone
INFN - Lecce

F. Ciocci, G. Dattoli, A. Dipace, A. Doria, G.P. Gallerano, L. Giannessi, E. Giovenale,
G. Messina, P.L. Ottaviani, S. Pagnutti, L. Picardi, M. Quattromini, A. Renieri, G. Ronci,
C. Ronsivalle, M. Rosetti, E. Sabia, M. Sassi, A. Torre, A. Zucchini
ENEA/FIS

J. Rosenzweig
UCLA

1 Aim of the experiment

The aim of the SPARC project is to promote an R&D activity oriented to the development of a high brightness photoinjector to drive SASE-FEL experiments. It has been proposed by a collaboration among ENEA-INFN-CNR-Università di Roma Tor Vergata-INFM-ST and funded by the Italian Government and INFN.

The main goals of the SPARC project are:

- the generation of a high brightness electron beam able to drive a Self Amplified Spontaneous Emission Free Electron Laser (SASE FEL) experiment in the green visible light, Seeding and Higher Harmonics Generation,
- the development of an ultra-brilliant beam photo-injector needed for the future SASE FEL-based X-ray sources, as for the recently funded 1 GeV 10 nm FEL project SPARX whose SPARC is become its test facility.

The SPARC injector will allow also investigations into the physics of ultra-short beams, plasma wave-based acceleration, and production of X-ray Compton back-scattering as reported in the PLASMON activity section.

2 Group activity in 2008

The year was mainly dedicated to complete the alignment of the undulator modules and the commissioning of the machine. For this stage of commissioning we have operated with a laser pulse with gaussian longitudinal profile of FWHM in the order of 6-8 ps. The bunch charge was between 200 pC up to 700 pC, mainly limited by the low (in the lower order of 10^{-5}) and not constant quantum efficiency of the cathode. Also several improvements in term of energy efficiency and stability has been achieved on the laser system. In the following we described the progress and the achievement in several subsystems.

Two main technical failures, both related with the SPARC plants, reduced the running time between July and mid November. At the beginning of July t he temperature of the power supplies room increased over the interlock limit. There is no refrigeration plant in this hall. Only in September was possible to start the machine. Suddenly a spike in the pressure of the water system resulted in the damage of the window of the RF circulator. While the circulator was unplugged and send in the US for the reparation an old RF circulator was found in Milan and replaced in the mid November.

2.1 Laser System

The research on the shaping of ultrafast laser pulses has been completed at the SPARC photoinjector of LNF-INFN. The promise of increasing the brightness of electron beams from RF (radio frequency) photoinjectors by using a flat top UV laser pulse to illuminate the cathode was the application inspiring the pulse shaping activity. Previously different pulse shapers in the IR have been experimentally characterized. The layout of the experimental setup is reported in Fig. 10. The pulse shapers were installed after the laser oscillator and before the amplification stages in order avoid energy losses and optical damages.

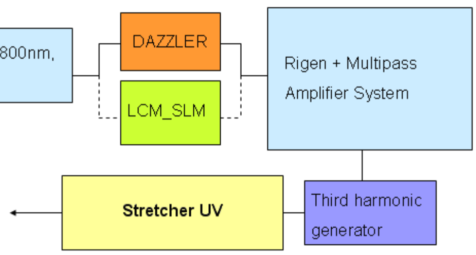

Figure 1: *Laser pulse shaper.*

We tested the programmable dispersive acousto-optic modulator (the DAZZLER) and the liquid crystal mask spatial light modulator (LCM-SLM) placed in a 4-f optical setup. Since these shapers are installed before the amplification and the third harmonic generator, the final UV pulse is affected by strong distortions. To improve the rise time of the flat top pulse we specifically designed an optical system based on the UV stretcher. This stretcher is designed in order to have a plane where the input wavelengths are spatially dispersed for a suitable spectral amplitude modulation. Beside, this apparatus permits, changing the distance between the gratings, the fine control of the final pulse length.

In such scheme the laser beam is diffracted 4 times by the gratings. Since the metal coated reflective gratings used so far, have a diffraction efficiency of 60% at the operating wavelength, the overall efficiency is less than 15%. The poor efficiency significantly limits the attainable charge and increases the energy demands on the laser system. At higher energy the laser energy fluctuations becomes larger and, moreover, the probability of optical damages grows significantly. During the 2008, to enhance the stretcher efficiency the metal coated reflective gratings have been replaced with transmission one. The new gratings are ruled on two mm thick fused silica substrate. The diffractive area is 30 by 30 mm and the grooves density is 4500per mm. The efficiency of this typology of grating is maximized for radiation linear polarized TE and can reach at the Littrow angle 90%. The final efficiency is therefore more than 50%. Moreover the available energy per pulse at the cathode could be easily tripled. To rotate the polarization from TM to TE a polarization rotation periscope has been installed upstream the UV stretcher.

The optical transport to the cathode has been improved in order to increase the flexibility in the laser beam control of the best transverse shape at the cathode. The optical transport has been designed in order to produce at the cathode the image of an iris used to select a hard edge flat top transverse shape. In the optical path a three lenses telescope has been designed and tested. This device permits the control of the spot dimension at the cathode maintaining the perfect image of the iris. The three lenses telescope is designed to permits a dimension variation more than a factor 3.

During the 2008 other improvement on the laser system has been achieved. An improvement on the laser room conditioning system and a new temperature setting point reduced the daily temperature variation, guaranteeing a more stable laser source operation. The control of the temperature reduced the long term drift in the laser energy and pointing. Beside, the optical table for the laser s ystem has been completely covered in order to avoid air turbulences and powder deposition on the optics. The cover mitigated the amplitude and the position jitter on short term time scale. In Fig. 2 is shown the comparison between the former and the actual situation.

2.2 RF

The synchronization of the SPARC photodiode laser to the RF reference is routinely monitored and adjusted in a slow feedback loop configuration by means of a pulse resonant stretching method sketched in the Fig. 3

The core of this system is the HV photodiode which converts a sample of the photocathode laser into an electrical pulse that impulsively excites free oscillations of a finely tuned resonant cavity. This system has been upgraded in 2008 by implementing a new photodiode (Photek PD025, Fig. 3) equipped with its own HV supply and capable to deliver electrical pulses of ≥ 1 kV peak and duration ≤ 200 ps FWHM, with an overall benefit in the signal-to-noise ratio in the phase detection process. The laser-to-RF jitter measured with this technique is typically 400 fs rms in operation,

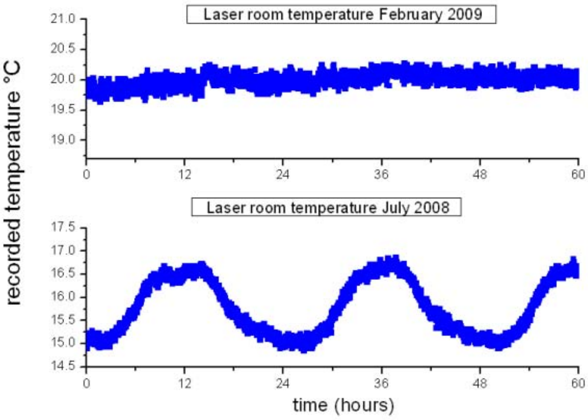

Figure 2: *Laser room temperature.*

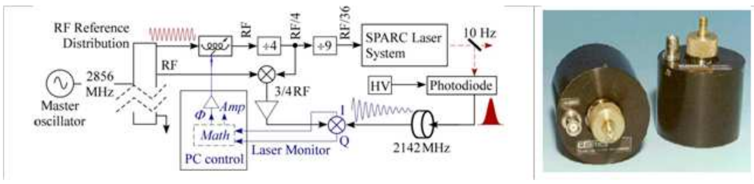

Figure 3: *Left:Sketch of the Laser to RF synchronization. Right: HV photodiode.*

and it is limited by the performances of the Synchrolock system keeping the laser oscillator phase-locked to the RF. To overcome this limitation we have tested a different architecture of the facility s ynchronization which is "laser driven" more than "RF driven". In this case the RF reference sine-wave is extracted from the laser oscillator pulse train with a high rep-rate photodiode followed by a tuned filter. The sketch of the test of this different architecture is shown in Fig. 4

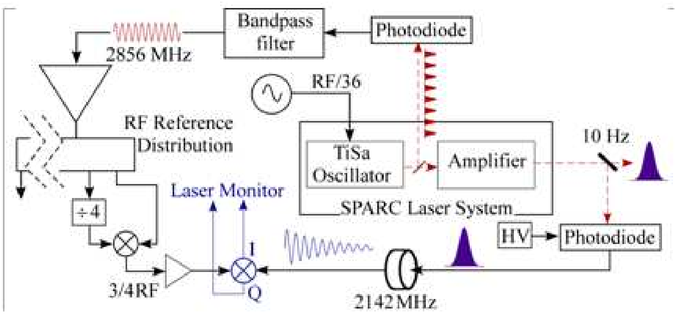

Figure 4: *Laser to RF jitter measuerements.*

The Synchrolock system performances are not crucial in this case, and the o verall laser-to-RF jitter is then reduced to 200 fs rms, mainly due to the s pecifications of the divider-by-4 prescaler board present in this configuration.

2.3 SPARC Commissioning

SPARC is a normal conducting accelerator. The RF gun is one of the most recent generation 1.6 cell S-band BNL/UCLA/SLAC type follow by 3 S-band traveling wave accelerator constant gradient structures. The power sources are the 45 MW peak, 2856 MHz klystron TH2128C. The Klystron n.1 feeds the the RF gun and the third accelerating structure with 3.6 μs RF pulses. Klystron n.2 feeds two high gradient accelerating sections through an energy compressor that allows to obtain 60 MW - 0.8 μs RF pulses. Around the first and the second accelerating structure several solenoids are placed to provide additional focusing both for velocity bunching and to match the beam envelope with the linac according with the invariant envelope scheme.

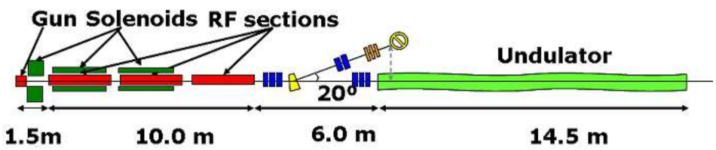

Figure 5: *SPARC layout.*

The undulator is composed by 6 sections of permanent magnet undulator, separated by 0.36 m gaps, and featuring single quadrupoles which focus the electron beam in the horizontal plane.

Every module contains 75 periods each one 2.8 cm length, with an undulator parameter kw = 1.4. The FEL will operate in self amplified spontaneous emission (SASE) mode at a wavelength of about 500 nm with an expected saturation length of about 10-12 m.

For this stage of commissioning we have operated with a laser pulse with gaussian longitudinal profile of FWHM in the order of 6-8 ps. The bunch charge was between 200 pC up to 700 pC, mainly limited by the low (in the lower order of 10^{-5}) and not constant quantum efficiency of the cathode.

Two main technical failures, both related with the SPARC plants, reduced the running time between July and mid November. At the beginning of July the temperature of the power supplies room increased over the interlock limit. There is no refrigeration plant in this hall. Only in September was possible to start the machine. Suddenly a spike in the pressure of the water system resulted in the damage of the window of the RF circulator. While the circulator was unplugged and send in the US for the reparation an old RF circulator was found in Milan and replaced in the mid November.

2.4 SPARC Diagnostic commissioning

SPARC is a R&D machine to produce high brightness beam and to conduct extensive studies on the beam dynamics. In order to achieve these goals a precise characterization of the beam parameters is needed. Here a brief review of our diagnostic tools.

2.5 Beam Envelope and transverse emittance

The beam envelope is measured in four different positions: one before the first accelerating module, 1181 mm far away from the cathode, two others positions are between the accelerating modules, and the last at the exit of the third module. The measurements of the beam envelope is mandatory in order to fulfill the requirements of the invariant envelope matching.

Downstream the last section several diagnostic tools for a full characterization of the beam parameters are installed. A triplet of quadrupoles is followed by the SPARC RF deflector, the dipole for the high energy measurement and the flags to evaluate the beam parameters (see Fig. 6).

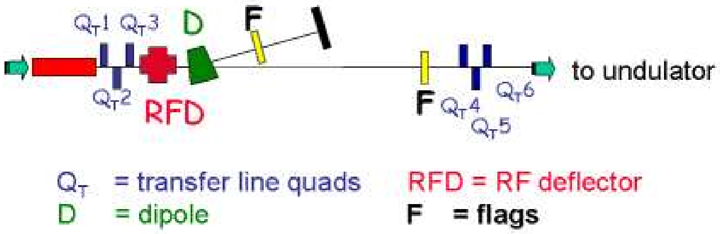

Figure 6: *Layout of the experimental area at 150 MeV.*

The quadrupoles are routinely used for the quadrupole scan in order to evaluate the transverse emittance. This technique allows, powering the RF deflector, also the investigation of the longitudinal phase space via the measurements of the slice emittance.

2.6 Longitudinal parameters

A preliminary measurement of slice emittance has been performed. The bunch charge was 300 pC, 5.3 FHWM bunch length, with a beam energy of 145 MeV. The result is consistent with a measurement of the projected emittance that gives (2.8±0.1) mm-mrad.

Referring to Fig. 6 only the quadrupoles named QT2 and QT3 have been used together in order to maintain the vertical dimension (i.e. the longitudinal resolution) constant during the scan. The slice length has been set to 150 μm i.e. about 0.5 ps.

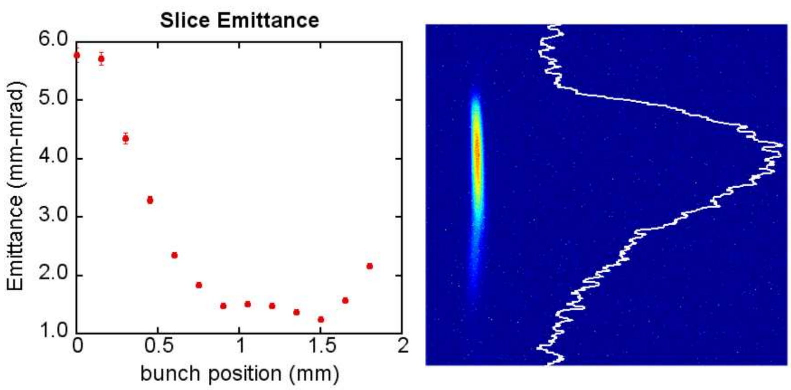

Figure 7: *Left:Slice emittance measurement. Right: Bunch length measurements.*

The evaluation of the bunch length is mandatory especially in the foreseen studies of the velocity bunching. The RF deflector is used for this task. The ultimate temporal resolution is affected not only from the deflecting voltage but also from the intrinsic vertical dimension of the beam size at the flag when the deflector is off. In the actual condition the temporal resolution is estimated to be around 1 ps.

In Fig. 7 a measurement with 300 pC charge is reported, giving a length of 7.7 ps FWHM equal to 5.5 mm on the flag.

2.7 Velocity bunching

Some preliminary tests of beam longitudinal dynamics in the Velocity Bunching regime have been also performed. Figure 8 shows the measured compression factor for a 250 pC beam vs the phase of the first traveling wave.

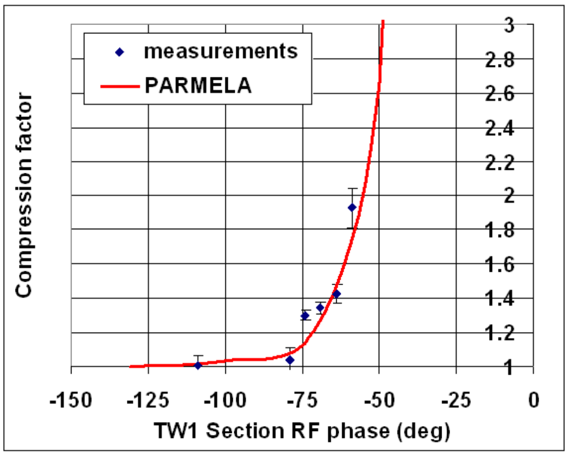

Figure 8: *Bunch length measurements versus accelerating phase in the first accelerating module.*

The reduction of the bunch length from 5 ps to 2.5 ps for a phase range variation of 20 degrees results to be in good agreement with PARMELA simulations.

The 2009 activities will be focused on the velocity bunching, with the goal of obtaining the compression of the bunch keeping small the transverse emittance; on the FEL studies, including saturation on the fundamental harmonic, seeding experiment and studies of the high order harmonic.

3 SPARX

In 2008 the team contributed also to the preparatory phase of the SPARX facility, which is in an advanced state of progress with the completion of the Technical Design Report (TDR), the preparation of the updated Scientific Case and the starting of the Consortium LUCE, being constituted by CNR, ENEA, INFN and the University of Roma Tor Vergata, which will take care of the construction and the operation of the source.

3.1 Machine description and Parameter list

SPARX-FEL facility will host two beamlines for each undulator source in order to maximize the users accessibility. The beamlines, optimized for high photon energy resolution and for short-pulse handling, have been designed for the following energy ranges:

1. VUV-EUV beamline: 40 -124 eV (10 -30.5 nm)
2. EUV - Soft X-ray beamline: 88.5 1240 eV (1 - 14 nm)
3. Soft-X-ray beamline: 1280 eV 2000 eV (0.6 1.2 nm)

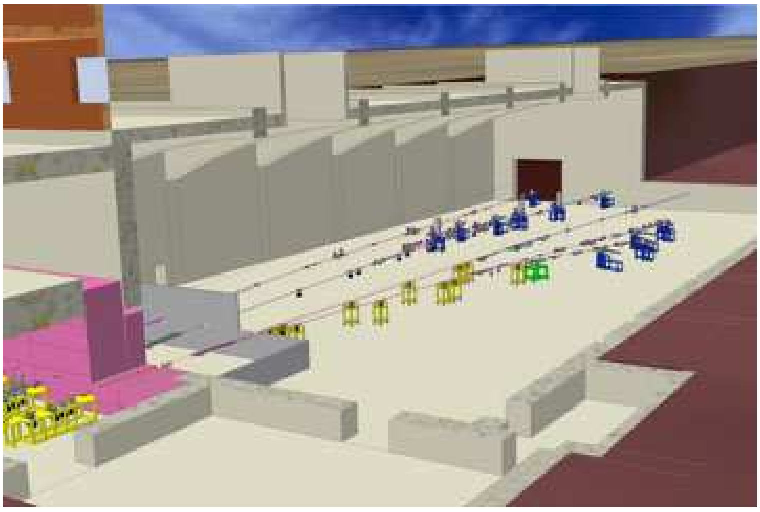

Figure 9: *SPARX Experimental hall.*

The photon beamlines are driven by the SPARX accelerator, which is meant to be realized in two phases with two different electron beam energies: one up to 1.5 GeV and the other up to 2.64 GeV. In order to reach SASE saturation in undulators of reasonable length, a peak current Ipk=1÷2.5 kA is needed for lower and higher energies respectively. The required final beam energy spread is 0.1% in each case and the machine is designed to operate at a repetition rate of 100 Hz. The main parameter list is reported in Table 1.

Table 1: Electron beam parameter list.

Energy	(GeV)	E	1÷1.5	2.4
Peak current	(kA)	I_{pk}	1	2.5
Normalized transverse emittance slice	(μm)	ϵ_n	1	1
Correlated energy spread	(%)	σ_δ	0.1	0.1
Radiation wavelength	(nm)	γ_r	40÷3	3÷0.2

A schematic lay-out of the machine is shown in Fig. 10.

SPARX acceleration and compression schematic layout using SPARC injector. A multistage Linac delivers the accelerated electron beams, at energies between 0.96 and 2.64 GeV, to three undulators through doglegs DL 1-2-3. The bunch compressors BC 1-2-3 are four-dipole chicanes, DG indicates diagnostic stations.

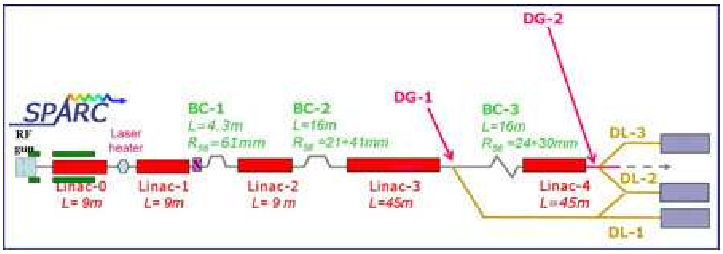

Figure 10: *SPARX acceleration and compression schematic layout using SPARC injector. A multistage Linac delivers the accelerated electron beams, at energies between 0.96 and 2.64 GeV, to three undulators through doglegs DL 1-2-3. The bunch compressors BC 1-2-3 are four-dipole chicanes, DG indicates diagnostic stations.*

References

1. A. Cianchi *et al.*, PRST-AB, 11, 032801 (2008).
2. A. Mostacci *et al.*, Review of Sci. Instr. **79**, 013303 (2008).
3. M. Boscolo *et al.*, Nucl. Instr. & Meht. A **593**, 106 (2008).
4. L. Giannessi *et al.*, Nucl. Instr. & Meht. A **593**, 132 (2008).
5. M. Boscolo *et al.*, Nucl. Instr. & Meht. A **593**, 137 (2008).
6. J. Rosenzweig *et al.*, Nucl. Instr. & Meht. A **593**, 39 (2008).
7. R. Boni at al. “Activities on High Brightness Photo-Injectors at the Frascati Laboratories, Italy”, Proc. of Linac08, Victoria, CDN.
8. F. Anelli *et al.*, “SPARC Control System Operation”, Proc. of PCaPAC08, Ljubljana, Slovenia.
9. M. Migliorati, G. Dattoli, A. Schiavi, and M. Venturini, “A four-dimensional Vlasov solver for microbunching instability in the injection system for X-ray”, contribution at 2008 European Particle Accelerator, Conference, pp. 1764-1766, Genova, Italy, June 2008.
10. C. Ronsivalle *et al.*, “Simulations of the Emittance Compensation in Photoinjectors and Comparison with SPARC Measurements”, Proc. of EPAC 2008, Genova, Italy.
11. V. Petrillo *et al.*, “Single Spike Operation in SPARC SASE-FEL” Proc. of EPAC 2008, Genova, Italy.
12. A. Cianchi *et al.*, “Preliminary Characterization of the Beam Properties of the SPARC Photoinjector”, Proc. of EPAC 2008, Genova, Italy.

13. V. Fusco *et al.*, “Spatial Autocorrelation for Transverse Beam Quality Characterization”, Proc. of EPAC 2008, Genova , Italy.

14. C. Vaccarezza *et al.*, “Slice Emittance Measurements at SPARC Photoinjector with a RF Deflector” Proc. of EPAC 2008, Genova , Italy.

15. M. Boscolo *et al.*, “A Possible THz Radiation Source with a Train of Short Pulses in the SPARC High Brightness Photoinjector”, Proc. of EPAC 2008, Genova , Italy.

16. M. Ferrario *et al.*, “Recent Results and Future Perspectives of the SPARC Project”, Proc. of EPAC 2008, Genova , Italy.

17. A. Gallo *et al.*, “Performances of the SPARC Laser and RF Synchronization Systems”, Proc. of EPAC 2008, Genova , Italy.

18. M. Ferrario *et al.*, “Recent Results Of The Sparc Project”, Proc. of FEL Conference 2008, Korea.

19. M .Boscolo at al. “Single spike experiments with the SPARC SASE FEL”, Proc. of FEL08 Korea.

General Information

Communication and Outreach

R. Centioni, V. Ferretti (Art. 15), L. Sabatini, S. Vannucci (Resp.)
Office for Education and Public Relations
Scientific Information Service

The "Laboratori Nazionali di Frascati dell'INFN" (INFN-LNF) provide basic education in Physics for the general public, students and teachers. The LNF Educational and Public Relation programmes are made possible by the enthusiastic involvement of the laboratory graduate students, postdocs, researchers, engineers and technicians.

1 Visiting LNF

`http://www.lnf.infn.it/edu/`

- *LNF Guided Tours* (about 3000 people). A well established tradition, for general public, students and teachers. A typical visit consists of: a brief historical presentation of the laboratory; a presentation of the activities on site and abroad; a visit to the "en plein air museum" and the experimental areas.
- *LNF Scientific Week and Open day* (650 visitors). Scientific Coordinator: P. Di Nezza. Most of LNF employees are in action to present their research center, answer questions and care for their guests. The standard format of the event provides for guided tours; conferences and public lectures; scientific videos;

2 Scientific Itineraries - Frascati Scienza

The aim is to offer a more complete view of the scientific institutions operating in the area and improve the communication with the general public. In collaboration with: CNR, ENEA Frascati, ESA-ESRIN Frascati, INAF, Frascati Scienza, Associazione Eta Carinae, Associazione Tuscolana Astronomia, Frascati and Castelli Romani Municipalities, International non-government organizations, University of Rome Tor Vergata.

3 Students' programme

- *LNF Stages for high school students.* Scientific Coordinators: F. Bossi, P. Gianotti.

  `http://www.lnf.infn.it/edu/stagelnf/`

  The aim is to enable students to acquire the knowledge and understanding of INFN research activities. The programme consists of:

  - Winter stages, 9 days: 34 students with 19 tutors;
  - EU Project Masterclasses 2008, 3 days: 33 students with 8 tutors;

- Summer stages, 2 weeks: 94 students with 36 tutors;
- Lectures at school by LNF researchers, 2-3 days: 371 students with 22 tutors.

- *Special Programme for Primary School: QUASAR.* Care of F. Murtas and B. Sciascia.

  `http://www.lnf.infn.it/edu/quasar/`

  First meeting with the children (age: 8 - 14) at their school to introduce the world of research and some concepts of modern physics. Then a visit to the Frascati National Laboratories by small groups. Total of children and teachers in visit: 520.

4 High school teachers' programme

- *"Incontri di Fisica".* Organizing Committee: P. Di Nezza (chair), D. Babusci, M. Calvetti, P. Campana, L.E. Casano, R. Centioni, C.O. Curceanu, V. Ferretti, S. Miozzi, L. Sabatini, S. Vannucci.

  `http://www.lnf.infn.it/edu/incontri/`

  The event consists in lectures for high-school science teachers and people involved in scientific research dissemination. The aim is to stimulate teachers' professional training and provide an occasion for interactive and hands-on contact with the latest developments in physics. 8th edition (October 1-3, 2008): 152 participants and 49 LNF Tutors (researchers, engineers and technicians).

- *Lezioni di Fisica.* Care of M. Calvetti, O. Ciaffoni, G. Di Giovanni and SIS Education and Public Relations.

  Live lectures by scientists for teachers and students avalaible at

  `http://www.lnf.infn.it/media/`

5 General public programme

- *Seminars*

  `http://www.lnf.infn.it/edu/seminaridivulgativi/`

  Upon request, LNF researchers gave seminars to high school students and the general public. The following is the list of the seminars in 2008:

  - G. Pancheri, "The questions of physics and the first matter and antimatter collisions in Italy", Liceo P.M. Vermigli (Zurich), February 17.
  - P. Di Nezza, "Notes on modern physics. Elementary particles physics", Lic. Sc. G. Galilei di Potenza, March 31.

Figure 1: *High school teachers programme: Incontri di Fisica. The picture has been taken during the talk given by prof. De Rujula (CERN).*

- P. Campana, "LHC: final frontier", Lic. Sc. G. Peano, Monterotondo (RM), April 1.
- E. Chiadroni, "SPARX, light of the future. Physics and applications", Lic. Sc. A. Landi, Velletri (RM), April 8.
- S. Miozzi,"Space and time in the Einstein Universe", Lic. Sc.Landi, Velletri (RM), April 10.
- G. Pancheri, "Gender issues in the EU: how Brussels is moving towards gender equity", March Meeting of the American Physical Society, St. Louis, April 12.
- G. Pancheri, "Gender issues in the EU and other stories", Boston University Seminar, Boston, April 24.
- G. Pancheri, "Activity of Frascati INFN, National Laboratories", Science Festival *Apriamo la mente 2008*, LNF, May 9
- G. Pancheri, "Bruno Touschek and the Frascati story: thirty years latery", LNF Spring School Bruno Touschek, May 12.
- F. Bossi,"Nuclear physics and elementary particle physics", Lic. Sc. F. d′Assisi, Roma, May 13.
- S. Miozzi, "Special Relativity", Lic. Sc. F. d′Assisi, Roma, May 15.

• *Bruno Touschek and Frascati Special activity.* Care of G. Pancheri.
The movie "Bruno Touschek and the art of physics", produced by INFN, was sent to the CERN Courier and received a very favourable review [1]. It has then been requested and sent to a number of physicists from various Laboratories around the world. The movie was

also presented at the Zurigo Italian High School Piermarin in February 2008 and at the LNF Spring School Bruno Touschek in May 2008.

The magazine Analysis prepared an issue about "50 anni dei Laboratori Nazionali di Frascati" dedicated to the history of Frascati INFN Laboratories, which was edited by Toni Baroncelli and G. Pancheri [2] and includes an article about theoretical physics activities in Frascati [3] since the arrival of Gatto and Touschek in the late '60s.

A contribution to a volume of recollections by italian physicists [4] includes an article by G. Pancheri with a tribute to Bruno Touschek's contribution to theoretical physics.

6 Events

- *European Researchers' Night.* Project Coordinator: Catalina Curcenau.

  `http : //www.lnf.infn.it/nottedellaricerca/`

  The event has been organized within the European Researchers' Night on September 26, 2008. About 600 visitors at LNF.

  An important feedback of the success of the event comes from the questionnaire (available on the web site http://www.infn.it/nottedellaricerca) addressed to investigate the achievement of the main purpose of the project and of the quality of the activities.

- *Christmas Concert.* Since 2002, in the week preceding Christmas, the LNF organize a Concert in the Bruno Touschek auditorium located in the High Energy building. In 2008 the concert has been held by Giovanna Marini and the "Corso di Canto di Tradizione Orale " di Monte Porzio Catone (RM).

Figure 2: *Christmas Concert, 18 December 2008 (INFN-LNF Photo).*

7 Conferences

For the the list of International Conferences, Workshops and Meeting hosted and/or organized by the LNF see next chapter.

References

1. C. Sutton "Bruno Touschek and the art of physics", CERN Courier, April 16, 2008, `http://cerncourier.com/cws/article/cern/33813/2`.
2. T. Baroncelli and G. Pancheri, Analysis **2+3**, 2 (2008).
3. M. Greco and G. Pancheri, Analysis **2+3**, 20 (2008).
4. G. Pancheri, *Maestri ed allievi nella fisica italiana del Novecento*, Ed. L. Bonolis, Pavia, La Goliardica Pavese, 2008.

CONFERENCES, WORKSHOPS and MEETINGS in 2008

International conferences, workshops and meetings hosted and/or organized by LNF:

1. *Alice EMCal Production* Meeting, LNF, 16-17 January, 2008.
2. Workshop on *Montecarlo, la fisica e le simulazioni a LHC*, LNF 18-20 February, 2008.
3. Workshop on *PANDA Grid*, LNF 5-7 March, 2008.
4. International Workshop on *e^+e^- collisions from ϕ to ψ* LNF 7-10 April, 2008; Proc. avalaible in Nucl. Phys. B (Proc. Suppl.) **181+182** (2008), Eds. C. Bini and G. Venanzoni.
5. Meeting on *Radiative corrections and generators for low energy hadronic cross section and luminosity*, LNF 11 April, 2008.
6. LNF Spring School *Bruno Touschek*, LNF 12-16 May, 2008.
7. *Alice Italia* Meeting, LNF 14-15 May, 2008.
8. Workshop on *Frontier objects in Astrophysics and Particle Physics*, Vulcano 25-31 May, 2008.
9. *Mini-Mac* Meeting, LNF 16-17 July, 2008.
10. International Workshop on *Compton Sources for X/γ rays: Physics and Applications*, Alghero 7-12 September 2008; Proc. will be published in Nucl. Instr. Meth A, Eds. M. Carpinelli and L. Serafini.
11. International Workshop on *Diffraction in High-Energy Physics*, La Londe (France) 9-14 September, 2008.
12. Workshop on *Strings and Strong Interactions*, LNF 18-19 September, 2008.
13. Workshop on *LC08: e^+e^- Physics at the TeV scale*, LNF 22-25 September, 2008.
14. Workshop on *WUVV08: The use of Synchrotron UV and Visible Radiation*, LNF 8-10 October, 2008.
15. *Nanoscience & Nanotechnology 2008*, LNF 20-22 October, 2008.
16. International Conference on *Theoretical and experimental aspects of the spin-statistic connection and related symmetries*, Trieste 21-26 October, 2008.
17. *Channeling 2008*, Erice 25 October/1 November 2008.
18. *CERN Accelerator School*, Monte Porzio Catone 2-14 November, 2008.
19. *Hiper WP12* Meeting, LNF 20-21 November, 2008.
20. Workshop on *High-harmonic seeding for present and future short wavelength Free-Electron Lasers (FELs)*, LNF 3-5 December, 2008.
21. Japan-Italy Collaboration Meeting on *Crab Factories*, 10-11 December, 2008;
22. Workshop on *SuperB Computing*, LNF, 16-17 December, 2008.

Publications

1 – Frascati Physics Series

(available at `www.lnf.infn.it/sis/frascatiseries/index.html`)

Volume XLVIII– Special Issue
Les Rencontres de Physique de la Vallée d'Aoste – Results and Perspectives in Particle Physics,
Ed.: M. Greco
La Thuile, Aosta Valley, February 24 - March 1, 2008
ISBN 978–88–86409–56–8

2 – LNF Frascati Reports

(available at `www.lnf.infn.it/sis/preprint/search.php`)

LNF-08–1(P)
D. Arnold *et al.*, "The INFN-LNF Space Climatic Facility", 10th ICATPP Conference on Astroparticle, Particle, Space Physics, Detectors and Medical Physics Applications, Villa Olmo (Como), 8-12 October 2007.

LNF-08–2(P)
R. M. Godbole, A. Grau, G. Pancheri, and Y.N. Srivastava, "Large Rapidity Gaps Survival Probabilities at LHC", Presented at ISMD07.

LNF-08–3(P)
D. Currie, S. Dell'Agnello, G. Delle Monache, M. Garattini, and R. Tauraso, "A New Approach to LAGEOS Spin Orientation and its Role IN General Relativity Measurements", Submitted to the 10th ICATPP Conference on Astroparticle, Particle, Space Physics, Detectors and Medical Physics Applications, 8-12 October 2007, Villa Olmo (Como), Italy.

LNF-08–4(P)
S. Bellucci, F Micciulla, and N. Pugno, "Properties of Nanocomposites Based on Resin and Carbon Nanotubes", Reserch Signpost, The Nanomechanics in Italy.

LNF-08–5(P)
R.M. Godbole, A. Grau, G. Pancheri, and Y.N. Srivastava, "Minijets, Soft Gluon Resummation and Photon Cross-Sections", Nucl. Phys. B **184**, 85 (2008).

LNF-08–6(IR)
S. Dell'Agnello *et al.*, "Fisica Fondamentale con la Missione Lunare MAGIA".

LNF-08–7(IR)
S. Dell'Agnello *et al.*, "Far Field Diffraction Pattern Test of LARES Retroreflectors and Thermal Characterization of LARES Bread-Boards at INFN-LNF".

LNF-08–8(P)
M. Pedio *et al.*, "A Nexafs Study of Nitric Oxide Layers Adsorbed from a Nitrite Solution Onto a Pt(111) Surface", Submitted to Journ. Chem. Phys.

LNF-08–9(P)
A. Marmigi, A. Spallone, F. Celani, P. Marini, and V. di Stefano, "Anomalous Heat Generation by Surface Oxidized Pd Wires in a Hydrogen Atmosphere", Presented at the, 8th International Workshop on Anomalies in Hydrogen-Deuterium Loaded Metals Catania, October 13-18, 2007, Submitted to World Scientific, CMNS Series, 2008.

LNF-08–10(P)
A. Spallone, A. Marmigi, F. Celani, P. Marini, and V. di Stefano, "A Review of Experimental studies about Hydrogen over-loading within Palladium wires (H–Pd ≥ 1)", Presented at the 8th International Workshop on Anomalies in Hydrogen–Deuterium Loaded Metals Catania, October 13-18, 2007, Submitted to World Scientific, CMNS Series, 2008.

LNF-08–11(P)
F. Celani *et al.*, "High Temperature Experiments, by Differential Reactor, on Deuterium Absorbed by HSA Pd_{black} γ Al_2O_3-Pd-$Sr(NO_3)_2$ Nanopowder", Invited paper at the 8th International Workshop on Anomalies in Hydrogen-Deuterium Loaded Metals, 13-18 October 2007, Cannizzaro (CT), Italy.

LNF-08–12(IR)
S. Dell'Agnello, G. O. Delle Monache, A. Boni, N. Intagletta, and M. Tibuzzi, "Design, Construction and SCF-Test of a Laser-ranged Test mass for the Deep Space Gravity Probe Mission", 3-Year Study on *Cosmology and Fundamental Physics (COFIS)* Funded by the Italian Space Agency.

LNF-08–13(P)
LNF Accelerator Division, Papers presented at PAC 2007.

LNF-08–14(NT)
A. Paoloni *et al.*, "Multi-Streamer Studies on Gas Mixtures for the OPERA RPCs".

LNF-08–15(TH)
C. Lo Surdo, "Fondamenti della Fisica-Matematica Classica, una Introduzione".

LNF-08–16(P)
F. Terranova, H. Kiriyama, and F. Pegoraro, "Bandwidth Enhancement for Parametric Amplifiers Operated in Chirped Multi-Beam Mode", Submitted to Optics Communications.

LNF-08–17(P)
A. Achilli, A. Grau, G. Pancheri, and Y. N. Srivastava, "QCD Contributions to the Froissart Bound for the Total Cross-Section", Presented at Hadron Structure'07, HS07, Modra-Harmonia, September 3-7, 2007.

LNF-08–18(P)
D. Hampai *et al.*, "Elemental Mapping and Micro-Imaging by X-Ray Capillary Optics", Optics Letters **33**, 2743 (2008).

LNF-08–19(Thesis)
J. Zdebik, "Merging and Splitting of Clusters in the Electromagnetic Calorimeter of the KLOE Detector".

LNF-08–20(IR)
AA.VV, *Activity Report 2007*.

LNF-08–21(IR)
V. Lucherini and T. Bressani, "KAIUM at DAΦNE ?".

LNF-08–22(IR)
A. Babaev *et al.*, "On Crystal-Assisted Processes by Means of 20-800 MeV e^-e^+ LNF Beams".

LNF-08–23(NT)
L. Quinteri, "Design of the Radiation Shielding Around the DAΦNE BTF Target".

LNF-08–24(NT)
L. Quinteri, "Feasibility Study of a Neutron Source at the DAΦNE BTF Facility".

LNF-08–25(IR)
M. Cordelli, R. Habel, A. Martini, and L. Trasatti, "Nerone Test at 2500 m depth".

LNF-08–26(IR)
A. Boni *et al.*, "Optical Far Field Diffraction Pattern Test of Laser Retroreflectors for Space Applications in Air and Isothermal Conditions at INFN-LNF".

LNF-08–27(P)
L. Benussi *et al.*, "Sensitivity and Environmental Response of the CMS RPC Gas Gain Monitoring System", Presented at the IEEE, 8-23 October 2008, Dresden, Germany.

LNF-08–28(P)
R.M. Godbole, A. Grau, G. Pancheri, and Y.N. Srivastava, "Total Photo-Production Cross-Section at Very High Energy", Submitted to European Journal of Physics C.

LNF-08–29(P)
L. Benussi *et al.*, "The CMS RPC Gas Gain Monitoring System: an Overview and Preliminary Results", Presented by L. Benussi at the RPC07, February 2008, Mumbai, India.

LNF-08–30(P)
Y. N. Srivastava, A. Achilli, R. Godbole, A. Grau, and G. Pancheri, "Photoproduction Total Cross-Sections at Very High Energies and the Froissart Bound".

LNF-08–31(P)
R.M. Godbole, A. Grau, G. Pancheri, and Y.N. Srivastava, "QCD and Total Cross-Sections: Photons and Hadrons".

LNF-08–32(Thesis)
S. Colafranceschi, "Uso dei Sensori in Fibra Ottica per Applicazioni Aerospaziali e per i Rivelatori dell'Esperimento CMS".

3 – INFN Reports

(available at `www.lnf.infn.it/sis/preprint/search.php`)

INFN–AE–08–1
P. La Rocca and F. Riggi, "Nuclear Photodisintegration in the Solar Field: Numerical Simulations of the Gerasimova-Zatsepin Effect".

INFN–TC–08–1
S. Barbanotti, M. Bonezzi, M. Todero, and N. Panzer, "Traction Tests for The Qualification of the TTF-ILC Composite Support Posts".

INFN–TC–08–2
M. Anghinolfi *et al.*, "Study of the Response of the NEMO-KM3 Detector Instrumented with Direction-Sensitive Optical Module".

INFN–TC–08–3
V. Diaz, P. Ciliberti, S. Levorato, and M. Bari, "New Monochromator and Sonar System - User Manual".

INFNTC–08–4
S. Andreozzi and M. Marzolla, "A Restful Approach to the OGSA Basic Execution Service Specification".

INFN–TC–08–5
A. Paccalini, G. Rivoltella, and G. Volpini, "A Thermal Conductivity Measurements at Cryogenic Temperatures: Hardware and Software Apparatustonio".

INFN–TC–08–6
P. Andreetto *et al.*, "Standards-Based Job Management in Grid Systems".

INFN–TC–08–7
F. Astuti *et al.*, "Characterization of Avalanche Photo Diodes for the First Super-Module of the ALICE Electromagnetic Calorimeter".

INFN–TC–08–8
M. Cresta, D. Piombo, and F. Pratolongo, "La Power Board per la Stringa Antares a Capo Passero".

INFN–TC–08–9
E. Energico and P. Parascandolo, "L' Amplificatore di Carica del Chip SER–09".

INFN–TC–08–10
A. Anastasio, A. Pandalone, and A. Vanzanella, "Scheda DWFD dellEsperimento EXPADES".

INFN–CCR–08–1
R. Alfieri and R. Covati, "Una Infrastruttura di Autenticazione e Autorizzazione Flessibile e Scalabile per una Comunitá Scientifica Locale".

INFN–CCR–08–2
M. Michelotto, "Worker Node per il Calcolo LHC".

INFN–CCR–08–3
V. Ardizzone, A. Calanducci, and E. Giorgio, "Rapporto sull′Attività Svolta nei due Corsi INFN per la Formazione GRID", Martina Franca (TA), 5-9 e 12-23 Novembre 2007.

INFN–CCR–08–4
R. Alfieri, R. Covati and E. Tagliavini, "Integrare il Calcolo Locale MPI nella FARM INFN-GRID".

SEMINARS in 2008

S. Dell'Agnello	INFN LNF
27-11-2008	*Probing gravity with the international lunar network and the proposed* ASI lunar mission MAGIA
M. Milanese	Politecnico di Torino
19-11-2008	*KiteGen project: High Altitude Wind Generation for Renewable Energy cheaper than Oil*
B. Bernstein	FNAL
13-11-2008	*Prospects for a High-Sensitivity Lepton Flavor-Violating Search at Fermilab*
A. Strumia	Pisa University
06-11-2008	*Model-independent implications of the positron, electron, anti-proton cosmic ray spectra on properties of Dark Matter*
S. Adler	Institute for Advanced Study (Princeton)
29-10-2008	*Can the flyby anomaly be attributed to earth-bound dark matter?*
M. Casolino	INFN & U. Tor Vergata
23-10-2008	*Precision Cosmic Ray Research in Space with PAMELA Experiment*
G. Stratan	Ist. Naz. Fisica ed Ingegneria Nucleare "Horia Hulubei", Bucarest
15-10-2008	*La Nozione di legge fisica nell'opera di Galileo Galilei*
W. Weise	Technische Universität München
13-10-2008	*Chiral SU(3) Dynamics and Antikaon-Nuclear Systems*
Uwe Becker	Fritz-Haber-Institut, Berlin
08-10-2008	*Entanglement in Space-Time: Suddenly this overview, big questions, small questions*
E. Borloni	Fondazione CNAO
19-09-2008	*Economia della salute: costruzione, gestione e analisi del Bilancio di un Centro di Adroterapia*
G. Dattoli	ENEA Frascati
11-09-2008	*Euler, Riemann, Ramunijan, Feynman, Dyson, Schwinger and Operational calculus*
S. Liuti	Univ. of Virginia, Charlottesville, VA
14-07-2008	*Hard Exclusive Reactions as Probes of Hadronic*
F. Sannibale	LBNL
10-07-2008	*Coherent Synchrotron Radiation Studies at the Advanced Light Source*
F. Sannino	Univ. of Southern Denmark
03-07-2008	*(Near) Conformal Technicolor: From Lattice to LHC and Cosmology*

R. Gunnella	U. Camerino
18-06-2008	*High temperature metallization of semiconductor surfaces studied by electron spectroscopies*
P. A. Lukin	BINP, Novosibirsk
17-06-2008	*BABAR Results on Hadronic Cross Sections with Initial State Radiation (ISR)*
Y.N. Srivastava	Univ. Perugia
11-06-2008	*Entropy, Memory and Information in Water Biophysical Basis of Water Memory*
J. R. Brucato	BINP, Novosibirsk
09-06-2008	*Organics on Stardust samples: Laboratory Hint of Astrobiology*
V. N. Makhov	P.N. Lebedev Physical Institute, RAS, Moscow
05-06-2008	*UV spectroscopy of rare earth ions in solids: recent studies and possible applications*
S. Bettoni	CERN
29-05-2008	*Stato del design magnetico dei quadrupoli del final focus per lo schema*
B.D. Josephson	U. of Cambridge, UK
27-05-2008	*The Fate of New Ideas: Nobel Prize or "Hell of the Heretic"?*
K. Rith	University of Erlangen-Nuremberg
26-05-2008	*The EMC effect - history and future*
E. Lamanna	U. Magna Graecia, Catanzaro
2-05-2008	*Percorsi formativi per l'insegnamento della fisica nel nuovo millennio*
A. Maratkanova	Physical-Technical Institute, Ural Branch of Russian Academy of Sciences
08-05-2008	*Nanostructured Fe-based materials obtained by mechanochemical synthesis in organic liquids*
A. Pullia	U. Milano Bicocca
04-04-2008	*Dark Matter search with a continuously sensitive Bubble Chamber*
H. de Kerret	College de France
19-03-2008	*Double Chooz experiment*
J. Purans	Juris Purans - Ins. of Solid State Physics, Riga
13-03-2008	*Near field X-ray spectromicroscopies: new tools for nanoscience*
G. Ranucci	INFN Milano
07-02-2008	*Risultati esperimento Borexino*
U. Schade	Bessy Berlin
16-01-2008	*THz Spectroscopy with Coherent Synchrotron Radiation*

Glossary

These are the acronyms used in each status report to describe personnel qualifications other than Staff Physicist:

Art 15	Term Contract (Technician)
Art. 23	Term Contract (Scientist)
Ass.	Associated Scientist
Ass. Ric.	Research Associate
Bors.	Fellowship holder
Bors. PD	PostDoc Fellow
Bors. UE	European Community Fellow
Dott.	Graduate Student
Laur.	Undergraduate Student
Loc. Coor.	Local Coordinator
Osp.	Guest Scientist
Perfez.	PostLaurea Student
Resp.	Local Spokesperson
Resp. Naz.	National Spokesperson
Specializ.	PostLaurea Student
Tecn.	Technician